SEDIMENTOLOGY OF THE UPPER CRETACEOUS (TURONIAN) CARDIUM FORMATION IN OUTCROP IN SOUTHERN ALBERTA

By

© WILLIAM LEWIS DUKE, B.S.

A Thesis

Submitted to the School of Graduate Studies

in Partial Fulfilment of the Requirements

for the Degree

Doctor of Philosophy

McMaster University

June 1985

SEDIMENTOLOGY OF THE CRETACEOUS CARDIUM FORMATION, ALBERTA

DOCTOR OF PHILOSOPHY (1985) McMASTER UNIVERSITY
(Geology) Hamilton, Ontario

TITLE: Sedimentology of the Upper Cretaceous (Turonian) Cardium Formation in Outcrop in Southern Alberta

AUTHOR: William Lewis Duke, B.S.
(Massachusetts Institute of Technology)

SUPERVISOR: Professor R. G. Walker

NUMBER OF PAGES: xxvi, 724

ABSTRACT

Cardium Formation exposures in Alberta consist of vertically juxtaposed thickening- and coarsening-upward cycles. Shallow-marine deposits exhibiting hummocky cross-stratification (HCS) dominate cycles. Locally, cycles record a marine to non-marine transition; they are interpreted as the deposits of a prograding storm-dominated shoreline. Sands were introduced into the basin by storms, and were transported in the proximal offshore region by geostrophically balanced bottom flows. Sharp contacts between cycles represent transgression surfaces; they display erosionally based, laterally extensive marine conglomerates. Locally, erosional transgressions removed non-marine deposits from the cycle tops over extensive distances normal to shoreline. Conglomerates were transported during transgressions, accumulating within a "hydrodynamic shadow" over the drowned shoreface of the preceding regressive episode.

A technique for paleohydraulic analysis of conglomeratic symmetrical ripples has been discussed, tested, and applied to Cardium occurrences; results suggest that associated examples of HCS were formed in the oscillatory-flow flat-bed field by previously unrecognized low-amplitude, three-dimensional orbital ripples.

ACKNOWLEDGMENTS

Funding for the research reported in this thesis was provided by the Natural Science and Engineering Research Council of Canada (operating grants to Roger Walker). Additional financial and logistic support was generously provided by Amoco Canada and Shell Canada. This support is most gratefully acknowledged. Amoco provided valuable helicopter time and logistic support; I am deeply indebted to Bill Richmond, Glen McMaster, Craig Nardon, and Adam Hettinger for these and other courtesies.

William Kramer, Andrew Bullock, Emidio Crapsi, and Gary Loosemore provided competent, tireless, cheerful, and forgiving field assistance; I was very lucky to have had their company and help. Likewise, I was exceptionally fortunate to have had the opportunity to examine several Cardium sections with Guy Plint, George Pemberton, Bob Frey, Dale Leckie, Doug Cant, Perry Glaister, Percy Strong, and John Knight, who generously shared their expertise. I extend my thanks to all these friends.

I thank Jack Whorwood for all the photographic assistance and stimulating conversation over the years, and Don Krebs, who made the plates for this thesis.

Courses and coversations with various McMaster workers have been enormously enriching; my deep appreciation is extended to Gerry "Doc" Middleton, Gerd

Westermann, Paul Clifford, Brian McCann, Mark Donelan, Guy Plint, Paul Smith, Dale Leckie, Rick Cheel, Brent Ainsworth, Dan Thompson, Larry Heaman, Rick Kusmirski, Lorne Rosenthal, Dave Taylor, Greg Nadon, Scott Furgeson, Ulrich Meier-Hart, Dave Collins, Pedro Moreno-Heinz, Randy Rice, Fereydon Gazhban, Don Keith, Karen Downing, Kathy Bergman, Marg Rutka, and many others.

I thank the faculty of the Department of Geosciences, the Pennsylvania State University, for the confidence they expressed in hiring me prior to the completion of this thesis. I am especially indebted to Rudy Slingerland, for his support, and C. Wayne Burnham, for his decision.

The topic of this thesis was suggested by Roger Walker, who supervised all aspects of the research. It is my sincere opinion that he provided the finest supervision any graduate student could ever receive, effecting that rare balance (so vital to intellectual growth) between active direction and the freedom to explore unlikely tangents. Given my numerous flights of fancy, maintenance of this balance testifies to a great patience and strength of character. Additionally, Roger provided many days on the outcrop dedicated to instruction in basic techniques and principles, an enormous enthusiasm and insight which inspired continuing effort, and skillful editing of a seemingly endless string of preliminary drafts. The suc-

cesses of this thesis are directly attributable to the high quality of this supervision, which shall serve as a pattern for my further work, and for which I am ever grateful.

Most importantly, I thank all my family, who formed and nurtured me, and provided the marvelous opportunities that have enriched my experience in life. I especially thank my mother, Lillian Hazel Duke, and my father, William Lewis Duke, who provided the firmest of foundations upon which are built my life, mind, and principles. I thank my father- and mother-in-law, Vincenzo and Vincenza Matteliano, and my brother- and sister-in-law, Calogero and Yian Wui Matteliano, who have continued and refined my development through their support and example.

Lastly, to my wife, Maria Agnese Matteliano, without whom none of this would have been possible or even worthwhile, and to our child, as yet unborn, this thesis is lovingly and gratefully dedicated.

"We have no right to isolated thoughts, whether truthful or erroneous. Our thoughts should grow out of our values with the same necessity as the fruit out of the tree. Our yeas and nays, our ifs and buts should all be intimately related and bear testimony to one will, one health, one soil, one sun. Supposing you find these fruits unpalatable? What concern is that of the trees...?"

-- F. W. Nietzsche

TABLE OF CONTENTS

	Page
CHAPTER 1. INTRODUCTION TO THIS STUDY, AND THE GENERAL NATURE OF ITS CONTRIBUTION	1
History of this study	1
Scientific justification for this study	5
Economic justification for this study	9
Specific objectives and methods	10
CHAPTER 2. THE CARDIUM FORMATION: BRIEF DESCRIPTION, CRITICAL REVIEW OF PREVIOUS WORK, AND SUMMARY OF THE PRESENT STUDY	15
Introduction	15
Brief description of the Cardium Formation	15
Origin of the name of the formation	17
Previous interpretations of depositional processes and environments	22

CHAPTER 3. STRATIGRAPHIC REVISIONS OF THE CARDIUM FORMATION AND ITS MEMBERS IN THE ALBERTA FOOTHILLS 40

Introduction 40

Internal inconsistencies of existing cycle and member correlations 46

Cycle vs. member correlations: Do Stott's cycles represent lithostratigraphic units? 49

Proposed revision of member stratigraphy based upon cycle correlations documented in this thesis 54

CHAPTER 4. DEFINITION AND PRELIMINARY INTERPRETATION OF FACIES 62

Introduction 62

Facies descriptions 66

Association 1. Mud-dominated marine facies 67

Facies 1SH 67

Facies 1BM 68

Facies 1GB 71

Facies 1UP 81

Association 1: Preliminary interpretation 91

Association 2. Interbedded hummocky cross-stratified sandstones and mudstone 94

Facies 2H1 96

Facies 2H2 112

Facies 2H3 120

Association 2: Preliminary interpretation 127

Association 3. Sand-dominated facies 129

Facies 3BS 129

Facies 3HA 132

Facies 3SW 153

Facies 3PL 172

Association 3: Preliminary interpretation 178

Association 4. Non-marine deposits 181

Facies 4VL 182

Facies 4VC 189

Facies 4IF 195

Facies 4SF 204

Association 4: Preliminary interpretation 215

Association 5. Marine conglomerates 217

Facies 5CV 218

Facies 5CB 225

Facies 5C1 231

Facies 5C2 236

Association 5: Preliminary interpretation 243

Brief summary of inferred depositional environments 245

CHAPTER 5. VERTICAL FACIES RELATIONSHIPS: THE DEFINITION AND PRELIMINARY INTERPRETATION OF CYCLES 246

Introduction 246

Note on statistical methods utilized herein 251

Generalized description of Cardium cycles 255

Facies sequence analysis, and the definition of cycle types 260

"Type examples" of Cardium cycles 289

Segregated Markov-chain analyses 291

Cycle type 1 301

Cycle type 2 302

Cycle type 3 305

Cycle type 4 323

Cycle type 5 324

Cycle type 6 339

Preliminary interpretation of Cardium cycles 345

Interpretation of variant cycles 360

Description and interpretation of selected features within their stratigraphic context 367

A preliminary interpretation of Cardium sequences, emphasizing features of the shoreline and lower coastal plain 376C

CHAPTER 6. LATERAL CORRELATION OF CYCLES, AND THE DEVELOPMENT OF A CONCEPTUAL MODEL FOR CARDIUM SEDIMENTATION 385

Introduction 385

Correlation of Cardium cycles: Gross relationships 386

Correlation of Cardium cycles: Detailed relationships 403

Development of a conceptual model for Cardium sedimentation: Assumptions and constraints 416

A conceptual model for Cardium sedimentation 424

Summary of the conceptual model developed in the preceding time series diagrams 462

Some variations on the basic facies geometry in the conceptual model 463

Tests of the conceptual model 472

CHAPTER 7: PALEOGEOGRAPHIC RECONSTRUCTIONS AND PALEOFLOW PATTERNS: DEFINITION OF LARGE-SCALE SHELF CIRCULATION DURING CARDIUM DEPOSITION 493

Introduction 493

Patterns of shelf circulation determined from paleoflow data: Implications for large-scale depositional processes 495

Paleogeographic reconstructions 503

A tentative extension of the findings of this thesis to subsurface Cardium fields 520

CHAPTER 8. EXTENDED DISCUSSION OF WAVE-FORMED STRUCTURES AND SEQUENCES IN THE CARDIUM FORMATION 527

Chapter outline and introduction 527

Notation used in this chapter 528

PART 1. Suggested processes for the origin of hummocky cross-stratification: A critical review 531

Introduction 531

Hummocky cross-stratification: Description 532

Inferred origin due to progressive surface gravity waves: Historical perspective 550

Inferred origin due to progressive surface gravity waves: Some recent suggestions 553

Suggested generative agents other than bottom flows resulting from progressive surface gravity waves 579

Summary and discussion 589

PART 2. Paleohydraulic analysis of conglomeratic symmetrical ripples 592

Introduction: Symmetrical ripples as paleohydraulic indicators 592

Symmetrical ripple morphology 593

Calculation of bottom orbital diameter from ripple parameters 597A

Determination of flow conditions in the boundary layer 606

Data sources 617

The definition of incipient motion 622

Empirical relationship governing onset of general motion under turbulent flow 624

Calculation of U_m^2/T^2 from ripple parameters 634

Determination of U_m^2 and T^2 635

Test of paleohydraulic method 640

Summary and discussion 652

PART 3. Application of paleohydraulic method to ancient occurrences of conglomeratic symmetrical ripples, and implications for the origin of hummocky cross-stratification 663

Introduction 663

Hummocky cross-stratification and conglomeratic symmetrical ripples 665A

Origin of conglomeratic symmetrical ripples 668

Structural sequences involving conglomeratic symmetrical ripples and hummocky cross-stratification: Summary 676

Structural sequences involving conglomeratic symmetrical ripples and hummocky cross-stratification: Qualitative interpretation 678

Structural sequences involving conglomeratic symmetrical ripples and hummocky cross-stratification: Quantitative interpretation 682

PART 4. Estimated bathymetry and storm-wave climate, and the hydraulic significance of vertical structural sequences in prograding shoreline deposits in the Cardium Formation 689

Introduction 689

Cycle thickness and paleobathymetry 689

Magnitude of storm waves incident at Cardium shorelines 692

Toward a hydraulic framework for the interpretation of vertical sequences developed in prograding shoreline deposits. 693

CHAPTER 9. SUMMARY OF THIS STUDY 698

Internal stratigraphy of the Cardium Formation 698

Large-scale sedimentology of the Cardium Formation 699

Nature and origin of various wave-formed structures 703

Improved technique for vertical facies analysis 705

AFTERWORD 706

REFERENCES 707

APPENDIX 1. FIELD GUIDE TO EXPOSURES OF THE CARDIUM FORMATION MEASURED FOR THIS STUDY

APPENDIX 2. MEASURED SECTIONS OF THE CARDIUM FORMATION

APPENDIX 3. FACIES-TRANSITION DATA

APPENDIX 4. FABRIC DATA FROM CONGLOMERATES IN THE CARDIUM FORMATION

APPENDIX 5. VECTOR MEANS OF PALEOFLOW DATA

APPENDIX 6. SUMMARY OF THE EXISTING STRATIGRAPHIC SYSTEM FOR THE CARDIUM FORMATION IN FOOTHILLS EXPOSURES

APPENDIX 7. SUMMARY OF THE REVISED STRATIGRAPHIC SYSTEM FOR THE CARDIUM FORMATION IN FOOTHILLS EXPOSURES

APPENDIX 8. AN ANNOTATED HISTORY AND BIBLIOGRAPHY OF HUMMOCKY CROSS-STRATIFICATION

APPENDIX 9. TABULATION OF THE DATA OF MANOHAR (1955) FOR THE ONSET OF INCIPIENT AND GENERAL MOTION OF SEDIMENT UNDER OSCILLATORY FLOW

LIST OF FIGURES

Fig.		Page
1-1	Location map of sections measured for this study	6
2-1	Map of the Cardium in subsurface	18
2-2	Stratigraphy of the Alberta Group	20
3-1	Member divisions of Cardium Formation	41
3-2	Cardium correlation diagram by Stott	47
3-3	Correlation diagrams for Cardium sections 5-37 and 5-45	51
4-1	Exposures of facies 1SH and 1GB	69
4-2	Exposures of facies 1GB	73
4-3	Bouma sequence	75
4-4	Exposures of facies 1UP	83
4-5	Exposures of facies 1UP	85
4-6	Block diagram of undulatory parallel lamination	87
4-7	Symmetrical ripples in association 2	95
4-8	Block diagram of sharp-based hummocky cross-stratification	97
4-9	Exposures of facies 2H1	101
4-10	Sole features in association 2	103
4-11	Trace fossils from associations 1 and 2	109
4-12	Exposures of facies 2H2	113
4-13	Exposures of facies 2H2	115

4-14	Exposures of facies 2H2	117
4-15	Exposures of facies 2H3	121
4-16	Trace fossils from facies 3BS	131
4-17	Block diagram of amalgamated hummocky cross-stratified sandstone	135
4-18	The four subfacies of amalgamated hummocky cross-stratified sandstone	137
4-19	Exposures of facies 3HA	143
4-20	Exposures of facies 3HA	145
4-21	Exposures of facies 3HA	149
4-22	Block diagram of swaley cross-stratification	155
4-23	Exposures of facies 3SW	157
4-24	Exposures of facies 3SW	159
4-25	Exposures of facies 3SW	161
4-26	Body fossils from Cardium Formation	171
4-27	Exposures of facies 3PL	175
4-28	Exposures of facies 4VL and 4VC	183
4-29	Root casts in associations 3 and 4	185
4-30	Exposures of facies 4IF	197
4-31	Exposures of facies 4SF	207
4-32	Exposures of facies 5CV	219
4-33	Exposures of facies 5CB	227
4-34	Exposures of facies 5C1	233
4-35	Exposures of facies 5C2	239
5-1	A typical thickening- and coarsening-upward cycle in the Cardium Formation	247

5-2	Classification scheme for Cardium cycles	257
5-3	Residual probability: Cardium Formation, all transitions	263
5-4	Simplified residual probability: Cardium Formation, all transitions	265
5-5	Confidence: Cardium Formation, all transitions	271
5-6	Significance: Cardium Formation, all transitions	273
5-7	Simplified residual probability: type 1 cycles	277
5-8	Confidence: type 1 cycles	279
5-9	Significance: type 1 cycles	281
5-10	Simplified residual probability: top-absent cycles	283
5-11	Confidence: top-absent cycles	285
5-12	Significance: top-absent cycles	287
5-13	Vertical juxtapositioning of like cycles	293
5-14	Key for simplified residual probability diagrams	295
5-15	Key for confidence diagrams	297
5-16	Key for significance diagrams	299
5-17	Normative type 1 cycle	303
5-18	Simplified residual probability: type 2 cycles	307
5-19	Confidence: type 2 cycles	309
5-20	Significance: type 2 cycles	311
5-21	Normative type 2 cycle	313
5-22	Simplified residual probability: type 3 cycles	315

5-23	Confidence: type 3 cycles	317
5-24	Significance: type 3 cycles	319
5-25	Normative type 3 cycle	321
5-26	Simplified residual probability: type 4 cycles	325
5-27	Confidence: type 4 cycles	327
5-28	Significance: type 4 cycles	329
5-29	Normative type 4 cycle	331
5-30	Simplified residual probability and confidence: type 5 cycles	333
5-31	Significance: type 5 cycles	335
5-32	Normative type 5 cycle	337
5-33	Simplified residual probability and significance: type 6 cycles	341
5-34	Normative type 6 cycle	343
5-35	Proximal-distal ordering of cycle types	347
5-36	Cycle relationships involving a minor split of non-marine sediment	363
5-37	A middle-absent cycle	365
5-38	Detailed vertical log for section GC-2	371
5-39	Gutter casts from associations 1 and 2	373
5-40	Shore-normal vertical profile for a wave-dominated sandy shoreline	377
5-41	Block diagram of Cardium shoreline and lower coastal plain	381
6-1	Location map of correlation diagrams	388
6-2	Correlation diagram 32	390

6-3	Correlation diagram S1	392
6-4	Correlation diagram D1	394
6-5	Correlation diagram D2	396
6-6	Correlation diagram D3	398
6-7	Correlation diagram D4	400
6-8	Correlations from Grande Cache area	404
6-9	Correlation diagram illustrating two different correlations of the same rocks	410
6-10	Regressive-transgressive episode of Cardium sedimentation: time 1	426
6-11	Regressive-transgressive episode of Cardium sedimentation: time 2	432
6-12	Regressive-transgressive episode of Cardium sedimentation: time 3	438
6-13	Regressive-transgressive episode of Cardium sedimentation: time 4	444
6-14	Regressive-transgressive episode of Cardium sedimentation: time 5	450
6-15	Shoreface translation, erosion, and aggradation	452
6-16	Regressive-transgressive episode of Cardium sedimentation: time 6	458
6-17	Regressive-transgressive episode of Cardium sedimentation: time 7	460
6-18	Examples of variability in conceptual model	464
6-19	Sediment distribution in subsurface Willesden Green field	470

6-20	Distribution of cycle-capping transgressive conglomerates by cycle type	478
6-21	Transgressive conglomerate thickness vs. thickness of association 3 sandstones for occurrences of cycle types 2 and 3	482
6-22	Transgressive conglomerate thickness vs. thickness of association 2 deposits for occurrences of type 4 cycles	484
6-23	Joint distribution by cycle type of fining-upward cycle caps and transgressive conglomerates	486
7-1	Comparison of vector mean orientation of symmetrical ripple crests and vector mean flow orientations	498
7-2	Development of a geostrophically balanced flow along an east facing shoreline in the northern hemisphere	504
7-3	Location map and pseudo-palinspastic base map for paleogeographic reconstructions	508
7-4	Data base and paleogeographic reconstruction of the Seebe-Cutpick regression	510
7-5	Paleogeographic reconstruction of the Sundre transgression	512
7-6	Data base and paleogeographic reconstruction of the Sundre-Cutpick regression	518
7-7	Pembina field in vertical cross-section	522

7-8	Subsurface Cardium paleogeography.	524
8-1	Order of discordant surfaces in hummocky cross-stratified beds	536
8-2	Classification of second order boundaries within hummocky cross-stratification	538
8-3	Flow-parallel profiles of ripples generated under oscillatory flow	595
8-3.5	Plot of λ_r/D vs. d_o/D for wave-formed ripples	597C
8-4	Relationship between fluid motion characteristics under progressive surface gravity waves	599
8-5	Variation in d_o^* with grain size for quartz-density particles	603
8-6	λ_r vs. D for recent ripples	611
8-7	"Measured" vs. "predicted" values of d_o for recent ripples	613
8-8	Jonsson diagram for determination of f_w and flow conditions in an oscillatory boundary layer	619
8-9	Data of Manohar (1955) for incipient few-particle displacement of quartz-density sediment	625
8-10	Comparison of data trends for incipient few-particle displacement	629
8-11	Data of Manohar (1955) for incipient few-particle displacement of quartz-density sediment	631

8-12	Nomogram for determination of U_M^* and T^* for straight-crested orbital vortex ripples formed under rough-turbulent oscillatory flow	637
8-13	"Measured" vs. "predicted" values of U_M for recent ripples	643
8-14	"Measured" vs. "predicted" values of T for recent ripples	645
8-15	Boundary-layer development in an oscillating-bed device	655
8-16	Vertical near-bed and intergranular water motion resulting from oscillatory flows	659
8-17	Exposures of conglomeratic symmetrical ripples formed within a prograding shoreline sequence	664
8-18	Exposures of conglomeratic symmetrical ripples capping a prograding shoreline sequence	6658
8-19	Graph of λ_M vs. D for ancient conglomeratic symmetrical ripples	672
8-20	Comparison of BPHFXM sequence with rare variant sequence (BRHFXM)	680
8-21	Calculated generative flow conditions for conglomeratic symmetrical ripples in the Cardium Formation and the Chungo Sandstone of the Wapiabi Formation	684
8-22	Calculated generative flow conditions for conglomeratic symmetrical ripples in the Moosebar-Gates transition	686

8-23 A tentative framework for the interpretation of vertical structural sequences observed in prograding shoreline sequences in the Cardium Formation 694

LIST OF TABLES

Table		Page
8-1	"Measured" values of generative wave parameters for recent ripples formed in a water depth of 18.3 m	607
8-2	"Predicted" values of generative wave parameters and depth for recent ripples	609
8-3	Relative error between measured and predicted values of generative fluid-motion characteristics for recent ripples	615
8-4	Characteristic parameters of ancient conglomeratic symmetrical ripples	666
8-5	Calculated fluid-motion characteristics of ancient conglomeratic symmetrical ripples	674

CHAPTER 1. INTRODUCTION TO THIS STUDY, AND THE GENERAL NATURE OF ITS OBJECTIVES

In the summer of 1978, I began an extensive field study of the Upper Cretaceous Cardium Formation in the Rocky Mountain Foothills of southern Alberta, Canada. The major results of this study are reported in this thesis. A brief history, justification, and summary of the methods and objectives of this study is presented in this chapter.

HISTORY OF THIS STUDY

In June, 1977, Roger Walker and Rein de Wit visited an outcrop of the Cardium Formation at Seebe, Alberta. Their preliminary survey of this exposure revealed that hummocky cross-stratification is well developed and present in abundance at this site, and their findings represent the first recognition of this structure within the Cardium Formation. At that time, hummocky cross-stratification was a relatively newly-recognized structure (see appendix 8). The term "hummocky cross-stratification" was first introduced in 1975 (Harms et al., 1975, p. 87). It was not until 1976 that hummocky cross-stratification was first

recognized in Alberta, when A. P. Hamblin identified the structure in the Jurassic Fernie-Kootenay transition (Hamblin, 1978).

During the summer of 1978, a preliminary examination by Walker and this author of Cardium sections 6-8 (Red Deer River) and 5-45 (Ram River) revealed that hummocky cross-stratification is ubiquitous over a wide area in the Alberta Foothills. Also, this preliminary work demonstrated that major problems exist in the member divisions defined by Stott (1963). Specifically, it was observed that these member divisions do not adequately reflect the basic subdivisions of the formation -- namely, the well developed coarsening-upward cycles which are present in each exposure. Very early into this study, therefore, the following three important points became obvious:

1) The interpretation of hummocky cross-stratification was recognized as being essential to an analysis of sedimentary processes and depositional environments in the Cardium Formation. Specifically, both the inferred origin(s) of the structure and the inferred method(s) of emplacement of the sands in which the structure is formed would constitute a major constraint on the inferred depositional processes and environments of the Cardium.

2) The need to revise the internal stratigraphy

(member divisions) of the formation was indicated by preliminary correlations. The identification of the proper units of correlation throughout the Foothills might also facilitate correlation between Foothills exposures and subsurface oil and gas fields.

3) Because previous investigators of Cardium depositional environments in the Foothills did not recognize the ubiquitous hummocky cross-stratification, previous interpretations of depositional environments were considered likely to be inadequate. Likewise, preliminary paleoflow measurements suggested that sediment transport within the Cardium was directed predominantly toward the southeast. This physical evidence contradicted previous suggestions of sediment dispersal toward the northeast (MacDonald, 1957; Stott, 1963, p. 137-141). These earlier suggestions were based upon regional thickness trends within the sandstones, not upon paleoflow indicators preserved in the rocks.

These preliminary observations each suggested the timeliness of a major re-examination of the Cardium Formation in the Foothills. Specifically, extensive field work would be required to determine: 1) regional variation within hummocky cross-stratified sandstones, 2) regional stratigraphic relationships within the formation, and 3) regional variation in depositional environments and

paleoflow patterns.

Thus, during the first field season (summer, 1978), it was decided to spend several additional field seasons measuring in detail as many Cardium exposures as possible. Field methods are described below. Three additional summer field seasons were spent in Alberta and British Columbia. Each of these was 14 to 16 weeks in duration.

Field work by the author was limited to an area of roughly 28,000 km²; this area contains the entire northern Foothills of Alberta (between the Athabasca River and the Alberta-British Columbia border) and the major part of the central Foothills (between the Athabasca and Bow Rivers). Additionally, the Cardium was measured in the Pouce Coupe area of British Columbia, northeast of the Alberta field area. In total, 28 complete or partial sections were measured by the author, and a few additional sections were briefly examined (Fig. 1-1).

South of this field area, several additional sections of the Cardium were measured by Walker (unpublished) and other students, specifically, B. H. Ainsworth (unpublished) and M. E. Wright (1980). Some of their findings have been incorporated within this thesis. These sections are located in the extreme southern portion of the central Foothills and throughout the southern Foothills between the Bow River and the Alberta-Montana border (Fig. 1-1). These southern sections were all

measured during the 1979 and 1980 field seasons.

Portions of the research summarized in this thesis have been presented in a preliminary form elsewhere (Hamblin et al., 1979; Duke et al., 1980; Duke, 1981; Duke, 1982a; Walker et al., 1983; Duke & Leckie, 1984; Leckie & Duke, 1984; Duke, 1985b). Additionally, a major paleogeographic and paleoclimatologic survey of all known examples of hummocky cross-stratification, originally intended to form a portion of this thesis, has already been published separately (Duke, 1985c), and will not be elaborated upon herein.

SCIENTIFIC JUSTIFICATION FOR THIS STUDY

Early in this study, it was recognized that a major re-examination of the Cardium Formation in the field would be scientifically interesting for at least five major reasons:

1) The Cardium Formation in the Alberta Foothills is an excellent and well exposed example of a shallow-marine sequence displaying abundant, well developed hummocky cross-stratification. Because this sedimentary structure is newly recognized and poorly understood, an extensive and detailed facies analysis of this unit would

Figure 1-1. Locations of measured sections utilized in this study. Filled circles represent sections measured by the author. Open circles represent sections measured by Roger G. Walker, Brent H. Ainsworth, and Marsha E. Wright. The dotted lines labelled A.R. and B.R. represent the Athabasca and Bow Rivers, respectively, and define the boundaries of the northern, central, and southern Foothills of Alberta. Detailed directions to sections measured by the author are presented in appendix 1, which also includes detailed location maps and outcrop photographs.

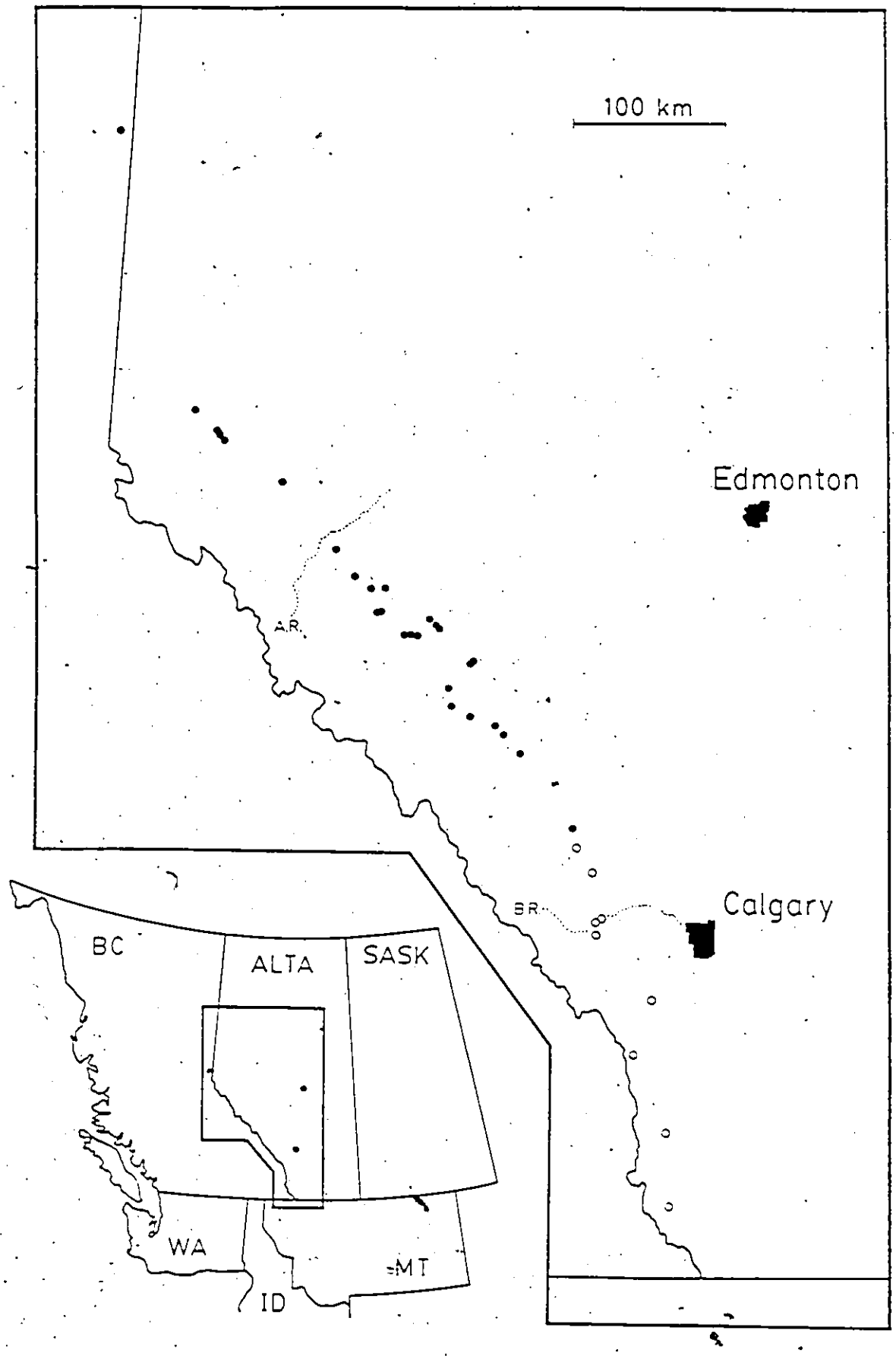
100 km
Edmonton
Calgary
A.R.
B.R.
BC
ALTA
SASK
WA
ID
MT

constitute a major contribution to the limited body of knowledge currently in existence on the environmental significance of hummocky cross-stratification. Additionally, a process-oriented analysis of structures and sequences developed in the Cardium Formation could possibly enhance our understanding of the processes which generate hummocky cross-stratification.

2) Because hummocky cross-stratification has been interpreted as a storm-generated structure, the abundance of this structure in the Cardium Formation suggests that major storms were common within the Western Interior Seaway during Cardium time. It was reasoned that a systematic study of the Cardium Formation might reveal something of the nature of violent storms during the non-glacial Cretaceous Period, and also might contribute to our knowledge of sedimentary processes associated with storm-dominated depositional systems.

3) Resedimented conglomerates were also recognized from the early outcrop examinations. There have been few systematic studies of resedimented conglomerates, especially those deposited in shallow-marine basins. A second major justification for this study, therefore, was to determine the processes of deposition of these conglomerates.

4) Shallow-marine sandstones are present within the Cardium Formation in the subsurface of the Alberta Plains.

These sand bodies form major hydrocarbon reservoirs, and their distribution is well documented by core and log data. A study of the Cardium in outcrop would possibly shed light upon the development of these sandstones.

5) Because the Cardium Formation is such an excellent example of storm-dominated shallow-marine sedimentation, a systematic facies analysis of this unit could provide a major part of a data base upon which a facies model for this style of sedimentation may eventually be erected.

ECONOMIC JUSTIFICATION FOR THIS STUDY

The Cardium Formation is one of the largest producers of oil and gas in Canada (Oil Pools of Western Canada, Geological Survey of Canada, Map 1559A, 1981). The formation produces from wells in both the Foothills (Ricinus field and minor stratigraphic traps) and the Plains (all other fields). The last systematic study of Cardium exposures throughout the Foothills was conducted between 1954 and 1957 (Stott, 1963) and was largely stratigraphic in nature. Thus, a re-examination of Cardium exposures at this time should provide industry with a long-overdue sedimentological framework for the interpretation of Cardium sand bodies, for the search for

new Cardium reservoirs, and for the planning of enhanced recovery programs.

Additionally, there are several other major reservoir sandstones in the Western Interior of North America and elsewhere which closely resemble the Cardium Formation in major respects (e.g., Gallup Sandstone of New Mexico; Campbell, 1971; Harms et al., 1975, chapter 5). A local depositional model developed from the Cardium Formation could serve as a preliminary facies model to aid in the interpretation and exploitation of these similar units.

SPECIFIC OBJECTIVES AND METHODS

The major goals of the field work conducted for the present study can be grouped under three headings:

1) Depositional environment. The primary objective throughout this study has been to determine depositional environments within the Cardium Formation from examination of Foothills exposures. In order to accomplish the primary objective, it was determined that the major emphasis of the study would be placed upon field work; accordingly, a full four summer-long field seasons were devoted to the detailed examination of the maximum number of exposures possible

over the maximum field area possible. This aspect of the investigation can be referred to as the extensive environmental survey. In order to evaluate the possibility of pronounced variation in depositional environment over short distances laterally, an area in the northern part of the central Foothills was selected for the examination of several closely spaced exposures (Fig. 1-1). The selection of an area for this intensive environmental survey was dictated by: 1) the recognition early in the study that major environmental variation was recorded in the central Foothills exposures, and 2) availability of closely spaced outcrop of suitable quality (see below). Where fortuitous combinations of outcrop and accessibility permitted, limited intensive surveys involving only a few exposures were conducted outside this designated target area (e.g., in the region of Grande Cache).

Although maximum coverage was a major goal, this priority primarily affected only the selection of outcrop, not the manner in which it was examined. Specifically, once an outcrop was selected for examination, it was systematically and thoroughly measured, and a vertical graphic log was drawn at the scale of 2 cm to the meter. Section measurement included a bed-by-bed examination for paleoflow indicators preserved in the rocks, including many tedious measurements of conglomerate fabric. Availability of supplies or transportation occasionally necessitated a

less thorough examination.

Another factor which controlled outcrop selection was the quality of exposure. Generally, the sections measured for this study represent the best available outcrop, being well exposed laterally and apparently undisturbed tectonically. This criterion was necessary for proper evaluation of primary structures and paleoflow indicators. Some exceptions were deemed necessary due to their environmentally critical location (e.g., section NR-1 on the North Ram River, which is poorly exposed and may be tectonically thinned).

Finally, a fifth summer field season was devoted to the examination of units similar in depositional style to the Cardium Formation, in an attempt to possibly refine and/or generalize environmental interpretations inferred for the Cardium Formation. Findings from this part of the study have not been explicitly incorporated into this thesis.

2) Origin of hummocky cross-stratification. The second major objective of field work was the accumulation of descriptive data concerning hummocky cross-stratification, with the intention of refining our knowledge of the processes which form the structure. Specifically, parameters of form-spacing, form-height, relationships between laminae and lamina-intersection

surfaces, and other basic descriptors were recorded wherever possible. This activity required only minimal outcrop-inspection time additional to that necessary for the primary objective. Some of the results of this aspect of the study have already been published elsewhere (Walker et al., 1983; Leckie & Duke, 1984; Duke & Leckie, 1984; Duke, 1985b, 1985c).

3) Conglomerate depositional processes. The third major objective of field work was the acquisition of conglomerate fabric data for use in determining the depositional processes of Cardium conglomerates. This activity, although time consuming, generally did not interfere with the primary objective: Most of the fabric data were obtained by the field assistant during the time that I was engaged in measurement of the section.

Fabric data were obtained using the Brunton compass and a ruler. Generally, the data collected included: 1) orientation of the A-B plane (i.e., the plane containing the long and intermediate axes), 2) rake of the long axis within the A-B plane, and 3) length of the long axis. Additionally, generalized clast shape was approximately determined visually, and regional bedding attitude was of course also recorded. These conglomerate fabric data are tabulated in appendix 4. Where present, sedimentary structures in Cardium conglomerates (such as graded bedding

and conglomeratic symmetrical ripples) were also examined in detail.

For reasons of space and time limitations, much of the fabric data collected have not been analyzed in detail for this thesis. Accordingly, the interpretations of Cardium conglomerates offered herein are based upon internal structures, facies sequences, lateral facies transitions, and the preliminary fabric data.

In addition to the field work described above, data from theoretical, experimental, and recent studies of oscillatory-flow bedforms were re-examined in detail. This re-examination has led to the development of a new technique for the paleohydraulic analysis of conglomeratic symmetrical ripples, and has permitted a narrowing of the range of possible hydrodynamic conditions under which some examples of hummocky cross-stratification were formed. This portion of my thesis work has been summarized in abstract form elsewhere (Duke & Leckie, 1984), and is presented in detail in chapter 3.

Finally, it is noteworthy that petrographic analysis was not included as a part of the present investigation; however, complete sample suites were collected for possible future studies. Sampling included mudstones for future micropaleontological identifications.

CHAPTER 2. THE CARDIUM FORMATION: BRIEF DESCRIPTION, CRITICAL REVIEW OF PREVIOUS WORK, AND SUMMARY OF THE PRESENT STUDY

INTRODUCTION

In this chapter, a brief description of the Upper Cretaceous (Turonian) Cardium Formation is provided for readers who are unfamiliar with its appearance in outcrop and its regional distribution. The origin of the name of the formation is then discussed, and there follows a detailed summary of previous work. This summary emphasizes previously published interpretations of depositional processes and environments of this unit. Interpretations developed from the present study are briefly summarized and contrasted with those from previous studies.

BRIEF DESCRIPTION OF THE CARDIUM FORMATION

The Cardium Formation is very well exposed throughout the Alberta Foothills. The formation can be traced in outcrop as far north as central British Columbia and the Peace River area of central Alberta (Stott, 1975);

to the south, it is probably also present in northern Montana (Stott, 1963). The unit extends to the northeast of this outcrop belt in the subsurface of the Alberta Plains. In the subsurface, the Cardium is present throughout the western half of southern Alberta (Fig. 2-1 -- see also chapter 7).

In the Alberta Foothills, the formation has an average thickness of approximately 100 m. Situated centrally within the Alberta group, the Cardium is underlain and overlain by hundreds of meters of dark grey to black marine shale (Fig. 2-2 -- see chapter 3 and appendix 7 for details of internal stratigraphy). The Cardium Formation is everywhere represented by one or more shallow-marine thickening- and coarsening-upward clastic sequences, or cycles. These cycles are largely composed of mudstones and sandstones; predominantly, the sandstones are hummocky cross-stratified. The number of coarsening-upward cycles tends to increase toward the central Foothills. Cycles typically are sharply bounded. As shall be demonstrated in this thesis, these cycles probably represent prograding, storm-dominated, shallow-marine and shoreline deposits. The sharp bounding surfaces probably represent periods of transgression; these surfaces typically are erosional or non-depositional, or are punctuated by conglomerate beds deposited during transgression.

Cycles in the southern Foothills do not contain non-marine deposits; the thick sandstones present within these southern exposures were deposited entirely within shallow marine environments. Further north, however, cycles typically are fully regressive (i.e., capped by non-marine deposits). The non-marine intervals within the Cardium thicken toward the northwest and the southwest. Non-marine beds are not present southeast of Cripple Creek in the central Foothills, but are present in every complete section northwest of this locality.

ORIGIN OF THE NAME OF THE FORMATION

The following history of the origin and establishment of the name "Cardium Formation" is summarized from the more comprehensive review by Stott (1963). The first published usage of the term "Cardium shales" is by Whiteaves (1895, p. 110), who identified fossils collected by J. Hector from Cretaceous marine rocks along Bow River. The Cardium Formation and surrounding strata contain in abundance several species of pelecypods formerly included in the genus Cardium; ironically, however, this genus recently has been redefined, and is now restricted to Europe and Africa (Thompson, no publication date given, p. 483). The name was restricted to the sandstones within

Figure 2-1. Map of Cardium reservoir fields, showing the subsurface depositional edge of the formation. K = Kakwa; E = Edson; C.C. = Carrot Creek; W.G. = Willesden Green; F = Ferrier; R = Ricinus; C = Caroline; G = Garrington; CR = Crossfield. After Walker (1983c, Fig. 1).

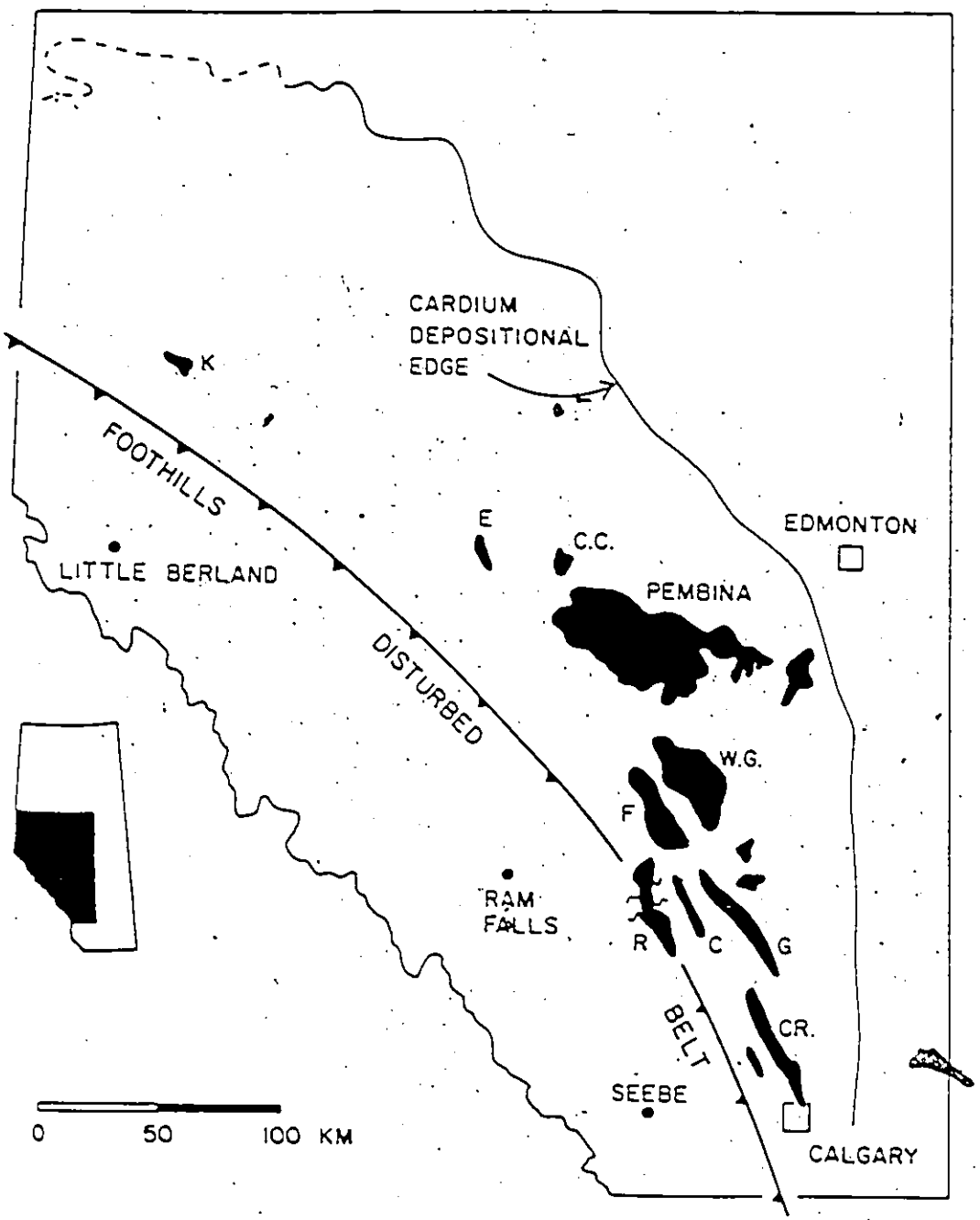
CARDIUM
DEPOSITIONAL
EDGE
K
FOOTHILLS
LITTLE BERLAND
E
C.C.
EDMONTON
PEMBINA
DISTURBED
W.G.
F
RAM
FALLS
R
C
G
BELT
CR.
SEEBE
CALGARY
0
50
100 KM

Figure 2-2. Stratigraphy of the Alberta Group in the Alberta Foothills (equivalent to the Colorado Group in the U.S.A.). Numbers at left are absolute ages in millions of years (Palmer, 1983). From Walker (1984, Fig. 2).

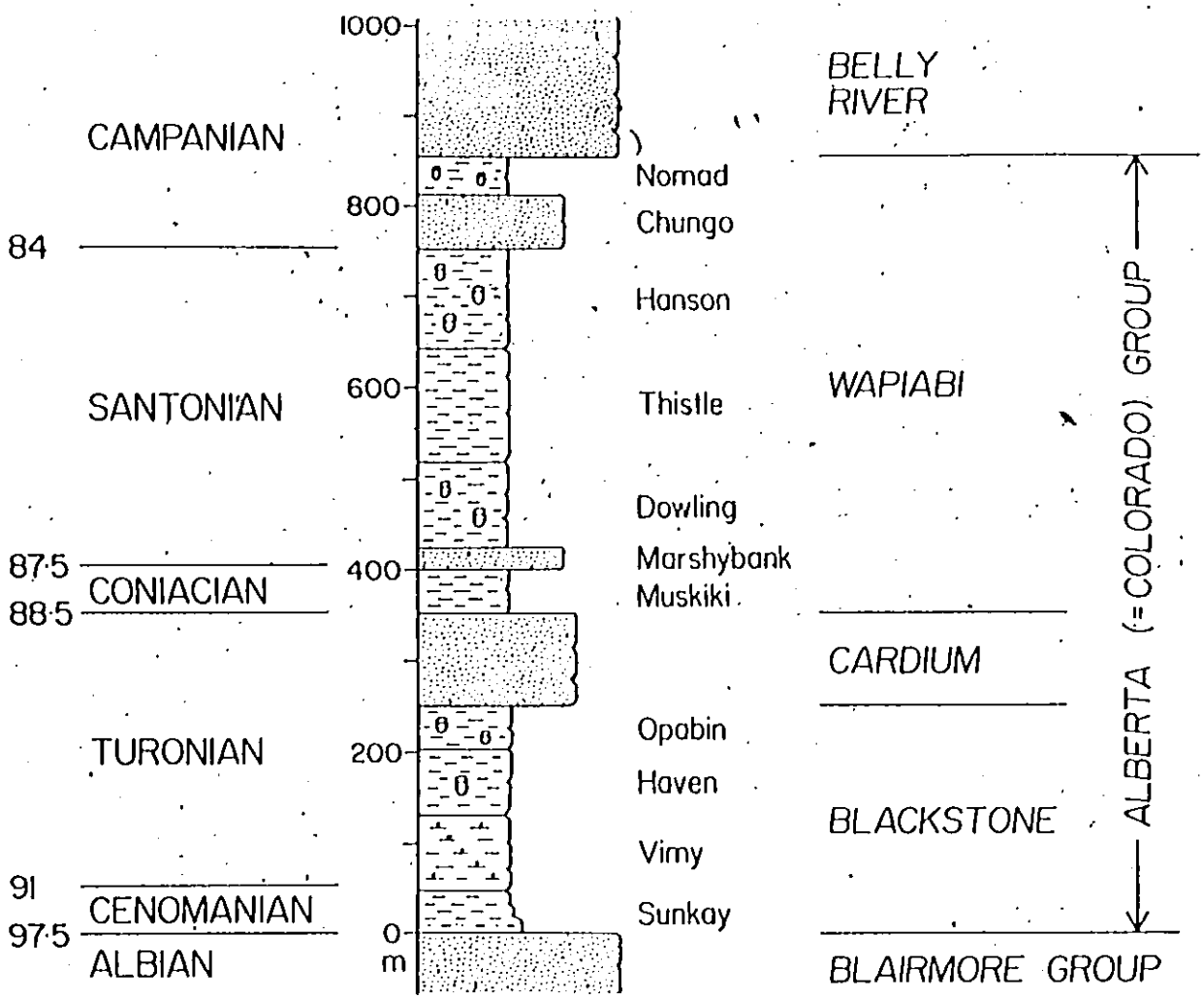
1000
800
600
400
200
0
m
CAMPANIAN
84
SANTONIAN
87·5
CONIACIAN
88·5
TURONIAN
91
CENOMANIAN
97·5
ALBIAN
Nomad
Chungo
Hanson
Thistle
Dowling
Marshybank
Muskiki
Opabin
Haven
Vimy
Sunkay
BELLY RIVER
WAPIABI
CARDIUM
BLACKSTONE
BLAIRMORE GROUP
ALBERTA (=COLORADO) GROUP

the Alberta Group by Cairnes (1907, p. 29); Rutherford (1927) assigned a formational rank to the Cardium sandstones, and thus the unit assumed more-or-less the boundaries and status that obtain at the present (as defined by Stott, 1963).

At various times, the name Bighorn Formation has been used instead of Cardium Formation. This name was introduced by Malloch (1911); unfortunately, it had been pre-empted by the Ordovician Bighorn dolomite of Wyoming. Despite the fact that paleontological names for stratigraphic units are discouraged by the approved rules of nomenclature, the Stratigraphic Committee of the Geological Survey of Canada has recommended that an exception be made in this instance, and that the long-standing name, Cardium Formation, be officially adopted (reported by Stott, 1963, p. 8).

PREVIOUS INTERPRETATIONS OF DEPOSITIONAL PROCESSES AND ENVIRONMENTS

The review presented below emphasizes modern interpretations of Cardium depositional environments. Readers who are interested in early studies of this unit (pre-1955) are referred to the excellent comprehensive review by Stott (1963, p. 3-9 and p. 53-81). A more recent

literature review, emphasizing modern sedimentological studies, has been presented by Walker (1983b). The following summary covers much the same material as was discussed by Walker (1983b), and accordingly is somewhat brief; however, this review places a greater emphasis on outcrop rather than subsurface studies.

A critical evaluation of previously suggested depositional processes and environments will be presented in a unified discussion following the brief literature summary below.

Literature Summary

Beach (1955). Following the first production of oil from the Cardium (at Pembina, Alberta, in 1953), Beach (1955) produced the first modern sedimentological interpretation, based largely upon lithological sequences observed from numerous well cuttings in the plains. He suggested a turbidity-current origin for the pebbles present at the top of the main Cardium sandstone, which appeared to be uniformly distributed over wide areas of the ancient sea floor.

De Wiel (1956). In a discussion of Beach (1955), De Wiel (1956) denied the turbidity-current explanation. His main objection (one which is commonly echoed today) was that the shallow slopes of the Cardium epicontinental sea

floor would have prevented turbidity-current transport of pebbles over long distances. The alternative offered by De Wiel was variation in relative sea-level; he preferred to interpret thick sandstones and conglomerates within the formation as being regressive deposits associated with shoreline progradation. In general, this is the alternative preferred in this thesis.

Beach (1956). In reply to De Wiel (1956), Beach (1956) advanced the idea that tsunamis might supply the energy necessary to generate the initial momentum required for turbidity currents. This is the first suggestion of an alternative to gravitational potential as a source of energy for the emplacement of coarse material far from shore within an epicontinental basin. This suggestion is important for three reasons:

1) It heralds the idea of an alternative to gravitational potential as an energy source for the generation of sediment-laden currents within shallow-marine basins.
2) It suggests a catastrophic phenomenon other than slope failure as the triggering agent for depositional events in the Cardium Formation.
3) It suggests the possibility of a "mixed-process" transport mechanism for coarse Cardium clastics.

Nielson (1957). The 1957 Alberta Society of Petroleum Geologists symposium on the Cardium produced varying sedimentological interpretations. Nielson (1957) concluded from a study of a great number of electric logs that the Cardium at Pembina was a shallow-marine offshore sand body, but no attempt was made to describe the mechanism by which this sand was deposited; however, the turbidity-current hypothesis was denied. It was suggested that the Cardium was deposited in a regressive environment, and that the lowermost portion of the formation (the majority of its thickness) was deposited below wave base, whereas the uppermost sand and conglomerate were deposited above wave base and were "exposed to the erosive effect of normal marine currents." The entire unit was then plunged into relatively deeper water. The interpretation of deposition during regression is supported by this thesis; however, Nielson (1957) does not suggest any specific mechanism whereby such an extensive sand body may be deposited offshore.

Michaelis (1957). This study was much more extensive and detailed than any previously discussed. Nearly 40 cores from Pembina wells were examined and compared with 60 outcrop sections in the Foothills. It is a great misfortune that Michaelis never published more of the results of his extensive work in the Foothills, for in

his correlations he correctly emphasized thickening- and coarsening-upward cycles as the basic subdivisional units of the formation and, unlike Stott (1963), he correctly recognized that the two major occurrences of non-marine deposits are separated by a marine cycle in the inner (southwestern) central Foothills.

Michaelis (1957) does not report the locations of the 60 sections examined in the Foothills, with the exception of two sections measured on Cardinal River and Canyon Creek (both located in the central Foothills). He recognized five major coarsening-upward cycles in these two sections, and he states that these five cycles can be correlated with reasonable confidence in all of the outcrop sections examined. This statement suggests that his field work was probably limited to the central Foothills and the northern part of the southern Foothills, where indeed five major cycles are present in most complete exposures. These cycles were correctly interpreted by Michaelis (1957) as regressive shoreline deposits separated by periods of transgression, and he also clearly perceived that the conglomerates at the tops of these cycles were deposited during transgression. This interpretation is in basic agreement with the one advanced in this thesis. Michaelis (1957) reports that only two of these cycles are fully regressive into non-marine deposits, another observation which is in basic agreement with results of the present

field study. The lowermost part of each cycle was inferred to have been deposited below wave base (again, in agreement with this thesis); however, specific environmental interpretations offered for the uppermost marine beds in these cycles (i.e., beach and tidal flat environments) are not in full agreement with the interpretations advanced by the present author. Whereas the beach interpretation is very broadly applicable to the tops of many of these cycles, tidal flat deposits generally are not present.

It is important to emphasize the significance of this early study, the magnitude of which has not been widely recognized by subsequent workers. Firstly, this paper summarizes the results of the most extensive sedimentological investigation of Cardium exposures ever undertaken prior to the present study. [The extensive field study by Stott, 1963, was essentially stratigraphic, not sedimentological.] Secondly, it is this author's opinion, supported by the data included in this thesis, that Michaelis (1957) demonstrates the clearest understanding of the nature of correlation within the Cardium of any work published prior to the 1980's. Although Stott (1963) also recognized coarsening-upward cycles within the Cardium, and considered them to be the basic subdivisions of the formation, the member scheme which he erected does not reflect this knowledge and has obscured these correlative cycles for the past twenty

years. Also, the cycles which Stott defined were not as accurate as those defined by Michaelis, as has been mentioned previously (see further discussion in chapter 3). Finally, Michaelis (1957) was the first to interpret these cycles as prograding shoreline deposits separated vertically by erosional transgression surfaces, and likewise was the first to use field evidence to demonstrate that Cardium conglomerates in the Foothills are associated not only with these transgression surfaces, but also with the relatively deeper-water deposits immediately overlying these surfaces. Thus, Michaelis (1957) was the first worker to recognize that most Cardium conglomerates were deposited during transgression.

In contrast to this interpretation of Foothills geology, Michaelis (1957) interpreted the Cardium in the Pembina field as a regressive offshore shoal sandstone capped with conglomeratic beach deposits, and he suggested that the entire Pembina field is correlative with the third major sedimentary cycle present in the central Foothills.

MacDonald (1957). In the last paper presented in the symposium proceedings of 1957, the stratigraphy and sedimentation of the Cardium in the northern Foothills was discussed. Both outcrop and subsurface well logs from this area were interpreted and correlated. This study is partially flawed because the Baytree Member of the Cardium

in the Peace River area has been incorrectly assigned to the Badheart Sandstone (Marshybank Member) of the Wapiabi Formation. The author concluded that the Cardium in this area consisted of a delta complex with northerly and northeasterly sediment dispersal.

Stott (1963). Between 1954 and 1957, D. F. Stott conducted an extensive and essentially stratigraphic examination of the Alberta Group throughout the Alberta Foothills. Following this study, Stott (1963) published what has since been universally regarded as the definitive statement of Cardium stratigraphy. Although he recognized and correlated laterally impersistent coarsening-upward cycles, Stott did not base his member stratigraphy upon cycle correlations; instead, he established a scheme of member divisions in which arbitrarily defined member boundaries cross cycle boundaries (see chapter 3). This member scheme was maintained and extended in a later summary of Cretaceous stratigraphy in British Columbia (Stott, 1975). Because Stott's member boundaries cross lithostratigraphically correlative cycle boundaries, the members defined by Stott do not represent physically correlative stratigraphic units.

The non-correlative member divisions established by Stott (1963) have recently been brought into question by Duke (1980) and Walker (1983a). This member scheme is

analysed in detail in chapter 3, where it is suggested that it be discarded. Also in that chapter, a new member scheme is suggested, based upon the cycle correlations of this author.

Stott's brief environmental interpretations emphasized beach environments for thicker sand bodies, with conglomerates forming transgressive "beach concentrates".

Berven (1966). In a study of the Cardium in the subsurface in the Crossfield-Garrington area, Berven (1966) recognized two separated offshore bars in the "lower Cardium" sandstone. No attempt was made to explain the conglomerate capping these sandstone bodies, although Berven stated that the sharp tops of the bars "may indicate a rapid transgression".

Michaelis & Dixon (1969). This study concentrated on the interpretation of primary physical and biogenic structures recognized in Cardium cores from several producing fields. The Cardium was interpreted as a tidal shoal complex. As demonstrated in later sections of this thesis, tidal deposits probably are absent or very rare in the Cardium.

A possible early recognition and storm interpretation of hummocky cross-stratification was included for "tabular laminated sandstones" recognized from most of the major reservoirs. Characterized by low-angle

plane-laminated sandstone concordantly overlying a planar erosional surface truncating the underlying low-angle lamina set, this structure was inferred to have been formed by "periodic planation during abnormal periods of high current activity, such as storms." Presumably the authors envisioned storm-enhanced tidal currents, consistent with their concept of a tidal shoal complex.

Sinha (1970). The subsurface Cardium in the Edson field was recognized as consisting of two thickening- and coarsening-upward clastic cycles grading from mudstone to sandstone and conglomerate. The lower cycle ("B" sandstone) was interpreted as a NW-SE trending "offshore bar with a flat base and a convex top" locally capped with conglomerates "deposited on a partly scoured and semi-consolidated upper surface of the sandstone". Based upon the macrofaunal and microfaunal assemblages and the abundance of plant remains, the upper cycle ("A" sandstone) was inferred to have been "deposited in shallow marine to brackish lagoonal environments associated with progradation of the shoreline".

Swagor et al. (1976). This paper ushered in a new era in the interpretation of Cardium depositional processes. The Cardium in the Carrot Creek Field was interpreted as an "offshore terrace bar" in which sediment accumulated at a break in slope. Conglomerate capping this

bar was inferred to have been deposited by storm-driven bottom flows; this is the first interpretation of storms as the primary depositional agents for offshore conglomerates. The authors envisioned transport of pebbles as bedload, an inferrence refuted by Wright & Walker (1981) but partially supported by this thesis. As shall be discussed in subsequent chapters, however, the "terrace bar" concept probably is wholly invalid; the asymmetrically tapered geometry of Cardium sand bodies is best interpreted as a shoreface (or "shoreface-attached") sand body modified by subsequent transgressive marine erosion (chapter 6).

Wright & Walker (1981). The excellent Cardium exposures at the Seebe and Horseshoe dams near Seebe, Alberta, were the subject of this study, which represents the first published interpretation of Cardium sedimentation by members of the McMaster Cardium group. It was demonstrated that the entire formation (including several thick sandstones consisting of numerous amalgamated beds) was deposited in shallow marine environments below fairweather wave base at these localities, as inferred from the ubiquitious hummocky cross-stratification within sandstones and the foraminiferal assemblage within mudstones. Further, it was demonstrated that conglomerate beds within the formation probably could not have been emplaced by tractional transport due to storms (as was

suggested for the Carrot Creek field by Swagor et al., 1976). Instead, these conglomerates were interpreted as having been transported in a dispersion above the bed by rapidly flowing turbidity currents. This latter interpretation was based upon calculations of transport time and the suite of sedimentary structures associated with these conglomerates.

Walker (1983a, 1983b, 1983c). These three papers present different aspects of a detailed subsurface study of the Cardium Formation in the Garrington, Caroline, and Ricinus areas. A subsurface member system was established for these three fields. It was shown that the formation in these fields consists of two thickening- and coarsening-upward, laterally persistent clastic cycles, composed of interbedded sandstones and mudstones and capped with thin conglomerates. The lower sandstones in the sequences were interpreted as turbidites; the upper sandstones probably are hummocky cross-stratified. [Note, however, that the recognition of hummocky cross-stratification from drill core must be considered somewhat tentative.] All sandstone and conglomerate-beds were inferred to have been deposited from shallow-marine turbidity currents.

The thicker sandstones present at the tops of cycles within producing fields extend in slightly reduced

or patchy form between the fields. This discontinuous sheet-like distribution was characterized by the term "ragged blanket" sand body. This geometry is similar to the inferred geometry of extensive shallow-marine sand bodies exposed in the southern and outer central Foothills (chapters 6 & 7).

At Ricinus only, a NW-SE oriented channel-fill sandstone erosionally truncates the upper sand body. It was suggested that sharp-based sandstone and conglomerate beds in this field are a minimum of 100 km from the nearest possible shoreline, and that these conglomerates and sandstones also were deposited by turbidity currents, which cut and filled the submarine channel. In this thesis, I have recognized the probability of extensive transgressive erosion of the tops of previously deposited Cardium sand bodies, and the removal of large thicknesses of non-marine and marine deposits capping these sand bodies. This recognition suggests a probable modification of the inferred turbidity-current origin for this channel and the coarse clastics within it (chapters 6 and 7).

Griffith (1981) and Keith (1985). These studies of the Cardium in the subsurface Ferrier field (Griffith) and Willesden Green field (Keith) reveal a different internal field geometry than that at Garrington-Caroline-Ricinus. Both of these fields consist of a series of prograding sand

bodies offlapping to the NE and capped with conglomerate. This "shingled-sand" geometry is similar to the inferred geometry of shoreline-proximal sand bodies throughout the northern Foothills and the inner central Foothills (see chapter 6 for further discussion).

These two studies provide an excellent descriptive base for the interpretation of these Cardium fields; this is especially true of the Keith study, which involved examination of over 1000 well cores and logs. Unfortunately, neither worker produced a "big picture" sedimentological interpretation of the documented field geometry. Based upon the data of these studies and my own data from the examination of Cardium exposures, I have advanced such an interpretation in chapter 6 of this thesis (see brief summary below).

Some Unresolved Problems Made Evident by this Literature Review, and Possible Resolutions Deriving From the Present Study

The preceding literature review highlights three important questions of Cardium sedimentation which have yet to be resolved:

1) Are thickening- and coarsening-upward clastic sequences in the Foothills and the subsurface best interpreted as prograding shoreline sequences,

offshore "shoals" (possibly shelf sand ridges), or both?

2) What sensible combination of processes can be invoked to account for the offlapping sands and conglomerates in the asymmetrically tapered sand bodies in the Carrot Creek, Ferrier, and Willesden Green fields?

3) How were coarse clastics transported to the offshore region; specifically, what role did shallow-marine turbidity currents play in Cardium deposition?

The study reported in this thesis is summarized briefly in the following paragraph; the assertions made below are defended in the remainder of this thesis.

My investigations suggest that shallow-marine sedimentation in the Cardium was dominated by the effects of storms. All Cardium cycles containing relatively thick sandstones (greater than a few meters in thickness) are best interpreted as partial or complete prograding shelf-to-shoreline sequences; the thick sandstones were deposited on the shoreface or as an extension of the shoreface in a proximal offshore setting. Of these sequences, those which are not capped with non-marine deposits are inferred to have been truncated by transgression: during transgression, erosion by the retreating shoreface locally removed previously deposited

non-marine sediments over a significant width (approximately 50 km or more) across the lowermost coastal plain. Minor cyclic developments, characterized by relatively thin sandstone/conglomerate bodies, were formed basinward of the position of maximum shoreline extent during regression (i.e., basinward of major regressive sand sheets); these sequences probably represent discontinuous shelf sand ridges formed during the latter stages of regression and/or the early stages of transgression. Transport of coarse clastics on the Cardium shelf was primarily due to geostrophically balanced flows generated by storms; there is no evidence for extensive deposition from turbidity currents. Asymmetrically tapered sand bodies and thick shallow-marine conglomerates with which they are locally capped (such as those documented by Swagor et al., 1976, Griffith, 1981, and Keith, 1985) were also formed in the sediments now exposed in the Foothills. These sand bodies and conglomerates were formed at or near the edge of major regressive sand sheets, probably by transgressive erosion of the edge of the sheet immediately following its deposition, as described above. The thick capping conglomerates represent eroded transgressive lag deposits; however, this coarse material was remobilized during transgression, and locally was resedimented over the drowned shoreface by flows which held it in a dispersion above the bed. The term "resedimented-lag" is herein

proposed for this type of coarse deposit.

The findings of this thesis summarized above suggest the following resolution to the three major questions which remain unanswered following a review of previous studies:

1) Thick coarsening-upward sequences in the Cardium Formation exhibiting sand-dominated intervals several meters in thickness were formed by progradation of a storm-dominated shoreline. Thinner coarsening-upward sequences were formed beyond the shoreline by the development and migration of shelf sand ridges formed under geostrophically balanced flows on the shelf.

2) Offlapping sands and capping conglomerates within subsurface Cardium fields are also present in the Foothills belt. This geometry is the result of transgressive erosion of a regressive sheet sand deposited by shoreline progradation.

3) Sediment was transported to (and on) the Cardium shelf by storm-generated, geostrophically balanced flows. Deposition from turbidity currents probably took place on a very limited scale only. There is no evidence for the generation of large turbidity currents on the Cardium shelf, or for the transport of coarse material for tens or hundreds of kilometers across the shelf by means of turbidity currents.

Details of these conclusions and associated implications are discussed in the following chapters.

CHAPTER 3. STRATIGRAPHIC REVISIONS OF THE CARDIUM FORMATION AND ITS MEMBERS IN THE ALBERTA FOOTHILLS

INTRODUCTION

In this chapter, the existing stratigraphy of the Cardium Formation (as defined by Stott, 1963, 1975 -- see Fig. 3-1) is shown to be inadequate for the following reasons:

1) The members of the Cardium defined by Stott (1963, 1975) are distinguished by arbitrary criteria and are each bounded by non-correlative surfaces.

2) Thickening- and coarsening-upward cycles present within the Cardium probably are better natural subdivisions of the formation, because these cycles are the smallest subdivisions which can be traced with confidence over large distances laterally. These cyclic developments are not reflected by the existing stratigraphy.

3) Large thicknesses of marine strata have been incorrectly identified by Stott (1963, 1975) as being non-marine in origin.

As a result of these stratigraphic and sedimentological

Figure 3-1. Summary diagram comparing existing and revised member divisions of the Cardium Formation. Upper panel shows the existing members (Stott, 1963, 1975); lower panel shows the revised scheme proposed herein. The revised members reflect the distinction between marine deposits (not stippled) and non-marine deposits (stippled). Interfingering between the Cardium and the Blackstone Formation drawn at the base of the Seebe Member is diagrammatic, as are minor cyclic developments superimposed upon the Wapiabi transgression. Note tongues of non-marine sediments protruding from the main body of the Cutpick Member (numbered). See text for further discussion.

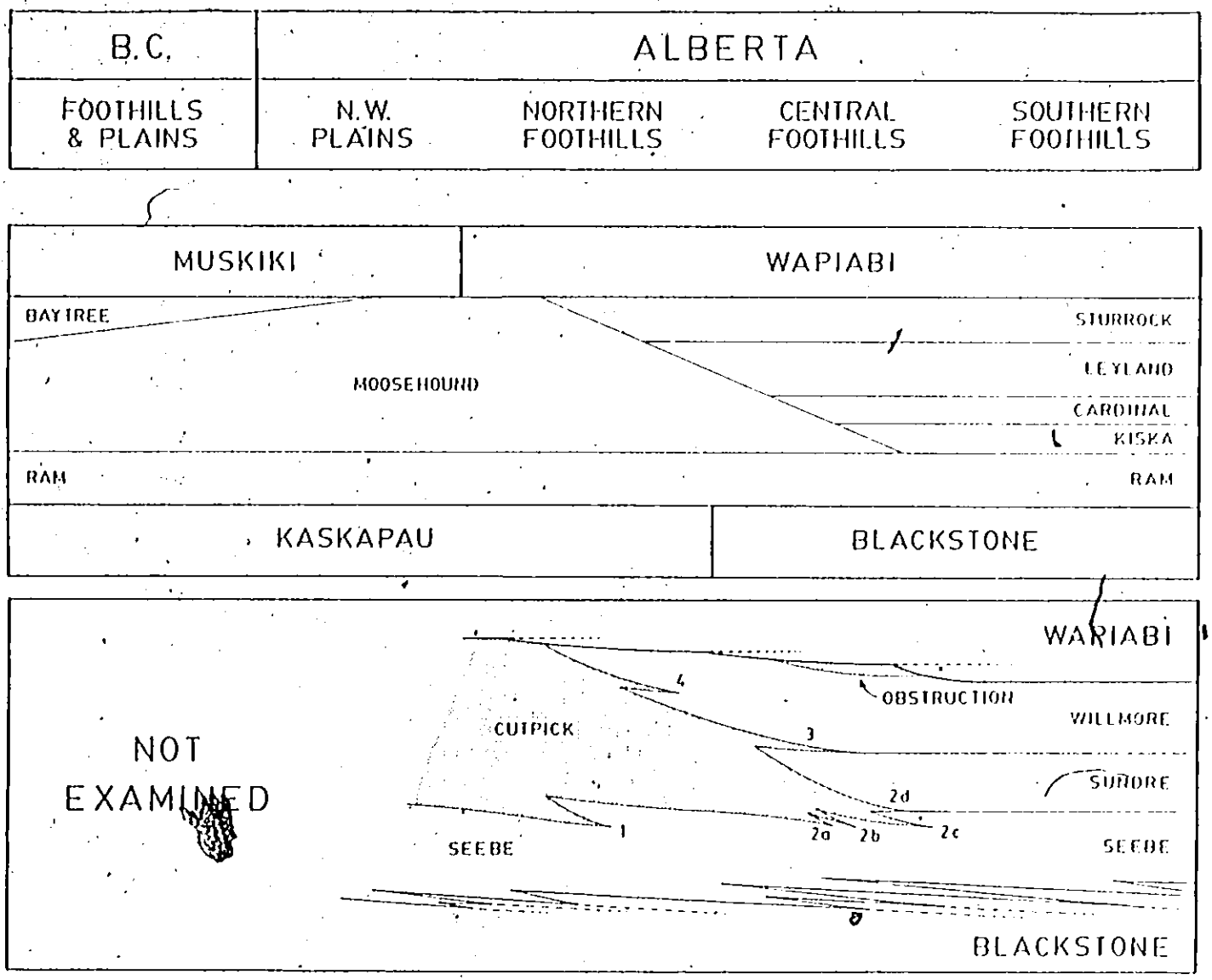
B.C.
ALBERTA
FOOTHILLS & PLAINS
N.W. PLAINS
NORTHERN FOOTHILLS
CENTRAL FOOTHILLS
SOUTHERN FOOTHILLS
MUSKIKI
WAPIABI
BAYTREE
MOOSEHOUND
STURROCK
LEYLAND
CARDINAL
KISKA
RAM
RAM
KASKAPAU
BLACKSTONE
NOT EXAMINED
WARIABI
OBSTRUCTION
WILLMORE
CUTPICK
SUNDRE
SEEBE
SEEBE
BLACKSTONE
4
3
2d
1
2a
2b
2c

problems, any correlations, isopach maps, or other geometrical constructs derived from the existing stratigraphy are not geologically significant, because they do not reflect physically correlative lithological units.

It is suggested that the existing stratigraphy be abandoned. A new member system is defined for the Alberta Foothills, based upon the lithologically correlative cycles which constitute sedimentologically natural subdivisions of the formation. The new member names have not been pre-empted by prior usage. There are six members in the revised stratigraphy; the member names are as follows:

Baytree Member

Obstruction Member

Willmore Member

Sundre Member

Cutpick Member

Seebe Member

In the revised member scheme (Fig. 3-1), the Seebe, Sundre, and Willmore Members contain marine deposits exclusively, whereas the Cutpick and Obstruction Members contain non-marine deposits exclusively. I did not examine the Baytree Member, which is restricted to the British Columbia Foothills and northwest Alberta (Stott, 1975); its environment of deposition is not known. This distinction between non-marine and marine deposits is not reflected by

the stratigraphic units defined by Stott (1963, 1975).

Each of the marine members in the revised stratigraphy contains at least one coarsening-upward cyclic development. The number of cycles present within each of these marine members varies on a regional basis. For example, the Sundre Member contains only one cycle throughout most of the central Foothills, whereas two cycles are present in the southern Foothills. Similarly, the Willmore Member contains two or more cycles in mountain-proximal sections in the inner Foothills, whereas outer Foothills sections contain only one coarsening-upward cycle in this member.

Several tongues or splits of non-marine deposits protrude from the non-marine Cutpick Member in the central Foothills. These Cutpick tongues have been numbered in figure 3-1. The largest of these are informally designated as the "Lower Tongue" (2) and the "Upper Tongue" (3); they protrude from the "Main Body" of this member. The Lower Tongue is the largest of the two.

Where outcrop control is relatively tight, several minor non-marine "splits" have also been recognized; I think it probable that additional unrecognized splits are present between the more widely spaced exposures (see further discussion in chapter 6). The small splits which have been recognized are informally designated as the "Grande Cache Split" (1), the "Canyon Creek Split" (2a),

the "Headwaters Split" (2b), the "Cripple Creek Split" (2c), and the "Little Berland Split" (4). The tip of the Lower Tongue is also labelled (2d).

Complex interfingering occurs between the Cardium and the Blackstone Formations, as has been depicted diagrammatically at the base of the Seebe Member. Also, minor regressive cyclic developments are superimposed upon the Wapiabi transgression; these generally cannot be traced with confidence between exposures, and are also depicted diagrammatically in figure 3-1.

The new internal stratigraphy outlined in this chapter can be used with great success in correlation between outcrop sections in the Foothills. Tentative correlations have also been established between outcrop and subsurface occurrences of the formation both in the Foothills and the Plains.

Important sedimentological implications of regional cycle and member correlations are discussed in detail in chapters 6 and 7.

The existing stratigraphy of the Cardium Formation as defined by Stott (1963, 1973) is summarized in appendix 6. Appendix 7 presents formal designations of type and reference sections, and definitional criteria for the recognition of the new members.

INTERNAL INCONSISTENCIES OF EXISTING CYCLE AND MEMBER CORRELATIONS

The inconsistent nature of the cycle and member correlations proposed by Stott (1963, 1975) for the Cardium Formation in Foothills exposures in Alberta was first recognized by R. G. Walker (pers. comm., 1979) and was described briefly by Duke (1981). A succinct demonstration of the problems with the existing stratigraphy has been presented previously by Walker (1983a, p. 15-16), from whom I quote below:

> The early history of Cardium nomenclature has been reviewed by Stott (1963, p. 3-9, 53-63). In 1963, he subdivided the Cardium into six members, from base upward the Ram, Moosehound (nonmarine), Kiska, Cardinal, Leyland and Sturrock (Stott, 1963, p. 10-11, 53-81). The correlation of these members was shown in a series of large figures (Stott, 1963, figs. 3-14).
>
> Stott also recognized a series of cycles, stating that, "cyclic units within individual members show a gradational change upwards from clay shale to siltstone. These cycles have been traced for great distances and are of value for the correlation within individual members, as is shown in the stratigraphic cross-sections (Figs. 3 to 14)" (Stott, 1963, p. 12).
>
> Part of Stott's Figure 5 is reproduced here in Figure 3 [this thesis, Fig. 3-2]. Formation boundaries are shown by continuous heavy lines, member boundaries by broken heavy lines, and cycle correlations by light continuous lines. The diagram is reproduced exactly as published by Stott. In several places, cycle boundaries cross member and even formation boundaries, which by definition are "mappable at the surface or traceable in the subsurface" (American Commission on Stratigraphic Nomenclature) and hence represent

Figure 3-2. Portion of a correlation diagram presented by Stott (1963, Fig. 5) of Cardium outcrop sections. Heavy solid lines show formation boundaries, heavy dashed lines show member boundaries, and light solid lines show boundaries of lithostratigraphically correlative coarsening-upward cycles. Note that cycle boundaries cross both member and formation boundaries, demonstrating that these stratigraphic units are not lithostratigraphically correlative. This diagram has also been figured by Walker (1983a), who recognized and discussed this stratigraphic problem.

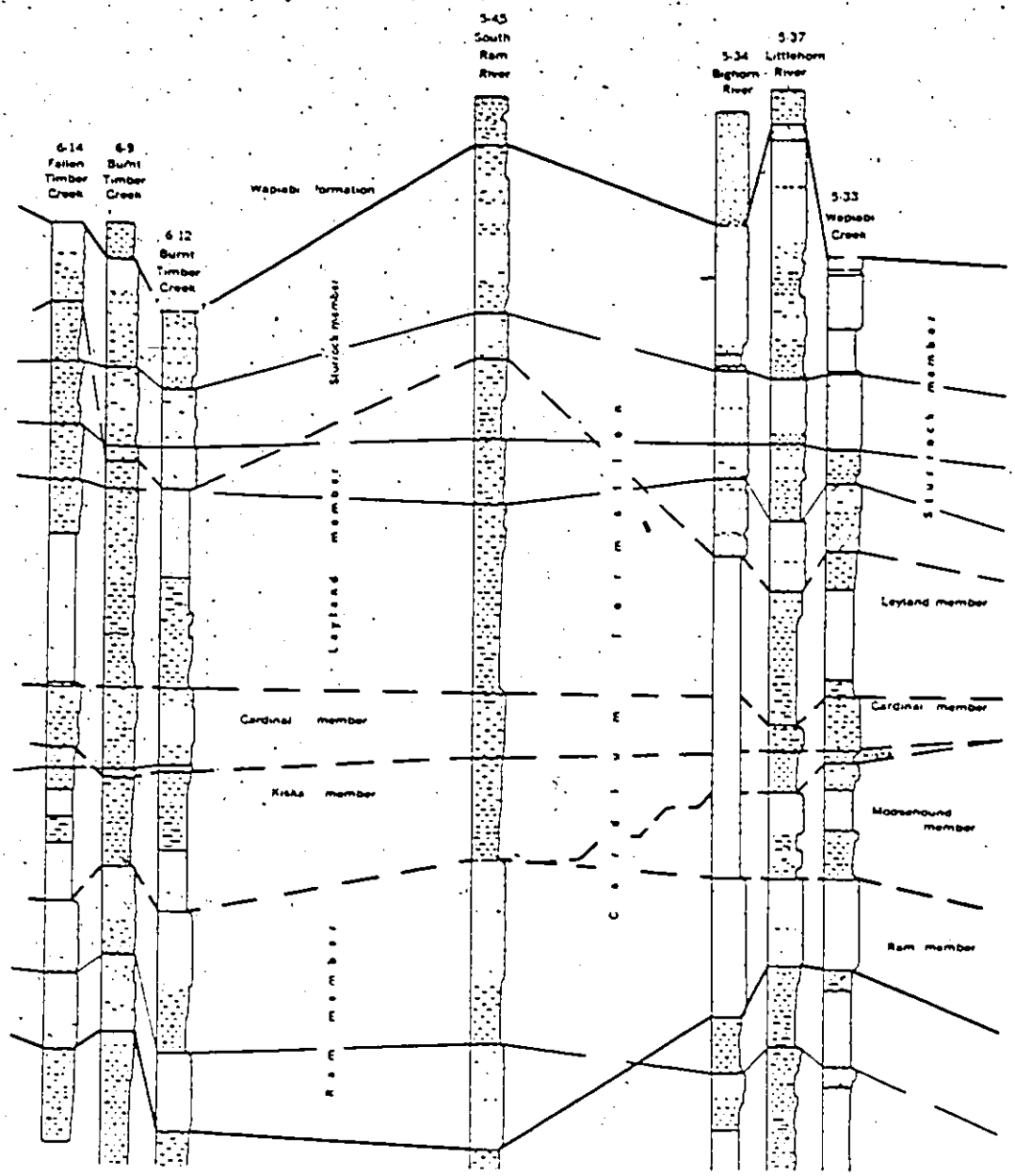
6-14
Fallen
Timber
Creek
6-9
Burnt
Timber
Creek
6-12
Burnt
Timber
Creek
Wapiabi formation
5-45
South
Ram
River
5-34
Bighorn
River
5-37
Littlehorn
River
5-33
Wapiabi
Creek
Sturrock member
Leyland member
Cardinal member
Kiska member
Ram member
Cardium formation
Sturrock member
Leyland member
Cardinal member
Moosehound
member
Ram member

> continuous rock bodies. Physically continuous rock bodies obviously cannot cross each other. Crossing boundaries are also present in Stott's Figures 5, 6, 8, 9, 10, 11 and 12. The work of W. L. Duke (1980, 1981 and pers. comm.), as part of a Ph.D. thesis in progress, has shown that depositional coarsening-upward cycles can indeed be correlated for long distances, and form the best basis for an internal stratigraphy within the Cardium....To avoid the problem of crossing rock bodies, I suggest that abandonment of the present member terminology be considered.

Figure 3-2 is a copy of Walker's figure 3 mentioned above, which in turn duplicates part of Stott's figure 5. This cross-section illustrates the stratigraphic difficulties described by Walker in the extract above.

CYCLE vs. MEMBER CORRELATIONS: DO STOTT'S CYCLES REPRESENT LITHOSTRATIGRAPHIC UNITS?

The preceding section has demonstrated the inconsistent nature of cycle boundaries and stratigraphic boundaries established by Stott (1963) for the Cardium Formation in the Alberta Foothills. It would appear that Stott regarded his cycles as true lithostratigraphic units (see extract from Walker quoted above); his cycle-crossing members and formations, therefore, could not represent lithostratigraphic units. Below I demonstrate that his cycle divisions (although better than his member divisions)

also do not represent true lithostratigraphic units, and therefore cannot be used as the basis for a revised stratigraphic system.

Figure 3-3 shows two differing correlation diagrams for Cardium sections 5-37 (Littlehorn Creek) and section 5-45 (Ram River). On the right are correlations defined by my own inspection of these exposures, showing the revised member terminology. Non-marine intervals are indicated with a stipple pattern. Member and formational boundaries are represented by heavy continuous lines; where cycle boundaries are not coincident with stratigraphic boundaries, the cycle boundaries are represented by light broken lines. Cycles are represented with curved arrows. In my correlation scheme for the Cardium, stratigraphic boundaries and cycle boundaries never cross one another.

Sections 5-37 and 5-45 were also measured by Stott (1963), whose logs of vertical lithological variation have been reproduced in figure 3-2. Close inspection of the two sets of graphic logs permits the transposition of Stott's member and cycle correlation lines to the graphic logs based upon my own work. This transposition is shown on the left in figure 3-3. The accuracy of these transpositions is further enhanced by detailed bed-by-bed comparison of Stott's measurements (Stott, 1963, p. 239-243 & 249-253) and my own measurements recorded in my field notes. Stratigraphic and cycle boundaries are depicted as on the

Figure 3-3. Correlation diagrams for Cardium sections 5-37 (Littlehorn Creek) and 5-45 (Ram River). Tick marks indicate intervals of 10 m. Diagram at left is after Stott (1963); diagram at right is based upon data in this thesis. Heavy solid lines represent stratigraphic boundaries; light broken lines represent cycle boundaries. Cycles are indicated by curved arrows. Stipple pattern indicates non-marine and/or lagoonal deposits. Three non-marine intervals were recognized in the present study. See text for discussion.

Note: Section 5-45 has been designated as the new type section of the Cardium Formation, due to ease of access; section 5-37 is the principal reference section (appendix 7).

STOTT, 1963

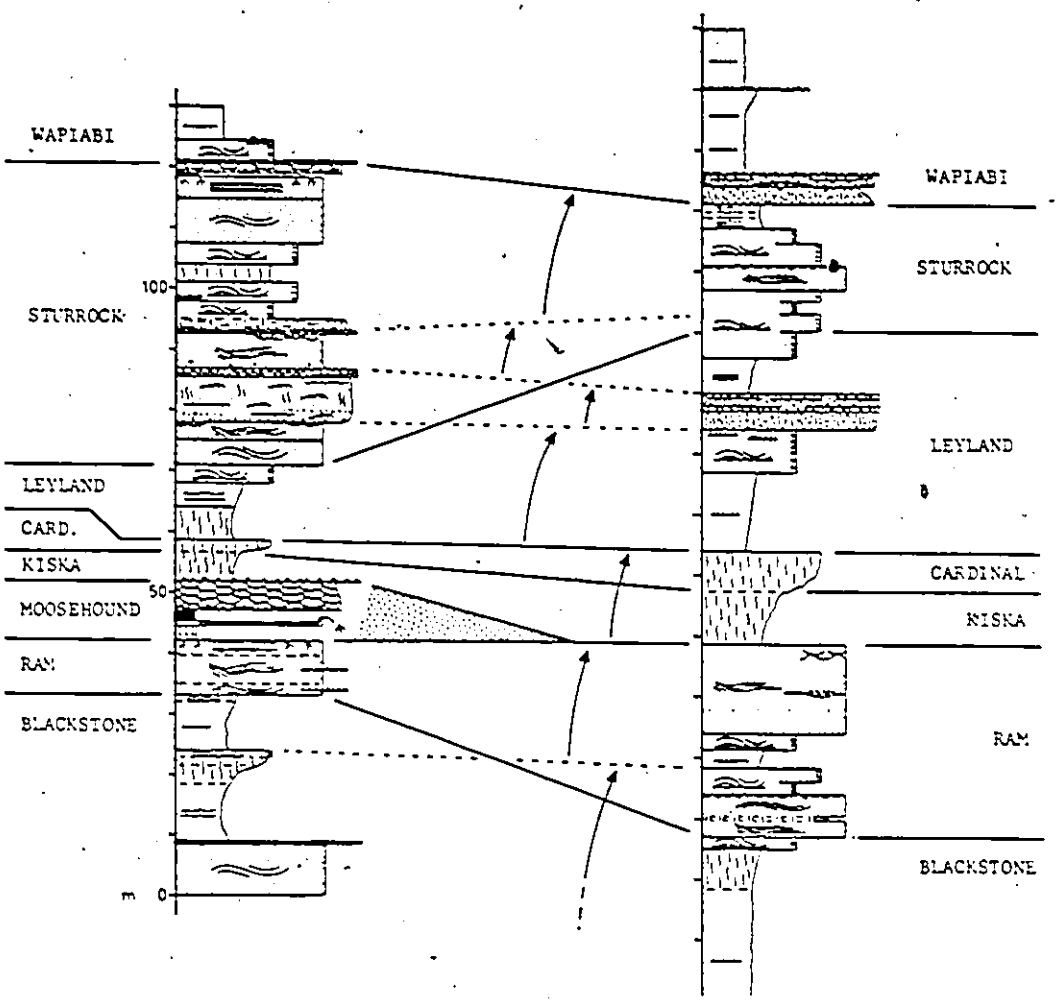

5-37 5-45

1 of

DUKE, 1985

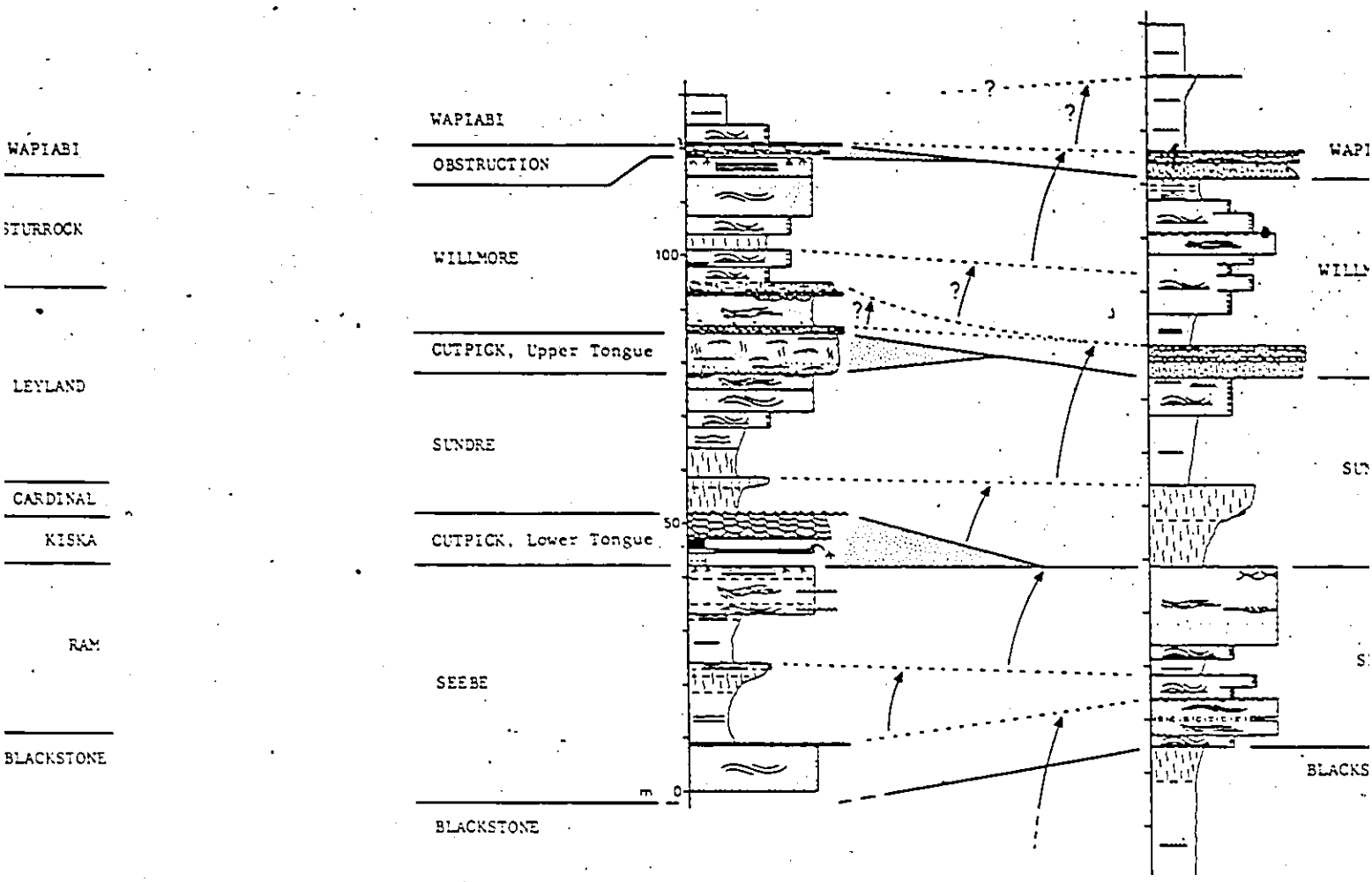

5-37 5-45

2 of 2

right; the member terminology is that of Stott.

This comparison serves once again to illustrate that Stott's members and formations do not appear to represent true lithostratigraphic units, no matter which set of cycle correlations is utilized. Additionally, only two of Stott's cycles are identical to those revealed in my own correlations for these sections. My own cycle correlations are based upon a comparison of: 1) cycle thickness and sequence, 2) sequences of lithologies within cycles, and 3) structure sequences within cycles involving a wide variety of primary sedimentary structures (both physical and biological), including paleoflow indicators. Detailed comparison of my own cycle correlations and those of Stott (1963) indicates that the newer set of correlations is demonstrably superior to the older set. [In all fairness, however, it should be stated that the correlation of minor cycles superimposed upon major cyclic developments is tentative in both systems. Three such minor cycles are indicated with question marks in figure 3-3 on the right.] Thus, the cycles defined by Stott (1963) probably do not represent true lithostratigraphic units; they therefore cannot be used to establish a new member stratigraphy.

PROPOSED REVISION OF MEMBER STRATIGRAPHY BASED UPON CYCLE CORRELATIONS DOCUMENTED IN THIS THESIS

The members established by Stott (1963) do not represent lithostratigraphically correlative subdivisions of the Cardium Formation. In this section, I abandon the existing stratigraphy in favor of a new system based upon revised cycle correlations.

Basis of Correlation and Member Divisions

The new internal stratigraphy for the Cardium Formation in the Alberta Foothills is based upon detailed correlation of depositional coarsening-upward cycles recognized in outcrop studies by myself (central and northern Foothills) and by R. G. Walker, B. H. Ainsworth, and M. E. Wright (southern Foothills). Lateral cycle relationships are discussed at length in chapter 6. Detailed cycle-correlation diagrams are presented in that chapter (see figures at beginning of chapter 6).

The correlation of Cardium cycles is hung primarily upon the first transition from marine to non-marine deposits, identified as the datum in the cycle-correlation diagrams of chapter 6. In the southern part of the central Foothills, the non-marine deposits tongue out; cycle correlations are carried further to the south (into the

southern Foothills) by comparing cycle number, thickness, and sequence (and the suite of sedimentary structures present within cycles, including paleoflow indicators) between the various exposures. Sedimentological implications of these correlations are discussed extensively in chapters 6 and 7; the reader is referred to these chapters for a more complete discussion of the sedimentological basis for these correlations. For the purpose of erecting the new stratigraphy defined below, these correlations will be taken as correct.

My field investigations indicate that the coarsening-upward depositional cycles present within the Cardium are the smallest subdivisional lithological units which can be traced with confidence over large distances between exposures in the Foothills. The interfingering of marine cycles and non-marine deposits permits the recognition and correlation of easily mappable subdivisions of the Cardium in Foothills exposures. These subdivisions, based upon the cycle-correlation diagrams of chapter 6, separate marine from non-marine sediments, and have been assigned member names as follows:

Baytree Member (environment unknown)

Obstruction Member (non-marine)

Willmore Member (marine)

Sundre Member (marine)

Cutpick Member (non-marine)

Seebe Member (marine)

These new names have not been pre-empted by prior usage, and have been reserved (pending publication and formal recognition) by the Geological Survey of Canada (T. Bolton, pers. comm., 1983). I did not examine the coarse conglomeratic sandstones of the Baytree Member present in northwest Alberta and the Foothills of British Columbia (Stott, 1975); thus, this member is in no way modified in the revised stratigraphy. However, the new stratigraphy totally replaces the Ram, Moosehound, Kiska, Cardinal, Leyland, and Sturrock Members proposed by Stott (1963) for the entire Foothills belt of Alberta.

An outline of the new stratigraphy is given below. Only the general nature of this revised system is described; the reader is referred to appendix 7 for formal type and reference section designations, and definitional criteria for the recognition of the new member and formational boundaries.

Summary of Revised Internal Stratigraphy: Formal Terminology

Regional stratigraphic relationships between the new members are illustrated diagrammatically in figure 3-1. This diagram emphasizes the distinction between marine and non-marine deposits, and indicates that the Cardium may be conveniently subdivided into six members:

Seebe Member. The Seebe Member is present in all exposures examined in this study. Depending upon local variability, one to three major marine cycles are present within the Seebe Member. This member consists of the marine deposits overlying the Blackstone-Kaskapau shales and underlying the lowest major body of non-marine deposits (Cutpick Member) present in the formation. In the southern part of the field area, non-marine deposits are not present; the Seebe is overlain in this area by the marine Sundre Member. The Seebe and Sundre Members may be distinguished by the correlation of their constituent cycles, as discussed above. Conglomerate is locally present at the Seebe-Sundre contact; this coarse sediment is included in the overlying Sundre Member.

Note that small tongues ("splits") of non-marine deposits from the Cutpick Member (e.g., the "Grande Cache Split", labelled "1" in Fig. 3-1) locally extend into the underlying Seebe Member. Note also that the transition

beds formerly included by Stott (1963) in the underlying Blackstone or Kaskapau Formations are herein included in the Seebe Member of the Cardium Formation.

Cutpick Member. The Cutpick Member represents the major non-marine (lagoonal and fluvial) member in Foothills exposures. This member is present in the central Foothills of Alberta and in more northerly exposures; where present, the Cutpick Member always overlies the Seebe Member. In the extreme northern Foothills and more northerly exposures, the Cutpick Member is vertically continuous (the "Main Body" -- Fig. 3-1); toward the south (in the southern part of the northern Foothills), the Cutpick divides into two major tongues of non-marine deposits which locally envelope the marine Sundre Member. These tongues are informally designated the Lower and Upper Tongues (Fig. 3-1, labelled "2" and "3", respectively). These two tongues of non-marine deposits pinch out in the southern part of the central Foothills.

The Upper Tongue and Main Body of the Cutpick Member are overlain by the marine cycle(s) of the Willmore Member throughout the Foothills (except in the extreme northern Foothills and further north, where the Cutpick beds are overlain by either the conglomeratic coarse sandstones of the Baytree Member or the basal marine deposits of the Wapiabi or Muskiki Formations).

The Lower Tongue of the Cutpick is everywhere overlain by the Sundre Member.

Again, note that small splits of the Cutpick Member may protrude into the underlying Seebe Member or the overlying Willmore Member (Fig. 3-1).

Sundre Member. The Sundre Member is present throughout the southern Foothills and all but the northernmost central Foothills. This member is composed locally of either one or two marine cycles. The cycles comprising the Sundre Member (and the member itself) are recognized and defined in the central Foothills, where they are completely enveloped by the two major tongues of the Cutpick Member. Further south, where the Cutpick tongues pinch out, the Sundre is traced by the correlation of cycles. The Sundre Member overlies the Seebe Member as stated previously, except in central Foothills exposures where it overlies the Lower Tongue of the Cutpick Member. In most central Foothills exposures, the Sundre is overlain by the Upper Tongue of the Cutpick; further south, it is overlain by the marine cycles of the Willmore Member. Locally, conglomerate marks the contact between the Sundre and Willmore Members; this conglomerate is always included in the Willmore Member.

Willmore Member. The Willmore Member is composed of one to three major marine cycles, depending upon local

variability. The Willmore has been traced throughout the Alberta Foothills to where it pinches out in the extreme northern Foothills. This member overlies the Main Body or Upper Tongue of the Cutpick Member where these units are present; in the south, it overlies the marine Sundre Member, and the contact is traced by the correlation of cycles. Locally, the Sundre-Willmore contact is marked by conglomerates; these are always included in the overlying Willmore Member.

One non-marine split was observed to extend into the Willmore Member from the laterally adjacent Cutpick Member (the "Little Berland Split", labelled "4" in Fig. 3-1). Other such splits are suspected to be present, but were not observed (see discussion in chapter 6).

The Willmore Member is everywhere overlain by the Wapiabi Formation, except in the inner central Foothills west of the Bighorn and Nikanassin Ranges, where it is overlain by the thin, non-marine Obstruction Member. Locally, the Willmore-Wapiabi contact is marked by conglomerates; these are always included as the basal beds of the overlying Wapiabi Formation.

Obstruction Member. The Obstruction Member is the thinnest member of the Cardium Formation, and it displays the smallest areal distribution. The Obstruction Member is composed of non-marine deposits overlying the Willmore

Member in the inner central Foothills west of the Bighorn and Nikanassin Ranges. The Obstruction is overlain by the marine Wapiabi Formation. Marine conglomerates present at the Obstruction-Wapiabi contact are always included in the Wapiabi Formation.

Baytree Member. The coarse conglomeratic sandstones of the Baytree Member are restricted to northeast British Columbia and northwest Alberta; this member was not examined in this study. The reader is referred to appendix 6 for a definition of this member, which has not been altered in the revised stratigraphy.

CHAPTER 4. DEFINITION AND PRELIMINARY INTERPRETATION OF FACIES

INTRODUCTION

In this chapter, facies within the Cardium Formation are defined and described, and preliminary environmental interpretations are advanced.

I have defined 19 distinct and homogeneous facies following the detailed examination of 28 Cardium exposures. The term facies is herein used in reference to the complete assemblage of primary characteristics of the rocks, both physical (lithology, sedimentary structures) and biological (trace and body fossils). It is purely descriptive and stratigraphically unconfined. For an extended discussion of the concept implied by the term facies, the reader is referred to Middleton (1973) and Walker (1984a).

Preliminary facies were defined following examination of only 11 Cardium exposures (Duke, 1980), when it became apparent that each exposure could be subdivided using these preliminary facies. As new exposures were examined, it was found that the preliminary facies were adequate to describe the bulk of the thickness of each exposure; however, modifications and additions to the

preliminary facies scheme were made whenever previously undescribed facies were encountered. The final scheme of 19 facies presented below adequately characterizes all rocks examined.

To help the reader determine the significance and interrelationships of the numerous facies, they have been grouped together into five associations. It is important to realize that facies are units of description which are in part arbitrarily defined. The associations defined below are simply groupings of similar facies (i.e., the associations represent less specific assemblages of characteristic features). It follows that an analysis based upon the five facies associations would define gross variations in environment of deposition, whereas an analysis based upon the 19 facies would reveal more subtle environmental variation.

A list of the five associations and the 19 facies is presented on the following page. The associations are numbered, and the facies are designated by a three-character combination of letters and numerals. Note that each of the facies designations begins with the same numeral as the association to which it belongs. The page number for the description of each facies is given in this listing.

Association 1. Mud-dominated facies (p. 67)

1SH: Non-bioturbated shale (p. 67)

1BM: Extensively bioturbated mudstone (p. 68)

1GB: Very thin graded beds (p. 71)

1UP: Very thin undulatory parallel laminated beds (p. 81)

Association 2. Interbedded sandstones and mudstone (p. 94)

2H1: Thin hummocky cross-stratified beds (p. 96)

2H2: Intermediate-thickness hummocky beds (p. 112)

2H3: Thick hummocky beds (p. 120)

Association 3. Sand-dominated facies (p. 129)

3BS: Extensively bioturbated sandstone (p. 129)

3HA: Amalgamated hummocky beds (p. 132)

3SW: Swaley cross-stratification (p. 153)

3PL: Parallel and low-angle planar lamination (p. 172)

Association 4. Facies containing coal, root casts, and/or abundant plant fragments (p. 181)

4VL: Variable lithology, lagoonal fauna (p. 182)

4VC: Variable lithology, coaly (p. 189)

4IF: Interbedded channel fill (p. 195)

4SF: Sandstone channel fill (p. 204)

Association 5. Marine conglomerates (p. 217)

5CV: Conglomerate veneer (p. 218)

5CB: Bioturbated conglomerate (p. 225)

5C1: Minor bedded conglomerate (p. 231)

5C2: Major bedded conglomerate (p. 236)

The following facies descriptions constitute the major data base of this study. Each facies is described separately. The facies descriptions are presented in greater detail than are the preliminary interpretations which follow each association description. These preliminary interpretations are presented at the level of associations, rather than at the detailed level of facies, in order to emphasize the similarities between the various facies of any one association. More detailed discussions are presented in the integrated interpretations of chapters 5 through 8.

Certain features (e.g., pot- and gutter-casts, hummocky cross-stratification) which are common to many facies are described in this chapter in a preliminary form only. Subtle variation in these features from facies to facies can best be described and interpreted only within their stratigraphic context. Accordingly, extended discussion of variation in these common features will be delayed to the end of chapter 5, following the discussion of vertical facies relationships.

A very brief summary of the association interpretations is presented at the end of this chapter (p. 245).

FACIES DESCRIPTIONS

The following pages describe each of the 19 facies defined by the author following examination of 28 exposures of the Cardium Formation. Note that the corresponding facies symbol used in the measured sections of appendix 2 is presented at the beginning of each facies description. These small diagrams have not been formally designated as figures; they are presented simply for the convenience of the reader.

A summary of the basic features which distinguish a particular facies is provided at the end of the longer facies descriptions.

Association 1. Mud-dominated marine facies.

This association is composed of facies consisting predominantly of shale and/or mudstone. Thin beds (generally <10 cm thick) of coarse siltstone and/or very fine sandstone are interbedded with mudstone in certain facies, but these coarse beds typically constitute much less than half of the thickness of any occurrence. Marine trace and body fossils are present in most occurrences. Shales and mudstones generally are dark grey to black; siltstones and sandstones are steel grey to rusty brown. Nodules of black chert or siliceous mudstone are present in the shales and mudstones of this association; these nodules generally are discoidal in shape, having widths of a few tens of centimeters and maximum thicknesses of a few to several centimeters. Nodules are black on fresh surfaces only; typically, they weather to a punky reddish-orange color due to the presence of siderite.

Facies 1SH ("Marine Shale"): Non-bioturbated marine shale or argillaceous mudstone.

This is the rarest facies in association 1, there being only eight occurrences. Average facies thickness is 5.0 m (range: 0.8 to 10.0 m).

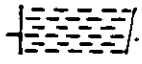

This facies is composed of dark grey to black, fissile shale and/or argillaceous mudstone (Fig. 4-1A). It is characterized by little or no bioturbation and the absence of sedimentary structures; however, rare horizontal laminations composed of delicate, thin (about 1 mm) silty layers are observed locally. Where bioturbation is present, biogenic structures consist of very thin oblique tubes resembling Chondrites. No body fossils have been observed in this facies.

Facies 1BM ("Bioturbated Mudstone"): Extensively bioturbated mudstone.

There were 32 occurrences of this facies encountered, having an average thickness of 5.2 m (range: 1.0 to 12.2 m).

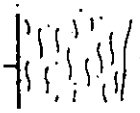

Lithologically, this facies is composed of mudstone (silty argillite to argillaceous siltstone) and sandy mudstone (<50% sand). Sand generally is very fine to fine grained.

Physical and biogenic structures. The mudstone is intensely bioturbated (Fig. 4-1B & 4-1C). It is characterized by a ropy, knotted texture in which certain

Figure 4-1. Examples of facies 1SH and 1GB.

A) Vertical section through an occurrence of facies 1SH. Note millimeter- to centimeter-scale "wispy" siltstone laminae. Section 7-1, 100 m level.

B) Vertical section through an occurrence of facies 1BM. Note absence of bedding and presence of ropy bioturbation texture. Individual biogenic structures are visible in this occurrence: "N" indicates nondescript burrows; "R" indicates subhorizontal Rhizocorallium. Coin is 2.4 cm in diameter. Section 5-37, 55 m level.

C) Vertical section through an occurrence of facies 1BM. Note how weathering differences affect appearance of outcrop. Thin, sharp-based siltstone bed immediately above coin is readily apparent in blocky area on right side of photo, but is traced only with difficulty in wacky area to the left. Coin is 2.4 cm in diameter. Section 5-45, 50 m level.

D) Vertical section through an occurrence of facies 1BM. Although completely bioturbated, decimeter-scale bedding is clearly evident in this exposure. Note concretion at bottom center of photo. Up is to the left. Section 7-1, 123 m level.

A
B
C
D

elements appear to be less argillaceous than others; however, in this characteristic occurrence, individual biogenic structures cannot be recognized due to the innumerable cross-cutting relationships. Locally, within favorably weathered exposures, numerous trace fossils can be recognized. These include Chondrites, Planolites, Teichichnus, and, less commonly, horizontal Rhizocorallium and Zoophycos (Fig. 4-1B; see also Fig. 4-11). Locally, Chondrites was observed to occur preferentially within pre-existing Teichichnus burrows. This characteristic assemblage of trace fauna is best attributed to a transitional or gradational interface between the Cruziana and Zoophycos ichnofacies (Frey & Pemberton, 1984).

In some occurrences, a crude horizontal bedding can be recognized by relatively subtle variation in lithology and/or weathering characteristics on a decimeter scale (Fig. 4-1D). Generally, no primary physical structures are visible in these occurrences, which also appear to be totally bioturbated. Locally, very small lenticles of very thin (about 1 cm) sharp-based siltstone or sandstone beds are preserved from bioturbation (Fig. 4-1C). These resemble the siltstone beds of facies 1GB described below. They may be apparently structureless or parallel laminated.

A complete spectrum exists between facies 1BM and facies 3BS (bioturbated sandstone). At several localities, the two facies are gradationally juxtaposed vertically. In

order to determine an approximate boundary between the two, an estimate of sand content was made in the field. The discriminative criterion used was the transition from sandy mudstone (<50% sand: facies 1BM) to argillaceous sandstone (>50% sand: facies 3BS). Bioturbated argillaceous siltstone was always included in facies 1BM.

Macrofossils. A few ammonites (genus Scaphites) were collected from this facies. Body fossils from the Cardium Formation are illustrated in figure 4-26.

Facies 1GB ("Graded Beds Facies"): Very thin sharp-based graded beds of siltstone or very fine sandstone.

This is the most commonly encountered facies in association 1, there being 75 occurrences. Average facies thickness is 7.1 m (range: 0.9 to 39.1 m).

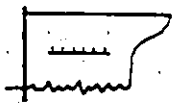

This facies is composed of very thin siltstones (rarely, very fine sandstones) about 0.5 to 5 cm (rarely, 10 cm) in thickness, interbedded with thicker mudstones and/or shales identical to the lithologies of facies 1BM or 1SH (Fig. 4-2). Mudstones typically are 2 to 10 cm thick.

Ratio of coarse to fine beds typically is low (about 1:5) but varies between about 1:2 to 1:10.

Lateral continuity of coarse beds. The thin siltstones of this facies at any one locality typically display varying degrees of lateral continuity (Fig. 4-2). Some beds, although only a few centimeters in thickness, are laterally continuous across several meters or tens of meters of outcrop (Fig. 4-2A & 4-2B). Other siltstone "beds" occur as isolated, lenticular deposits only a few centimeters wide (Fig. 4-2C & 4-2E). Most are intermediate in lateral continuity, being traceable over only a few decimeters (Fig. 4-2D & 4-2G). In some cases, this lateral pinch-out appears to be a primary feature (Fig. 4-2C & 4-2E); in many cases, however, it is obviously attributable to the pervasive bioturbation associated with the interbedded finer material (Fig. 4-2G).

Bases of coarse beds. Siltstone beds are characterized by very sharp, flat bases (Fig. 4-2) which rarely possess oriented sole marks (grooves, scratches, rare prods). Less commonly, bases are gradational over a few millimeters.

Internal structures within coarse beds. Coarse beds within facies 1GB commonly display a gradational vertical color change from siltstone into overlying

Figure 4-2. Examples of facies 1GB in sections normal to bedding.

A) A typical exposure. Note lateral continuity of thin beds. Section 7-1, 10 m.

B) Alternation between shale and graded or parallel laminated silt/sandstones produces the typical "ribby" appearance of this facies. Section 4-21, 15 m.

C) Sharp-based silt/sandstone beds display parallel lamination or asymmetrical ripple cross-lamination in this section. Ripple foresets indicate flow from left to right. Scale is 15 cm long. Section 7-1, 15 m.

D) These thin, sharp-based coarse beds are apparently structureless or crudely laminated. Section 4-19, 53 m.

E) Discontinuous asymmetrical ripple trains ("starved" ripples) are present at various levels in this interval near the base of section 5-45. Foresets and asymmetry indicate flow to left. Tape is extended 23 cm.

F) This thick coarse bed displays the ascending vertical sequence: sharp-base, plane parallel lamination, asymmetrical ripple cross-lamination. Foresets indicate flow to left. Scale in centimeters and inches. Section WA-1, 57 m.

G) In this example, bioturbation has disrupted the thin coarse beds, which probably were fairly continuous originally. Scale is 15 cm long. Section 5-39, 5 m.

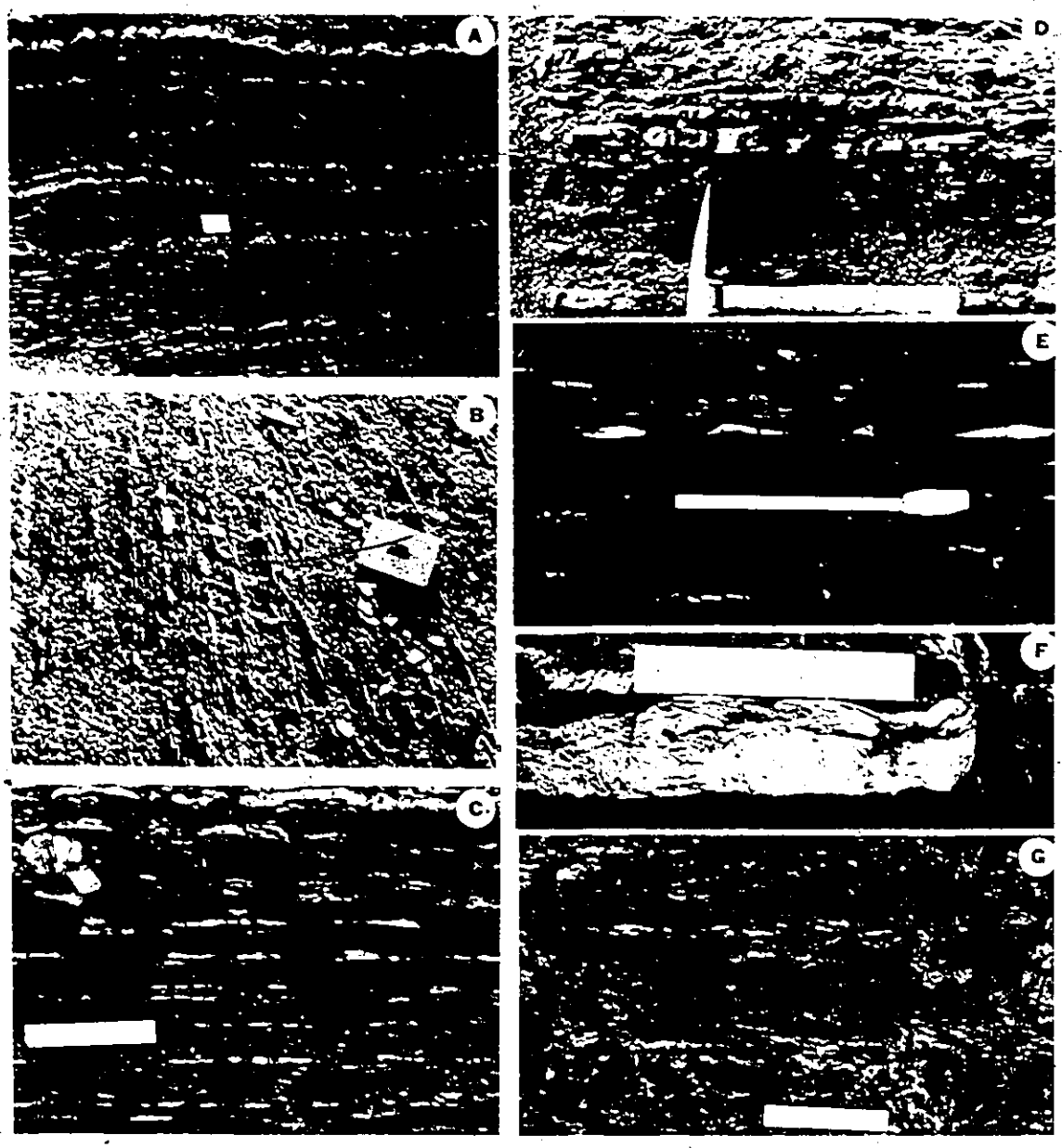
A
B
C
D
E
F
G

mudstone, suggestive of graded bedding (Fig. 4-2G); many other beds display parallel lamination (e.g., lower beds in Fig. 4-2C). Commonly, coarse beds consist of single sets of small-scale asymmetrical ripple cross-lamination (Fig. 4-2C & 4-2E); in these cases, the asymmetrical ripple form typically is preserved. It is in beds such as these that the primary lenticularity previously mentioned is developed. In such cases, numerous disconnected ripples ("starved ripples") commonly occur at the same stratigraphic horizon.

Another fairly common internal feature of siltstone beds in this facies is the vertical sequence upward from the sharp base into parallel lamination and finally asymmetrical ripple cross-lamination (Fig. 4-2G). This sequence tends to be developed in the thicker siltstones and sandstones. It is in beds such as these that the previously mentioned sole marks are best developed and the coarsest grain sizes (very fine sandstone) are observed.

Descriptively, the structure sequences described above constitute partial Bouma sequences (Fig. 4-3). Complete Bouma sequences are very rare in this facies; typical observed sequences in an approximate order of abundance are BE, AE, BCE, CE, ABE, CDE, BCDE, BDE. Structural sequences from this facies are further discussed in subsequent chapters.

Small scours filled with very fine sandstone are

Figure 4-3. The Bouma sequence, a facies model describing classical turbidites, proppsed by Arnold Bouma (1962). Figure from Walker (1984c, Fig. 4).

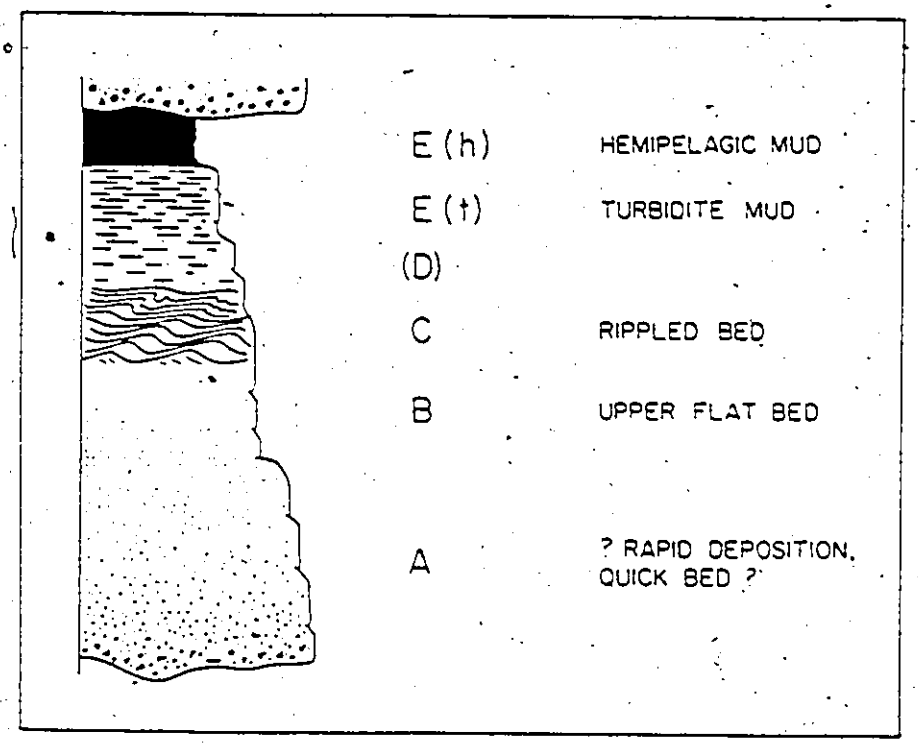
E (h)
HEMIPELAGIC MUD
E (t)
TURBIDITE MUD
(D)
C
RIPPLED BED
B
UPPER FLAT BED
A
? RAPID DEPOSITION, QUICK BED ?

infrequently encountered within this facies. These scours may occur at the bases of the siltstones previously described, but more commonly occur as isolated pods within mudstone. They have flat tops and concave, sharply erosive bases and sides. These scours have a distinctive geometry; they are 10 cm to 1 m in width and 10 to 50 cm in maximum eroded depth. In the third dimension, these scours have lengths generally in excess of 1 to a few meters (the maximum exposed lengths commonly observable in outcrop), although some of them are more nearly equant. Internally, sandstone within these scours is apparently structureless, parallel laminated, or low-angle cross-laminated. These features have been termed gutter-casts and pot-casts by previous workers; because they are also present in facies 1UP, 2H1, 2H2, and 2H3, they will be described and discussed in detail at the end of chapter 5.

Tops of coarse beds. Tops of graded or parallel laminated beds typically are gradational into overlying mudstone. Beds capped with asymmetrical ripples typically have sharp upper contacts (Fig. 4-2C, 4-2E, & 4-2F). The upper contacts of any type of bed, however, commonly are so extensively bioturbated as to make it impossible to determine the primary nature of the upper contact (Fig. 4-2G).

Conglomerate "stringers". A rare feature of this

facies is the occurrence of "stringers" of very coarse sand, granules, or small pebbles of varicolored chert (grain sizes ranging from about 1 mm to 5 cm; average approximately 1 cm). These stringers generally consist of bands or rows of widely dispersed, matrix-supported clasts, usually no more than one or two clast diameters in thickness; coarse clasts generally are separated from one another by several grain diameters. The matrix of these very matrix-rich beds is usually extensively bioturbated. In some cases, granules and pebbles occur in thicker beds (several clast diameters in thickness) and are clast-supported. In these examples, the matrix often is sandy or contains both sand and mud, and the beds are sharp-based and may be graded. These latter clast-supported pebble beds commonly are only slightly disrupted by bioturbation. All of the above-mentioned coarse-grained thin beds or bands occupy a special stratigraphic position; they are most frequently found within facies 1GB (or 1UP -- see below) within close stratigraphic proximity to an underlying conglomeratic facies (facies 5CB, 5CV, 5C1, or 5C2). In several instances, a gradational contact is present between facies 5C1 and an overlying occurrence of facies 1GB exhibiting thin conglomerate beds. Due to their special relationship with the conglomeratic facies, an expanded description and discussion of these pebble bands will be presented

following the discussion of vertical facies relationships (chapter 5).

Biogenic structures. The thin siltstone beds are usually disrupted to varying degrees by nondescript oblique biogenic tubes penetrating the entire bed (Fig. 4-2G). These are usually mudstone-filled, but sandstone-filled oblique tubes have also been observed. These tubes typically are cylindrical, possessing no ornamentation, and are usually 0.5 to 1 cm in diameter. Tops of siltstone beds occasionally display horizontal traces of various sorts, of which Gyrochorte is the most abundant recognizable form. It is always preserved in convex epirelief. Planolites has been observed in concave epirelief.

The interbedded mudstones of this facies often are extensively bioturbated (see description of identical mudstones of facies 1BM). Recognized biogenic structures include Chondrites, Planolites, and Teichichnus. As with facies 1BM, this trace-fauna assemblage suggests a transitional interface between the Cruziana and Zoophycos ichnofacies (Frey & Pemberton, 1984). Trace fossils from associations 1 and 2 are illustrated in figure 4-11.

Macrofossils. Ammonites (genus Scaphites) and Inoceramus have been found within this facies at many places. One Inoceramus valve (from an occurrence of facies

1GB immediately overlying an inferred transgression surface) was encrusted with bryozoans (Fig. 4-26). Body fossils from the Cardium Formation are illustrated in figure 4-26.

Summary: Basic distinguishing features. The basic distinguishing features which identify any single occurrence of facies 1GB are listed below:

1) Occurrences consist of mudstone interbedded with very thin beds of coarse siltstone and/or very fine sandstone.
2) Trace and body fossils indicate a marine origin at a gradational interface between the Cruziana and Zoophycos ichnofacies.
3) The thin interbeds of siltstone/sandstone (0.5 to about 5 cm thick) generally are extensive laterally. Bases of beds are sharp and locally display directional sole marks. Internally, coarse beds display graded bedding, parallel lamination and/or asymmetrical ripples. Isolated ("starved") asymmetrical ripples encased in mudstone are locally abundant. Sequences of structures within beds correspond to partial Bouma sequences; typical sequences in order of abundance include BE, AE, BCE, CE, ABE, CDE, BCDE, BDE.
4) Wave-formed structures are absent from this facies.

Facies 1UP ("Undulatory Parallel Lamination"): Very thin, sharp-based, undulatory parallel laminated siltstones and very fine sandstones.

This is another commonly encountered facies (63 occurrences). Average facies thickness is 4.1 m (range: 0.4 to 28.2 m).

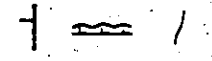

This facies consists of siltstones and/or very fine sandstones about 3 to 10 cm in thickness, interbedded with sediments identical to those of facies 1SH, 1BM, and/or 1GB (see "Interbedded Material" subheading below). Ratio of coarse beds to interbedded material is similar to or somewhat greater than that of facies 1GB, averaging about 1:4 or 1:3 (Fig. 4-4 & 4-5). Internally, however, the coarse beds of facies 1UP possess a distinctive undulatory lamination which differs markedly from the internal structures of coarse beds within facies 1GB.

Lateral continuity of coarse beds. Facies 1UP siltstones and sandstones typically are laterally continuous across an outcrop several meters wide; however, many beds pinch out over a few meters laterally, but may reappear at the same stratigraphic level slightly further along strike (Fig. 4-4A). All beds display an undulatory pinch-and-swell character, typically varying by several

centimeters in thickness over a few tens of centimeters laterally (Fig. 4-4B, 4-4D, & 4-4H). Although bioturbation is responsible for some of this lateral variability (e.g., uppermost coarse bed in Fig. 4-4B), lateral variation in thickness appears to be a primary feature of all of these beds.

Bases of coarse beds. Siltstone/sandstone beds typically have very sharp, flat bases (Fig. 4-4 & 4-5) which rarely possess oriented sole marks (grooves, scratches, rare prods). Less commonly, the bases are very gently undulatory with very broad, extremely low-angle erosional scours (Fig. 4-5A, 4-5D, & 4-5I). Rarely, these beds are associated with numerous small sandstone-filled scours 10 cm to 1 m in width and 10 to 50 cm in maximum eroded depth. Internally, scour fill is apparently structureless, parallel laminated, or undulatory parallel laminated; in some of the larger occurrences, the scour fill appears to be hummocky cross-stratified (see further discussion below). These scours often occur at the bases of siltstone/sandstone beds, but may occur isolated with finer grained material; in such occurrences, they have erosive, concave bases and flat tops, and resemble "gutter-" and "pot-casts" (see discussion at end of chapter 5).

Internal structures within coarse beds. The thin

Figure 4-4. Examples of facies 1UP in sections normal to bedding. Coin is 2.4 cm in diameter, ruler is 15 cm long.

A) A typical exposure. Note lateral continuity of pinching and swelling coarse beds. Section 5-45, 100 m.

B) A sharp-based, pinching and swelling coarse bed (center) and a heavily bioturbated bed (top). Note essentially flat lamination in central bed above hammer, and vertical color gradation at right. Section 5-8, 23 m.

C) In vertical succession, this bed displays a sharp base, shale rip-up clasts in basal laminae, planar parallel lamination, and symmetrical ripple cross-lamination.

D) Note superficial erosional features at top of coarse bed at center of photo. Section 5-19, 28 m.

E) In ascending vertical sequence, uppermost bed in photo displays a somewhat gradational base, flat to very gently curved lamination, and symmetrical ripple cross-lamination. Section 4-21, 50 m.

F) Small mud-filled superficial scour and convex lamination at top of a coarse bed. Section 4-21, 50 m.

G) Note low-angle cross-lamination and convex-upward upper surface of this coarse bed. In plan, upper surface displays 3-D undulatory topography. Section 5-39, 47 m.

H) Symmetrical, convex-upward (ripple?) form capping a coarse bed. Section 4-21, 50 m.

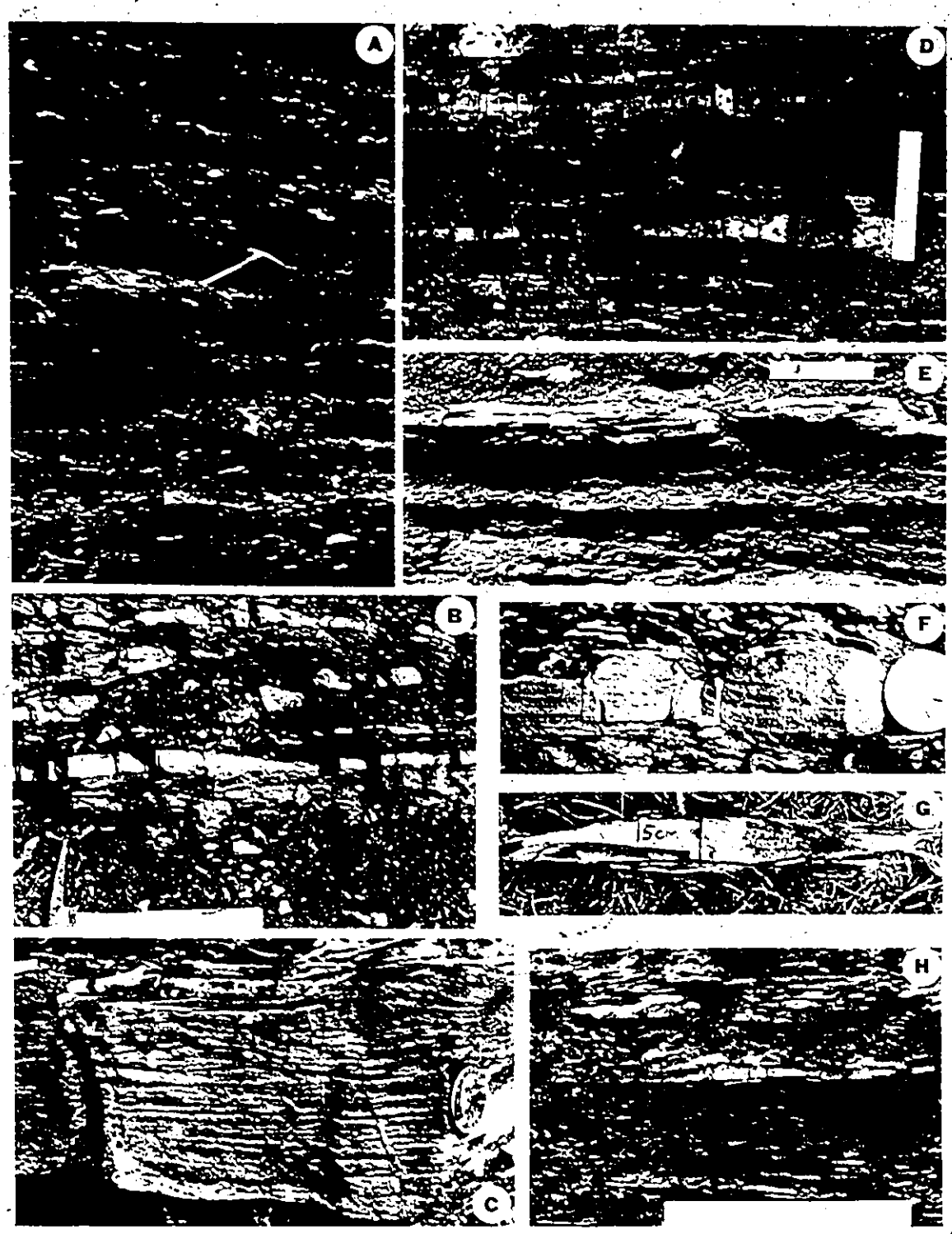
A
D
E
B
F
G
15cm
C
H

siltstone/sandstone beds of facies 1UP commonly are graded; locally, coarse beds have upper contacts which are gradational into mudstone/shale (Fig. 4-4B & 4-5F). Coarse beds display pinching and swelling parallel lamination (Fig. 4-4B; 4-5E, & 4-5F), with relatively rare, very low-angle intersecting laminae (about 3° to 5°) suggestive of hummocky cross-stratification (Fig. 4-4F, 4-4G, 4-5G, & 4-5H). The broadly curved parallel lamination may be concave upward (Fig. 4-5G, central portion of bed at center of photo) or convex upward (Fig. 4-4G, 4-5E, & 4-5H); usually both senses of curvature occur in the same bed (Fig. 4-5G, and detail of same bed in 4-5H). Form-wavelengths of these gently curved laminae are difficult to determine; generally, form-wavelengths range from approximately 20 to 50 cm. A definition sketch of this type of lamination is presented as figure 4-6. I shall refer to this sedimentary structure as "undulatory parallel lamination".

Some coarse beds included within this facies are graded but display no lamination or only a crude lamination (Fig. 4-4B), and some show true parallel lamination and/or asymmetrical ripples (Fig. 4-5A, and detail in 4-5C). Beds displaying these structures are included within facies 1UP only when bounded above and below by numerous beds possessing undulatory parallel lamination; wherever many such beds are grouped together in a vertical sequence in

Figure 4-5. Examples of facies 1UP in sections normal to bedding. In all photographs, coin is 2.4 cm in diameter. All examples are from section 5-45, 156 to 159 m level.

A) Vertical section displaying a variety of coarse beds.

B) Detail of bed above coin in photo A. At right, note truncation of most of the laminae (dipping to the left) by one or two sandstone lamina(e) dipping to the right.

C) Detail of beds at top of photo A, showing isolated asymmetrical ripple and overturned (current-deformed) sandstone laminae. Ripple asymmetry, ripple foresets, and overturned laminae all indicate flow to the right.

D) Superficial erosion of a coarse bed (at center).

E) Another superficially eroded bed.

F) Vertical section showing termination of laminae at the base of a coarse bed, very low-angle cross-lamination in lower part of bed at left, and gently curved to flat lamination throughout most of the thickness of the bed.

G) Prominent low-angle, curved lamination and laminae intersections. See detail in photo H.

H) Detail of bed in photo G. Note low-angle, curved intersection of laminae at center of bed, overlain by intersection-concordant, convex-upward laminae.

I) Vertical section showing bioturbated coarse beds. Note scour at base of lower bed. Scale is 15 cm long.

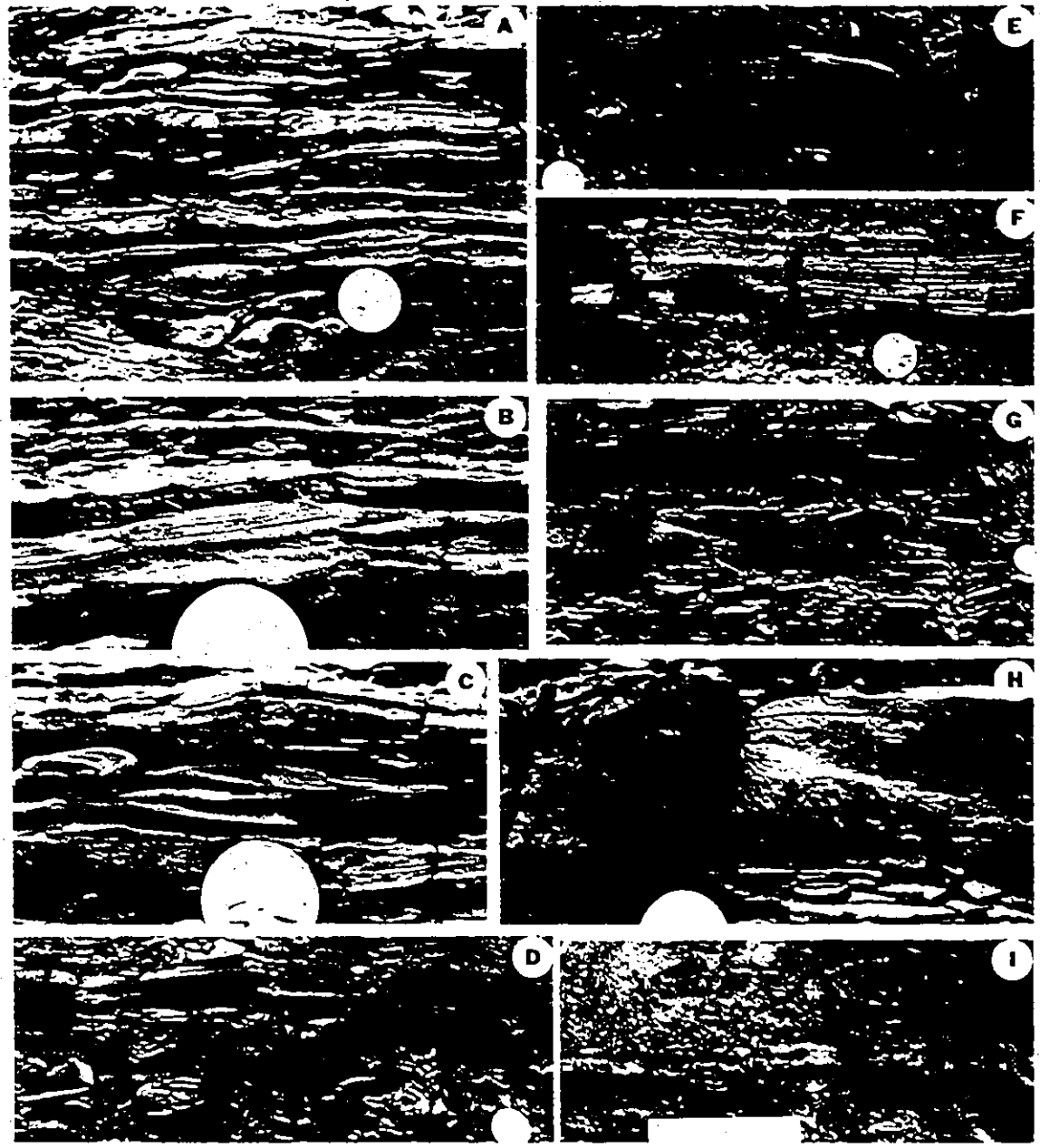
A
B
C
D
E
F
G
H
I

excess of a few tens of centimeters in thickness, the facies designation 1GB is used and the interval would be separated from an overlying or underlying facies 1UP occurrence.

Tops of coarse beds. Tops of undulatory parallel laminated beds are variable in character. Most occurrences display superficial erosional surfaces which truncate internal lamination (Fig. 4-4D, 4-5B, 4-5D, 4-5E, & 4-5G).

As previously mentioned, tops of beds are locally gradational over a few millimeters or centimeters into mudstone (Fig. 4-4B). Less commonly, sharp, flat upper surfaces are present, often slightly modified by bioturbation (Fig. 4-5F). Even less frequently, small-scale, two-dimensional symmetrical ripples (oscillation or wave ripples) are present on the upper bedding surface (Fig 4-4C & 4-4E). Both trochoidal ripples (possessing sharp crests and broad, flat troughs) and sinusoidal ripples are encountered; spacings are usually about 7 to 9 cm, but range up to about 15 cm. Rarely, three-dimensional convex-upward forms resembling sinusoidal symmetrical ripples are encountered at the tops of beds (Fig. 4-4H); these possess an irregular hummock-and-swale morphology and have spacings similar to those of the two-dimensional ripples described above (7 to 9 cm). In a few, rare examples, the upper surfaces of undulatory

Figure 4-6. Block diagram illustrating major morphological features of undulatory parallel lamination.

LAMINAE NEARLY PARALLEL
LOCALLY, VERY-LOW-ANGLE INTERSECTIONS

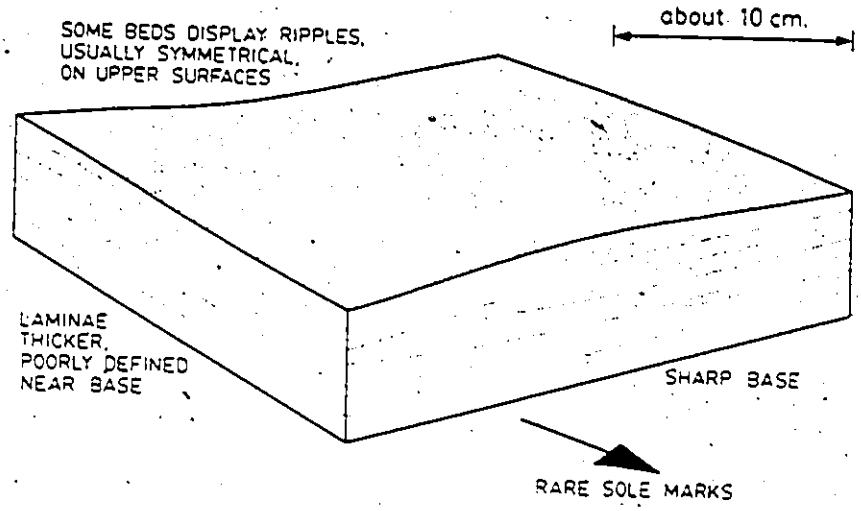

parallel laminated beds display small-scale asymmetrical ripples (current ripples) having spacings of approximately 5 to 20 cm.

Conglomerate "stringers". As in facies 1GB, facies 1UP occurrences locally exhibit thin conglomerate beds (see facies 1GB above). These are further discussed within their stratigraphic context at the end of chapter 5.

Biogenic structures. Biogenic structures from facies 1UP are identical to those from facies 1GB described above, with one exception: In facies 1GB, Gyrochorte is present in convex epirelief only, whereas in facies 1UP, it occasionally is also observed in concave hyporelief. Again, this trace-fauna assemblage suggests a transitional interface between the Cruziana and Zoophycos ichnofacies (Frey & Pemberton, 1984). Trace fossils from associations 1 and 2 are illustrated in figure 4-11.

Macrofossils. A few ammonites (genus Scaphites) were collected from facies 1UP. Pelecypod molds (genus Cardium) were very rarely observed from the bases of coarse beds within this facies. Body fossils from the Cardium Formation are illustrated in figure 4-26.

Summary: Basic distinguishing features. The basic distinguishing features which identify any single occurrence of facies 1UP are listed below:

1) Occurrences consist of mudstone interbedded with very thin beds of coarse siltstone and/or very fine sandstone.

2) Trace and body fossils indicate a marine origin at a gradational interface between the Cruziana and Zoophycos ichnofacies.

3) The thin interbeds of siltstone/sandstone (3 to 10 cm thick) generally are extensive laterally. They have sharp bases which locally display directional sole marks. Many pinch and swell in thickness. Internally, coarse beds display low-angle, undulatory parallel lamination, and are locally capped with symmetrical ripples. Asymmetrical ripples are present locally.

Association 1: Preliminary Interpretation

The presence of marine trace and body fossils and the dominance of shale/mudstone suggest an offshore origin for the facies of association 1. Specifically, the dominance of hemipelagic mudstones and the trace-fauna assemblage (transitional between the Cruziana and Zoophycos ichnofacies) both indicate minor agitation of bottom waters far from the source of clastic material.

The thin interbedded siltstones and sandstones of facies 1GB and 1UP are sharp-based and fining-upward, indicating sudden introduction of coarse silt and very fine sand into a basin dominated by slow deposition of hemipelagic muds. This interpretation is strongly supported by the sequences of structures observed in many coarse beds (especially those of facies 1GB), which corroborate deposition under waning unidirectional flow. Structures in these beds commonly record a vertical transition from upper to lower flow-regime bedforms. In fact, many of these beds display partial or (rarely) complete Bouma sequences generally associated with deposition from subaqueous turbidity currents; however, a turbidity-current origin is contra-indicated by paleoflow data (chapter 7). The complete absence of wave-formed structures in all facies other than 1UP is consistent with the inferred offshore depositional setting below the

influence of surface gravity waves.

The undulatory parallel laminated beds of facies 1UP are transitional (both descriptively and stratigraphically) between the current-dominated beds of facies 1GB and the wave-dominated hummocky cross-stratification of association 2; as such, they probably represent wave-influenced deposition from unidirectional flows in depths of water near effective storm wave-base. Depending upon the local storm-wave climate, storm wave-base may be a few tens to over 100 meters in depth. Depth in this facies could not have been much shallower than effective storm wave-base, because not all coarse beds in this facies exhibit inferred wave-generated structures. In fact, many beds between individual undulatory parallel laminated beds typically reveal a dominance of current-generated structures.

Note that the transitional setting between the Cruziana and Zoophycos ichnofacies is fully supportive of the inferred depositional setting in water depths approximating effective storm wave-base. The Cruziana ichnofacies is characteristic of deposition "below daily wave-base but not storm wave-base," whereas the Zoophycos association represents deposition "below storm wave-base to fairly deep water" (Frey & Pemberton, 1984, Table 2). Thus, a transitional setting would imply deposition in water depths approximating effective storm wave-base.

N.B.: As this thesis is being completed (Spring 1985), a major debate exists within the geological community concerning the possibility of forming turbidity currents on shallow epicontinental and pericontinental shelves (such as the Mesozoic Western Interior Seaway, in which the Cardium sediments were deposited). This issue will be addressed in detail for the Cardium Formation in particular in chapter 7.

Association 2. Interbedded hummocky cross-stratified sandstones and mudstones.

This association is composed of sharp-based hummocky cross-stratified siltstones and sandstones (roughly 15 to 220 cm in thickness) interbedded with shale and/or mudstones (Fig. 4-7A & 4-7B). Many hummocky beds are capped with small-scale symmetrical ripples (Fig. 4-7B to 4-7G). The fine-grained deposits between hummocky beds commonly contain very thin siltstones and/or sandstones identical to those of association 1 (Fig. 4-7A). All siltstones and sandstones are composed predominantly of quartz and chert grains; generally, grain size is no larger than lower fine sand size. Marine trace and body fossils are present in most occurrences. Medium-scale high-angle cross-bedding formed by submarine megaripples (dunes) or sandwaves is entirely absent from this association.

Siltstones and sandstones of this association are steel grey to rusty brown in color; shales and mudstones are dark grey to black. Typically, sideritic chert or siliceous mudstone nodules identical to those of association 1 are present within the thicker shaly intervals.

Figure 4-7. Association 2: General bedding characteristics and plan-view exposures of symmetrical ripples.

A) A typical exposure. Up is to the right. Most beds are essentially tabular; one pinches out toward top of outcrop (large arrow at bottom right). Weathering characteristics do not make this exposure particularly well suited for viewing laminae; nevertheless, four convex-upward hummocks (arrows pointing right) and three concave-upward swales (arrows pointing left) are clearly discerned. Hammer for scale. Section 5-19, 30 m.

B) Thickening- and coarsening-upward sequence developed in an occurrence of association 2. Field book (top center) for scale. Section 4-23, 128 m.

C) Sinusoidal symmetrical ripples capping a hummocky bed. Seebe Member at section 5-45.

D) Trochoidal symmetrical ripples capping a hummocky bed. Scale is 15 cm long. Seebe Member at section 5-5.

E) Trochoidal symmetrical ripples capping a hummocky bed. Seebe Member at section 5-45.

F) "Ladderback" interference ripples (left) and slightly asymmetrical (combined-flow?) ripples (right) capping the same hummocky bed. Seebe Member at section 5-45.

G) Oblique plan view of three-dimensional, trochoidal to sinusoidal symmetrical ripples capping a hummocky bed. Scale is 30 cm long. Seebe Member at section 5-45.

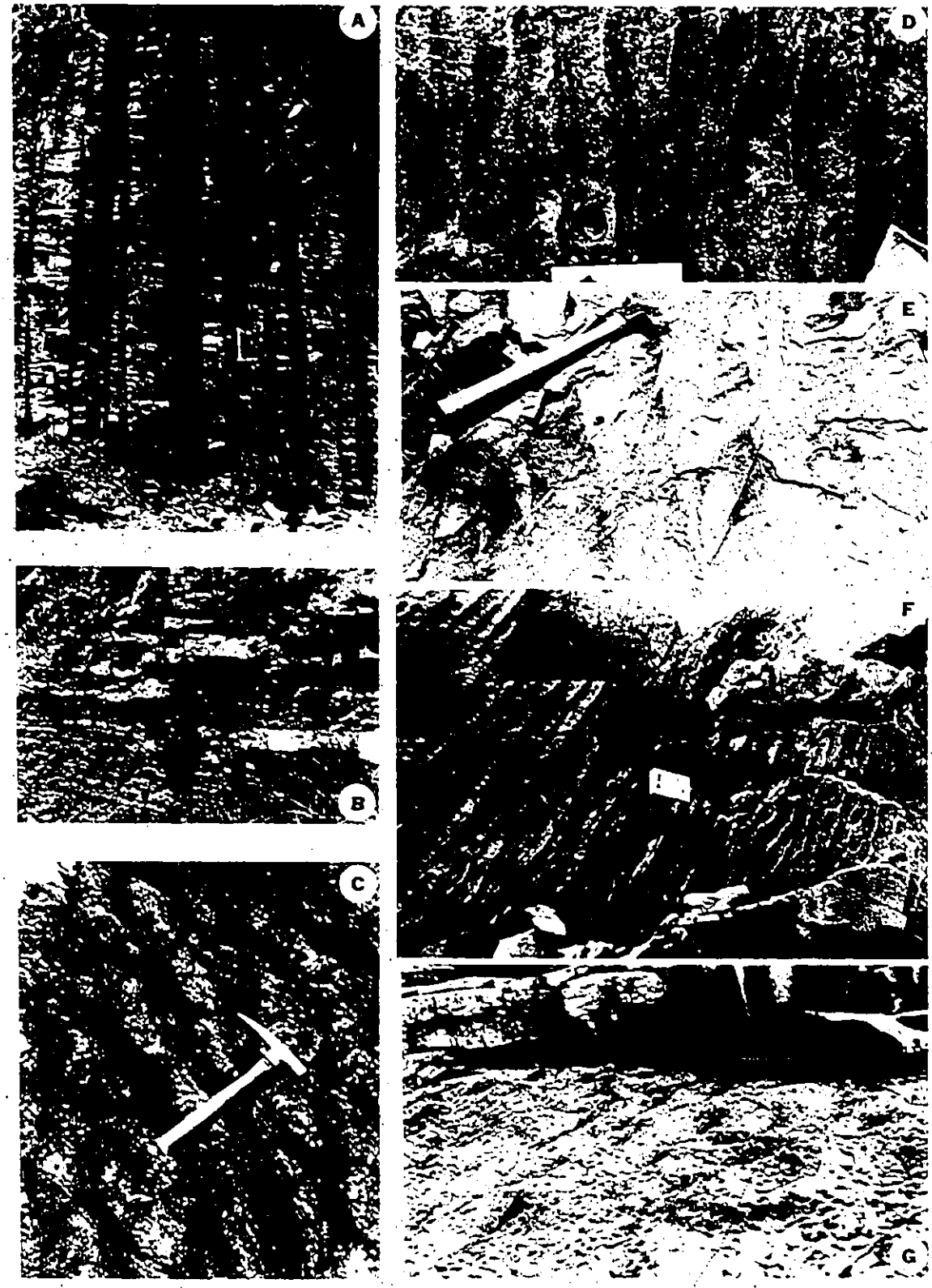
A
B
C
D
E
F
G

Facies 2H1 ("Thin Hummocky Beds"): Thin (<20 cm) sharp-based hummocky cross-stratified siltstones and sandstones interbedded with mudstones.

This is the most commonly encountered facies within the Cardium Formation (84 occurrences). Average facies thickness is 2.5 m (range: 0.5 to 8.5 m).

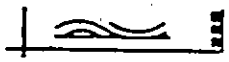

This facies consists of hummocky cross-stratified coarse siltstones/very fine to fine sandstones interbedded with sediments identical to those of facies 1UP, 1GB, 1BM, and/or 1SH. High-angle cross-bedding in sets thicker than a few centimeters is entirely absent from this facies.

Extended discussion of hummocky cross-stratification from this and other facies is presented in chapters 5 and 8. The brief description presented here is intended to familiarize the reader with only the major features of this structure in this facies. See figure 4-8 for a block diagram illustrating the major morphological features of the structure.

Thicknesses of hummocky cross-stratified beds within facies 2H1 range from about 10 to 20 cm. By definition, sharp-based hummocky beds having thicknesses predominantly in excess of 20 cm are classified within

Figure 4-8. Block diagram illustrating the major morphological features of sharp-based hummocky cross-stratification. Letters at right indicate divisional sequence in the right-hand corner of the block; a discussion of these divisions is deferred to chapters 5 and 8. From Duke (1985c, Fig. 1).

LOW-ANGLE TRUNCATIONS & TERMINATIONS

LOW-ANGLE CURVED LAMINAE, BOTH CONCAVE- AND CONVEX-UPWARD

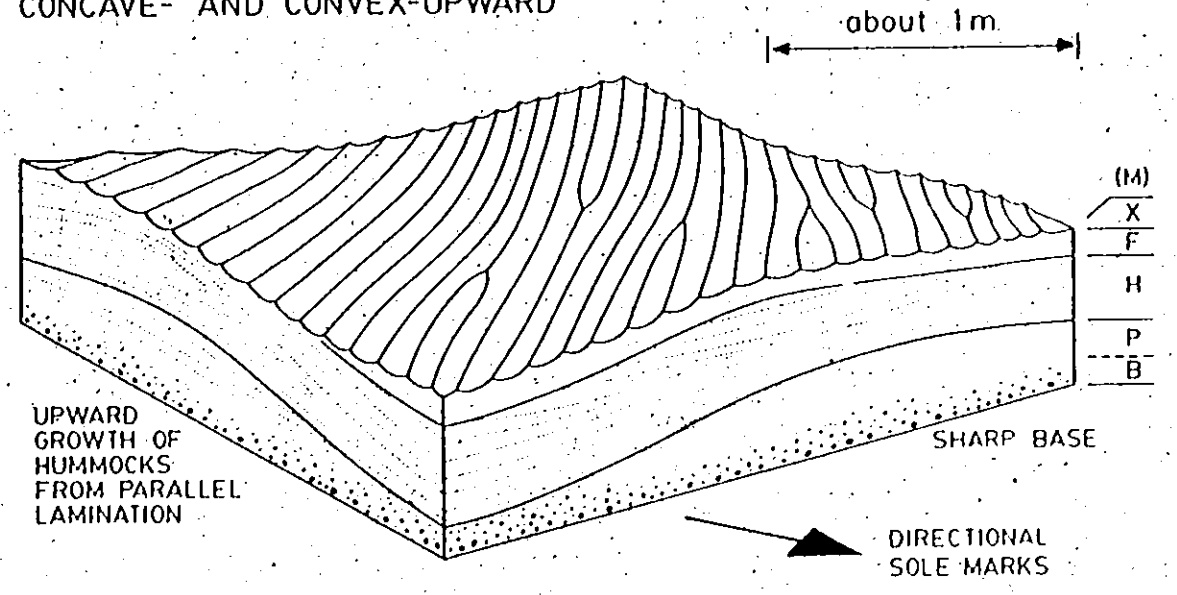

facies 2H2 or 2H3. This arbitrary distinction reflects a fairly natural break in bed thickness (evident in Fig. 4-7B).

Geometry of hummocky beds. Sharp-based hummocky cross-stratified siltstones and sandstones of facies 2H1 typically display an essentially tabular morphology on the outcrop scale (e.g., thinner hummocky beds in Fig. 4-7A & 4-7B). This tabular bed geometry is in many instances slightly or greatly modified by one or more of the following (Fig. 4-9; see similar features in illustrations of facies 2H2):

1) preservation of a hummock/swale topography at the tops of beds (Fig. 4-9A),
2) wavey or irregular superficial scouring at the tops of beds (Fig. 4-9B & 4-9D),
3) localized shallow scouring at the bases of beds (Fig. 4-9A),
4) extensive step-wise scouring or channelling at the bases of beds,
5) lateral depositional pinch-out (as in the case of the thin bed in Fig. 4-7A).

The first three factors listed above generally result in only minor local departures from a tabular geometry. These deviations are on the order of a few tens

of centimeters or a few meters in width, and only a few centimeters or tens of centimeters in thickness.

The fourth factor listed above, step-wise scouring or channelling, generally results in a laterally extensive variation in bed thickness, on the order of a few tens of centimeters.

Locally, hummocky beds of facies 2Hl are laterally impersistent. Over a few meters or tens of meters along strike, some examples thin to near zero thickness, but thicken again further along strike. Other beds are observed to pinch out entirely along strike. This major lateral variation in thickness is due to pronounced step-wise scouring or channelling, pronounced superficial erosion, and/or lateral depositional pinch-out.

Rarely, hummocky cross-stratification of facies 2Hl occurs <u>within</u> large gutter-casts. This relationship is further discussed in chapter 5.

<u>Bases of hummocky beds</u>. Hummocky beds within facies 2Hl typically have very sharp bases displaying oriented or directional sole marks (grooves, scratches, prods, rare flutes -- Fig. 4-10). The sharp bases usually are regionally flat; less commonly, they are gently undulatory (Fig. 4-9A). Rarely, sharp bases are irregularly scoured in a step-wise fashion. Maximum eroded depth may be as great as a few tens of centimeters in these

Figure 4-9. Vertical sections through hummocky cross-stratified sandstones from facies 2H1 (except photo A). Scale bar is 15 cm long.

A) Low-angle undulatory lamination in a thin, isolated lens of hummocky sandstone within facies 1UP (section WA-1, 68 m). Note sharp basal contact, shallow basal scour at base, steeper internal scour, flattening of laminae toward top of bed, and gradational upper contact with mudstone (especially evident at right).

B) A very low-angle internal intersection is evident in this sharp-based bed, approximately 3 cm above the basal contact at top of scale. A pronounced superficial erosional surface of irregular relief is indicated by the dotted line. Note shallowly inclined Ophiomorpha burrow above scale. Section 6-8, 73 m.

C) Hummocky sandstone interbedded with abundant, thin, symmetrical-rippled sandstones similar to those of facies 1UP. Section 5-45, 65 m.

D) An unusual hummocky sandstone in which laminae dip fairly consistently in a single direction (i.e., to the right) with respect to regional bedding. Note superficial erosional truncation of laminae at the sinusoidal upper surface of this sandstone. Also note mottled, largely bioturbated mudstone above sandstone, similar to that of facies 1BM. Section 6-8, 56 m.

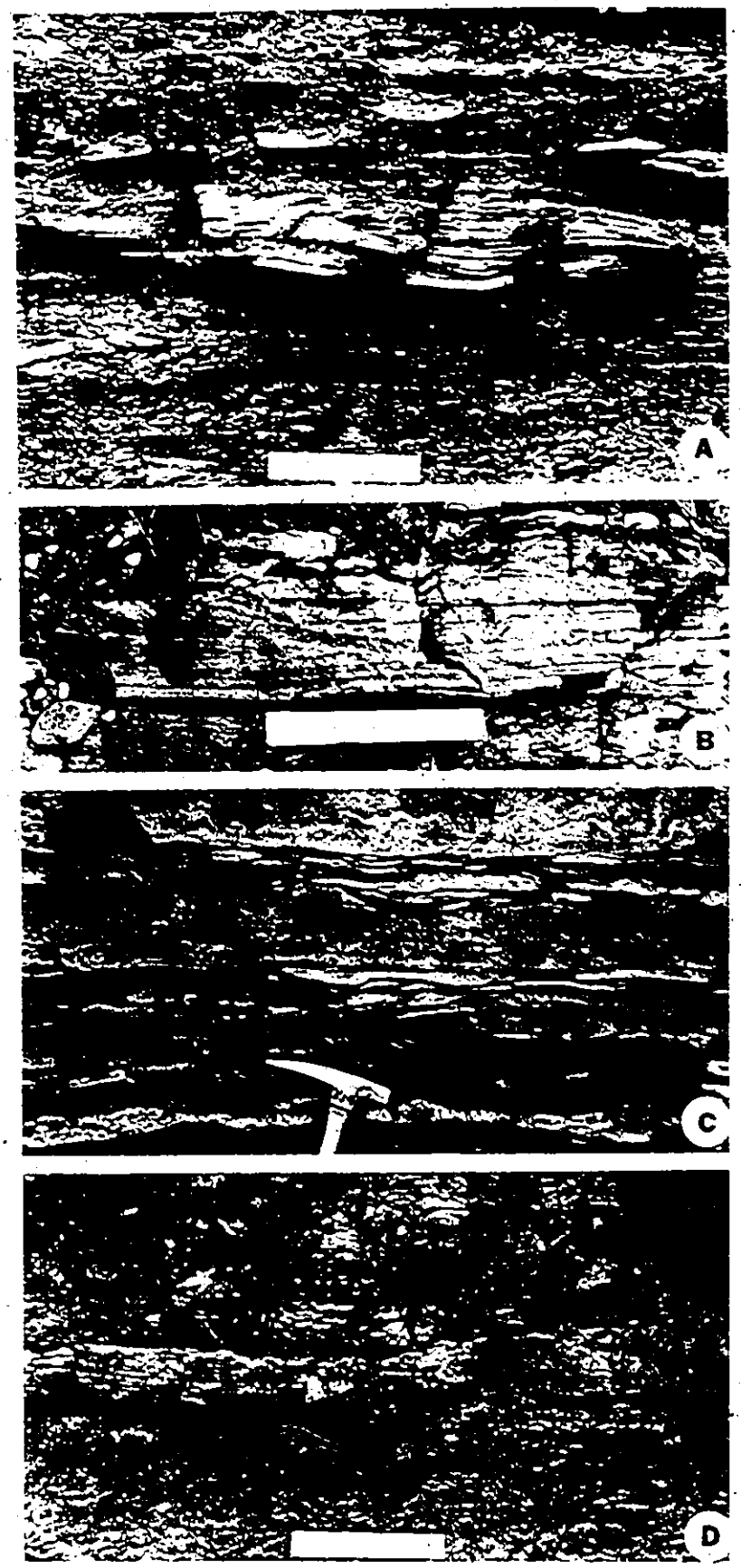
A
B
C
D

cases, and is commonly associated with local thickening of an individual bed beyond the 20 cm cut-off for typical thicknesses of hummocky cross-stratified beds in this facies. Molds of disarticulated shells (predominantly Cardium shells) are occasionally observed at or near the bottoms of the coarse beds; where present, they rarely appear in great profusion on the soles of beds in a hydrodynamically stabilized, convex-upward position (Fig. 4-10D). More typically, only a few shell molds are observed on these basal surfaces; these also appear in a convex-upward position. These shell molds often serve as useful paleoflow indicators: In many occurrences, shells are aligned at the base of the bed. In such a situation, the umbo is inferred to have acted as an "anchor" pointing in the up-current direction. Flat shale rip-up clasts a few centimeters long are also frequently present near the bases of hummocky beds (Fig. 4-10C); rarely, rip-up clasts are present higher within the bed. Very rarely, scattered granules and pebbles (maximum diameter about 0.5 cm) are found at the bases of hummocky beds; also, a thin graded or apparently structureless interval may be present above the base, and/or a thin parallel laminated interval (see Walker et al., 1983, and chapter 8 of this thesis).

Internal structures within hummocky beds.

Internally, hummocky cross-stratified beds commonly are

Figure 4-10. Primary physical sole features from the sharp bases of hummocky cross-stratified sandstones in association 2. All photographs show the bases of beds as viewed from below.

A) Elongate, very shallow ridges and depressions resembling current lineations. Lineation orientation is roughly parallel to the hammer handle. Note that the large biogenic structures do not appear to have been modified by this flow, suggesting their formation post-dated the emplacement of the sand. Section 5-19, 74 m.

B) Oriented sole markings (primarily grooves) found in float at section 5-39. Coin is 2.4 cm in diameter.

C) Impressions of abundant shale rip-up clasts in the basal laminae of a hummocky sandstone bed found in float at section 5-45. Scale is 15 cm long.

D) Oblique view looking upward of the sharp base of a hummocky sandstone. Note scattered Cardium valves in a convex-upward position (especially obvious at right). Scale in millimeters and inches. Section 5-45, 140 m.

E) View of an elongate step-wise scour at the base of a hummocky bed (again, looking up-section). At right, base scours down from a stratigraphically higher level away from the camera. Scour feature is elongate from 10 o'clock to 4 o'clock in this view. Coin (center left) is 2.4 cm in diameter. Willmore Member, section 5-45.

A
B
C
D
E

graded in their upper parts, or display gradational interlamination with overlying mudstone or shale (Fig. 4-9A). As has been previously mentioned, a thin graded, apparently structureless, or parallel-laminated interval may be present above the base of a bed. Scattered shale rip-up clasts are occasionally encountered dispersed throughout these beds; often, these are concentrated near the base.

In comparison with the other hummocky facies described below, the scale of hummocky cross-stratification in facies 2H1 is relatively small. The hummocky form in facies 2H1 is characterized by relatively low values of form-spacing, the distance (measured parallel to regional bedding) separating two laterally adjacent hummocks (or two laterally adjacent swales). Form-spacings in this facies range between about 50 and 200 cm. Similarly, values of form-height (the vertical distance separating the crest of a hummock from the trough of an adjacent swale, measured normal to regional bedding) are also relatively low. Form-heights in facies 2H1 range from a few centimeters to about 15 cm. Low-angle cross-lamination within these beds ranges from 0° to about 15°; typical values are 10° or less (Fig. 4-9).

Additional description and interpretation of the internal structures of hummocky cross-stratified beds is presented in chapters 5 and 8 (see also Walker et al.,

1983).

Tops of hummocky beds. Tops of hummocky cross-stratified beds within this facies commonly are extensively bioturbated and display no preserved lamination; these extensively bioturbated upper parts of beds are characterized by a ropy or mottled structure resulting from numerous non-descript cross-cutting burrows. In less extensively bioturbated examples, lamination is locally preserved at the tops of beds, and numerous different trace fossils may be identified (see description below). Very often, tops of beds which are only slightly modified by bioturbation are covered with small-scale symmetrical ripples (Fig. 4-7). The spacing between ripples is relatively constant on any one bed; however, spacing values vary from bed to bed, ranging between about 5 and 15 cm. Crests of symmetrical ripples usually are sharp, with broad, flat troughs (trochoidal ripples); less frequently, both crests and troughs are round and broad (sinusoidal ripples). Tuning-fork bifurcations are occasionally observed. Favorable bedding-plane exposures reveal that symmetrical ripple crests generally are perfectly straight to very gently curved over distances of a few to as many as 15 m. Occasionally, however, radii of curvature as small as 1 or 2 m have been observed; such curvature persists over short distances only, resulting in

arcs of about 70° maximum being described by ripple crests. Although symmetrical ripples locally display internal cross-lamination indicating lateral translation of the ripple form (combined-flow ripples, Harms et al., 1975, p. 58), true asymmetrical (current) ripples have never been observed capping hummocky cross-stratified beds within this facies. Rarely, small-scale three-dimensional sinusoidal ripples cap hummocky beds (Fig. 4-7G).

In addition to the bioturbated and symmetrical rippled tops of beds described above, tops of hummocky beds are very commonly very sharp and regionally flat; examples of this type of upper bedding contact between underlying sandstone and overlying mudstone typically display superficial erosional truncation of underlying sandstone laminae. Many examples display thin, flat, platy interbeds of siltstone/sandstone and shale/mudstone (Fig. 4-9A & 4-9B); mud-filled scours may also be present at the eroded tops of beds (Fig. 4-9C).

Finally, the tops of hummocky beds in this facies locally preserve an original depositional hummock/swale topography. Beds of this sort often exhibit minor superficial scouring and/or a veneer of symmetrical ripples.

Biogenic structures within hummocky beds. As noted above, tops of hummocky beds commonly are extensively

bioturbated, displaying a ropy or mottled structure resulting from numerous non-descript cross-cutting burrows (generally vertical or oblique to bedding). In less bioturbated examples, both lamination and individual burrows may be observed throughout the thickness of the bed. The tops of these latter beds typically display numerous horizontal traces, of which Gyrochorte (preserved in convex epirelief), Muensteria, and Palaeophycus are the most abundant. Horizontal Rhizocorallium and Zoophycos are observed at the tops of beds within this facies, as are low-density vertical burrows resembling Skolithos, Cylindrichnus or Rosselia, Diplocraterion, and/or (rarely) Ophiomorpha (Fig. 4-9B). Locally, escape (?) burrows penetrate hummocky beds (Fig. 4-11E).

Bases of hummocky beds in this facies also very commonly display biogenic structures, locally in great abundance. Unlike tops of beds, however, vertical and oblique structures are only rarely encountered at the bases of beds. Horizontal traces include Planolites, Palaeophycus, numerous nondescript burrows, and rare Thalassinoides. Gyrochorte (preserved in concave hyporelief) is a commonly encountered ichnogenus. At one locality, a single example of Spirorhaphe was observed. Trace fossils from associations 1 and 2 are illustrated in figure 4-11.

Interbedded material. Interbedded between hummocky cross-stratified siltstones and sandstones of facies 2H1 is fine-grained material which is distinctly similar to the deposits of facies 1UP, 1GB, 1BM, or 1SH described above. Within any one occurrence of facies 2H1, the material interbedded between hummocky cross-stratified beds may or may not be consistently similar to one or another of these four types.

The most commonly encountered type of material interbedded between hummocky siltstone/sandstones consists of regularly and thinly interbedded shale or bioturbated mudstone and thin (1 to 5 cm) sharp-based siltstones and/or sandstones (Fig. 4-9A & 4-9C). Typically, these thin coarse beds are undulatory parallel laminated, and they rarely are capped with symmetrical ripples; therefore, interbedded material typically resembles the deposits of facies 1UP. Less commonly, the thin coarse beds are apparently structureless or graded, or display parallel lamination and/or true current ripples. In this case, the interbedded material resembles facies 1GB deposits. These types of interbedded deposits generally lie upon hummocky beds which are not extensively bioturbated.

Extensively bioturbated mudstone or sandy mudstone (equivalent to facies 1BM deposits -- Fig. 4-9B & 4-9D) generally lies upon hummocky beds which are extensively bioturbated in their upper parts; however, bioturbated

Figure 4-11 (in two plates). Some common trace fossils in sandstones from associations 1 and 2. In all photos, scale is in centimeters and inches, and is 15 cm long. Unless otherwise stated, coin is 2.4 cm in diameter.

A) Sole view of Diplocraterion.

B) Sole view of Planolites. Coin is 1.9 cm in diameter.

C) Internal bedding-plane with Chondrites.

D) Internal bedding-plane with unidentified trace.

E) Escape (?) burrows through a hummocky sandstone. Note local bending of laminae upward around burrows.

F) Mud-filled burrow penetrating thin bed at top of photo.

G) Plan view of Gyrochorte at top of sandstone.

H) Plan view of Gyrochorte at top of sandstone.

I) Gyrochorte (1) and larger Palaeophycus (2) in plan view at top of sandstone. Note symmetrical ripples.

J) Palaeophycus (1) and Thalassinoides (2) in plan view at top of sandstone.

K) Skolithos, Cylindrichnus, and/or Rosselia in plan view at top of sandstone.

L) Large, steeply inclined structure in plan view at top of sandstone. Note symmetrical ripples.

M) Detail of L. Note concentric rimming and possible recolonization of filling within large structure. Also note Muensteria (1) and Cylindrichnus (2).

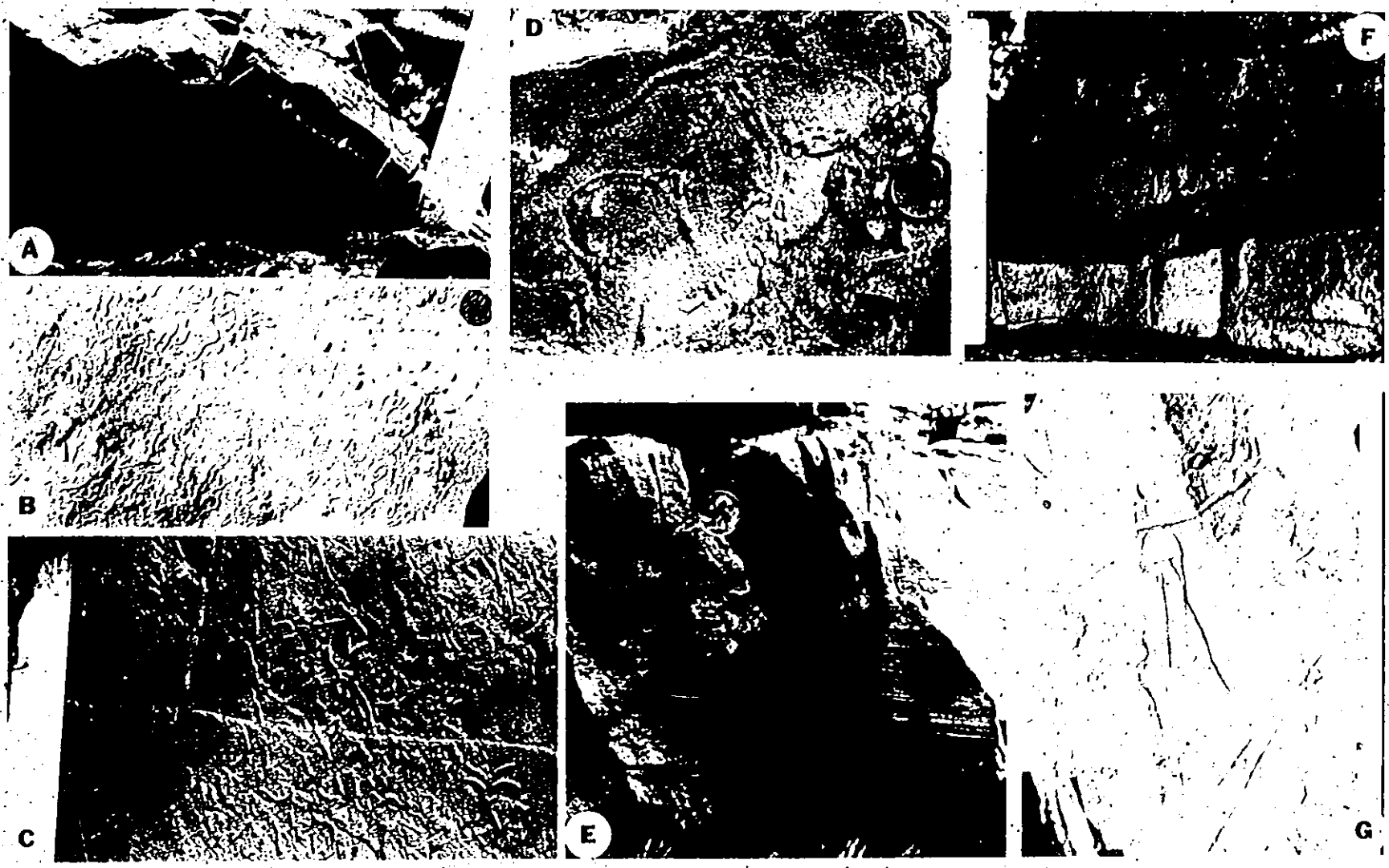
A
B
C
D
E
F
G

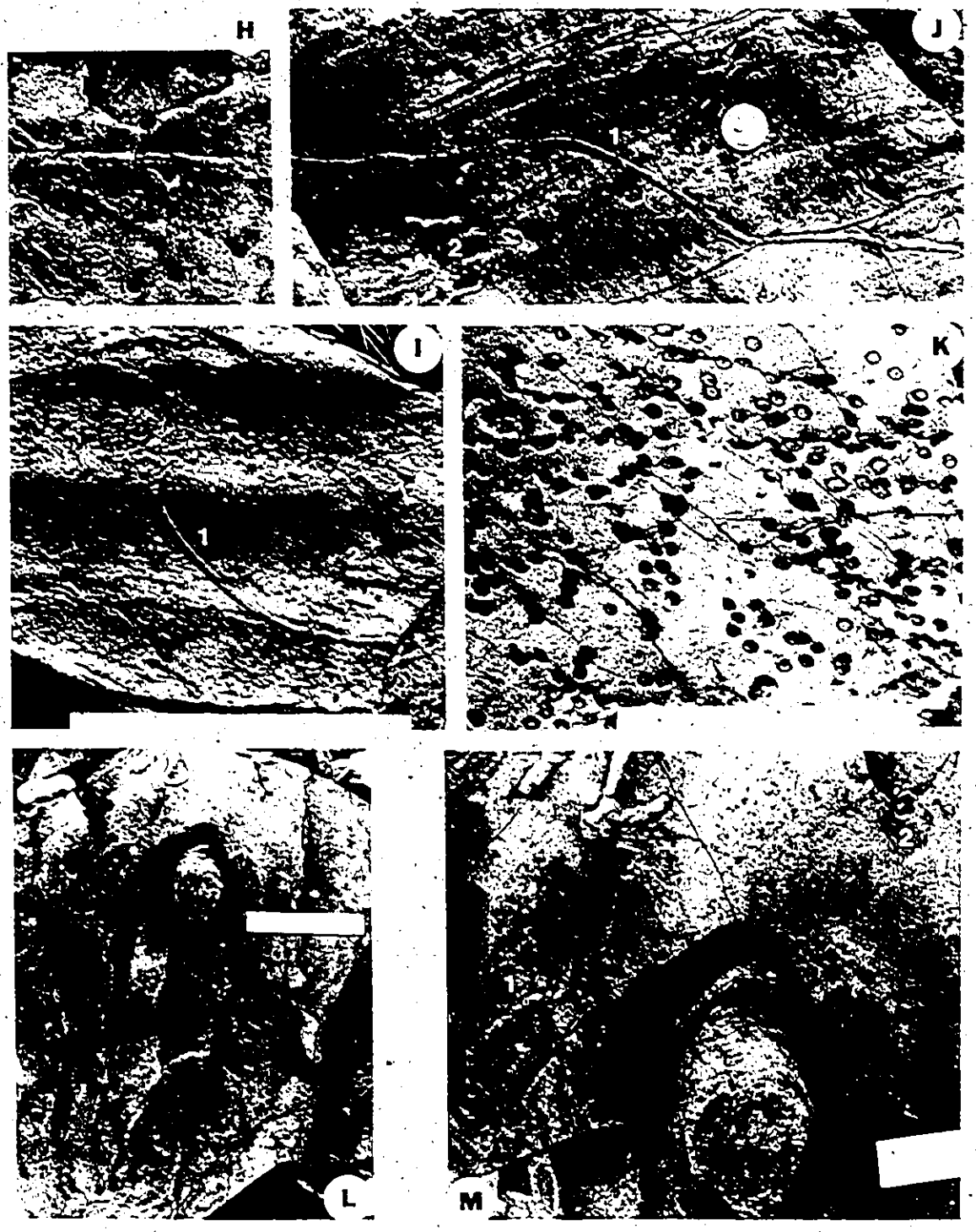
H
J
1
2
I
1
K
L
M
1

mudstone may lie upon less extensively bioturbated hummocky beds.

Biogenic structures within interbedded material. Fully bioturbated mudstones generally do not reveal identifiable trace fauna other than irregular vertical and oblique burrows having diameters of approximately Ø.5 to 2 cm and occasional well preserved Chondrites. Less bioturbated fine-dominated deposits typically reveal a large number of trace fauna, including Chondrites, Planolites, rare Teichichnus, and Gordia. The thin undulatory parallel laminated, parallel laminated, and rippled siltstones/sandstones between hummocky beds commonly display Gyrochorte, both in convex epirelief and concave hyporelief.

Ichnofacies classification. The lithology-controlled alternation between the two assemblages of trace fauna described above is typical of the Cruziana ichnofacies (Frey & Pemberton, 1984).

Macrofossils. The megascopic body fossil most commonly encountered within facies ZHl is the pelecypod Cardium, which is almost invariably preserved as molds of disarticulated shells, usually present at the bases of hummocky cross-stratified siltstone/sandstone beds. Shell molds appear on the soles of beds in a hydrodynamically

stabilized convex-upward position. Several ammonites (genus Scaphites) were also observed within this facies. Body fossils from the Cardium Formation are illustrated in figure 4-26.

Summary: Basic distinguishing features. The basic distinguishing features which identify any single occurrence of facies 2H1 are listed below:

1) Occurrences are composed of interbedded hummocky cross-stratified siltstone/sandstones and shale/mudstone.
2) Hummocky beds are sharp-based.
3) Hummocky beds are predominantly less than 20 cm in thickness.
4) Trace and body fossils indicate a marine origin within the Cruziana ichnofacies.

Facies 2H2 ("Intermediate-Thickness Hummocky Beds"):

Sharp-based hummocky cross-stratified sandstones of intermediate thickness (20 cm to 100 cm) interbedded with mudstones.

This a commonly encountered facies (75 occurrences) having an average thickness of 2.5 m (range: 0.4 to 11.1 m).



Facies 2H2 is similar to facies 2H1 previously described; however, the hummocky cross-stratified beds generally are thicker and coarser than those of the previous facies. Hummocky cross-stratified beds of facies 2H2 consist exclusively of sandstone (very fine to lower fine sandstone; very rarely, medium or coarse sandstone), except in the upper parts of some beds, which grade into siltstone. These sandstones range in thickness from about 20 cm to no greater than 1 m. By definition, sharp-based hummocky beds having thicknesses predominantly less than 20 cm are classified within facies 2H1, whereas those having thicknesses in excess of 1 m are classified within facies 2H3. These arbitrary distinctions reflect fairly natural breaks in bed thickness.

An extended discussion of hummocky cross-stratification from this and other facies is presented in chapters 5 and 8. Figure 4-2 is a definition sketch of

Figure 4-12. Vertical sections of sharp-based hummocky cross-stratified sandstones from facies 2H2.

A) Bed showing very sharp base, preserved convex-upward hummocky form at top of bed, and small-scale symmetrical ripples in cross-section at top of bed (at center and right). Note thin sandstones within interbedded material. Section GC-2, 30 m.

B) Tabular bed with internal lamination revealing two hummocks separated by a swale. Field book for scale at center of swale. Section 4-43, 152 m. From Duke (1985c, Fig. 1).

C) Bed with lateral variation in thickness. Up is to the right. Note internal convex-upward laminae defining a hummocky form, the crest of which is above the 15 cm scale bar at center of photo. Section SC-1, 97 m.

D) Typical outcrop appearance. Up is to the left. Note sharp, flat bases of sandstones, and gently undulatory and sharply scoured tops of sandstones. Hammer at center left for scale. Section 5-45, 140 m.

E) Sharp undulatory base of this bed may be due in large part to differential compaction, as indicated by conformable curvature of underlying material. Note low-angle, curved laminae and intersections, and symmetrical ripples at top of bed at right. Both coins are 2.4 cm in diameter. Willmore Member, section 5-45.


A
B
C
D
E

hummocky cross-stratification.

Geometry of hummocky beds. The bedding geometry of hummocky cross-stratified sandstones in facies 2H2 is similar to that of facies 2H1 described above. Beds in both facies are dominantly tabular in nature, but tend to be more variable in thickness laterally in facies 2H2 (Fig. 4-12). The noteworthy differences between the two facies are discussed below.

Bases of hummocky beds. Hummocky beds within facies 2H2 typically have very sharp bases which closely resemble those of facies 2H1 beds. Oriented or directional sole marks (Fig. 4-10B) are much more common on the basal surfaces of facies 2H2 beds.

The sharp bases of facies 2H2 usually are regionally flat (Fig. 4-12A, 4-12B, & 4-12D) to gently undulatory (Fig. 4-12C & 4-12E). Locally, bases are irregularly scoured in a step-wise fashion (Fig. 4-13A & 4-13C). Pronounced step-wise scouring and/or channelling is much more commonly encountered in facies 2H2 than in facies 2H1. Likewise, maximum eroded depth of these scours or channels generally is greater in facies 2H2, typically ranging between about 10 cm and 50 cm.

As in facies 2H1, disarticulated shell molds (predominantly Cardium molds) are commonly observed at or near the bottoms of hummocky beds (Fig. 4-10D). These

Figure 4-13. Details of lamination within hummocky cross-stratified sandstones in facies 2H2.

A) Prominent convex-upward hummock filling a concave-upward erosional depression (base of sandstone bed). Note step-wise scouring at base (especially evident at right, where the bed thins to 15 cm). Section 5-45, 152 m.

B) Prominent convex-upward laminae thickening over a hummock. Scale bar is 15 cm long. Section 5-45, 152 m.

C) Step-wise scouring at the base of a hummocky sandstone. Note that broad convex-upward laminae in upper part of bed terminate non-erosionally against underlying sandstone laminae. Section 5-45, 153 m.

D) Thick interval of parallel lamination (division P) at the base of a sandstone in a sequence of hummocky beds. Note extreme bioturbation of upper part of bed. Coin is 2.4 cm in diameter. Seebe Member at section 5-45.

A
B
C
D

shell casts are more common in this facies than in facies 2H1; where present, they usually appear in great profusion on the soles of beds in a hydrodynamically stabilized, convex-upward position. Flat shale rip-up clasts a few centimeters long are also frequently present near the bases of hummocky beds in facies 2H2 (Fig. 4-10C). Rarely, scattered granules and pebbles (maximum diameter about 0.5 cm) are found at the bases of hummocky beds; this rare coarse component is more common in this facies than in facies 2H1. A thin graded or apparently structureless interval may be present above the base, and/or a thin parallel laminated interval. Typical sequences of structures observed in hummocky sandstones from facies 2H2 are indicated in figure 4-14. See Walker et al. (1983) and chapter 8 of this thesis for detailed discussion of divisional sequences in hummocky cross-stratified sandstones.

Internal structures within hummocky beds.

Internally, hummocky cross-stratified sandstones within this facies commonly are graded in their upper parts, and graded, structureless, and/or parallel laminated intervals may be present above the base of a bed. The hummocky form in facies 2H2 is characterized by intermediate form-spacings and form-heights (i.e., values are greater than in facies 2H1, smaller than in facies 2H3). In facies

Figure 4-14. Sequences of structural divisions in three sharp-based hummocky cross-stratified sandstones from facies 2H2. Bed "C" is a rare example of a hummocky sandstone capped with a thick rippled interval (division X). In this bed, note that the lowest ripple forms overlying the hummocky interval are slightly asymmetrical, and foresets indicate translation of the ripple form to the left (combined-flow ripples?). Stratigraphically higher ripple forms in this bed are symmetrical, and foresets indicate vertical accumulation of sediment with little or no translation of the ripple form. In "A", coin is 2.4 cm in diameter. In "C", scale is in centimeters and inches. Divisional terminology is that of Walker et al. (1983).

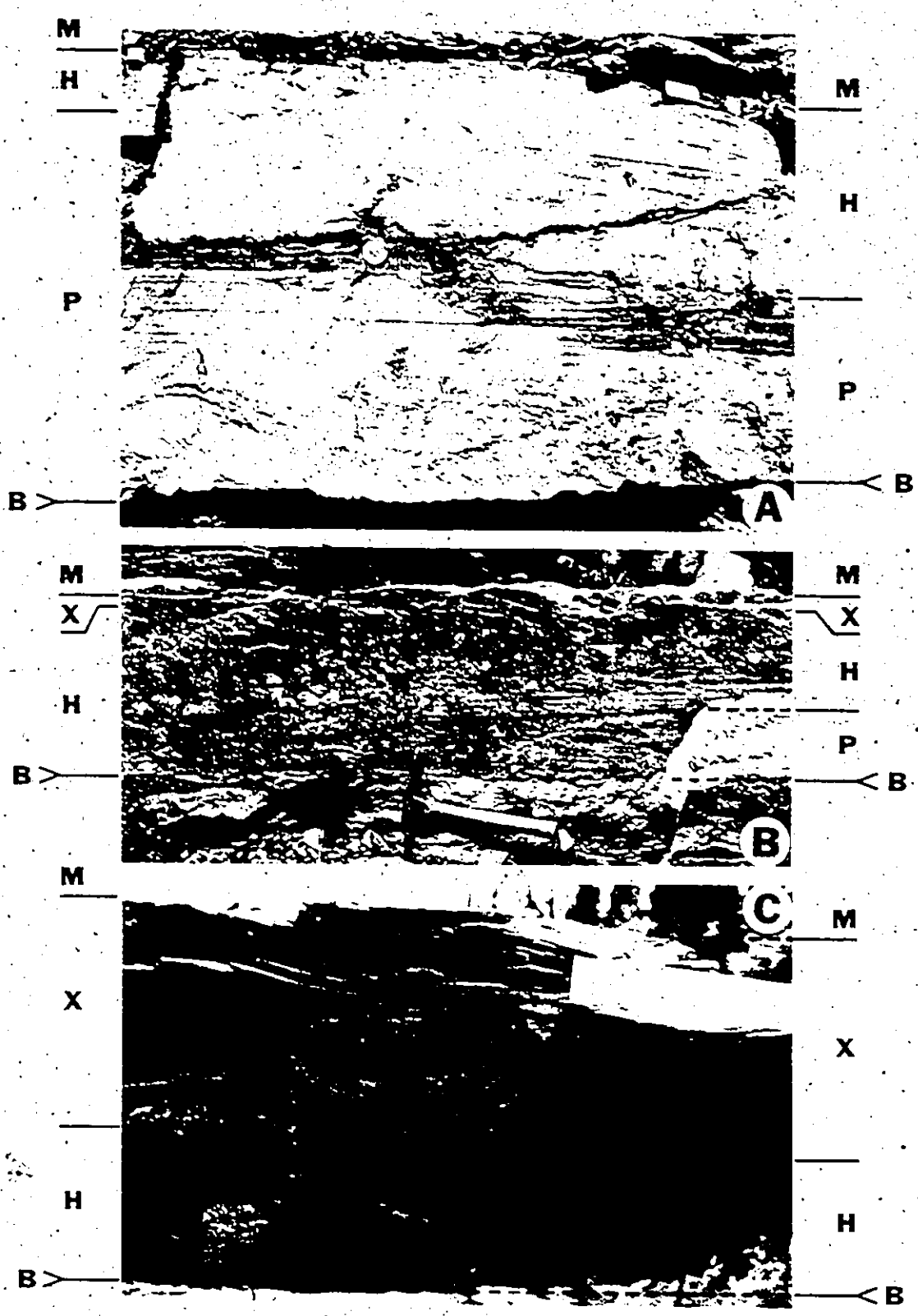
M
H
P
B
A
M
H
P
B
M
X
H
B
B
M
X
H
P
B
M
X
H
B
C
M
X
H
B

2H2, form-spacings range between about 100 and 400 cm. Form-heights range from a few centimeters to about 25 to 30 cm, and the characteristic concave-convex form is best developed in this facies (Fig. 4-12, 4-13, & 4-14). Low-angle cross-lamination within these beds ranges from 0° to a rare maximum of about 25°; typical maximal values are on the high end of this distribution (15° to 20°). A more detailed description and interpretation of the internal structure of hummocky cross-stratified beds is presented in chapters 5 and 8.

Tops of hummocky beds. Tops of hummocky cross-stratified sandstones within this facies are more-or-less identical to those of facies 2H1 described above.

Biogenic structures within hummocky beds. Biogenic structures within the hummocky beds of this facies are more-or-less identical to those of facies 2H1 described above.

Interbedded material. The interbedded mud-dominated material between the hummocky cross-stratified sandstones of facies 2H2 is in most respects identical to that of facies 2H1. Typically, this interbedded material is similar to the deposits of facies 1UP, 1GB, 1BM, or 1SH described above, as is the

interbedded material of facies 2H1. There is a difference in one major respect, however: the interbedded material of facies 2H2 is commonly somewhat sandier than that of facies 2H1, and typically contains thin hummocky beds similar to the thinnest hummocky cross-stratified sandstone/siltstone beds of facies 2H1 (Fig. 4-12).

Biogenic structures within interbedded material. The biogenic structures within the mud-dominated material between the hummocky sandstones of facies 2H2 are more-or-less identical to those of facies 2H1 described above.

Macrofossils. The megascopic body fossils present within facies 2H2 are identical to those present within facies 2H1 described above (Cardium, Scaphites). Body fossils from the Cardium Formation are illustrated in figure 4-26.

Summary: Basic distinguishing features. The basic distinguishing features which identify any single occurrence of facies 2H2 are listed below:

1) Occurrences are composed of interbedded hummocky cross-stratified siltstone/sandstones and shale/mudstone.
2) Hummocky beds are sharp-based.
3) Hummocky beds are predominantly greater than 20 cm

and less than 100 cm in thickness.

4) As in facies 2H1, trace and body fossils indicate a marine origin within the Cruziana ichnofacies.

Facies 2H3 ("Thick Hummocky Beds"): Thick (>100 cm) sharp-based hummocky cross-stratified sandstones.

This facies was encountered 24 times. These occurrences have an average thickness of 3.6 m (range: 1.0 to 12.1 m).

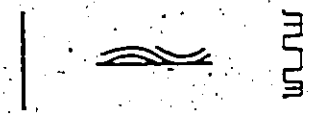

Facies 2H3 is similar to facies 2H2 and 2H1 previously described; however, the hummocky cross-stratified, very fine to fine sandstones which characterize this facies are greater than 100 cm in thickness (Fig. 4-15). The thickest sharp-based hummocky sandstones present in the Cardium Formation are included in facies 2H3; the maximum observed thickness of a sharp-based hummocky bed is 2.3 m.

A basic description of hummocky cross-stratification is presented under facies 2H1 above. An extended discussion of hummocky cross-stratification from this and other facies is presented in chapters 5 and 8. Figure 4-8 is a definition sketch of hummocky cross-stratification.

Figure 4-15. Vertical sections through hummocky cross-stratified sandstones from facies 2H3.

A) Two sharp-based, hummocky cross-stratified sandstones, each of which is greater than 1 m in thickness, are present in the lower portion of this photograph (between the two white bars). For scale, these two beds together are 2.4 m thick. These two beds have come very close to amalgamation, being separated by only a few centimeters of platey, sandy mudstone. In this photograph, hummocky cross-stratification is clearly visible throughout the lowest bed and only at the top of the second bed; at the exposure, however, hummocky cross-strata can be clearly discerned throughout both beds. Close examination of laminae suggests that each of these two beds is best interpreted as a separate depositional event (i.e., neither of them represents an amalgamated unit of multiple depositional events). In contrast, the thick bed overlying these two hummocky sandstones <u>does</u> represent an amalgamated sand body (facies 3HA); it <u>is</u> composed of multiple, separate depositional events, as inferred from erosionally-based conglomerate lags present in the body. Section GC-2, 140 m.

B) Outcrop view of a single sandstone from facies 2H3 (arrowed). Trace of minor fault is dashed. For scale, this bed is 1.5 m thick. Section 4-19, 137 m.

240 cm
A
B

Geometry of hummocky beds. Hummocky cross-stratified sandstones within this facies occur in beds which are essentially tabular on the outcrop scale. Bases are sharp and typically are regionally flat. Generally, tops of beds in this facies also are flat; in many occurrences, however, tops of beds preserve the hummock/swale depositional topography. Superficial preservation of depositional topography is more common in this facies than in either of the preceding facies.

It is noteworthy that step-wise basal scouring/channelling is rare in hummocky beds of facies 2H3; however, those examples displaying such erosional features exhibit the largest maximal values of eroded depth, on the order of 100 cm.

Bases of hummocky beds. The bases of sandstone beds in facies 2H3 are more-or-less identical to the bases of hummocky beds in the other facies of this association (however, see comments under "geometry of hummocky beds" above).

Internal structures within hummocky beds. The internal structures within hummocky beds of this facies are similar in most respects to the internal structures in beds of facies 2H1 and 2H2 described above; however, the scale of hummocky cross-stratification is generally larger in facies 2H3. Form-spacing ranges between approximately 100

cm and 700 cm, and generally is larger than in the other facies of this association. On the other hand, form-height ranges from only a few centimeters to about 30 cm, roughly the same range as in facies 2H2. Thus, maximum dip within hummocky sandstones of facies 2H3 is generally less than about 10°, which also is less than in facies 2H2.

Hummocky sandstones of this facies locally exhibit basal chert-pebble conglomerate lags and/or relatively thick (roughly 10 cm to 40 cm) basal divisions which are either apparently structureless or essentially parallel laminated (Walker et al., 1983; this thesis, chapter 8).

Tops of hummocky beds. Tops of hummocky cross-stratified sandstones within this facies are more-or-less identical to those of facies 2H1 and 2H2 described above; however, the preservation of original depositional hummock/swale topography is more common in facies 2H3 than in the other facies of this association.

Biogenic structures within hummocky beds. Biogenic structures within the hummocky beds of this facies are more-or-less the same as those of facies 2H1 and 2H2 above. In addition to these traces described above, note that vertical or oblique Ophiomorpha burrows are occasionally observed within the thicker beds of this facies, and the bases of these beds locally display horizontal traces resembling Ophiomorpha or Thalassinoides. Thalassinoides

is also present in the other facies of this association, but it was observed more frequently in facies 2H3. Also, the tops of all hummocky beds in facies 2H3 exhibit Skolithos, Rosselia, and/or Cylindrichnus burrows much more commonly than in the other facies of this association; these burrows are locally present in relatively higher densities (roughly 1 burrow per 10 cm^2).

Interbedded material. The interbedded mud-dominated material between the thick (>100 cm) hummocky cross-stratified sandstones of facies 2H3 is in most respects identical to that of facies 2H2. Typically, this interbedded material is similar to the deposits of facies 1UP, 1GB, 1BM, or 1SH described above, as is the interbedded material of facies 2H2 and 2H1; however, mudstones from both facies 2H2 and 2H3 commonly are somewhat sandier than the interbedded mudstones of facies 2H1. Additionally, the major hummocky sandstones that characterize facies 2H3 (i.e., those thicker than 100 cm) typically are interbedded in any one occurrence of the facies with numerous thinner hummocky beds similar to those of facies 2H2 and 2H1. These minor hummocky beds between the thicker beds typically are similar to or somewhat thicker than those of facies 2H2, having characteristic thicknesses of roughly 20 to 100 cm.

Biogenic structures within interbedded material. The biogenic structures within the mud-dominated material between the hummocky sandstones of facies 2H3 are more-or-less identical to those of facies 2H1 and 2H2 described above.

Ichnofacies classification. As in facies 2H1 and 2H2 above, trace fauna from the interbedded lithologies of facies 2H3 indicate deposition within the Cruziana ichnofacies; however, the increased relative abundance of structures such as Ophiomorpha, Thalassinoides, and Skolithos indicates deposition in slightly more agitated water, possibly shallower and more proximal to shore than in either of the other facies of association 2, and possibly transitional into the Skolithos ichnofacies (see Frey & Pemberton, 1984).

Macrofossils. Locally, casts of the pelecypod genus Cardium are present at the bases of hummocky beds within this facies, occasionally in great profusion. Body fossils from the Cardium Formation are illustrated in figure 4-26.

Summary: Basic distinguishing features. The basic distinguishing features which identify any single occurrence of facies 2H3 are listed below:

1) Occurrences of this facies are composed of

interbedded hummocky cross-stratified sandstones and shale/mudstone.

2) Hummocky beds have sharp bases.

3) Occurrences of this facies contain one or more hummocky beds thicker than 100 cm. These meter-plus sharp-based beds do not exhibit obvious amalgamation surfaces. In cases involving more than one meter-plus bed, these thick beds usually are stratigraphically separated from one another by mudstone and a few hummocky beds which are thinner than 100 cm.

4) The thickest non-amalgamated, sharp-based hummocky cross-stratified sandstone observed in the Cardium Formation has a thickness of 220 cm. Thus, the beds that characterize facies 2H3 have thicknesses on the order of 1 to 2 m.

5) Trace and body fossils indicate a marine origin within the Cruziana ichnofacies, possibly transitional into the higher-energy Skolithos ichnofacies.

Association 2: Preliminary Interpretation

Numerous previous workers (e.g., Gilbert, 1899; Campbell, 1966; Harms et al., 1975; see appendix 8 for further references) have inferred that hummocky cross-stratification is probably formed by unusually large storm waves, especially in examples where the structure occurs in sharp-based sandstones interbedded with mudstones (as in association 2). In their study of the Jurassic Fernie-Kootenay transition, Hamblin & Walker (1979) further refined this interpretation, suggesting that interbedded deposits of this sort were deposited in water depths between fairweather and storm wave-base, as outlined for the Cardium Formation below.

The large thicknesses of bioturbated mudstone present between hummocky sandstones in association 2 indicate relatively long periods of quiescence between major episodes of sand deposition. The "normal" or "background" sediment deposited in this association during fairweather conditions was hemipelagic mud and thin siltstones or sandstones (generally displaying symmetrical ripples and/or undulatory parallel lamination) indicating a reduced wave climate relative to the major hummocky sandstones. This indicator of quiet fairweather conditions largely isolated from coarse clastic input suggests offshore sedimentation <u>below</u> both fairweather wave-base and

any possible tidal influences.

The hummocky cross-stratified sandstones themselves, and the symmetrical ripples which commonly mantle them, indicate that unusually large waves generated by storms produced fairly powerful bottom flows in this association; thus, a water depth well above storm wave-base is indicated. The sandstones of association 2 are therefore best interpreted as episodically deposited storm deposits, and association 2 is best interpreted as representing deposition in water depths below fairweather wave-base but above storm wave-base.

For comparative purposes, note that fairweather wave-base along the U.S. Atlantic Shelf is approximately 10 to 15 m (Walker, 1979a); storm wave-base varies between a few tens of meters and over 100 m, depending upon the specific storm-wave climate.

The inferred depositional setting is fully consistent with the Cruziana assemblage of trace fauna observed in this association. This ichnofacies suggests deposition "below daily wave-base but not storm wave-base" (Frey & Pemberton, 1984, Table 2).

Association 3. Sand-dominated facies.

This association consists of thick quartz/chert sandstones with only minor components of other lithologies. Marine trace and/or body fossils are present in all facies. Sandstones generally are light grey to steel grey on fresh surfaces; they commonly weather to buff yellow or bright orange-red due to siderite cement. The sandstones of facies 3PL, however, contain abundant silica cement, and weather to a light grey or white color. Tops of facies 3PL occurrences typically display abundant root casts.

Facies 3BS ("Bioturbated Sandstone"): Extensively bioturbated sandstone, argillaceous sandstone, and/or silty sandstone.

This facies occurred 19 times in this study. Average facies thickness is 2.7 m (range: 0.7 to 6.6 m).

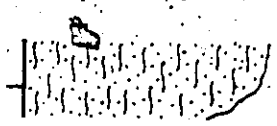

Lithologically, this facies is composed of very fine to fine sandstone (typically, argillaceous and/or silty sandstone). A complete spectrum exists between this facies and facies 1BM (bioturbated mudstone). At numerous localities, the two facies are gradationally juxtaposed

vertically. In order to determine an approximate boundary between the two, an estimate of sand content was made in the field. The discriminative criterion used was the transition from sandy mudstone (<50% sand: facies 1BM) to argillaceous sandstone (>50% sand: facies 3BS). Bioturbated argillaceous siltstone was always included in facies 1BM.

Bioturbation and bedding. Facies 3BS is characterized by intense bioturbation which has completely destroyed any sedimentary structures and has resulted in a ropy or knotted texture. Commonly, individual biogenic structures are not recognizable; in many occurrences, however, a variety of recognizable ichnogenera have been observed (Fig. 4-16); these commonly include Chondrites, Teichichnus, Palaeophycus and Planolites. At a few localities, Chondrites was observed to occur preferentially within pre-existing Teichichnus burrows. Horizontal Rhizocorallium, Thalassinoides, and Zoophycos are locally abundant; Muensteria and Diplocraterion are uncommon. This assemblage is approximately equivalent to the Cruziana ichnofacies (Frey & Pemberton, 1984).

Suggestions of thick, pinching-and-swelling bedding (less than or equal to about 1 m thickness) are locally visible through the bioturbation. This bedding is highlighted by variation in the intensity of bioturbation,

Figure 4-16. Trace fossils from facies 3BS. In all photographs, coin is 2.4 cm in diameter, and scale bar (in centimeters and inches) is 15 cm long.

A) Mottled to homogeneous appearance of facies 3BS in a V section normal to bedding. Millimeter-scale white blebs are Chondrites. To the left of the coin, fine lamination is visible in a lenticle of preserved bedding roughly 10 cm wide. Larger white patches are Teichichnus.

B) Mottled outcrop (section normal to bedding) with preserved lenticles of thin beds near coin.

C) Bedding-plane exposure of Thalassinoides.

D) Bedding-plane exposure of distinctly lined Palaeophycus. Lining is apparent in individual at lower center of photo.

E) Bedding-plane exposure of large Thalassinoides identical to those attributed to lobsters by Pemberton et al. (1984).

F) Sole view of numerous burrows, including Diplocraterion at lower center of photo.

G) Bedding-plane exposure of horizontal Rhizocorallium.

H) Bedding-plane exposure of Muensteria.

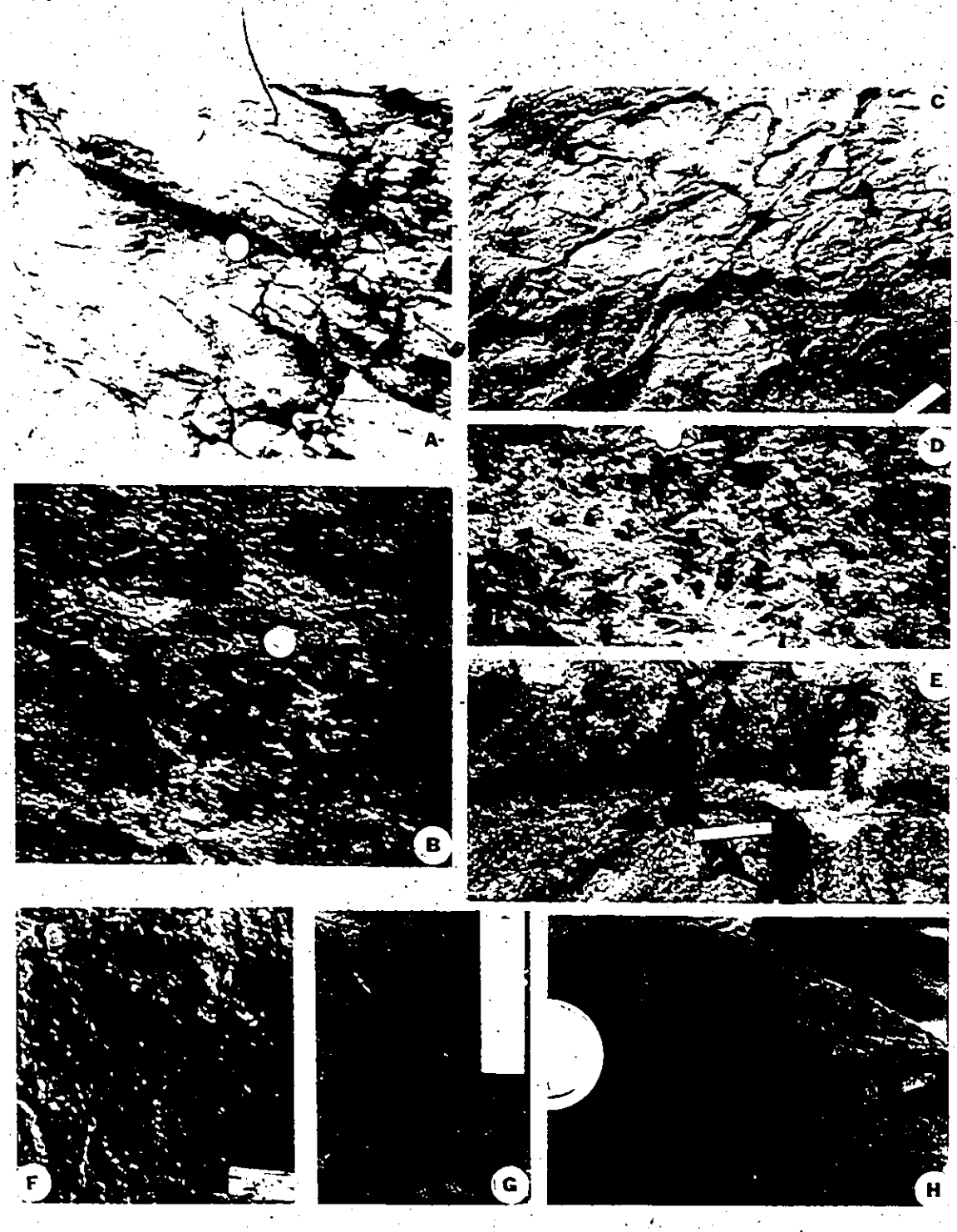
A
B
C
D
E
F
G
H

and is suggestive of the bedding style associated with hummocky cross-stratification. No other sedimentary structures have been observed within this facies, with the exception of rare, thin, isolated lenticles of sub-horizontal sandstone laminae which have escaped complete biological reworking (Fig. 4-16A & 4-16B). Where present, these lenticles are typically only a few centimeters in width.

Macrofossils. No megascopic body fossils have been observed within this facies.

Facies 3HA ("Amalgamated Hummocky Sandstones"):

Amalgamated hummocky cross-stratified sandstones.

This is the most commonly encountered facies within association 3, there being 54 occurrences. Average thickness is 4.5 m (range: 0.5 to 12.2 m).

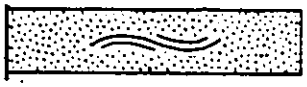

Composition and internal structures. This facies consists of thick, very fine to fine sandstone bodies. Medium sand occurs locally. Sandstones generally are a few meters thick; each occurrence of this facies represents a

single thick sand body. The thinner occurrences of this facies generally have been truncated by an overlying transgression surface (see chapter 5). Lenses of shale or mudstone commonly are present within these thick sandstones. Granules and pebbles occur locally.

Internally, sandstones of facies 3HA are predominantly hummocky cross-stratified. Unlike the hummocky facies of association 2, the mudstone/shale interbedded between sandstones is not continuous across the outcrop, but rather occurs either as isolated lenses within a thick sand body, or is absent entirely. The fine-grained deposits of this facies are discussed in detail below.

The thick hummocky cross-stratified sandstones of this facies consist of numerous individual beds which are <u>amalgamated</u>. Each of these amalgamated beds represents a sandstone/mudstone couplet similar to those in association 2; however, in facies 3HA, each of the flows emplacing sand has eroded through the underlying mudstone (either entirely or in part), bringing the sandy part of the couplet into erosional contact with the sandy part of the previously deposited underlying couplet. Each couplet may therefore be regarded as a separate depositional unit; these units are herein termed <u>amalgamation units</u>. A block diagram illustrating the major morphological features of amalgamated hummocky cross-stratification is presented as figure 4-17. This figure illustrates a thick amalgamated

sand body consisting of five separate amalgamation units.

Considerable variation exists within amalgamated hummocky cross-stratified sandstones. Observations from the Cardium Formation and other units studied by the author, and published descriptions of additional units containing amalgamated hummocky beds (e.g., Dott & Bourgeois, 1982) indicate that there are four basic types of amalgamated sequences (Fig. 4-18). Variation in the internal structures within individual amalgamation units is the criterion used to distinguish the four subfacies. Gradations between the four basic types are common.

Each of the four subfacies is described in detail below, following a general description of certain aspects of the facies as a whole.

General description of hummocky cross-stratification. Hummocky cross-stratification is generally larger in scale within facies 3HA than within any of the interbedded hummocky facies of association 2 described above. Form-spacing of the structure within facies 3HA is locally as great as 10 m; typical values range between 3 and 6 m. Form-height ranges between approximately 10 and 60 cm.

Recognition of amalgamation units, and descriptive terminology. As stated above, facies 3HA is characterized by thick amalgamated sand bodies composed of numerous

Figure 4-17. Block diagram illustrating major morphological features of amalgamated hummocky cross-stratified sandstone (facies 3HA).

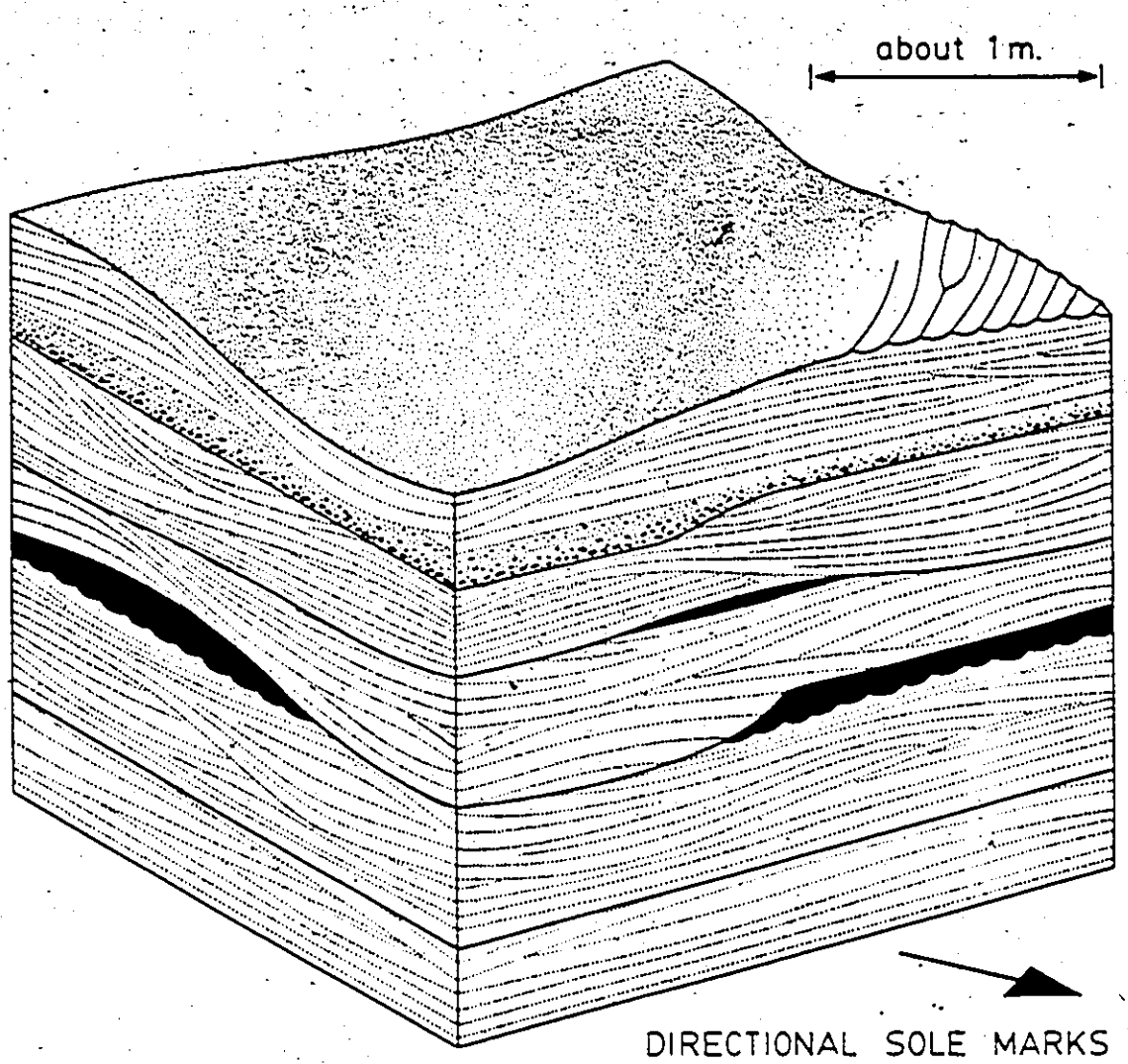

DIRECTIONAL SOLE MARKS
FROM BASES OF SANDSTONES
OVERLYING MUDSTONE LENTICLES



Figure 4-18. Diagram of sections normal to bedding illustrating the major morphological distinctions between the four basic types, or subfacies, of amalgamated hummocky cross-stratified sandstone.

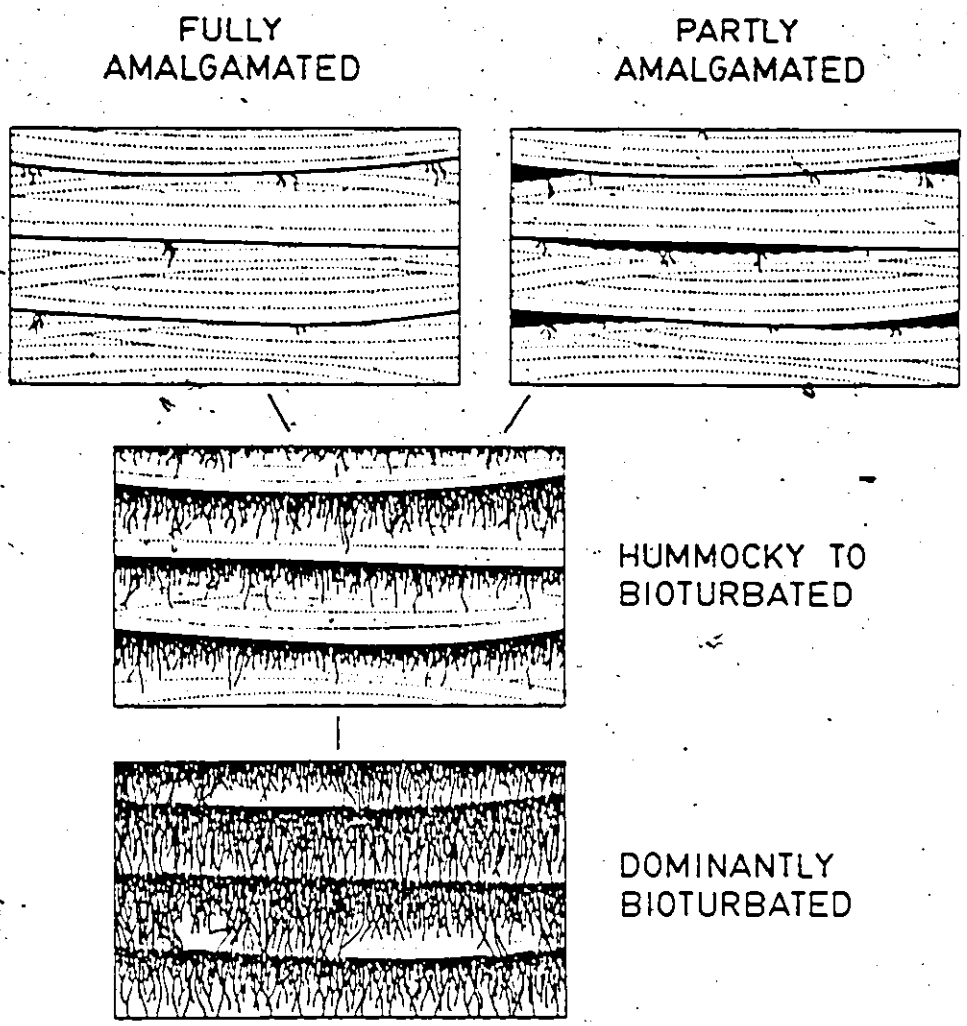
FULLY
AMALGAMATED
PARTLY
AMALGAMATED
HUMMOCKY TO
BIOTURBATED
DOMINANTLY
BIOTURBATED

amalgamation units. Although the internal structures within these amalgamation units are variable, they have certain basic features in common. Most amalgamation units are tabular and laterally extensive, although they tend to pinch and swell somewhat in thickness laterally. Individual amalgamation units are recognized by means of the amalgamation surfaces which bound them both above and below (Fig. 4-17 & 4-18). These surfaces are equivalent to the first-order boundaries (sensu Dott & Bourgeois, 1982) at junctions between different lithologies (i.e., junctions between sandstone and mudstone) in association 2 (compare with Fig. 4-8; also, see part 1 of chapter 8, which includes a detailed discussion of the hierarchy of boundary surfaces within hummocky cross-stratification). In all but the most limited of exposures, amalgamation surfaces generally are easily distinguished from less extensive second-order surfaces, or intersections between sandstone laminae (except in subfacies 1, where this distinction commonly is difficult to make -- see below). Depending upon the subfacies in question, amalgamation surfaces can be recognized by one or more of the following characteristic features:

1) Truncation of underlying sandstone laminae over extensive distances laterally (i.e., several meters).

2) Truncation of underlying shale/mudstone lenses.

3) Truncation of underlying biogenic structures.

4) Presence of oriented sole marks on base of sandstone immediately overlying an amalgamation surface.

5) Concentration of coarse material (e.g., pebbles, shells) as a basal lag immediately overlying an amalgamation surface. This basal lag frequently displays imbrication and/or grading; locally, conglomeratic symmetrical ripples are also developed (see chapter 8).

6) Presence of apparently structureless, graded, and/or plane parallel laminated sandstone immediately overlying an amalgamation surface.

These criteria for the recognition of amalgamation units are further discussed below and in part 1 of chapter 8. Sequences of structures observed within hummocky beds of this and all other facies are discussed in detail in part 3 of chapter 8.

Subfacies descriptions. As stated above, there are four basic intergradational subfacies of amalgamated hummocky cross-stratified sandstones (Fig. 4-18). These are listed on the following page:

1) Fully amalgamated sandstones.

2) Partly amalgamated sandstones.

3) Hummocky-to-bioturbated amalgamated sandstones.

4) Dominantly bioturbated amalgamated sandstones.

The first two subfacies are recognized on the basis of lithology and primary physical structures within individual amalgamation units; the last two are recognized by vertical sequences of physical and biogenic structures within these units. Suggested gradational relationships between the subfacies are illustrated diagramatically by the connecting lines in figure 4-18.

Each of the four subfacies are described in detail below. It should be noted that no attempt has been made to represent the various subfacies in the measured sections of appendix 2, nor has subfacies variation been incorporated in the Markov chain analysis of chapter 5.

Subfacies 1: Fully amalgamated sandstones. In subfacies 1 (fully amalgamated sandstones) there are no preserved lenses of mudstone or shale (Fig. 4-19B, 4-19D, 4-20B, & 4-20C). This subfacies is composed exclusively of sandstone which is predominantly hummocky cross-stratified; pebbles are present locally (Fig. 4-20B & 4-20C).

The absence of mudstone lenses below amalgamation surfaces makes it difficult in some examples of this subfacies to distinguish between amalgamation surfaces and

second-order boundaries within individual amalgamation units. In cases where a prolonged depositional hiatus cannot be inferred with confidence, amalgamation surfaces cannot be confidently distinguished, and all laminae intersections must be assigned a second-order rank (see discussion of hierarchy in chapter 8, part 1). In most examples, however, this distinction can be made with a fair degree of confidence. Unlike those second-order surfaces which do not represent the amalgamation of separate depositional events, the inferred amalgamation surfaces (i.e., inferred first-order surfaces) within this subfacies typically:

1) truncate underlying biogenic structures,
2) are overlain by sandstone containing mudstone rip-up clasts,
3) are overlain by chert pebble lag deposits (commonly graded, imbricated, or capped with conglomeratic symmetrical ripples), and/or
4) are overlain by structureless, graded, or parallel laminated sandstone. Thick (up to approximately 40 cm) parallel laminated sandstone intervals above first-order truncation surfaces are relatively common in this subfacies (Fig. 4-20A).

In contrast, second-order surfaces do not truncate biogenic structures and typically are overlain by hummocky sandstone

Figure 4-19. Examples of amalgamated hummocky cross-stratification (facies 3HA).

A) A thick example in a section normal to bedding. Occurrence consists of two different subfacies. More resistant beds (immediately above the person) occupying the lower third of this occurrence represent an example of subfacies 3 (hummocky-to-bioturbated amalgamated sandstones). Hummocky cross-stratification is preserved in basal portions of amalgation units in this interval. Upper two-thirds of facies 3HA at this locality is predominantly bioturbated; preserved laminae are rare. This interval represents subfacies 4 (dominantly bioturbated amalgamated sandstones). Seebe Member, section 6-8.

B) Lower half of photo shows oblique plan view and cross-sectional view of a thick example of subfacies 1 (fully amalgamated sandstones). Photo is rotated relative to present horizon (see arrowed person). Note broadly undulatory (hummocky) plan surfaces and associated low-angle internal cross-strata. Seebe Member, section BL-1.

C) Hummocky surface within occurrence of subfacies 2 (partly amalgamated sandstones). Note mudstone lens on right behind hammer handle. Willmore Member at section 4-43.

D) Concave-upward swale overlain by convex-upward hummock in an occurrence of subfacies 1 (fully amalgamated sandstones). Scale is 15 cm. Seebe Member, section BL-1.

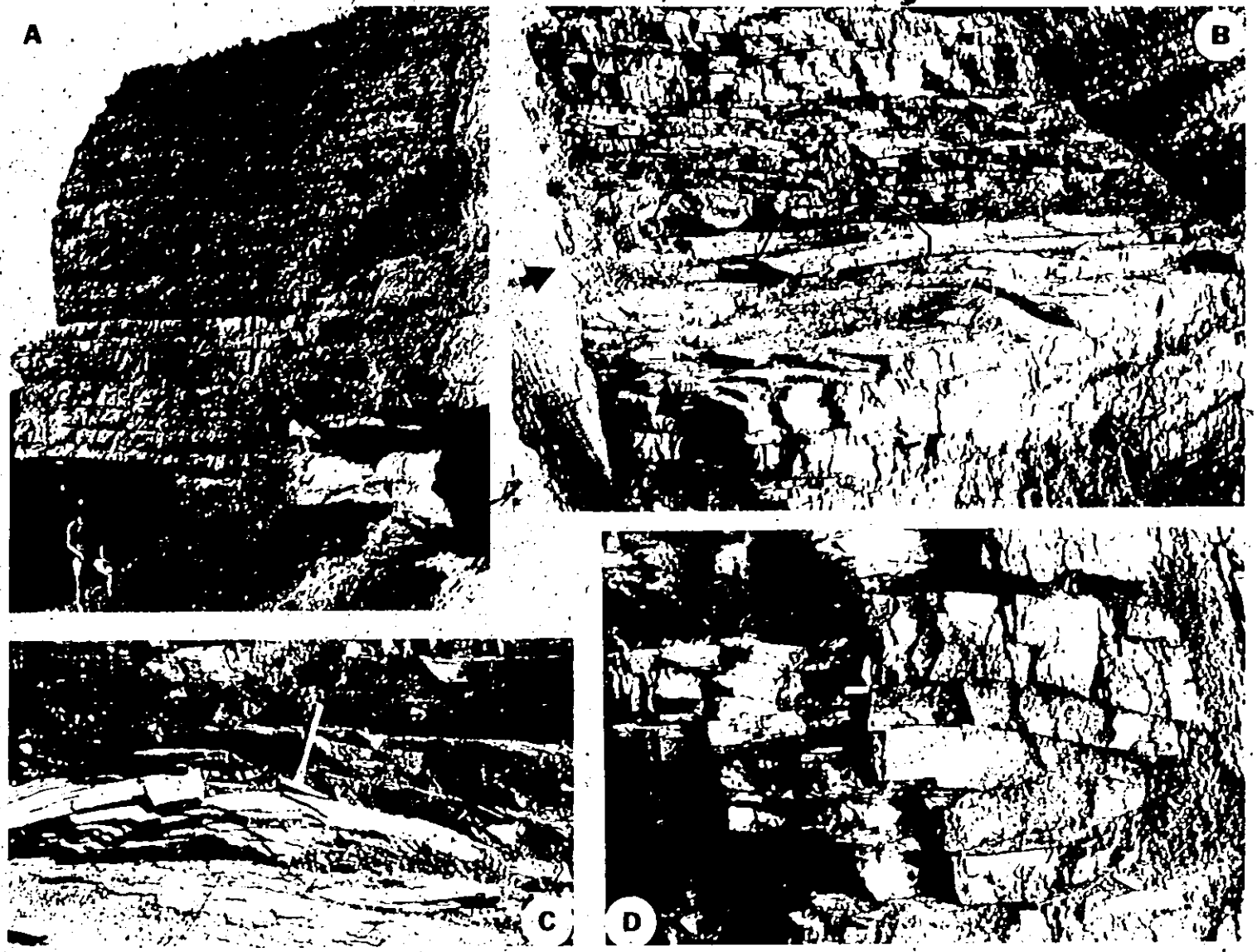
A
B
C
D

laminae which do not contain either mudstone rip-up clasts or abundant gravel clasts. Additionally, in extensive exposures of this subfacies, it is relatively easier to distinguish between these two types of surfaces because the amalgamation surfaces are laterally extensive across the entire outcrop, whereas second-order surfaces usually can only be traced a few meters or less laterally (see chapter 8, part 1).

As illustrated in figure 4-18, biogenic sedimentary structures below amalgamation surfaces either are absent or are present in abundances low enough to permit recognition of all primary lithological variation and physical sedimentary structures present throughout the sandstone body. Low abundances of biogenic structures is one of the definitional criteria for this subfacies. Biogenic structures in this and all other subfacies are described under a separate subheading following the subfacies descriptions.

Subfacies 2: Partly amalgamated sandstones. In subfacies 2 (partly amalgamated sandstones) lenses of mudstone or shale are present below most or all amalgamation surfaces; thus, these surfaces may be confidently assigned a first-order ranking (see discussion of hierarchy in chapter 8, part 1). This is the most commonly encountered subfacies within examples of facies

Figure 4-20. Basal contacts of amalgamation units in facies SHA in sections normal to bedding.

A) In this example of subfacies 2 overlain by subfacies 1, basal contacts of amalgamation units are inferred using two different criteria. Behind book, an amalgamation surface is recognized where sandstone overlies a mudstone lens (subfacies 2). Note biogenic structures in mudstone. Above book, two (three?) amalgamation surfaces are recognized by chert-pebble lags, and a fourth is recognized by a change in sandstone grain size associated with color change at top of photo. Absence of mudstone in this interval is definitional criterion for assignment to subfacies 1. Section SD-1.

B) Amalgamation units defined by thick chert-pebble lags. Note gradational contact between pebbles and sandstone in this example of subfacies 1. Scale is 15 cm long. Section GC-2, 53 m.

C) In this example, one amalgamation surface is defined by mudstone behind 15 cm scale bar, and another above it is defined by conglomerate lag. Note gradation between conglomerate and overlying hummocky sandstone, and pebbles incorporated within hummocky cross-strata.

D) An amalgamation surface (behind book) defined by a thin lens of platey, argillaceous sandstone. Note gutter-casts at this contact. Section 4-19, 74 m.

A
B
C
D

3HA, accounting for a large majority of occurrences.

In this subfacies, first-order boundaries are easily distinguished from second-order boundaries in all but the most limited of exposures. This ease of identification is due largely to the presence of the mudstone lenses (Fig. 4-19C, 4-20A, 4-20C, & 4-20D), which unequivocally define periods of quiescence between episodes of sand deposition. Identification of individual beds is also facilitated by the well developed sequences of structures within the sandy parts of individual beds (divisions B, P, H, F, and X).

Bases of sandstones commonly display oriented sole marks where they lie upon mudstone lenses. Molds of oriented, stabilized Cardium valves are also locally present at bases of sandstones, often in great profusion.

Pebble lags identical to those in subfacies 1 are locally observed overlying bases of amalgamation units within this subfacies. Mudstone rip-up clasts typically are very abundant above bases of beds in this subfacies.

Bases of beds within this subfacies are overlain by sandstone which typically is either parallel laminated or hummocky cross-stratified; rarely, a thin structureless or graded interval is present above the base. The major part of each individual sandstone bed within this subfacies generally is hummocky cross-stratified. Tops of individual sandstones may display "flat" lamination and/or symmetrical

ripples.

Tops of individual sandstone/mudstone couplets typically display numerous biogenic structures (Fig 4-20A). These generally are sharply truncated by an overlying erosional basal surface. By definition, bioturbation in this subfacies (as in subfacies 1) is never great enough to obliterate most primary physical structures or primary lithological variation.

Mudstone/shale lenses lie upon the sandy parts of individual sandstone/mudstone couplets. These lenses typically have a maximum thickness of about 10 to 30 cm, and usually are no wider than 3 to 5 m (see examples in Fig. 4-19 & 4-20). Spacing between lenses at the same stratigraphic level generally is rather large (many meters or tens of meters); often, no more than one lens can be observed at any level over the width of a limited exposure. In these cases it is probable that some percentage of first-order amalgamation surfaces will not display underlying mudstone lenses over the width of exposure. However, the distinction between first- and second-order boundaries can frequently be made with confidence on the basis of pebbles, rip-up clasts, truncated biogenic structures, etc. (see above).

Subfacies 3: Hummocky-to-bioturbated amalgamated sandstones. This subfacies is distinguished by the

vertical sequence of primary and biogenic sedimentary structures. Subfacies 3 consists of numerous tabular couplets of laminated sandstone and bioturbated sandstone or argillaceous sandstone (Fig. 4-19A & 4-21D). Many beds pinch and swell in thickness laterally; average thickness of individual couplets is approximately 40 to 80 cm.

As in subfacies 1 and 2, bases of individual beds are sharp and erosional; typically, bases are flat to gently undulatory, but may be steeply scoured in a step-wise fashion. No chert-pebble lags have been observed overlying the sharp basal surfaces in this subfacies.

Sandstone overlying basal surfaces typically is hummocky cross-stratified; locally, the basal zone is parallel laminated. Thick basal intervals of parallel laminated sandstone (up to approximately 40 cm) are fairly common in this subfacies (Fig. 4-21D). Rarely, the basal zone is apparently structureless or graded. Typically, the laminated intervals of beds in this subfacies consist entirely of hummocky cross-stratification, parallel lamination, or the vertical sequence: parallel lamination overlain by hummocky cross-stratification. Overlying the basal laminated sandstone interval, an interval of extremely bioturbated sandstone or argillaceous sandstone completes the couplet. This bioturbated sandstone is characterized by a ropy or knotted texture resulting from numerous cross-cutting burrows. Contacts between laminated

Figure 4-21. Additional features of facies 3HA.

A) An occurrence of subfacies 1 in a section normal to bedding. Note sandstone rip-up clasts at center right. Scale (next to clasts) is 15 cm long. See detail in B.

B) Detail from photo A of large sandstone rip-up clasts incorporated within hummocky laminae. These are the largest clasts observed within hummocky sandstones in the Cardium Formation. Section 4-23, 132 m.

C) Oblique plan view of elongate erosional furrow at the base of a sandstone amalgamation unit in subfacies 2. Beds are dipping toward camera. Eroded mudstone lens is present in shadow behind hammer. Willmore Member at section 4-43. Compare with similar feature from association 2 (Fig. 4-12E, 4-13A, & 4-13C).

D) Beds from subfacies 3 seen in a section normal to bedding. Up is to the right. Prominent amalgamation unit to left of scale displays a sharp base overlain by hummocky cross-strata which are difficult to see in this photograph. In turn, the laminated interval is gradationally overlain by intensely bioturbated sandstone, which is sharply overlain by another amalgamation unit (behind scale). Note plane parallel lamination above base of final unit. Scale (in centimeters and inches) is 15 cm long. Seebe Member at section 5-45.

A
B
C
D

sandstone and overlying bioturbated intervals are always gradational due to bioturbation which increases in intensity upward through the couplet. Within the intensely bioturbated interval, no physical structures are preserved.

The specific nature of biogenic structures within this subfacies is discussed in further detail below.

Subfacies 4: Dominantly bioturbated amalgamated sandstones. Subfacies 4 (dominantly bioturbated amalgamated sandstones -- Fig. 4-19A) represesents a much more intensely bioturbated version of subfacies 3 described previously. This is the rarest of the four subfacies. Average thickness of individual amalgamation units is similar in subfacies 3 and 4 (approximately 40 to 80 cm). In subfacies 4, the laminated sandstone divisions of amalgamation units are much thinner and typically are not laterally continuous, but rather are lens-shaped. Some amalgamation units do not display any laminated sandstone, but rather are thoroughly bioturbated throughout their thickness.

The decreased abundance and lenticular distribution of laminated sandstone within this subfacies is due directly to an increase in bioturbation. Subfacies 3 and 4 represent distinctive reference points along a gradational spectrum ranging from subfacies 1 and 2 (in which bioturbation is negligible) and fully bioturbated sandstone

(facies 3BS previously described). Subfacies 4 is equivalent to the "'amalgamated' burrowed zones" of Bourgeois (1980) and the "bioturbated-type amalgamated sequence" of Dott and Bourgeois (1982).

Biogenic structures. The association of biogenic structures present within amalgamated hummocky cross-stratified sandstones is variable, depending upon the subfacies of a particular occurrence.

Subfacies 1 and 2 contain biogenic structures similar to those of association 2 (interbedded hummocky sandstones and mudstones); however, due to erosion of the upper parts of sandstone/mudstone couplets, these traces are present in much lower abundances (especially in subfacies 1). Typically, the forms present within sandstones or at sandstone/mudstone boundaries include Gyrochorte, Planolites, Skolithos, Rosselia, and/or Cylindrichnus, and Thalassinoides; additionally, vertical and oblique Ophiomorpha burrows are highly abundant in a few occurrences. Within mudstone lenses, Chondrites, Planolites, Rhizocorallium, and Teichichnus are common.

Subfacies 3 and 4 generally reveal intense bioturbation (nondescript vertical and oblique burrows) in which individual structures are not generally recognizable; however, Ophiomorpha, Chondrites, and/or Planolites are observed locally. This assemblage of biogenic structures

probably is best assigned to a Skolithos ichnofacies transitional with the Cruziana ichnofacies (Frey & Pemberton, 1984).

Macrofossils. A few ammonites (genus Scaphites) have been observed within this facies. Molds of Cardium valves are present in great abundance at the bases of many amalgamation units within this facies; often, these shells appear in a hydrodynamically stabilized convex-upward position, and they usually display a systematic orientation. Inoceramus valves were observed locally. Body fossils from the Cardium formation are illustrated in figure 4-26.

Summary: Basic distinguishing features. The basic distinguishing features which identify any single occurrence of facies SHA are listed below:

1) Occurrences consist of very fine to fine sandstones several meters in thickness. Shale/mudstone lenses are present locally.
2) Sandstones are hummocky cross-stratified, consisting of numerous amalgamated sandstone/mudstone couplets. Erosional amalgamation has resulted in partial or complete removal of the mudstone intervals (see Fig. 4-17).
3) Occurrences contain marine trace and body fossils.

Locally, intense bioturbation is extensively developed, and hummocky cross-stratification can be recognized only near the bases of amalgamation units. In extreme cases, only small lens-shaped intervals of hummocky cross-stratification can be recognized. Where bioturbation is less intense, recognizable burrows indicate deposition within the Skolithos to Cruziana ichnofacies.

Facies SSW ("Swaley Sandstone"): Swaley cross-stratified sandstone, a variant of hummocky cross-stratification.

This facies was encountered 39 times. These occurrences have an average thickness of 4.5 m (range: 1.3 to 14.6 m).

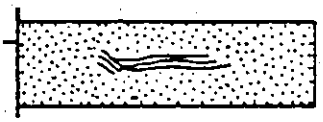

Composition and internal structures. This facies consists predominantly of thick, very fine to fine siliciclastic sandstone bodies. Sandstones are always thicker than 1 m; the thin occurrences typically have been truncated by a post-depositional transgression (chapter 5). Each occurrence of this facies represents a single thick sand body. Granules and pebbles of varicolored chert occur locally.

Internally, sandstones of facies 3SW are swaley cross-stratified. A generalized description of this newly recognized sedimentary structure is provided below.

Swaley cross-stratification: Generalized description. The term "swaley cross-stratification" was introduced informally by Duke (1980) to distinguish a variant of hummocky cross-stratification from the Cardium Formation in which swales are preferentially preserved and hummocks are rare or absent. Descriptions and photographs of the structure from a variety of units are provided by Leckie & Walker (1982), Walker (1982), Walker et al. (1983), Taylor & Walker (1984), and Duke (1985c). A block diagram illustrating the major morphological features of swaley cross-stratification is presented as figure 4-22.

Examples of the features described in this paragraph are illustrated in figures 4-23, 4-24, and 4-25. Swaley cross-stratification is characterized by superimposed, concave-upward, shallow, low-angle scours about 0.5 to 5 m wide (rarely up to 10 m wide) and a few tens of centimeters deep. Scours cut into one another and into intercalated units of subhorizontal (flat or extremely low-angle) quasi-planar parallel lamination. Dips of cross-strata within the shallow scours rarely exceed 10°. The broad, low-angle scours contain curved stratification which generally follows the basal surface of the scour,

Figure 4-22. Block diagram illustrating major morphological features of swaley cross-stratification.

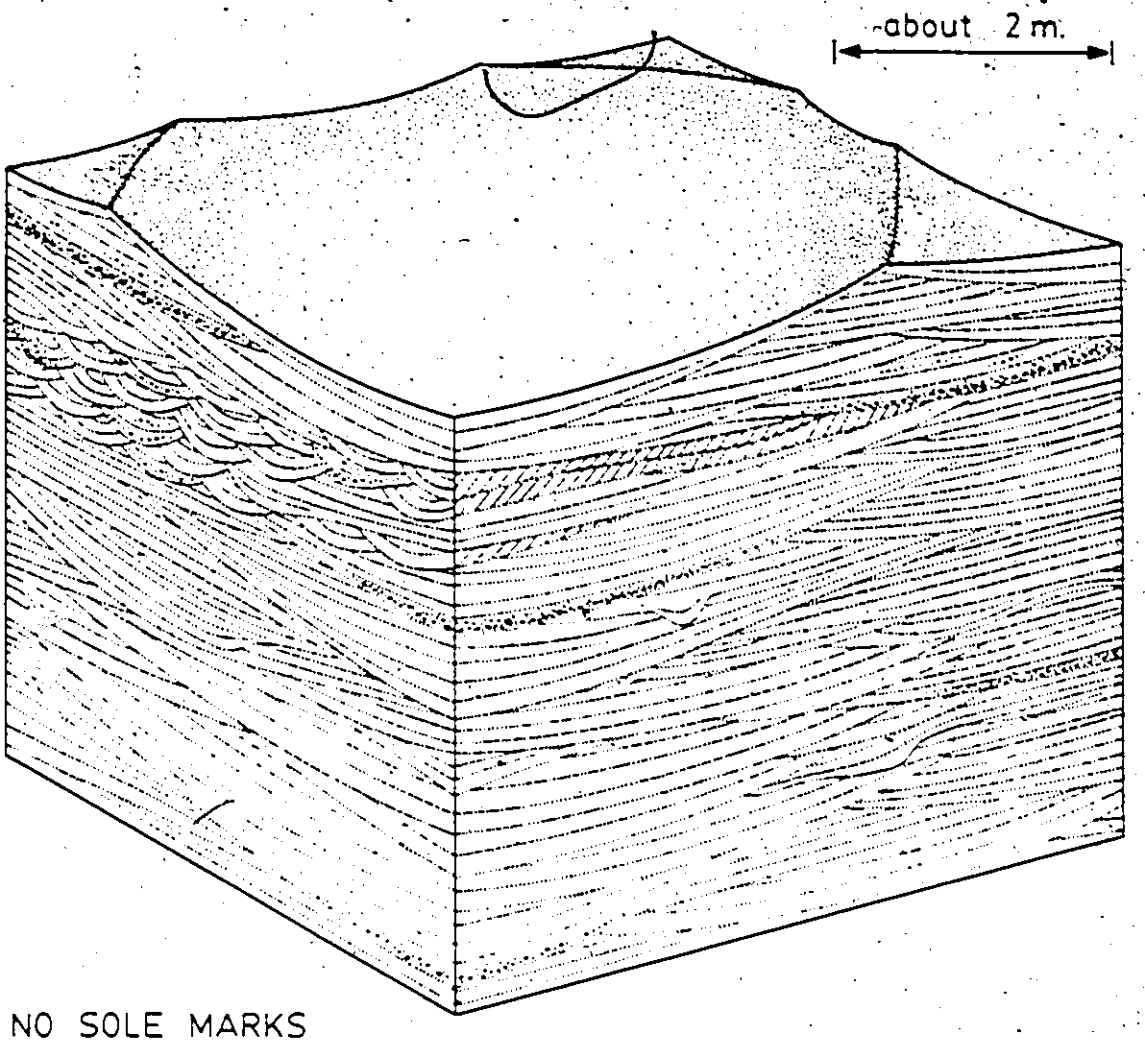

NO SOLE MARKS
NO MUDSTONE
HUMMOCKS RARE OR ABSENT
SYMMETRICAL RIPPLES VERY RARE OR ABSENT

LENTICLES OF MEDIUM-SCALE TROUGH CROSS-BEDDED SANDSTONE LOCALLY PRESENT

NO EVIDENCE FOR AMALGAMATION OF BEDS OR EPISODIC SEDIMENTATION

Figure 4-23. Examples of swaley cross-stratification (facies SSW). Note platey appearance of weathered surfaces and absence of mudstone lenses within swaley intervals (A, B, & C).

A) Vertical section through vertical transition from amalgamated hummocky cross-stratification (below) to swaley cross-stratification (above). Person points to sharp base of final obvious amalgamation unit, where hummocky cross-strata overlie bioturbated sandstone. Note broad, low-angle, convex-upward laminae in this 30 cm hummocky bed. About 60 cm above base of this bed are the first swaley cross-strata. Facies SSW occupies upper half of photo; note low-angle concave-upward scours, roughly concordant laminae in scours, and smaller, steeper, one-sided scours. Section WA-1, 73 m.

B) Swaley scour fill in vertical section. Section 5-45, 56 m.

C) A thick swaley interval in vertical section, showing relatively thick parallel laminated intervals and low-angle swaley scours. Note preferred dip direction within scours (to the right). Section GC-2, 45-48 m.

D) Bedding surface in swaley sandstone (plan view), showing cm-scale coalified wood fragments (rectangular depressions). Coin is 2.3 cm wide. Section 5-45, 87 m.

E) A thick, isolated set of high-angle cross-strata within swaley sandstone (vertical section). Section 5-45, 88 m.

A
1
B
C
D
E

but may flatten upward somewhat within the scour. The largest concave-upward scours often possess slightly undulatory bases; overlying sandstone laminae more-or-less follow these gently undulatory erosional bases. In some occurrences, pebbles and granules are concentrated locally within sandstone laminae at the bottoms of the swaley scours; coarse grains may also be widely disseminated throughout the sandstone filling these scours. In plan view, scours are three-dimensional and radially symmetrical, and in all respects resemble the swales present in the other hummocky cross-stratified facies of associations 2 and 3 (hence the name of this style of cross-stratification). Angle of dip of cross-strata within swales does not vary systematically with direction; similarly, there is no preferred direction of cross-strata dip within occurrences of this facies. As a consequence of this geometry, vertical sections through swaley cross-stratified sandstones appear similar regardless of their plan-view orientation.

An extremely important feature of virtually all occurrences of swaley cross-stratification is the presence of a few low-angle, convex-upward, three-dimensional laminae, forming isolated, three-dimensional hummocks within a sand body dominated by intersecting swales (Fig. 4-23A, 4-25A, & 4-23C).

Swaley cross-stratification is distinctly

Figure 4-24. Examples of swaley cross-stratification (facies SSW) in sections normal to bedding.

A) A two-meter-thick swaley sandstone truncated by transgression and overlain by mud-dominated deposits of association 1. Note broad, shallow, swaley scour delineated by hammer and book, abundant biogenic structures penetrating into sandstone from overlying mudstone, and a concentration of smaller, steeper scours in sandstone below hammer. See details in B and C.

B) Detail of sandstone in A. Note dominance of horizontal to very low-angle, curved laminae, and smaller scours with steeper erosional relief. Also note flattening of laminae toward the top of one of the steeper scours (near shadow at lower left). In a very limited exposure (i.e., too small to recognize broad scours such as the one in photo A), a swaley sandstone such as this might easily be confused with trough cross-bedding. Tape is extended 61 cm. Section 6-8, 132 m.

C) Detail of sandstone in A, showing mudstone-filled biogenic structures (predominantly sub-horizontal Rhizocorallium) extending from overlying mudstone. Scale is 15 cm long. Section 6-8, 132 m.

D) Isolated set of high-angle cross-strata in a swaley sandstone. Note low-angle curved laminae both above and below the high-angle set. Coin is 2.4 cm in diameter.

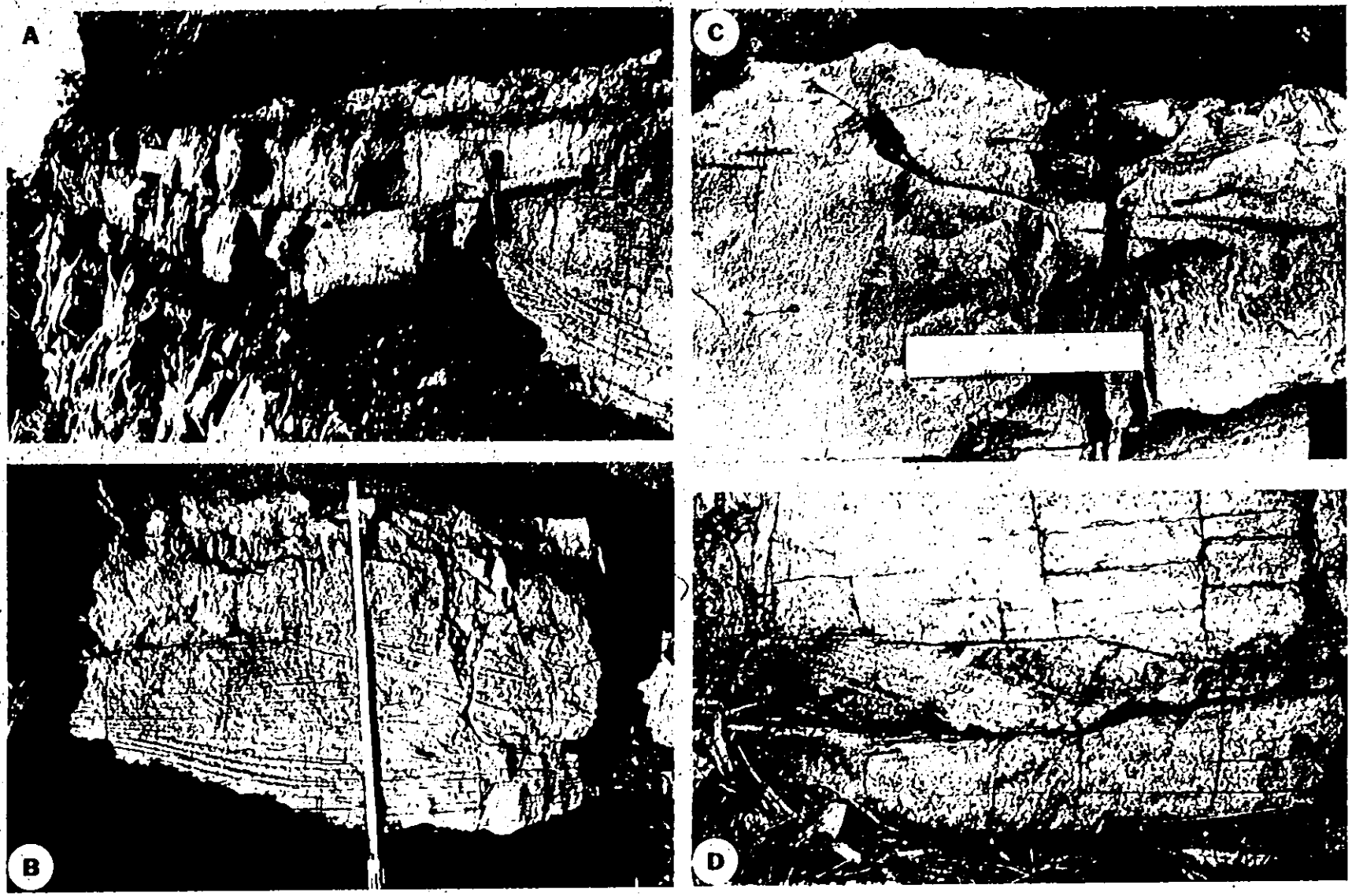
A
B
C
D

dissimilar to more familiar high-angle cross-stratification (e.g., trough cross-bedding). Angles of cross-stratification typically are much lower than angle-of-repose cross-bedding, and the random orientation of dip direction is unlike the preferred dip direction present in high-angle cross-bedding. The differences between trough cross-bedding and swaley cross-stratification were further discussed and illustrated by Walker (1982).

Despite the aforementioned differences between swaley cross-stratification and various forms of high-angle structures, it is important to note that many occurrences of swaley cross-stratified sandstones contain locally developed high-angle cross-strata (Fig. 4-23E, 4-24B, & 4-24D). These fairly rare high-angle cross-strata (as developed in the Cardium Formation) are described in detail under a separate subheading below.

Duke (1985a) was the first worker to note that swaley cross-stratified sandstones generally do not show evidence of amalgamation, and therefore are best interpreted as being deposited under temporally continuous or quasi-continuous bottom flows. The distinction between a thick amalgamated (or episodically deposited) sandstone and a thick non-amalgamated (or quasi-continuously deposited) sandstone is critical to the interpretation of temporal variation in near-bed hydrodynamic processes and, accordingly, depositional environment. There are several

Figure 4-25. Details of lamination in swaley cross-stratified sandstone (facies 3SW). In all photographs, sections are normal to bedding and coin is 2.4 cm in diameter.

A) Low- to moderate-angle swaley cross-strata. As is typical of this structure, the width of swales in this exposure is much greater than the width of this photograph. Note small, isolated, convex-upward hummock at center left. Also note very low-angle discordances along lamina at base of coin and elsewhere. Section 5-45, 150 m.

B) Area adjacent to photo A above, showing intersections of swales. Note very low-angle discordances within upper swale fill, and small-scale, low-angle scour fill at lower right. Section 5-45, 150 m.

C) Low-angle swale intersections similar to those in A and B. This exposure permits viewing of sections normal to bedding and to one another; outcrop has the same appearance regardless of orientation of vertical section. Hammer handle for scale. Section 5-45, 58 m.

D) Close-up of very rare small-scale symmetrical ripple within a swaley sandstone. Section normal to crest orientation. Section 5-45, 150 m.

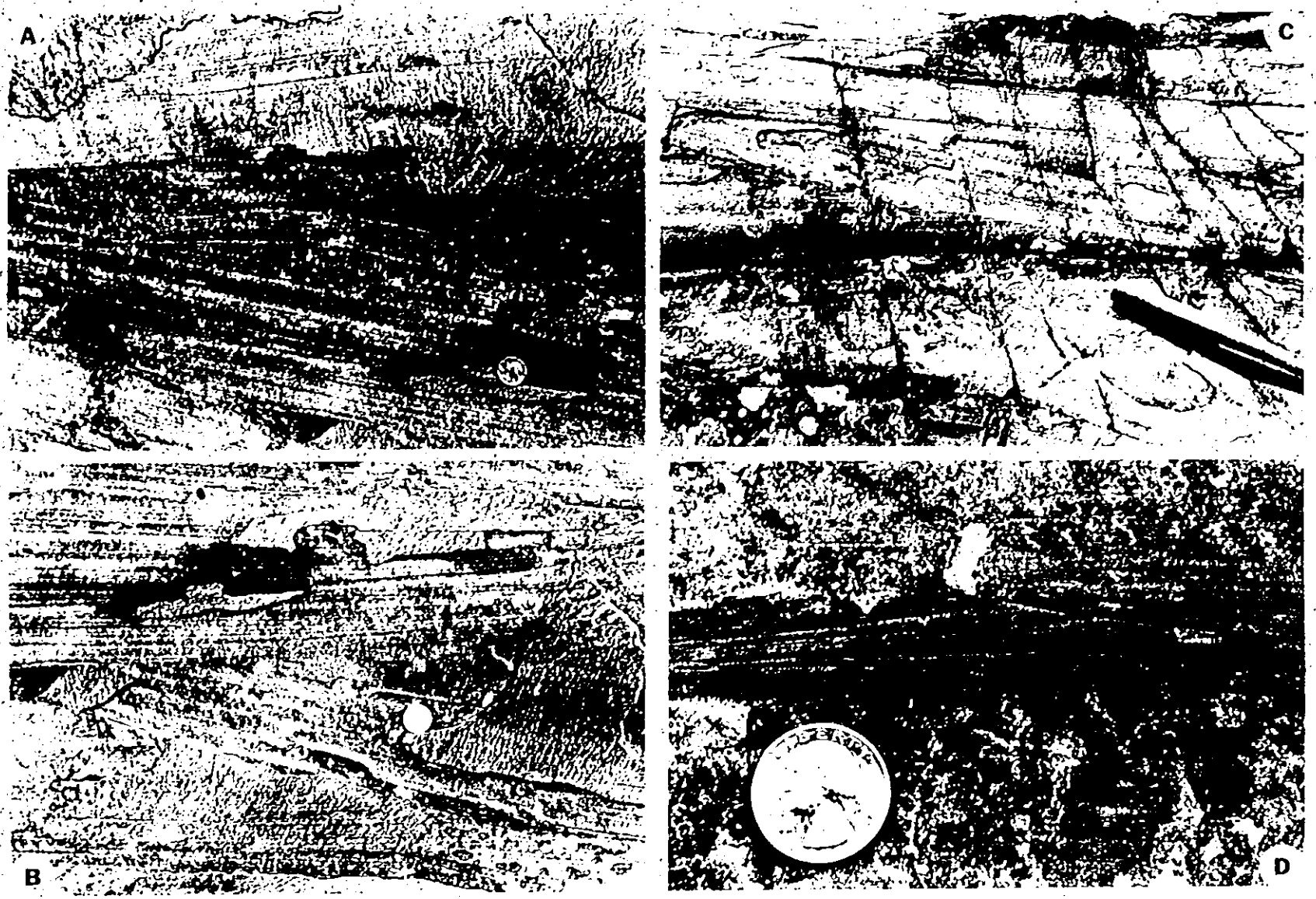
A
B
C
D

lines of evidence (largely negative evidence) which support the interpretation of continuous or quasi-continuous deposition of thick swaley cross-stratified sandstones:

1) Mudstone lenses usually are absent from swaley cross-stratified sand bodies; where present, these lenses are rare and thin, and typically occur near the gradational basal contact of a swaley sandstone where it lies upon hummocky cross-stratified sandstone (see further discussion in the facies interpretations which follow, and in chapters 5 and 10).

2) Mudstone rip-up clasts are seldom observed within swaley sandstones; most occurrences do not contain such clasts.

3) Erosional contacts within swaley cross-stratified sandstones cannot be traced more than a few meters laterally, in marked contrast to the typically extensive erosional surfaces present in amalgamated hummocky cross-stratified sandstones.

4) Extensively bioturbated intervals generally are not present within swaley cross-stratified sandstones. Rarely, however, swaley sandstones are extensively bioturbated by vertical and oblique Ophiomorpha burrows, or similar forms (see further discussion below).

The preceding generalized description of swaley cross-stratification serves equally well as a basic

description of examples from the Cardium Formation. Certain additional details, largely specific to Cardium occurrences, are further discussed below.

High-angle cross-strata. As noted above, swaley cross-stratification is overwhelmingly dominated and characterized by low-angle cross-stratification; however, many occurrences of thick sand bodies dominated by swaley cross-stratification contain locally developed high-angle cross-strata. This high-angle stratification may be classed within three categories:

1) steep one-sided scours,
2) irregular, isolated, trough-shaped scours,
3) lenticular intervals of medium-scale trough cross-bedding.

The steep one-sided scours are illustrated in the block diagram (Fig. 4-22) and in figure 4-23A. These scours may be steeper than the angle of repose. They typically scour approximately 10 to 30 centimeters deep into low-angle swaley cross-stratification. They are one-sided (i.e., laminae overlying the erosional surface flatten laterally and vertically and do not describe a trough shape). One-sided scours are rare; they do not appear to show a preferential orientation with respect to other paleoflow indicators. These scours typically are

filled with very fine to fine sandstone identical to the surrounding swaley sandstone.

Isolated trough-shaped scours are irregular in cross-sectional geometry. These scours typically are steep-sided, but do not generally exceed the angle of repose. Scours typically are trough-like in cross-section, but unlike typical trough cross-bedding, both the erosional surface and the overlying laminae which parallel this surface may be somewhat undulatory (Fig. 4-24B & 4-25A). Scours are isolated, occurring individually or in small groups of just a few scours. These features scour into low-angle swaley cross-stratification and one another. Scours are a few tens of centimeters deep and generally less than 1 m wide. Limited three-dimensional exposures suggest that laminae within these scours may be either radially symmetrical or may display a preferred infilling direction similar to the infilling geometry of trough cross-bedding. These scours typically are filled with very fine to fine sandstone identical to the surrounding swaley sandstone.

The third type of high-angle cross-strata encountered within swaley cross-stratified sandstones is medium-scale trough cross-bedding. In these occurrences, the high-angle structure is morphologically identical to the numerous examples of trough cross-bedding reported from a variety of depositional settings by numerous workers

(compare with Harms et al., 1982, Fig. 3-10). Individual cosets of trough cross-bedding within swaley cross-stratified sandstones generally are a few tens of centimeters thick and less than 1 m in width; however, they may be as thick as 60 cm and as wide as 3 m. Trough cross-beds occur in groups of cross-cutting cosets which typically form large lenses of trough cross-bedded sandstone within even larger swaley cross-stratified sand bodies. Unlike the other scours described above, lenses of trough cross-bedding within swaley sand bodies are generally formed in fine to medium sandstone slightly coarser than the surrounding swaley strata.

The basal surfaces of trough cross-bedded lenses are erosional and typically scour many tens of centimeters to a few meters deep into the swaley sandstone. Laterally, trough cross-bedding commonly passes gradationally into and is intercalated with typical swaley cross-stratification. Within limited exposures, these lenses of trough cross-bedding may traverse an entire outcrop; the largest such lenticular body was traced a few hundred meters laterally across an extensive exposure (section 4-21) before passing gradationally into swaley cross-strata; the total lateral extent of this occurrence could not be determined due to erosion of the outcrop at the other end. Thus, the original width of this lenticular trough cross-bedded sand body was greater than a few hundred

meters. The greatest observed thickness of trough cross-bedding within swaley cross-strata (approximately 7 m) was also observed in the occurrence at section 4-21. In more typical occurrences, trough cross-bedded lenses are only about 1 m thick or less.

It should be re-emphasized that high-angle cross-strata of the types described above are not a necessary or common feature of swaley cross-stratified sandstones. The characteristic morphology of swaley cross-stratification is a low-angle variant of hummocky cross-stratification described under the preceding subheading. It should also be noted that any or all of the three types of high-angle cross-strata may be present or absent in any one occurrence of swaley cross-stratification.

Biogenic structures. Internally, biogenic structures within swaley cross-stratified sandstones are extremely rare. Vertical and oblique Ophiomorpha is occasionally present in low/moderate abundance, and small Terebellina burrows are observed locally. Where facies 3SW is erosionally transgressed by mud-dominated deposits of association 1, abundant biogenic structures (often, mud-filled Rhizocorallium and associated forms) penetrate into the sandstone from the overlying mudstone (Fig. 4-24A & 4-24C).

Basal surfaces of facies JSW occurrences locally display abundant horizontal trace fauna (Thalassinoides, horizontal Ophiomorpha, and Planolites). Such abundant basal-contact bioturbation is restricted to occurrences which immediately overlie mudstone.

Where facies JSW is overlain by a thin occurrence of facies JPL, root casts originating from the top of facies JPL rarely penetrate through the entire thickness of that facies and into the upper parts of the underlying swaley sandstone.

The assemblage of trace fauna described above is representative of the Skolithos ichnofacies (Frey & Pemberton, 1984).

Bases of sandstones. Basal contacts of facies JSW typically are either very sharp or gradational, depending upon the lithology of the underlying facies. Where facies JSW lies upon sandstone, the contact is usually gradational (Fig 4-23A). This gradation reflects the fact that sandstones underlying facies JSW are always hummocky cross-stratified, and it typically is difficult to distinguish a sharp transition from one variant of hummocky cross-stratification to another. Extensive bioturbation is usually not present at these sandstone-sandstone transitions.

Where facies JSW lies upon mudstone, the contact is

always sharp, but commonly is extensively bioturbated (see above). Rarely, directional sole marks are observed at sharp, non-bioturbated bases; however, sharp, flat, non-bioturbated bases <u>without</u> sole markings are more common.

<u>Tops of sandstones</u>. Tops of swaley cross-stratified sandstones have a variable aspect, depending upon the nature of the overlying facies. One aspect of great importance in the interpretation of the mode of genesis of the structure is worthy of note. In several of the coarsening-upward cycles present in various Cardium exposures, the uppermost facies present locally is facies SSW, and these swaley cross-stratified sandstones commonly are blanketed by deeper-water mudstones following an inferred deepening at the site of deposition (e.g., Fig. 4-24A). In such occurrences, the original sand-bed topography may possibly be preserved at the tops of the swaley cross-stratified sand bodies (however, superficial erosion is most common -- see further discussion in chapter 5). In one such example, however, the topography below the transgression surface is characterized by abundant positive-relief hummocks (as well as negative-relief swales), unlike the swale-dominant internal structure of swaley sand bodies. This occurrence suggests the possibility of an origin for swaley cross-stratification

due to the post-depositional truncation of prominent hummocks (but see reservations discussed in chapter 5).

In cycles in which swaley sandstones are overlain by inferred beach deposits (facies 3PL), the width of swaley scours gradually increases upward while the apparent depth of erosion in these scours diminishes upward, leading to a gradual reduction in the angle of cross-stratification and a gradational transition to the planar parallel lamination of facies 3PL.

Macrofossils. Megascopic body fossils are very rare from this facies. One ammonite (genus Scaphites) was collected from this facies. Molds of Cardium valves commonly are concentrated near the bottom of swaley scours, and valves of Pinna or Atrina were observed in one occurrence. Body fossils from the Cardium Formation are illustrated in figure 4-26.

Summary: Basic distinguishing features. The basic distinguishing features which identify any one example of facies 3SW are listed below:

1) Occurrences are composed of thick, very fine to fine sandstone. Mudstone lenses and rip-up clasts are absent or rare.
2) Sandstones of this facies are dominated by a distinctive variant of hummocky cross-stratification

known as swaley cross-stratification. This structure is dominated by low-angle (<10°), curved cross-strata which typically form equant, concave-upward, erosionally intersecting swales several meters wide. Rare hummocks are present locally, as is quasi-planar, very-low-angle to flat stratification.

3) There typically is no evidence for amalgamation of episodic sand deposits within examples of swaley cross-stratification.

4) High-angle scours and trough cross-bedded lenses are locally present within swaley sandstones. Trough cross-bedded lenses are formed in fine to medium sandstone which is slightly coarser than the host material.

5) Trace fossils (predominantly Ophiomorpha) and body fossils indicate a marine origin within the Skolithos ichnofacies.

Figure 4-26. Body fossils from the Cardium Formation.

A) This section normal to bedding displays a death(?) assemblage of Inoceramus valves in swaley cross-stratified sandstone. Note thin chert-pebble lags. Scale is 15 cm long. Section 5-4, 44 m.

B) Inoceramus encrusted with bryozoans from an inferred transgression surface (association 1 immediately overlying a conglomerate veneer capping a sandstone of association 3). Bryozoans are visible near center of photo, above the "8" on the ruler. See detail in photo C. Scale in centimeters.

C) Detail of encrusting bryozoans in photo B. Scale in centimeters.

D) Disarticulated valves formerly classed within the pelecypod genus Cardium. These valves occur in a convex-upward position on the base of a sandstone from association 3. Coin is 2.4 cm in diameter.

E) Scaphites from association 1. These ammonites are most commonly encountered (often in abundance) at inferred transgression surfaces; they are especially common at surfaces bounding minor cycles present in the basal transition beds of the Wapiabi.

F) An ammonite from the Blackstone-Cardium transition interval at section 5-45.

A
B
C
D
E
F

Facies 3PL ("Parallel and Planar Lamination"): Thick parallel laminated sandstone and low-angle divergent sets of planar laminated sandstone.

This facies occurred 34 times in this study. Average facies thickness is 1.9 m (range: 0.6 to 6.8 m).

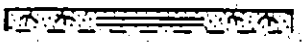

Composition and internal structures. Occurrences of facies 3PL consist of well-sorted, very fine to medium sandstone. Most occurrences consist of fine sandstone. Sandstones typically are very white in color, rarely steel grey, but never predominantly rusty red (even on weathered surfaces). This characteristic color is unlike that of any of the other sand-dominated facies. In all occurrences, sandstones are extremely hard and tough (much more so than the sandstones of other facies) due to abundant silica cement. Each occurrence of this facies represents a single thick sand body. There are no shale/mudstone lenses or scattered shale rip-up clasts within these sandstones; however, in a very few of the thicker occurrences, the outcrop is traversed by one or two thin, continuous shale beds (rarely, coaly shale). Also very rare within this facies are small, shallow channels (about 1 m wide, 10 to 30 cm eroded depth) filled with chert pebbles and/or shale rip-up clasts (approximately 0.5 to 2 cm diameter).

Carbonaceous root casts are typically present at the top of occurrences of this facies (see below).

Internally, sandstones commonly are delicately parallel laminated throughout the exposure (Fig. 4-27A & 4-27B); less frequently, they are entirely or in part composed of low-angle (less than 12°) divergent sets of planar parallel laminae (Fig. 4-27C) with set thicknesses of about 30 to 50 cm. In either case, individual sets of laminae generally can be traced for several meters. Very rarely, widely dispersed scattered chert pebbles occur along parallel laminae within this facies. These pebbles may be as large as 4 cm. At one location (section 4-21), parallel lamination grades laterally (over roughly 1 km of exposure) into trough cross-bedding similar to that of facies 3SW. With the exception of this trough cross-bedding, there are no curved laminae within sandstones of this facies. Lense-shaped masses and horizons of apparently structureless (bioturbated?) sandstone are present locally.

Biogenic structures. With the exception of root casts (further dicussed below under "Tops of sandstones"), biogenic structures are extremely uncommon within this facies. Animal-generated structures are most common along the basal surfaces of facies 3PL sandstones (i.e., along the contact between facies 3PL and the underlying facies).

This high abundance of burrows at the basal contact is most commonly observed in occurrences of facies 3PL which immediately overlie mudstone. Occurrences which overlie sandstone typically do not show extensive basal-contact bioturbation. Where basal-contact bioturbation is present, the dominant forms are horizontal burrows; commonly encountered forms include Thalassinoides, horizontal Ophiomorpha, and Planolites. Internally, facies 3PL sandstones typically are devoid of animal-generated biogenic structures; however, vertical and oblique Ophiomopha burrows are locally abundant, and a single crude Diplocraterion was observed in one occurrence of facies 3PL. This assemblage of structures is characteristic of the Skolithos ichnofacies (Frey & Pemberton, 1984).

Tops of sandstones. It has been mentioned previously that the upper parts of facies 3PL sandstones commonly display root casts, most typically in great abundance. In fact, 24 (71%) of the 34 occurrences do indeed display root casts in their upper parts. These root casts may penetrate up to 2 m through the sandstone from the upper bedding surface; typically, however, they penetrate only 30 to 70 cm.

In a few instances, root casts are so abundant that they have completely bioturbated the upper parts of sandstones, totally obliterating any sedimentary structures

Figure 4-27. Examples of facies 3PL in sections normal to bedding (except photo D).

A) Parallel lamination capping a coarsening-upward sequence. Up is to the left. Notebook (circled) lies upon hummocky cross-stratified sandstone, which is overlain by parallel lamination of facies 3PL (contact indicated by arrow at top of photo). At extreme left, parallel laminated sandstone is immediately overlain by recessive coaly shales of association 4 (not visible in photo). Section 4-19, cycle 6.

B) This parallel laminated sandstone is locally rooted and is immediately overlain by 16 cm of recessive shaly coal from association 4 (not visible in photo). Scale is 15 cm long. Section 5-39, 51 m.

C) Flat, planar, parallel lamination overlain by low-angle, divergent sets of planar parallel lamination within a single occurrence of facies 3PL. This is a relatively thick occurrence of this facies. Facies 3PL overlies facies 3SW at the top of the person's head, and is in turn overlain by bioturbated sandstone just visible at top of photo. Section WA-1, 70 m.

D) Plan view of heavily rooted upper surface of an occurrence of facies 3PL. This surface is immediately overlain by rooted mudstones of association 4. Scale at center of photo is 15 cm long. Section 4-13, 28 m.

A
B
C
D

that may have been present prior to rooting.

Root casts from facies 3PL sandstones typically are thin and hair-like (diameter 2 mm or less) vertical and oblique shafts filled with carbonaceous material. Locally, the diameter of these vertical and oblique features may be as great as 2 to 3 cm; these larger root casts are filled completely with coal. Downward branchings are common, as is a downward decrease in the diameter of these features.

Upper contacts of facies 3PL sandstones (i.e., upper facies contacts) are generally sharp and regionally flat. Where rooting is abundant, the upper bedding surface is bumpy and irregular; favorable bedding-plane exposures reveal a characteristic pattern of radiating and irregularly arranged elongate bumps and hollows (Fig. 4-27D). These bumpy surfaces generally are dark brown to red in color.

Bases of sandstones. Basal contacts of facies 3PL typically are either very sharp or gradational, depending upon the lithology of the underlying facies. Where facies 3PL lies upon another sandstone facies, the contact is occasionally gradational, but may be sharp. Biogenic structures generally are not present in either situation. However, where facies 3PL lies upon mudstone or shale, the contact is always sharp and commonly is marked by the animal-generated bioturbation described above. All basal

contacts of facies 3PL occurrences are regionally flat. No sole-marks have been observed on the bases of sandstones in this facies.

Macrofossils. No megascopic body fossils (other than root casts) have been observed within this facies.

Summary: Basic distinguishing features. The basic distinguishing features which identify any single occurrence of facies 3PL are listed below:

1) Occurrences are characterized by well-sorted, hard, silica-cemented sandstones. Grain size ranges from very fine to medium sandstone. Most occurrences consist of fine sandstone.
2) Shale/mudstone lenses are absent from this facies.
3) Sandstones display delicate, horizontal parallel lamination and/or low-angle (less than 12°) divergent sets of planar parallel lamination.
4) Tops of sandstones commonly display abundant root casts.
5) Marine trace fauna indicate formation within the Skolithos ichnofacies.

Association 3: Preliminary interpretation

The thick sandstones of association 3 are marine in origin, as indicated by abundant trace and body fossils. A probable association with the foreshore and shoreface is indicated by: 1) the relative abundance of sand in this association, and 2) the dominance of trace fauna from the Skolithos ichnofacies, indicative of shifting substrates (Frey & Pemberton, 1984, Table 2).

In chapter 5, figure 5-40 (p. 378) shows a typical shore-normal profile for a sandy shoreline, on which the foreshore, shoreface (or nearshore), and offshore regions are located and defined. The foreshore includes the shoreline region between mean low- and high-tide water levels; foreshore deposits are exposed to swash from incident waves. The shoreface lies between the mean low-tide water level and effective fairweather wave-base, approximately the maximum depth to which normal local wave conditions agitate the substrate. The offshore region lies in depths below fairweather wave base.

Under normal fairweather conditions, the mudline will extend from the offshore region to a depth approximating fairweather wave-base; in shallower waters, fairweather-wave agitation prevents mud deposition. Under more energetic storm conditions, mud can be eroded and resuspended below fairweather wave-base, possibly to depths

as great as storm wave-base, and sand can be transported to the offshore region. Thus, lithological boundaries cannot be expected to conform precisely with the boundaries of the various regions defined above, due to the lateral and bathymetric shifting of these boundaries as the wave climate varies. The nearshore-offshore transition in ancient prograding shoreline sequences must therefore be defined on the basis of a facies analysis, not on the basis of lithology alone.

The sand bodies of association 3 are inferred to form within the foreshore, shoreface, and proximal offshore shelf regions, and to extend continuously across these regions, reflecting the erosion (by storms) of proximal offshore muds deposited under fairweather conditions (see chapter 5 for evidence of continuity). These sandstones may therefore be termed <u>shoreface-attached sand bodies</u>. An alternate interpretation involves formation of some of these thick sandstones within shoreface-detached proximal shelf sand ridges or bars. Distinction between these two alternative interpretations requires knowledge of vertical and lateral facies relationships; this discussion will be delayed to chapter 5 and subsequent chapters.

The foreshore interpretation is restricted to facies 3PL, which exhibits parallel and low-angle planar lamination characteristic of the surf zone (foreshore region). This interprtation is enhanced by the presence of

abundant root casts at the tops of occurrences, indicative of subaerial exposure or extremely shallow water depths.

The trace fauna assemblage in facies 3SW, 3HA, and 3BS of this association, ranging from the Skolithos ichnofacies to a transitional Skolithos-Cruziana assemblage, is also consistent with the inferred shoreface to shallow offshore depositional setting (Frey & Pemberton, 1984).

Amalgamated hummocky cross-stratification and the related variant, swaley cross-stratification (facies 3HA and 3SW, respectively), suggest a storm-dominated depositional environment. As in association 2, the amalgamated hummocky sandstones of association 3 are inferred to represent deposition in depths between fairweather and storm wave-base (i.e., offshore); however, the increased abundance of both sand and chert pebbles relative to association 2 suggests conditions in which storm events were more energetic and/or frequent, consistent with a more proximal offshore setting. The depositional environment of swaley cross-stratification is less clear, but the absence of evidence for episodic deposition suggests a more energetic environment, probably within the shoreface region. This interpretation is further supported by locally abundant chert pebbles within swaley sandstones, and will be examined further within the context of facies sequences in subsequent chapters.

Association 4. Deposits of variable lithology containing abundant plant fragments and/or coals and root casts.

This association is composed of deposits of variable lithology, ranging from calcareous mudstones to pebbly, very coarse quartz-chert sandstones to coals (Fig. 4-28A). Marine indicators are absent, except in the case of facies 4IF and certain occurrences of facies 4VL, where trace fauna indicating a probable marine affinity are present in greatly reduced densities and varieties compared to previously described, lithologically similar marine facies. Occurrences of facies 4VL also contain symmetrical ripples and an invertebrate fauna indicating deposition in fresh or brackish water. All occurrences of this association contain thin coals (Fig. 4-28A), abundant and very well developed root casts (Fig. 4-28E), and/or very abundant macerated plant debris and coalified wood fragments, some of which are over 1 m in length.

Facies 4VL ("Variable Lithology, Lagoonal"): Deposits of variable lithology (dominantly coaly, calcareous mudstone) containing a brackish- to fresh-water fauna, burrowing, and/or symmetrical ripples.

There are 16 occurrences of this facies. Average facies thickness is 1.5 m; thickness ranges from 0.4 to 3.1 m.



Lithology. This facies is characterized by the interbedding of variable lithologies. Coals, plant fragments, and/or root casts are abundant in all lithologies. Most occurrences are slightly calcareous throughout much or all of their thickness. Typically, the dominant lithology is clayey, coaly, calcareous mudstone interbedded with a variety of lithologies; these include coals, siltstones, very fine to fine sandstones, and/or (rarely) pebbly, poorly sorted (fine to coarse) sandstones. These coarse clastics typically are muddy, coaly, and/or calcareous; in marked contrast with other facies, sandstones in facies 4VL typically are greenish, indicating reducing conditions.

Coals in this facies tend to be relatively thin (1-15 cm) and laterally extensive across the entire width of exposure. They usually are soft, and locally are papery and contain thin shales. Coals very commonly lie upon

Figure 4-28. Common features of mud-dominated deposits in association 4 (i.e., facies 4VL and 4VC).

A) Facies 4VL in a section normal to bedding. Up is to the left. Dark interval is a relatively thick shaly coal. Note typically poor exposure. Section 4-43, 96 m level (Seebe-Cutpick contact).

B) Section normal to bedding through a 50 cm high-angle cross-bedded sandstone from facies 4VC. Note caliche-like deposit (interpreted as a paleosol) at top of bed. Scale is 15 cm long. Cutpick Member at section 4-43.

C) Typical bedding-normal outcrop of rooted, clayey mudstone with thin siltstones and sandstones. This is facies 4VC; very similar deposits with invertebrate remains are classed in facies 4VL. Field book for scale.

D) Lined burrows from sandstones in facies 4VL. Sample at left is a section normal to bedding; sample at right is a plan view. Scale in centimeters and inches. Section 5-22, 69.5 m level.

E) Coalified root casts in a section normal to bedding from facies 4VL. Up is to the left. Hammer iron is at tip of decimeter-scale cast (1); hair-like casts are present above this (2).

A
B
C
D
E
2
2

rooted horizons.

Bedding characteristics. Due to the soft nature of the mudstones which dominate this facies, occurrences usually are very poorly exposed. Beds within facies 4VL generally are tabular and thin (15-75 cm or less). Bedding is defined by lithological variation (i.e., each bed has a different lithology). Beds generally are tabular and laterally extensive across the width of outcrop. Beds generally do not pinch and swell, and channelization was not observed. Contacts between beds generally are gradational; however, bases of siltstones and sandstones locally are relatively sharp, or very sharp and scoured (Fig. 4-29B). Tops of beds everywhere are regionally flat, and generally are gradational.

Small cyclic developments are locally present within facies 4VL. The only common developments consist of interbedded siltstone/sandstones and mudstones, forming thickening- and coarsening-upward sequences about 1 to 2 m in thickness (Fig. 4-29C). Where present, these cycles always occupy a unique stratigraphic position relative to surrounding facies within prograding sequences: They occur at the top of facies 4VL occurrences immediately below inferred backbeach deposits (commonly, facies 3PL).

Physical structures. Primary physical structures within bedding generally are absent in occurrences of

Figure 4-29. Examples of coarse beds in associations 3 and 4 which display root casts. All sections are normal to bedding.

A) Typical millimeter-scale (diameter) coalified root casts penetrating an argillaceous sandstone from facies 4VL. Scale is in centimeters. Section 5-19, 64 m.

B) Typical centimeter-scale coalified root casts from the top of a parallel laminated sandstone (facies 3PL). Coin is 1.9 cm in diameter. Section ND-1, 42 m.

C) Thickening- and coarsening-upward sequence roughly 1 m in thickness formed by parallel laminated and symmetrical-rippled sandstones interbedded with mudstones in facies 4VL. Scale is 15 cm long. This interval is interpreted as a lagoon to backbeach sequence, based in part on stratigraphic context (see below). Note robust, downward branching, centimeter- to decimeter-scale coalified root casts, which penetrate over 50 cm from the upper surface of the uppermost thick sandstone bed in this interval. This surface is located roughly 20 cm above the scale (top of photo); a thin, discontinuous coal is present on the upper surface of the bed from which these root casts originate. This interval is overlain by facies 4VC and underlain by a rooted, parallel laminated sandstone (facies 3PL) capping a major fully regressive cycle. Section 5-4, 60 m.

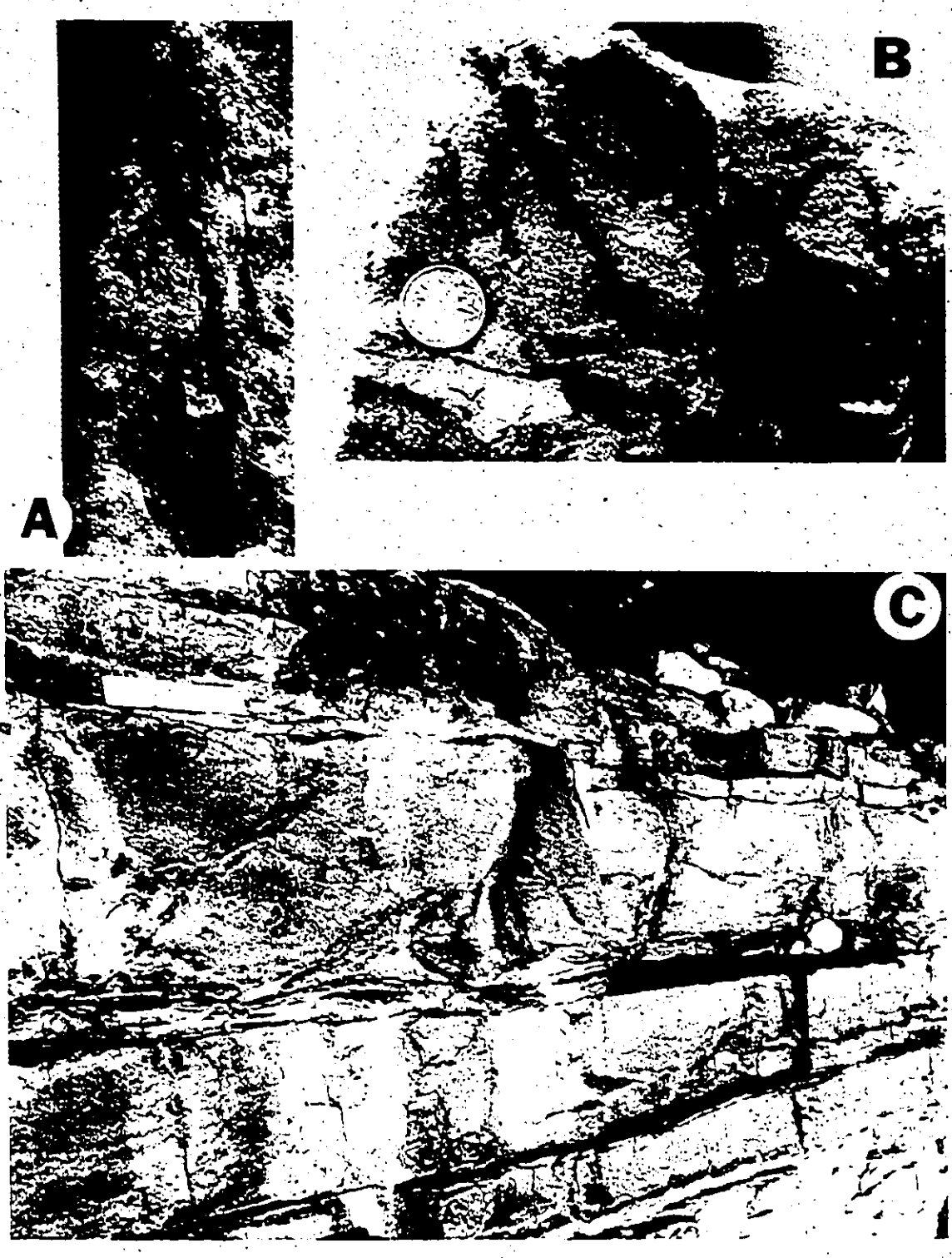
A
B
C

facies 4VL, in part because many occurrences consist entirely of mudstone. Many occurrences do contain coarser deposits (siltstone and/or sandstone); commonly, these beds are also largely structureless, or display crude lamination (Fig. 4-29A), often disturbed by rooting. Other siltstone or sandstone beds are structureless due in part to bioturbation by animals. Distinct ripples (both asymmetrical and straight-crested symmetrical ripples) are present at the tops of several coarse beds in this facies; internally, some beds display small-scale trough cross-lamination.

Biogenic structures. Biogenic structures within facies 4VL include both plant-generated and animal-generated varieties.

Root casts are plant-generated structures. They are extremely abundant in all lithologies; tops of siltstones and sandstones generally display the highest abundance of root casts (Fig. 4-29A & 4-29C). They vary from slender structures (0.1-1.5 cm in diameter and a few centimeters to a few decimeters in length) to robust structures (5-10 cm in diameter and approximately 1 m in length). All root casts contain coal. Numerous downward branchings of root casts were observed.

Animal-generated structures include various nondescript vertical and oblique lined tubes, often curved

(Fig. 4-28D). Horizontal tubes are less common. Thalassinoides was observed at section 5-4. All burrows have diameters of a few millimeters to approximately 1 cm. Burrows are not generally present ubiquitously, but they are found locally in every lithology, usually in low density. High-density burrowing is restricted to siltstones, sandstones, and pebbly sandstones, where it generally is confined to the basal contacts. I have not attempted to classify this assemblage in terms of ichnofacies.

Macrofossils. Macrofossils of both plant and animal origin are abundant within facies 4VL.

Plant macrofossils are the most abundant varieties: these include root casts, leafy and woody debris, and coals. Root casts are described under "biogenic structures" above. Plant fragments include very abundant macerated material and abundant blade-like leaves of grasses, sedges, or other grass-like plants. Wood fragments are coalified and were not identified: these fragments commonly are a few centimeters or tens of centimeters long, and generally are restricted to the bases of siltstones, sandstones, and pebbly sandstones. Coals are described under "lithology" above.

Animal macrofossils include various invertebrate fauna. Fauna are restricted to mudstones, and include

various thin-shelled pelecypod genera. Identified forms include Corbicula, Corbula, and (?)Modiolus.

Summary: Basic distinguishing features. The basic distinguishing features which identify any single occurrence of facies 4VL are listed below:

1) Occurrences typically are characterized by a variable lithology (dominated by clayey, coaly, calcareous mudstone) including calcareous and/or clayey and/or coaly mudstones, siltstones, and/or sandstones or pebbly sandstones, and coals.
2) Lithology varies over short distances vertically (average bed thickness is 15 to 75 cm).
3) Beds generally are laterally continuous and tabular across the width of outcrop.
4) Contacts between lithologies generally are gradational.
5) Macerated wood fragments and blade-like leaf remains are abundant throughout all lithologies.
6) Coalified wood fragments are locally concentrated near the bases of siltstones and sandstones.
7) Abundant, well developed root casts generally are present throughout the mudstones and at the tops of the siltstones and sandstones.
8) Trace fossils, largely restricted to siltstones and sandstones and their contacts with adjacent

mudstones, are present in low to moderate abundances in many occurrences. Traces generally consist of nondescript vertical, oblique, and horizontal simple tubes, many of which are lined.

9) An invertebrate fossil assemblage is present in most occurrences. This assemblage probably indicates brackish- to fresh-water environments.

10) Straight-crested symmetrical ripples and/or asymmetrical ripples are locally present capping siltstone/sandstone beds in several occurrences.

Facies 4VC ("Variable Lithology, Coaly"): Coaly deposits of variable lithology (dominantly coaly mudstone) which do not contain invertebrate fauna, burrowing, or symmetrical ripples.

There are 48 occurrences of this facies. Average facies thickness is 3.4 m; thickness ranges from 0.2 to 17.9 m.

Lithology. This facies is characterized by a complex interbedding of variable lithologies. Unlike facies 4VL, none of these lithologies is calcareous, excepting certain rare, thin (<20 cm) horizons present locally. In most occurrences, the greater part of the

thickness consists of clayey, coaly mudstone (Fig. 4-28C). Interbedded with mudstones in most occurrences are muddy and/or coaly siltstones and/or sandstones (Fig. 4-28B), and coals. Plant fragments and root casts are abundant in all lithologies. The thicker (decimeter-scale) sandstones in this facies are locally capped with caliche-like intervals rich in carbonate cement (Fig. 4-28B). These deposits are interpreted as paleosols.

As in facies 4VL, coals in facies 4VC tend to be relatively thin (1-15 cm) and laterally extensive across the entire width of exposure. They usually are soft, and locally are papery and contain thin shales. Coals commonly lie upon rooted horizons.

Bedding characteristics. Beds within facies 4VC generally are thin (15-75 cm or less). Bedding is defined by lithological variation (i.e., each bed has a different lithology). Cyclic developments within this facies were not discerned. Beds generally are tabular and laterally extensive across the width of outcrop. Contacts between beds generally are gradational; however, bases of siltstones and sandstones locally are relatively sharp, or very sharp and scoured. Locally, coarse beds are lenticular, filling small erosional channels a few meters wide and a few decimeters deep. Tops of beds are everywhere regionally flat and gradational.

Physical structures. Small-scale physical structures are relatively rare within all lithologies. Siltstones and sandstones generally are apparently structureless or graded, having gradational upper contacts with mudstones. Asymmetrical ripples and small-scale trough cross-lamination are locally present within coarse beds; medium-scale, high-angle cross-bedding is rare (Fig. 4-28B).

No symmetrical ripples were observed within this facies. Absence of symmetrical ripples is one of the features which distinguishes this facies from facies 4VL.

On a larger scale, gently inclined lateral accretion surfaces are locally present within siltstones and sandstones of this facies (see discussion of similar features in facies 4SF below). These features typically are defined by subtle grain size variation, or by alternations between coarse material and mudstone.

Biogenic structures. No biogenic structures other than root casts have been observed in this facies. Root casts are essentially similar to those of facies 4VL above. Rooting is present in all lithologies, but is most abundant at the tops of siltstones and sandstones.

Absence of animal-generated biogenic structures is one of the features which distinguishes this facies from facies 4VL. See further discussion below.

Macrofossils. No macrofossils other than woody and leafy debris, root casts, and coals have been observed in this facies. Plant fragments include very abundant macerated material and abundant blade-like leaves of grasses, sedges, or other grass-like plants. Decimeter- and meter-scale wood fragments are coalified and were not identified; these are generally restricted to the bases of siltstones and sandstones. Root casts are described under "biogenic structures" above; coals are described under "lithology" above.

The absence of lagoonal/fresh-water body fossils is one of the features which distinguishes this facies from facies 4VL described above.

Summary: Basic distinguishing features. The basic distinguishing features which identify any single occurrence of facies 4VC are listed below:

1) Each occurrence contains a wide variety of lithologies dominated by coaly, clayey mudstone. Lithologies include coal, clayey mudstones and siltstones, muddy and/or silty very fine to fine sandstones, and coaly examples of the preceeding clastic lithologies. Note that, unlike facies 4VL, pebbly medium to coarse sandstones were not observed in this facies, and calcareous cements are restricted to very rare, very thin intervals

locally.

2) Lithological variation occurs over short distances vertically (average bed thickness is 15 to 75 cm).

3) Contacts between lithologies are generally gradational. Locally, siltstones and sandstones have sharp bases.

4) Beds are generally tabular; locally, however, siltstones and sandstones possess scoured bases, or fill very small channels a few meters wide. Note that channelling was not observed in facies 4VL.

5) Typically, primary physical structures within bedding are absent. Siltstones and sandstones typically display "crinkled" lamination, probably a secondary structure resulting from soil development. Asymmetrical ripples, small-scale trough cross-lamination, and lateral accretion surfaces are present locally within siltstones and sandstones. Unlike facies 4VL, no symmetrical ripples are present in this facies.

6) Macerated wood fragments and grass-like leaves are abundant throughout all lithologies.

7) Coalified wood fragments are locally concentrated near the bases of siltstones and sandstones.

8) Abundant, well developed root casts are generally present throughout the mudstones and at the tops of the siltstones and sandstones.

9) Animal-generated biogenic structures are not present in any occurrences.

N.B.: Facies 4VC is distinguished from facies 4VL by the absence in the former of invertebrate fauna, trace fossils, and symmetrical ripples. Additional contrast is provided by lithology: Facies 4VC occurrences generally are not calcareous, and pebbly sandstones were not observed within this facies. However, absence of evidence is not evidence of absence; in this context, it is noteworthy that some of the mudstone beds of facies 4VL are identical to those of facies 4VC in that they contain no positive evidence for a marine affinity, but they differ in that they are closely overlain and underlain by beds which do contain such evidence. Thus, the distinction between these two facies is tenuous in some places. In some occurrences, facies 4VC may in fact represent lagoonal deposits from an environment identical to that of facies 4VL.

Facies 4IF ("Interbedded Channel Fill"): Weakly bioturbated channel-fill deposit consisting of interbedded mudstones and (pebbly) sandstones.

This is the rarest facies encountered in this study, there being only 3 occurrences. Average facies thickness is 7.2 m (range: 6.3 to 7.7 m).



Lithology. This facies consists of interbedded mudstones and sandstones. The coarse beds range from very fine sandstone to very coarse pebbly sandstone. Maximum grain sizes observed in the three occurrences are:

Section CU-1: fine sand.

Section 4-19: medium sand.

Section 5-37: very coarse pebbly sandstone (pebbles up to 1.5 cm).

Both mudstones and sandstones contain fairly abundant macerated plant debris.

Bedding characteristics. Vertically, the sandstone/mudstone ratio is somewhat variable in all occurrences, averaging approximately 50% to 75%. All three occurrences of this facies consist of an interbedded,

overall thinning- and/or fining-upward sequence. The upper surfaces of all three occurrences are essentially planar and regionally flat.

All occurrences have erosional basal contacts (Fig. 4-30); at sections CU-1 and 4-19, the exposure reveals a channellized basal contact (see below). Channellization can only be inferred for the third occurrence. I shall first describe the large-scale channel geometry visible in two occurrences, and then describe the bedding characteristics of the material filling all three channels.

Discrimination between various erosional basal-contact geometries is difficult in outcrop studies of ancient rocks, due to the largely two-dimensional geometry of natural exposures. It is necessary to develop explicit and definitive criteria for the recognition and classification of the possible geometric relationships. Three possible geometries which could result in superficially similar exposures are:

1) an erosionally-based, tabular unit with localized, radially symmetrical or non-oriented scouring at the basal contact;
2) an erosionally-based, tabular unit with localized, elongate, oriented scouring at the basal contact;
3) an erosionally-based channel fill with localized, elongate, oriented scouring at the basal contact.

Figure 4-30. Examples of facies 4IF (interbedded channel fill), seen in sections normal to bedding (except photo C).

A) In this occurrence from section 4-19, up is to the left. Note angular relationship between erosional, channelized base and underlying non-marine deposits (dashed line). Field book below basal contact for scale. See additional photographs of this occurrence in B, C, & D.

B) Detail of basal sandstones from occurrence in A. Note angular basal contact (dashed line) and high-angle cross-bedding on inclined surface at lower left.

C) Sole view of biogenic structures near base of occurrence shown in A and B. Scale is 15 cm long.

D) A slightly different view of the occurrence in A, B, & C. Note multiple channels within this example, and extension of lateral accretion surfaces to the top of the occurrence (at left). This example is erosionally transgressed by mud-dominated deposits of association 1. Field book (circled) for scale.

E) Channellized base of occurrence at section CU-1. Up is to the right. Field book at bottom center of photo for scale.

A
B
C
D
E

In the first situation, non-oriented scours can probably be distinguished in extensive exposures by measuring the orientation of the sides of the scours. It may be very difficult to distinguish between the second and third situations, however -- in both cases, basal scours would appear oriented when several were measured, and a channelized sand body might appear to be tabular in nature if the outcrop extent is much less than the scale of the channel.

The only relatively certain method for the determination of a channellized geometry requires extensive (or favorable) exposures in which: 1) the inclination of the erosional basal surface relative to regional bedding attitude varies monotonically over the width of exposure (several meters or more), and 2) measured paleoflow directions from the base of the channel and/or within the channel fill are directed essentially at right angles to the dip of the channel wall.

These criteria for the tentative recognition of channellization in two-dimensional exposures are present in the two exposures of facies 4IF at sections 4-19 (Fig. 4-30A, 4-30B, & 4-30C) and CU-1 (Fig. 4-30C). In these occurrences, maximum inclination of the channellized base (relative to regional bedding) is about 25°; minimum inclination is 0°. Observed depth of erosion is a few meters in both occurrences.

Relative to regional bedding attitude, the lower beds in the two distinctly channelized occurrences (both sandstones and mudstones) dip in the same direction as the erosional channel base, but their magnitude of dip is less than that of the basal surface. Thus, the lower channel-fill beds pinch out against the channel floor/wall. Vertically, bedding inclination diminishes upward, and the upper beds of the channel fill are either regionally flat (sections CU-1 and 5-37) or inclined only a few degrees relative to the flat top of the channel fill (section 4-19). This geometry indicates a minor lateral component of accretion of sediment, largely restricted to the lower portion of the channel fill. Thickness of sandstone beds generally increases down-dip into the channel at the base; superimposed upon this trend is a tendency to pinch and swell in thickness laterally. Sandstones have a maximum thickness of about 50 cm; they average approximately 10 to 30 cm.

The third example (section 5-37) has an erosional, scoured base, but is essentially tabular over the extent of the exposure. In this occurrence, it is impossible to distinguish between the second and third geometries listed above. A channel geometry can only be tentatively inferred for this occurrence.

Physical structures. In contrast with the

interbedded sandstones and mudstones of associations 1 and 2, sole marks were only rarely observed on the sharp bases of sandstones in facies 4IF. Many sandstones of this facies are either graded or apparently structureless. Many display parallel lamination, either planar or gently pinching and swelling. Locally, small-scale asymmetrical ripple forms or trough cross-lamination are present in abundance within sandstones; at section 5-37, both asymmetrical and symmetrical ripples are present aburdantly. Medium-scale trough cross-bedding, dipping obliquely toward the channel wall (relative to regional bedding), was observed at the base of one occurrence (section 4-19, Fig. 4-30C).

Mudstones are either structureless or display wispy silt streaks. Small, shallow, silt-filled scours are locally present within mudstones.

Biogenic structures. Biogenic structures are locally abundant within all three occurrences of this facies. These structures are found in both sandstones and mudstones, and may be classified as plant-generated (sediment disturbance associated with rooting) or animal-generated (burrows).

Root casts were observed in only one occurrence (section CU-1). Sediment disturbance due to rooting is negligible in this occurrence. Root casts are confined to

the gradational upper contact of this occurrence and the overlying mudstones of facies 4VC, from which facies these roots apparently penetrate. This example of root casts is further discussed in the "note on stratigraphic context" below.

Animal-generated burrowing is locally abundant in all occurrences. Rare nondescript vertical and oblique burrows, Skolithos, and Planolites are scattered in low to moderate density throughout both sandstones and mudstones; abundant burrowing is confined to beds at or near the channellized base. In these localized zones of relatively high-density burrowing, the most common structures are vertical forms resembling Skolithos; horizontal forms resembling Planolites are also abundant on the bases of sandstones. A few forms resembling Teichichnus and Diplocraterion were observed. This assemblage of biogenic structures is characteristic of the Skolithos ichnofacies.

Macrofossils. No megascopic body fossils of animal origin were observed within facies 4IF; however, macerated plant debris is present in both occurrences. At two localities (sections CU-1 and 5-37), a large concentration of coalified woody material is present immediately above the channellized base. This material consists of decimeter-scale log fragments incorporated within the basal sandstones of the occurrence.

Note on stratigraphic context. At section CU-1, facies 4IF lies approximately 6 m above beach deposits (facies 3PL); the intervening material consists of rooted lagoonal/non-marine clayey mudstones (facies 4VL and 4VC). At this locality, facies 4IF is overlain by additional rooted mudstones, with roots penetrating down into the channel fill.

At section 4-19, facies 4IF occurs at a regional transgression, where it is underlain by rooted deposits and overlain by marine shales of facies 1SH.

Facies 4IF also occurs at a regional transgression at section 5-37, where it erosionally overlies upper shoreface to nearshore sandstone (facies 3SW) and is erosionally truncated by marine conglomerates of association 5.

Facies sequences are discussed briefly in the preliminary interpretations below, and more fully in chapter 5.

Summary: Basic distinguishing features. The basic distinguishing features which identify any single occurrence of facies 4IF are listed below:

1) Occurrences have an erosional channellized base (channelization can only be demonstrated unequivocally in favorable exposures).
2) The channel fill consists of thin, sharp-based, very

fine to very coarse sandstones (locally pebbly) interbedded with mudstone. Sole marks appear to be relatively rare.

3) The interbedded channel fill forms an overall thinning- and/or fining-upward sequence.

4) Internal lamination of sandstones consists of small-scale trough cross-lamination, parallel lamination, and/or graded bedding. Many sandstones are apparently structureless. Medium-scale trough cross-bedding occurs locally.

5) Sandstones are locally capped with straight-crested symmetrical ripples.

6) Animal-generated bioturbation (nondescript vertical and oblique burrows, many of which are lined) are present in very low density throughout the occurrence. Locally abundant burrowing (dominantly Skolithos, with Planolites in lower density, and rare Diplocraterion or Teichichnus) is confined to beds at or near the channellized base.

7) Abundant macerated wood fragments are present throughout the channel fill. Large coaly wood fragments are locally present in great abundance at the channellized bases.

Facies 4SF ("Sandstone Channel Fill"): Non-bioturbated, fining-upward channel-fill deposit consisting predominantly of fine sandstone to very coarse (pebbly) sandstone.



There are 16 occurrences of facies 4SF, having an average facies thickness of 4.9 m (range: 0.8 to 17.4 m).

Lithology. Each occurrence of this facies is composed predominantly of coarse clastic material, typically forming a fining-upward sequence. In most occurrences, dominant grain size ranges from fine sand to very coarse and/or granular sand. All occurrences of this facies contain sandstone at least as coarse as medium sand size. Sands typically are relatively poorly sorted in comparison with other sandstone facies. Pebbly sandstone and siltstone is present locally, as are beds of sandy or clayey coal.

Most pebbles in this facies are formed of varicolored chert. Sandstone pebbles are present locally, as are pebble-sized mudstone rip-up clasts and coalified wood fragments.

Sands are composed predominantly of quartz and varicolored chert, with a small but significant percentage of pink feldspar grains. Many occurrences contain fairly

abundant macerated plant material locally.

Rocks of this facies tend to be very well cemented and unusually hard, but generally not as hard as those of facies 3PL. Silica and siderite are the dominant cements. One occurrence is slightly calcareous. Some occurrences weather to a light grey color, but most are orange to bright orangey-red, due presumably to the siderite.

Lithological sequence. Typically, any single occurrence of facies 4SF forms a single fining-upward bed. The coarsest lithology is generally concentrated at the base, in approximately the basal 10% of the facies thickness. Typically, this basal interval consists of pebbly or granular medium to very coarse sandstone. The central 80% of the thickness of the occurrence is typically composed of medium sandstone fining upward gradually to fine sandstone. The uppermost 10% of the occurrence typically grades upward from fine to very fine sandstone (locally, to coarse siltstone). Superimposed upon this fining-upward trend in some occurrences are decimeter- to meter-thick, subtle, symmetrical coarsening- and fining-upward departures from the general trend.

Bedding characteristics. All occurrences of facies 4SF possess sharp erosional bases (Fig. 4-31B) which locally display oriented directional sole marks. All examples display shallow scours at their basal contacts, on

the order of a few meters wide and at least a few tens of centimeters in eroded depth. Extensive exposures generally reveal deep channellization at the basal contact. Criteria used to determine the presence of a channelled base are discussed under the description for facies 4IF above. Tops of occurrences generally are regionally flat and gradational into the overlying facies.

There are two major types of bedding within occurrences, corresponding to a large degree with the presence or absence of lateral accretion surfaces.

Typically, occurrences of this facies do not display lateral accretion surfaces; in these examples, each occurrence represents a single fining-upward bed (Fig. 4-31A, 4-31C, & 4-31D). Amalgamation surfaces and other prominent bedding planes were not observed, except at the very base of a few occurrences, where multiple, laterally extensive scour drapes indicate a composite or amalgamated sequence (see further discussion below). All vertical structure sequences (discussed below) exhibit essentially gradational contacts in these occurrences. Further, some examples which do display lateral accretion surfaces also exhibit fairly gradational vertical trends, suggesting quasi-continuous depositional conditions.

Most examples which do display large-scale lateral accretion surfaces over some large percentage of their thickness also exhibit an obvious composite or amalgamated

Figure 4-31. Examples of facies 4SF (sandstone channel fill) in sections normal to bedding.

A) Large-scale trough cross-bedding formed in medium-grained, slightly feldspathic sandstone. Note high-angle cross-strata and prominent erosional truncation of laminae in this section transverse to inferred flow direction. Scale is 15 cm long. Section 5-22, 67 m.

B) Sharply erosional basal contact of facies 4SF. Up is to the right. Very coarse to granular pebbly sandstone overlies fine marine sandstone. Note shale rip-up clasts. Scale is 15 cm long. Section PC-1, 12 m.

C) Medium- to large-scale trough cross-bedding formed in medium to coarse sandstone. Note uniform dip direction in cosets. Flow to the right in this flow-parallel section. Note 15 cm interval of plane parallel lamination immediately above hammer iron. Section ND-1, 47 m.

D) Same occurrence as in C, seen in flow-transverse section oriented roughly 90° to outcrop in C.

E) A thin example of facies 4SF. Prominent lateral accretion surfaces dip to right relative to regional bedding (sharp base of occurrence). Surfaces defined by alternation between sandstone and coaly mudstone. This example is overlain and underlain by rooted mudstones (association 4). Note thin non-marine sand at top of photo. Field book (circled) for scale. Section 4-23, 82 m.

A
B
C
D
E

bedding sequence (Fig. 4-31E). In examples of this sort, the units of amalgamation define the lateral accretion surfaces, and often extend obliquely across nearly the entire thickness of the occurrence. The amalgamation units typically begin with basal surfaces which vary locally, being gradational at some places and sharply erosional elsewhere. Erosional contacts are more common near channel bases; gradational contacts are more common near the tops of channels. These surfaces are overlain by sandstones which commonly contain mudstone rip-up clasts and/or coaly plant fragments near their bases. Each sandstone fines upward, passing gradationally into coaly mudstone and/or soft sandy coal to complete the amalgamation unit. Typically, amalgamation units are on the order of 25 cm to 100 cm in thickness (Fig. 4-31E); they generally thicken obliquely downward into the channel. Similarly, sandstone is relatively more abundant (and mudstone and coal less abundant) near the channel base. Typically, physical structures within sandstones also vary over the channel depth (see below); it is noteworthy, however, that many sandstones within amalgamation units are apparently structureless.

Physical structures. Typically, a vertical succession of primary physical structures is developed within any single occurrence of this facies. Internal

structure sequences are discussed under the following heading; individual types of structures are described separately in the following paragraphs.

1) Sole marks. Oriented sole marks (scratches and grooves) are fairly common from the bases of occurrences of facies 4SF. Locally, oriented directional marks are present (prods and flute casts).

2) Scour drapes. Scour drapes are mantles of medium to coarse (pebbly) sandstone which overlie the scoured basal contact of many occurrences. These drapes are either normally graded, or they display crude lamination or thin bedding. Stratification within these drapes generally conforms to the geometry of the basal scour surface, although there is a tendency for strata to flatten upward. Locally, multiple scour drapes are present above basal scours, suggesting an episodically repeated scouring process. These scour drapes probably were deposited from a high-concentration turbid bottom flow during the process of substrate erosion; they represent aggradation over an irregular topography during modified upper-stage plane-bed transport conditions.

3) Planar parallel lamination. Planar parallel lamination in this facies (Fig. 4-31C) is inferred to result from aggradation during upper-stage plane-bed transport (compare with Harms et al., 1982, Fig. 3-12).

4) Medium- and large-scale trough cross-bedding. Trough cross-bedding (Fig. 4-31A, 4-31C, & 4-31D) is inferred to result from aggradation accompanying the migration of large three-dimensional asymmetrical ripples (called "dunes" if formed under unidirectional flows, "megaripples" if formed under complex marine flows). Compare with figure 3-10 of Harms et al., (1982).

5) Small-scale trough cross-lamination. Small-scale trough cross-lamination is inferred to result from aggradation accompanying the migration of three-dimensional small asymmetrical ripples ("current" ripples). The angle of climb of these ripples was relatively low in comparison with #6 below (see Harms et al., 1982, Fig. 3-7B & 3-7C).

6) Climbing asymmetrical ripple cross-lamination. Climbing asymmetrical ripple cross-lamination is inferred to result from aggradation accompanying the migration of three-dimensional small asymmetrical ripples ("current" ripples). The angle of climb of these ripples was relatively high compared with #5 above (see Harms et al., 1982, Fig. 3-7D).

7) Lateral accretion surfaces. Lateral accretion surfaces (Fig. 4-31E) are inferred to result from the lateral migration (due to aggradation on an inclined surface) of a point bar within a subaqueous channel (see Harms et al., 1982, chapter 5).

Structure sequences. Typical vertical sequences of sedimentary structures are listed below. Note that large-scale lateral accretion surfaces are not included in this sequence listing, although they are present in some examples, and that sequences are listed from top to bottom:

Section 5-22 38.5 - 43.9 m	Section 5-22 51.4 - 69.0 m	Section 4-43 77.9 - 81.5 m
TXL	TXB	TXL + CRXL
TXB	TXB + PPL	TXB
PPL + TXB	TXB	SD
TXB	SD	
TXB + SD		

Where TXL = small-scale trough cross-lamination, CRXL = climbing asymmetrical ripple cross-lamination, PPL = planar parallel lamination, TXB = medium-scale trough cross-bedding, and SD = scour drapes, all described above.

The three vertical sequences listed above are representative of those observed in other occurrences. These structural sequences generally are consistent with an upward decrease in boundary shear stress (or mean flow velocity) in each occurrence (compare with Harms et al., 1982, Fig. 2-4). Note that this inferred upward decrease in flow strength is also consistent with the observed

fining-upward grain-size variation.

Biogenic structures. Root casts have been observed in numerous occurrences of this facies (Fig. 4-29C). Where present, root casts always cap channel sandstones, as described above.

In one occurrence (section 5-22, 43.7 m), a few small structures of problematic origin were observed at the gradational upper contact of this facies and overlying coaly mudstones assigned to facies 4VC. It is not clear whether these poorly defined, millimeter-wide, horizontal features actually represent animal-generated traces, and if so, whether they were formed by terrestrial or aquatic animals. With this single tentative exception, no animal-generated biogenic structures were observed in this facies.

Macrofossils. No macrofossils other than root casts, coalified wood fragments, thin sandy coals, and macerated leafy and woody fragments have been observed in this facies.

Root casts (where present) always cap channel sandstones. Decimeter- to meter-scale coalified wood fragments tend to be concentrated just above the channellized bases of sandstones. Thin sandy coals are locally present overlying laterally accreted sandstone beds, thus defining lateral accretion surfaces. Macerated

plant debris generally is concentrated at the bases of channels, but locally is present within "pockets" higher up within the channel fill in several occurrences.

Summary: Basic distinguishing features. The basic distinguishing features which identify any single occurrence of facies 4SF are listed below:

1) Occurrences are characterized by a distinctive, poorly sorted, medium to coarse sandstone, which locally is pebbly, coaly, and/or slightly feldspathic. Occurrences generally are at least a few meters thick.
2) Bases of sandstones are sharp and erosional, and locally are demonstrably channellized. Oriented directional sole marks are present locally.
3) Occurrences fine upward from (pebbly) coarse sandstone to medium sandstone. Fine sandstone or siltstone may be present at the top of occurrences.
4) A wide variety of primary tractional physical structures generally is present.
5) Structure sequences (and grain-size variation -- see #3 above) indicate an upward decrease in boundary shear stress and flow strength in each occurrence.
6) Lateral accretion surfaces are present in many occurrences.

7) Root casts are present at the regionally flat tops of many occurrences.

8) Macerated wood fragments are abundant, especially near the bases of occurrences.

9) Large coalified wood fragments (tens of centimeters in length) typically are present near the bases of occurrences.

10) Occurrences do not contain body fossils, animal-generated trace fossils, symmetrical ripples, or any other marine indicators.

Association 4: Preliminary Interpretation

With the exception of facies 4IF (described separately below) and certain occurrences of facies 4VL, occurrences of association 4 do not contain marine fauna or bioturbation. Most occurrences display root casts and abundant plant debris or coals. Thus, a lagoonal or non-marine origin can be inferred on paleontological grounds for all facies other than facies 4IF. This interpretation is substantiated in facies 4VL by generally weak bioturbation and a fresh- to brackish-water invertebrate faunal assemblage; the presence of lined burrows in some occurrences probably indicates at least a partial marine affinity, because terrestrial insects are not known to line their burrows (R. W. Frey and S. G. Pemberton, pers. comm., 1980).

The thick, poorly sorted, medium to coarse pebbly sandstones of association 4 (facies 4SF) are best interpreted as the fill of fluvial channels, probably shallow distributary channels in many occurrences (based upon their generally small thickness and close vertical proximity to beach and lagoonal facies). A fluvial interpretation is consistent with the assemblage of internal sedimentary structures (channellized bases, parallel lamination, trough cross-bedding, small-scale trough cross-lamination, lateral accretion surfaces, and

root casts capping the sandstones) and the general fining-upward nature of the thick sandstones.

The interbedded channel-filling sandstones and mudstones of facies 4IF display bioturbation attributable to marine fauna, but these biogenic structures occur in lower density than commonly is found in the demonstrably marine facies previously described. Additionally, traces are characteristic of the Skolithos ichnofacies, suggesting a relatively more energetic environment. Occurrences of facies 4IF are tentatively interpreted as estuarine (or possibly tidal) channel deposits. This interpretation is consistent with the relatively great abundance of wood fragments (compared with the marine facies) and the concentration of biogenic structures near the channel base, in what were presumably the deepest and most saline waters present within the estuarine channel. This interpretation is further supported by the stratigraphic context of the three occurrences (all are present immediately above nearshore, beach and/or lagoonal sediments, and two are present at regional transgression surfaces).

Association 5. Marine conglomerates.

This facies association contains coarse material deposited in a shallow marine environment. Lithologically, most occurrences consist of chert-pebble conglomerates with sandy, granular, or muddy matrix material; commonly, the matrix contains all of these grain sizes. Marine deposition is indicated by marine trace and body fossils, and by stratigraphic context (see chapter 5).

Fabric of these conglomerates was measured at numerous locations. Conglomerate fabric data are summarized in appendix 4.

N.B.: Facies 5CB, 5C1, and 5C2 described below are intergradational, and distinctions between these facies can occasionally be somewhat difficult. Likewise, facies 5C1 and certain of the facies in association 1 are also intergradational, as was discussed in the description of association 1. These intergradational relationships are discussed preliminarily in the following descriptions, and in further detail following the discussion of vertical facies relationships in chapter 5. An extended interpretation of certain Cardium conglomerates is presented in chapter 8.

Facies 5CV ("Coarse Veneer"): Very thin conglomerate veneers.

This is the most commonly encountered facies in association 5 (31 occurrences). Facies thickness is negligible; occurrences typically are only a single clast diameter in thickness.

All occurrences of this facies consist of an erosion surface (in several cases, possibly just a non-depositional surface) overlain by scattered pebbles or granules of varicolored chert (Fig. 4-32). Rarely, one or a few cobbles are also encountered within this veneer (Fig. 4-32A), and a few occurrences are composed predominantly of chert cobbles ranging up to 20 cm in maximum diameter. Cobble lithology is discussed in detail below. In a few occurrences, chert granules and very coarse sand are the dominant component of the veneer, and very small pebbles constitute only a very minor component. Clasts are commonly widely spaced over erosion surfaces (Fig. 4-32A & 4-32B); thus, a large percentage of the surface may be devoid of clasts. Locally, clasts are closely packed over the entire surface. In one occurrence (section BD-1, 37 m level), patches of coarse sand and granules are scattered

Figure 4-32. Examples of facies SCV (very thin conglomerate veneers). All occurrences cap thickening- and coarsening-upward sequences.

A) Plan view of scattered pebbles and small cobbles of varicolored chert, present as a veneer over a thick marine sandstone of association 3. Shale chips at bottom of photo are derived from fine-grained marine deposits which immediately overlie this veneer. Scale is 15 cm long. Section 4-21, 120 m.

B) A band of pebbles and small cobbles seen in a section normal to bedding. Pens point to larger clasts. This occurrence separates interbedded hummocky sandstones and mudstones (association 2, underlying) from mud-dominated marine deposits (association 1, overlying). Note that pebble band immediately overlies very silty mudstone, and is immediately overlain by less silty mudstone. Section 4-23, 39 m.

C) Oblique plan view of the top of a cycle. Relative to photo, beds dip at shallow angle toward the camera and to the left. Thick beds to right of hammer are conglomerates of facies SC2; these are overlain by a thin pebble veneer at end of hammer handle. This veneer has a sandy matrix, and is overlain by mud-dominated deposits of association 1. Section 5-45, 156 m.

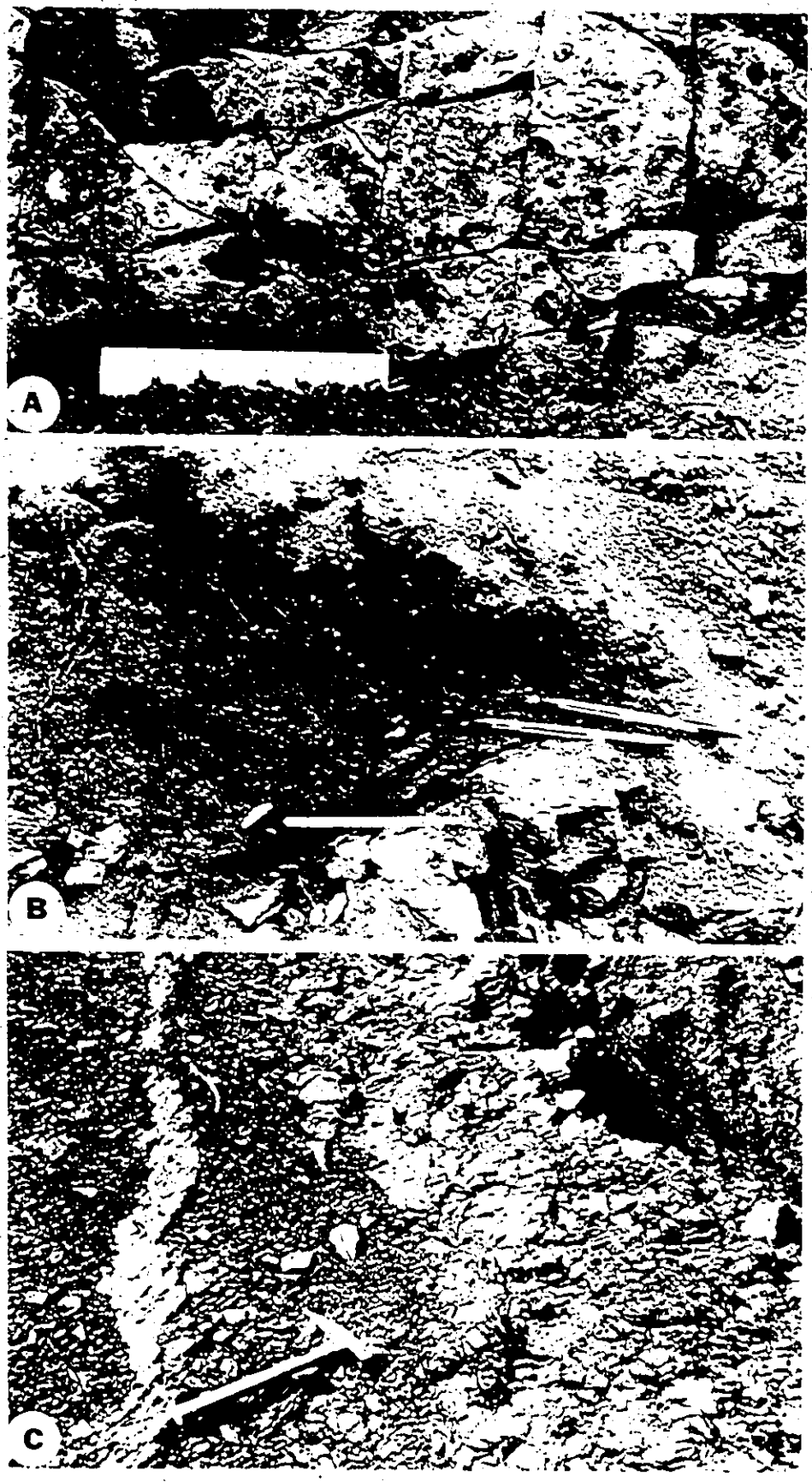
A
B
C

over the erosion surface along with sparsely scattered, small pebbles and reworked Ophiomorpha burrows. These Ophiomorpha burrows are identical to those found in place within the underlying sandstone.

Erosion surfaces. The surfaces underlying the pebble veneers of facies SCV can usually be identified as erosional by one or more of the following characteristic features:

1) Erosion surfaces usually lie upon sandstones within which laminae are erosively truncated by the basal surface of the veneer.

2) Long, linear grooves are occasionally present in the tops of underlying sandstones, immediately below the pebble veneer. These grooves are always aligned with one another; they commonly are steep-sided (i.e., steeper than the angle of repose), suggesting that the underlying sandstone was cohesive (due to early cementation) prior to development of the erosion surface.

3) Negative-relief structures resembling positive-relief flute casts are locally (rarely) present on the upper surfaces of sandstones underlying pebble veneers, again suggesting erosion of partially consolidated sand.

4) The previously mentioned occurrence of reworked Ophiomorpha burrows within a pebble veneer strongly suggests removal of a significant thickness of sand from

the deposit immediately underlying that veneer.

5) In the pebble-dominated occurrences, pebbles usually are well sorted. Locally, well-sorted pebble veneers contain one or a few cobbles much larger than the typical grain size of the occurrence. The lithology of most of these cobbles suggests that they were originally formed as nodules within fine-grained sediment (see further discussion below). Such an origin implies extensive erosion of penecontemporaneously deposited shale/mudstone prior to formation of the pebble veneer.

Coarse veneer. The coarse material overlying the erosion surface of facies 5CV varies in grain size from coarse sand and granules to cobbles. All coarse clasts are composed of varicolored chert, regardless of grain size. Most facies 5CV occurrences are composed predominantly of pebbles.

Pebble- and cobble-dominated occurrences are rarely greater than one or two grain diameters in thickness. Sand/granule occurrences, however, may be several (about 5 to 20) diameters in thickness. In these occurrences, the sand and granules generally are patchily distributed; rare small pebbles typically are present also.

In the pebble-dominated occurrences, the distribution of clasts over the erosion surface is variable. Typically, these veneers display many fewer

pebbles/square meter than would be present if the clasts were closely spaced over the surface. Thus, a large percentage of the erosion surface may be devoid of pebbles. Although pebbles may locally be imbricated one against the other, pebble-dominated occurrences of facies 5CV are never greater than two diameters in thickness.

Cobble-dominated occurrences are closely packed and approximately one clast diameter in thickness; in these occurrences, cobbles are well-sorted and consist of varicolored chert. However, most cobbles in this facies, as in all other facies of association 5, occur as isolated large clasts within a pebble-dominated veneer which otherwise is well-sorted. These cobbles commonly consist of black siliceous material which resembles the nodules encountered in the marine shales/mudstones throughout the entire formation. This siliceous material may be black chert or siliceous mudstone. Unlike the other clasts, these cobbles typically exhibit a punky, reddish-orange weathering rind similar to the rind found on in situ nodules. This rind probably consists largely of siderite. These cobbles are best interpreted as erosional remnants of a thick, locally eroded shale/mudstone interval.

Matrix of coarse veneers and relationship with overlying facies. The intervening material between coarse clasts within facies 5CV typically bears a distinct

similarity to the rocks of the immediately overlying facies. Facies 5CV conglomerates are always overlain by mud-dominated facies of association 1. The matrix of a coarse veneer rarely consists of argillaceous sandstone or sandy mudstone; typically, the matrix is mudstone or shale identical in appearance to the overlying mudstone or shale. Furthermore, thin silty laminae within this mudstone occasionally are observed to drape over immediately underlying chert clasts.

Biogenic structures. Reworked Ophiomorpha burrows from this facies have previously been described. Additionally, the matrix of coarse veneers occasionally contain in situ nondescript vertical and oblique burrows (0.5 to 2 cm diameter).

Macrofossils. Several ammonites (genus Scaphites) were observed within pebble veneers of facies 5CV. One of these (at section 5-22, 38 m level) was vertically embedded (i.e., the plane of symmetry of the coil was roughly normal to bedding). Vertically embedded ammonites can sometimes be used as paleodepth indicators; however, it is likely that this shell was emplaced as a clast, and no paleobathymetric significance is inferred. Inoceramus and Cardium valves also are common; in one occurrence, an Inoceramus valve encrusted with bryozoans (Fig. 4-26) was closely associated with a veneer.

Note on stratigraphic context. All examples of facies 5CV occur at the tops of coarsening-upward cycles. However, the converse is not true -- not all cycle tops are capped with facies 5CV. Occurrences of this facies lie upon knife-sharp erosion surfaces which separate cycles. As further discussed in subsequent chapters, these contacts are inferred to represent erosional transgression surfaces associated with rapid local or regional deepening within the basin.

Summary: Basic distinguishing features. The basic distinguishing features which identify any single occurrence of facies 5CV are listed below:

1) Occurrences consist of a thin veneer of granules and/or pebbles (locally, cobbles), usually no more than a single clast diameter in thickness, overlying an erosion surface.
2) Clasts may be densely packed or widely scattered over the erosion surface.
3) All examples of this facies occur immediately above erosional boundaries between cycles.
4) Cobbles are present locally as sparsely scattered, unusually large clasts within pebble-dominated occurrences. These cobbles are inferred to have originally formed as nodules within penecontemporaneously deposited fine-grained

sediments.

Facies 5CB ("Bioturbated Conglomerate"): Thick units of intensely bioturbated argillaceous pebbly sandstone or sandy pebbly mudstone.

This facies was encountered only 4 times in this study. Thickness ranges from 1.9 to 3.0 m (average: 2.6 m).

Facies 5CB is composed of exceedingly intensely bioturbated material (Fig. 4-33). It always represents a thorough mixture of sediments of highly variable grain sizes (Fig. 4-33C); lithologically, occurrences of this facies may be described either as argillaceous, pebbly sandstones or sandy, pebbly mudstones, depending upon abundance of sand-sized material. The sand fraction of the matrix often is very coarse and may contain a large percentage of granule-sized grains (Fig. 4-33C).

Largest clasts. Small cobbles are the largest clasts observed within this facies; maximum diameter varies between 0.4 and about 7 cm. Large clasts generally are well-rounded, oblate to prolate, varicoloured chert; their abundance is usually very low, representing only a few

percent of the volume of the rock (i.e., these are very matrix-rich matrix-supported conglomerates). In some occurrences, larger clasts are locally grouped together abundantly in small, equant "pockets" (roughly 10 to 30 cm in width, slightly less in thickness; see Fig. 4-33D). Within these pockets, the abundance of large clasts is as high as approximately 30%, and clast-clast contacts have been observed.

Matrix and biogenic structures. The matrix between clasts is a variable mixture of clays, silt, sand, and (locally) granules (Fig. 4-33C). The coarser grains of the matrix are composed of varicolored chert and quartz. Typically, the matrix has a ropy, knotted, or mottled texture characteristic of intense bioturbation. Nondescript vertical and oblique burrows are abundant. On a centimeter scale, sand/granule content varies widely within the matrix: patches of sand and granules may define irregular centimeter-scale vertical, oblique, or horizontal burrows. Irregular, large, horizontal and slightly oblique burrows, referable to the ichnogenus Thalassinoides, can occasionally be distinguished (2 to 10 cm diameter, 15 to 100 cm in length). These burrows are locally observed to be branching. In some occurrences (Fig. 4-33E), they are morphologically identical to the "subway tunnel" burrows observed within Cardium sandstones at Seebe by Wright &

Figure 4-33. Examples of facies 5CB (bioturbated conglomerate). All sections are normal to bedding (except G).

A) Bands of concretions in pebbly, gritty, sandy mudstone. Note ropey or mottled appearance of outcrop. Section 5-45, 125 m.

B) Blocky weathering pattern of facies 5CB (resistant bed forming the ridge). Same occurrence as A.

C) Gritty, sandy matrix of facies 5CB. Note mottled texture and absence of lamination. Coin is 2.4 cm in diameter. Section 5-45, 162 m.

D) A concentrated "pocket" of large clasts. Scale is 15 cm long. Same occurrence as C.

E) Large horizontal Thalassinoides. Coin is 2.1 cm in diameter. Same occurrence as A & B.

F) Inoceramus fragments. Scale is 15 cm long. Same occurrence as C & D.

G) Plan view of a portion of a large coalified wood fragment. Coin is 2.4 cm in diameter. Same occurrence as A, B, & E.

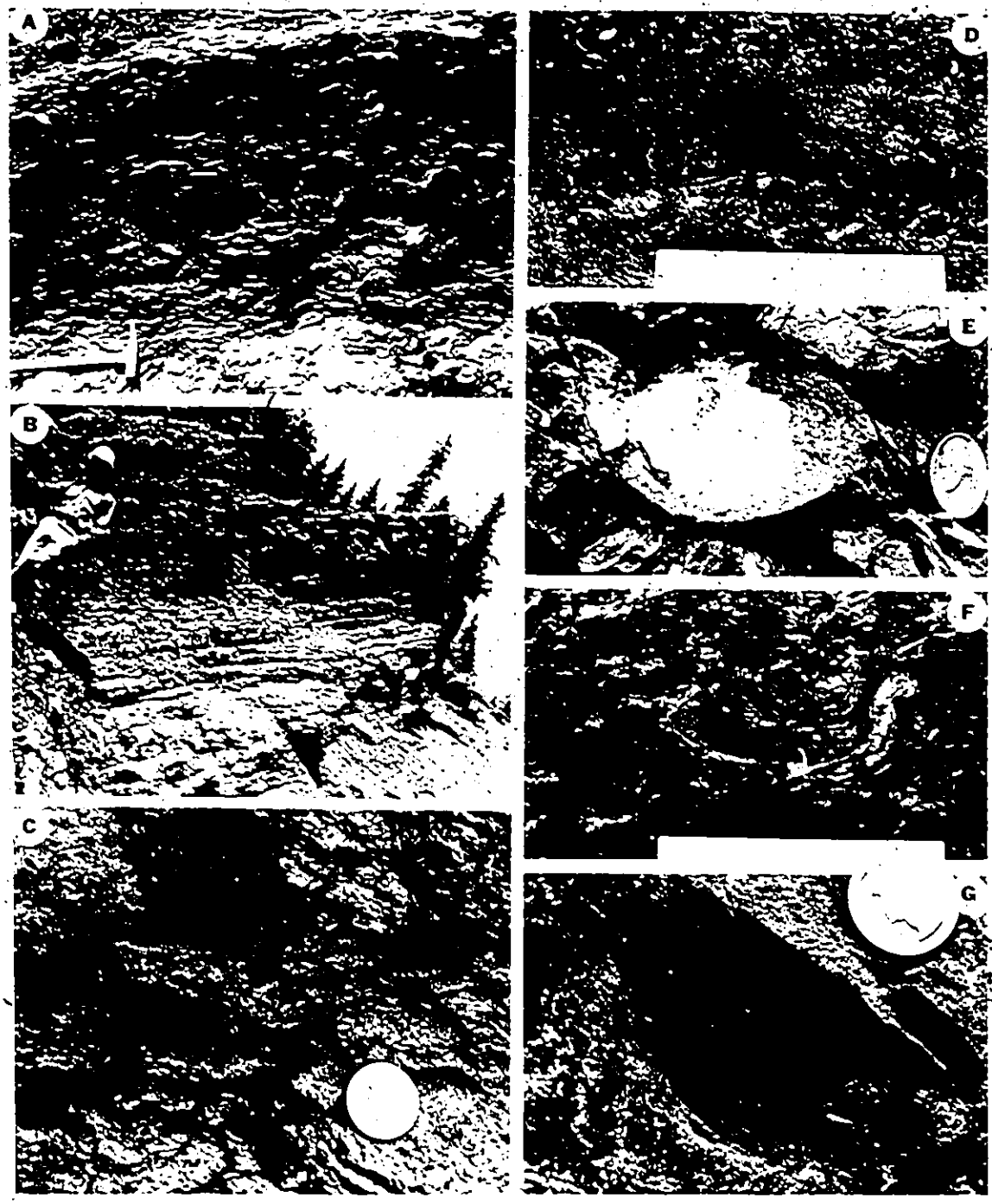
A
B
C
D
E
F
G

Walker (1981, Fig. 11 -- see further discussion by Pemberton et al., 1984, who suggested an origin due to the extinct lobster Linuparus canadensis). Problematic Ophiomorpha burrows are observed locally. Some of the large, irregular burrows in this facies apparently are lined with granules or small pebbles.

The difficulty in recognizing many of the biogenic structures in this facies is probably in part attributable to the coarse grain size of the sediment. The general dominance of large vertical and oblique structures, including Ophiomorpha and Thalassinoides, suggests that this assemblage probably is best referred to the Skolithos ichnofacies (Frey & Pemberton, 1984).

Lenticles of bedded siltstone/sandstone are locally preserved from bioturbation within the matrix of some occurrences of facies 5CB. These lenticles are remnants of thin (2 to 10 cm), sharp-based, parallel and undulatory parallel laminated beds.

Crude bedding. Typically, facies 5CB deposits possess an extremely crude bedding. This bedding often resembles that of facies 5C1 or 5C2 (see below), and a gradational spectrum between the three facies can be inferred from the many intermediate examples present within occurrences of these facies. There are two types of crude bedding within facies 5CB:

1) Bedding within the matrix, consisting of lenticles of bedded siltstone/sandstone, has been described above. This type of bedding bears a distinct similarity to that of facies 5C1 and 5C2, which in turn is similar to facies 1GB occurrences which contain thin "stringers" of coarse material. These inter-relationships are discussed further under a separate heading below.

2) Bedding involving clasts and matrix is similar to that of facies 5C2. This type of bedding occurs on a larger scale than that described above, and these two types of bedding co-exist in some occurrences. Bedding involving clasts and matrix is usually very crude, and consists of horizontal bands or rows in which pebble abundance is increased slightly over that of the surrounding material. Usually, only a few such bands are present, and these have a thickness of roughly 30 cm. Interbedded material with lower pebble abundance has a similar or greater thickness. Bands of concretions are present locally (Fig. 4-33A)

Macrofossils. Megascopic body fossils from this facies include abundant Inoceramus fragments from every occurrence (Fig. 4-33F). On average, and very approximately, one or two such fragments are observed per square meter of outcrop surface. Additionally, at one location (section 5-45, 136 m level) a carapace fragment of the decapod Linuparus was collected from this facies. This

fragment resembles the Linuparus canadensis carapace collected by Wright and Walker (1981, Fig. 13) at Seebe.

Abundant wood fragments are present in each occurrence of this facies; some of these coaly fragments are up to 20 cm long and 3 cm wide (Fig. 4-33G).

Summary: Basic distinguishing features. The basic distinguishing features which identify any single occurrence of facies 5CB are listed below:

1) Occurrences are composed of intensely bioturbated argillaceous pebbly sandstone or sandy pebbly mudstone.
2) All occurrences are exceedingly intensely bioturbated. Typically, the rock has a ropy or knotted texture. Poorly defined burrows, some very large, are occasionally recognizable. The assemblage of biogenic structures is probably best interpreted as representative of the Skolithos ichnofacies.
3) A marine origin is indicated by abundant Inoceramus fragments in most examples.
4) Coalified wood fragments are locally abundant.

Facies 5Cl ("Minor Bedded Conglomerate"): Thin sharp-based beds of conglomerate (generally matrix-supported) within mudstone or pebbly mudstone.

I encountered 12 occurrences of this facies. Average facies thickness is 0.4 m (range: 0.1 to 0.8 m).

This facies is composed of thin, laterally extensive beds (or equant, localized "pockets") of conglomerate in mudstone (Fig. 4-34). Mudstone is the dominant lithology. Conglomerate consists of oblate to prolate pebbles (usually 0.5 to 2 cm long-axis diameter) and granules of varicolored chert. Rarely, mudstones are sandy (always coarse to very coarse varicolored sands, probably composed largely of chert) or "gritty" (i.e., containing dispersed granules, also composed of varicolored chert).

Bedding characteristics of conglomerates. Conglomerate beds generally are very extensive laterally (across the entire width of outcrop -- locally, several hundred meters), yet are only a few clast diameters in thickness (roughly, a few centimeters to a decimeter thick). Pebbles typically are not in contact with one another (i.e., they are matrix-supported). Locally,

pebbles are widely dispersed, constituting only a small percentage of the volume of a conglomerate bed. Such beds may be termed matrix-rich. In most occurrences, however, the pebble abundance is significantly higher; within many of these thin conglomerate beds, pebbles occupy approximately 50% of the rock volume. In these "concentrated" or clast-rich conglomerate beds, the mudstone matrix typically is very sandy. In several of these beds, pebbles are actually in contact with one another (clast-supported); the matrix of these beds generally is very fine to fine sand. Thus, as pebble abundance increases, so does the mean grain size of the matrix material within conglomerate beds. The more highly concentrated pebble beds typically exhibit sharp bases, and "coarse-tail" grading within the pebble size range is developed locally (i.e., pebbles become less numerous upward into the overlying mudstone).

The matrix-rich, matrix-supported conglomerate beds exhibit a somewhat variable geometry. In many instances, the rather diffuse nature of these conglomerates causes them to appear as thin bands or "stringers" of pebbles widely scattered along certain horizons within an otherwise homogeneous mudstone (Fig. 4-34C). Locally, equant "pockets" of pebbles within mudstone are present: these often occur below conglomerate bands, apparently representing load-balls formed by the localized foundering

Figure 4-34. Examples of facies SC1 (minor bedded conglomerates), seen in sections normal to bedding. Scale is 15 cm long.

A) Thin, sharp-based pebble bed showing coarse-tail grading. Note relief on basal surface due to localized erosion and possible loading. Clasts are supported by one another at base of bed, and by matrix material at top of bed. Note widely dispersed pebbles and granules in underlying mudstone.

B) Thin, sharp-based, graded bed of clast-supported pebbles overlying sandstone. This bed is too thick to be classified as a veneer (facies SCV) and too thin to be included within facies SC2 (major conglomerates).

C) Widely dispersed pebbles within a mudstone bed. Note concentration of pebbles at base of bed (behind scale), resulting in coarse-tail grading.

A
B
C

of a pebble band into underlying quick mud.

Mudstones between conglomerate beds. The mudstone-dominated sediments between conglomerate beds of facies 5C1 typically are identical in every major feature with the deposits of facies 1SH, 1BM, 1GB, and/or 1UP. Most commonly, these deposits are identical to facies 1GB, and include thin, sharp-based siltstone/sandstone beds exhibiting Bouma sequences. Rarely, a thin graded interval at the base of these Bouma sequences contains grit and/or coarse sand. The more intensely bioturbated occurrences, resembling facies 1BM, are locally gritty or sandy as in facies 5CB. See further discussion under "Note on stratigraphic context" below.

Biogenic structures. Biogenic structures within this facies typically resemble those of association 1 (transitional between the Zoophycos and Cruziana ichnofacies). Locally, however, vertical and oblique Ophiomorpha burrows are also present in low to moderate abundance.

Macrofossils. Ammonites (genus Scaphites) were observed in several occurrences of facies 5C1. Body fossils from the Cardium Formation are illustrated in figure 4-26.

Note on stratigraphic context. As mentioned in the

description of facies 1GB, conglomerates of facies 5C1 commonly are overlain gradationally by facies 1GB or 1UP, in which are locally developed thin, sparsely scattered conglomerate beds or "stringers". Likewise, the distinction between sparsely conglomeratic deposits of association 1 and mudstone-rich deposits of facies 5C1 is at places somewhat arbitrary. Generally, deposits which contain over 1 m of non-conglomeratic mudstone between thin conglomerate stringers have been separated from facies 5C1 and included in the appropriate facies of association 1. These relationships are further discussed and interpreted in chapter 5.

Summary: Basic distinguishing features. The basic distinguishing features which identify any single occurrence of facies 5C1 are listed below:

1) Conglomerates of this facies are interbedded with mudstones. Conglomerates generally are present in thin, laterally extensive, matrix-rich, matrix-supported pebbly horizons: the matrix is mudstone. Locally, pebbles occur in thin, sharp-based, matrix- or clast-supported beds, occasionally graded; the matrix is sandstone in these beds. Conglomerate beds generally are only a few centimeters thick. Loading of conglomerate into mudstone is present locally.

2) Conglomerate beds are separated by centimeters or decimeters of mudstone-dominated sediment similar to that of association 1 (most typically, similar to facies 1GB or 1UP).

3) The trace fauna assemblage is similar to that of association 1 (transitional between the Zoophycos and Cruziana ichnofacies); locally, however, fairly abundant vertical and oblique Ophiomorpha also are present.

4) This facies exhibits intergradational relationships with facies 5CB and 5C2, as well as with facies of association 1.

Facies 5C2 ("Major Bedded Conglomerate"): Thick sharp-based beds of conglomerate (generally clast-supported conglomerate).

I encountered 20 occurrences of this facies. Average facies thickness is 2.5 m (range: 0.9 to 7.2 m).

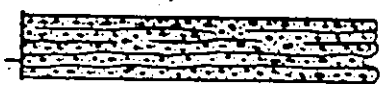

This facies is composed of thick beds of conglomerate, locally interbedded with mudstone (generally gritty and/or sandy) or argillaceous sandstone (generally gritty). In other occurrences, conglomerate is not

generally is gritty. In other occurrences, conglomerate is not interbedded with finer material, but occurs either as a single discrete bed or as a composite or amalgamated unit consisting of numerous discrete conglomerate beds (Fig. 4-35, second plate; see also the sections discussing conglomeratic symmetrical ripples in chapters 5 and 8). Conglomerate beds interbedded with mudstones typically are several centimeters to a few decimeters in thickness; in some examples, conglomerate occurs as an amalgamated bed a few meters in thickness. Conglomerate consists of oblate to prolate pebbles (usually 0.5 to 5 cm long-axis diameter) and granules of varicolored chert. In some examples, cobbles of varicolored chert also are present (Fig. 4-35H). These cobbles have measured lengths up to 12 cm; some broken clasts were observed which originally may have been as long as about 20 cm.

Bedding characteristics of conglomerates.

Typically, each occurrence of facies SC2 has an erosional basal contact with the underlying facies (Fig. 4-35C & 4-35F). Criteria for the recognition of an erosion surface have been reviewed under the description of facies SCV above. Erosion of the underlying material is made even more obvious in facies SC2 by 1) injection of conglomerate along underlying sandstone laminae below the erosional contact (Fig. 4-35F), and 2) incorporation within

occurrences of facies SC2 of large rip-up clasts or blocks of the underlying lithology (Fig. 4-35E).

The conglomerates of facies SC2 occur in discrete, laterally extensive beds which locally exhibit a variety of sedimentary structures. Occurrences of conglomerates in this facies invariably display sharp bases (Fig. 4-35F); locally, elongate scours or sole marks are present at the bases of beds. Conglomerate beds typically are normally graded and/or imbricated; pebbles usually are clast-supported (Fig. 4-35F & 4-35H). Matrix typically is gritty sandstone or gritty argillaceous sandstone; in some occurrences, however, matrix material is gritty or sandy mudstone. Tops of conglomerate beds either 1) are erosionally truncated by an overlying sharp-based conglomerate, 2) pass gradationally into pebbly, gritty mudstone or sandstone (see below), or 3) are sharp, locally displaying conglomeratic symmetrical ripples (chapters 5 and 8) with characteristic spacings of approximately 1 m. Internally, conglomeratic symmetrical ripples occasionally reveal crude cross-stratification indicating vertical aggradation with or without lateral migration of the symmetrical ripple form. Chapter 8 includes a quantitative paleohydraulic analysis of these ripples.

Mudstones and sandstones between conglomerate beds. In occurrences of facies SC2 in which sharp-based

Figure 4-35 (two plates). Examples of facies SC2 (major bedded conglomerates). All photos show sections normal to bedding (except E, G, & H).

A) Conglomerates and sandstones interbedded with mudstone. Up is to right. Book rests on sandy conglomerate; next bed up is hummocky sandstone. Section 4-43, 168 m.

B) Thick sharp-based conglomerates interbedded with mudstone and thin, gritty sandstones. Section 5-45, 165 m.

C) Thick sandy conglomerates and pebbly sandstones interbedded with mudstones and thin, gritty sandstones (indicated by pens). Up is to right. Section 5-19, 95 m.

D) Sharp-based gritty sandstones and small burrows between conglomerates shown in C. Coin diameter is 2.4 cm.

E) Plan view of pebbly sandstone from occurrence in B; note small pebbles (lower right) & outline of large sandstone clast (left of pen). Pen indicates large wood fragment.

F) Sharply erosional basal contact of conglomerate over sandstone. Up is to right. Note injection of pebbles into sandstone at center of photo, and sharp top of conglomerate. Scale is 15 cm long. Section BD-1, 5 m.

G) Oblique plan view of conglomerate bed sharply overlying sandstone. Note large cobbles. Section 5-19, 85 m.

H) Plan view of part of bed in G. Note bimodal size distribution in this clast-supported conglomerate, with long axes of cobbles up to 12 cm. Scale is 15 cm long.

D
A
C
B

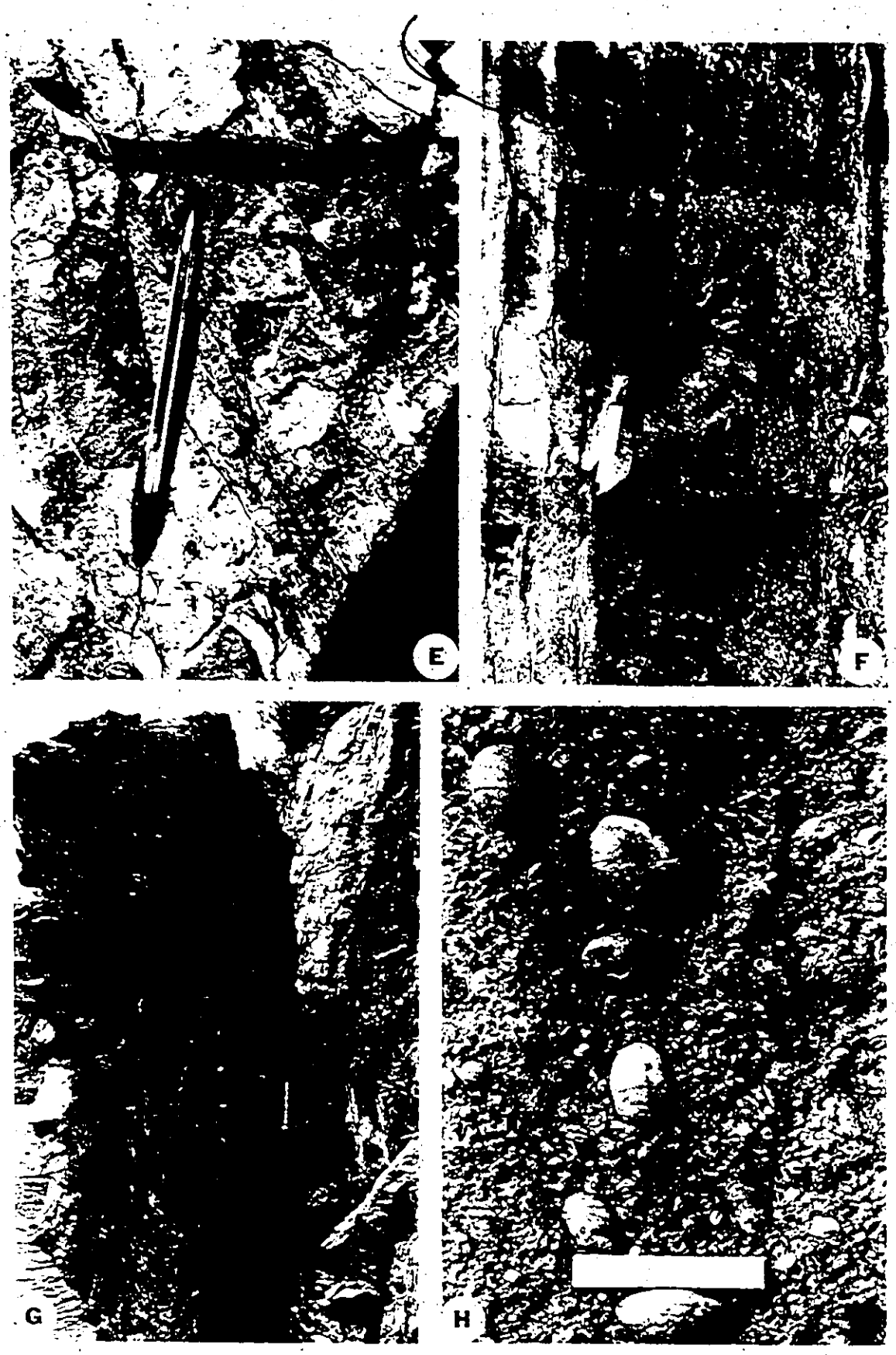
E
F
G
H

conglomerate beds are interbedded with finer material, that material typically is similar to the bioturbated pebbly sandstone/mudstone of facies 5CB (Fig. 4-35D). In most cases, interbedded material consists of extensively bioturbated argillaceous gritty sandstone; it represents a mixture of all grain sizes between clay and granules. Thin, sharp-based sandy or gritty beds typically are preserved from complete bioturbation (Fig. 4-35B, 4-35C, & 4-35D); locally, sandstone beds are 10 cm or more in thickness, and are hummocky cross-stratified (Fig. 4-35A). Less frequently, bioturbated mud-size material is dominant (gritty sandy mudstone). In many cases, interbedded material is sparsely pebbly; usually, these rare pebbles are significantly smaller than the pebbles within the conglomerate beds.

Biogenic structures. Where present, biogenic structures within this facies generally are large and ill-defined; smaller forms are also commonly present in the interbedded sandstones and/or mudstones (Fig. 4-35D). The larger forms are identical to those of facies 5CB above; they probably are best referred to the Skolithos or Cruziana ichnofacies, and are restricted to the mudstones and sandstones present locally between bedded conglomerates. Bioturbation such as this suggests an intergradational relationship between facies 5CB (without

bedded conglomerates) and facies 5C2 (bedded conglomerates present).

Macrofossils. Inoceramus and ammonite fragments are present locally within facies 5C2. The Inoceramus fragments are restricted to bioturbated finer materials; the ammonite fragments are rare, and were restricted to a few of the bedded conglomerates. Body fossils from the Cardium Formation are illustrated in figure 4-26.

Abundant coalified wood fragments similar to those of facies 5C3 are common within both the bioturbated finer materials and the coarser conglomeratic beds (Fig. 4-35E).

Summary: Basic distinguishing features. The basic distinguishing features which identify any single occurrence of facies 5C2 are listed below:

1) Conglomerates of this facies occur in thick, laterally extensive, sharp-based beds which typically are graded and/or imbricated. Bed thickness typically is several centimeters to a few decimeters; locally, beds are a few meters thick. Conglomerate beds are locally capped with conglomeratic symmetrical ripples.
2) In many occurrences, conglomerate beds are separated by centimeters or decimeters of relatively finer bioturbated material similar to that of facies 5C3

-- a heterogeneous mixture of mud, sand, granules, and (locally) scattered pebbles.

3) The assemblage of trace fauna within the interbedded bioturbated material is similar to that of facies 5CB (large and small, generally ill-defined vertical, oblique, and horizontal structures, possibly representative of the Skolithos or Cruziana ichnofacies).

4) Coalified wood fragments generally are present in abundance.

5) This facies exhibits intergradational relationships with facies 5CB and 5C1.

Association 5: Preliminary Interpretation

The assemblage of abundant trace and body fossils within association 5 unequivocally indicates a marine depositional environment for these conglomerates.

Characteristic facies sequences (discussed in chapter 5) likewise unequivocally indicate that many of these marine conglomerates are associated with periods of transgression (see below).

The occurrence of multiple sharp-based, graded beds suggests active transport of conglomerate during periods of transgression. As shall be discussed in chapter 7, fabric data from many of these conglomerates indicate a long-axis-parallel imbrication, in which the A-axis is parallel to the flow direction inferred from imbrication. This type of imbrication suggests transport of coarse clasts as a dispersion above the bed, rather than by tractional rolling in contact with the bed (Walker, 1984c). Dispersion of pebbles and development of a good imbrication fabric indicate deposition from powerful unidirectional flows. The local development of conglomeratic symmetrical ripples at the tops of association 5 occurrences indicates local modification by powerful oscillatory flows.

The above evidence suggests that transgressions within the Cardium which are marked by the conglomerates of association 5 appear to be divided into two phases:

1) During the onset of transgression, pronounced erosion took place on a local or regional scale, as indicated by the erosional basal contacts of the various conglomeratic facies and by other evidence of local cycle truncation (chapter 5).

2) Erosion was followed by a depositional period during which time the rate of deposition was probably greatly reduced (relative to regressive periods), as indicated by extensive bioturbation. Conglomerates were deposited within the basin from powerful unidirectional flows, and were locally modified by powerful oscillatory flows.

The probable source of pebbles during transgression, therefore, may be either from erosion of underlying material and/or from some other source, possibly the transgressing shoreline. In either case, conglomerates have been extensively transported and redeposited; they do not represent simple erosional lag deposits. Reflecting this possible mixed-mode origin (discussed further in later chapters), I propose the term <u>resedimented-lag deposits</u> be introduced in reference to the conglomerates of this association.

BRIEF SUMMARY OF INFERRED DEPOSITIONAL ENVIRONMENTS

Association 1. Hemipelagic mudstones and very thin siltstones and sandstones deposited in a distal offshore setting.

Association 2. Interbedded mudstones and storm-deposited sandstones from an intermediate offshore setting.

Association 3. Thick shoreface-attached sandstones deposited in the storm-dominated proximal offshore to foreshore regions.

Association 4. Lagoonal, fluvial, and lower coastal plain (non-marine) deposits.

Association 5. Marine conglomerates, most of which were deposited during transgression as resedimented lags.

CHAPTER 5. VERTICAL FACIES RELATIONSHIPS: THE DEFINITION AND PRELIMINARY INTERPRETATION OF CYCLES

INTRODUCTION

In this chapter, I discuss vertical facies sequences observed in exposures of the Cardium Formation, and their relationship to the major cyclic developments ubiquitous within this formation.

All exposures studied consist of one or more clastic marine cycles. Typically, these cycles are thickening- and coarsening-upward; locally, however, certain cycles are symmetrical, such that they first thicken and coarsen upward in their lower part, and then thin and fine upward in their upper part. In these symmetrical cycles, the lower thickening/coarsening interval is always much thicker than the upper thinning/fining interval.

Cycles are a few meters to a few tens of meters in thickness. They are sharply bounded, well developed, and immediately obvious in the field (Fig. 5-1; see also the photographs in appendix 1).

Internally, cycles display a variety of essentially similar facies sequences. Because most exposures consist

Figure 5-1. A completely typical thickening- and coarsening-upward cyclic development in the Cardium Formation (cycle 7, section 7-1). Person at basal boundary of cycle (at right) for scale; his hand is on the basal contact with an underlying cycle. Note upward increase in sandstone thickness and abundance, accompanying an upward decrease in mudstone thickness and abundance. Also note minor cyclic development near center of photograph superimposed upon the general trend. Many additional cycles (both single developments and multiple, vertically juxtaposed developments) are illustrated in appendix 1.



of several cycles juxtaposed vertically, these exposures typically display a sequence of facies which obviously is largely repetitive. There are two basic approaches which one can bring to the analysis of cyclicity in natural phenonmena: 1) cyclicity can be objectively determined by means of statistical analysis, or 2) cyclicity can be determined by the subjective synthesis of observations. With respect to cyclic sequences in sedimentary rocks, the most widely employed statistical technique is that of Markov-chain analysis (specifically, a one-step embedded Markov-chain analysis -- see below). On the other hand, a subjective analysis usually consists of the worker's conceptual synthesis (or "gut feeling") regarding the nature of cyclicity in the unit examined.

Both statistical and subjective syntheses of data have their advantages and pitfalls. Statistical techniques carry the advantage of rigorous numerical solution; they are best applied to situations in which preferred transitions are only slightly more common than random, and thus are difficult to detect subjectively. The problem of non-ergodic sedimentary processes (i.e., processes involving systematic spatial and/or temporal variation not accommodated within a statistical averaging process) is inherent in any analysis; likewise, concurrent multiple data trends involving the same transition elements (in this case, facies) are especially difficult to detect in a

one-step analysis such as those commonly employed. Multi-step analyses increase resolution, but are much more difficult to construct. Thus, although numerically rigorous, the statistical techniques can sometimes be of limited value; in exceptional cases, they may even be very misleading. By way of illustration, consider a situation involving pronounced inhomogeneous and/or non-stationary processes (i.e., processes involving systematic spatial and temporal variation, respectively) yielding a non-ergodic data base, in which, for example, fining-upward cycles are vertically and/or laterally juxtaposed with coarsening-upward cycles composed of the same facies as transition elements. A one-step statistical treatment of a similar number of each type of cycle could produce near zero observed-minus-random transition probabilities, whereas in actuality, the facies are arranged in strongly non-random sequences.

On the other hand, the subjective synthesis of field data following careful comparison of measured sections can be useful in evaluating systematic vertical or lateral variability within <u>obviously</u> cyclic sequences. Such analysis inevitably is frought with personal bias, however, and it is of little value in complicated sequences, or sequences with transition probabilities approaching random values.

The Cardium Formation is perhaps typical of most

clastic units in that cyclicity is immediately apparent even to the casual observer (Fig. 5-1 & appendix 1), but a fairly wide variation in facies sequence exists within these cyclic developments (see below). In such a situation, one may easily be lulled into the belief that a subjective synthesis may be adequate, although this may well be an incorrect assumption. Regarding the application of statistical techniques, the problem of non-ergodic depositional processes is a major concern in Foothills sections (e.g., non-marine facies are restricted to the northern half of the field area, and thick marine sandstones are best developed in mountain-proximal inner Foothills sections); likewise, at least two basically different types of cycles appear to be developed in most exposures (i.e., fully bioturbated vs. weakly bioturbated cycles -- see below). Perhaps of even greater concern is the observation (mentioned above) that both thickening- and coarsening-upward sequences and thinning- and fining-upward sequences composed of the same facies elements are present in numerous exposures. In a one-step analysis, these sequences will act in effect to cancel one another partially, thus falsely increasing the apparent randomness of sequences.

To summarize these introductory remarks, it seems prudent in my analysis of vertical trends within the Cardium to attempt to integrate the objectivity of

statistical techniques with the geological insight developed over several years of involved study on my part. To that end, I shall first present my subjective synthesis of field data, and then compare these results to those of the Markov-chain analysis. This procedure will lead to the recognition of a set of cycle "types" characteristic of the Cardium Formation in Foothills exposures. Facies defined in chapter 4 will then be re-interpreted in light of observed facies sequences, following a re-description of certain features best considered within their stratigraphic context. Finally, preliminary environmental interpretations of the typical facies sequences associated with different cycle types will then be assigned.

NOTE ON STATISTICAL METHODS UTILIZED HEREIN

For the statistical analysis of vertical facies relationships within the Cardium, I have employed an iterative proportional fitting technique developed by Powers & Easterling (1982). This technique was developed to produce a more accurate random-transition matrix for one-step embedded Markov-chain analyses in which self-transition (e.g., facies A to facies A) is denied. Random transition probability is subtracted from observed transition probability to yield residual probability (p_r).

This residual probability may be either positive or negative, and offers a relative indicator of preferred facies sequences within the sample set.

Statistical significance for individual transitions was evaluated using the method advocated by Harper (1984). In this method, the significance of each set of transitions from one facies to any one other facies is evaluated by calculating the binomial probability for randomly encountering the observed number or a greater number of transitions. This probability is subtracted from unity to give the statistical confidence (c) of each transition for which residual probability is positive. Details of both procedures may be determined from the original papers or from the code of program "Markov" (available from the author -- see further discussion below).

Universally, Markov-chain analysis has been employed in sedimentary geology to determine characteristic sequences of facies, lithologies, etc. The purpose is to recognize underlying patterns within complex vertical sequences; to filter the signal from the obscuring noise. The goal is to descern geologically significant vertical sequences. However, statistical significance and geological significance are very different concepts. The methods described above may result both in high residual (observed minus random) probability and statistical confidence for transitions which are not geologically

significant to a normative determination. In particular, these techniques cannot discriminate between significant non-random transitions which occur rarely, and those which occur commonly. An illustrative example of this problem is discussed in detail later in this chapter.

Traditionally, the only way to determine the normative significance of any particular transition has been to subjectively re-examine the data. Herein I have developed a simple quantitative method which represents an improvement over this technique. The new method is described below.

The procedure outlined below is utilized as a final "filter" following the determination of non-random transitions having high confidence values (utilizing the methods of Powers & Easterling, 1982, and Harper, 1984). It is applied only to those transitions which have arbitrarily defined high values of both residual probability and statistical confidence. The procedure is to calculate the total number of observed transitions from facies i to facies j for all transitions, and to compare these figures to the total number of transitions observed. The more commonly observed transitions are geologically more significant to a normative determination than are those less commonly observed, assuming the same or similar residual probability and statistical confidence.

The probability of encountering a particular

transition (say, from facies i to facies j) can be written as $p_{i,j}$ and is given by

$$p_{i,j} = n_{i,j} / T$$

where $n_{i,j}$ is the number of transitions from facies i to facies j, and T is the total number of transitions in the data set. The mean of all positive (i.e., non-zero) probability values may be written as p^*; this value represents a benchmark to which individual transition probabilities may be compared. The "relative transition probability" ($r_{i,j}$) for the transition from facies i to facies j is given by

$$r_{i,j} = p_{i,j} - p^*$$

The relative transition probability r is herein referred to as the significance parameter. Positive values of significance correspond to transitions which are more common than the mean; those with negative values are less common. This quantity permits comparison of transitions which have equally (or similarly) high values of both residual probability and statistical confidence. Use of this significance parameter is illustrated below, and is discussed in detail later in this chapter.

It is important to emphasize that the significance parameter r is meant to have a narrowly-defined application; specifically, it is used only to eliminate

from a normative sequence those transitions which are relatively rare in comparison with other transitions, according to some arbitrarily defined cut-off value of r. [Usually this value is zero.] The eliminated transitions are not to be regarded as having no geological significance; rather, they are simply of reduced significance to a normative sequence.

A self-explanatory, user-interactive BASIC program (program "Markov") was written by the author to handle all statistical computations outlined above. A listing for program Markov is available from the author.

GENERALIZED DESCRIPTION OF CARDIUM CYCLES

Before I subjectively define a set of cycle types for the formation, a few additional generalized remarks regarding the nature of Cardium cycles is in order.

As stated above, thick coarsening-upward cycles constitute the bulk of Cardium sediment in each exposure examined. Typically, each cycle displays knife-sharp contacts with the underlying and overlying cycles; these contacts commonly are erosional.

Cardium cycles generally appear to be either "complete" or "truncated" versions of a single basic facies sequence. This basic "complete" cycle is described in the

generalized terms of facies associations below.

Complete cycles begin in the mud-dominated facies of association 1. A thickening- and coarsening-upward tendency is generally well-developed in the very thin siltstones and sandstones of these mud-dominated deposits. Association 1 is overlain by interbedded sandstones and mudstones of association 2. Typically, these sandstone beds also thicken- and coarsen-upward, and they in turn are overlain by the thick sandstones of association 3. Non-marine deposits of association 4 cap complete cycles. Cycles typically display sharp upper contacts which locally are accentuated by the marine conglomerates of association 5; locally, thin intervals of thinning- and fining-upward deposits may also be present at the tops of cycles. These deposits in turn are immediately overlain by the basal mudstones of the overlying cycle (association 1).

The sequence described above represents a <u>fully regressive</u> "<u>complete</u>" <u>cycle</u> (Fig. 5-2, left), in which is recorded a depositional transition from marine to non-marine sediments. The return to offshore muds, generally marked by a knife-sharp erosional contact, represents a transgression of the sea probably accompanied by decimeters or meters of shoreface and floodplain erosion. The subject of shoreface erosion during transgression has been discussed in detail by Curray (1964) and, more recently, in a series of papers by Swift (see

Figure 5-2. One scheme for the classification of Cardium cycles. Top-absent cycles are by far the most abundant; cycle "types" defined in this chapter are based upon variation within the top-absent group (including one fully regressive type). The rarer middle- and bottom-absent types (and combinations of these attributes) are ignored in the scheme of six cycle types proposed herein. Nevertheless, these rarer types have great sedimentological significance. See text for further discussion.

ANY TYPE OF CYCLE MAY BE CAPPED WITH TRANSGRESSIVE CONGLOMERATES AND/OR THINNING- AND FINING-UPWARD INTERVALS, IN EITHER ORDER.

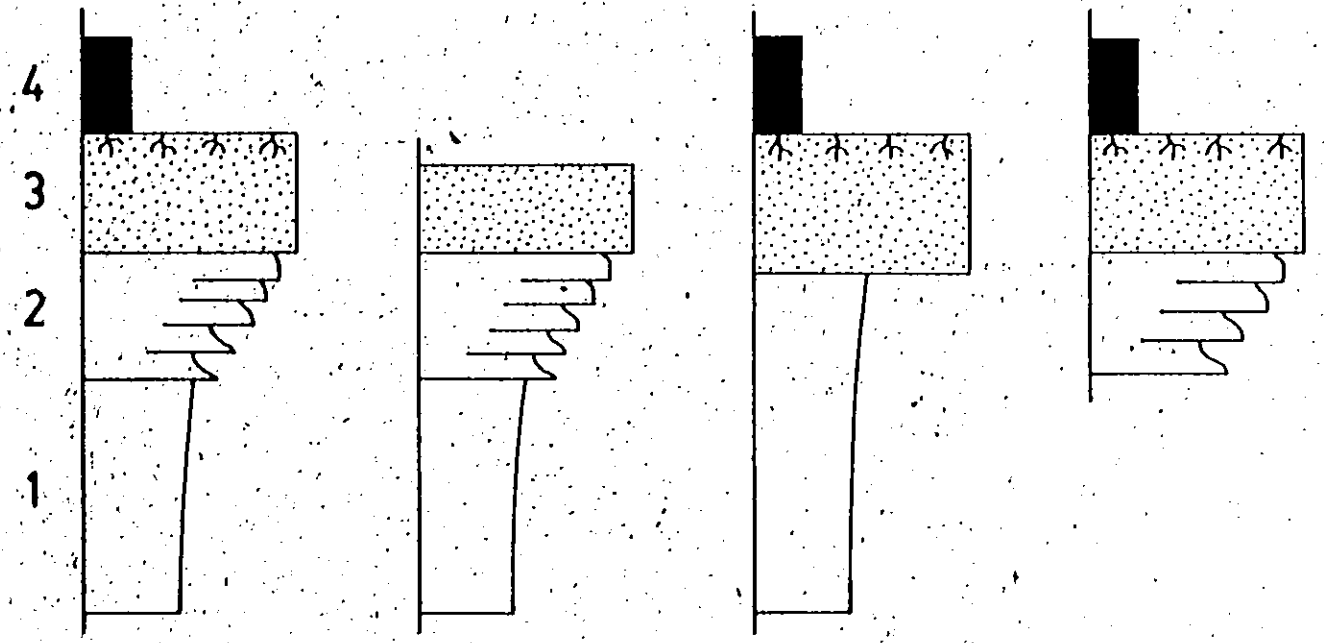

FULLY REGRESSIVE "COMPLETE" CYCLES

TOP-ABSENT CYCLES

MIDDLE-ABSENT CYCLES

BOTTOM-ABSENT CYCLES

summary by Swift, 1976); further discussion will be provided in chapter 6.

Various partial or "incomplete" versions of the basic cycle are present within the formation. Incomplete cycles are illustrated diagrammatically in figure 5-2. Coarsening-upward cycles beginning in association 1 may be sharply terminated at any level (i.e., within any association). Partial or incomplete cycles which begin in association 1 but do not record a transition to non-marine sedimentation may be termed top-absent cycles. Coarsening-upward cycles which are fully regressive but do not commence with association 1 are termed bottom-absent cycles. Cycles which display an abrupt transition from association 1 to association 3 are termed middle-absent cycles. Of course, various combinations of absent associations within cycles are possible, and are observed rarely. An example of a cycle truncated both at the top and the bottom is also illustrated in figure 5-2.

The majority of Cardium cycles are complete or top-absent varieties. For this reason, the subjective cycle-classification scheme described below is based upon variation within the top-absent group, and the presence or absence of associations 1 or 2 lower in the cycle does not come into consideration. The sedimentological significance of those few cycles which are bottom- or middle-absent will be discussed following the basic cycle-type descriptions.

FACIES SEQUENCE ANALYSIS, AND THE DEFINITION OF CYCLE TYPES

Following preliminary field work for this study, several different types of cycles were subjectively defined, each type consisting of a typical facies sequence (R. G. Walker, pers. comm., 1979; Duke, 1980). The preliminary set of cycle types defined by Duke (1980) has been modified below, following a subjective synthesis of all field observations. This modified classification of cycles defines typical facies sequences within the Cardium Formation.

Following detailed examination of 28 Cardium exposures containing 134 major cyclic developments, I have subjectively recognized six basic cycle types (see below).

Subjective Classification of Cycle Types

I have subjectively recognized six different types of cycles within the Cardium Formation. All six types defined below are generally thickening- and coarsening-upward; note, however, that examples of each type are locally capped with marine conglomerates and/or thinning- and fining-upward intervals:

Cycle Type 1: Fully regressive coarsening-upward cycles which terminate with low-angle planar or parallel laminated sandstone (facies SPL)

and/or non-marine deposits of association 4.

Cycle Type 2: Coarsening-upward cycles which terminate with swaley cross-stratified sandstone (facies 3SW).

Cycle Type 3: Coarsening-upward cycles which terminate with amalgamated hummocky cross-stratified sandstones (facies 3HA).

Cycle Type 4: Coarsening-upward cycles which terminate with interbedded mudstones and hummocky cross-stratified sandstones of association 2.

Cycle Type 5: Coarsening-upward cycles composed entirely of the mud-dominated facies of association 1.

Cycle Type 6: Coarsening-upward cycles which are extensively bioturbated throughout their entire thickness. Rarely, these cycles display thin, less strongly bioturbated intervals in which various facies of association 1 are recognizable. Type 6 cycles always commence with bioturbated mudstone (facies 1BM) and terminate with bioturbated sandstone (facies 3BS).

The six cycle types defined above are described more fully

in a subsequent section. Below, I shall utilize Markov-chain analysis in an attempt to rigorously corroborate this set of subjectively recognized cycle types.

Markov-Chain Analysis

The results of Markov-chain analysis are presented in the remainder of this chapter in the form of numerous spider's web diagrams (see below). The original data from which these diagrams were constructed are summarized in tabular form in appendix 4.

Figure 5-3 is the residual (observed-minus-random) probability diagram for facies transitions in the Cardium Formation. This diagram is based upon 595 observed facies transitions (all that were observed). Figure 5-3 shows all and only those facies transitions which occur statistically more frequently than if all transitions were random; it is extremely complicated, owing to the large number of facies involved. A simplified version is presented as figure 5-4, in which are shown only those transitions with high residual probabilities. Before spending time examining the complete residual probability diagram, it is advisable that one first become familiar with the simplified diagram, which will be discussed first below.

With three exceptions, the simplified residual

Figure 5-3. Residual probability diagram for all observed transitions in the Cardium Formation. This diagram is "complete" in that it shows all transitions with positive residual probabilities; it does not show transitions with residual probabilities less than or equal to zero. See text for discussion.

CARDIUM FORMATION, ALL TRANSITIONS

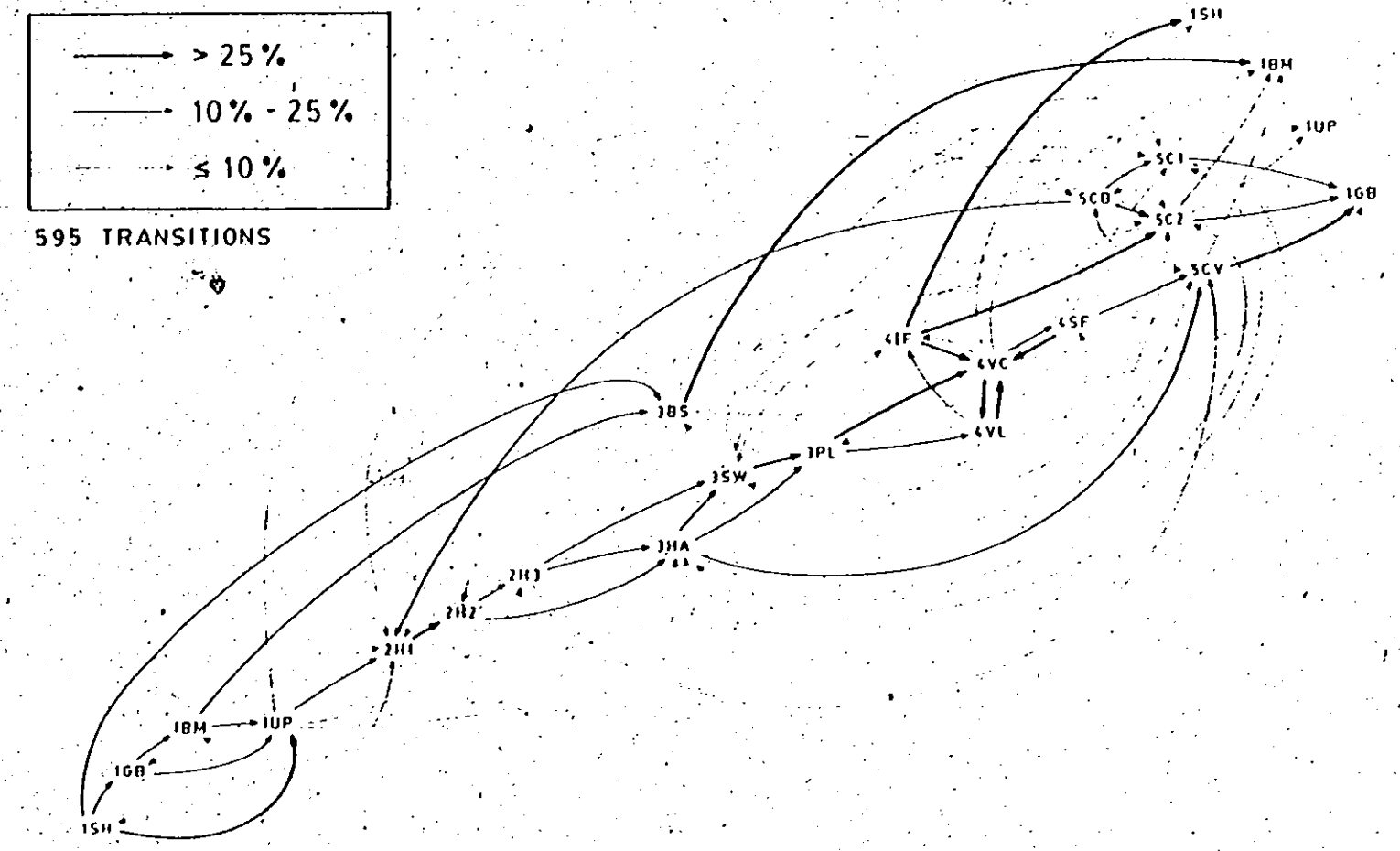

Figure 5-4. Simplified residual probability diagram for all observed transitions in the Cardium Formation. See text for discussion.

CARDIUM FORMATION, ALL TRANSITIONS

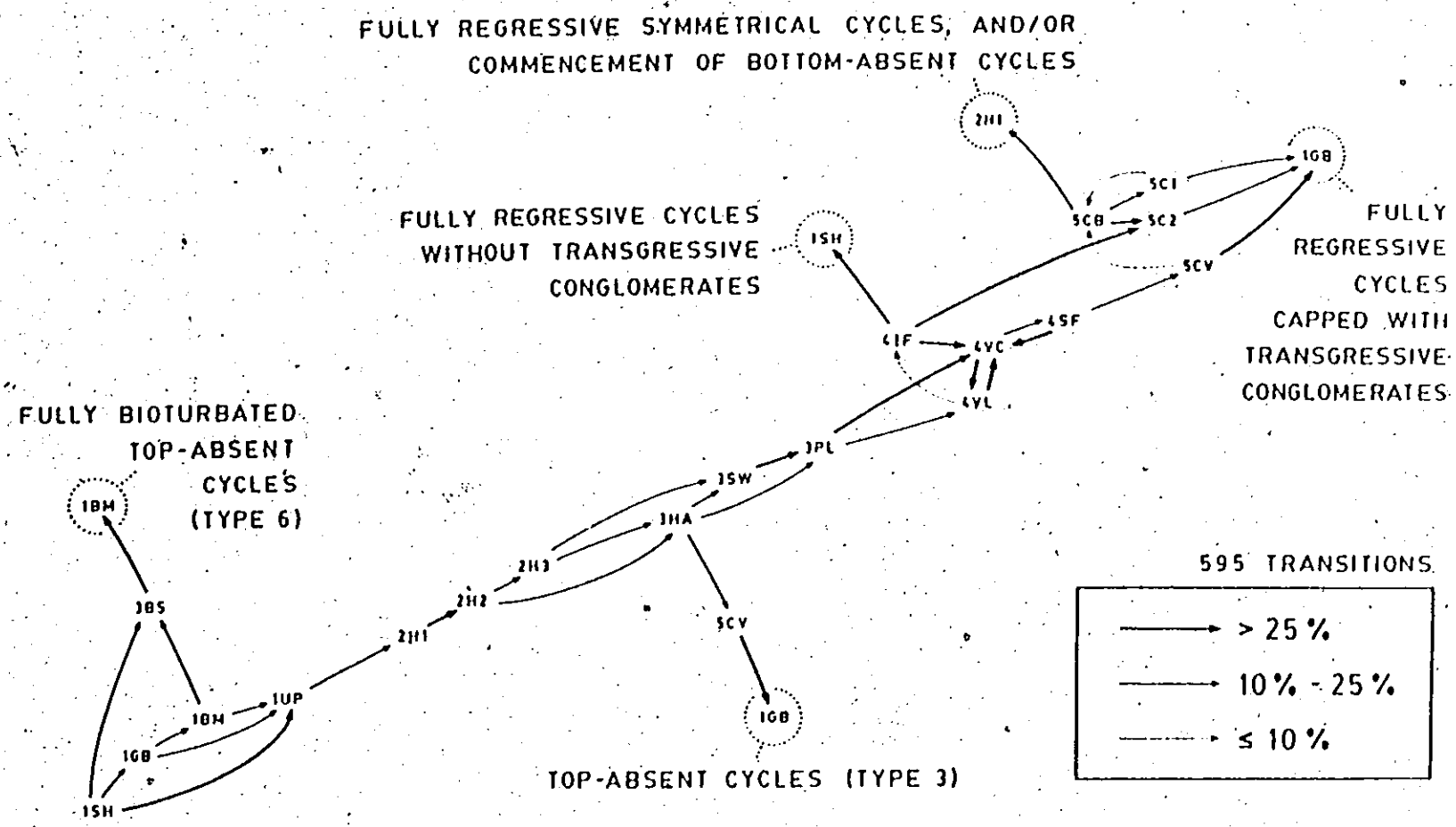

probability diagram (Fig. 5-4) shows only those transitions with residual probabilities greater than 10%. The three exceptions were included to permit entry into facies 5CB and 4IF, which do not lie over any facies with probability greater than 10%. These three low-probability transitions are those with the highest values which allow entry to these two facies. Examination of this diagram reveals five broad categories of cyclicity, each of which is discussed below.

Beginning in association 1 at the lower left of the diagram, the first cyclic sequence is labelled "fully bioturbated top-absent cycles (type 6)". Coarsening-upward cycles of this sort are terminated in facies 3BS, and are underlain by various facies of association 1. In these cycles, facies 3BS completes the sequence with a return to facies 1BM of association 1.

Another top-absent cycle is the next coarsening-upward sequence encountered in this diagram; it is labelled "top-absent cycles (type 3)". Cycles of this sort likewise begin in various facies of association 1, which are overlain by facies of association 2, which in turn are overlain by facies 3HA. The cycle is completed with the vertical transition through marine conglomerates of facies 5CV into facies 1GB of association 1.

The third cycle type encountered on figure 5-4 is labelled "fully regressive cycles without transgressive

conglomerates", and includes, in ascending order, various facies from association 1, 2, 3, and 4. This is a type 1 cycle. The cycle is completed with the transition back to facies 1SH of association 1. Because this cycle begins in association 1 and ends in association 4, it may be regarded as a "complete" cycle.

The fourth cyclic sequence, labelled "fully regressive symmetrical cycles, and/or commencement of bottom-absent cycles", is open to a variety of different interpretations. These cycles also are fully regressive (type 1), but are not "complete" in that they do not return to the mud-dominated deposits of association 1. Strictly interpreted, these cycles commence in facies 2H1 of association 2, coarsen upward through association 2 into associations 3, 4 and 5, and then return to facies 2H1; thus, they are bottom-absent cycles. However, because this is only a one-step analysis, it is probable that included in this type of cyclic development are fully regressive "complete" cycles overlain by bottom-absent cycles. Likewise, it is probable that the occurrences of cycles terminating in facies 2H1 include some examples of the symmetrical cycles described above; in these occurrences, facies 2H1 would represent the base of a thinning- and fining-upward cap of inferred transgressive deposits. The relationships between these various possibilities will be clarified in subsequent sections of this chapter.

Finally, the fifth cycle type recognized in this diagram is labelled "fully regressive cycles capped with transgressive conglomerates". These are "complete" type 1 cycles displaying, in ascending order, various facies of associations 1, 2, 3, and 4; they terminate with trangressive conglomerates (various facies of association 5) overlain by facies 1GB of association 1.

Having become familiar with the simplified residual probability diagram, it is now possible to examine the complete diagram (Fig. 5-3) more easily. Note in this figure that many of the low-probability arrows indicate transitions from facies of associations 1, 2, or 3 into facies of association 5; these correspond to various varieties of top-absent cycles (types 2 to 6). Examples include the transitions from 1UP to 5CB, from 2H3 to 5CV, and from 3SW to 5C2. A few of the other arrows indicate transitions opposite in sense to the more probable transitions; these probably correspond in part to the thinning- and fining-upward cycle caps previously mentioned. Examples of these transitions include those from facies 2H3 to 2H1, and from 1UP to 1SH.

Figure 5-5 shows transitions which have residual probabilities in excess of 10% and statistical confidence values of 90% or more. It is noteworthy that there are several other transitions not shown on this diagram which are statistically confident at this high level, but have

residual probability values less than 10%. Such transitions (although statistically confident) probably are not geologically significant to a normative determination because their observed probability values are very close to being random; however, I emphasize that the 10% cut-off was arbitrarily chosen to simplify the facies relationships. Figure 5-5 is largely similar to figure 5-4, but reveals that the sequence termination corresponding to symmetrical and/or bottom-absent cycles is not statistically confident at this high level.

Finally, figure 5-6 shows facies relationships following application of the final "significance filter" developed in this thesis. Facies 4IF (three occurrences only) has been eliminated in this step, and relationships within association 5 have been somewhat simplified. Close comparison of the simplified residual probability diagram (Fig. 5-4), the confidence diagram (Fig. 5-5), and the significance diagram (Fig. 5-6) permits the recognition of a standard facies sequence, presented along the main diagonal of figure 5-6. This diagonal represents the standard Cardium facies sequence.

This first level of facies sequence analysis corroborates the subjective recognition of coarsening-upward cycles as the major repetitive components of the formation; additionally, this analysis confirms the existence of cycle types 1, 3, and 6. A more refined

Figure 5-5. "Confidence" diagram for all observed transitions in the Cardium Formation. See text for discussion.

CARDIUM FORMATION, ALL TRANSITIONS

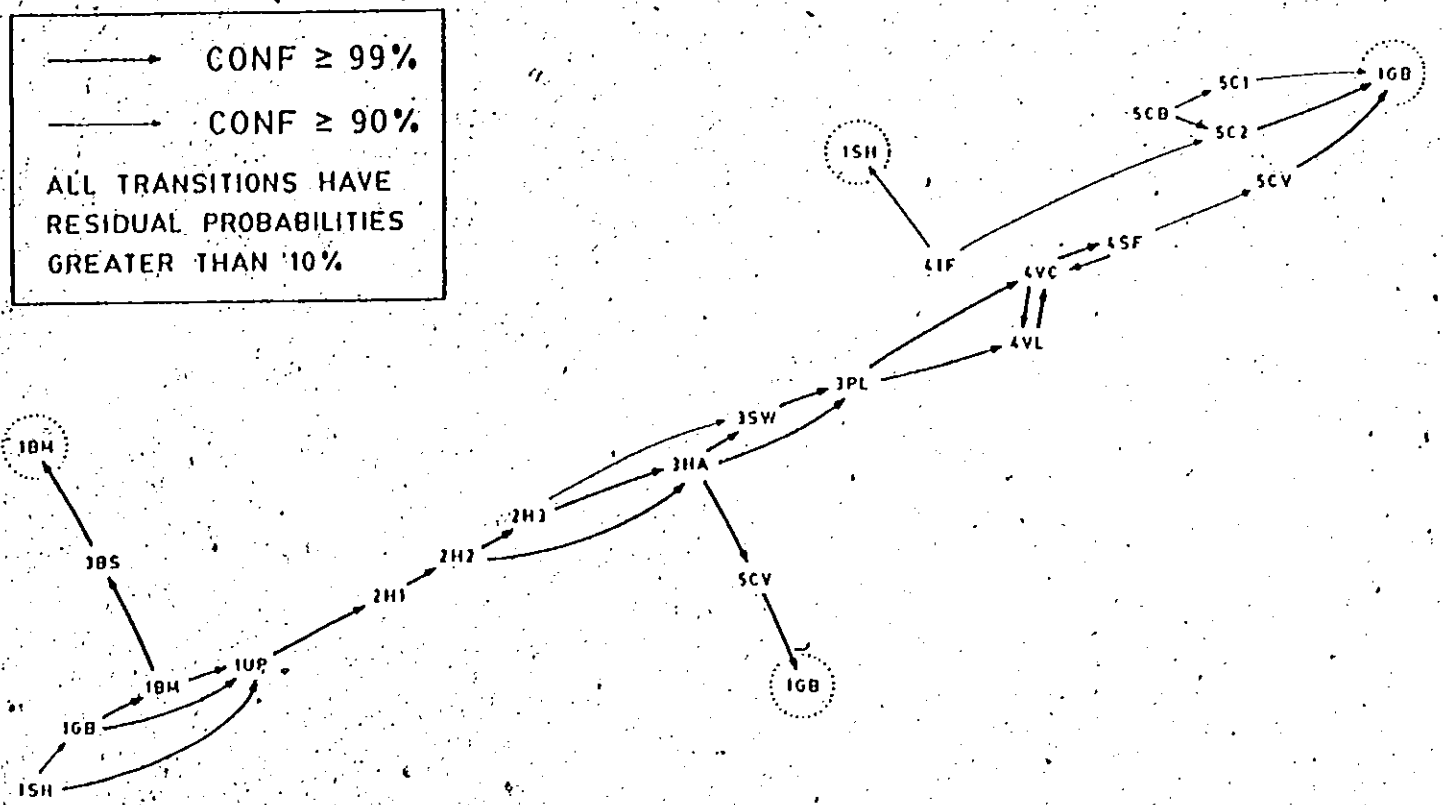

Figure 5-6. "Significance" diagram for all observed transitions in the Cardium Formation. See text for discussion.

CARDIUM FORMATION, ALL TRANSITIONS

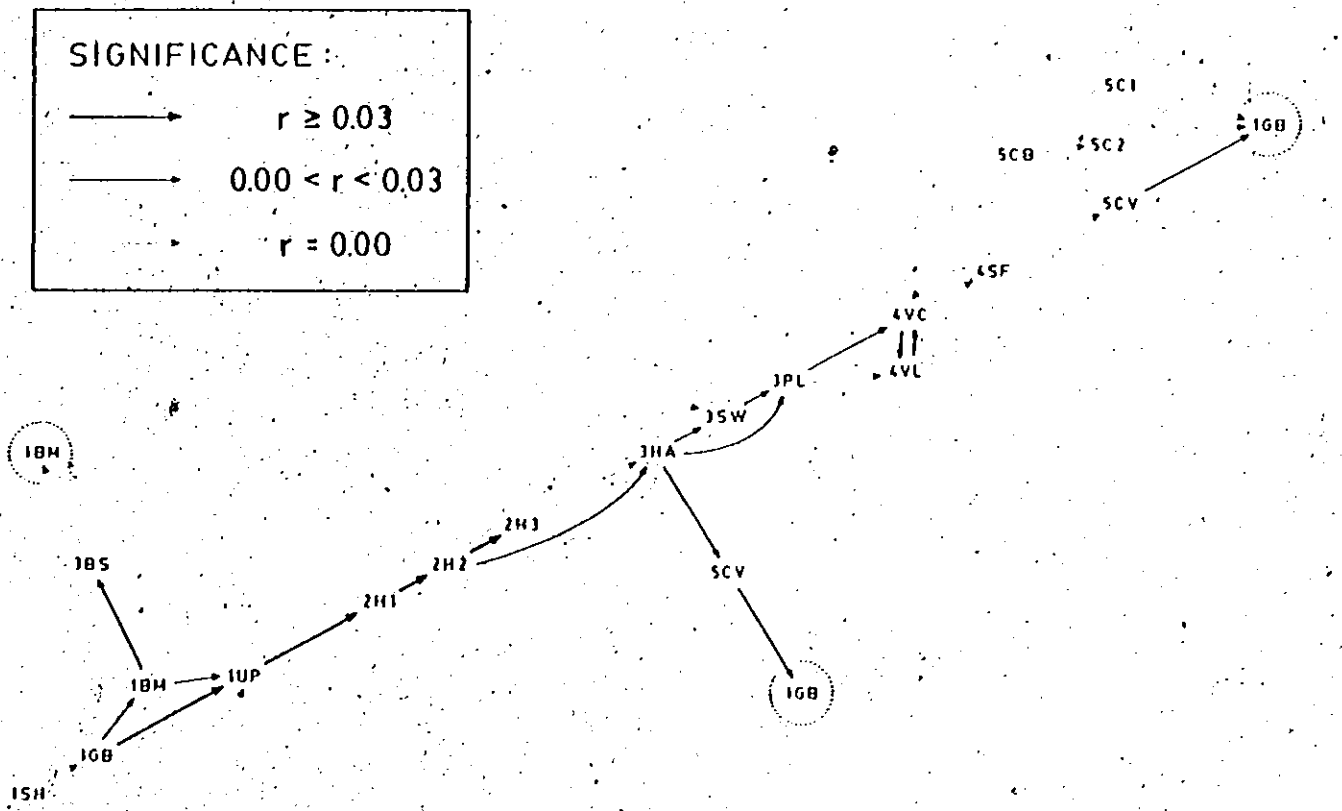

ALL NEGATIVE VALUES OF r ELIMINATED
ALL RESIDUAL PROBABILITIES > 10%
ALL CONFIDENCE VALUES ≥ 90%

analysis of facies transitions is presented below.

Segregated Markov-Chain Analyses: Countering the Effects of Non-Ergodic Data

As was mentioned previously, it can be demonstrated that Cardium deposition was controlled by processes which were strongly non-ergodic; systematic variations in the controlling processes can be expected to obscure certain facies relationships within the data set. The most obvious problem concerns the indiscriminate sampling both from fully regressive cycles and from cycles which do not display non-marine deposits. Distinction between these two groups of cycles is a simple matter, and offers an immediate method whereby the blurring of facies relationships due to inhomogeneity and/or non-stationarity may be minimized. Accordingly, I have divided the sample set into two groups of cycles, based upon the occurrence or absence of non-marine facies (including all facies of association 4 and the foreshore deposits of facies 3PL). The two segregated data sets are totally non-overlapping; each can be subjected to a separate Markov-chain analysis. The resuting data are tabulated in appendix 4. It is noteworthy that this segregation of cycles will dramatically reduce the number of transitions observed <u>between</u> cycles, simply because fully regressive cycles and

"incomplete" cycles commonly are vertically juxtaposed, and the transitions between them must be disregarded in the segregated analyses. However, the internal sequences within the two separate groups can be expected to be enhanced.

The results of these two analyses are presented as spider's web diagrams (Fig. 5-7 to 5-12). First, let us consider the fully regressive type 1 cycles.

Figure 5-7 is the simplified residual probability diagram for fully regressive type 1 cycles, showing only the most probable transitions. These relationships are further simplified in figure 5-8, which shows only those transitions which have residual probabilities greater than 10% and are statistically confident at 90% or more. Finally, the significance filter (Fig. 5-9) again eliminates facies 4IF and simplifies relationships within the conglomerates.

The facies relationships within fully regressive (type 1) cycles only (Fig. 5-9) are essentially similar to those within the Cardium as a whole (Fig. 5-6), with the major exception that marine conglomerates of association 5 occur within fully regressive coarsening-upward intervals. This facies sequence is discussed in further detail in the next section of this chapter.

The simplified residual probability diagram for all top-absent cycles is presented as figure 5-10. This

Figure 5-7. Simplified residual probability diagram for fully regressive type 1 cycles only. See text for discussion.

FULLY REGRESSIVE CYCLES ONLY

215 TRANSITIONS
18 FACIES

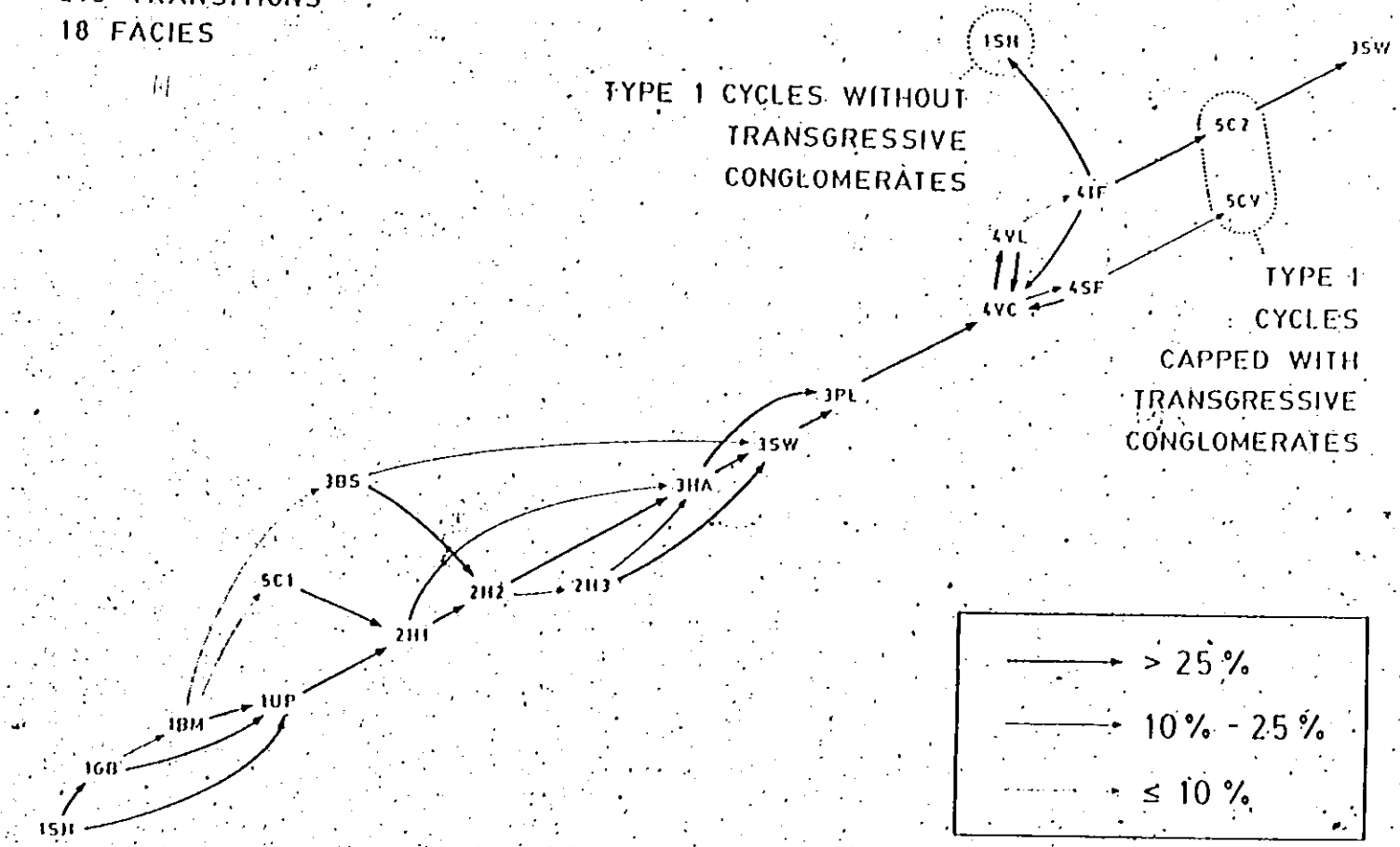

Figure 3-8. "Confidence" diagram for fully regressive type 1 cycles only. See text for discussion.

FULLY REGRESSIVE CYCLES ONLY

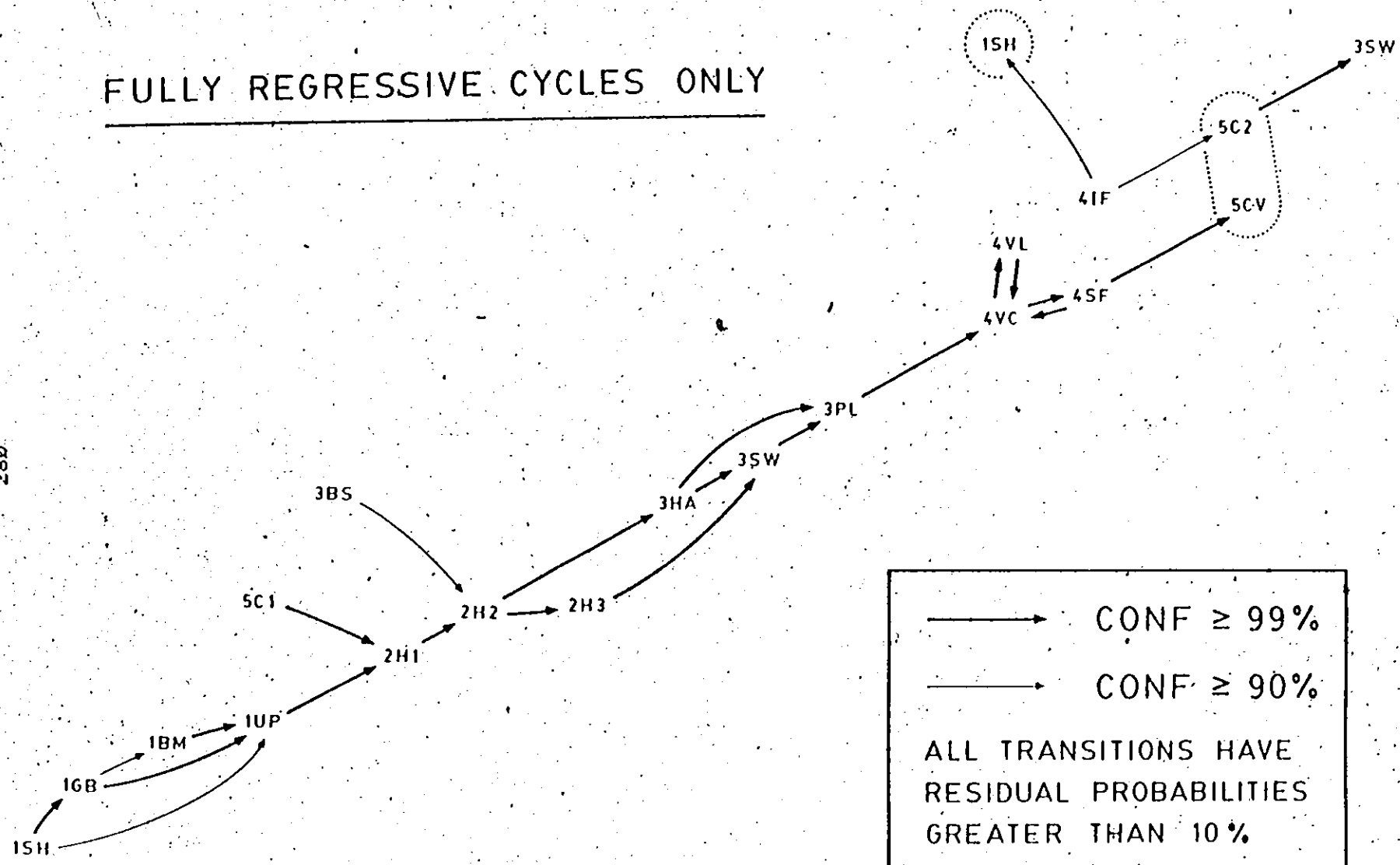

Figure 5-9. "Significance" diagram for fully regressive type i cycles only. See text for discussion.

FULLY REGRESSIVE CYCLES ONLY

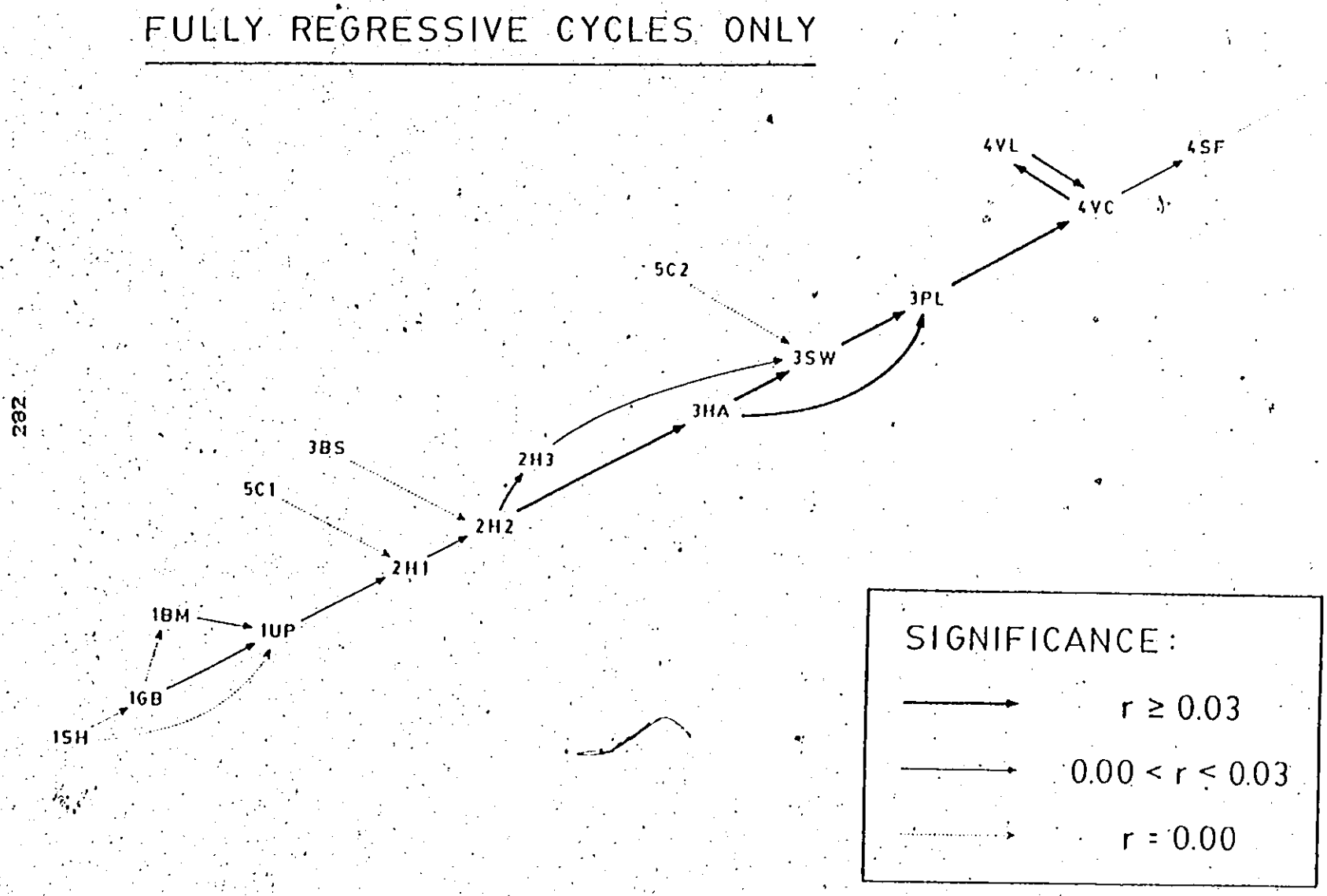

Figure 5-10. Simplified residual probability diagram for top-absent cycles only. See text for discussion.

TOP-ABSENT CYCLES ONLY

352 TRANSITIONS
14 FACIES

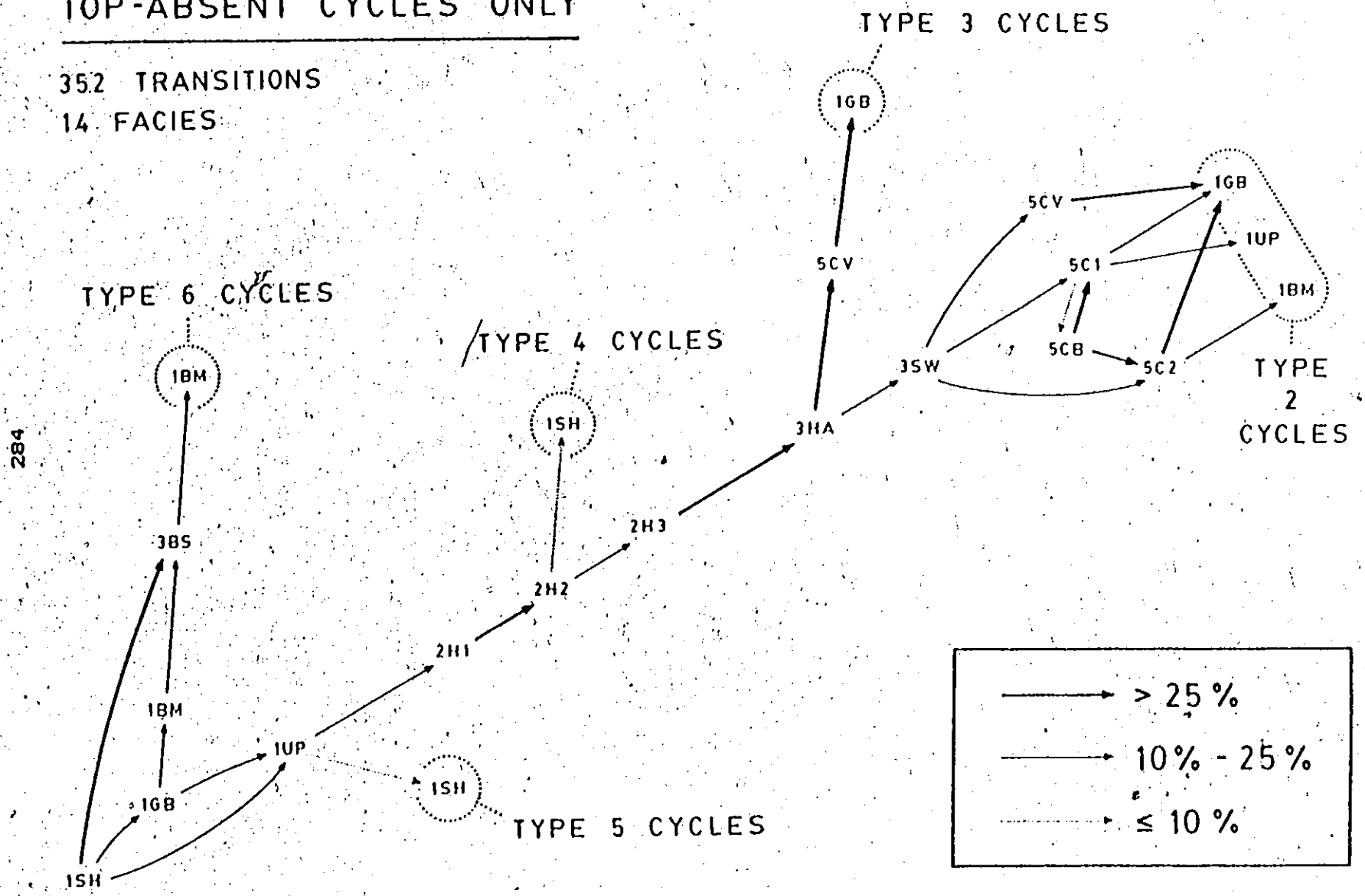

Figure 5-11. "Confidence" diagram for top-absent cycles only. See text for discussion.

TOP-ABSENT CYCLES ONLY

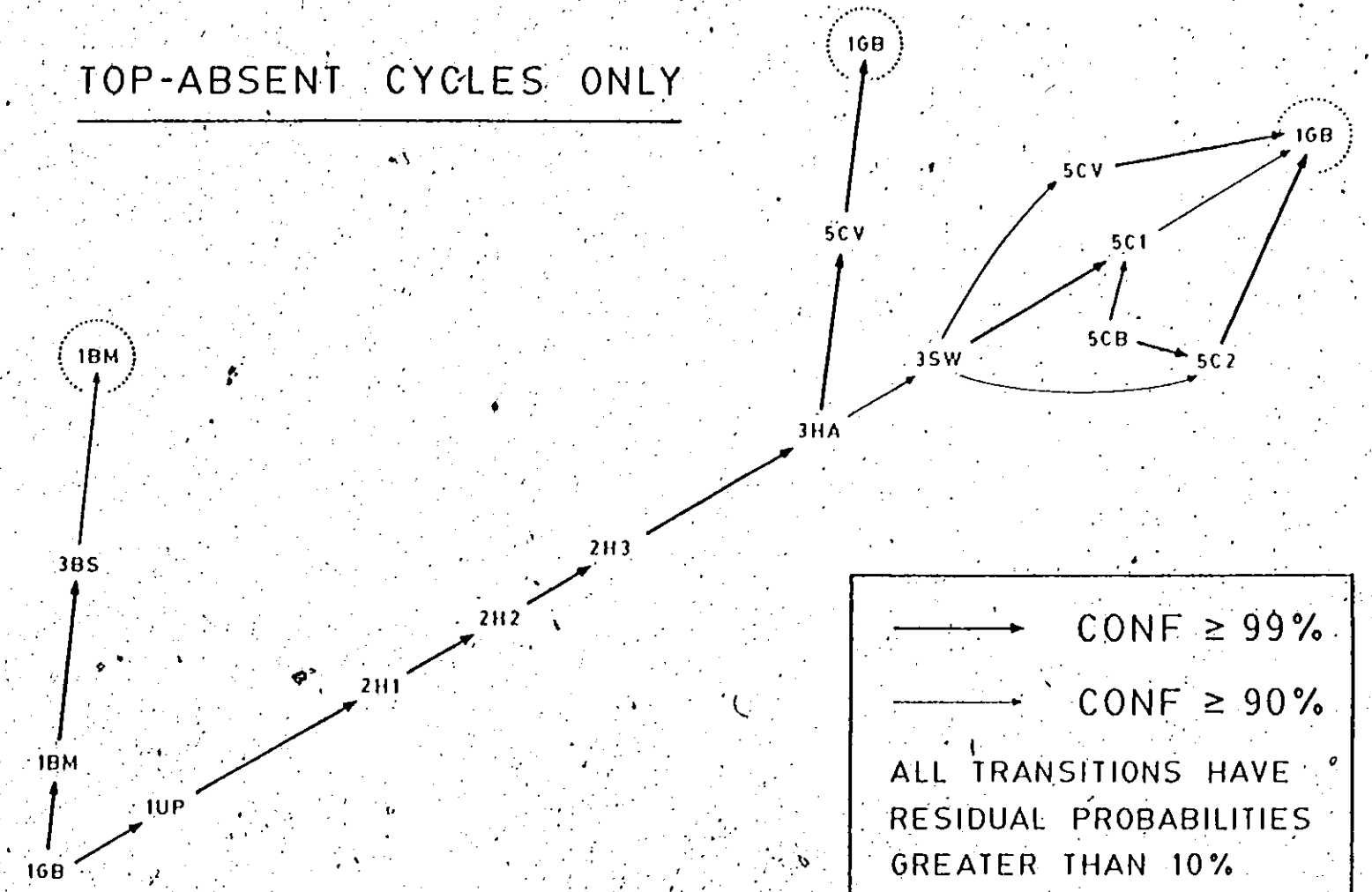

Figure 5-12. "Significance" diagram for top-absent cycles only. See text for discussion.

TOP-ABSENT CYCLES ONLY

ALL NEGATIVE VALUES OF r ELIMINATED
ALL RESIDUAL PROBABILITIES > 10%
ALL CONFIDENCE VALUES ≥ 90%

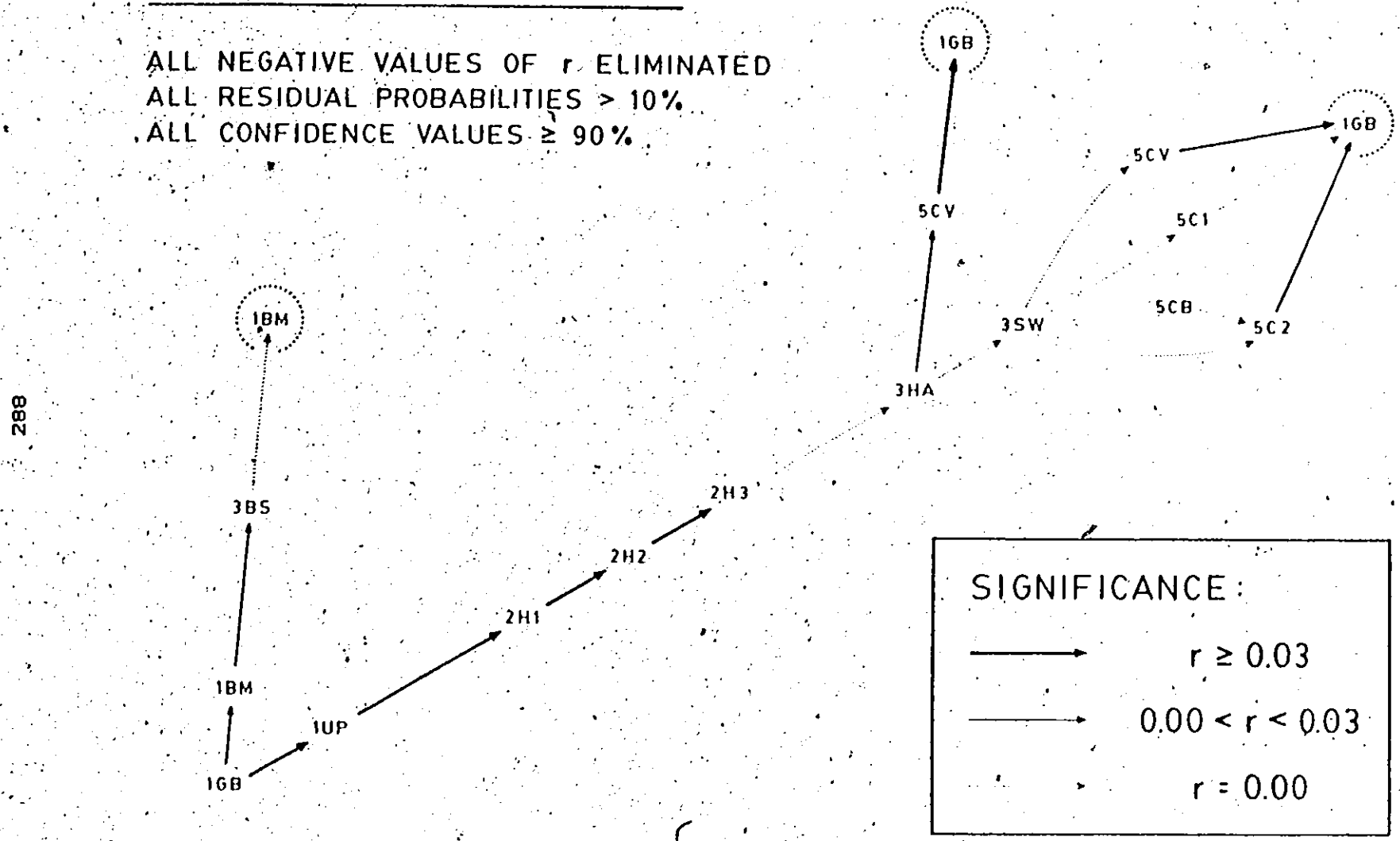

diagram shows five separate cycle terminations; these correspond to cycle types 2 through 6. The confidence diagram for these transitions (Fig. 5-11) reveals that only cycle types 2, 3, and 6 are statistically confident at the 90% level or higher. The significance diagram (Fig. 5-12) confirms the normative significance of these three cycle types.

The presence of all five of the subjectively recognized top-absent cycle types on the simplified residual probability diagram (Fig. 5-10) suggests that these types of cycles are indeed present within the formation, and serves as a rigorous confirmation of the subjective synthesis of data. In the following section of this chapter, the statistical analysis is further refined.

"TYPE EXAMPLES" OF CARDIUM CYCLES

In this section, a "type example" of each cycle type is described in further detail, accenting typical facies sequences and thicknesses. Each of these "type examples" is compared to a synthetic cycle determined by means of Markov-chain analyses (described below).

Synthetic cycles representing normative facies sequences were constructed using the "thickness-of-underlying" matrices in appendix 4. These matrices give

the average facies thickness associated with individual transitions (e.g., for the transition from facies A to facies B, the associated element of the thickness-of-underlying matrix lists the mean thickness of all occurrences of facies A which are immediately overlain by facies B).

Each type-example cycle has been selected on the basis of: 1) similarity of facies sequence within the type example, as compared with the normative facies sequence for that cycle type, 2) quality and accessibility of exposure, 3) similarity of thickness of the type example, as compared with the thickness of the synthetic cycle constructed from the normative facies sequence for that cycle type, and 4) similarity of thicknesses of individual facies within the type example, as compared with mean facies thicknesses in the corresponding synthetic cycle.

As mentioned above, 134 major cyclic developments were observed in the field. This tabulation does <u>not</u> include minor coarsening- and thickening-upward cyclic developments superimposed upon a general coarsening and thickening trend (e.g., the two minor cycles superimposed upon cycle #4 in section 4-21 -- see appendix 2). The following descriptions are based upon the subjective synthesis of observations from these 134 major cycles. Data for subjectively recognized cycles are summarized on the following page:

CYCLE TYPE	NUMBER OF OCCURRENCES	MEAN THICKNESS (RANGE), m
1	34	34.8 (9.5 to 78.7)
2	14	20.8 (4.0 to 52.2)
3	22	15.1 (3.1 to 41.7)
4	42	16.2 (3.7 to 36.0)
5	13	11.9 (3.7 to 20.0)
6	9	12.7 (6.7 to 18.7)
ALL CYCLES:	134	20.5 (3.1 to 78.7)

Individual cycles are listed by type in appendix 4.

Segregated Markov-Chain Analyses for Individual Types of Cycles

The recognition of all six types of cycles in the preceding statistical analyses justifies proceeding with a segregated Markov-chain analysis for each of the six cycle types. These segregated analyses are presented below.

Preliminary computer runs were conducted in which data were handled in two different ways:

1) The top of each cycle was considered as a break in section, unless immediately overlain by a cycle of the same type. This is the manner in which the two previous segregated analyses were

conducted.

2) Cycles were artificially juxtaposed vertically. In this procedure, tops of cycles exposed at the upper contact were considered to be immediately overlain by the next cycle of the same type if and only if the following cycle was exposed at the lower contact (Fig. 5-13). Cycle sequence was determined by random selection. A break in section was placed in cases where the transition was between two occurrences of the same facies.

The preliminary computer runs indicated that artificial vertical juxtapositioning of cycles resulted in much more realistic transitions at the tops of cycles, thus better representing the first facies encountered within cycles. These results (i.e., those of method 2 described above) are presented under the next heading. [Except for type 1 cycles. Differences between the two methods of analysis were minor for type 1 cycles; thus, the results summerized in figures 5-7 to 5-9 (using method 1 above) were used in the construction of the synthetic cycle for cycle type 1.]

On the spider's web diagrams which follow, the key for weighting of arrows is identical to that used in the preceding diagrams (Fig. 5-3 to 5-12). The keys for all of the remaining diagrams are reproduced as figures 5-14, 5-15, and 5-16.

Figure 5-13. Diagram illustrating method of artificial vertical juxtapositioning of like cycles. See text for discussion.

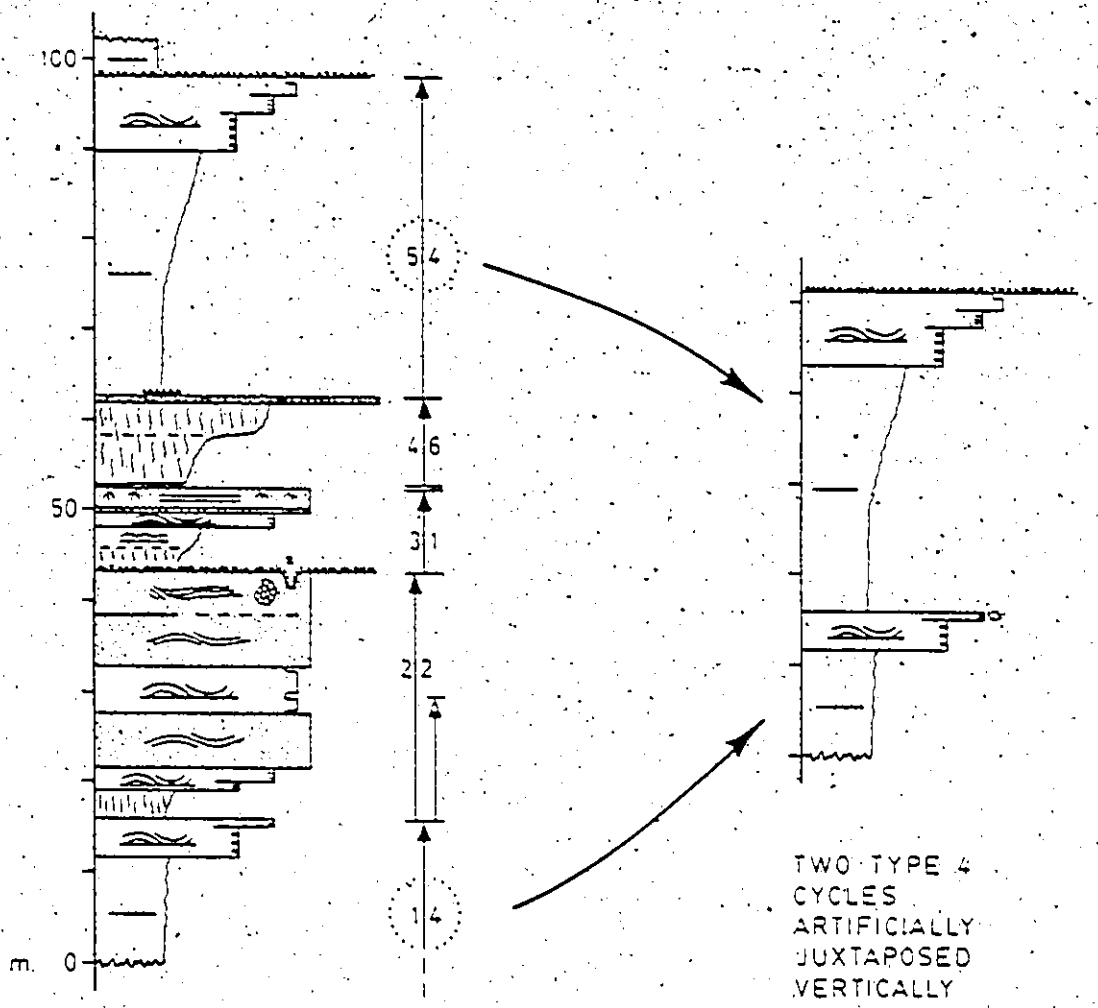

SECTION 5-39
BLACKSTONE RIVER



Figure 5-14. Key for the weighting of arrows in all of the simplified residual probability diagrams which follow. This weighting scheme is identical to the one used in previous simplified residual probability diagrams. See text for discussion.

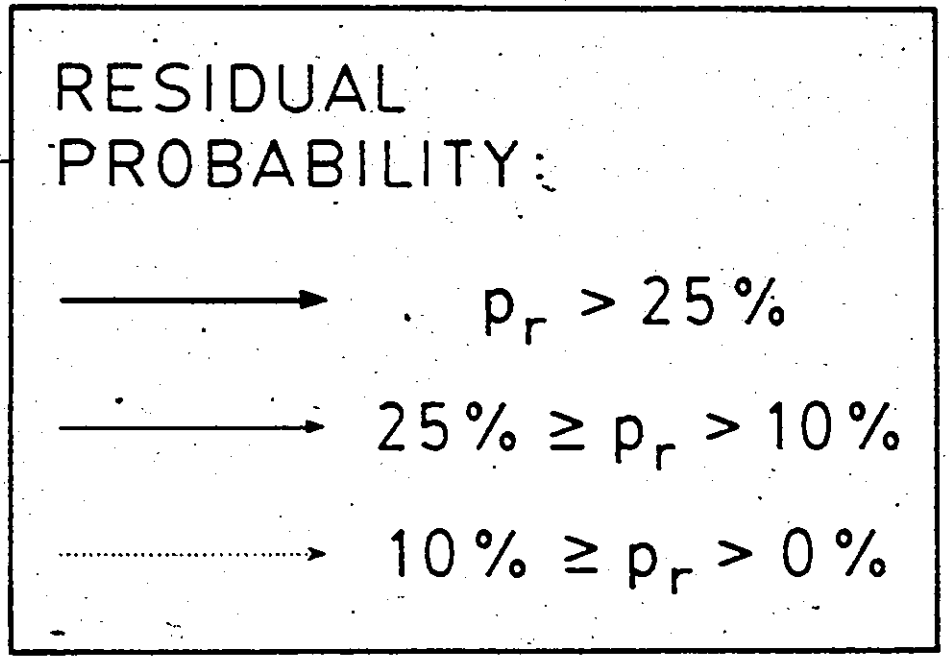
RESIDUAL
PROBABILITY:
$p_r > 25\%$
$25\% \geq p_r > 10\%$
$10\% \geq p_r > 0\%$

Figure 5-15. Key for the weighting of arrows in all of the "confidence" diagrams which follow. This weighting scheme is identical to the one used in previous "confidence" diagrams. See text for discussion.

CONFIDENCE:

→ $c \geq 99\%$

→ $99\% > c \geq 90\%$

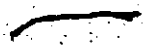

Figure 5-16. Key for the weighting of arrows in all of the "significance" diagrams which follow. This weighting scheme is identical to the one used in previous "significance" diagrams. See text for discussion.

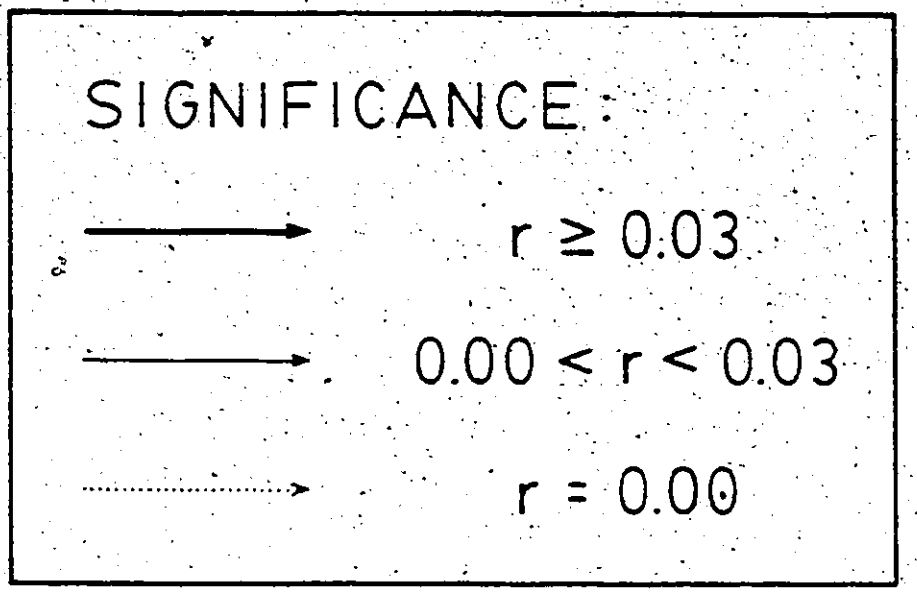
SIGNIFICANCE:
r ≥ 0.03
0.00 < r < 0.03
r = 0.00

Cycle Type 1 ("Fully Regressive Cycles")

Of the 134 observed cycles, 34 examples (25%) are classified as type 1. These 34 examples have an average thickness of 34.8 m (range: 9.5 to 78.7 m). The lower marine interval of these cycles has an average thickness of about 22.3 m; the non-marine interval (association 4 only) has an average thickness of about 12.5 m.

Six of these 34 cycles (18%) are capped with marine conglomerates of association 5 and/or symmetrical thinning- and fining-upward marine deposits overlying the non-marine deposits of association 4. Of these six cycles, all are capped with transgressive conglomerate, and two also display a symmetrical cap associated with this conglomerate.

The simplified residual probability, confidence, and significance diagrams for type 1 cycles only have previously been presented as figures 5-7, 5-8, and 5-9, respectively. These figures indicate that the most typical type 1 facies sequence (from the base of one cycle to the base of the next cycle) is as follows:

1GB > 1UP > 2H1 > 2H2 > 3HA > 3SW > 3PL >
4VC >> 4VL >> 4VC > 4SF > 1GB

The double arrows from facies 4VC to 4VL and from 4VL back to 4VC indicate that there may be more than one vertically

stacked couplets of these two facies (e.g., 4VC > 4VL > 4VC > 4VL > 4VC, etc.). The normative number of such transitions cannot be determined statistically by means of a one-step analysis, but can be determined subjectively by a re-examination of the original data. This subjective survey suggests that one such couplet probably is best representative of these cycles; thus, the normative sequence of facies for type 1 cycles becomes:

1GB > 1UP > 2H1 > 2H2 > 3HA > 3SW > 3PL > 4VC > 4VL > 4VC > 4SF > 1GB

Figure 5-17 is a vertical graphic log of this synthetic sequence; thicknesses were derived from the thickness-of-underlying matrix for these transitions (appendix 4). This synthetic sequence can be compared with the designated type example of cycle type 1 (cycle number 2, section GC-1, Grande Cache Highway Roadcut -- inset of Fig. 5-17). The synthetic cycle has a thickness of __._ m, similar to the mean thickness of cycles (34.8 m). The thickness of the type example is somewhat greater (42.9 m).

Cycle Type 2 ("Swaley Cycles")

Of the 134 observed cycles, 14 examples (10%) are classified as type 2. These 14 examples have an average

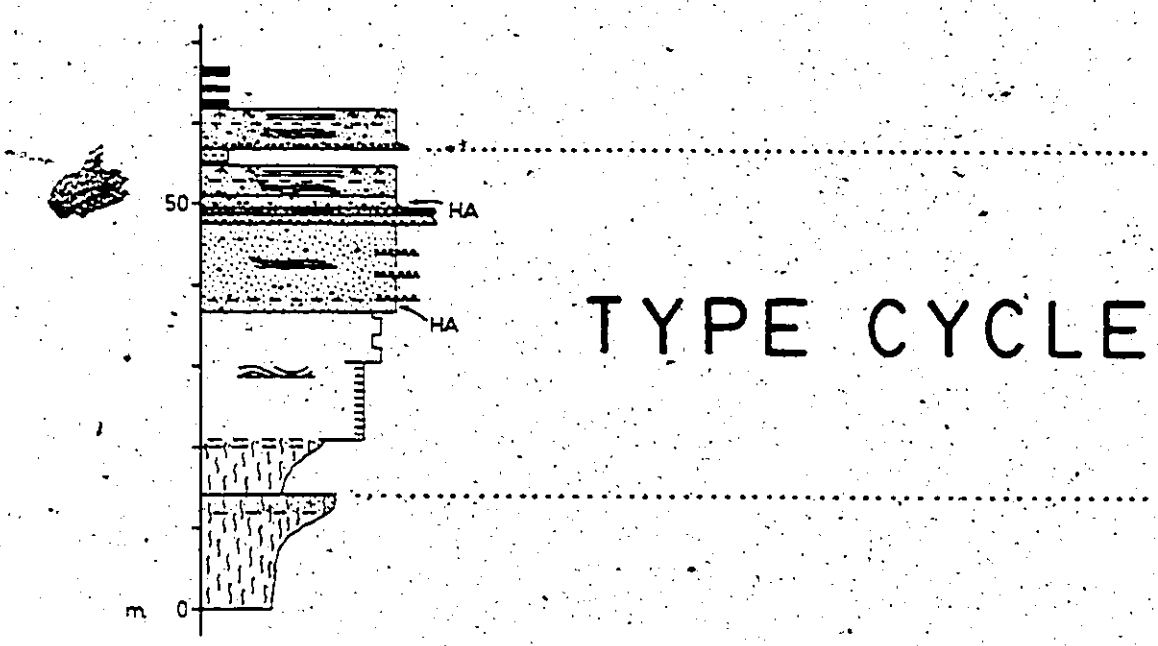

Figure 5-17. Synthetic (i.e., normative) type 1 cycle. Inset diagram shows the type example for this cycle type; tick marks on type example indicate 10 m intervals. See text for discussion.

TYPE 1 CYCLES

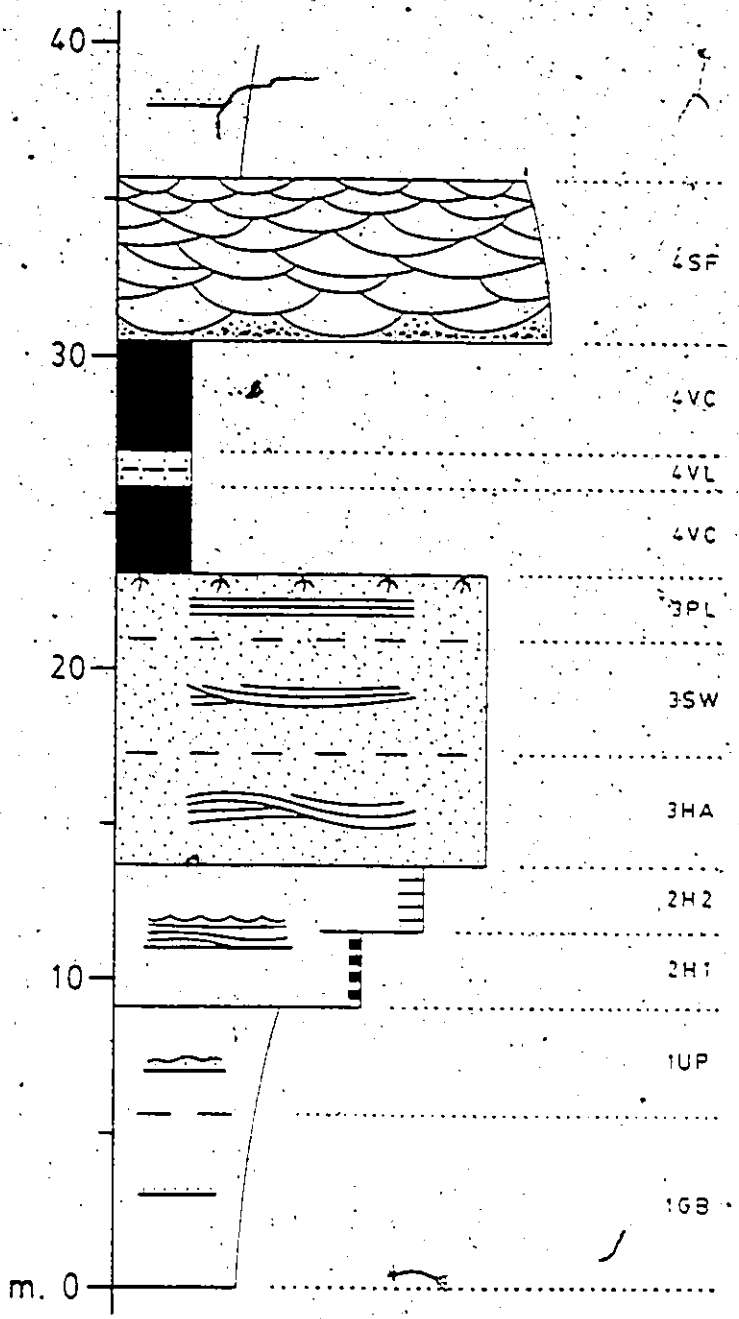

SYNTHETIC
CYCLE

thickness of 20.8 m (range: 4.0 to 52.2 m).

The simplified residual probability, confidence, and significance diagrams for type 2 cycles only are presented as figures 5-18, 5-19, and 5-20, respectively. These figures indicate that the most typical type 2 facies sequence (from the base of one cycle to the base of the next cycle) is as follows:

1GB > 1BM > 2H1 > 2H2 > 2H3 > 3HA > 3SW > 5CV > 1GB

Figure 5-21 is a vertical graphic log of this synthetic sequence; thicknesses were derived from the thickness-of-underlying matrix for these transitions (appendix 4). This synthetic sequence can be compared with the designated type example of cycle type 2 (cycle number 4, section 4-43, Mackenzie Creek -- inset of Fig. 5-21). The synthetic cycle has a thickness of 25.3 m, similar to the mean thickness of cycles (20.8 m). Note that the thickness of the type example (51.8 m) is much greater than either of these values. The mean cycle thickness is somewhat smaller than the synthetic cycle thickness, due to the inclusion of bottom- and middle-absent cycles in the calculation of the mean value.

Cycle Type 3 ("Amalgamated Hummocky Cycles")

Of the 134 observed cycles, 22 examples (16%) are

classified as type 3. These 22 examples have an average thickness of 15.1 m (range: 3.1 to 41.7 m).

The simplified residual probability, confidence, and significance diagrams for type 3 cycles only are presented as figures 5-22, 5-23, and 5-24, respectively. These figures indicate that the most typical type 3 facies sequence (from the base of one cycle to the base of the next cycle) is as follows:

1BM > 2H1 > 2H2 > 2H3 > 3HA > 5CV > 1BM

Figure 5-25 is a vertical graphic log of this synthetic sequence; thicknesses were derived from the thickness-of-underlying matrix for these transitions (appendix 4). This synthetic sequence can be compared with the designated type example of cycle type 3 (cycle number 1, section MS-1, Mason Creek -- inset of Fig. 5-25). The synthetic cycle has a thickness of 20.9 m, similar to the mean thickness of cycles (15.1 m); again, the thickness of the type example (approximately 42 m) is much greater than either of these values. The mean cycle thickness is somewhat smaller than the synthetic cycle thickness, due to the inclusion of bottom- and middle-absent cycles in the calculation of mean thickness.

Figure 5-18. Simplified residual probability diagram for type 2 cycles only. See text for discussion.

TYPE 2 CYCLES ONLY

81 TRANSITIONS

13 FACIES

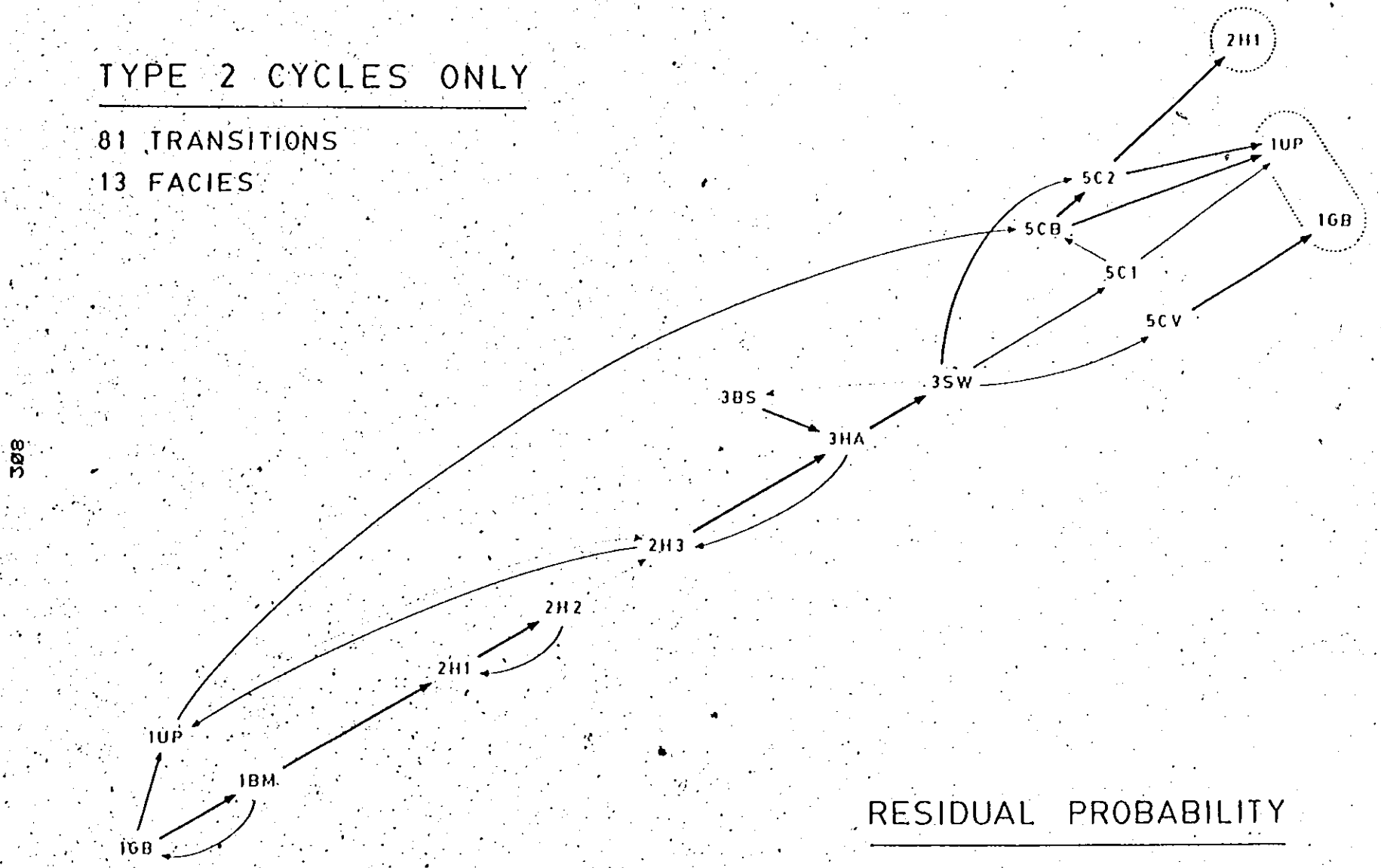

RESIDUAL PROBABILITY

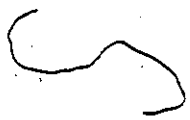

Figure 5-19. "Confidence" diagram for type 2 cycles only. See text for discussion.

TYPE 2 CYCLES ONLY

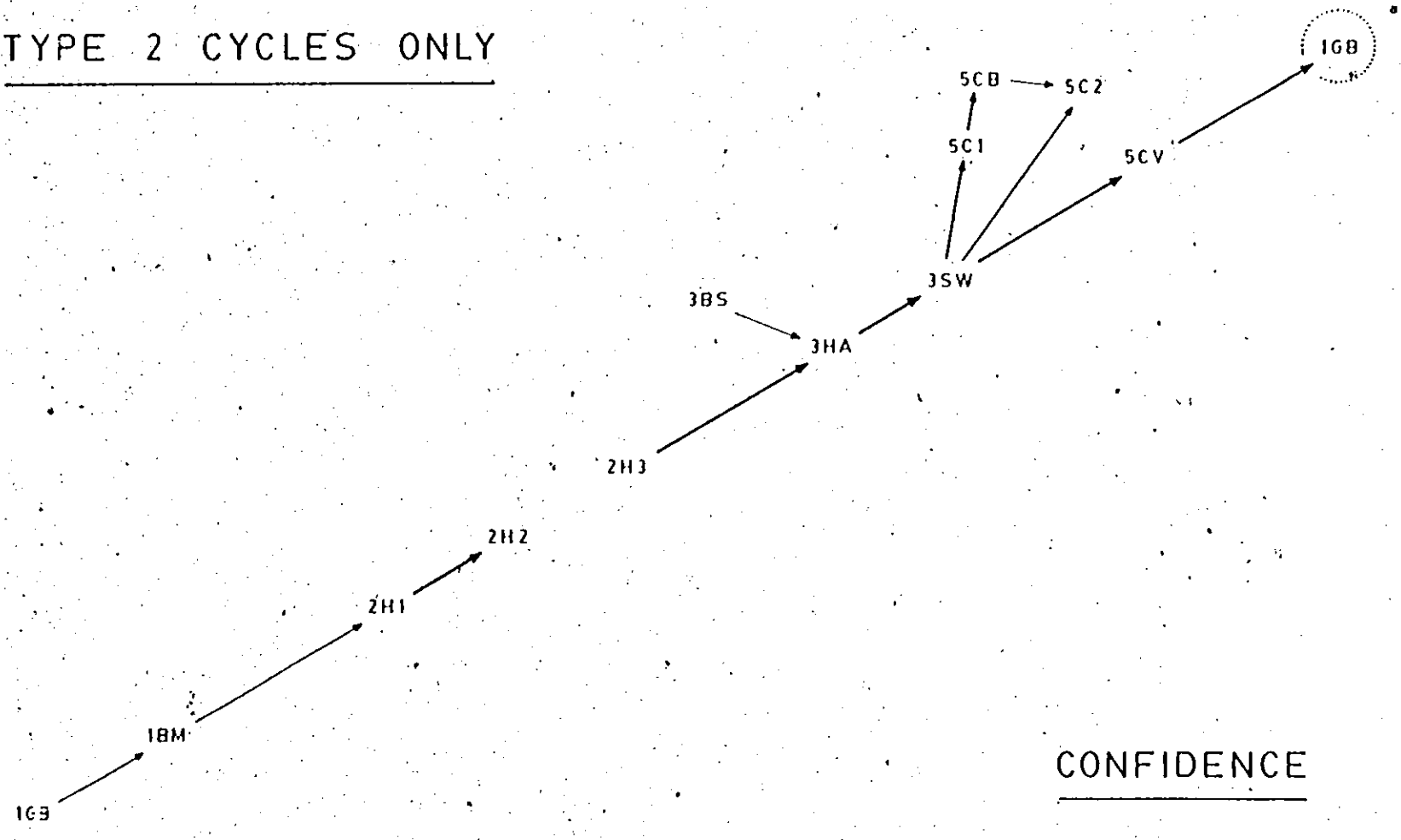

CONFIDENCE

Figure 3-20. "Significance" diagram for type 2 cycles only. See text for discussion.

TYPE 2 CYCLES ONLY

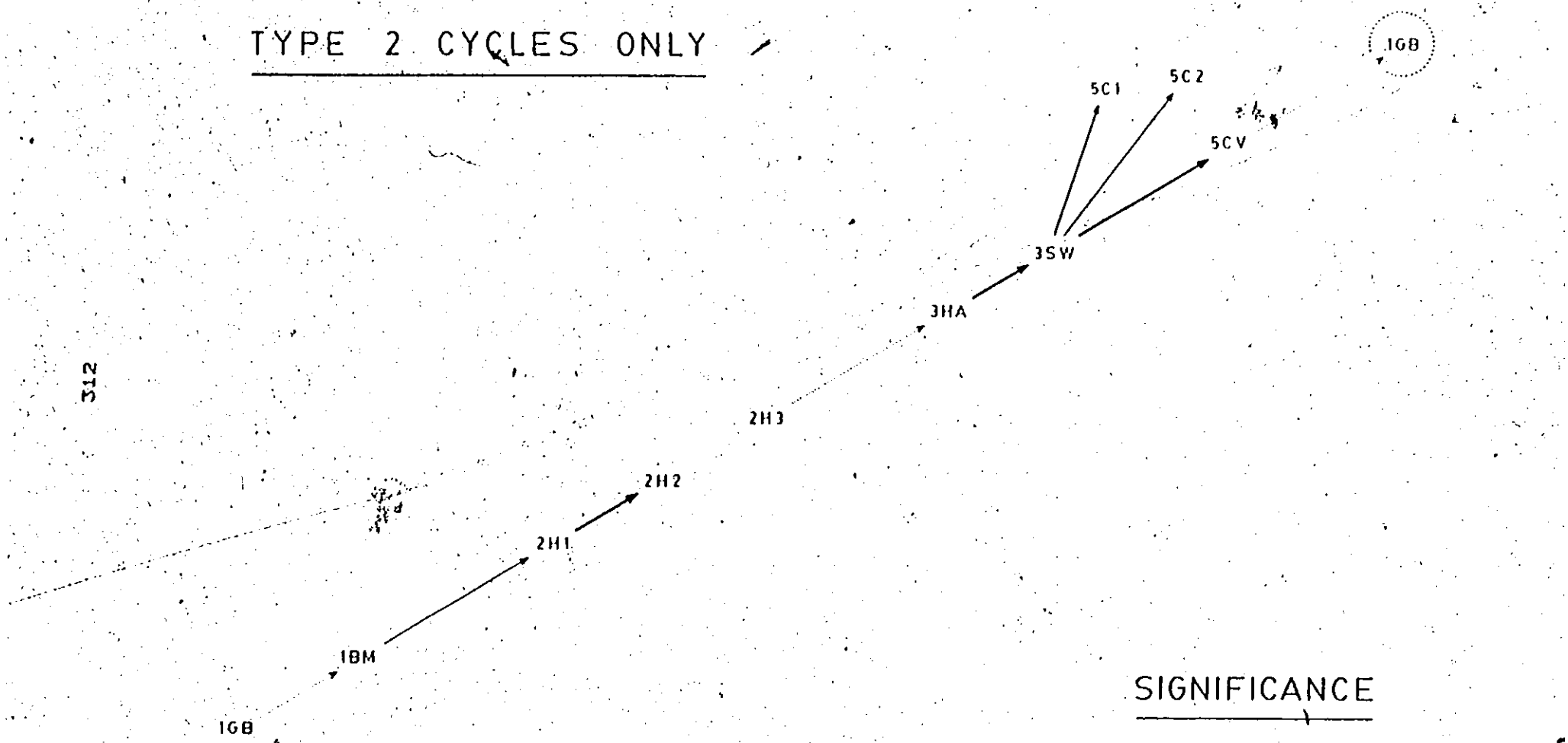

SIGNIFICANCE

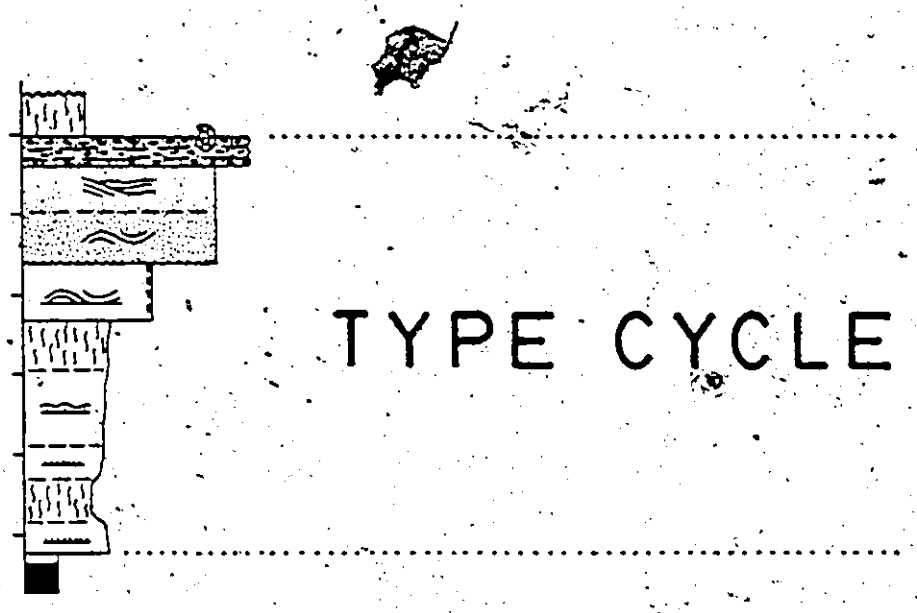

Figure 5-21. Synthetic (i.e., normative) type 2 cycle. Inset diagram shows the type example for this cycle type; tick marks on type example indicate 10 m intervals. See text for discussion.

TYPE 2 CYCLES

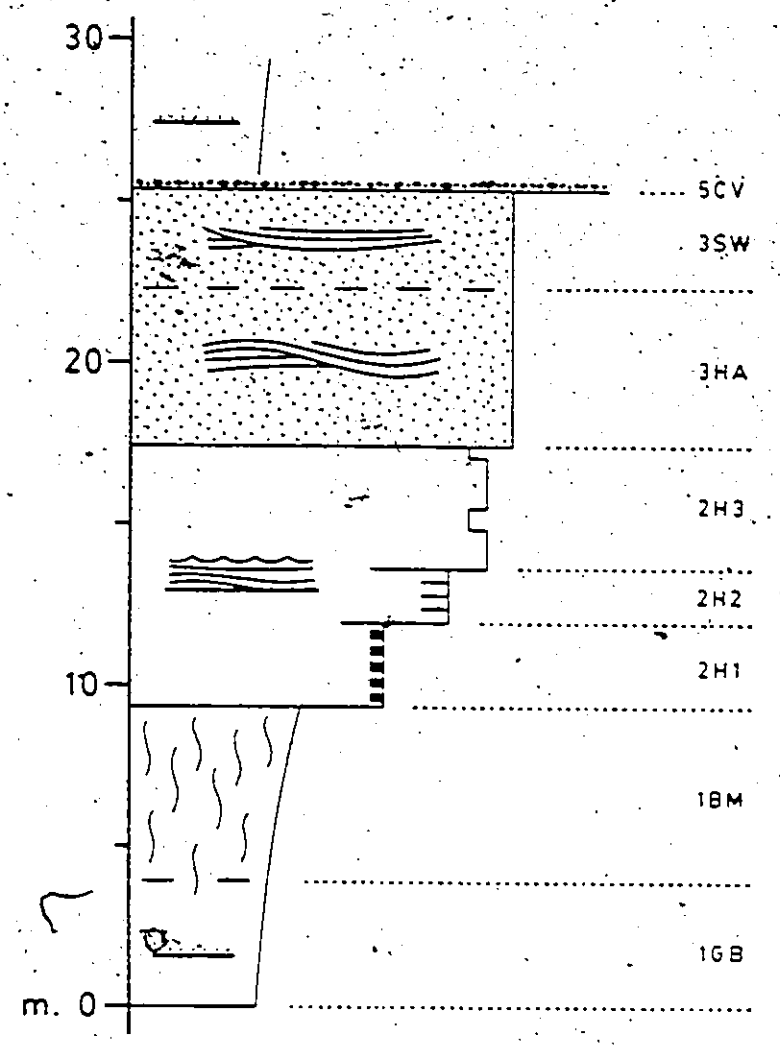

SYNTHETIC
CYCLE

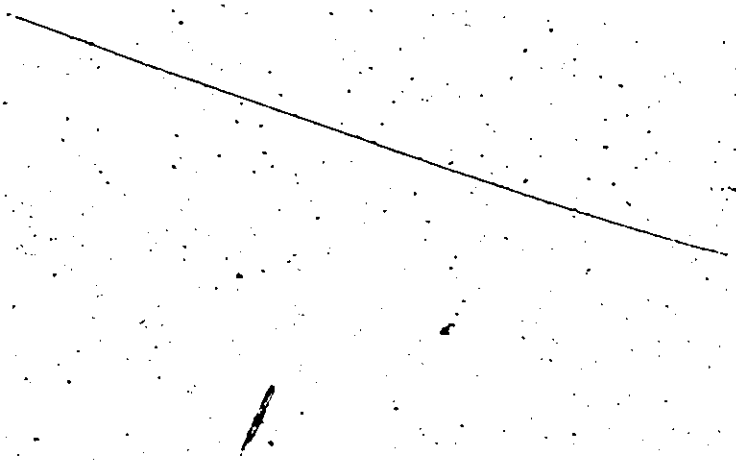

Figure 5-22. Simplified residual probability diagram for type 3 cycles only. See text for discussion.

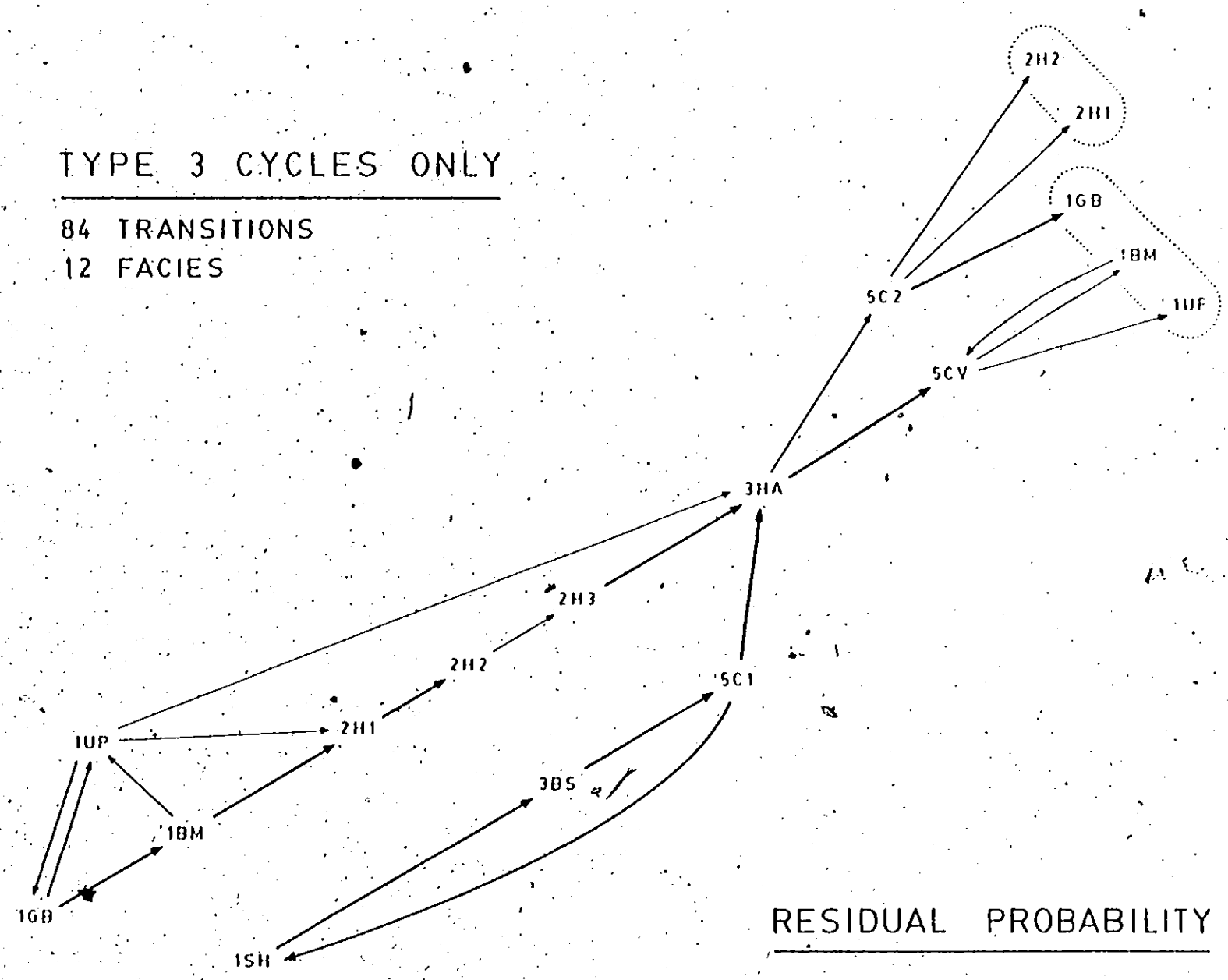
TYPE 3 CYCLES ONLY
84 TRANSITIONS
12 FACIES
2H2
2H1
1GB
1BM
1UF
5C2
5CV
3HA
2H3
2H2
5C1
1UP
2H1
3BS
1BM
1GB
1SH
RESIDUAL PROBABILITY

Figure 5-23. "Confidence" diagram for type 3 cycles only. See text for discussion.

TYPE 3 CYCLES ONLY

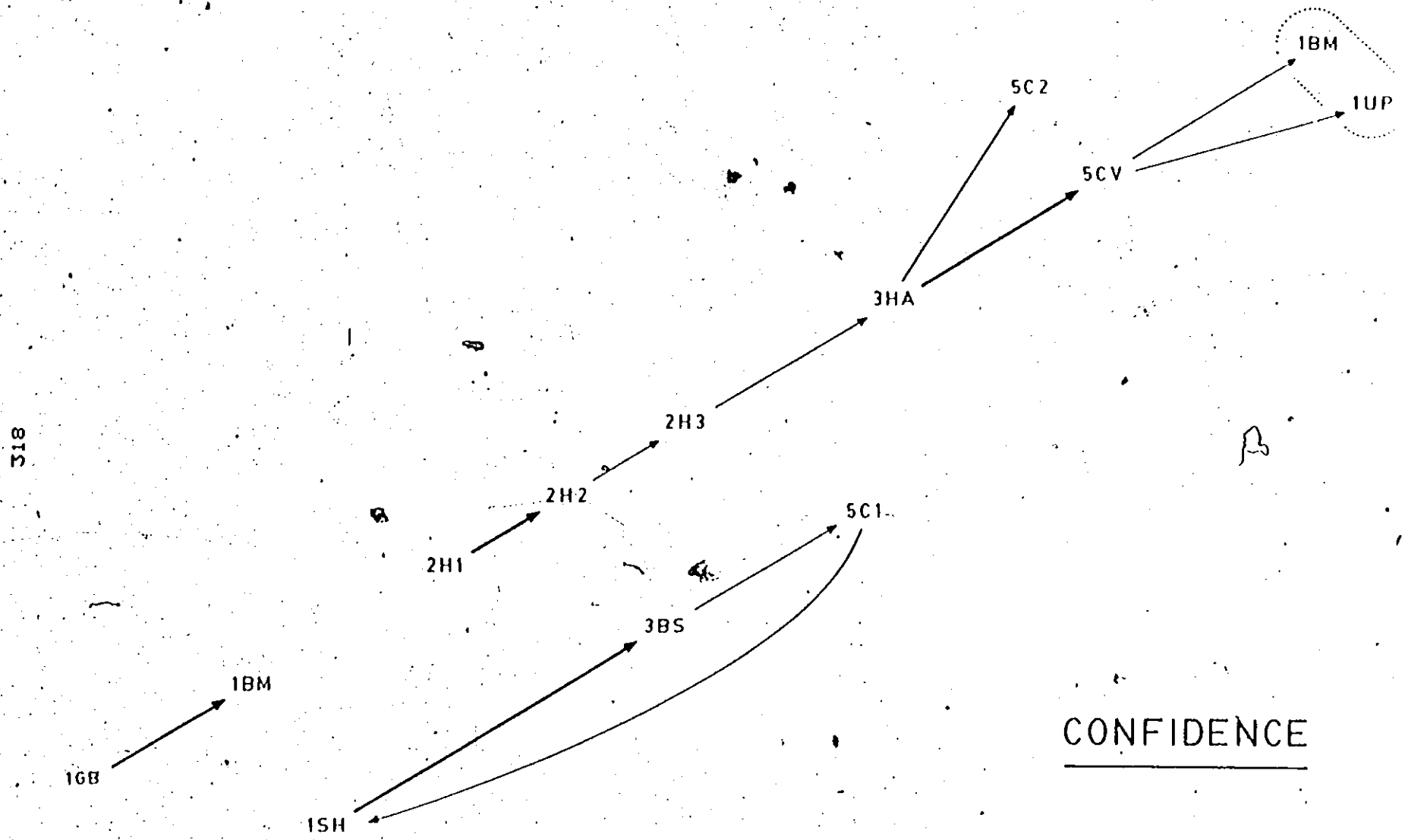

318

CONFIDENCE

Figure 5-24. "Significance" diagram for type 3 cycles only. See text for discussion.

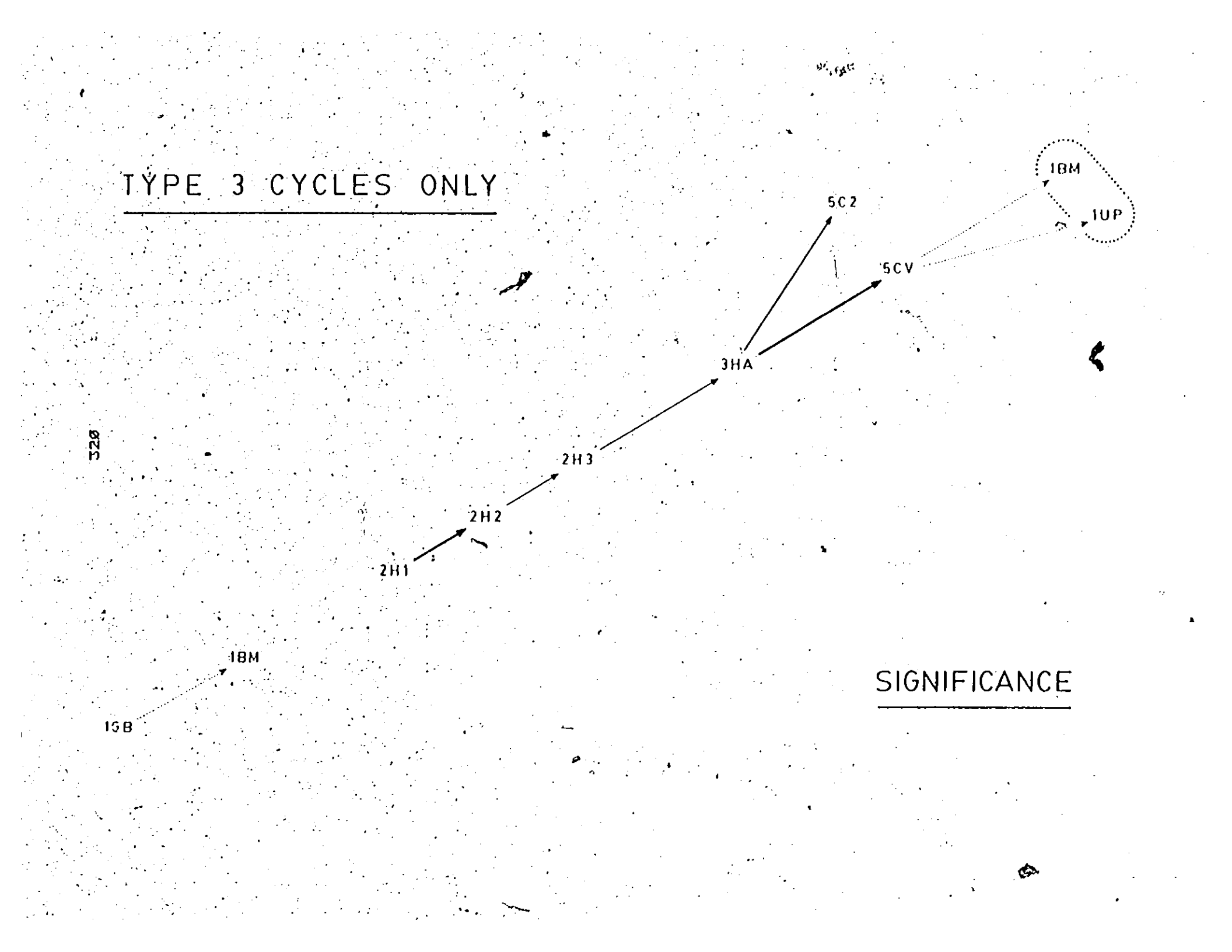
TYPE 3 CYCLES ONLY
1BM
1UP
5C2
5CV
3HA
2H3
2H2
2H1
320
1BM
1GB
SIGNIFICANCE

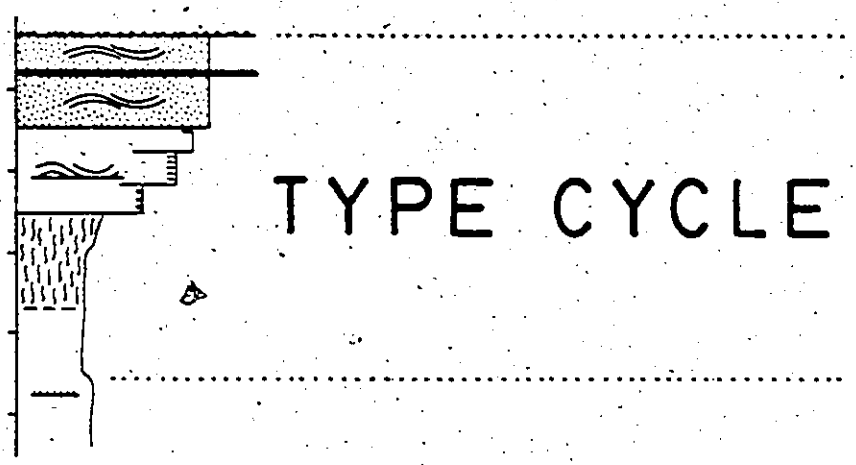

Figure 5-25. Synthetic (i.e., normative) type 3 cycle. Inset diagram shows the type example for this cycle type; tick marks on type example indicate 10 m intervals. See text for discussion.

TYPE 3 CYCLES

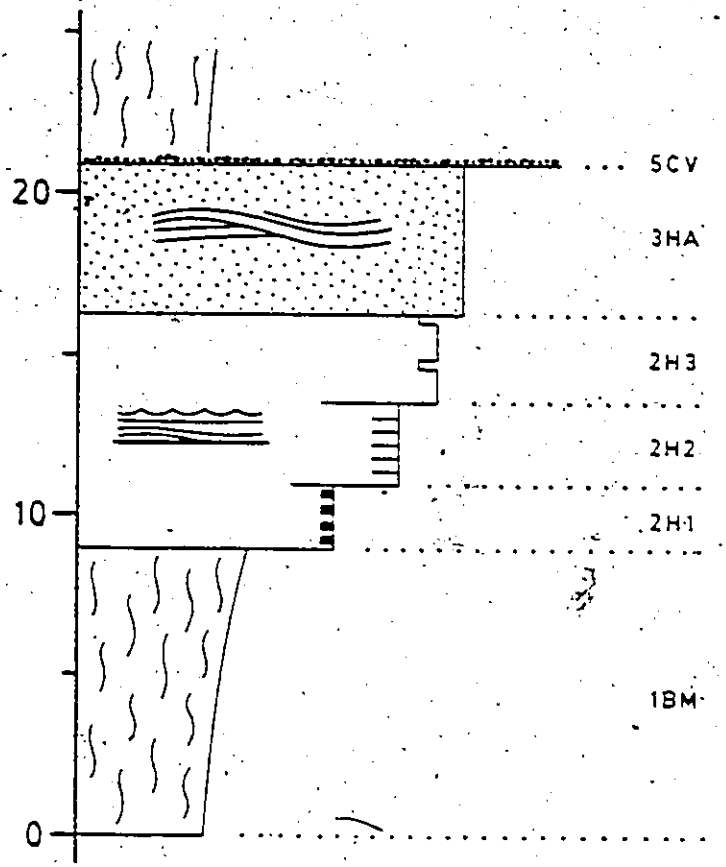

SYNTHETIC
CYCLE

Cycle Type 4 ("Interbedded Hummocky Cycles")

Of the 134 observed cycles, 42 examples (31%) are classified as type 4. These 42 examples have an average thickness of 16.2 m (range: 3.7 to 36.0 m).

The simplified residual probability, confidence, and significance diagrams for type 4 cycles only are presented as figures 5-26, 5-27, and 5-28, respectively. These figures indicate that the most typical type 4 facies sequence (from the base of one cycle to the base of the next cycle) is as follows:

1GB > 1UP > 2H1 > 2H2 > 2H3 > 5CV > 1GB

Figure 5-29 is a vertical graphic log of this synthetic sequence; thicknesses were derived from the thickness-of-underlying matrix for these transitions (appendix 4). This synthetic sequence can be compared with the designated type example of cycle type 4 (cycle number 5, section 5-39, Blackstone River -- inset of Fig. 5-29). A photograph of the type cycle is presented as figure A1-19C. Note that the synthetic cycle has a thickness of 18.8 m, similar to the mean thickness of cycles (16.2 m). The mean thickness of type 4 cycles is slightly smaller than that of the synthetic cycle, due to the many type 4 cycles which terminate in facies 2H2 or 2H1, or are bottom-absent. Thickness of the designated type example

(34.8 m) is much greater than either the synthetic or the mean cycle thickness.

Cycle Type 5 ("Mud-Dominant Cycles")

Of the 134 observed cycles, 13 examples (10%) are classified as type 5. These 12 examples have an average thickness of 11.9 m (range: 3.7 to 20.0 m).

Figure 5-30 shows the simplified residual probability and confidence diagrams for type 5 cycles only; figure 5-31 is the significance diagram. These figures indicate that the most typical type 5 facies sequence (from the base of one cycle to the base of the next cycle) is as follows:

1GB > 1UP > 1BM > 5CV > 1GB

Figure 5-32 is a vertical graphic log of this synthetic sequence; thicknesses were derived from the thickness-of-underlying matrix for these transitions (appendix 4). This synthetic sequence may be compared with the designated type example of cycle type 5 (cycle number 6, section 5-45, Ram River -- inset of Fig. 5-32). Note that the synthetic cycle has a thickness of 13.2 m, similar to both the mean thickness of cycles (11.9 m) and the thickness of the type cycle (14.0 m). The mean thickness of type 5 cycles is slightly smaller than that of the

Figure 5-26. Simplified residual probability diagram for type 4 cycles only. See text for discussion.

TYPE 4 CYCLES ONLY.

150 TRANSITIONS
11 FACIES

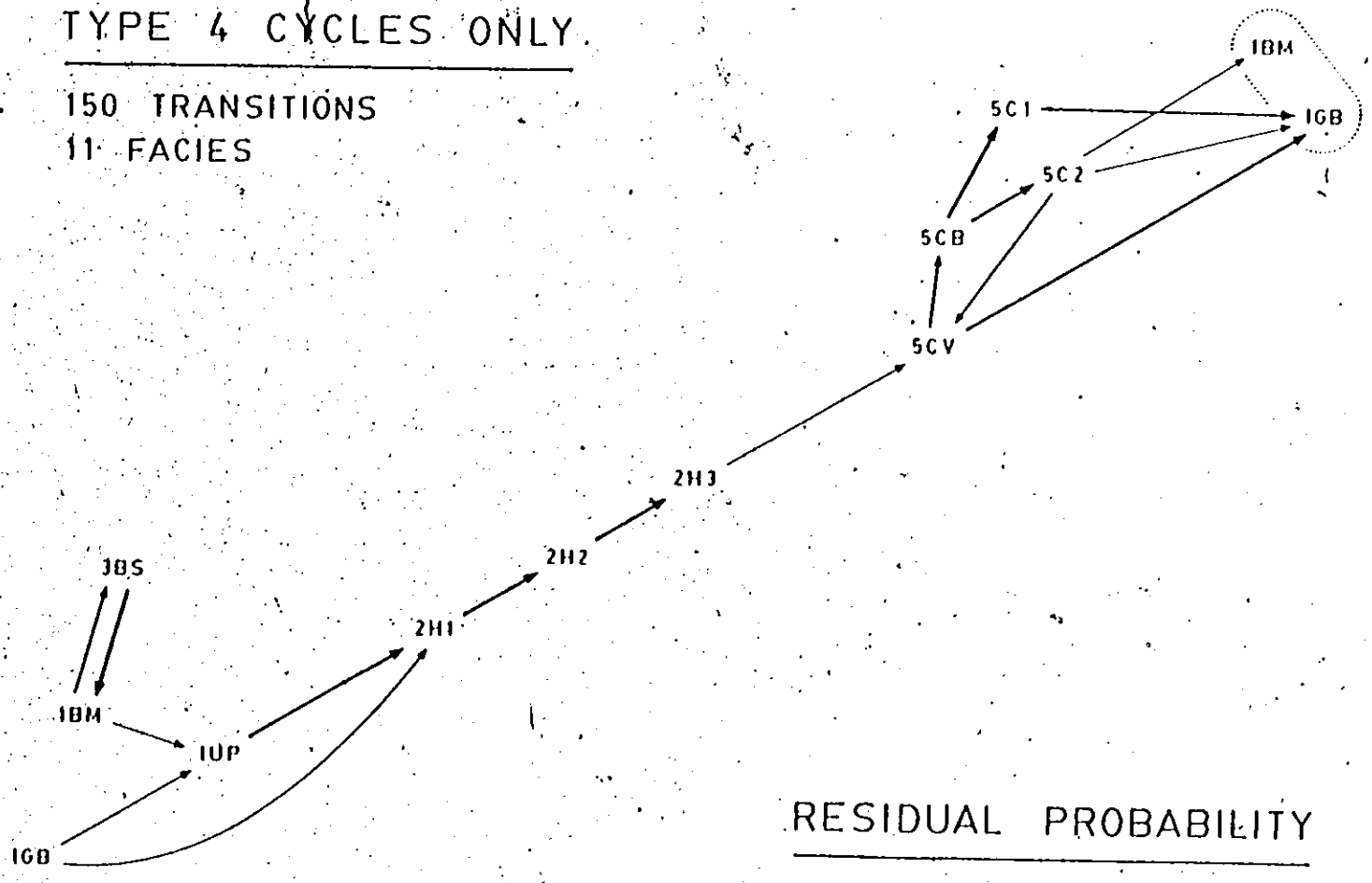

RESIDUAL PROBABILITY

Figure 5-27. "Confidence" diagram for type 4 cycles only.

See text for discussion.

TYPE 4 CYCLES ONLY

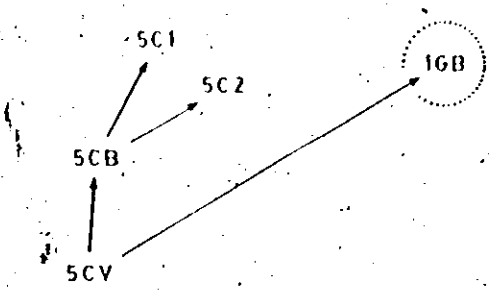

328

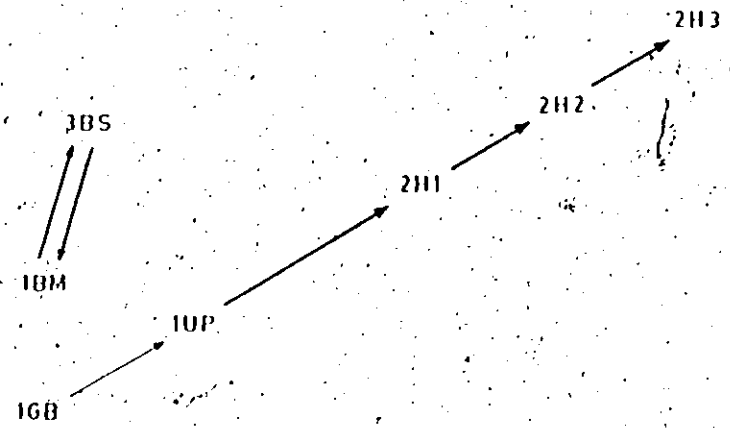

CONFIDENCE

Figure 5-28. "Significance" diagram for type 4 cycles only. See text for discussion.

TYPE 4 CYCLES ONLY.

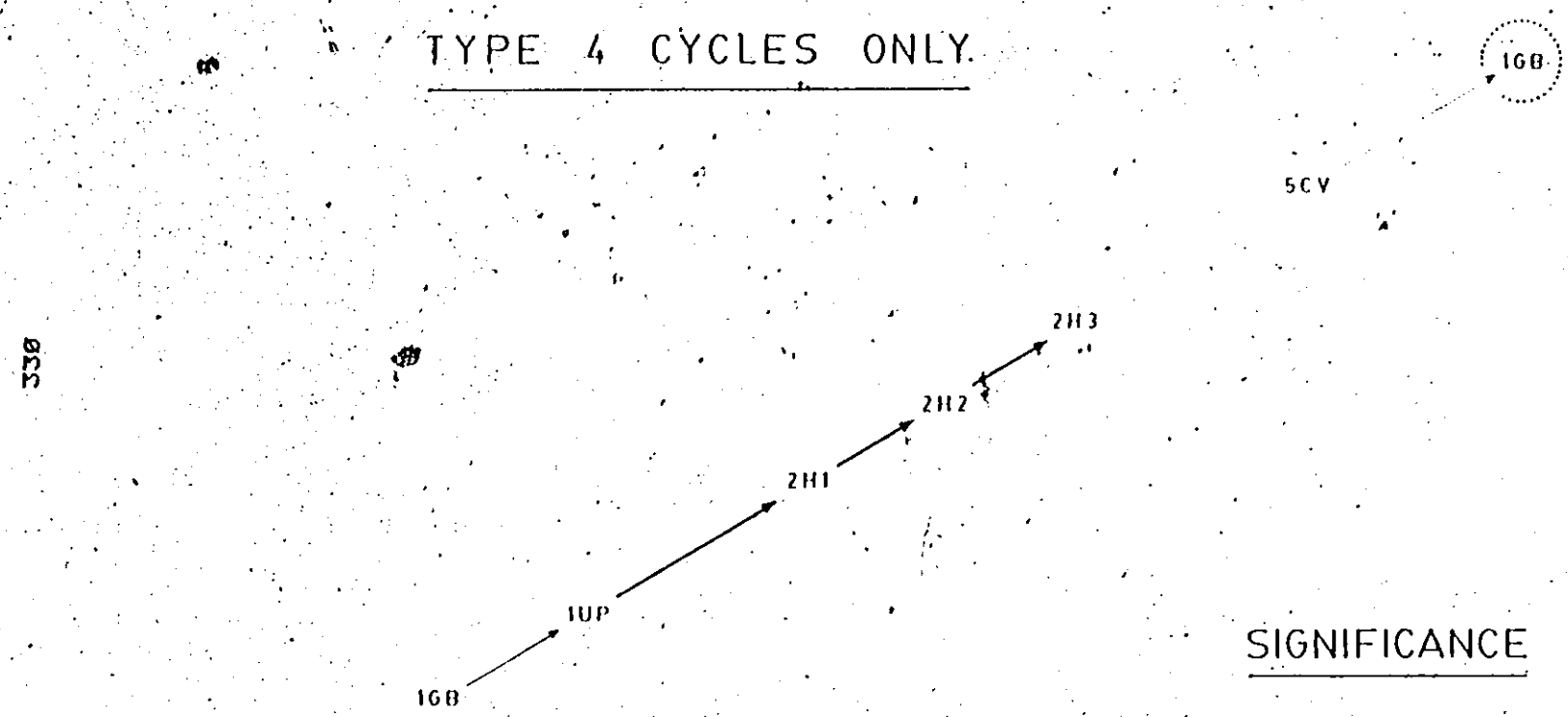

SIGNIFICANCE

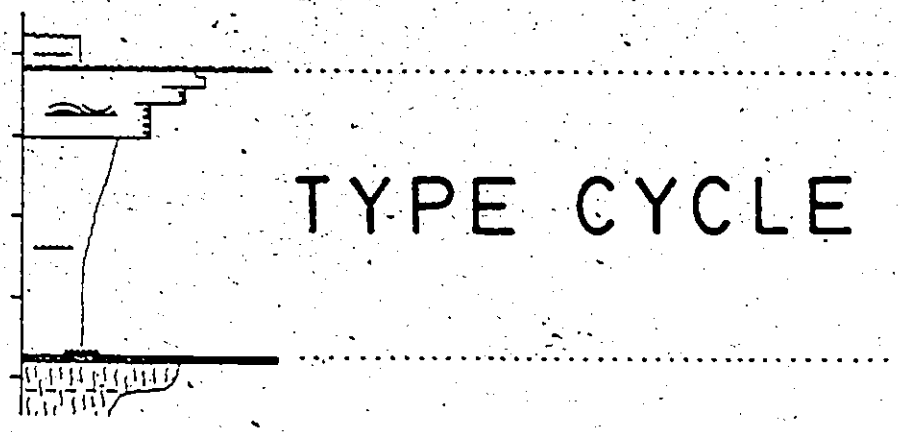

Figure 5-29. Synthetic (i.e., normative) type 4 cycle. Inset diagram shows the type example for this cycle type; tick marks on type example indicate 10 m intervals. See text for discussion.

TYPE 4 CYCLES

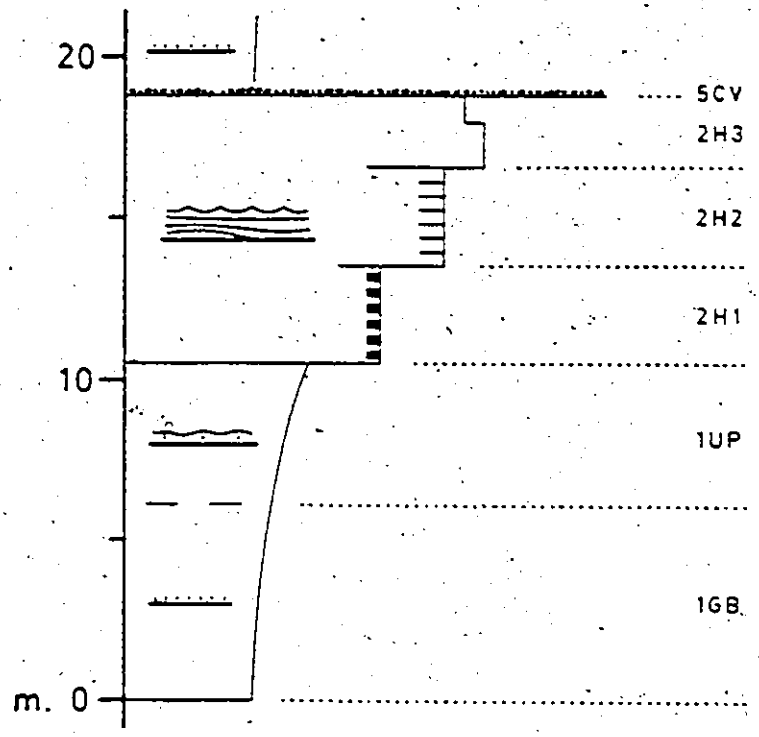

SYNTHETIC
CYCLE

Figure 5-30. Simplified residual probability and "confidence" diagrams for type 5 cycles only. See text for discussion.

TYPE 5 CYCLES ONLY

25 TRANSITIONS
6 FACIES

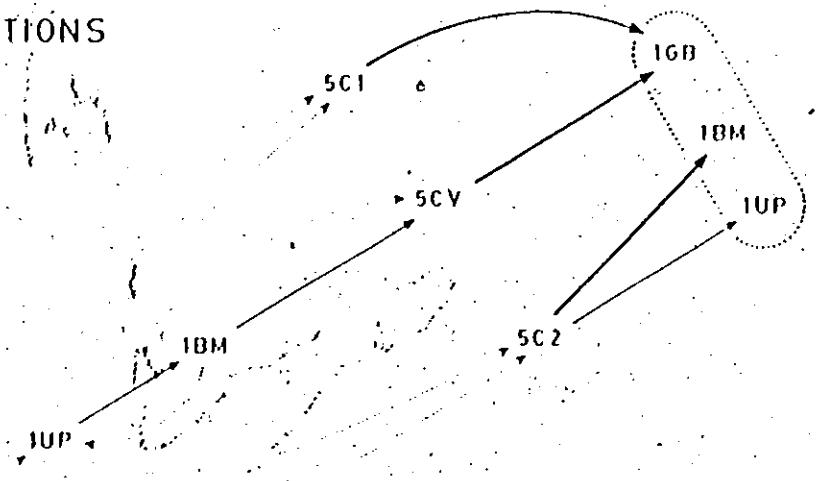

RESIDUAL PROBABILITY

ALL POSITIVE RESIDUALS SHOWN

CONFIDENCE

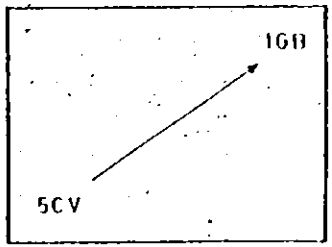

Figure 5-31. "Significance" diagram for type 5 cycles only. See text for discussion.

TYPE 5
CYCLES ONLY

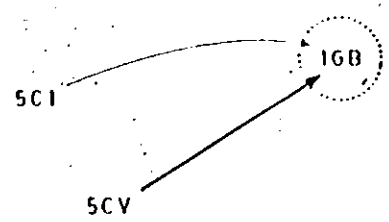

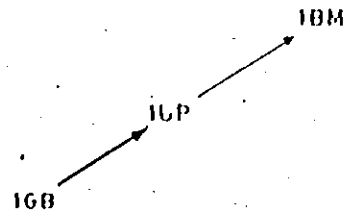

SIGNIFICANCE

ELIMINATED VALUES ≤ -0.02
ALL POSITIVE RESIDUALS CONSIDERED
CONFIDENCE IGNORED

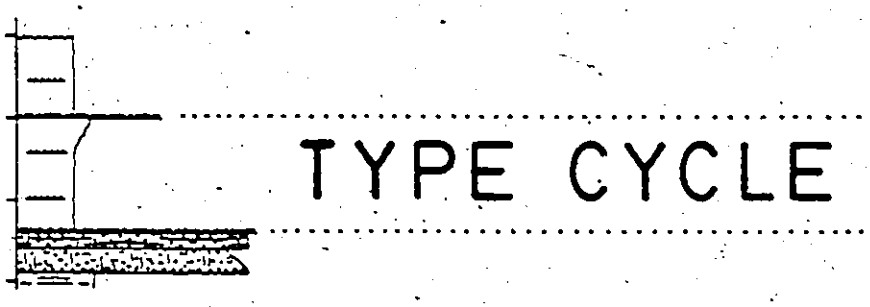

Figure 5-32. Synthetic (i.e., normative) type 5 cycle. Inset diagram shows the type example for this cycle type; tick marks on type example indicate 10 m intervals. See text for discussion.

TYPE 5 CYCLES

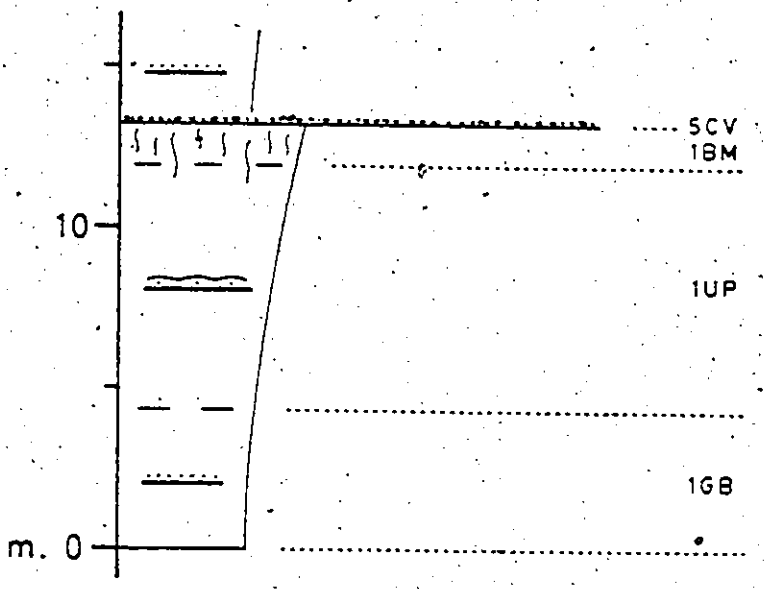

SYNTHETIC
CYCLE

synthetic cycle, probably due largely to partial development of some cycles (e.g., those in which facies 1UP is absent).

Cycle Type 6 ("Fully Bioturbated Cycles")

Of the 134 observed cycles, 9 examples (7%) are classified as type 6. These 9 examples have an average thickness of 12.7 m (range: 6.7 to 18.7 m).

The simplified residual probability and significance diagrams for type 6 cycles only are presented in figure 5-33. No confidence diagram was drawn, because all transitions had a confidence value less than 75%. These diagrams indicate that the most typical type 6 facies sequence (from the base of one cycle to the base of the next cycle) is as follows:

1BM > 3BS > 1BM

The data for type 6 cycles summarized in figure 5-33 provides an excellent example of the utility and validity of the "significance filter" developed in this thesis. The residual probability diagram indicates relatively high transition probabilities for transitions involving facies that occur only once or twice (i.e., those involving conglomerates of association 5 or non-bioturbated facies from association 1). It does <u>not</u> indicate a high value for

the transitions from 1BM to 3BS and from 3BS back to 1BM, despite the fact that they occur very commonly; this is because the majority of type 6 cycles consist of these two facies only. Transitions involving exactly two facies only will always appear exactly random. It is for this reason also that confidence values are so low in this set of transitions.

In the significance diagram, however, only the transition from 1BM to 3BS has a high value; this follows from the fact that this transition occurs so commonly. Thus, the application of this filter to those transitions with positive residuals allows determination of transitions significant in a normative sequence. Note that the transition from 3BS back to 1BM had a non-positive residual probability, and therefore was not subjected to the significance filter. However, the inclusion of this transition is necessary to complete the cycle (i.e., to indicate that facies 3BS represents the last facies in the normative sequence, a fact strongly indicated by the subjective inspection of cycles).

Figure 5-34 is a vertical graphic log of the synthetic sequence; thicknesses were derived from the thickness-of-underlying matrix for these transitions (appendix 4). This synthetic sequence can be compared with the designated type example of cycle type 6 (cycle number 3, section 5-45, Ram River -- inset of Fig. 5-34). Note



Figure 33. Simplified residual probability and "significance" diagram for type 6 cycles only. Confidence values are too low to warrant an illustration. See text for discussion.

TYPE 6 CYCLES ONLY

22 TRANSITIONS
6 FACIES

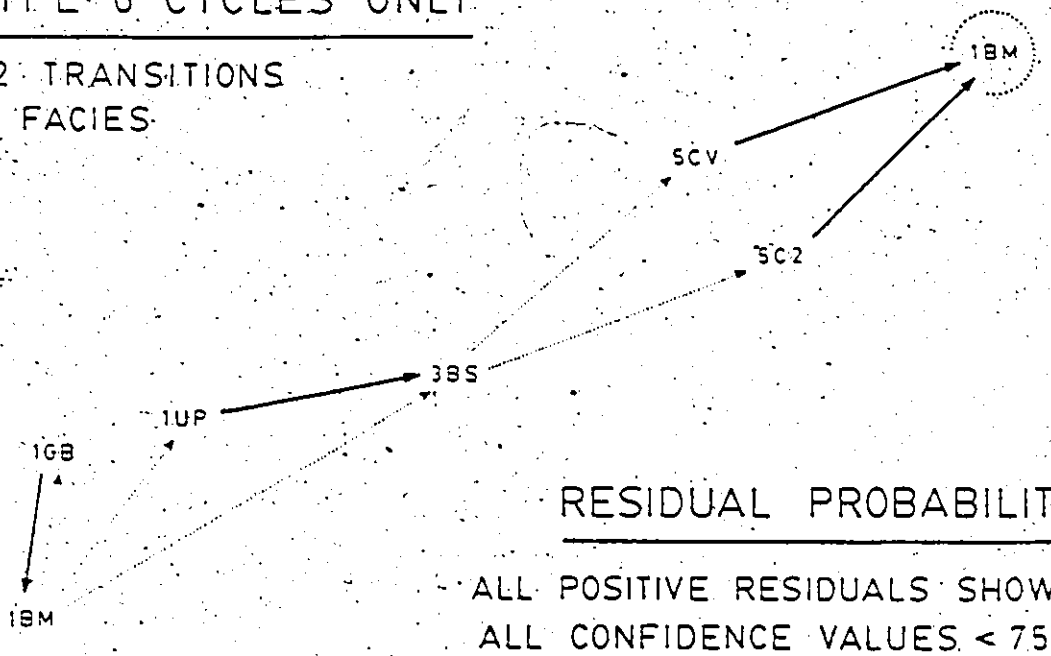

RESIDUAL PROBABILITY

ALL POSITIVE RESIDUALS SHOWN.
ALL CONFIDENCE VALUES < 75 %

TYPE 6 CYCLES ONLY

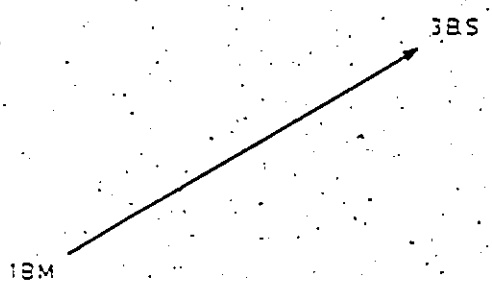

SIGNIFICANCE

ELIMINATED VALUES ≤ -0.05
ALL POSITIVE RESIDUALS CONSIDERED
CONFIDENCE IGNORED

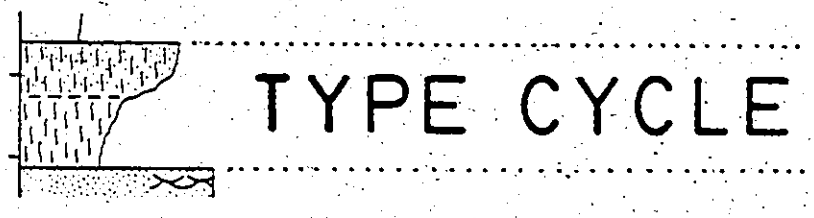

Figure 5-34. Synthetic (i.e., normative) type 6 cycle. Inset diagram shows the type example for this cycle type; tick marks on type example indicate 10 m intervals. See text for discussion.

TYPE 6 CYCLES

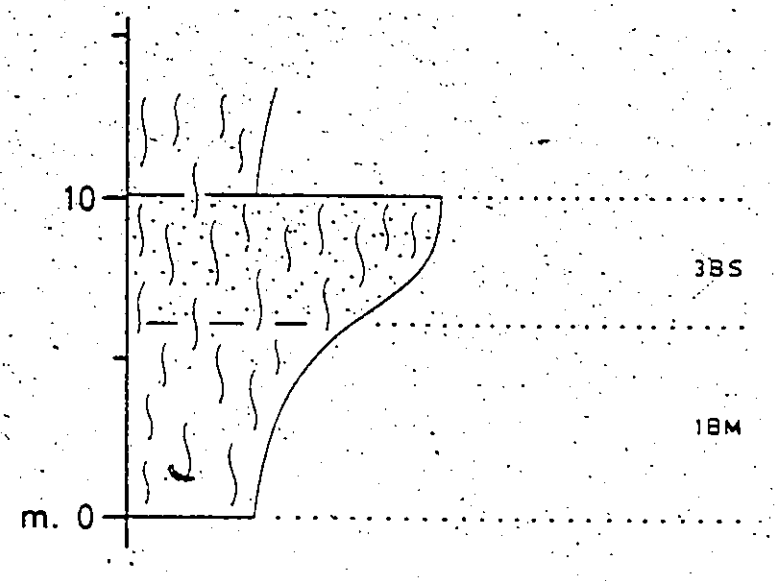

SYNTHETIC
CYCLE

that the synthetic cycle has a thickness of 10.1 m; again, this thickness is similar to the mean thickness of cycles (12.7 m), but is somewhat less than the thickness of the type cycle (15.1 m).

The utility of the significance filter in the analysis of type 6 cycles (see discussion above) is illustrated equally well in the analyses of the other cycle types in the Cardium Formation. Examining the type 3 cycle diagrams, for example, we see that the significance filter (Fig. 5-24) eliminates a lower branch of the residual and significance diagrams (Fig. 5-22 & 5-23) leading to facies 3HA. The eliminated branch involves a set of facies which occur very rarely in these cycles, but happen to be vertically juxtaposed (thus resulting in high residual probability and confidence values). This branch is of no significance to a normative analysis; its elimination again demonstrates the utility and validity of the significance filter.

PRELIMINARY INTERPRETATION OF CARDIUM CYCLES

Proximal-Distal Relationships

Having defined the six basic types of cycles recognized in this study, a comparison of their salient

features permits tentative interpretation of their origin and sedimentary significance.

The synthetic cycles represent typical sequences and thicknesses better than the type examples do, as illustrated in the preceding section. The six synthetic summary sequences are compared to scale in figure 5-35, and a tentative proximal-distal ordering of the terminal facies is assigned. This ordering was determined as follows:

The vertical sequence of facies in cycle type 1 clearly represents a regressive sequence, in that it records a gradual transition from marine mudstones through marine sandstones into non-marine deposits of variable lithology. The nature of Cardium shorelines has not yet been specified; however, the vertical sequence of facies in the type 1 cycle probably reflects a gradational upward decrease in water depth and increase in proximity to shore. Both of these relationships are supported by the preliminary interpretations of chapter 4; briefly summarized, the upward increase in maximum grain size and amount of coarse material per unit thickness, the increase in abundance and scale of wave-generated structures, and the variation in biological assemblages are all consistent with these conclusions.

Having assigned tentative proximal-distal relationships to the various facies by means of their ordering in cycle type 1, it is now possible to arrange the

Figure 5-35. Tentative proximal-distal ordering of the cycle types. Cycles are represented by their respective synthetic cycles, and are ordered according to proximality of the final deposits preserved. In this arrangement, cycle type 1 is most proximal; type 5 is most distal. Type 6 cycles cannot be ordered with any confidence. Note increase in cycle thickness with increasing proximality. Bracketed area indicates my subjectively assigned location in this scheme of the thickest transgressive conglomerates and the best-developed thinning- and fining-upward intervals. Tick marks on sections indicate 5 m intervals. See text for discussion.

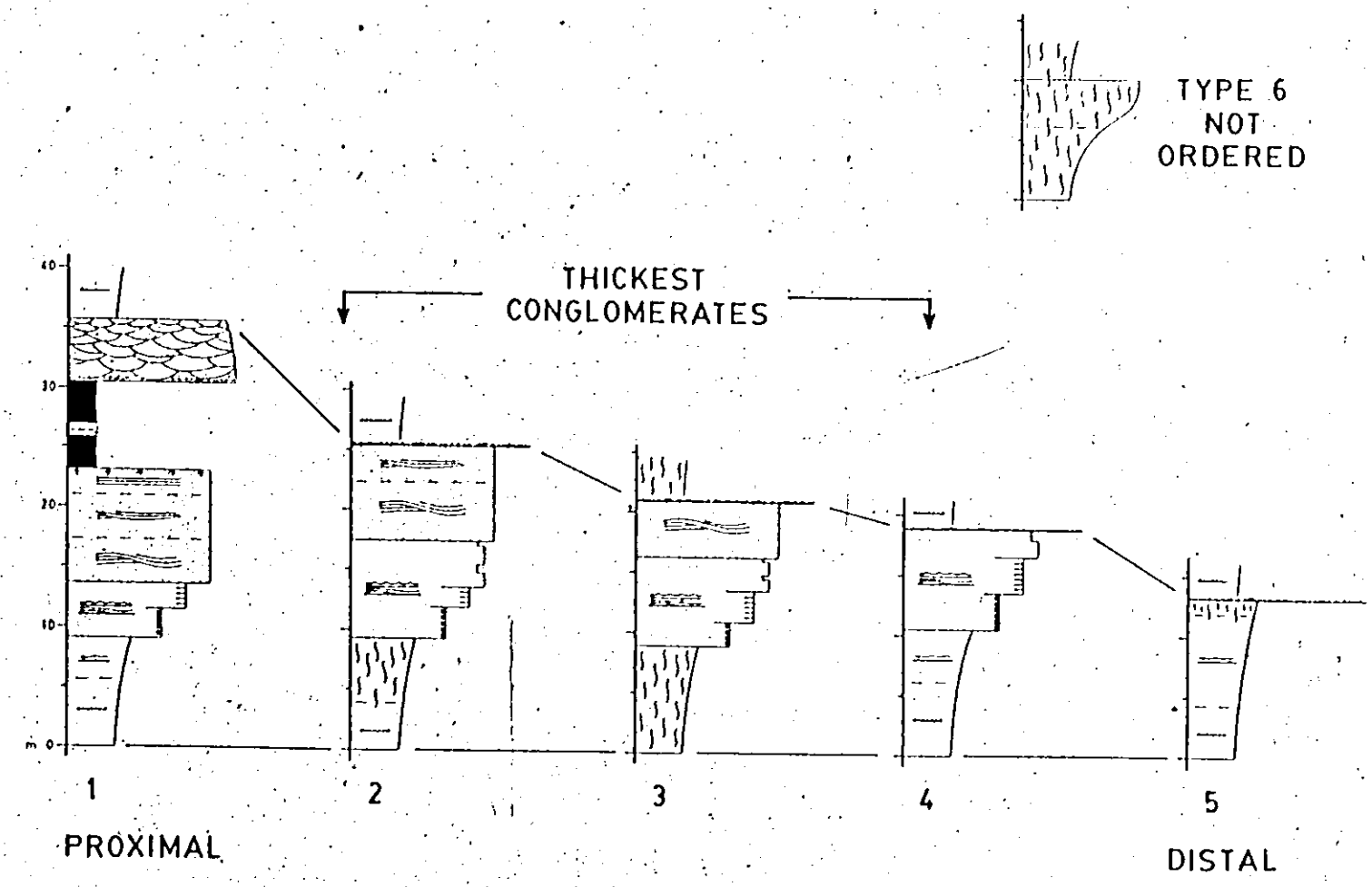
TYPE 6
NOT
ORDERED
THICKEST
CONGLOMERATES
40
30
20
10
m 0
1
2
3
4
5
PROXIMAL
DISTAL

various fully marine cycles (types 2 to 6) in order of the most proximal facies present, namely, the final characterising facies below the inferred transgressive surface. [Note that herein I use the term "transgressive" in reference to deposits or sequences that record a relative deepening, either local or regional, regardless of the depositional environment of the underlying deposits.] This arrangement of cycles by their maximum proximality is indicated in figure 5-35; conveniently, increasing maximum proximality is reflected by decreasing cycle-type number (with the possible exception of cycle type 6, which is difficult to arrange -- see below). According to this arrangement, an increasingly proximal position corresponds with an increased synthetic cycle thickness; proximality also is reflected by the mean thicknesses of each cycle type (see preceding section).

The fully bioturbated cycles (type 6) may represent something of an anomaly in comparison with the other weakly bioturbated cycle types. Although they are the thinnest cycles, the sand content, maximum sand size, and the thickness of (relict) bedding at the top of type 6 cycles commonly is greater than at the top of type 5 cycles; locally, these variables are greater in type 6 cycles than in many type 4 cycles. Thus, the position of type 6 cycles in the proximal-distal scheme above has been omitted (see chapters 6 and 7 for further discussion).

Figure 5-35 also indicates my own placement (subjectively determined) of the location in this proximal-distal scheme of those cycles which display the thickest transgressive conglomerates and the best-developed thinning- and fining-upward cycle caps. These features shall be discussed further in chapters 6 and 7.

Significance of Variable Stratigraphic Position of Transgression Surface

Comparison of the six synthetic cycles in figure 5-35 clearly reveals a very close similarity in the sequences and thicknesses of those facies present in more than one cycle type. Thus, these cycles can be regarded as differentially truncated versions of a single basic facies-sequence motif. The truncation surface corresponds to the inferred transgression surface in each case. What geological interpretations can we assign to this type of truncation geometry? Three possible interpretations involve:

1) unconformity between cycles,

2) erosional contact between cycles, and

3) non-depositional contact between cycles.

Given the consistantly concordant relationship between bedding in vertically juxtaposed cycles, any possible

unconformity present between cycles would be described as a disconformity or paraconformity, depending upon, respectively, the presence or absence of erosional relief. Although some hiatus is undoubtedly present between cycles, the lengths of time are much too small to warrent use of these terms, given that the entire formation (more or less) was deposited within only a fraction of the Turnian stage (Fig. 2-2).

Although bedding between cycles is consistently concordant, it is noteworthy that a slight angular discordance may be present between bedding in the uppermost Cardium and the basal Wapiabi beds at the exposure on Littlehorn Creek (section 5-37). Stott (1963, p. 87) also recognized this geometry. Close inspection of this contact suggests that the angular relationship is due to the depositional pinch-out of the overlying beds against the underlying transgressive surface. Note that these beds form a thinning- and fining-upward symmetrical cycle cap overlying non-marine depposits; inferred transgressive deposits of this sort display the least lateral persistance within the formation, consistent with the interpretation of depositional pinch-out.

Having eliminated the likelihood of unconformable relationships within the formation, the development of cycle truncations can be confidently attributed to

sedimentological (i.e., non-structural) processes only. Two extreme interpretations of the truncated geometry of Cardium cycles is possible: 1) The various levels of truncation may represent differential erosion of the same great thickness of sediment, to produce the final assemblage of six cycle types, or 2) this assemblage may result from lateral variation in sediment accumulation (and cycle development) prior to a non-erosional transgression. In reality, of course, a combination of both erosion and non-deposition may have been involved in the development of Cardium cycles. The relative importance of these two factors in the formation of the different cycle types will be estimated below, based upon a variety of evidence and reasoning.

Evidence of erosion. Evidence of pronounced erosion at the upper contacts of cycles is present in many examples, but is largely confined to cycle types 2 and 3, which terminate in the thick shoreface (or shoreface-attached) sandstones of association 3. Erosional features are locally present at the tops of type 1 cycles, also. Erosional features are associated with the sharp transgressive surfaces, or occur at the base of transgressive conglomerates of association 5. Virtually no evidence for an exceptional degree of erosion is present at the tops of any examples of type 4, 5, or 6 cycles (see

further discussion below). The various features indicating pronounced erosion of upper cycle boundaries are summarized and described below:

1) Truncation of underlying sandstone laminae by superficial transgression surfaces is almost universal in cycle types 2 and 3 (see below); note, however, that superficial erosion is a distinctly common feature of most hummocky beds, and may not indicate extreme erosion in the special case of the last bed in a coarsening-upward sequence.

In the context of this discussion, an observation from chapter 4 is perhaps worthy of elaboration. A single type 2 cycle was observed in which swaley cross-stratified sandstone, immediately overlain by a transgression surface at which no conglomerate was present, exhibited well developed positive-relief hummocks at the upper cycle boundary. Two interpretations of this unusual geometry are possible: First, swaley cross-stratification may form by penecontemporaneous erosion into and preferential removal of topographically higher hummocks, thus preferentially preserving swales. During rapid transgression, subsequent erosion of the last hummocks formed did not occur. Second, the last structures found in this particular cycle may have formed in deeper water <u>after</u> the commencement of transgression; thus, the superficial hummocks may actually

represent structures from a hummocky (not swaley) facies. In fact, both alternatives may be true. In the context of the present discussion of erosion, the interpretive alternatives of preserved hummocks below a transgression surface is of great importance, for their preservation implies non-erosion if the first interpretation is accepted, whereas in the second interpretation, the hummocks merely indicate remobilization of sand during transgression (very like the symmetrical caps discussed in detail below). In this case, the hummocks may in fact obliterate evidence of transgressive erosion. It being the case that all (or at least most) other tops of cycle types 2 and 3 show evidence of erosion, I suggest that the second interpretation is more likely.

2) Erosional relief on the order of tens of centimeters or more is locally observed on the tops of cycle types 2 and 3, but has never been observed at the top of any other cycle type. This type of erosional relief is generally restricted to gutter-like elongate scours or furrows (see below), but may also take the form of broad, shallow scours in the underlying sandstone. These features generally are filled with either conglomerate or mudstone.

3) Aligned erosional furrows are observed locally at the tops of cycle types 2 and 3. These erosional features generally are long and straight; their sides typically are much steeper than the angle of repose,

suggesting partial consolidation of the underlying sandstone (see further discussion below). In examples where conglomerates are present at transgression surfaces, these scours are beneath the conglomerate, with which they usually are filled. In examples where conglomerates are not present, the scours generally are filled with mudstone (locally, sandstone). The mudstone typically contains thin beds of siltstone or sandstone, indicating an episodic filling of pre-existing erosional furrows (i.e., the flows that cut the features were not the same as those that filled them). Large furrows of this type, from the top of a cycle at the Bighorn Damsite outcrop (section BD-1), have been described and figured by Krause & Nelson (1984, Fig. 11), who offered no specific interpretation of their origin.

4) Reworked Ophiomorpha burrows were observed within a transgressive conglomerate veneer (facies SCV) at the top of one type 2 cycle (cycle # 4, section BD-1, Bighorn Damsite). These burrow fragments, composed of siderite cemented sandstone, are identical to in situ burrows within the swaley cross-stratified sandstone immediately underlying the transgressive conglomerate veneer.

Accumulation of a significant amount of these burrows, especially where preserved within a conglomerate bed, implies erosion and removal of vast amounts of the

sand matrix in which they were formed. The burrow fragments themselves are generally a few centimeters long and wide, indicating an absolute minimum of a few centimeters erosion; however, it is more likely that the burrows were fragmented and/or hydrodymanically sorted by the erpding flows, and that the total amount of erosion was much greater.

Extent of erosion: Conceptual limitations. It is reasonably easy to accommodate the possibility of transgressive erosion and removal of previously deposited nearshore, beach, and/or lower coastal plain sediments. As summarized by Swift (1976), the onlap of the sediment-starved nearshore zone during transgression can be expected to produce such erosion (see further discussion in chapter 6). However, it is conceptually difficult to imagine a process whereby transgressive erosion could account for the removal of several meters of sediment deposited far offshore. The superposition of a transgressive, erosional nearshore zone over previously deposited nearshore (and, possibly, beach and non-marine) sediments can not be expected to cause deep erosion to distal offshore deposits without the addition of extensive tectonic uplift. There is no direct evidence (e.g., angular discordances or massive subaerial erosional relief between cycles) for periods of extensive uplifting in the

Cardium sequences examined. In situations in which major periods of uplift are not involved, transgressive erosion cannot be invoked to remove sediments originally deposited far offshore. The absence of erosional features at the tops of Cardium cycles composed exclusively of offshore sediments is consistent with the non-depositional truncation of these cycles, rather than truncation by means of transgressive or subaerial erosion.

Thickness variation within transgressive conglomerates. The preceding discussion suggests that only non-deposition or subaerial and/or transgressive erosion could reasonably account for the absence of tens of meters of sediment at the tops of cycle types 4, 5, and 6. What are some of the consequences of these two alternatives?

Non-deposition (and little or no erosion) associated with the passive termination of sedimentation during transgression would not be expected to produce thick erosional lag conglomerates at the tops of cycle types 4, 5, and 6. Erosion (either subaerial or submarine) would be expected to produce extensive conglomerates at the tops of these cycles. Thus, the distribution of cycle-capping conglomerates suggests a test for this distinction between processes.

Figure 5-35 shows the subjectively determined distribution of well developed cycle-capping conglomerates.

These conglomerates are best developed over cycle types 2 and 3, conceptually consistent with transgressive erosion of nearshore and proximal offshore sediments. Cycle types 4, 5, and 6 exhibit fewer and thinner conglomerates than the other top-absent cycles, consistent with the absence of associations 3 and 4 in these cycles due to non-deposition, rather than erosion. These conglomerates shall be further discussed in chapter 6.

Evidence of extended periods of submarine non-deposition. Transgression surfaces capping cycle types 4, 5, and 6 generally exhibit positive evidence for extended periods of exposure at the sediment-water interface, implying long intervals of non-deposition during transgression. This evidence consists of: 1) heavy siderite cementation at the tops of many of these cycles, 2) a great abundance of ammonites at the tops of these cycles locally, and 3) the local development of firmgrounds at these cycle tops, indicated by the presence of Inoceramus encrusted with bryozoans (Fig. 4-26).

Evidence of transgressive deposition. The thinning- and fining-upward caps locally present at the tops of cycles are best interpreted as having been deposited during transgression. These transgressive deposits are best developed at the tops of cycle types 2 and 3, as indicated in figure 5-35. Transgressive

deposition at the tops of these cycles is inconsistent with a suggestion of penecontemporaneous transgressive erosion at the same locality. These fining-upward intervals (locally capped with conglomerates) are best interpreted as being composed of sediment deposited during transgression which was eroded from laterally adjacent shallower waters more proximal to shore (possibly from lower-numbered cycles, including type 1 cycles). These transgressive deposits were deposited in deeper waters beyond the influence of actively eroding bottom flows (chapter 6).

Summary: Origin of truncated cycles. The various forms of truncated (i.e. top-absent) cycles defined by vertical facies analysis represent variously truncated forms of a prograding shoreline sequence. This sequence is completely developed in type 1 cycles. The other cycle types can be interpreted as developing due to lateral variation during transgression in the combined effects of erosion, non-deposition, and sedimentation. Extensive subaerial erosion is contra-indicated (see above).

Lateral variation in the relative importance of deposition and erosion (see above) suggests that landward translation of the shoreface profile during transgression was the major factor controlling the development of Cardium cycles. Accordingly, evidence of erosion is confined largely to the tops of cycle types 2 and 3, due to the

general restriction of major transgressive erosion to areas of the shoreface (especially the upper shoreface). Thus, the development of Cardium cycles probably was controlled largely by tectonoeustatic processes governing rates of change in relative sea level, rather than by sedimentologic processes alone (see further discussion in chapters 6 and 7). The inferred tectonoeustatic control of cycle development is consistent with the ability to correlate most Cardium cycles regionally, as will be discussed in chapter 6.

INTERPRETATION OF VARIANT CYCLES

As previously stated, absence of associations 1 and/or 2 from cycles displaying associations 3, 4, and/or 5 is a fairly common variation from the normal complete or top-absent cycle sequences described above. These common variant cycles are interpreted below.

Bottom-Absent Cycles

An individual cycle which does not commence in association 1 (termed a "bottom-absent" cycle -- Fig. 5-2) is best interpreted as representing deposition following a transgression of a locally restricted nature. By this I

mean, specifically, that the transgression was not sufficiently extensive to remove the source (i.e., the shoreline) to a position where only mud-dominated facies might be deposited at this particular site of deposition. This is not to say that the transgression must have been less extensive than the norm; rather, the effect of the transgression was simply less great at this particular site of deposition, very proximal to shore. The geometry of this interpretation is best illustrated by means of a diagram (Fig. 5-36). In this diagram, the bottom-absent cycle is placed in a more shoreline-proximal position following transgression than is a correlative "complete" cycle. As shall be demonstrated in chapter 6, the lateral correlation of cycles supports this interpretation most strongly.

Note that bottom-absent cycles tend to occur in vertically juxtaposed groups (as, for instance, the cycles present in section BD-1 at the Bighorn Damsite), supportive of the interpretation of formation due to oscillations of sealevel in a shoreline-proximal setting. They are most common in inner Foothills sections and northern Foothills sections, again supporting the inferred proximal setting (see chapters 6 and 7 for further discussion).

Middle-Absent Cycles

Middle-absent cycles are those in which association 2 is absent, but both associations 1 and 3 are present. Middle-absent cycles commence in association 1; these mud-dominated deposits are immediately and erosionally overlain by the thick sandstones of association 3. The resulting vertical profile shows an abrupt, step-wise coarsening-upward trend (Fig. 5-2 & 5-37), rather than the smoothly continuous profile typical of most cycles. The basal contact of association 3 is erosional; channelling and/or basal pebble lags are present locally.

Middle-absent cycles are the rarest variant present in Foothills sections. Originally, I interpreted this variant as representing a shallow-marine, shore-normal channel incised in the lower shoreface. The general absence of other shoreface channels was thought to reflect the localized nature of these features; alternatively, evidence of channels higher on the shoreface might have been erased by the subsequent shifting of sand due to wave activity.

Whereas the channel interpretation suggested above remains plausible for Foothills exposures, a much more appealing interpretation for middle-absent cycles has been developed from the detailed study of the Cardium in the subsurface of the Kakwa area, conducted by Guy Plint at

Figure 5-36. Diagram illustrating a vertical section normal to shoreline, based upon the correlation of measured sections in the Grande Cache area (appendices 1 and 2). These sections indicate the relationships (in a minor transgressive-regressive pulse superimposed upon a major regressive episode) between normal complete cycles, bottom-absent cycles, and cycles which are both bottom- and middle-absent. See text of this chapter (and, especially, chapter 6) for discussion.

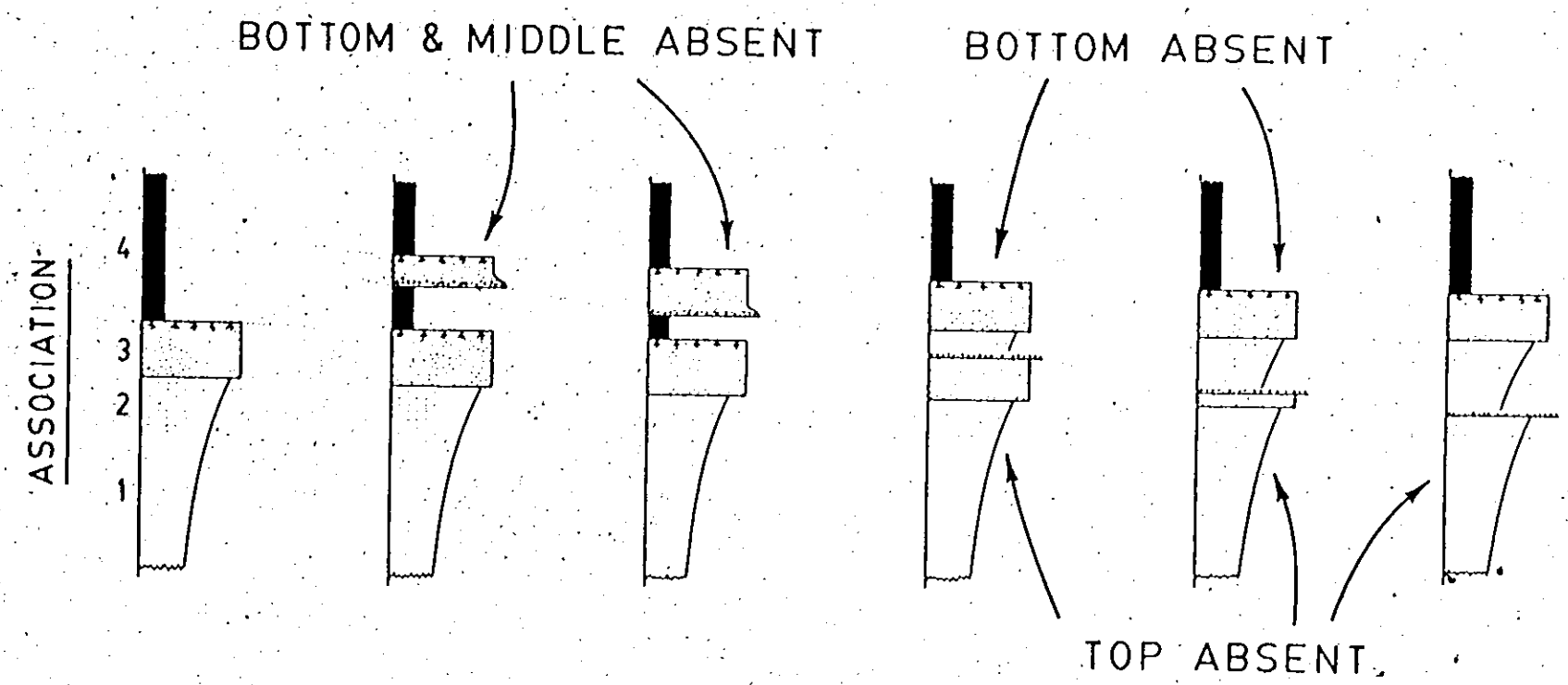
BOTTOM & MIDDLE ABSENT
BOTTOM ABSENT
ASSOCIATION
4
3
2
1
TOP ABSENT

Figure 5-37. Part of a middle-absent cycle seen in a section normal to bedding, showing a typically sharp contact between mud-dominated deposits of association 1 and sandstone of association 3. Up is to the right. Note gutter casts within mud-dominated deposits of facies 1UP. Cycle 3, section 5-37. See text for discussion.



McMaster University (pers. comm., 1984 & 1985). At Kakwa, the Cardium contains several cycles. The lower of these is the thickest and best developed; it represents a tens-of-meters thick, fully regressive cycle correlative for great distances laterally. This cycle closely resembles the major cyclic development present in the northern Foothills exposures, with which it probably is correlative. Areally extensive, closely spaced well cores and logs enabled Plint to map lateral variation within this cycle, revealing a NNW-SSE paleoshoreline orientation. Both complete and middle-absent developments are present within the cycle; these two types occur in three laterally adjacent, NNW-SSE trending bands parallel to shore. These three bands traverse the entire area of study (approximately 50 km). The innermost (western) band exhibits complete cycles. The central band (roughly 15 km in width parallel to shore) exhibits middle-absent cycles. The outer (eastern) band again exhibits complete cycles.

At Kakwa, the arrangement of variant cycles is inconsistent with the interpretation of a lower shoreface channel oriented perpendicular to shore. Rather, Plint attributes the observed areal zonation to an unusually rapid drop in relative sea level, accompanied by shoreface erosion (during subsequent progradation) of interbedded sandstones and mudstones previously deposited in a proximal offshore setting. I favor this interpretation for

middle-absent cycles in Foothills exposures, also.

DESCRIPTION AND INTERPRETATION OF SELECTED FEATURES WITHIN THEIR STRATIGRAPHIC CONTEXT

In this section, I describe and interpret certain primary features common to more than one facies defined in this study. These integrated descriptions and interpretations are presented to emphasize similarities between the facies, and to accent various subtle differences that exist between them. This discussion is presented within the stratigraphic and sedimentological context of the cycles in which these features occur. All observations are then integrated in an overview of Cardium shoreline sequences.

Hummocky Cross-Stratification

Typically, hummocky cross-stratified sandstone beds in regressive Cardium sequences show a variety of systematic vertical trends in basic descriptors (see chapter 3, part 3, for a quantitative discussion). In thickening- and coarsening-upward sequences, the scale of hummocky cross-stratification (specifically, the

characteristic form-spacing of undulatory laminae) increases upward gradationally and monotonically. This upward increase in scale probably reflects shoaling, and an increase in near-bottom orbital diameter associated with storm-generated surface gravity waves.

Also, vertical shoaling sequences generally record distinct variation in the morphology of hummocky cross-stratification. Specifically, the ratio of form-height to form-spacing first increases and then decreases upward. The increase in this ratio is of course associated with an increase in the maximum angle of cross-stratification attained within hummocky beds; thus, the maximum angle of cross-strata dip first increases and then decreases as one ascends through a typical regressive sequence. The maximum values of cross-strata dip and form-height:form-spacing ratio generally occur in facies 2H2, in beds having thicknesses of about 30 to 70 cm. These maxima correspond with those beds which display the best development and preservation of the hummock-swale geometry characteristic of this structure.

Ascending through regressive sequences, the associated tendencies toward increased form-spacing and decreased form-height:form-spacing ratio (in facies higher than facies 2H2) typically proceeds to the gradational contact between swaley cross-stratified sandstones (facies 3SW) and beach sandstones (facies 3PL). Immediately below

such contacts, the amplitude of very low-angle, concave-upward swales is so subtle as to be practically impossible to photograph: Such swales may be several meters in width, yet only a few centimeters in maximum eroded depth.

It is possible (probable?) that the vertical trends described above represent the record of structures formed within the gradational boundaries between stable, oscillatory-flow bed configurations (see extensive discussion in chapter 8). The vertical trends possibly correspond to increased values of near-bed orbital velocities associated with shoaling at a wave-dominated shoreline.

Pot- and Gutter-Casts

Figure 5-38 is a detailed vertical graphic log through the major fully regressive cycle (cycle #2) at section GC-2 (Grande Cache Railway Roadcut). This log is reproduced directly from my field notes. This cycle illustrates important stratigraphic relationships involving pot- and gutter-casts and hummocky cross-stratified sandstones in the Cardium Formation.

In this and other regressive sequences in the formation, it is apparent that gutter-casts greatly outnumber pot-casts where these features were observed.

The physical scale of gutter-casts in these sequences generally increases upward, as is revealed in this log (but see additional discussion below). Orientation of gutter-casts is similar to flow directions obtained from other paleoflow indicators in all sequences examined (appendix 2). These other indicators include sole marks from vertically adjacent hummocky cross-stratified beds which appear tabular on the outcrop scale.

A complete gradational spectrum between gutter-casts and tabular sandstones is apparent at section GC-2; gutter-casts gradually increase in size and thickness vertically, until the scale of channelization approaches and exceeds the scale of outcrop in this and other exposures (Fig. 5-38 & 5-39A). The sandstone filling gutter-casts is undulatory parallel laminated or hummocky cross-stratified in all sandstone-filled occurrences; the scale of undulations in these occurrences increases with the increase in scale of the gutter-casts themselves. Rarely, gutter-casts are filled with interbedded sandstones and mudstones; these sandstone beds are either hummocky cross-stratified or undulatory parallel laminated, and symmetrical ripples are locally observed.

The preceding descriptions suggest that gutter-casts in the Cardium Formation were formed in conjunction with the storm-generated flows inferred to

Figure 5-38. Detailed vertical graphic log for section GC-2 (Grande Cache, Railway Roadcut), photocopied directly from my field notes. Facies subdivisions for this section may be obtained by comparison with vertical graphic log of appendix 2. Tick marks are in meters. See text for discussion.

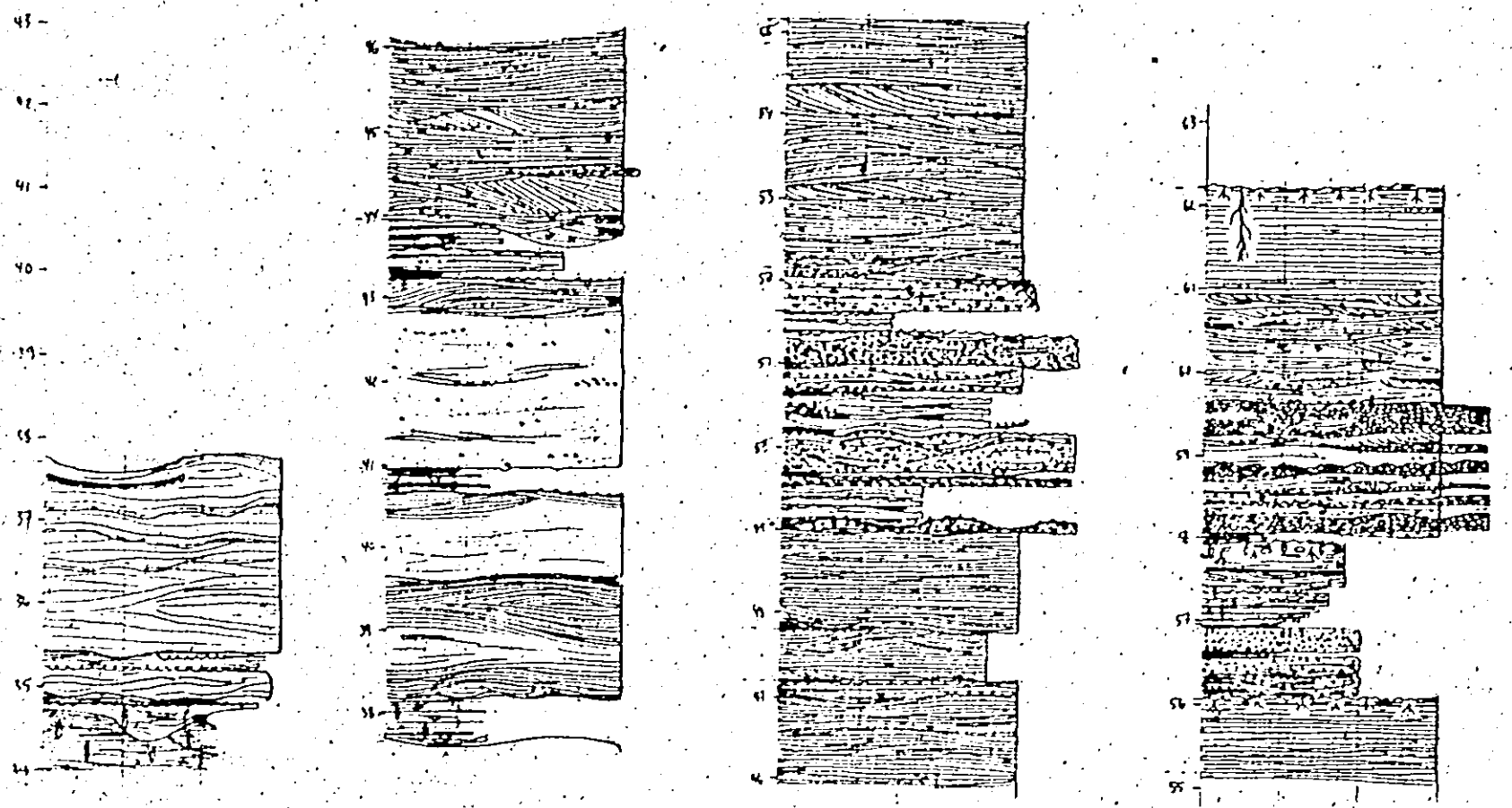

104

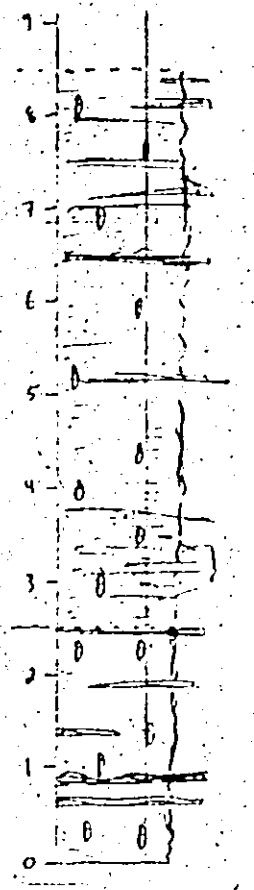

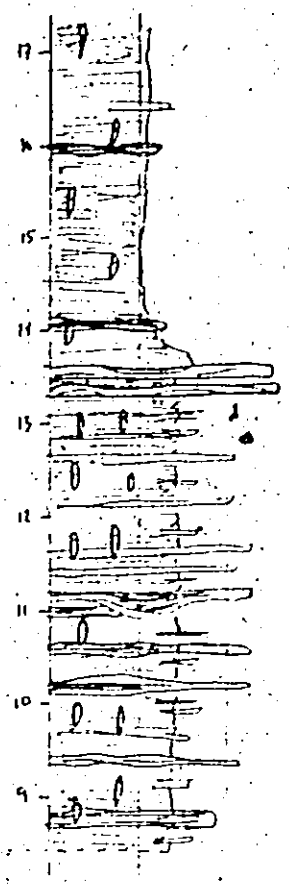

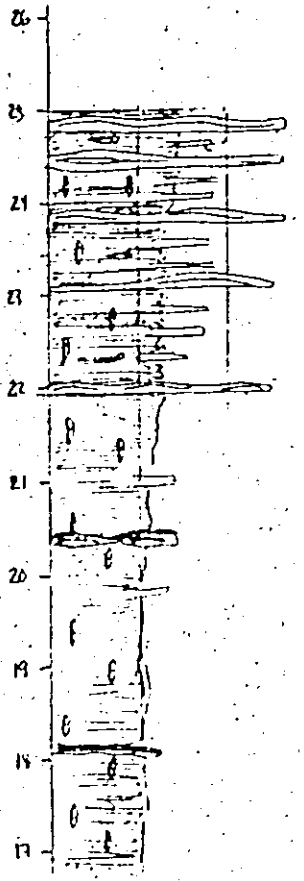

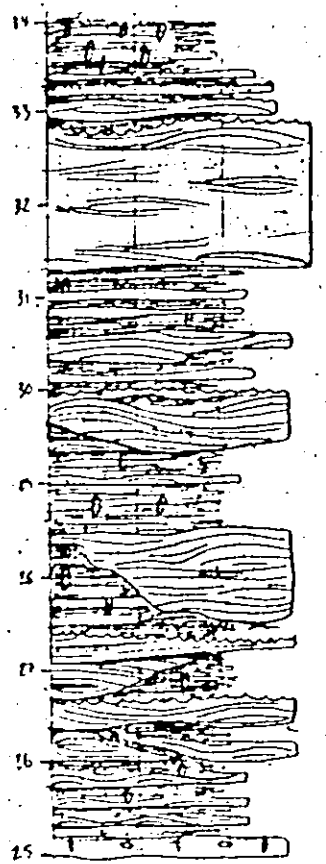

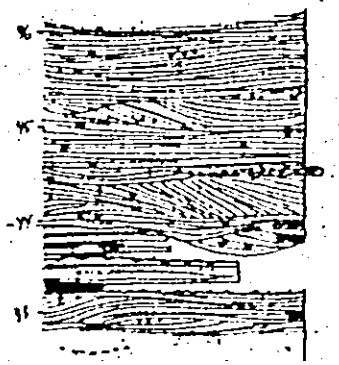

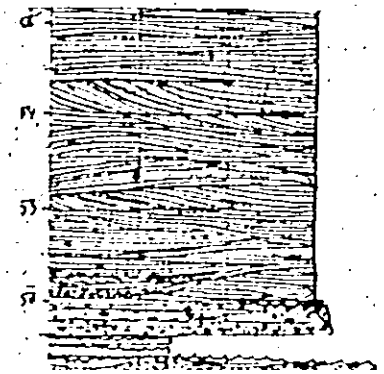

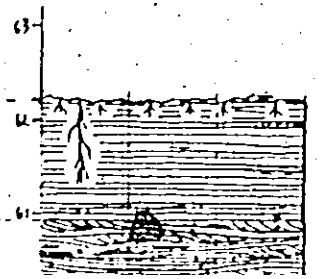

emplace tabular hummocky beds. The tabular beds themselves may represent extreme examples of similar channelized features, with much larger width/thickness ratios than is present in the demonstrably channelized gutter-casts. The presence of some smaller-scale channel features at the bases of certain tabular beds suggests an alternative interpretation, in which a large-scale sheet flow (forming a tabular bed) degenerates down-current into isolated, localized flows concentrated at the sea bed. Localized flows cut and fill channels having a maximum scale approximated by the largest gutter-casts observed in outcrop: these channel-forming flows decrease in scale basinward (down-current). In this alternate scenario, the tabular beds do not represent very wide, large-scale channel features.

A major deviation from the typical vertical pattern of gutter-cast scale variation (described above) is present in a few regressive cycles locally. Figure 5-39C clearly reveals an upward <u>decrease</u> in gutter-cast scale in one such sequence. Such rare sequences often involve several (10 or more) individual gutter casts at differnt stratigraphic levels; their variation cannot reasonably be attributed to random variation, but rather reflects a systematic upward decrease in scale. Such a decrease may possibly indicate that some storm-generated sheet flows, as they flow basinward, degenerate into localized channelized flows

Figure 5-39. Gutter-casts from associations 1 and 2, as seen in sections normal to bedding.

A) Large gutter-casts from section GC-2. Interval figured is between 25 and 31 m (compare with detailed log, Fig. 5-38). Note upward increase in gutter-cast scale, and upward gradational transition from channelized morphology to tabular morphology. See detail in photo B.

B) Detail from A, showing large gutter-cast at 27 m level (above notebook) and left edge of larger, more nearly tabular occurrence at 28.4 m (at upper right of photo).

C) Coarsening-upward sequence in which the scale of gutter-casts decreases upward; much thinner tabular beds in the same interval increase in scale upward. Section 4-21, cycle 2, 103-107 m. See D to F for detailed photos.

D) Detail of hummocky cross-stratification and thin mudstone layer within lowest, largest gutter-cast present in cycle shown in C. Scale is 15 cm long.

E) Obligue view of same gutter-cast shown in C & D. Note erosional longitudinal terracing at base, and cross-sectional profile revealed in the slightly displaced block which supports the 15 cm scale.

F) Close-up of one of the higher, smaller gutter-casts (below notebook in C) in cycle 2 at section 4-21. Note vertical sequence from hummocky cross-stratification to symmetrical ripples with mudstone partings.

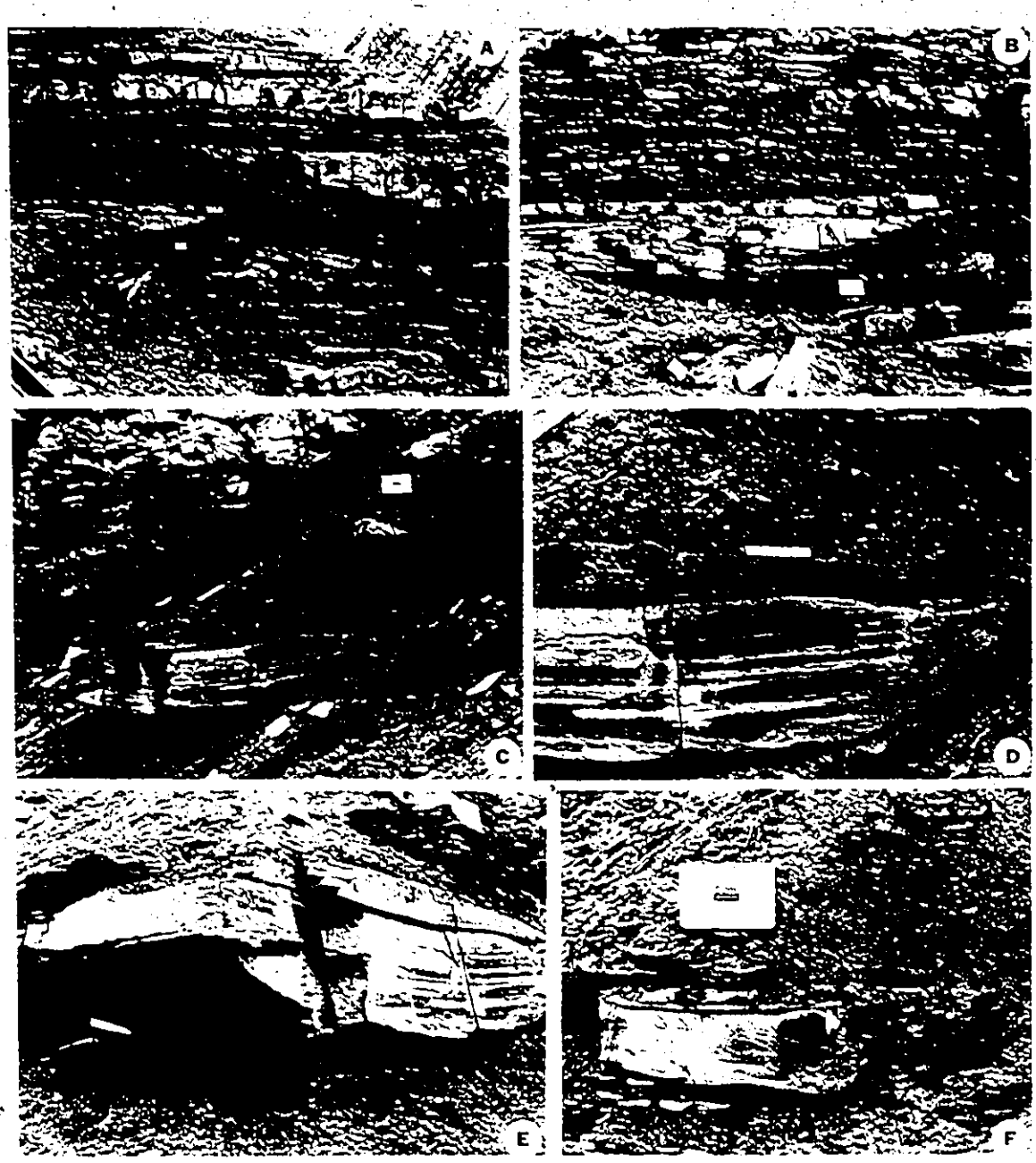
A
B
C
D
E
F

which coalesce downstream prior to their eventual decay and termination.

Occurrence of *Cardium* Valves

Various pelecypod species formerly classified under the genus name *Cardium* are abundant in the Cardium Formation. These species are thought to have populated the nearshore zone (G. E. G. Westermann, pers. comm., 1980). *Cardium* is most commonly encountered within association 2 and facies 3HA, which I interpret as proximal offshore deposits (chapter 4). However, all occurrences of *Cardium* in these deposits consist of disarticulated valves; where present, they almost invariably occur as convex-upward molds on the bases of sandstones overlying mudstones (association 2) or at the bases of amalgamation units (facies 3HA). No *Cardium* individuals were observed in life position. This characteristic mode of preservation strongly suggests that these valves were physically transported to their site of occurrence; they represent a locally allocthonous death assemblage.

I infer that *Cardium* valves in these facies were transported to the offshore zone from their habitat in the nearshore zone (as were the hummocky cross-stratified sands in which they occur) by storm-generated bottom flows. This interpretation is strongly supported by: 1) the general

increase in abundance of Cardium valves at the bases of sandstones as one ascends vertically through offshore deposits in regressive sequences (i.e., Cardium abundance in offshore deposits increases toward the nearshore zone), and 2) the presence of Cardium valves in many occurrences of facies 3SW (swaley cross-stratified sandstone), which I interpret as storm-influenced nearshore deposits.

Occurrence of Conglomeratic Symmetrical Ripples

Conglomeratic symmetrical ripples in the Cardium Formation occur only within facies 5C2. These bedforms are robust features (spacings are on the order of 1 m) inferred to have been generated in a high-energy wave environment (Duke & Leckie, 1984). The distribution of these occurrences (i.e., occurrences of facies 5C2 which display conglomeratic symmetrical ripples) is essentially bi-modal: They appear within inferred shoreface-attached sand bodies deposited during regression (as at section GC-2 -- see Fig. 5-38) and at transgression surfaces capping cycles, within resedimented-lag conglomerates (e.g., ripples capping cycle #2 at the Seebe Damsite outcrop; Wright & Walker, 1981). Extended discussion and illustration of conglomeratic symmetrical ripples will be presented in chapter 8 of this thesis.

The distribution of these wave-formed ripples

strongly suggests a high-energy, wave-dominated depositional setting for the Cardium shoreface, during both regressive progradation and transgressive re-working.

Occurrence of Conglomerate "Stringers"

As was mentioned in the facies descriptions of chapter 4, thin beds or "stringers" of pebbles are present locally within the mud-dominated deposits of association 1 where these deposits directly overlie transgressive conglomerates capping an underlying cycle. Several examples of these stratigraphic relationships are illustrated in the vertical graphic logs of appendix 2 (e.g., cycle 4, section 4-13; cycle 4, section 5-39; cycle 10, section 6-8). The ascending vertical transition from sand-dominated nearshore deposits (and/or non-marine deposits) below a sharp contact to mud-dominated offshore deposits above that contact clearly records a marine transgression, or a least a relative deepening within the basin. As I have discussed above, and as shall be discussed in greater detail in chapter 6, the thick conglomerates present locally at these contacts between cycles are best interpreted as being deposited during transgression. This interpretation is based upon a variety of evidence, including:

1) the presence of marine trace and body fossils within

cycle-capping conglomerates, including those which lie directly upon non-marine deposits,

2) the presence of conglomeratic symmetrical ripples within cycle-capping conglomerates, indicating wave-reworking and transport in relatively shallow water depths (typical of the sandy shoreface) during the early phases of transgression (see chapter 8),

3) the occurrence of thick cycle-capping conglomerates overlying thinning- and fining-upward intervals of clearly transgressive deposits at the tops of cycles locally, and

4) the deposition of cycle-capping conglomerates over a basal erosion surface.

There is no evidence for the the deposition of these thick cycle-capping conglomerates during the regression which produced the underlying cycle; however, the interpretation of transgressive deposition of cycle-capping conglomerates is strongly supported by the stratigraphic positioning of the conglomerate stringers. The occurrence of thin pebble beds overlying the main body of a transgressive conglomerate, appearing as discrete beds within the mud-dominated basal deposits of the next marine cycle, clearly indicates the association of these pebbles with the deposits of the overlying cycle. These sequences also indicate that pebbles were capable of being transported and

deposited (or re-deposited) in the deepest waters of the Cardium basin during transgression or the earliest phases of the subsequent regression.

A PRELIMINARY INTERPRETATION OF CARDIUM SEQUENCES, EMPHASIZING FEATURES OF THE SHORELINE AND LOWER COASTAL PLAIN

As mentioned above, the six basic cycle types defined in this chapter are best interpreted as differentially truncated versions of a prograding shoreline sequence. As has been inferred in previous studies of similar sequences, the ubiquitous abundance of hummocky cross-stratification and other wave-formed structures strongly suggests that the Cardium shoreline and shelf were dominated by waves -- specifically, storm waves and associated storm processes (see literature summary by Duke, 1985c). The general absence of tractional current-formed structures contra-indicates a strong tidal influence (Walker, 1984b).

Figure 5-40 shows a typical shore-normal profile for a sandy, wave-dominated shoreline. In chapter 4 (p. 178-179), I discussed the relationship between the location of the fairweather mudline and the upper limit of preserved mud deposits in ancient storm-dominated prograding

Figure 5-40. Shore-normal vertical profile for a wave-dominated sandy shoreline. Note location of ichnofacies. From Walker (1984b, Fig. 9). See text for discussion.

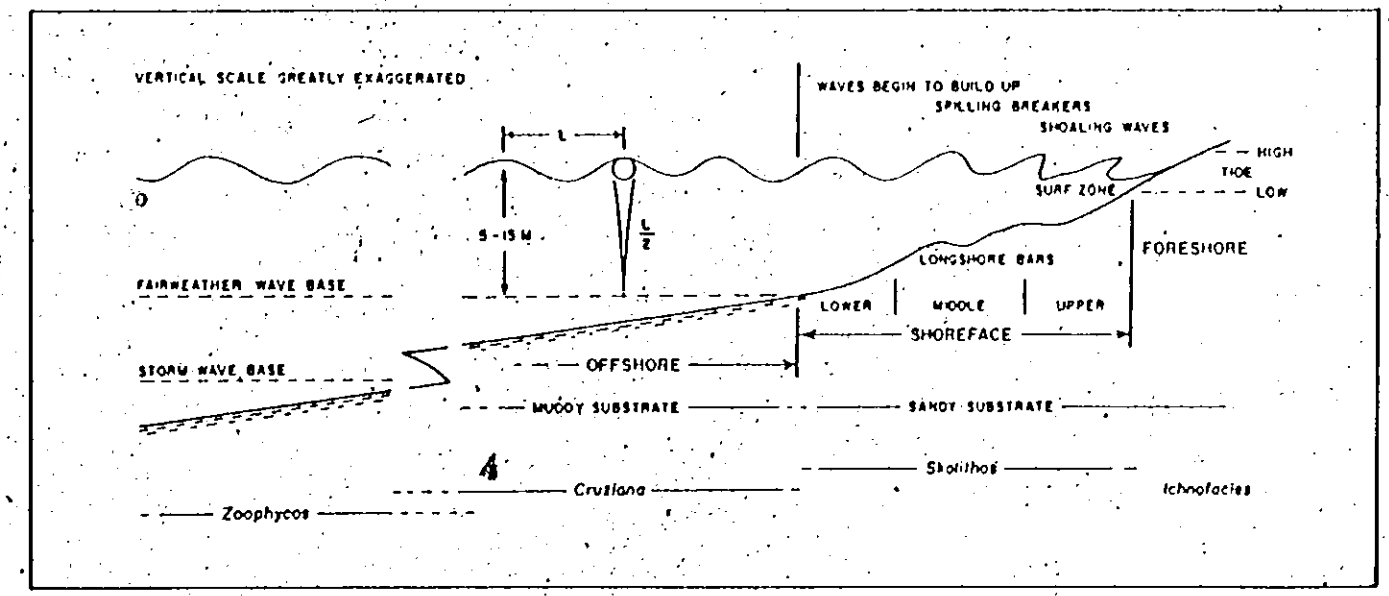
VERTICAL SCALE GREATLY EXAGGERATED
WAVES BEGIN TO BUILD UP
SPILLING BREAKERS
SHOALING WAVES
L
HIGH
TIDE
LOW
SURF ZONE
5 - 15 M
L/2
FORESHORE
LONGSHORE BARS
FAIRWEATHER WAVE BASE
LOWER
MIDDLE
UPPER
SHOREFACE
STORM WAVE BASE
OFFSHORE
MUDDY SUBSTRATE
SANDY SUBSTRATE
Skolithos
Cruziana
Zoophycos
Ichnofacies

shoreline sequences. Briefly summarized, the highest preserved mud lens within these ancient sequences will not generally correspond with the position of the ancient mudline, but rather will have been deposited in a proximal offshore setting at some depth below both the mudline and the fairweather nearshore zone (or shoreface, in the terminology of Walker, 1984b). This inferrence is based on the erosional removal of previously deposited muds (indicated by ubiquitous mudstone rip-up clasts) within facies JHA (amalgamated hummocky sandstones). In the Cardium, such mudstone clasts are present even in subfacies 1 of facies JHA, in which no in situ mudstone deposits are preserved. The offshore depositional setting suggested for the final in situ mudstone deposits is of course strengthened by their occurrence within a "classic" hummocky association (i.e., episodically deposited amalgamated beds with well developed hummocks, as opposed to quasi-continuously deposited, hummock-poor swaley sandstones -- see below).

In contrast, facies JSW (swaley cross-stratified sandstones) generally contains no evidence for mud deposition. This, coupled with the lack of evidence for episodicity in the deposition of thick swaley sandstones, suggests that the offshore-nearshore transition of figure 5-40 is best assigned to the hummocky-swaley contact in ancient sequences (see the normative type 1 sequence, Fig.

5-17). In fully regressive Cardium sequences where swaley cross-stratification is absent, this transition is best assigned to the hummocky-planar contact (i.e., the contact between facies 3HA and facies 3PL), and the nearshore zone is inferred to have been very restricted bathymetrically during fairweather conditions.

The nature of offshore sedimentation during Cardium time constitutes the subject of most of the remainder of this thesis. In the following paragraphs, however, I shall discuss sedimentation at the Cardium shoreline and on the lower coastal plain. The observations and assertions made below are supported by cycle correlations and paleoflow patterns discussed in subsequent chapters.

Figure 5-41 is a block diagram illustrating the major morphological features of the Cardium shoreline and lower coastal plain. A microtidal setting is inferred from the absence of tractional structures from most sequences, excepting those displaying unusually coarse-grained (i.e., sandy) lagoonal deposits. The absence of extensive lagoonal and backbeach deposits in most fully regressive cycles (Fig. 5-17) indicates that lagoons along the shoreline were small and localized. Thus, a strand-plain setting with minor coastal lagoons is inferred, and has been represented in figure 5-41. A probable modern analog is the wave-dominated coast of Nayarit, Mexico (Curray & Moore, 1964; Curray et al., 1969).

Figure 5-41. Block diagram illustrating the major morphological features of the Cardium shoreline and lower coastal plain. Numbers refer to various facies and associations:

1) Transgressive conglomeratic resedimented-lag deposit, capping underlying cycle.
2) Association 1 (mud-dominated marine deposits).
3) Association 2 (sharp-based hummocky sandstones).
4) Facies 3HA (amalgamated hummocky sandstones).
5) Facies 3SW (swaley nearshore sandstones).
6) Facies 3PL (foreshore sandstones).
7) Facies 4VL (lagoonal deposits).
8) Facies 3PL (backbeach sandstones).
9) Facies 4VC (lower coastal plain overbank deposits).

Two different types of channels are also indicated (C1 and C2). See text for discussion.

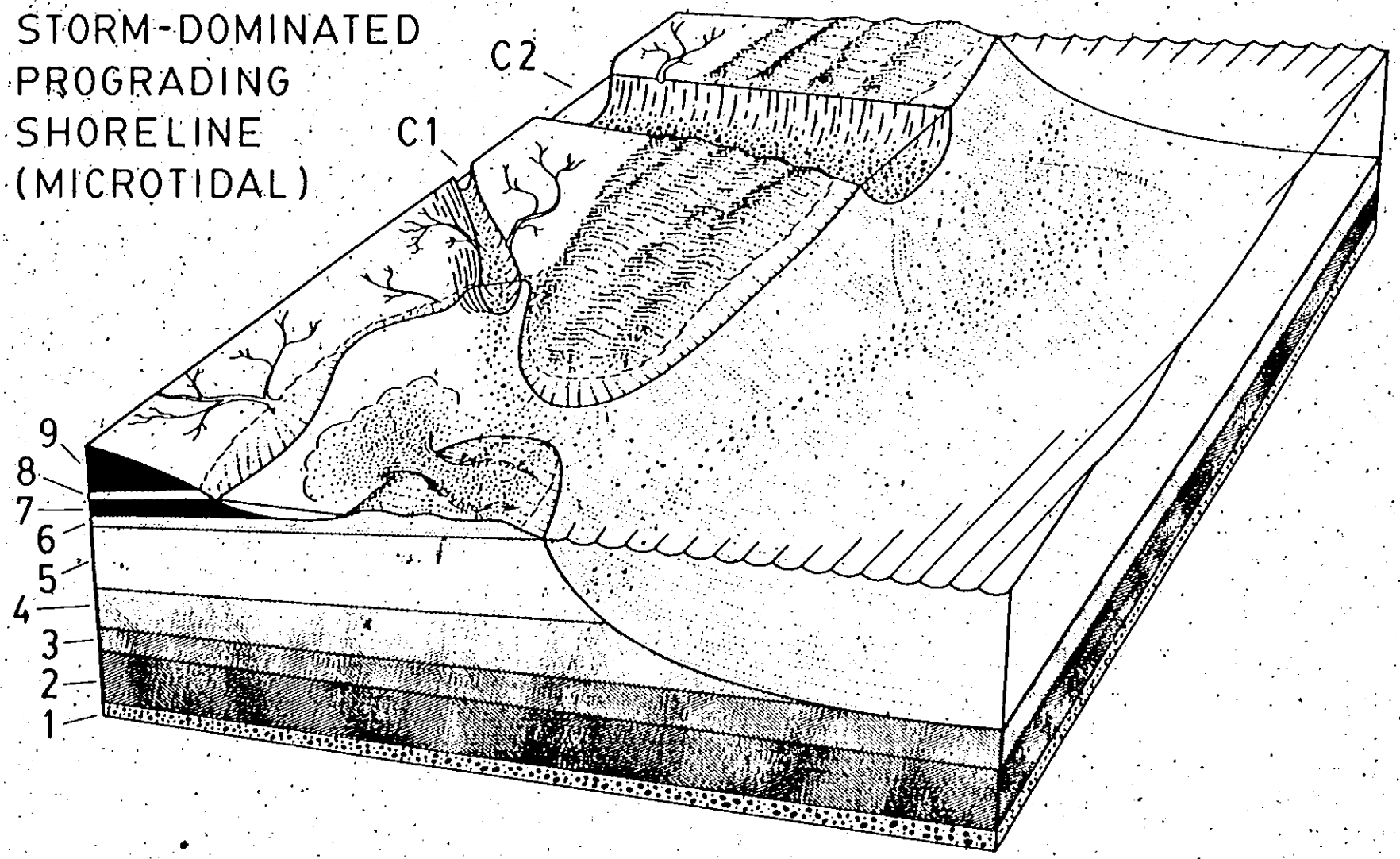
STORM-DOMINATED
PROGRADING
SHORELINE
(MICROTIDAL)
C2
C1
9
8
7
6
5
4
3
2
1
382

Figure 5-41 indicates two sources for coarse material to Cardium lagoons: overwash and fluvial distributary plain channels. These minor channels are labelled C1. Inferred overwash deposits (medium sands, some of which are pebbly) are preserved from bioturbation locally; these are the thin, sharp-based, rippled sandstones described in chapter 4. The lower coastal plain minor distributary channels are present in facies 4VC; the largest and coarsest of these minor channels were included in facies 4SF. I infer that some of these channels (most?) debauched into coastal lagoons.

Sequences displaying good evidence for lagoons and backbeach deposits include cycle #3, section 5-19 (Little Berland River) and cycle #3, section 5-37 (Littlehorn Creek). In both instances, major fully regressive marine cycles exhibit foreshore beach deposits overlain by coaly and/or bioturbated lagoonal intervals 1 or 2 m in thickness, which in turn are overlain by thin occurrences of facies 3PL (backbeach swash-zone sandstones) and then distributary plain overbank fines.

Major distributary fluvial channels (labelled C1) generally are observed <u>above</u> beach deposits in prograding sequences, separated from marine deposits by a few decimeters or meters of lagoonal and/or flood plain fines. In a few instances, however, the bases of these channels erode into marine sandstones of facies 3SW or 3HA (e.g.,

section PC-1; see Fig. 4-31B). In these instances, I infer that previously deposited beach sands have been erosionally removed, probably by lateral channel migration during periods of extreme discharge.

Very rarely, fluvial channels erode into offshore mud-dominated deposits (e.g., section WA-1). These unusual facies sequences probably are best attributed to rapid drops in relative sea level accompanied by channel incision through the shoreface, as has been discussed above.

CHAPTER 6. LATERAL CORRELATION OF CYCLES, AND THE DEVELOPMENT OF A CONCEPTUAL MODEL FOR CARDIUM SEDIMENTATION

INTRODUCTION

In this chapter I discuss the lateral correlation of Cardium facies and cycles, and the distribution of sandstones and conglomerates over local and regional distances. The correlation of cycles provides a conceptual framework for interpretation of the large-scale sedimentary processes active during deposition, and permits detailed interpretation of the processes controlling the geometry and distribution of sandstone and conglomerate bodies both in the Foothills and in the subsurface. The major control of Cardium sedimentation inferred from the distribution of facies and cycles is tectonoeustatic sea-level fluctuation, which resulted in distinct episodes of progradation and transgressive erosion of a storm-dominated sandy shoreline. Major sandstones in the formation were initially deposited as shoreface-attached sand bodies; these were modified during subsequent transgression, and locally were mantled with a resedimented-lag conglomerate of great lateral extent.

CORRELATION OF CARDIUM CYCLES: GROSS RELATIONSHIPS

The locations of the measured sections shown in the correlation diagrams are indicated in figure 6-1. Thirty-eight exposures are correlated in these diagrams. These 38 sections include the 28 exposures measured by the author, and nine exposures measured by R. G. Walker, M. E. Wright, and B. H. Ainsworth in the southern field area. These additional nine sections are indicated by two-letter designations. Also, one sedimentologically important section (section CL-1) is included in the correlation diagrams; this exposure was briefly examined by the author, and could only be measured at the facies-association level due to time constraints imposed by logistical considerations.

The correlation diagrams (Fig. 6-2 to 6-7) show lateral relationships between the various measured sections at the level of facies associations. An arbitrary horizontal datum has been drawn at the Seebe-Cutpick contact; the Seebe-Sundre contact extends this datum to exposures where the Cutpick is absent. On these diagrams, the actual distance between sections is shown at the bottom of the figures for exposures which are known to be located on the same thrust sheet; thus, these distances represent original separation of these exposures during their deposition.

The correlation diagrams have been discussed previously (chapter 3) within the context of the revised member stratigraphy defined for the formation. In that chapter, I stated that transitions from marine to non-marine sediments provided the basis for the correlation of most cycles, and that correlations could confidently be extended beyond the limit of preserved non-marine deposits on the basis of similarities of cycle type, thickness, and position within the formation.

This fairly mechanical approach to the lithostratigraphic correlation of cycles provides a perfectly reasonable (and frequently employed) method for the determination of gross lateral relationships between cycles (see further discussion below). The correlation diagrams successfully define three major (i.e., regionally correlative) regressive or progradational phases of sedimentation which are vertically juxtaposed within the formation; these have been depicted diagramatically in figure 3-1. These three regressive phases are each terminated by a regional transgression; as determined in chapter 5, transgressions typically are accentuated by marine conglomerates and/or thin intervals of thinning- and fining-upward offshore deposits (Fig. 5-2). The three major regressive phases and their overlying transgressions are herein termed episodes; these episodes are intermediate in rank between individual Cardium cycles (first-order

Figure 6-1. Map showing location of correlation diagrams figured in this chapter (Fig. 6-2 to 6-7). All measured sections are involved in these diagrams, permitting the correlation of cycle, member, and formational boundaries between any two sections.

Left panel indicates real locations of sections (i.e., locations prior to restoration). Central panel indicates locations after pseudo-palinspastic restoration. In this diagram, the Foothills belt has been expanded roughly 2.5 times, with some consideration given to relative offset along major thrusts. The actual locations (relative to fixed positions in the Plains) of section 6-28 at the Seebe Damsite (labelled SD on these maps) and section 5-45 at Ram River were determined palinspastically (Walker, 1983c, Fig. 21). Right panel indicates lines of correlation diagrams.

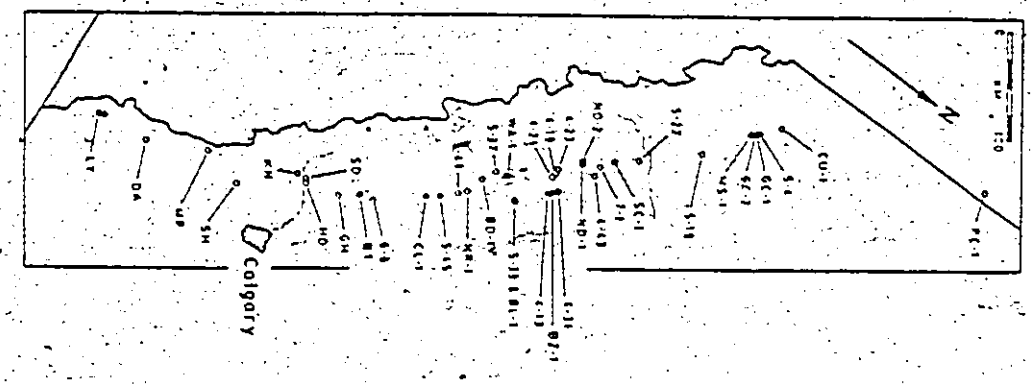
Colgory

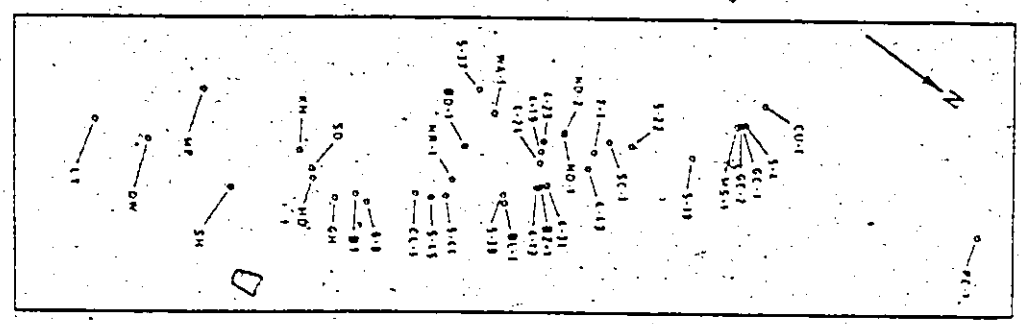

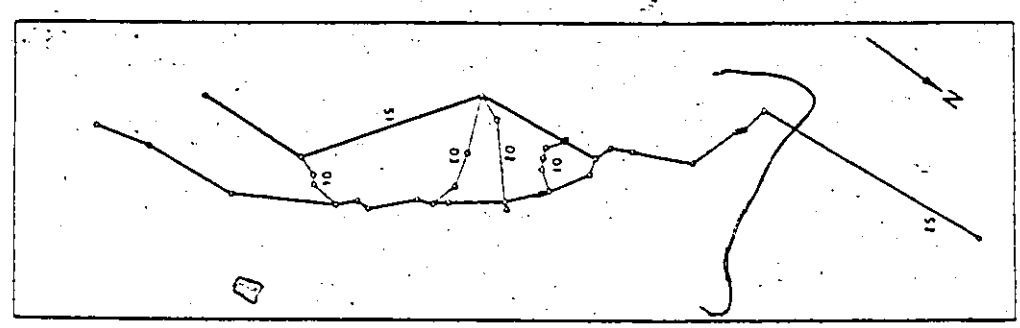

KEY:

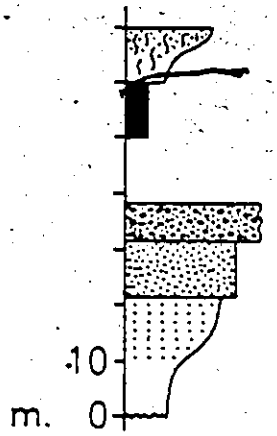

TYPE 6 CYCLE
ASSOCIATION 4
covered interval
ASSOCIATION 5
ASSOCIATION 3
ASSOCIATION 2
ASSOCIATION 1

Figure 6-2. Correlation diagram S2. See figure 6-1 for location of measured sections. This is the major mountain-parallel correlation diagram of this thesis, running from section PC-1 (Pouce Coupe, British Columbia) to section LY (Lynx Creek, near the Alberta-Montana border). Sections indicated by a two-letter designation (at southern end of diagram) were measured by R. G. Walker and B. H. Ainsworth. Formation and member boundaries are indicated by solid lines; many of these are coincident with cycle boundaries. Additional cycle correlations are indicated by dotted lines. See text for discussion.

NW

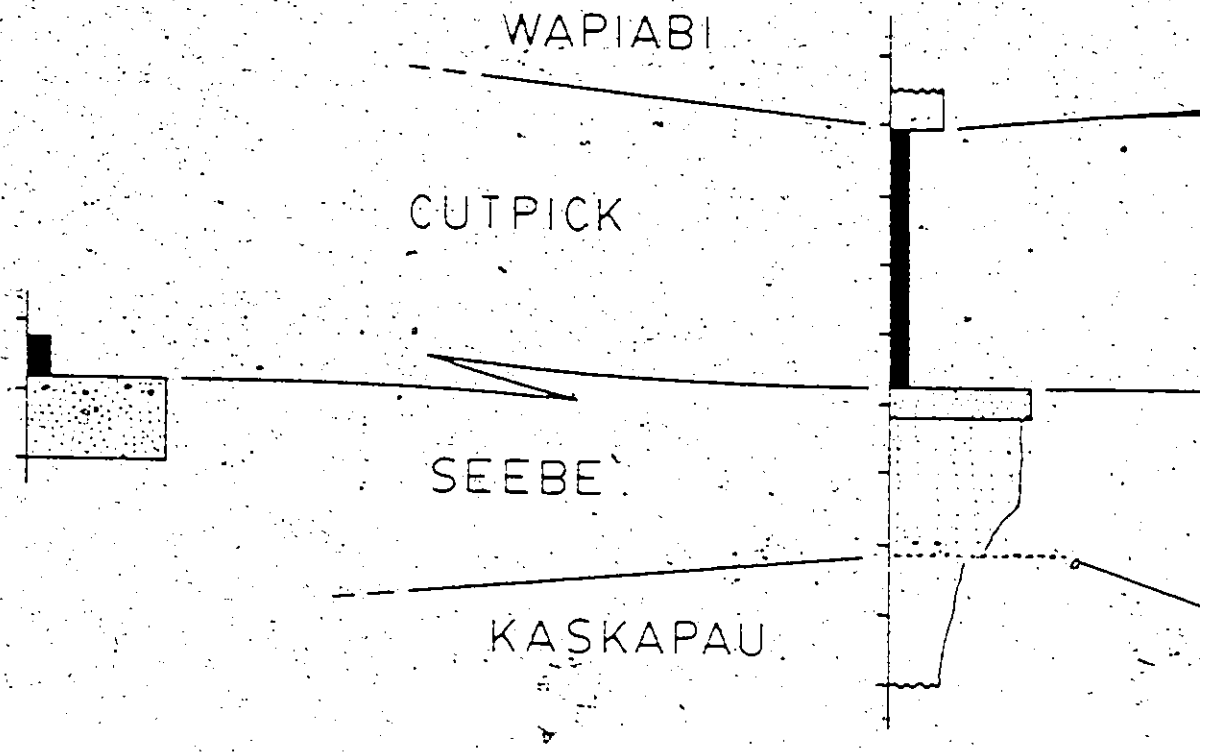

1 of

PC-1
POUCE
COUPE

CU-1
CUTPICK
HILL

2 of

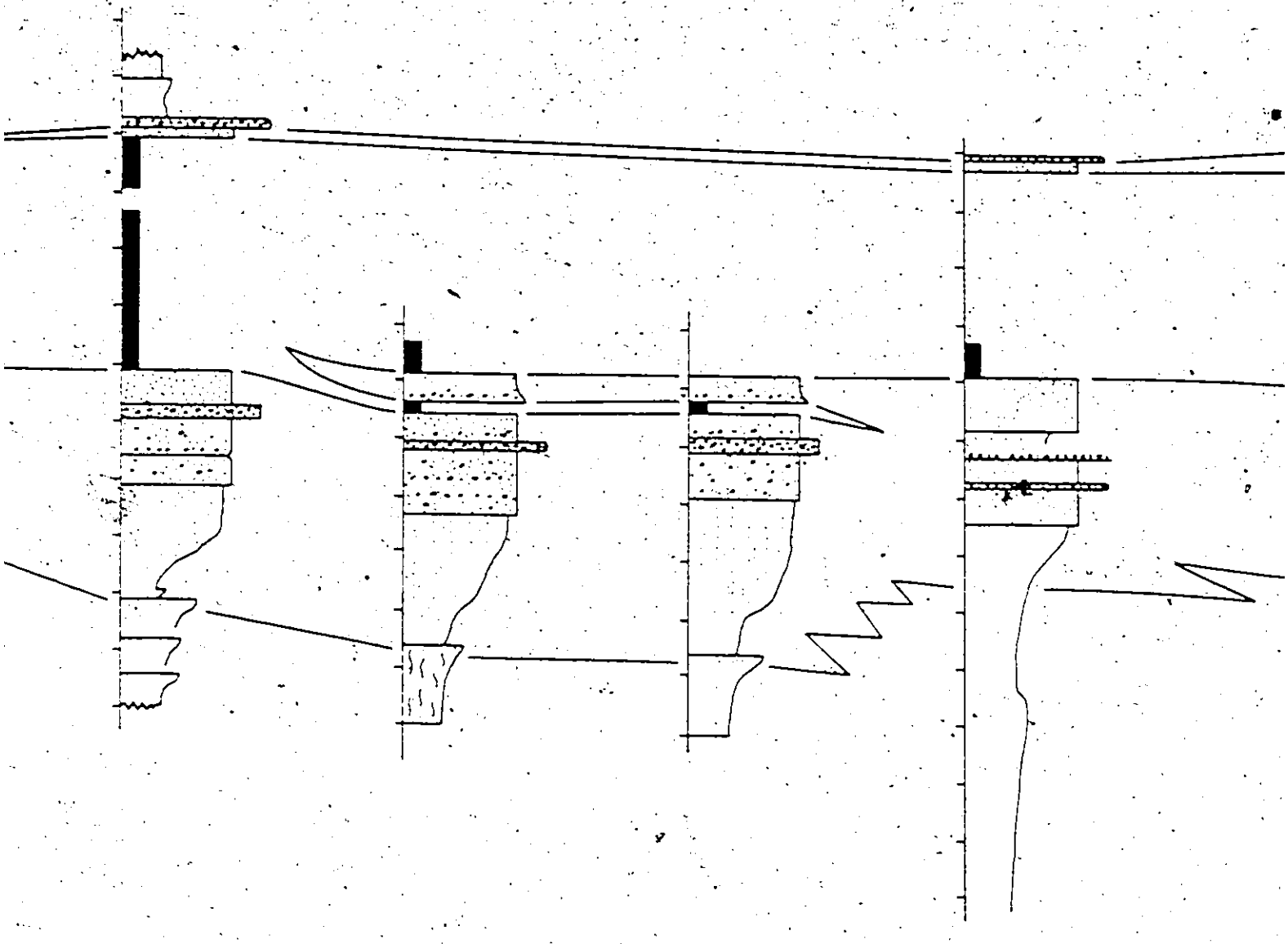

5-4
MUSKEG RIVER

GC-1
GRANDE CACHE HWY.

GC-2
GRANDE CACHE RR.

MS-1
MASON CREEK

1 km | 100 m | 8 km

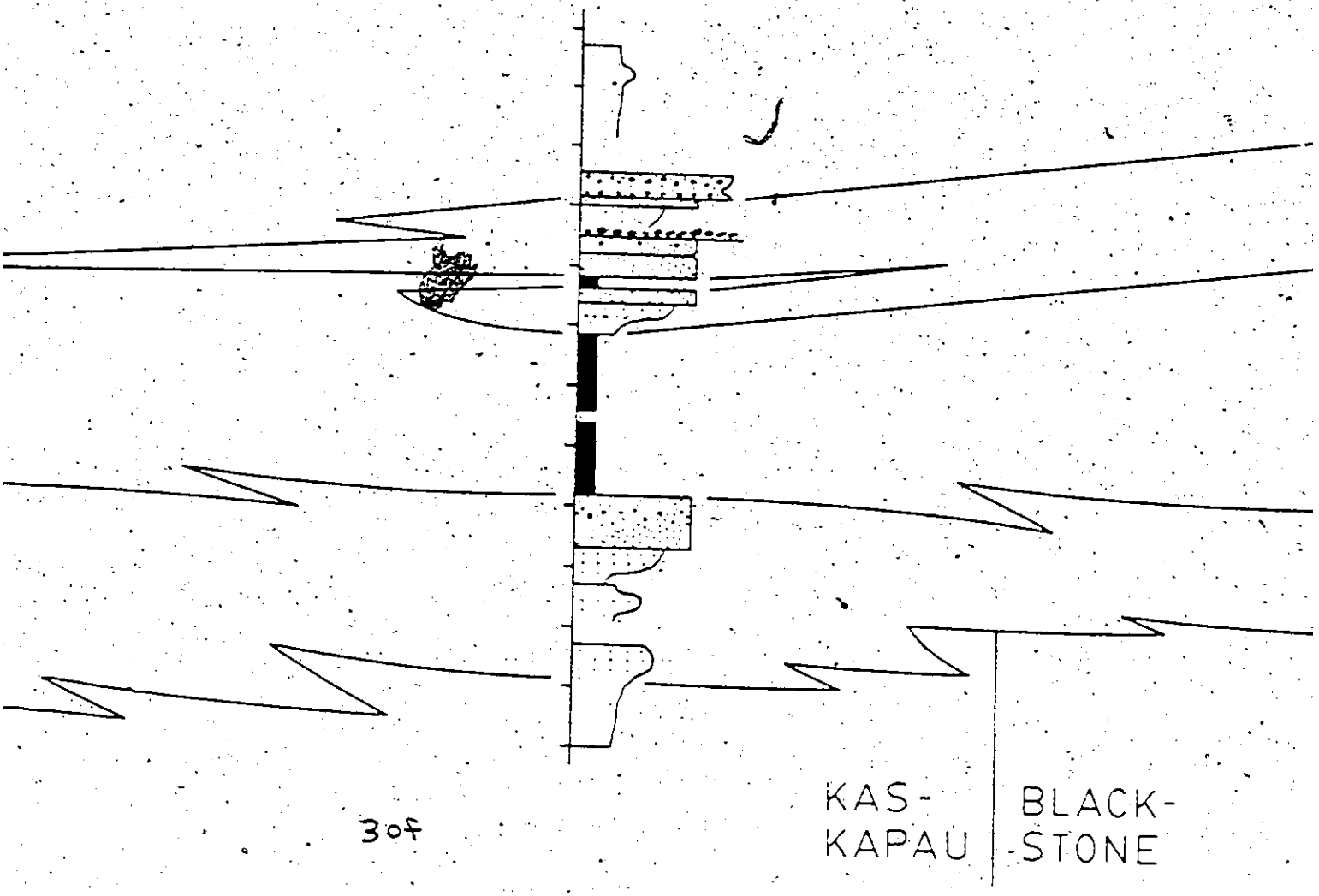

3 of

5-19
LITTLE
BERLAND R.

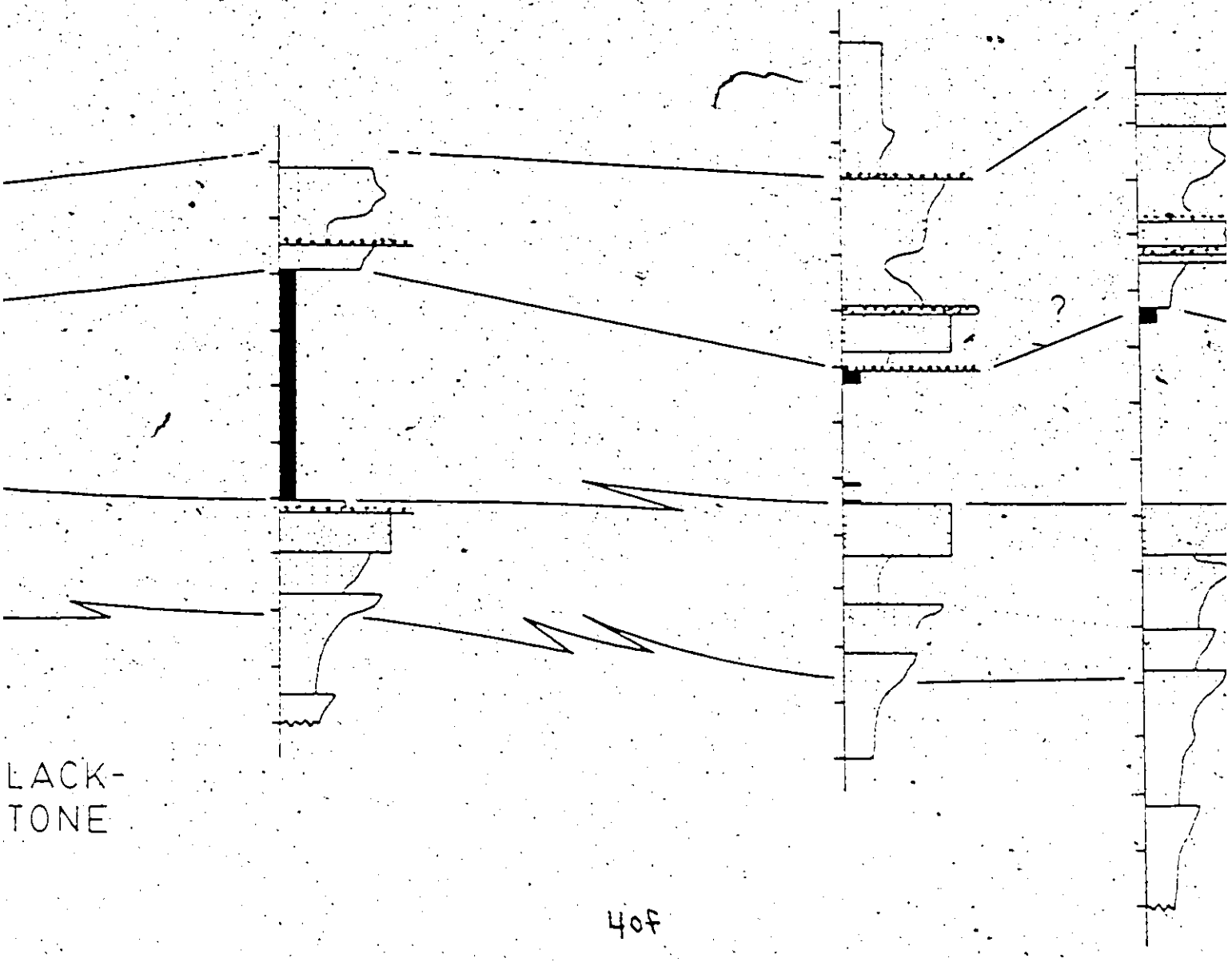

LACK-
TONE

4of

5-22
MASKUTA
CREEK

SC-1
SPHINX
CREEK

7-1
McLE
RIVE

13 km

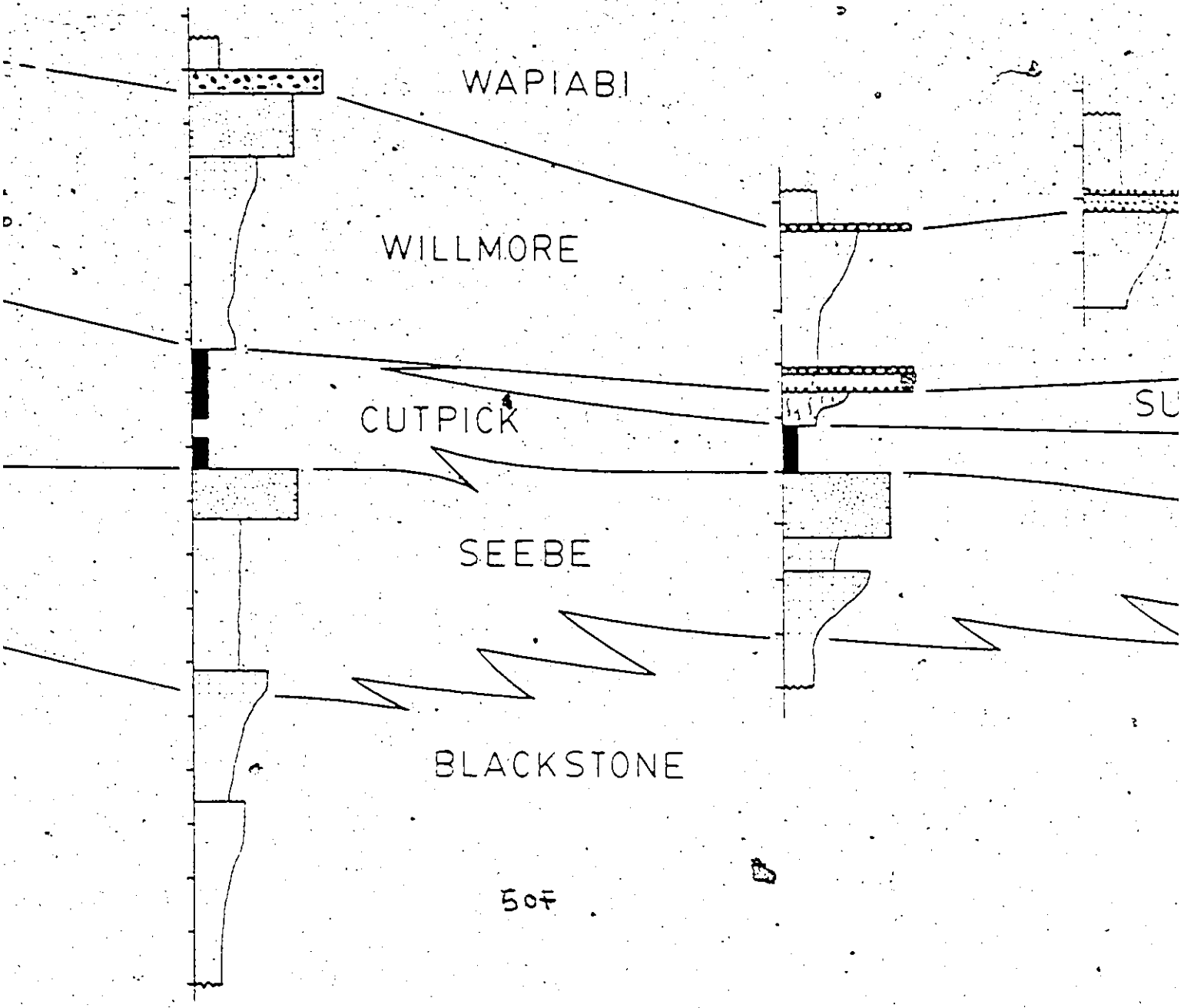

50↑

4-43
MacKENZIE
CREEK

4-31
CARDINAL
RIVER

BZ-1
BRAZE
RIVER

4 km

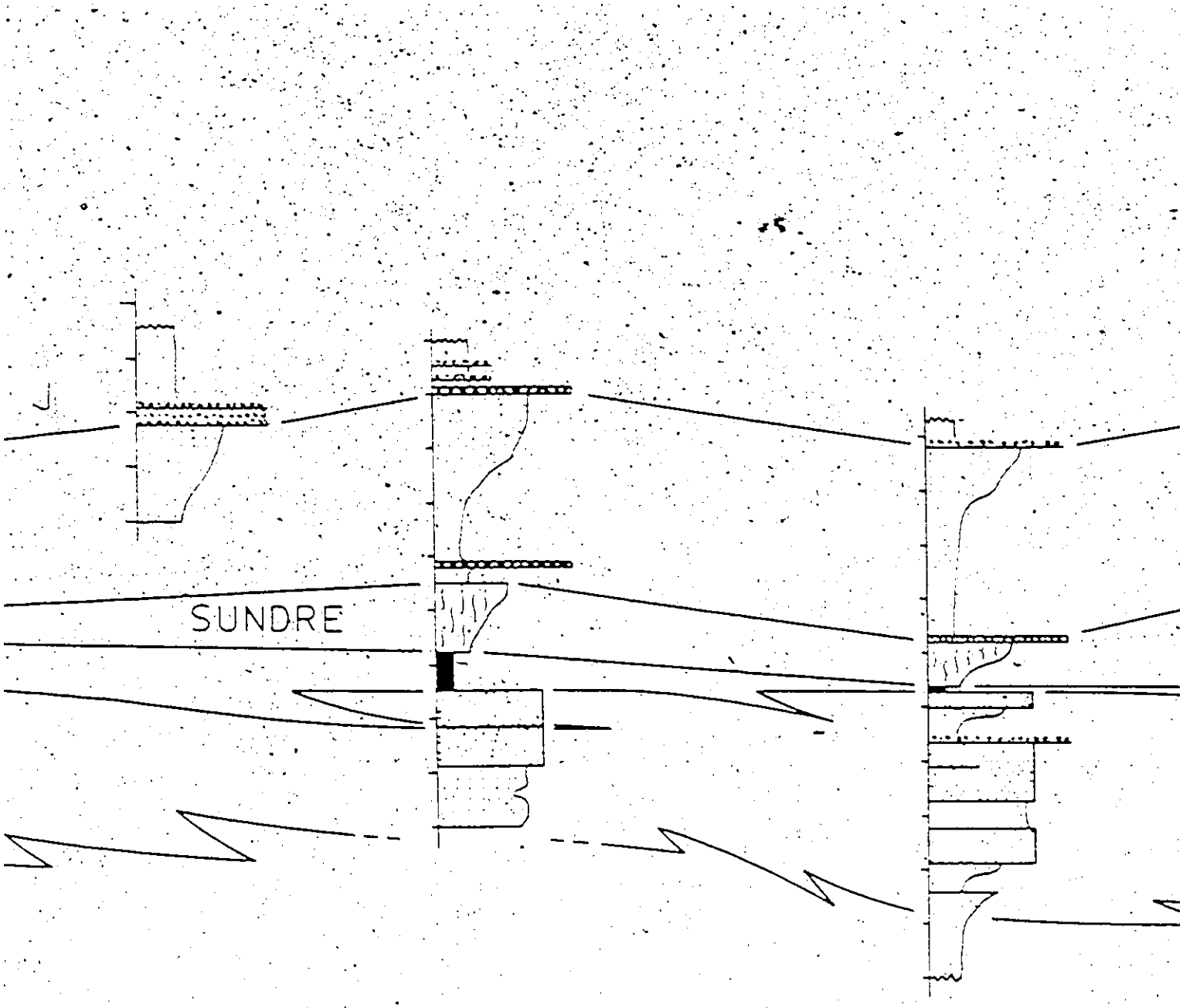

6 of

BZ-1
BRAZEAU
RIVER

4-13
CANYON
CREEK

5-39
BLACKSTONE
RIVER

AL

km

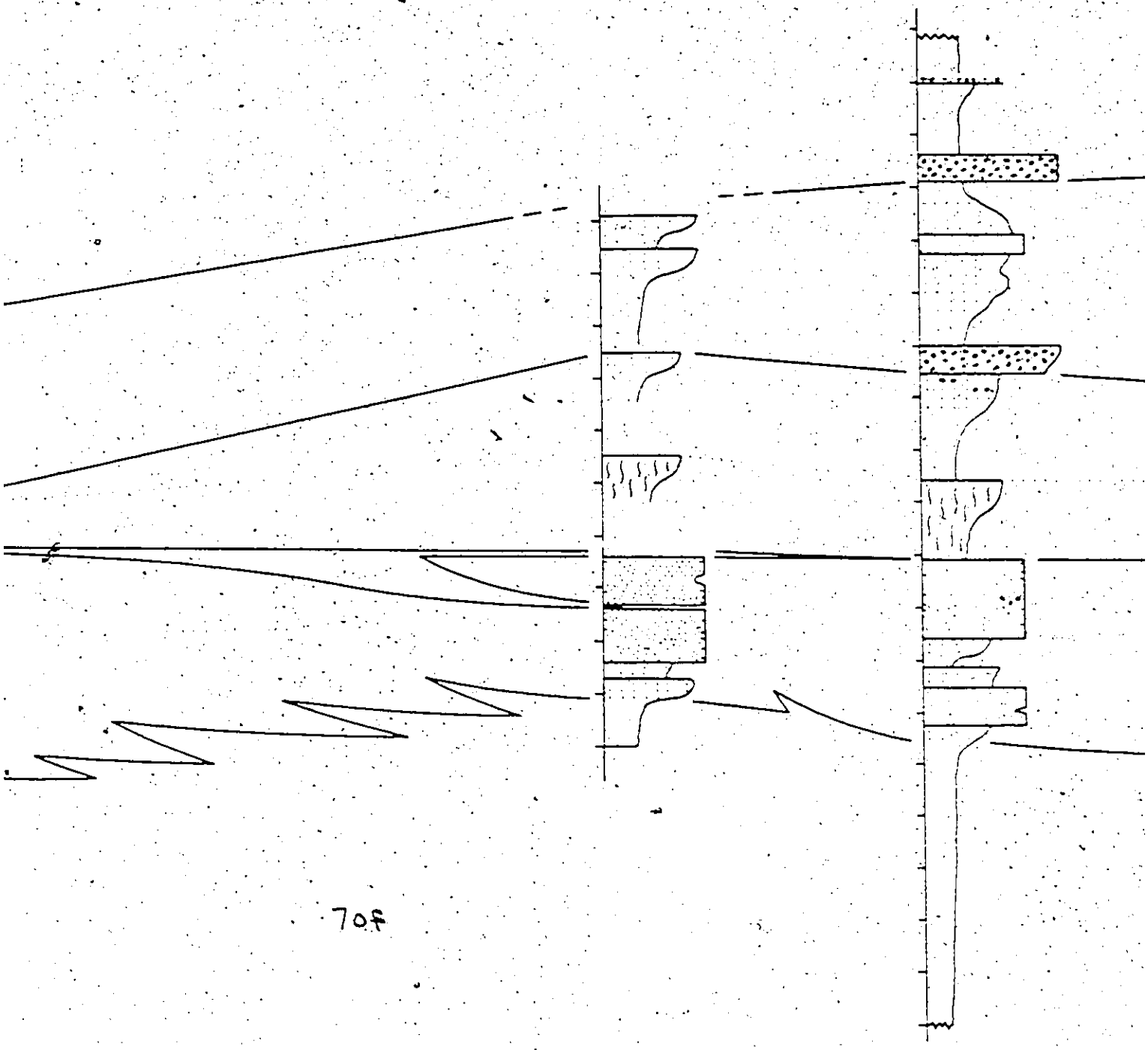

7 of

E

5-41
CRIPPLE
CREEK

5-45
RAM
RIVER

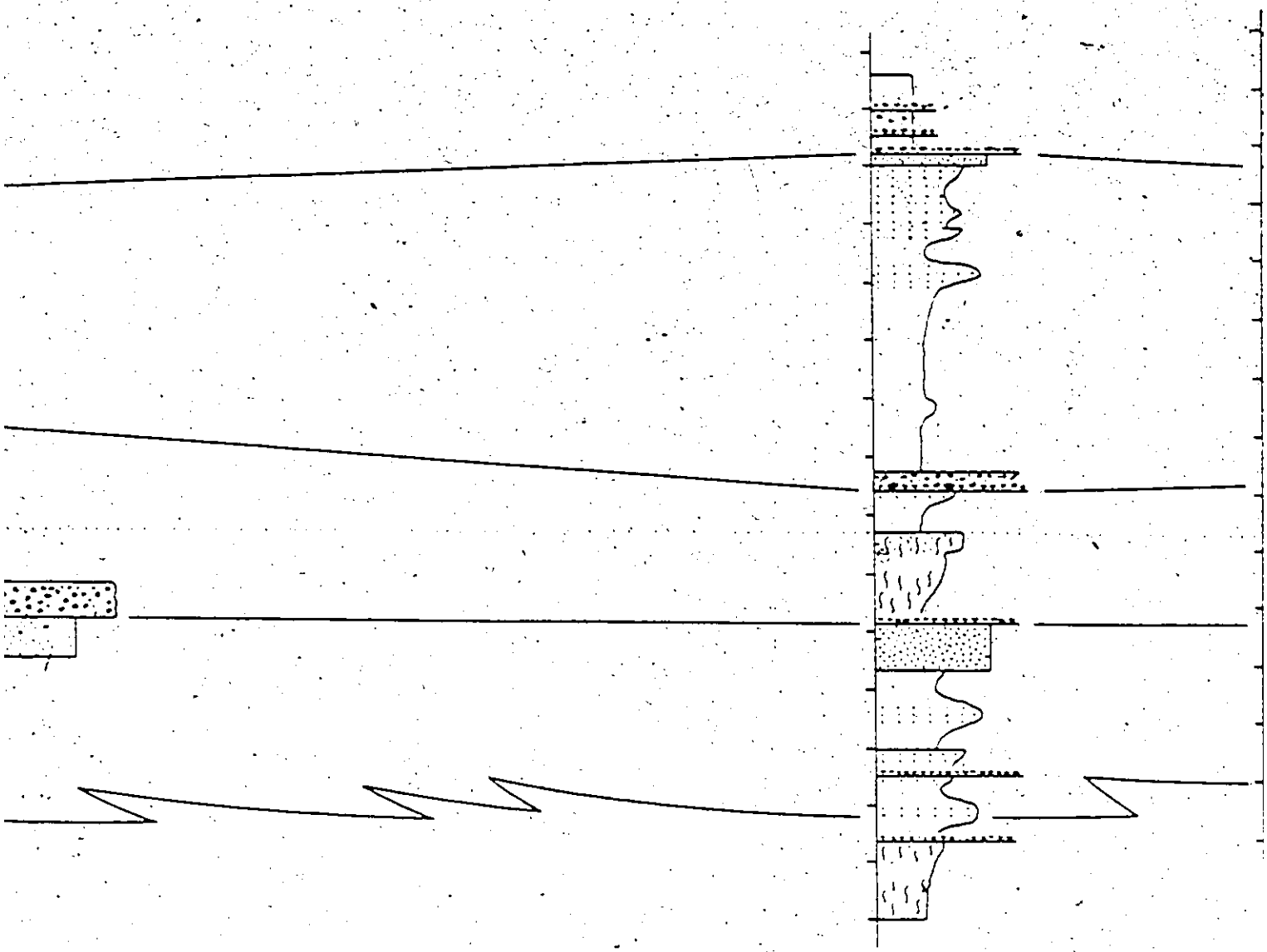

8 of

L-1
EARWATER
VER

6-8
RED DEER
RIVER

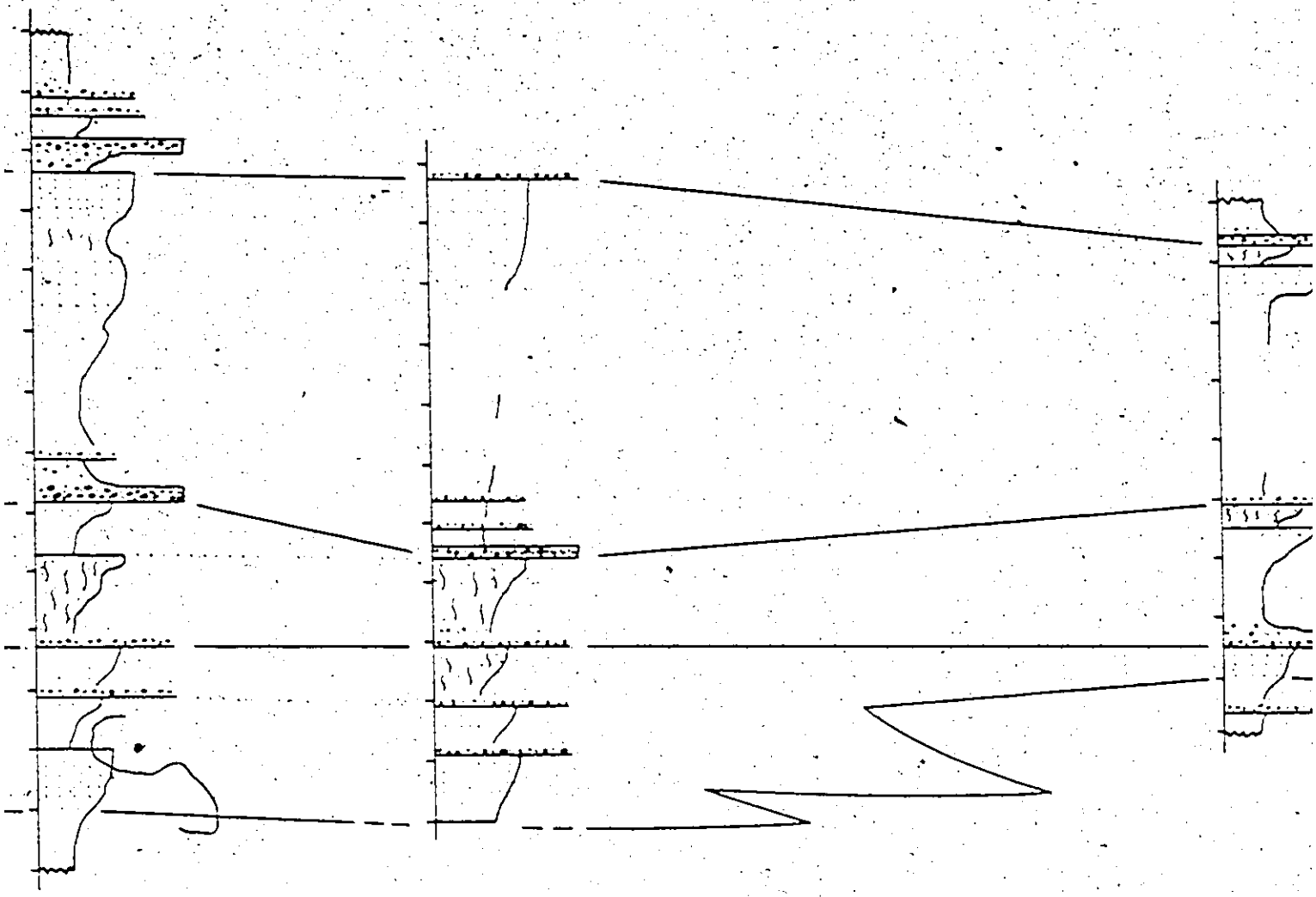

BT
BURNT
TIMBER CR.

GH
GHOST
RIVER

SH
SHE
RIV

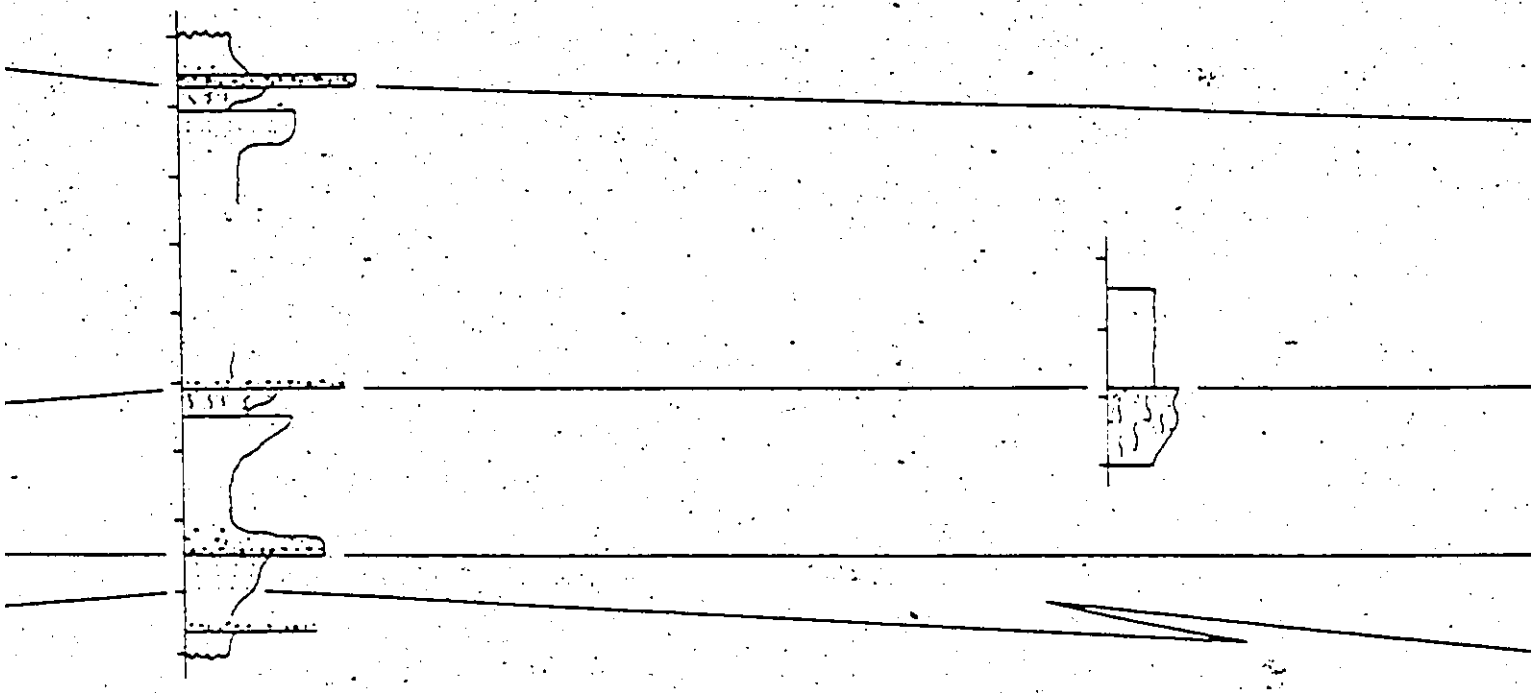

10 of

SH
SHEEP
RIVER

DW
DRYWOOD
RIVER

S

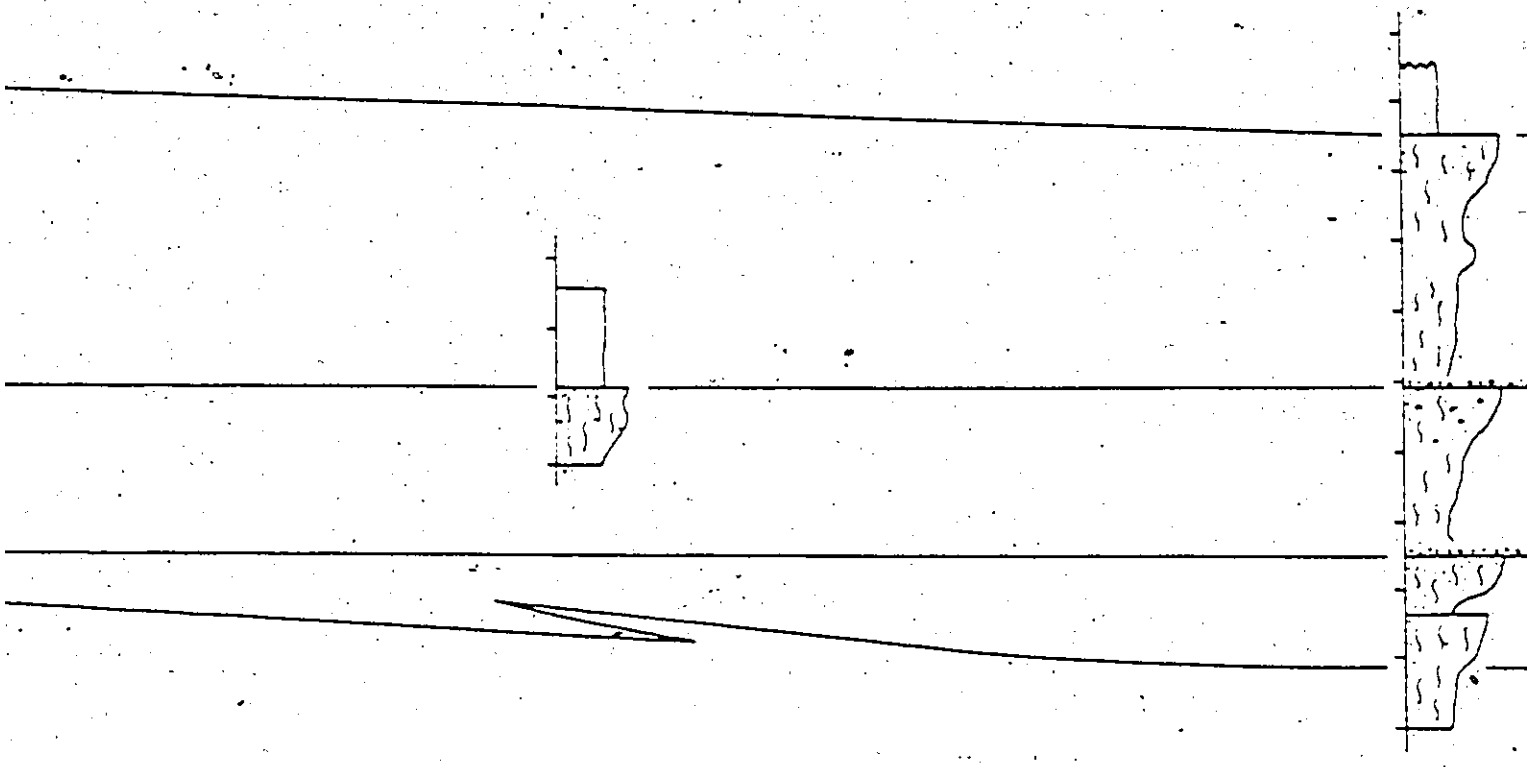

!!of

DW
DRYWOOD
RIVER

LY
LYNX
CREE

SE

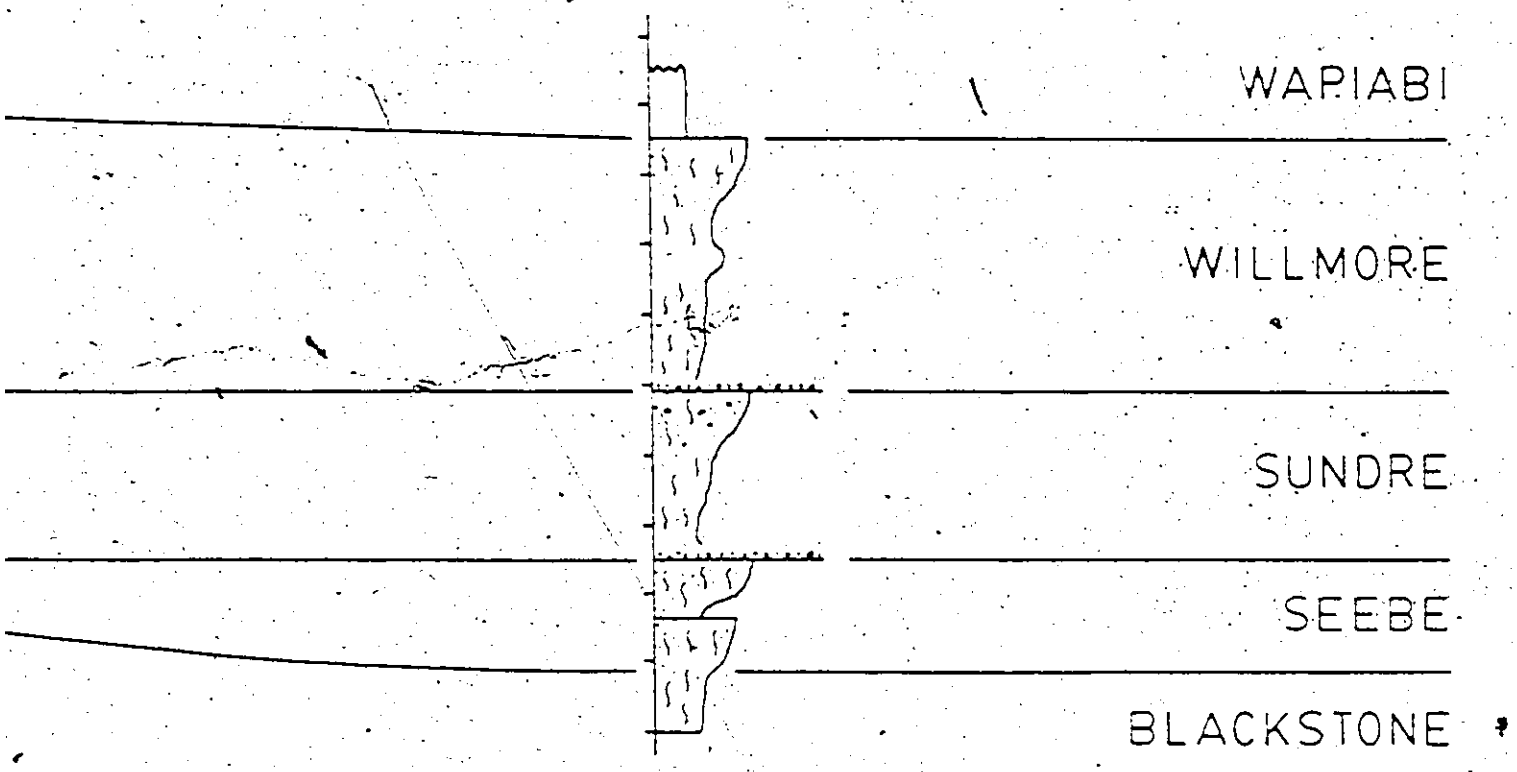

12 of 12

LY

LYNX
CREEK

D

KEY:

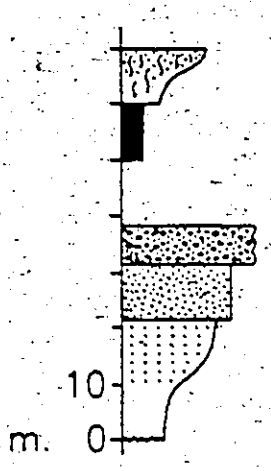

TYPE 6 CYCLE
ASSOCIATION 4
covered interval
ASSOCIATION 5
ASSOCIATION 3
ASSOCIATION 2
ASSOCIATION 1

Figure 6-3. Correlation diagram S1. See figure 6-1 for location of measured sections. This mountain-parallel correlation diagram runs from section 7-1 (where it joins line S2) to section MP; this represents an inner Foothills cross-section in a more source-proximal position than represented in line S2. Sections indicated by a two-letter designation (at southern end of diagram) were measured by R. G. Walker and B. H. Ainsworth. Formation and member boundaries are indicated by solid lines; many of these are coincident with cycle boundaries. Additional cycle correlations are indicated by dotted lines. See text for discussion.

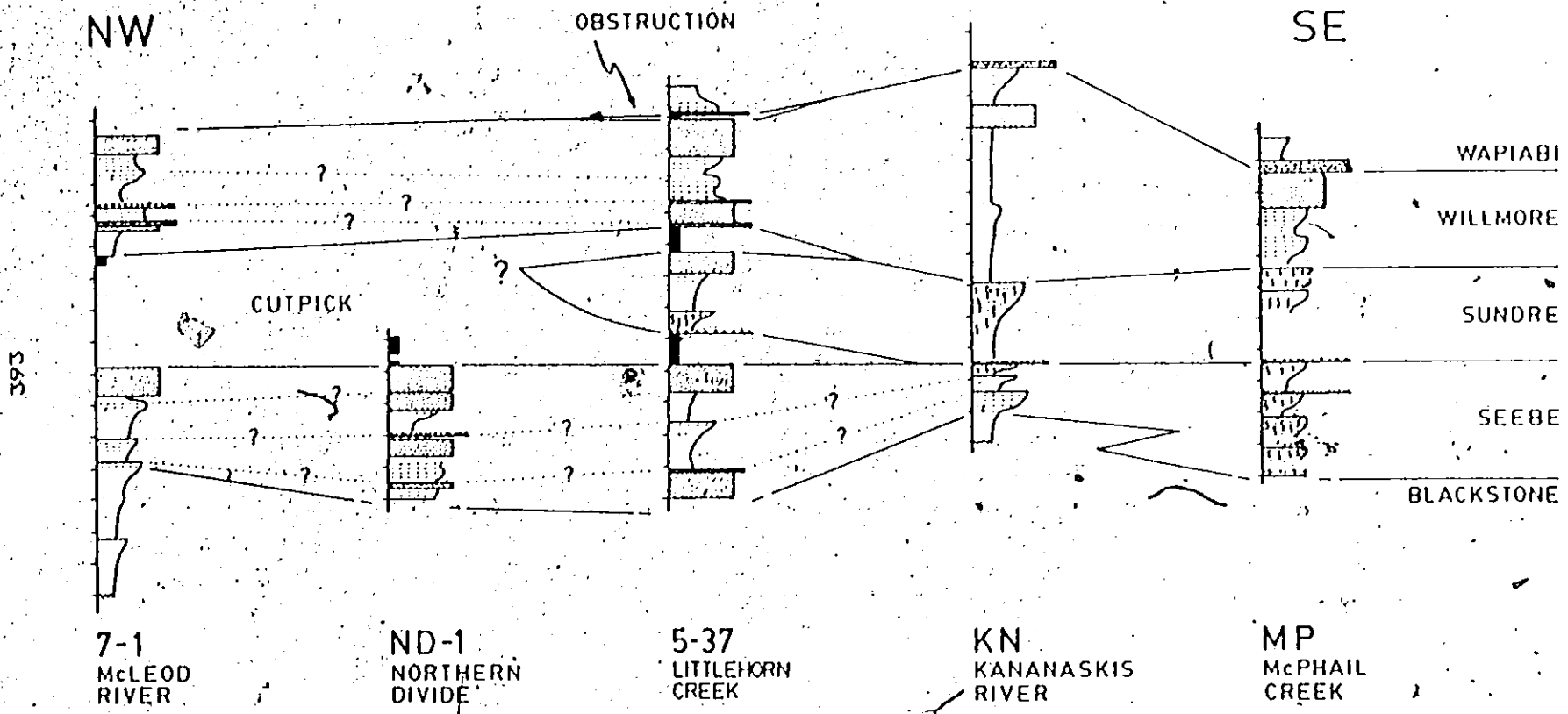
NW
OBSTRUCTION
SE
CUTPICK
WAPIABI
WILLMORE
SUNDRE
SEEBE
BLACKSTONE
7-1
McLEOD
RIVER
ND-1
NORTHERN
DIVIDE
5-37
LITTLEHORN
CREEK
KN
KANANASKIS
RIVER
MP
McPHAIL
CREEK

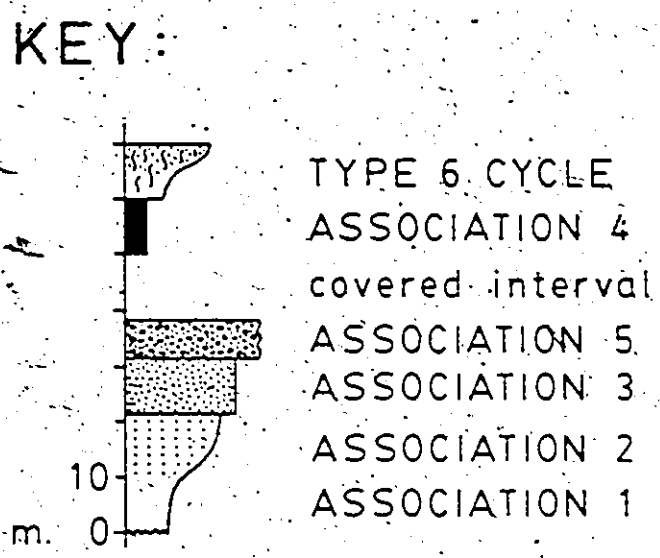

Figure 6-4. Correlation diagram D1. See figure 6-1 for location of measured sections. This mountain-normal correlation diagram runs from section ND-2 to section 4-31; it joins both line S1 and line S2. Formation and member boundaries are indicated by solid lines; many of these are coincident with cycle boundaries. Additional cycle correlations are indicated by dotted lines. See text for discussion.

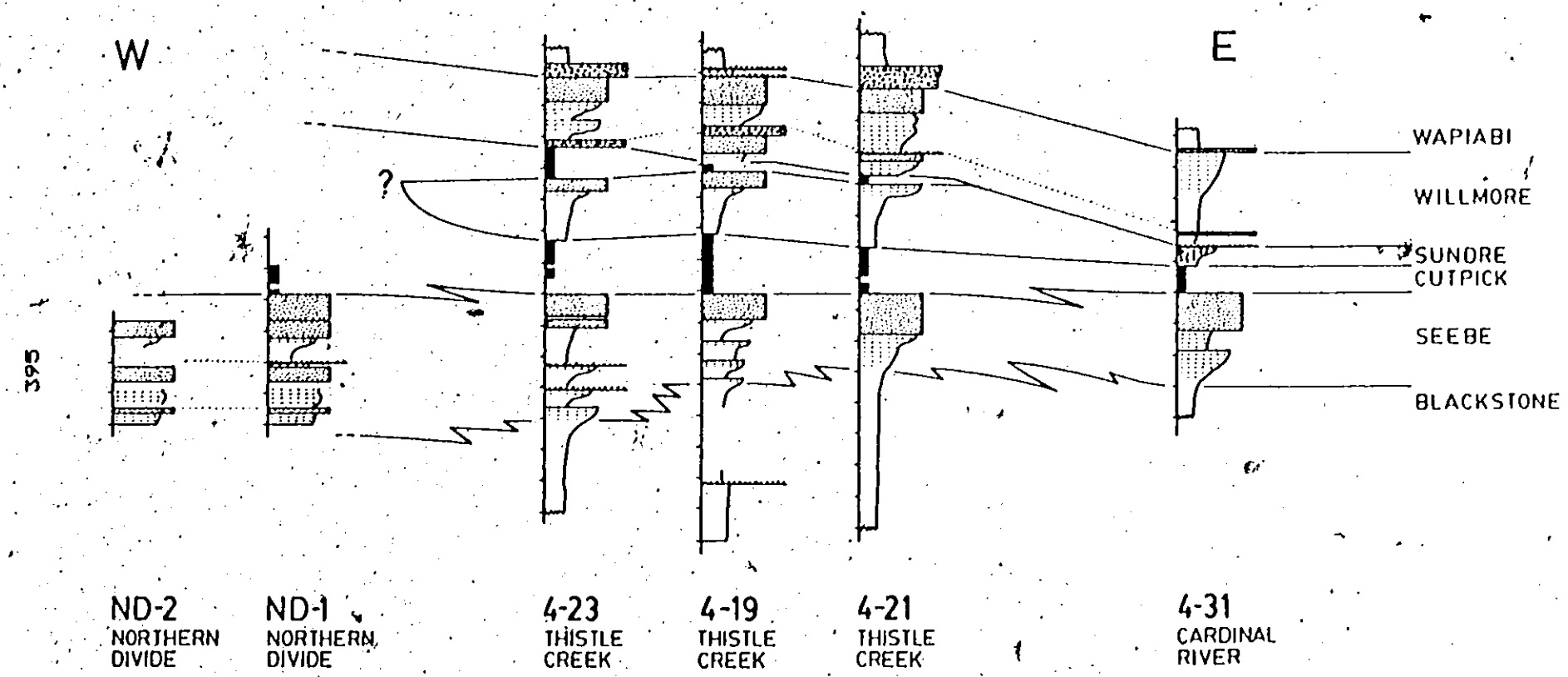
W
E
?
395
WAPIABI
WILLMORE
SUNDRE
CUTPICK
SEEBE
BLACKSTONE
ND-2
NORTHERN
DIVIDE
ND-1
NORTHERN
DIVIDE
4-23
THISTLE
CREEK
4-19
THISTLE
CREEK
4-21
THISTLE
CREEK
4-31
CARDINAL
RIVER
3 km

KEY:

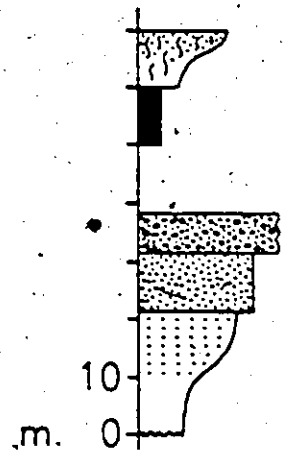

TYPE 6 CYCLE
ASSOCIATION 4
covered interval
ASSOCIATION 5
ASSOCIATION 3
ASSOCIATION 2
ASSOCIATION 1

Figure 6-5. Correlation diagram D2. See figure 6-1 for location of measured sections. This mountain-normal correlation diagram runs from section 5-37 to section BL-1; it joins both line S1 and line S2. Formation and member boundaries are indicated by solid lines; many of these are coincident with cycle boundaries. Additional cycle correlations are indicated by dotted lines. See text for discussion.

SW

NE

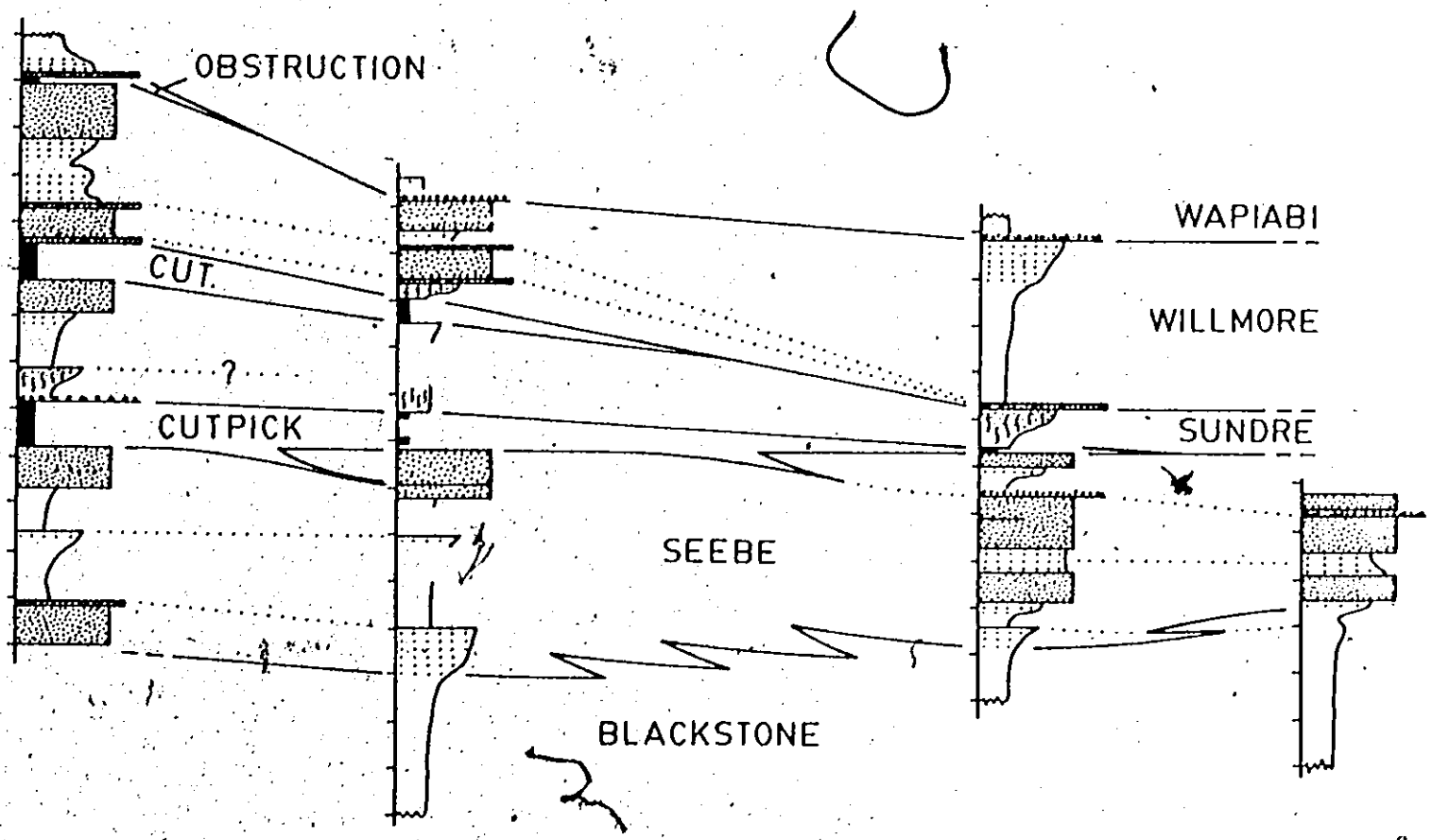

397

5-37
LITTLE HORN CREEK

WA-1
WAPIABI CR., S. FORK

5-39
BLACKSTONE RIVER

BL-1
BLACKSTONE RIVER

KEY:

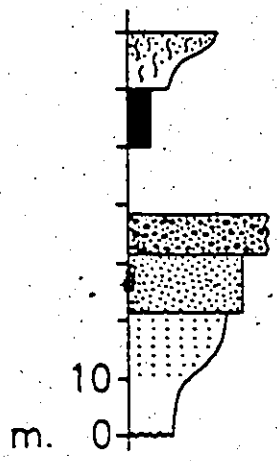

TYPE 6 CYCLE
ASSOCIATION 4
covered interval
ASSOCIATION 5
ASSOCIATION 3
ASSOCIATION 2
ASSOCIATION 1

Figure 6-6. Correlation diagram D3. See figure 6-1 for location of measured sections. This mountain-normal correlation diagram runs from section 5-37 to section 5-45; it joins both line S1 and line S2. Formation and member boundaries are indicated by solid lines; many of these are coincident with cycle boundaries. Additional cycle correlations are indicated by dotted lines. Note that section NR-1 is suspected of being tectonically thinned. See text for discussion.

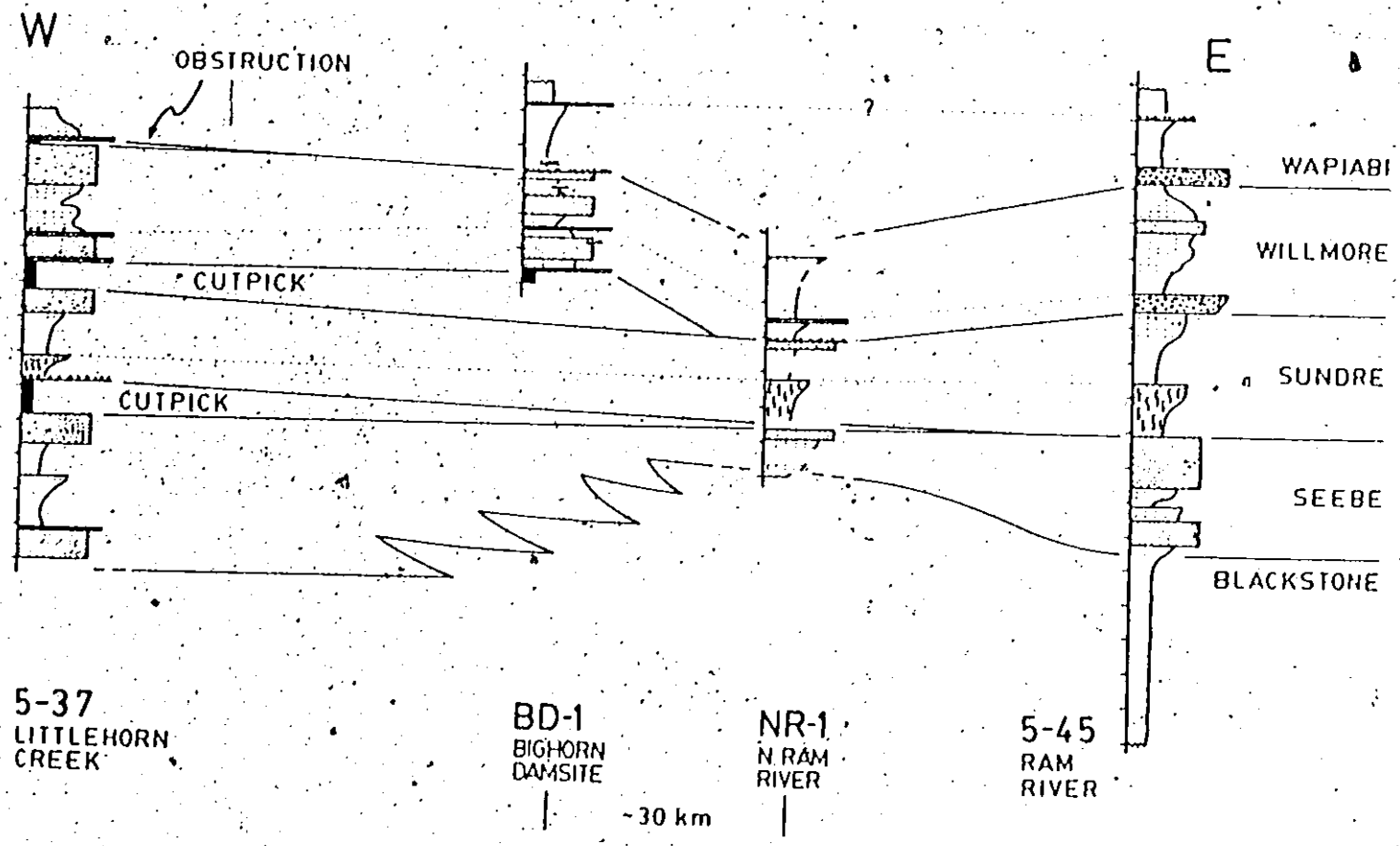
W
OBSTRUCTION
E
WAPIABI
WILLMORE
CUTPICK
CUTPICK
SUNDRE
SEEBE
BLACKSTONE
5-37
LITTLEHORN
CREEK
BD-1
BIGHORN
DAMSITE
~30 km
NR-1
N RAM
RIVER
5-45
RAM
RIVER

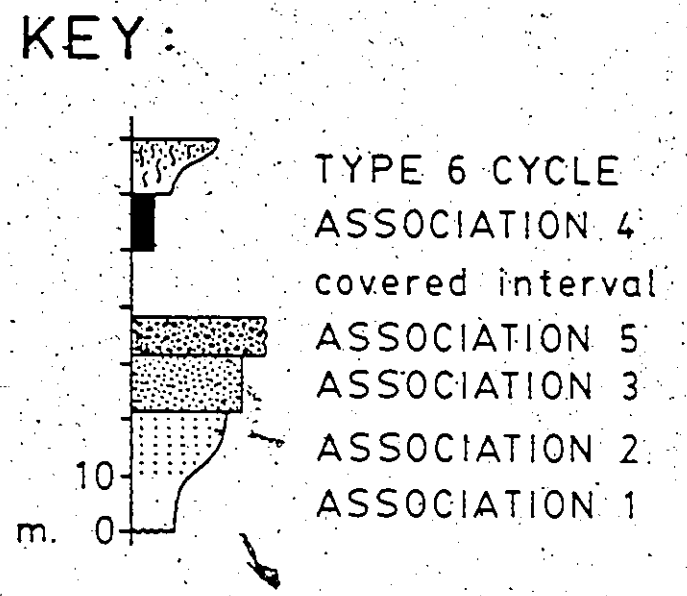

Figure 6-7. Correlation diagram D4. See figure 6-1 for location of measured sections. This mountain-normal correlation diagram runs from section KN to section GH; it joins both line S1 and line S2. Sections KN and GH were measured by R. G. Walker and B. H. Ainsworth; sections 6-28 and 6-22 were measured by M. E. Wright and R. G. Walker. Note on the location map (Fig. 6-1) that sections 6-28 and 6-22 are designated by the letters SD and HD, respectively. Formation and member boundaries are indicated by solid lines; many of these are coincident with cycle boundaries. Additional cycle correlations are indicated by dotted lines. See text for discussion.

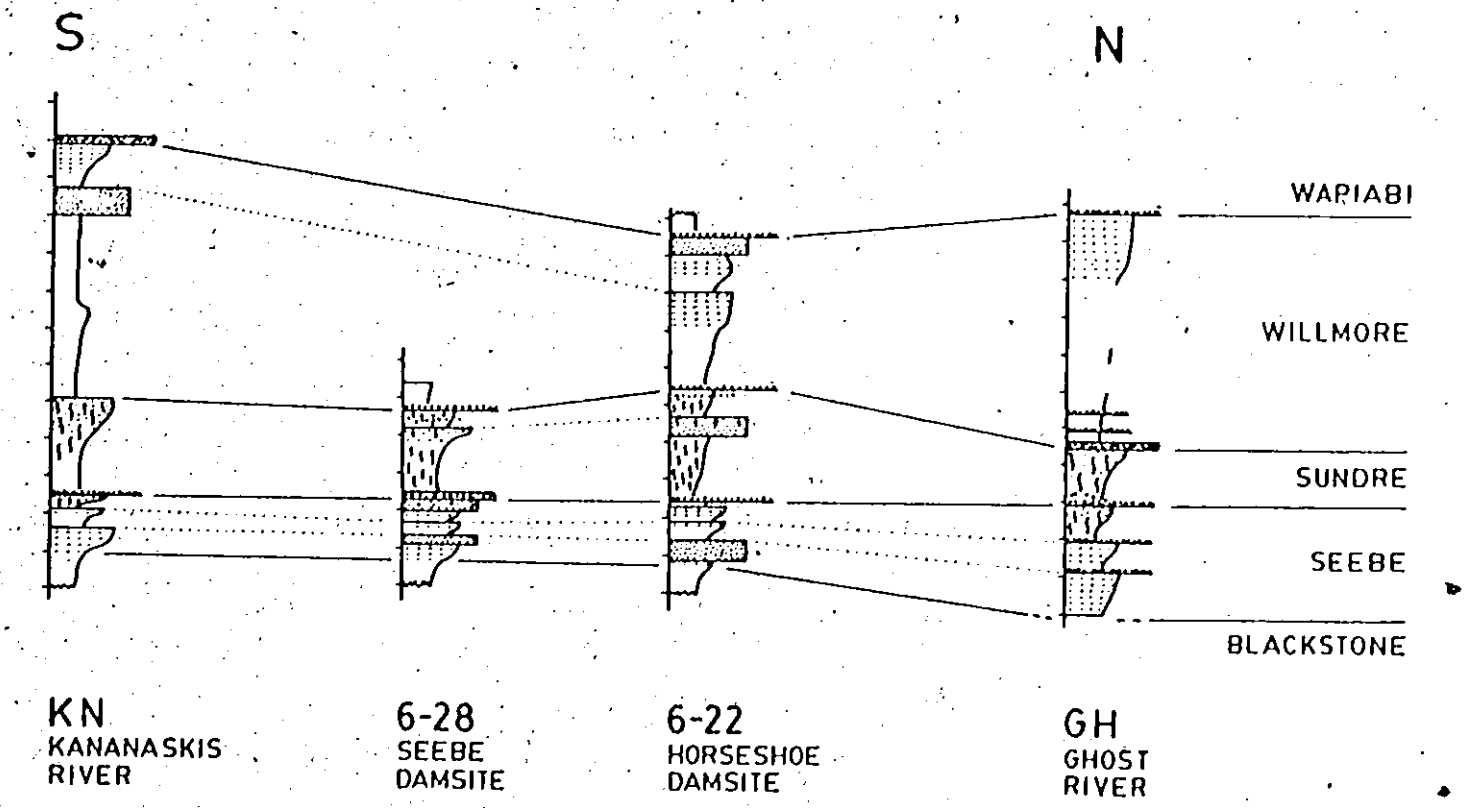
S
N
WAPIABI
WILLMORE
SUNDRE
SEEBE
BLACKSTONE
KN
KANANASKIS
RIVER
6-28
SEEBE
DAMSITE
6-22
HORSESHOE
DAMSITE
GH
GHOST
RIVER

cycles) and the entire formation itself, which, together with the underlying and overlying mud-dominant formations, represents a second order of cyclic sedimentation within the Alberta basin. The three episodes of sedimentation may be informally designated in terms of the revised member stratigraphy, which has been defined so as to reflect these three episodes. In descending order, these designations are as follows:

Episode 3: Wapiabi Transgression
Willmore-Obstruction Regression

Episode 2: Willmore Transgression
Sundre-Cutpick Regression

Episode 1: Sundre Transgression
Seebe-Cutpick Regression

Each of these regressive-transgressive episodes (depicted diagramatically in figure 3-1, and in detail in the correlation diagrams) displays local variability, as recorded by laterally impersistent cyclicity superimposed upon the regionally correlative regressive phase of sedimentation. Some of this variability was indicated in figure 3-1 in the form of minor tongues of non-marine sediment protruding from the main body of the Cutpick Member. It is this local variability which holds the key to the interpretation of Cardium sedimentation in both the

Foothills and the Plains, particularly:

1) the development of minor sedimentary cycles,
2) the development and distribution of sand bodies, and
3) the distribution of Cardium conglomerates and their relationship to sand bodies within the formation.

The development of local variability is examined in detail in the following section.

CORRELATION OF CARDIUM CYCLES: DETAILED RELATIONSHIPS

Minor Transgressions

Superimposed upon each of the three major regressive episodes of sedimentation are minor (i.e., locally developed) transgressive pulses. These are best illustrated where they involve cycles displaying a vertical transition to non-marine sediments, but can also be recognized in relationships between fully marine cycles.

Figure 6-8 shows part of correlation diagram S2 (Fig. 6-2), involving closely spaced exposures in the Grande Cache area. This diagram illustrates one of the minor transgressive pulses superimposed upon a regressive episode of regional extent. Individual facies are represented in this figure, rather than facies associations

Figure 6-8. Correlations involving closely spaced exposures from the same thrust sheet in the Grande Cache area. Note: 1) the "Grande Cache Split" of non-marine sediments (dark stipple) protruding into the underlying Seebe Member, 2) the conglomerate-covered transgression surface overlying this split, and 3) lateral variation in cycle occurrence, position, thickness, and type over a distance of only 9 km. Solid lines are formational and member boundaries, dotted lines are cycle boundaries, and squiggles indicate individual beds which probably are correlative. Note that the true lithostratigraphically correlative extent of the Seebe Member (indicated by light stipple) is difficult to determine without very closely spaced exposures such as these; for convenience of mapping in the field, the base of this member is drawn at the base of the "transition interval", which locally is not a truely correlative surface (see appendix 7 for a detailed discussion of stratigraphy). See text for further discussion.

SECTION 5-4
SECTION GC-1
SECTION GC-2
SECTION MS-1

only. The four sections represented on this diagram are from a single thrust sheet; thus, the distances between them represent true NE-SW separation during deposition.

The correlations of figure 6-8 illustrate two offlapping cyclic developments separated by an erosional transgression. The transgression has produced a conglomeratic lag deposit separating these cycles, and a small "split" of non-marine deposits at the top of the lower cycle extends from the Cutpick Member into the Seebe Member (Fig. 6-8). The fortuitous preservation and excellent exposure of the relatively small Grande Cache split provides important insight into the nature of processes that controlled both conglomerate deposition and the development of cyclicity within the Cardium -- insight which significantly affects the conceptual framework (or "working model") for the interpretation of sedimentary processes in the Cardium. The principal concepts affected include:

1) correlation of individual cycles between widely spaced outcrops,
2) factors controlling development of cyclicity,
3) origin of conglomerate beds deposited in both transgressive and regressive settings, and
4) distinction between lateral extent of preserved non-marine deposits and lateral extent of the

ancient shoreline.

Each of these four points is discussed in detail in the following paragraphs.

Correlation of cycles. The observation of major regressive cycles that pinch out over short distances laterally has great implications for the correlation of similar cycles occurring within the same regressive episode. The uppermost marine cycle below the Cutpick Member at section 5-4 (Muskeg River) is replaced by a new offlapping cycle of similar appearance and proportions at section MS-1 (Mason Creek), over a distance of only 9 km (Fig. 6-8 & A1-4). Let us assume that this dimension is typical of deposits resulting from minor transgressive pulses elsewhere in the formation. An average distance between exposures measured for this thesis is about 25 km (disregarding structural shortening); thus, the limit of resolution is generally of much greater magnitude than the features we are trying to detect -- too large to permit confident correlation of individual cycles within a single regressive episode (except in rare instances of closely spaced exposures on the same thrust slice, as in the Grande Cache area). By implication, it is possible (probable?) that numerous minor transgressions and minor tongues of non-marine sediment such as those observed in the Grande Cache area have not been detected in the course of field

work for this thesis. This situation is illustrated diagramatically in figure 6-9, which shows two very different patterns of cycle correlation depending upon variation in the amount of available exposure. In this conceptualization, the lack of tight outcrop control results in an over-simplification of cycle relationships. This situation accounts for the reservations mentioned in the discussion of gross cycle relationships above.

I am convinced that lack of exposure has resulted in such over-simplification on the correlation diagrams, at least in some parts of the study area (e.g., around the boundary between the northern and central Foothills, where outcrop is particularly limited, and between the Alberta and British Columbia exposures). Thus, tenuous cycle correlations abound in the correlation diagrams (indicated—by question marks), and several highly questionable correlations have been omitted entirely. Note, however, that the correlation of major regressive episodes (as understood and defined above) is probably very well established: Individual cycles of local extent, not properly resolved on the cycle-correlation diagram, are superimposed upon much more extensive regressive episodes of regional extent. Outcrop control is orders of magnitude smaller than these regional sedimentation episodes.

Development of cyclicity. The conceptual framework

which emerges from the above discussion provides an interpretion of the origin of cyclicity within any of the three major regressive episodes in the formation. The major control is minor or local variation in sea level. Local sea-level fluctuation probably resulted from local variation in the combined effects of sedimentation rate, subsidence rate, and (to a much lesser extent than in the major sedimentation episodes) eustatic sea-level changes; these local fluctuations were confined to limited areas and/or time intervals. This interpretation is consistent with the observation that most Cardium cycles are either fully regressive or top-absent varieties (chapter 5). As discussed in chapter 5, top-absent cycles probably form due to a combination of incomplete development prior to transgression, and/or partial erosion during transgressive retreat of the shoreface (i.e., submarine erosion).

Conglomerate deposition. The distribution of Cardium conglomerates deposited within regressive episodes is consistent with the conceptualization developed above. In particular, this interpretation can readily account for locally developed transgressive conglomerates (as illustrated in Fig. 6-8 and the correlation diagrams). Further, this conceptualization also accommodates the apparent "patchy" distribution of transgressive conglomerates at the tops of some cycles within these

Figure 6-9. Conceptual diagram illustrating two different correlations of the same rocks.

The upper correlation chart and interpretive panel diagram shows the correct correlation, based upon six closely spaced exposures (A, A', B', B, C, and D). Two non-marine tongues (NMT) are recognized: One is fully documented (between A and B), the other is inferred (between C and D) from less complete exposure.

The lower interpretation would result if sections A' and B' were not examined, and the areally restricted non-marine tongues were not recognized. This interpretation leads to an incorrect and overly extended set of cycle correlations.

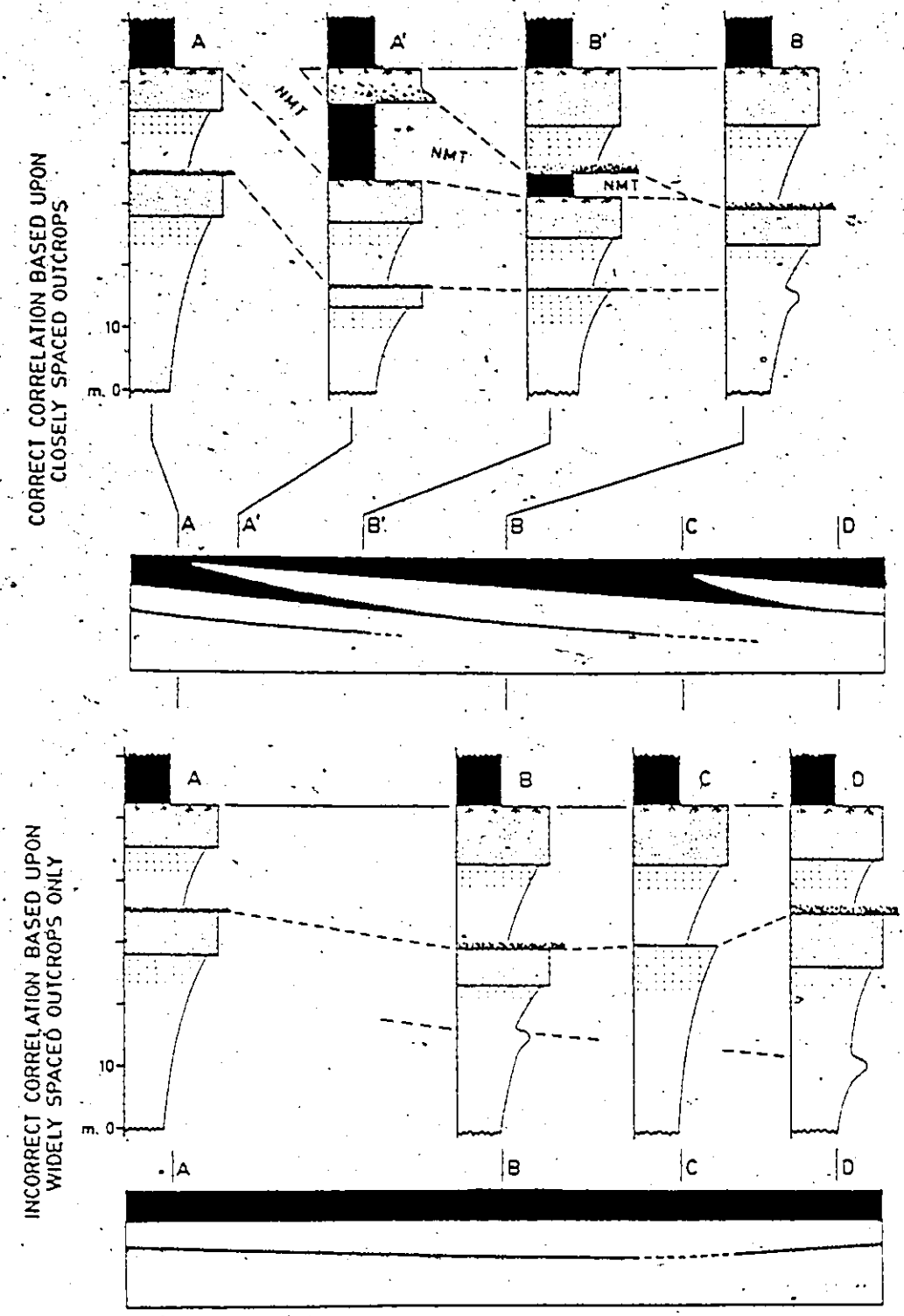
CORRECT CORRELATION BASED UPON
CLOSELY SPACED OUTCROPS
A
A'
B'
B
NMT
NMT
NMT
10
m. 0
A
A'
B'
B
C
D
INCORRECT CORRELATION BASED UPON
WIDELY SPACED OUTCROPS ONLY
A
B
C
D
10
m. 0
A
B
C
D

episodes. Patchy conglomerates of this sort appear to be correlative over relatively large distances, based upon widely spaced exposures (e.g., patchy conglomerates capping lower cycles in diagram D1, Fig. 6-4). In most cases, however, it is probable that neither the cycles nor the conglomerate caps are truely correlative (as illustrated in the conceptual diagram, Fig. 6-9).

Note that the minor transgressive phases described above cannot account for the major conglomerates present at the tops of major sedimentation episodes correlative over relatively large distances regionally (see correlation diagrams). Locally, these latter conglomerates tend to be much thicker than can reasonably be accounted for by the inferred mechanism of lag concentration during minor trangressions, and their distribution is significantly more extensive and complex. These regionally correlative transgressive conglomerates are discussed in detail later in this chapter.

Shoreline extent. As outlined above, the occurrence of shoreface erosion during minor transgressions (forming conglomerate lags) has major implications for the determination of ancient Cardium shorelines. Specifically, the final seaward extent of beach and/or non-marine deposits probably does not correspond with the final basinward position of the ancient shoreline: Transgressive

erosion probably removes these deposits over an undetermined distance landward from the final shoreline position.

Transgressive erosion is thought to have been more extensive during the major transgressive episodes. The post-depositional removal of upper shoreface and/or lower coastal plain deposits during subsequent transgressive erosion is discussed in detail later in this chapter.

Multiple Occurrences of Minor Transgressions

In chapter 3, figure 3-1 was used to diagramatically illustrate the occurrence of multiple minor regressive-transgressive pulses present at the southernmost extreme of the Cutpick Member; these are shown more precisely in the correlation diagrams. In addition to the Grande Cache Split (which does <u>not</u> occur at the tip of the Lower Tongue), diagram S2 (Fig. 6-2) reveals several additional non-marine splits which <u>are</u> present at the tip of this tongue. In particular, this diagram reveals separate non-marine splits at section 4-13 (the Canyon Creek Split) and section 5-41 (the Cripple Creek Split). These are separated by at least one more probable split, at section 5-39 on the Blackstone River; however, no non-marine deposits were actually observed enclosed within the Seebe Member at this outcrop. The Headwaters Split is

present in section WA-1 on diagram D2 (Fig. 6-5), and the inferred Blackstone River Split also is represented. The distal extremity of the Lower Tongue is also seen in both diagrams.

These multiple splits or lips at the tip of the Lower Tongue of the Cutpick are recognized in the southern part of the central Foothills, where outcrop control is the best in the study area. The recognition of an anomolously high number of splits in this area may in part be a function of availability of exposure; however, the occurrence of abundant splits at the extreme end of the preserved body of non-marine sediments is theoretically reasonable (see further discussion below). Note that a similar situation exists in the Chungo Sandstone Member of the overlying Wapiabi Formation (Rosenthal, 1983).

The concentration of numerous minor splits at the tip of the Lower Tongue of the non-marine Cutpick Member is conceptually reasonable within the basic framework of a major regression followed by a major transgression. These splits suggest the following generalized scenario for the movement of the Cardium shoreline during the Seebe-Cutpick episode. (N.B.: This scenario probably is also applicable to the two overlying episodes -- see further discussion below.):

1) The shoreline prograded basinward during a

relatively stable period of stillstand or slowly dropping sea-level, forming the cycles of the Seebe-Cutpick regressive episode. This period of steady progradation saw the advancement of the shoreline from the northern Foothills to its southernmost position in the southern part of the central Foothills. Progradation was occasionally interrupted by minor transgressions, forming very small splits of non-marine deposits such as the one recognized in the Grande Cache area (described above).

2) The shoreline oscillated within a narrow region in the southern part of the central Foothills during the early phase of a tectonoeustatic transgression of at least regional extent. This period of oscillation saw the development of the numerous minor splits present at the end of the Lower Tongue of the Cutpick Member. Shoreline oscillation probably was due to complex variations and interactions involving the rate of sediment supply, subsidence rate, and eustatic sea-level.

Note that subsequent transgressive erosion may have totally eliminated evidence for certain of these shoreline oscillations. This possibility, coupled with the incomplete nature of the natural exposures, suggests the possibility that many more splits were developed during this period than were preserved and recognized. Note also that the vertical juxtaposition of several minor splits

possibly requires a net upward vertical translation of the shoreface profile (and hence vertical aggradation of sediment) within this narrow region in the central Foothills. These observations are important in the further development later in this chapter of a conceptual model of sedimentation involving the major transgressive conglomerates.

3) A major tectonoeustatic transgression caused shoreline retreat back through the central and northern Foothills; formation of a major transgressive conglomerate took place at this time (see detailed discussion later in this chapter).

Following this transgression, two additional regressive-transgressive episodes of similar extent took place; these are recognized as the Sundre-Cutpick and Willmore-Obstruction regressive episodes. The events in each of these two episodes are thought to have been similar to those in the Seebe-Cutpick episode described above.

DEVELOPMENT OF A CONCEPTUAL MODEL FOR CARDIUM SEDIMENTATION: ASSUMPTIONS AND CONSTRAINTS

Below, I develop a conceptual model for sedimentation within the Cardium Formation. This model

will be founded upon a variety of data both from the outcrop and from a number of subsurface studies. This model is intended to act as a local facies model (or process-response model) for the Cardium both in the Foothills and in the subsurface in the Plains; as such, it is predicated on the assumption that Cardium sedimentation was essentially similar, or at least closely related, throughout the formation. This assumption will be defended below.

Implications of the model so developed will then be examined. The predicted effects on sedimentation arising as a logical consequence of the model will serve as a test of the hypothetical mode of origin.

Constraints on Sedimentation

A variety of data from outcrop and the subsurface serve as constraints of any analysis of Cardium sedimentation. In the following paragraphs I have tried to identify the major constraints that must be considered. Comments concerning the nature of the Cardium in the subsurface are summarized from previously published studies, and from on-going studies conducted by McMaster Cardium workers (R. G. Walker, G. Plint, D. Keith, K. Bergman). In the following paragraphs, personal communications from these McMaster workers will be

attributed to the "McMaster Cardium Group".

1) Coarsening-upward sequences. Thickening- and coarsening-upward cycles are ubiquitous throughout the Cardium, both in outcrop and in the subsurface. A variety of related facies sequences are present in these cycles. Sequences present in outcrop have been rigorously summarized in chapter 5; subsurface facies sequences are essentially identical (Walker, 1983c; pers, comm., McMaster Cardium Group, 1984). On the basis of facies sequences alone, all Cardium cycles can generally be interpreted as complete or top-absent variations of prograding storm-dominated shoreline deposits. Note that the top-absent cycles may result due to superficial erosion and/or non-deposition of their upper parts (see discussion in chapter 5).

2) Three regressive-transgressive episodes. As described above in this chapter, the Cardium in outcrop is composed of three vertically juxtaposed regional regressive episodes separated by transgression surfaces. The first of these regressive-transgressive episodes contains the most pronounced regressive interval in the Foothills (the Seebe-Cutpick episode). The third episode does not exhibit as pronounced a phase of regression, but is capped with the most widespread transgressive horizon (the Wapiabi transgression), and the most widespread transgressive

resedimented-lag conglomerate.

The three major episodes of sedimentation are thought possibly to correspond with three regressive-transgressive episodes present in many of the Plains oil fields. From base to top, these are the B, A, and Cardium zone developments. Note, however, that such a correlation is extremely tentative at this stage in the ongoing studies.

3) Offlapping cyclicity superimposed upon regional regressions. As described above in this chapter, locally developed cyclicity is superimposed upon each of the three regressive episodes in outcrop sections. These cycles display an offlapping relationship (see correlation diagrams). Offlapping cyclicity is also present in sand bodies within many Cardium subsurface fields (e.g., Ferrier, Willesden Green, and possibly Pembina --.see further discussion below).

4) Minor conglomerates deposited during regression. Minor accumulations of conglomerate deposited during regression are present within regressive cycles exposed throughout the Foothills. These conglomerates accumulated within lagoons (as washovers and/or small channel deposits), within shoreface sandstones (as plunge pool concentrates), and within thin offshore storm-event beds (either as basal lags of sandy beds or as thin sharp-based

conglomerate beds).

5) Minor conglomerates concentrated during minor transgressions of local extent. As discussed in detail above, minor conglomerates are present within regressive episodes in the Foothills as resedimented-lag concentrates capping transgressions of local extent, such as the one in the Grande Cache area (Fig. 6-8).

6) Numerous minor transgressions preceded major transgressions. As discussed in detail above, numerous minor-local transgressions apparently preceded major regional transgressions in the Foothills (see correlation diagrams and the summary of Fig. 3-1).

7) Major conglomerates restricted to regional transgression surfaces. As shall be demonstrated below, the major conglomerates present within the Cardium Formation are generally restricted to the three major transgression surfaces capping the three sedimentation episodes in the Foothills. Major conglomerates in the subsurface also are apparently restricted to regional transgression surfaces (Walker, 1983c; pers. comm., McMaster Cardium Group, 1984).

8) Lateral extent of major conglomerates. As indicated on the correlation diagrams above, and as shall be discussed in detail below, major conglomerates present

at regional transgressions enjoy a widespread distribution unlike the localized distribution of minor conglomerates deposited during regressions or minor transgressions.

9) Evidence of shallow-water deposition of major conglomerates. The major conglomerates present at regionally correlative transgression surfaces display a wide variety of evidence for deposition: 1) in a marine environment, 2) in very shallow water depths, and 3) in close proximity to shoreline. Abundant marine trace and body fossils confirm marine deposition (chapter 4). Paleohydraulic analysis of locally developed conglomeratic symmetrical ripples with spacings on the order of 1 m indicates deposition in very shallow water depths on the order of meters or a few tens of meters (chapter 8). Deposition of these conglomerates within close proximity to shoreline is suggested by: 1) the coarse grain size, 2) the trace fauna, and 3) the abundance of large (decimeter-scale) coalified wood fragments (chapter 4).

In the subsurface, many major Cardium conglomerates were also deposited in a marine environment. Although it is impossible to recognize meter-scale symmetrical ripples in core, the abundance of large wood fragments observed in subsurface conglomerates in some fields (pers. comm., McMaster Cardium Group, 1984) also suggests deposition in shallow water close to shore.

10) Asymmetrically tapered geometry of sand bodies. Several studies of Cardium fields in the subsurface, utilizing excellent control available from numerous well cores and logs, have demonstrated that many Cardium sand bodies possess a similar geometry (see detailed discussion below). In its simplest form, this geometry consists of either: 1) a tabular sand body terminated at the seaward extreme by a seaward-dipping surface oriented roughly parallel to the inferred paleoshoreline, or 2) a broadly tapered, flat-bottomed, convex-upward sand body elongate roughly parallel to the inferred paleoshoreline; the landward-dipping surface on the landward side of the body is much less steeply dipping than the seaward-dipping surface on the seaward side of the body.

In more complex instances, the geometry in a Cardium field consists of several such sand bodies shingled in an offlapping relationship (see further discussion below).

This commonly repeated, large-scale geometry has been attributed to offshore asymmetrical shoals (Sinha, 1970) or shelf "terrace bars" (Swagor, 1975). These interpretations are discussed below. I shall refer to Cardium sand bodies exhibiting this large-scale geometry as "asymmetrically tapered sand bodies", a non-genetic descriptive name. As I shall demonstrate below, evidence from outcrop suggests that these sand bodies do not form as

either offshore shoals or terrace bars, but rather as shoreface-attached regressive sand bodies modified during a post-depositional transgression.

ii) Asymmetrical conglomerate caps. Asymmetrically tapered sand bodies commonly display asymmetrical conglomerate caps. These capping conglomerates are asymetrical in that they are thicker on the steeply inclined, seaward-dipping, seaward side of the sand body; likewise, these conglomerates commonly are largely restricted to the steep seaward side of the sand body, and the top of the body near its seaward edge (Swagor, 1975; Griffith, 1981; Keith, 1985; pers. comm., McMaster Cardium Group, 1984).

Defence of the Assumption that Cardium Sedimentation was Similar in the Foothills and the Plains Regions

The basic assumption in the following development of a conceptual model for large-scale processes of sedimentation in the Cardium Formation is that these processes and the resulting large-scale features in the formation were essentially similar in the Foothills and the Plains regions. This assumption is necessary in order to develop a unified model for Cardium sedimentation. In my opinion, the development of such a model cannot be accomplished based on only one set of data (i.e., outcrop

data or subsurface data) because both data sets are inherently incomplete. Happily, however, the nature of these omissions is different in the two data sets; thus, a combination of outcrop and subsurface data permits development of a more-or-less complete picture of Cardium sedimentation.

The eleven points summarized above as the basic constraints on Cardium sedimentation reveal many of the essential similarities in the Foothills and the Plains regions. Specifically, factors 1, 2, 3, 7, 8, and 9 are essentially identical in the two regions, strongly supporting the basic assumption in the following analysis. All of the other factors may be present in both regions, but the evidence is somewhat equivocal. In my opinion, a sufficiently high degree of similarity exists in the formation in these two regions to justify proceding with the unified interpretation, utilizing data aquired from both areas.

A CONCEPTUAL MODEL FOR CARDIUM SEDIMENTATION

The conceptual model which follows represents an attempt to reconcile all eleven of the points listed above. This model is presented as a series of diagrams (Fig. 6-10 to 6-17), representing different times in the development of

an asymmetrically tapered sand body. The diagrams are drawn perpendicular to both the ancient shoreline and the elongation direction of the sand body; the vertical scale is greatly exaggerated. Each of these time-series diagrams is keyed to the following text by a sequence of letters.

Time 1: Steady Regression (Fig. 6-10)

Figure 6-10 represents the steady progradational phase of a Cardium shelf-to-shoreline sequence. Progradation took place during a relatively stable interval of slowly falling sea level (A) and/or stillstand. In this and the following diagrams, note that progradation is considered to take place over a flat, horizontal surface (B); however, any pre-existing topographic relief would probably have influenced the pattern of sedimentation (see further discussion below). As the shoreline prograded, the following facies associations were deposited in vertical succession:

Facies association 1 (C -- mud-dominated facies, colored grey) was deposited first, representing the most distal offshore deposition of storm-transported coarse clastic debris (thin siltstones and sandstones). Deposition was generally below effective storm wave-base.

Facies association 2 (D -- interbedded hummocky cross-stratified sandstones and mudstones, colored light



Figure 6-10. Time 1 in the conceptualized development of a regressive-transgressive episode of sedimentation in the Cardium Formation. See text for discussion.

TIME 1: STEADY REGRESSION, SHORELINE PROGRADES

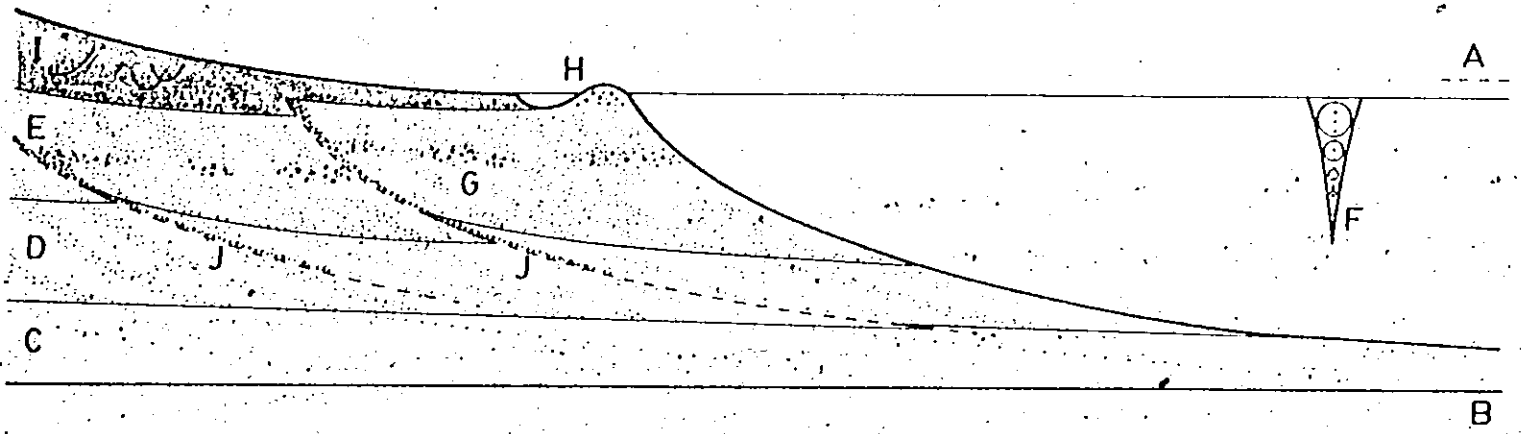

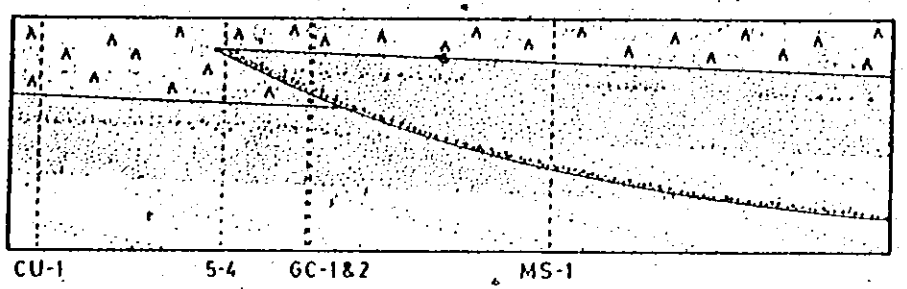

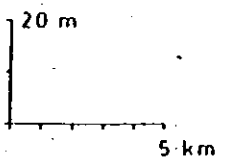

GRANDE CACHE NON-MARINE SPLIT OF THE CUTPICK MEMBER

427

yellow), represents storm-dominated deposition in a more proximal inner-shelf environment above storm wave-base.

Facies association 3 (E -- thick marine sandstones, colored dark yellow) represents the advance of a shoreface (or "shoreface-attached") sand body several meters to a few tens of meters in thickness. The upper part of this thick sandstone was deposited in water depths near or above effective fairweather wave base (facies 3SW and 3PL), as indicated by the diagrammatic representation of wave-orbital water trajectories (F). The base of this thick sandstone can be considered as the base of the "preserved" shoreface. Note, however, that mud deposition probably was extensive in the lower part of this sandy interval; much of this mud was removed by erosionally-based sandy storm deposits in a proximal offshore position (facies 3HA -- amalgamated hummocky sandstones). The inclusion within association 3 of sandstones deposited in the offshore zone below the mud-line is the basis for the interpretation indicated by the term "shoreface-attached sand body". No interpretation of plan-view geometry is signified by the use of this term. Plunge-pool conglomerate concentrates (G) are developed locally in a nearshore setting within association 3. Also, a small barrier/lagoon system (H) is represented at the shoreline, with localized lagoonal conglomerates concentrated during barrier progradation. Lagoonal conglomerates in the

Cardium may have been supplied either by barrier overwash or from fluvial channels entering the lagoon at the backbeach. Note that many Cardium sequences do not display lagoonal and backbeach deposits; Cardium lagoons probably did not extend along the entire shoreline, which in many places consisted of accretionary beach ridges without lagoons (chapter 5).

Facies association 4 (I -- lagoonal and non-marine deposits, colored green), records the transition from marine to non-marine sedimentation in this prograding sequence. Lower flood-plain deposits consist dominantly of mud; fluvial distributary channel deposits are encountered locally.

In the conceptual diagram of time 1, the steady progradation reflected by the coarsening-upward facies pattern is twice interrupted by minor transgressive pulses (J). These minor transgressions are of local extent only. As discussed above, the best real-world example of a local transgressive pulse is the Grande Cache non-marine split of the Cutpick Member; this split is drawn to scale in the lower panel of figure 6-10, where the vertical exaggeration is less severe than in the conceptualization. This lower panel gives the reader a better visualization of the low angles involved in these relationships than does the conceptual diagram. These relationships are discussed in

greater detail in the preceding section of this chapter.

Time 2: Early Transgression (Fig. 6-11)

By time 2, a series of minor transgressive-regressive pulses, closely spaced in time, have already occurred. These pulses immediately precede a major period of transgression commencing at time 3, and therefore are developed near the outermost basinward extent of the shoreline associated with this regressive episode. As discussed in detail above, the evidence for these closely-spaced oscillations of shoreline position immediately prior to a major tectonoeustatic transgression is the presence of numerous minor non-marine splits at the ends of non-marine tongues in the Cardium and other Western Interior Mesozoic units. The net accumulation of sediment required to preserve these minor splits implies a net rise in sea level prior to time 2 (A).

The inset series (Fig. 6-11) diagrammatically illustrates the sequence of events leading to the development of the vertically juxtaposed splits at the end of a non-marine tongue in the Cardium. This series of diagrams represents times intermediate between time 1 and 2; the series emphasizes developments in the nearshore and lower coastal plain, where minor transgressive-regressive pulses are expected to have the most prominent effects.

The hypothesized sequence of events and their effects are described below:

Panel 1 of the inset shows a shoreline prograding during stillstand or sea-level fall, with fluvial distributary channels on the lower floodplain (a). The situation in this panel is equivalent to conditions at time 1.

Panel 2 illustrates the effects of a single minor transgression. During transgression, a portion of the shoreface, shoreline, and lower coastal plain is eroded; a minor transgressive lag conglomerate (a) is developed by this erosion. The advance of the sea and accumulation of sediment on the retreating coastal plain result in a reduction of slope across the lower coastal plain; the associated reduction in hydraulic head results in abandonment of coarse fluvial distributary channels, and the deposition of a certain thickness of flood-plain and/or lagoonal muds across the lower coastal plain (b -- indicated by root symbols).

Panel 3 illustrates renewed progradation during stillstand or sea-level fall. A new system of fluvial distributaries (a) is incised in the lower coastal plain as relatively greater hydraulic gradients are re-established.

Panel 4 represents a second minor transgression, with formation of a second transgressive lag (a) and a

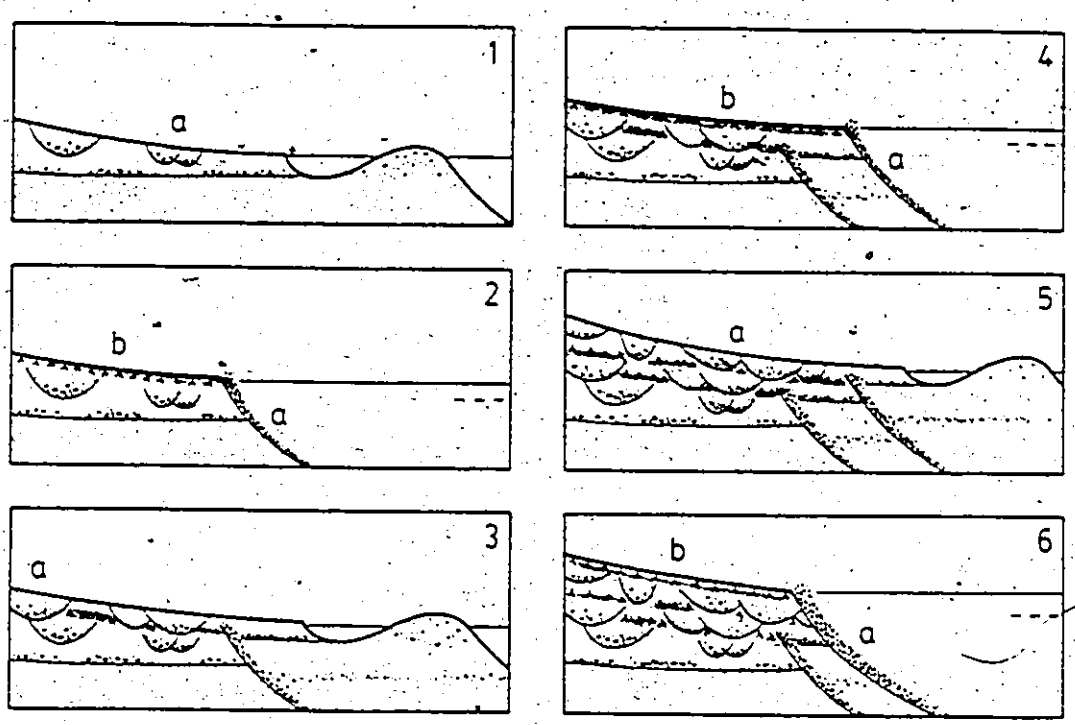

SEE NON-MARINE INTERVAL ON MASKUTA CREEK FOR AN EXAMPLE OF FLUVIAL DISTRIBUTARY CHANNELS INTERBEDDED WITH LAGOONAL DEPOSITS.

Figure 6-11. Time 2 in the conceptualized development of a regressive-transgressive episode of sedimentation in the Cardium Formation. Inset diagram is on this page. See text for discussion.

TIME 2: STILLSTAND / EARLY TRANSGRESSION
VERTICAL AGGRADATION

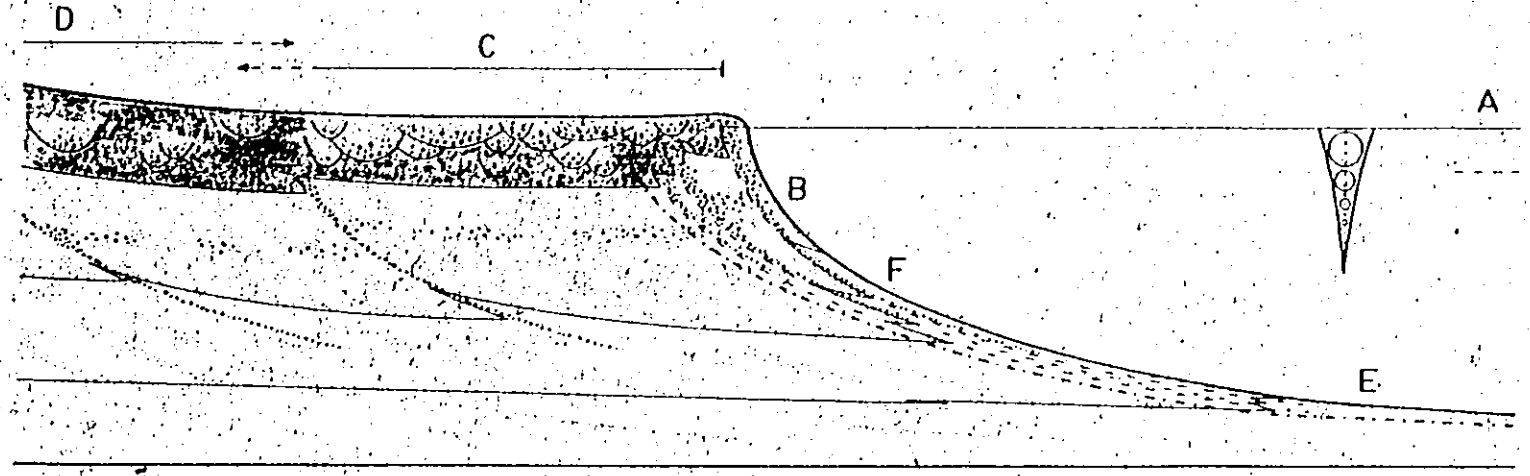

433

second coastal-plain mud blanket (b) similar to those shown in panel 2.

Panel 5 illustrates development of a new fluvial channel system (a) during a third period of progradation.

Finally, panel 6 illustrates a third minor transgression. This transgressive pulse differs from the two preceding it in that the associated transgressive erosion has been sufficiently extensive to cut back to the lag deposit formed during the immediately preceding transgressive pulse. Accordingly, the lag formed by this final minor transgression (a) is somewhat thicker than those illustrated previously, because it contains the selectively sorted coarse component of two minor regressive pulses, rather than one only. Note that a third coastal-plain mud deposit (b) has also been formed during this transgressive pulse.

The sea-level fluctuations discussed above have given rise to the distribution of sedimentary features illustrated in the diagram of time 2 (Fig. 6-11), which shows lithological variation over a larger cross-sectional area than represented in the inset. This diagram suggests that these shoreline oscillations can reasonably be expected to result in a dramatic concentration of conglomerate in close proximity to the shifting shoreline; this coarse material will be concentrated in a belt ranging

from the proximal offshore to the lower coastal plain, as discussed below.

The multiple minor transgressive lags have concentrated conglomerate in the nearshore to proximal offshore region (B), as illustrated in the inset series. Minor conglomerate lags deposited within regressive episodes in the formation rarely extend to within facies association 1 further offshore (chapter 5 and correlation diagrams of this chapter). Additionally, multiple transgressions and regressions have resulted in abandonment and re-establishment of fluvial distributary channels across the lower coastal plain, within the region delineated by the lower arrow (C). It is probable that minor fluctuations in sea level have not had a profound influence upon the coarser fluvial channels on the upper coastal plain (D); it is possible that these shoreline oscillations result in a net increase in the amount of coarse material deposited on the lower coastal plain relative to the upper plain. Thus, it is hypothesized that multiple shoreline oscillations prior to a major tectonoeustatic transgression result in a concentration of coarse material within the viscinity of the final shoreline position at maximum regression.

Of critical importance to the testing of the hypothetical developments outlined in this time series is the following prediction of effects at the base of the

shoreface: The multiple shoreline oscillations have accompanied a net rise in sea level (A); this net rise will result in the landward shifting of facies zones. These minor landward offsets will not be readily apparent far offshore (as at E), but will become progressively more pronounced at shallower depths. In particular, the landward offset of the base of the preserved shoreface (F) will be easily recognizable in outcrop. The minor fluctuations described above, superimposed upon a net transgression, will result in a thin interval of finer sediments being deposited upon the thick sandstones at the seaward extremity of the base of the preserved shoreface (at F). These finer sediments will record an overall thinning- and fining-upward tendency, but may be composed of even thinner "packages" of sediment displaying either a coarsening-upward or unvarying vertical profile, depending upon the relative "blurriness" of grain-size variation below the preserved shoreface during the minor shoreline oscillations.

As discussed below, sediments subsequently deposited over the thinning- and fining-upward interval briefly described above will result in a distinctive vertical facies sequence which cannot be conveniently interpreted by any process other than the one outlined in this time series. The presence at different stratigraphic levels within the Cardium of this distinctive facies

sequence strongly supports the hypothetical depositional process advanced in this chapter.

An additional effect of the multiple shoreline oscillations preceding time 2 has been pronounced vertical aggradation on the lower coastal plain and in the nearshore region, as indicated by the relative elevations of the profile at time 2 and the profile at time 1 (represented by the dot-dash line on figure 6-11). This aggradation has resulted in a broad and flat lower coastal plain at time 2. As depicted in the next diagram, continued transgression must at some point rapidly overtop the lower coastal plain due to this reduction in slope (and the inability of coastal-plain sedimentation to match the rise in sea level).

Time 3: Rapid Transgression (Fig. 6-12)

Time 3 illustrates the onset of an extensive, erosional transgression (A) over the previously deposited prograding shoreline sequence associated with the major regressive episode now terminated. This dramatic change in the effects of transgression is due to a combination of: 1) acceleration in the rate of tectonoeustatic sea-level rise, and/or 2) the inability of sedimentation on the lower coastal plain, made more nearly horizontal by vertical aggradation during the shoreline oscillations of time 2, to

Figure 6-12. Time 3 in the conceptualized development of a regressive-transgressive episode of sedimentation in the Cardium Formation. See text for discussion.

TIME 3: RAPID TRANSGRESSION, SHOREFACE EROSION

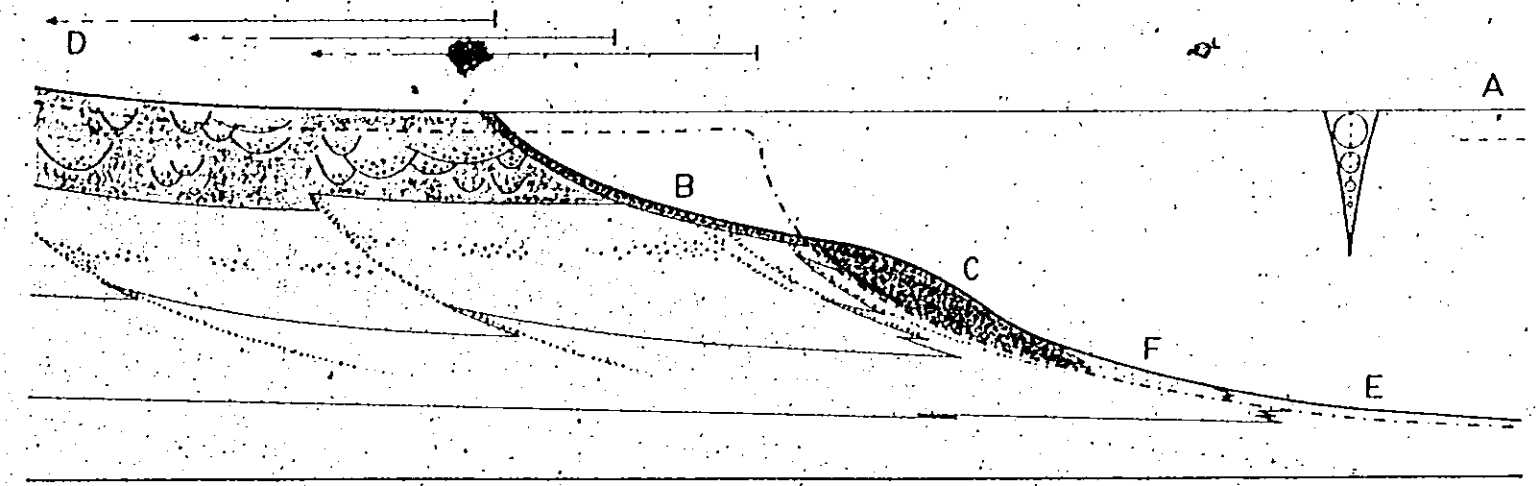

SEE CYCLE 5, SECTION 5-45, FOR AN EXAMPLE OF THIS UNUSUAL CYCLE CAP.

keep pace with the rise in sea level.

As this major transgression advances, a new shelf profile (B) develops by erosion of previously deposited sediment, particularly: 1) the overthickened, mud-dominated lower coastal plain deposits, including a series of fluvial distributary channels, and 2) the uppermost shoreface deposits, including the thickest portion of the previously formed multiple transgressive lags. The bulk of these previously deposited sediments is advected beyond the nearshore region due to this erosion; it is re-deposited in the proximal to distal offshore region. In the particular setting considered herein, this sediment is re-deposited on the drowned shoreface of the immediately preceding prograding shoreline (C), in what can be considered a "hydrodynamic shadow" below the influence of waves, formed at the break in slope on the developing transgressive shelf. A major transgressive lag deposit (colored red) is developed by this transgressive erosion. However, this conglomerate is <u>not</u> a simple transgressive lag, for it has been extensively transported (with a component of motion directed offshore) and resedimented in part in the offshore region during development of the new shelf profile. I shall refer to this deposit as a "resedimented-lag conglomerate"; preliminary fabric analyses (not presented herein) suggest deposition from a dispersion above the bed in many examples.

Note that the thickness of resedimented-lag conglomerate relative to other sediments has been greatly exaggerated in figure 6-12 for purposes of clarity.

Landward retreat of the transgressing shoreline leads to the abandonment of fluvial channels further and further back on the lower coastal plain, as indicated by the vertical sequence of horizontal arrows (D). Generally, therefore, periods of transgression probably do not supply vast amounts of coarse material to the shoreline, and the thick conglomerates deposited at times of major tectonoeustatic transgressions in the Cardium cannot have been transported to the shoreline during transgression. The only reasonable source for the thick transgressive conglomerates capping many Cardium cycles (see chapter 5) is the process of transgressive erosion and resedimentation suggested herein.

Note that I have indicated a progressive offshore fining of sediment accumulated on the shelf during transgression, with mud (E -- colored grey) being deposited further offshore than pebbly sandstones (F -- colored light red) and sandy conglomerates (C -- colored red).

At the base of the diagram, I have indicated a real-world example of the unusual stratigraphic sequence developed by time 3 over the toe of the drowned regressive shoreface. The fifth cycle at section 5-45 on Ram River (appendix 2) shows an unusually thin shoreface sandstone

overlain by a thick interval of thinning- and fining-upward shelf storm deposits, which in turn are overlain by thick marine conglomerates followed by distal offshore mudstone/shale. This unusual sequence of facies (and other examples like it) cannot be readily interpreted in simple terms of regressive coarsening, transgressive fining, and transgressive lag development, because there is no potential source of pebbles within the fining-upward interval from which a lag might be developed. However, this sequence is fully consistent with the interpretation of resedimented-lag conglomerates developed herein. Note also that multiple conglomerates associated with fining-upward sequences (between the shoreface sandstone and the thick transgressive conglomerate above the arrow in figure 6-12) are predicted by the model developed herein (at G), and are in fact observed in this position in real sequences (see further discussion later in this chapter).

Time 4: Minor Regression (Fig. 6-13)

This diagram has two purposes: 1) to illustrate the probable absence of major modifications imparted to the pattern of deposition by a minor regression superimposed upon the major tectonoeustatic transgression, and 2) to suggest a possible mechanism for the delivery of "new" conglomerate to the Cardium shoreline during transgression.

By the term "new conglomerate" I refer to coarse material which has not been erosionally exhumed from underlying regressive deposits, but instead has been brought to the shoreline across the coastal plain by surface processes.

At time 4, a minor drop in sea level (A) is superimposed upon the still-developing major transgression; this fluctuation may possibly represent a shoreline oscillation equivalent to or greater than those which heralded the onset of transgression at time 2. The drop in sea level causes an increase in the hydraulic gradient across the coastal plain, activating a system of fluvial distributary channels (B -- see further discussion below). The drop in sea level also causes erosion in the nearshore to proximal offshore regions on the newly-developed transgressive shelf profile (C). This erosion performs further hydrodynamic sorting of the resedimented-lag conglomerate deposited before time 4; some of this material is reworked further seaward to develop an offlapping "shingle" of marine conglomerate deposited in the "hydrodynamic shadow" (at D). These modifications do not significantly affect the general relationships between facies present at time 3.

A possible source of "new" conglomerate supplied to the shoreline during a period of overall transgression can be illustrated by means of this diagram; the concept from which this possible source is suggested has been developed

Figure 6-13. Time 4 in the conceptualized development of a regressive-transgressive episode of sedimentation in the Cardium Formation. See text for discussion.

TIME 4: MINOR REGRESSION

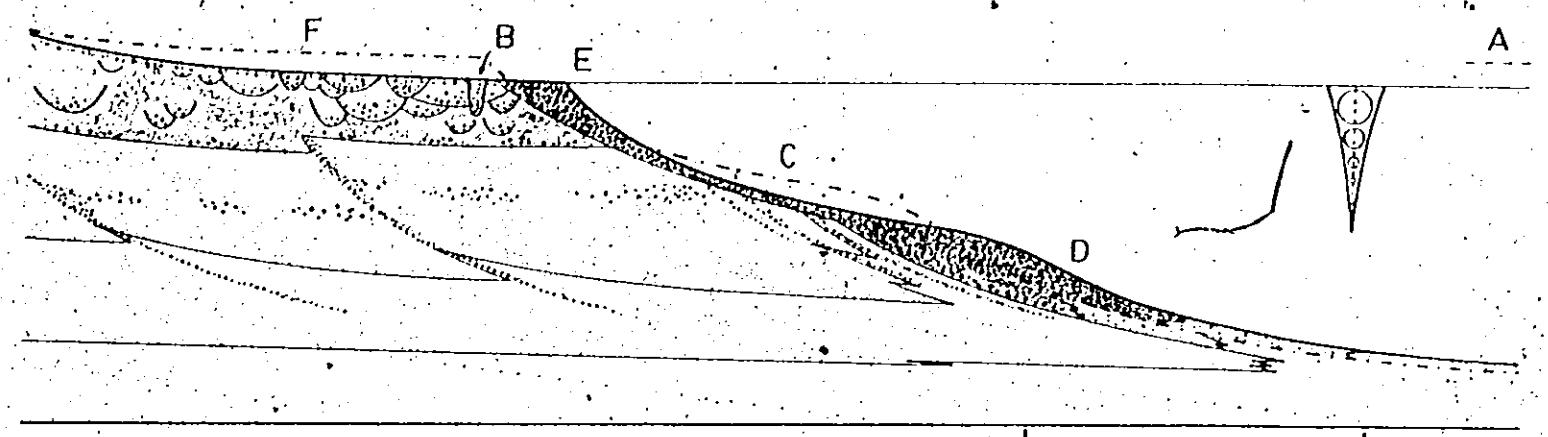

by Guy Plint in his study of the subsurface Cardium in the Kakwa area (G. Plint, pers. comm., 1985). In this conceptualization, a rapid and pronounced drop in sea level results in an extreme increase in the hydraulic gradient across the lower coastal plain. Although this increase may be relatively short-lived, it results in deep incision of river channels on the lower coastal plain (B). Incision of these channels leads to a sharp increase in river slope across the plain and the delivery of large volumes of coarse material to the shoreline, possibly forming temporary conglomeratic beach deposits (E) which can be reworked by storms to transport conglomerate to the shelf. Another possible factor is the erosional stripping of the uppermost deposits of the elevated coastal plain, represented by the profile change (F) on the lower coastal plain from time 3 to time 4. If such superficial erosion is large enough to dissect previously deposited channel sediments, an additional source of coarse material to the shoreline can be made available.

Support for this hypothetical origin for a temporally restricted supply of coarse material to the Cardium shoreline derives from the observation of fluvial distributary channels incised into the upper shoreface of some regressive sequences, both in the subsurface (at Kakwa) and in outcrop (e.g., sections WA-1 and 5-22). Incised channels of this sort typically remove beach and

nearshore deposits, and rarely remove an entire shoreface sequence (as at 5-22). Evidence against this origin is the observation that major Cardium conglomerates are restricted to transgression surfaces, leading to the conceptual difficulty in arguing for a close temporal association between major transgressions and episodes of pronounced sea-level fall. Future work may determine that such pronounced coincident extremes of sea level are conceptually reasonable, or at least justified on the basis of observational data; pending this development, the hypothetical origin of transgressive conglomerates preferred by this author is the resedimented-lag concept advanced above. It is noteworthy, however, that the two mechanisms are not mutually incompatible; both may have operated simultaneously in the development of some Cardium sequences.

At the base of the diagram, I have indicated two real-world examples of unusual stratigraphic sequences developed by time 4 over the toe of the drowned regressive shoreface. These are genetically related to the facies sequence from the fifth cycle at section 5-45 on Ram River, discussed under "Time 3" above. The significance of each of these sequences will be discussed more fully at the end of this chapter.

Time 5: Continued Transgression (Fig. 6-14)

Time 5 represents the continuance of the major tectonoeustatic transgression (A) interrupted by the minor regression of time 4. In this diagram, the shoreline has retreated far back along the lower coastal plain (B), leaving a transgressive lag deposit of relatively great lateral extent (colored red) deposited over a broad transgressive shelf terrace (between C and C' -- see further discussion below). Note that this lag thins in a direction away from the basin center, for two reasons:

1) As the transgression proceeds, the shoreline retreats back up the coastal plain away from the position of maximum basinward extent of the underlying regressive shoreline. Thus, the transgressing shoreline progresses beyond the region on the lowermost coastal plain in which the preceding minor shoreline oscillations have resulted in vertical stacking of multiple distributary channels; the source of coarse material for transgressive reworking therefore diminishes as transgression across the lower coastal plain proceeds.

2) Paleoflow data (discussed in chapter 7) confirms the suggestion implicit in this conceptual time series that storm reworking of lag material transports coarse detritus in a direction with an offshore component. Throughout the

continuing transgression, therefore, the effect of storm-generated currents over the shelf terrace has been to rework this lag material from shallower waters proximal to shore to deeper waters toward the center of the basin. Some of this material becomes relict in deeper water on the terrace (between C and C'); the finer fraction of the lag may be transported as far as the hydrodynamic shadow at or below the break in slope (seaward of C') where it accumulates in a less agitated environment (at D or further basinward).

The diagram for time 5 presents an opportunity to discuss variation in the stable shelf profile during progradation and transgression. Previous workers have emphasized the concept of the stable profile of a shelf formed in unconsolidated material as representing a large-scale substrate response to the complex hydrodynamic conditions of the shallow-marine environment (see review by Swift, 1976 -- especially his Fig. 18, reproduced herein as Fig. 6-15). In this conceptualization, the shelf geometry (particularly, the increase in water depth with distance from shore) can be regarded as being controlled by sediment grain size, sediment availability, and some characterization of the rate of energy expenditure at different depths on the shelf. The qualitative relationships are most clearly understood by considering

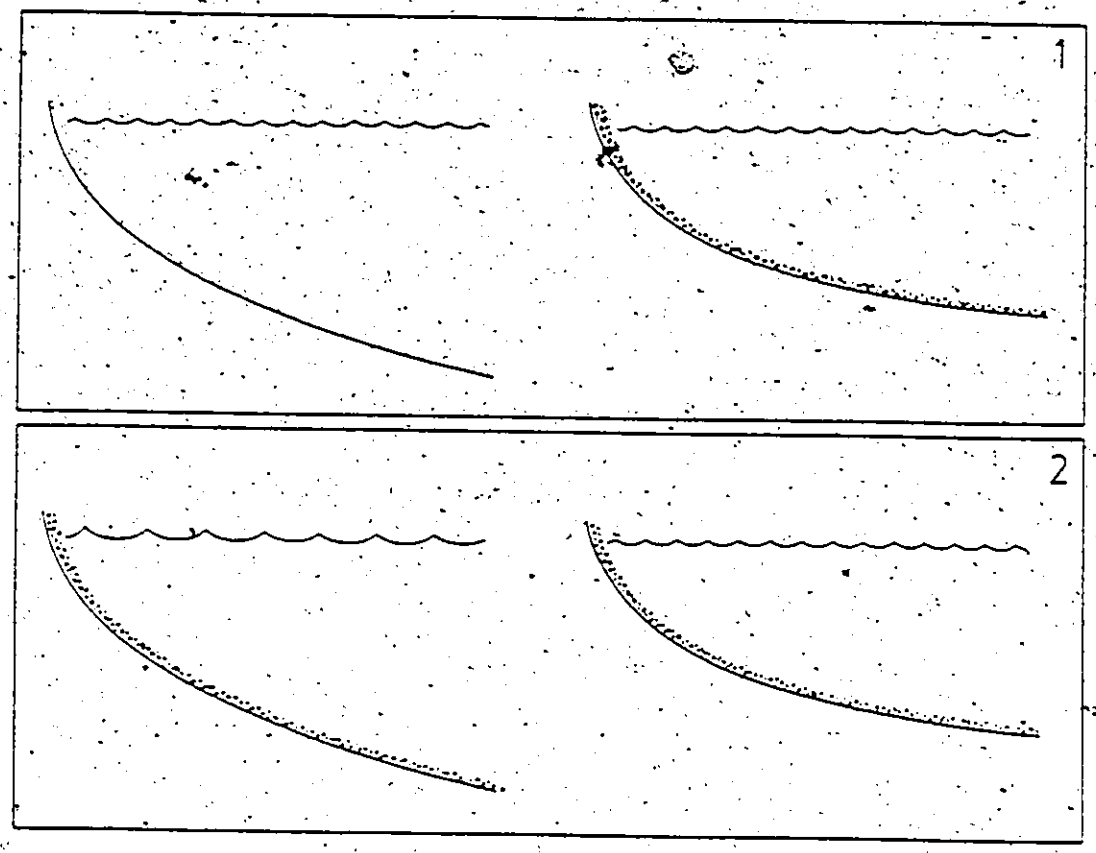

Figure 6-14. Time 5 in the conceptualized development of a regressive-transgressive episode of sedimentation in the Cardium Formation. Inset diagram is on this page. See text for discussion.

TIME 5: CONTINUED TRANSGRESSION

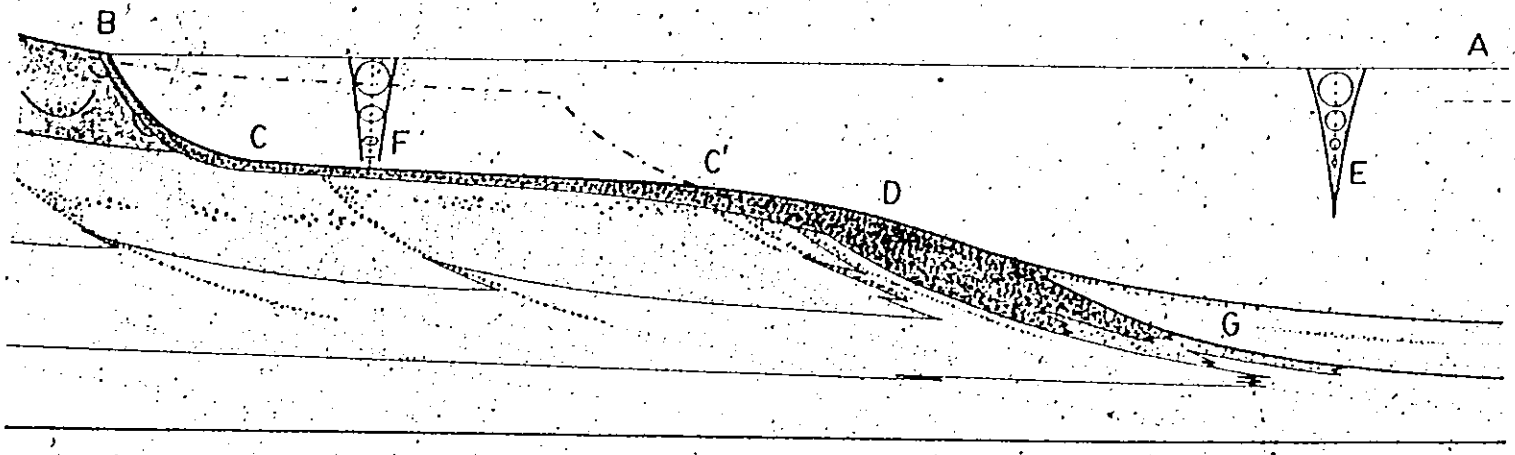

Figure 6-15. Shoreface translation and associated erosion and/or aggradation on the shoreface during various modes of regression or transgression. From Swift (1976, Fig. 18) after Curray (1964).

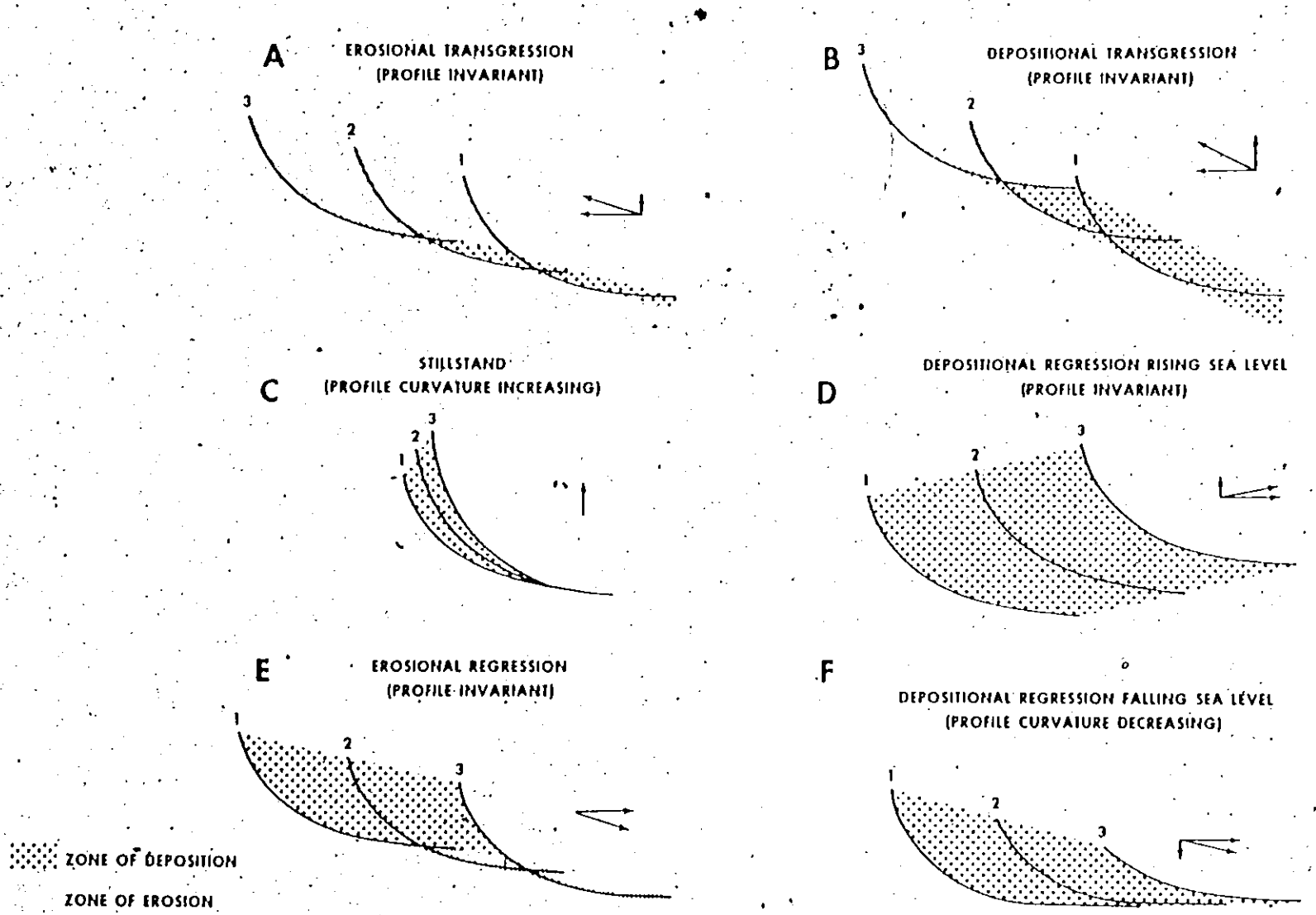
A
EROSIONAL TRANSGRESSION
(PROFILE INVARIANT)
3
2
1
B
DEPOSITIONAL TRANSGRESSION
(PROFILE INVARIANT)
3
2
1
C
STILLSTAND
(PROFILE CURVATURE INCREASING)
3
2
1
D
DEPOSITIONAL REGRESSION RISING SEA LEVEL
(PROFILE INVARIANT)
3
2
1
E
EROSIONAL REGRESSION
(PROFILE INVARIANT)
1
2
3
F
DEPOSITIONAL REGRESSION FALLING SEA LEVEL
(PROFILE CURVATURE DECREASING)
1
2
3
ZONE OF DEPOSITION
ZONE OF EROSION

transgressive erosion of abundant unconsolidated material. In the inset diagram for time 5, panel 1 indicates two different shelf profiles formed in different grain sizes (sand vs. gravel) under the same hydraulic regimes. Depth on the gravelly shelf is shallower at any specified distance from shore than is depth on the sandy shelf, a reflection of the inability of the shelf hydraulic regime (held constant in both cases) to erode gravel to the same depth as sand. In panel 2, grain size is held constant, but energy expenditure is varied. On the right, a low-energy regime is unable to erode to the same depth as is a high-energy regime.

The simple concepts outlined above have major significance for the modification of Cardium sand bodies during the development of a stable transgressive shelf profile. The presence of a relatively thick conglomeratic lag deposit suggests that substrate response during transgression probably was quite different than during the preceding progradational phase of sedimentation, at which time the substrate was characterized by finer grain sizes (very fine to fine sand). Assuming relatively similar hydraulic regimes, the situations during transgression and regression were analogous to those in panel 1 of the inset for time 5. Specifically, the sandy shelf profile stable during regression probably was significantly steeper than the gravelly shelf profile stable during transgression.

Both of the shelf profiles discussed above asymptotically approach the horizontal in deeper waters far from shore. The nearly horizontal floor of the gravelly transgressive shelf lay in shallower water depths than the floor of the sandy regressive shelf. This difference is illustrated qualitatively at time 5 by the wave orbitals over the distal offshore (E) and over the transgressive shelf terrace (F). On this terrace, the orbitals are drawn to suggest water depths in which the substrate is more-or-less continuously agitated during fairweather wave conditions; this suggestion is supported by calculations of water depth derived from conglomeratic symmetrical ripples formed in transgressive lag deposits (chapter 8). Wave activity in such shallow depths over the transgressive shelf terrace would effectively suspend muds derived at the eroding shoreline; during storms, eroded muds, silts, and sands might be flushed off the platform to accumulate in a distal offshore position (below E). Thus, the break in slope becomes progressively less pronounced as the transgressive accumulation of sediment proceeds.

Note (at G) that I have suggested the possibility of thin conglomeratic "stringers" within the distal offshore muds accumulating during transgression. These stringers are equivalent to those discussed in chapter 4 in the descriptions of associations 1 and 5; their position relative to the major conglomeratic lags is confirmed by

the correlation of cycles both in outcrop and in the subsurface (see correlation diagrams and chapter 7). These thin pebbly bands are thought to have been derived from the major mass of conglomerate (on the break in slope) during episodes of extreme agitation during storms.

Time 6: Continued Transgression (Fig. 6-16)

The transgressive rise in sea level (A) has continued to time 6. The shoreline has retreated off the left side of the page, leaving the patchy landward extremity of the reworked resedimented-lag veneer to pinch-out just at the edge of the page (B). Due to the increase in water depth, wave-orbital motion during fairweather conditions is very feeble at the sediment-water interface over the transgressive terrace (C); at this time, fine-grained sediments may be beginning to accumulate on the terrace between times of storm actvity. However, most of this material is swept from the terrace by these storms, and accumulates basinward of the break in slope (now very much subdued). This accumulation of fine material seaward of the break in slope (D to D') leads to vertical aggradation on the sea floor. If the sea floor aggrades at a rate faster than the rate of sea-level rise, the sediment-water interface will enter progressively shallower water depths. The effect of wave scour during storm

conditions may cause an upward increase in the abundance and thickness of storm-lag concentrates within the fine-grained material (D to D'). Fluctuations in the two rates (i.e., sea-level rise and sediment accumulation) may result in the development of small-scale cyclicity in these fine-grained deposits, as has been observed both in outcrop and in the subsurface (see correlation diagrams, and further discussion below and in chapter 7).

Time 7: Inundation (Fig. 6-17)

By time 7, transgression has continued (A) to the point that the entire sand/conglomerate body in the area of the diagram has become a relict feature. The continued deposition of hemipelagic muds has completely obliterated the break in slope; the sea floor is now relatively plain and flat across the diagram. Note the presence of some conglomerate stringers within muds deposited over the smothered terrace (B), formed by the episodic erosion of newly-deposited mud to incorporate storm-transported pebbles from the terrace top within laterally adjacent muds on the terrace.

The lettered intervals at the bottom of the diagram of time 7 will be used to refer the reader to segments of this hypothetical deposit when considering real-world sequences in the Cardium later in the thesis.

Figure 6-16. Time 6 in the conceptualized development of a regressive-transgressive episode of sedimentation in the Cardium Formation. See text for discussion.

TIME 6: CONTINUED TRANSGRESSION

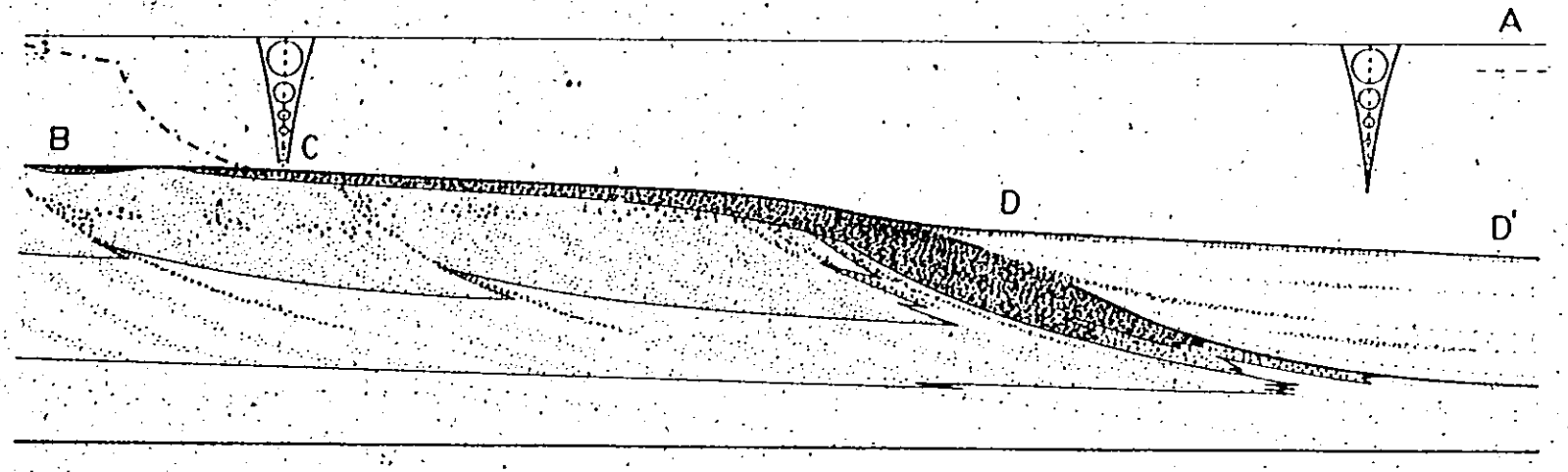



Figure 6-17. Time 7 in the conceptualized development of a regressive-transgressive episode of sedimentation in the Cardium Formation. See text for discussion.

TIME 7: INUNDATION, DEPOSITION OF MUD

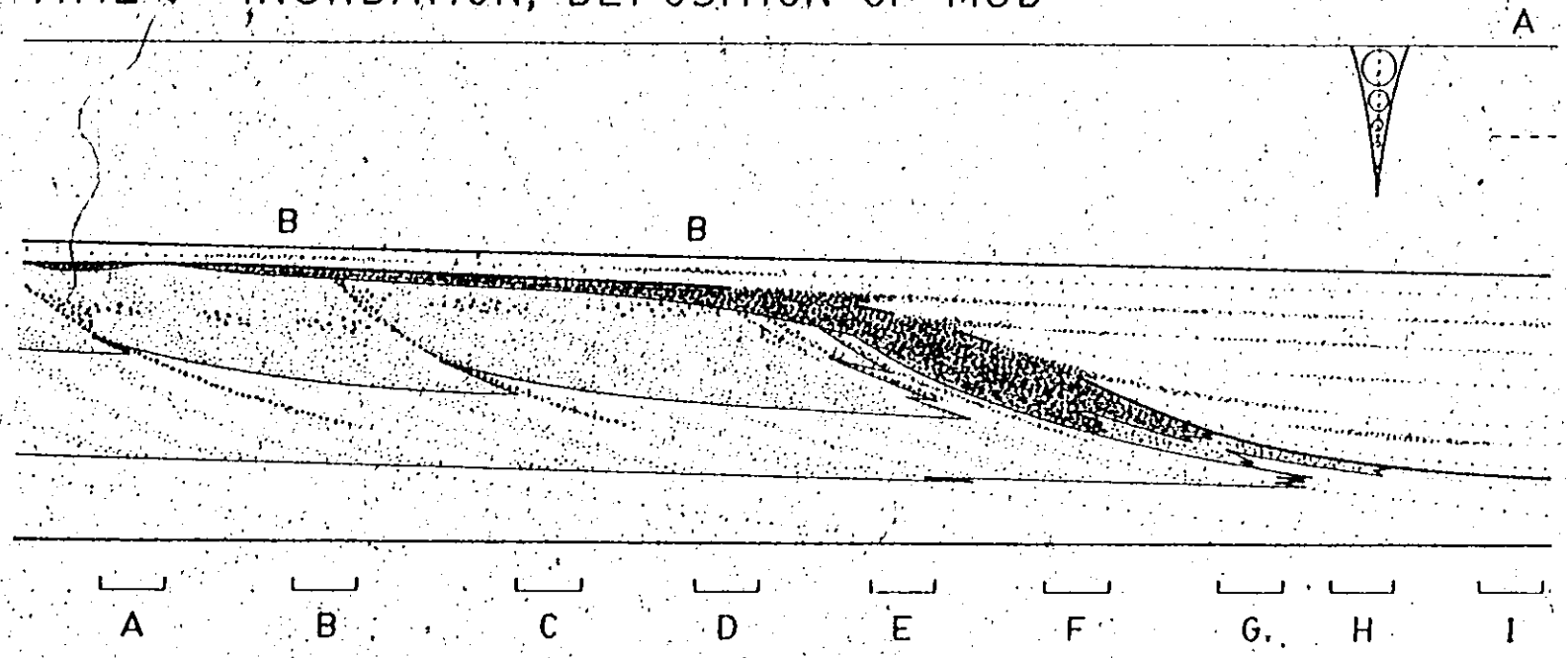

SUMMARY OF THE CONCEPTUAL MODEL DEVELOPED IN THE PRECEDING TIME SERIES DIAGRAMS

The conceptual sequence of depositional events discussed in the preceding section has produced an asymmetrically-tapered marine sand body with an asymmetrical conglomerate cap. This conglomerate is thicker on the basinward (steep) slope of the body. No non-marine deposits have been preserved in this body, which is entirely encased in marine muds (except on the landward side of the body, off the time-series diagrams to the left -- these deposits have yet to be discussed).

The resulting facies geometry represented at time 7 (Fig. 6-17) was produced by the sequence of major depositional events briefly summarized below:

1) Progradation of a shelf-to-shoreline sequence deposited the bulk of sediment preserved within the final body as a coarsening-upward sand sheet of great lateral extent.

2) At the onset of a major tectonoeustatic transgression, multiple oscillations of the shoreline concentrated abundant coarse sediment near the basinward edge of the regressive sand sheet.

3) A major transgression of this regressive

sequence was accompanied by erosional truncation of the upper part of the sequence and the removal of non-marine deposits. A resedimented-lag conglomerate of great lateral extent was formed during transgression, with the thickest conglomerate being deposited in a "hydrodynamic shadow" on the drowned shoreface at the steep basinward edge of the regressive sand sheet.

4) Inundation and de-activation of the coarse deposit (during the continuing transgression) was accompanied by deposition of an encapsulating "blanket" of hemipelagic muds over the sand and conglomerate.

SOME VARIATIONS ON THE BASIC FACIES GEOMETRY IN THE CONCEPTUAL MODEL

Two-Dimensional Variability (Fig. 6-18)

Figure 6-18 represents several possible variations on the basic conceptualization developed in the time-series diagrams above. It is noteworthy that the model as presented above is strictly two-dimensional; the same is true of the slightly more complicated variations of figure 6-18. Localized modifications resulting from sediment transport normal to the plane of the page (parallel to shore) have not been considered in either the model or

Figure 6-18. Three possible examples of two-dimensional variability in the conceptual model developed in this chapter. See text for discussion.



these variations; shore-parallel flows can be expected to result in further complications of the basic conceptual summary diagram of time 7 (Fig. 6-17).

The variations (Fig. 6-18) represent inferred facies geometries resulting from varying the combination, sequence, duration, and intensity of the same factors as were imagined for the original time-series diagrams. Each of these geometries (and a host of other variations) is considered to be equally as legitimate as the basic geometry summarized at time 7 (Fig. 6-17). Note that conglomerate thickness has again been greatly exaggerated relative to the thicknesses of other sediment types.

In the upper panel diagram, where the major regressive episode shows a pattern of offlapping cyclicity (developed in two sequences from sand to conglomerate), the second offlap sequence is the result of a pronounced period of regression superimposed upon the major transgression at a time equivalent to time 4 in the original series of diagrams. The second conglomerate is a product of transgressive reworking of coarse material concentrated by multiple minor transgression-regression pulses recorded in the underlying sand deposit. Note also that a third regressive pulse lies upon the major body of coarse material at the upper left on the upper panel.

In the central panel, the major transgressive conglomerate is split into two vertically juxtaposed

tongues at its basinward extreme; due to the deposition of a large amount of offshore mud during the early stages of the transgression (at a time equivalent to time 3 in the original series of diagrams). The lower tongue is continuous further out into the basin (far beyond the break in slope), reflecting the possible generation of sediment-laden density underflows on the relatively steep slopes of the drowned regressive shoreface. Note also the preservation of non-marine deposits (colored green) below the transgressive conglomerate over the top of the terrace, and the development of pronounced thicks and thins within this conglomerate. Variation in the thickness and distribution of the conglomerates on the terrace might reflect the original distribution of coarse material in the eroded regressive deposits, or it might result from constructional features (such as shelf ridges or channels) formed on the transgressed terrace, or both.

The lower panel diagram shows the greatest deviation from the conceptual norm. In this instance, transgressive conglomerate is distributed over a smaller area than in the preceding diagrams. This "patch" of transgressive conglomerate has acted as an armoring against deep transgressive erosion into the underlying sands; thus, the armored area stood as a major topographic high on the transgressing shelf, located just landward of the break in slope. [Note, however, that the vertical scale is greatly

exaggerated; the topographic high may have been on the order of meters over a width of tens of kilometers. See further discussion in chapter 7.] This topographic high has acted as a dam against the transport of fine-grained sediments into the distal offshore; hence the preservation of the break in slope in the mud blanket overlying and encasing the coarse sediments. This differential transgressive erosion of a previously deposited progradational sand sheet is the process by which convex-topped sand bodies in the Cardium in the subsurface are envisioned to have been formed.

Three-Dimensional Variability, and Interaction of Multiple Regressive Episodes

In addition to the type of variability outlined above, additional complications in the basic sedimentation pattern are possible if flows parallel to shoreline are considered. As shall be demonstrated in chapter 7, the dominant pattern of flow in the offshore region was essentially parallel to the inferred paleoshoreline, with an oblique offshore component; these offshore currents probably were in geostrophic balance. Thus, a greater range of variability is to be expected than has been represented in the preceding figures. This greater variability is due to the possible formation and migration

of transgressive (and possibly regressive) shelf sand or gravel ridges or shoals.

Likewise, the preceding diagrams have illustrated the case of one regressive episode only. Further complications would arise if remnant sea-floor topography (as is preserved in the lower panel of figure 6-18) were to influence deposition during a second regressive episode.

Considering the multitude of possible influences and responses, many of which certainly have not been properly or completely considered herein, it is abundantly clear that the conceptual model developed in this chapter may serve only as a very general observational guide and framework for interpretation in the Cardium Formation. Nevertheless, this local model does offer several possibilities for critical tests against the rock record. Some of these tests will be conducted below.

It is important to emphasize that the internal facies geometry predicted by the preceding conceptual development is essentially similar to that described in the subsurface Ferrier and Willesden Green fields by Griffith (1981) and Keith (1985), respectively. This subsurface geometry is illustrated in figure 6-19. Differences between outcrop and subsurface depositional patterns are discussed in chapter 7.

Figure 6-19. Plan view distribution of sediments, and two vertical cross-sections across the subsurface Willesden Green field. After Keith (1985).

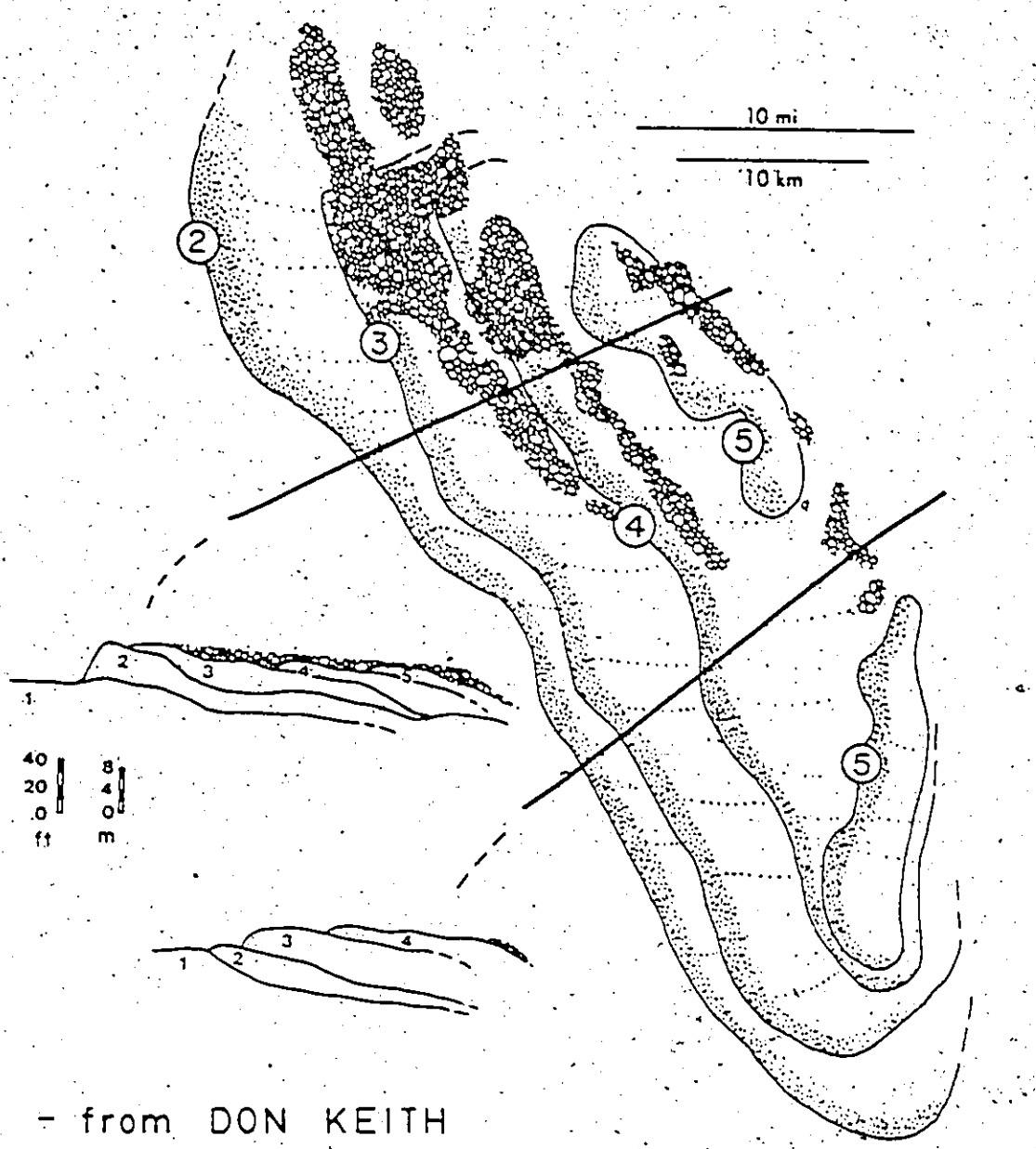

- from DON KEITH

TESTS OF THE CONCEPTUAL MODEL

Vertical Sequences Predicted by the Model

The first set of tests of the conceptual model developed herein concerns the joint occurrence in vertical sequences of one or more of the following:

1) anomalously thin shoreface sandstones,
2) rare thinning- and fining-upward sequences,
3) anomalously thick marine conglomerates,
4) inferred transgression surfaces, and
5) "multiple" transgressive conglomerates -- see below.

The most obvious implied relationships in the conceptual model developed in the preceding figures are that coarsening-upward cycles in the Cardium were deposited during regression, and that marine conglomerates in the formation should be best developed at transgression surfaces. The preferred vertical facies sequences of chapter 5 confirm this to be the case. However, these were two of the basic observations which served as constraints on the construction of the model; therefore, the inferred deposition of Cardium cycles during regression, and the preferential occurrence of marine conglomerates at transgression surfaces, cannot be invoked as testable

predictions of the conceptual model.

In contrast with the above, the occurrence of thinning- and fining-upward intervals in the formation can serve as a test of the model. As was indicated in chapter 5, rare fining-upward intervals of inferred offshore sediments locally cap Cardium cycles. This observation was not used in the construction of the model; rather, the existence of these intervals (at least locally preserved) is predicted as a logical consequence of the sequence of events in the conceptual model (see preceding sections).

The conceptual model suggests a number of tests involving fining-upward intervals, transgressive conglomerates, and other features; in vertical sequences, certain associations of features are predicted by the conceptual model. As seen in the final time-series diagram (Fig. 6-17), thinning- and fining-upward intervals should be preferentially associated with inferred transgression surfaces, transgressive conglomerates (especially, thick transgressive conglomerates and "multiple" conglomerates -- see below), cycles capped with shoreface and shoreface-attached sandstones (especially, those capped with anomalously thin sandstones of this sort), and, less commonly, cycles capped with sharp-based hummocky cross-stratified sandstones of association 2.

Additionally, both fining-upward intervals and thick transgressive conglomerates should preferentially

occur over the basinward edges of prograding shoreface-attached sand sheets (i.e., where these sand sheets thin and pinch out). Fining-upward caps should also be recognizable basinward of the edge of these sand sheets, where distal-offshore, mud-dominated facies (association 1) lie upon proximal-offshore, sharp-based hummocky facies (association 2).

The conceptual model developed in this chapter, as summarized in figure 6-17, suggests the following eleven generalized predictions involving associations of features in vertical sequences. [Predictions involving lateral cycle relationships and vertical relationships between cycles are discussed in a later section.] Each of these eleven predictions can serve as a test of this model:

1) Transgressive conglomerates should be most common over shoreface-attached sandstones (i.e., over cycle types 2 and 3).
2) The thicker examples of transgressive conglomerates should be most common over shoreface-attached sandstones (again, cycle types 2 and 3).
3) The thicker occurrences of transgressive conglomerates should lie upon anomalously thin shoreface-attached sandstones (i.e., in cycle types 2 and 3, conglomerate thickness should be inversely proportional to thickness of shoreface-attached

sandstones).

4) In contrast with the above, the thicker occurrences of transgressive conglomerates in type 4 cycles should lie upon anomalously thick intervals containing sharp-based hummocky sandstones (i.e., in type 4 cycles, conglomerate thickness should be directly proportional to thickness of hummocky intervals).

5) Locally, fining-upward intervals should have been formed and preserved at inferred transgression surfaces; however, these intervals should not have been as extensive laterally as either transgression surfaces in general or conglomerates deposited at transgression surfaces. Therefore, cycles capped with fining-upward intervals should be much less common than either sharp-topped cycles or any cycles capped with conglomerate.

6) Although rare, fining-upward cycle caps should be most common at the tops of cycle types 2, 3, and 4.

7) Although rare, fining-upward cycle caps should be associated with transgressive conglomerates more commonly than are cycles which are not capped with fining-upward intervals.

8) Transgressive conglomerates associated with rare fining-upward cycle caps should be anomalously thick.

9) Rare fining-upward cycle caps should be associated with "multiple" marine conglomerates (i.e., stratigraphically separated marine conglomerate facies occurring at two or more levels at or near the transgressed upper contact of a cycle -- see Fig. 6-17).

10) Where rare fining-upward cycle caps lie upon shoreface and shoreface-attached sandstones, these sandstones should be anomalously thin.

11) Where rare fining-upward cycle caps lie upon occurrences of association 2 (sharp-based hummocky sandstones), these occurrences of association 2 should be anomalously thick.

It is important to emphasize that local variability is inherent in the conceptual model (e.g., Fig. 6-18); thus, the above predictions are thought to be applicable only in a statistically generalized sense. How do observations from Foothills exposures compare with these predictions of the model? In chapter 5, I reported the subjective observation of a positive correlation between truncated shoreface-attached sandstones, fining-upward intervals, and anomalously thick transgressive conglomerates. This subjective observation is in agreement with some of the preceding predictions of the conceptual model. All of the these predictions are put to quantitative tests below.

Predictions 1 and 2. Figure 6-20 shows the distribution of cycle-capping, transgressive conglomerates (association 5) by cycle type. Graph A of this figure is a frequency distribution, showing the number of occurrences of each cycle type which display transgressive conglomerates. Graph B is a percentage-frequency distribution, showing the percentage of each group capped with conglomerates. In this figure, single hatchure represents thin conglomerates (those less than 3 m in thickness; usually much less than 1 m thick). This ornament includes all occurrences of conglomerate veneers (facies 5CV) only one or a few clast diameters thick. The double hatchure in this figure represents occurrences which are thicker than 3 m (up to about 9 m maximum); note that any of these occurrences may represent transgressive conglomerates which are divisible into two or more facies (as, for example, the occurrence capping cycle number 5 at section 5-45 on Ram River, consisting of the ascending vertical sequence from facies 5CB to 5C2 to 5CV).

These distributions corroborate the model predictions numbered 1 and 2 above; namely, that truncated shoreface and shoreface-attached sandstones (cycle types 2 and 3, respectively) are those most likely to display transgressive marine conglomerates (especially, thick conglomerates).

Figure 6-20. Distribution of cycle-capping transgressive conglomerates by cycle type. Single hatchure indicates conglomerate thickness less than 3 m; double hatchure indicates conglomerate thickness greater than 3 m.

A) Frequency distribution by cycle type.

B) Percentage-frequency distribution by cycle type.

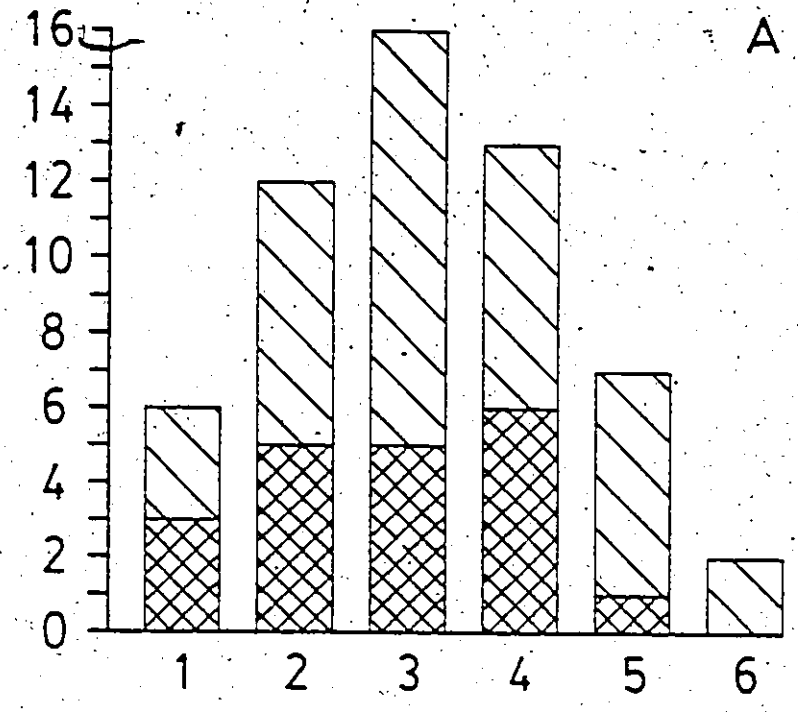
A
16
14
12
10
8
6
4
2
0
1
2
3
4
5
6

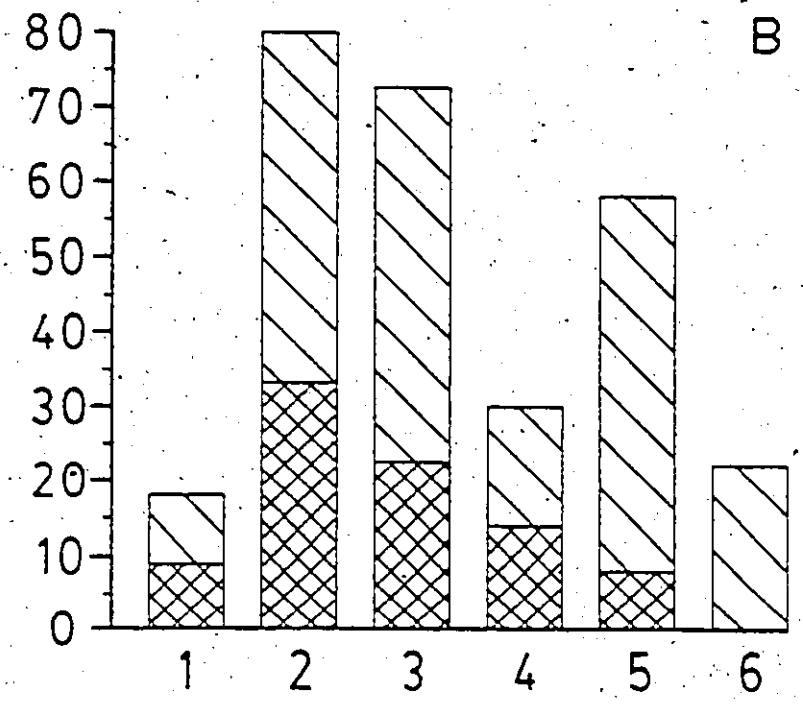
B
80
70
60
50
40
30
20
10
0
1
2
3
4
5
6

Prediction 3. How does the thickness of conglomerates capping cycles of types 2 and 3 compare with the thickness of the underlying shoreface and shoreface-attached sandstones? In total, 36 examples of these two cycle types were observed in this study; of these, 28 were capped with conglomerate. Conglomerate thickness is plotted against thickness of shoreface and shoreface-attached sandstone for all type 2 and 3 cycles in figure 6-21. Although widely scattered, these data indicate an indirectly proportional relationship between sandstone and conglomerate thickness, consistent with prediction number 3 of the conceptual model.

Prediction 4. How does the thickness of conglomerates capping type 4 cycles compare with the thickness of the underlying hummocky intervals (i.e., intervals containing interbedded mudstones and hummocky cross-stratified sandstones)? In total, 42 examples of type 4 cycles were observed in this study; of these, 13 were capped with conglomerate. Conglomerate thickness is plotted against thickness of hummocky intervals for all type 4 cycles in figure 6-22. Although scattered, these data indicate a directly proportional relationship between sandstone and conglomerate thickness, consistent with prediction number 4 of the conceptual model.

Prediction 5. The distribution by cycle type of

occurrences of cycles displaying thinning- and fining-upward caps is shown in figure 6-23. Graph A of this figure is a frequency distribution, showing the number of occurrences of each cycle type which display fining-upward intervals of this sort. Graph B is a percentage-frequency distribution, showing the percentage of each group capped with these intervals. This figure indicates that thinning- and fining-upward intervals are present at the tops of cycles locally, and thus can be inferred to have been deposited during transgression. Comparing figures 6-20 and 6-23, note that cycle-capping thinning- and fining-upward intervals (17 occurrences) are much less common than either: 1) cycles capped with conglomerate (56 occurrences) or 2) sharp-topped cycles without fining-upward caps (134 - 17 = 117 occurrences). These data confirm the fifth prediction of the model listed above.

Prediction 6. Figure 6-23 also indicates that fining-upward cycle caps statistically are most common at the tops of cycle types 2, 3, and 4, overlying shoreface sandstones, shoreface-attached sandstones, and proximal offshore sandstones, respectively. This observation corroborates prediction number 6 of the conceptual model.

Predictions 7 and 8. The ornamentation superimposed on the distributions of fining-upward cycle

Figure 6-21. Transgressive conglomerate thickness vs. thickness of association 3 sandstones for occurrences of cycle types 2 and 3. Conglomerate thickness equal to zero indicates absence of conglomerate; all facies 5CV (coarse veneer) occurrences have been assigned a thickness of 10 cm. Lines drawn through data are best-fit linear regressions. Solid line includes all points. Broad-dash line includes all cycles with conglomerate present. Short-dash line includes all cycles capped with conglomerates thicker than 50 cm. In each case, slope is negative. Negative correlation coefficient and slope are greatest for all cycles capped with conglomerate (i.e., excluding all and only those cycles without conglomeratic caps).

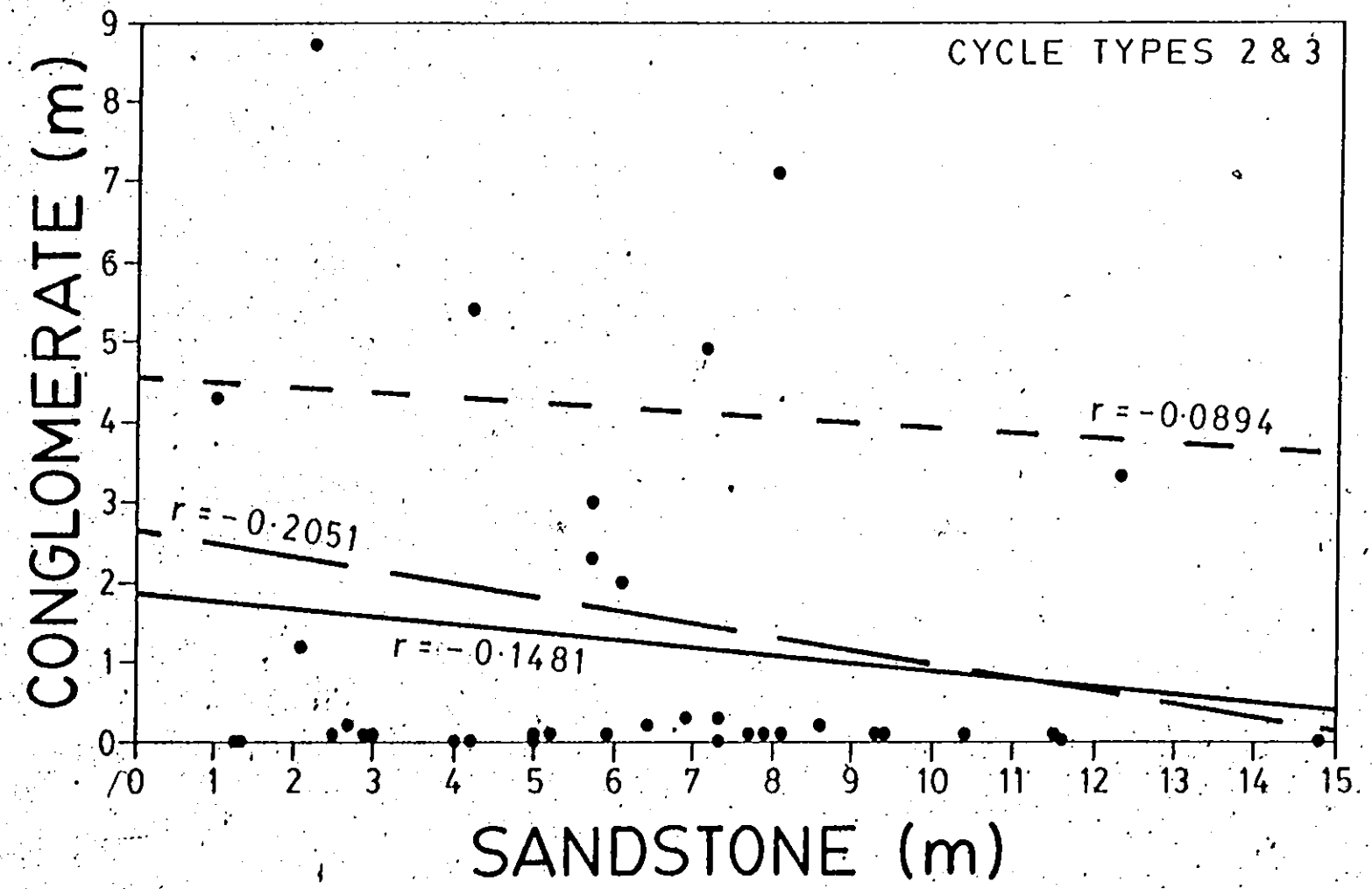
CYCLE TYPES 2 & 3
CONGLOMERATE (m)
SANDSTONE (m)
r = -0·0894
r = -0·2051
r = -0·1481
0
1
2
3
4
5
6
7
8
9
10
11
12
13
14
15

Figure 6-22. Transgressive conglomerate thickness vs. thickness of association 2 deposits for occurrences of type 4 cycles. Conglomerate thickness equal to zero indicates absence of conglomerate; all facies 5CV (coarse veneer) occurrences have been assigned a thickness of 10 cm. Lines drawn through data are best-fit linear regressions. Solid line includes all points. Broad-dash line includes all cycles with conglomerate present. Short-dash line includes all cycles capped with conglomerates thicker than 50 cm. In each case, slope is positive. Correlation coefficient and slope are greatest for all cycles capped with conglomerate (i.e., excluding all and only those cycles without conglomeratic caps).

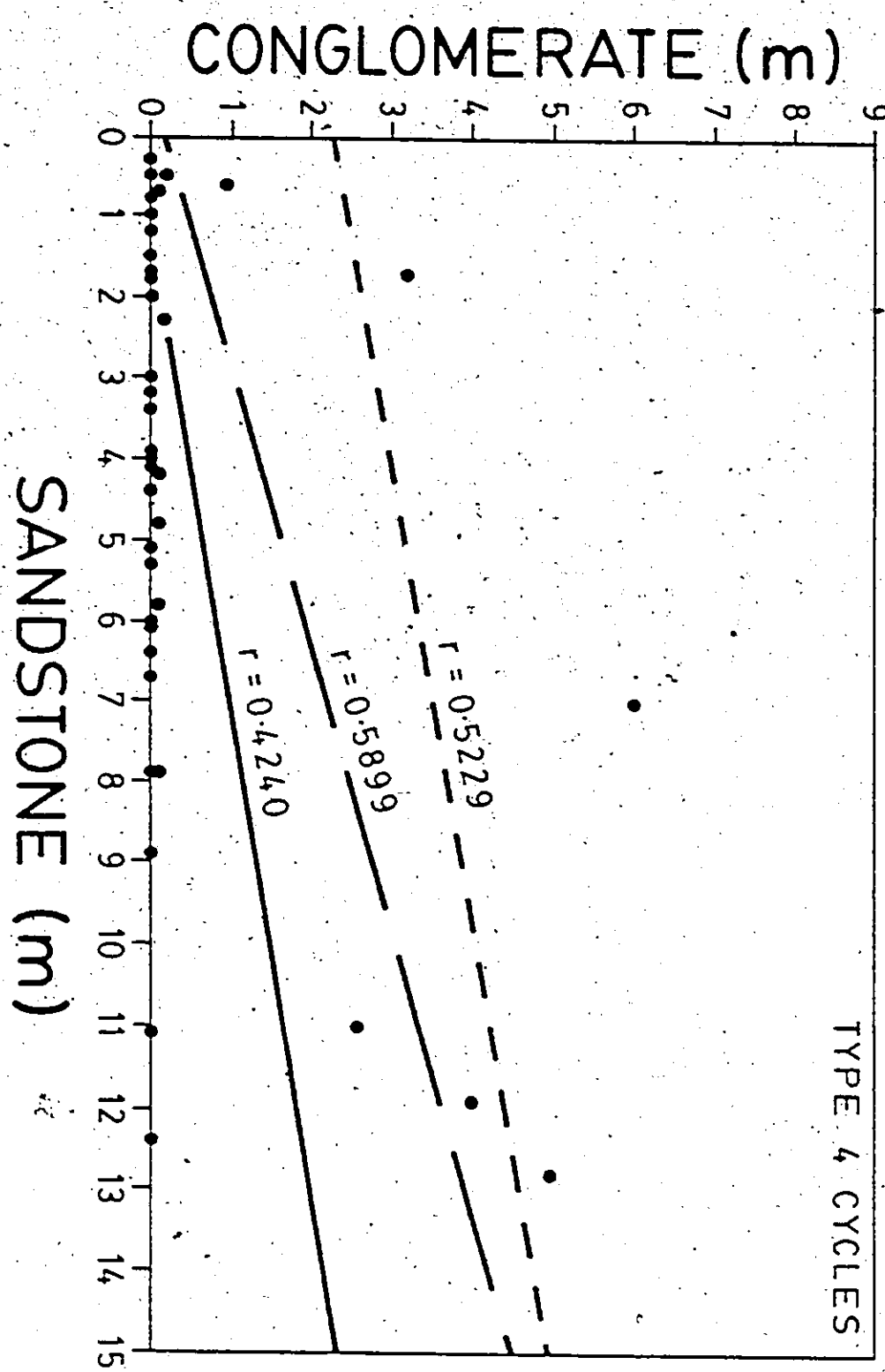
CONGLOMERATE (m)
SANDSTONE (m)
r = 0·5229
r = 0·5899
r = 0·4240
TYPE 4 CYCLES

Figure 6-23. Joint distribution by cycle type of thinning- and fining-upward cycle caps and cycle-capping transgressive conglomerates. All cycles capped with thinning- and fining-upward intervals are included in this graph. Hatchure pattern indicates thickness of associated transgressive conglomerate; pattern significance as in figure 6-20. Absence of hatchure indicates absence of conglomerate.

A) Frequency distribution by cycle type.

B) Percentage-frequency distribution by cycle type.

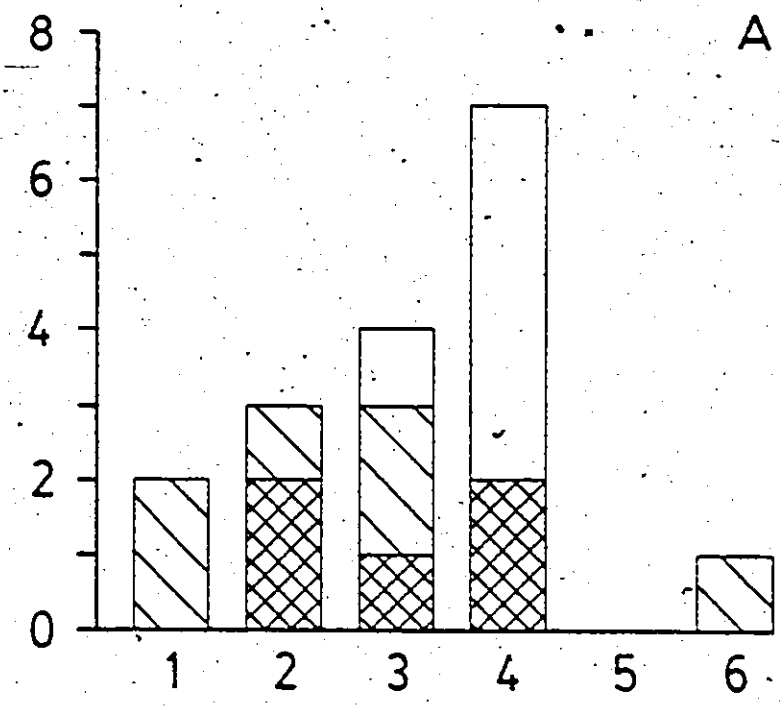
A
8
6
4
2
0
1
2
3
4
5
6

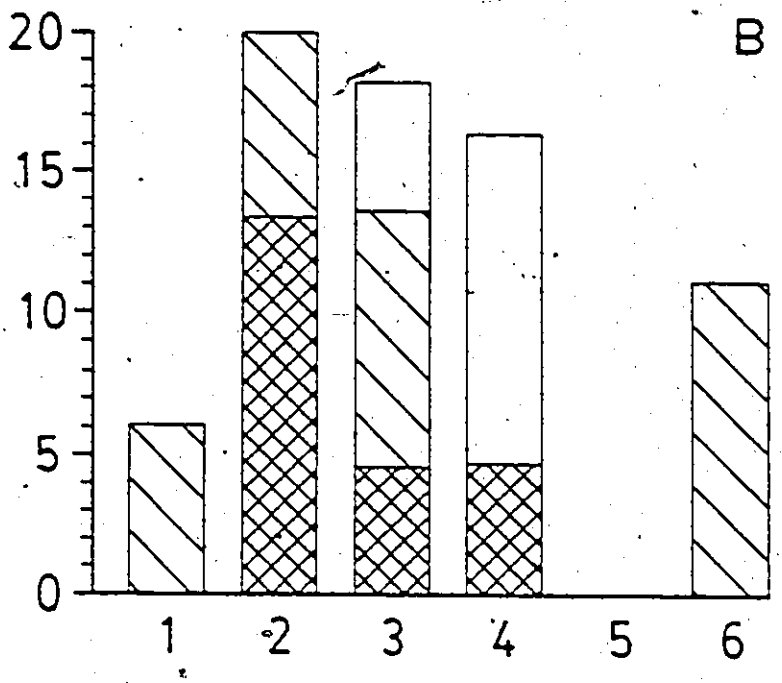
B
20
15
10
5
0
1
2
3
4
5
6

cycle caps (Fig. 6-23) indicates occurrences which also display transgressive conglomerates. The significance of the hatchure patterns is the same as in figure 6-20 described above. The joint distribution of fining-upward intervals and transgressive conglomerates (Fig. 6-23) indicates that these features have a greater-than-random probability of occurring together in the same cycle. There were 134 major cyclic developments examined in this study. Of these, 56 (42%) display conglomeratic caps; thick conglomerates are present at the tops of 20 cycles, representing 15% of all occurrences (Fig. 6-20a). Only 17 cycles (13% of all occurrences) display fining-upward caps. Of these 17 cycles, 11 (65%) display conglomeratic caps, and 5 (29%) display thick conglomerates. Thus, when compared with cycles in general, those cycles which display thinning- and fining-upward intervals at their tops have roughly a 50% greater probability of being capped with conglomerate, and a 90% greater probability of being capped with thick conglomerates. These data confirm yet another two predictions of the conceptual model; namely, that thinning- and fining-upward intervals at the tops of cycles are likely to be associated with transgressive conglomerates in general (prediction number 7) and thick transgressive conglomerates in particular (prediction number 8).

Prediction 9. Six of the 17 occurrences of fining-upward cycle caps are associated with "multiple" transgressive conglomerates. This type of conglomerate has been defined above. Only a few of the 117 sharp-topped cycles display multiple conglomerates of this sort. The common association of fining-upward intervals and multiple conglomerates corroborates prediction number 9.

Prediction 10. Cycle types 2 and 3 display shoreface sandstones of association 3 with average thicknesses of 7.1 m and 5.6 m, respectively. Taken together, the average thickness is 6.2 m. Those occurrences of cycle types 2 and 3 capped with fining-upward intervals display shoreface sandstones with average thicknesses of only 6.1 m and 5.1 m, respectively. Taken together, the average thickness of shoreface sandstones in these occurrences is 5.5 m. These data confirm prediction number 10: Where fining-upward cycle caps are present above shoreface-attached sandstones, these sandstones are relatively thin.

Prediction 11. Type 4 cycles display deposits of association 2 with an average thickness of 4.6 m. Equivalent deposits in occurrences capped with fining-upward intervals have an average thickness of 5.6 m. These data confirm prediction number 11: Where fining-upward cycle caps lie upon the deposits of association 2, these deposits are relatively thick.

The preceding paragraphs demonstrate that each of the eleven predictions of the depositional model is supported by trends and associations observed in vertical sequences from the Cardium Formation in outcrop. Thus, these vertical sequences can be regarded as conforming with the conceptual model developed in this chapter.

Lateral Cycle Relationships Predicted by the Model

The most critical tests of the conceptual model developed herein involve lateral variability within correlative Cardium cycles. The dominant, generalized implications of the model (Fig. 6-17) for lateral cyclic relationships are:

1) Thick prograding-shoreline sandstones should display well developed multiple cyclicity (due to shoreline oscillations) at their extreme basinward position.
2) Thick prograding-shoreline sandstones should be terminated at their extreme basinward position by an offlapping sheet of transgressive conglomerate.
3) The transgressive conglomerate should be thickest over shoreface-attached sandstones (and/or proximal offshore deposits), not non-marine deposits.
4) The transgressive conglomerate should be overlain by (and/or intertongue with) mud-dominated offshore deposits, in which may also be developed an

offlapping cyclicity, or cyclicity due to vertical aggradation.

The prograding sand sheet of the Seebe Member displays all of these characteristics, as can be verified by close inspection of correlation diagram S2 (Fig. 6-2). Moving from northwest to southeast, the Seebe is everywhere composed predominantly of a single major sand body; however, approaching the terminus of this body in the southern part of the central Foothills, a number of different major sand bodies appear in the Seebe Member. These are associated with offlapping splits of non-marine deposits, consistent with the oscillations of the shoreline inferred in the model.

Also moving from northwest to southeast, overlying transgressive conglomerates (included in the Sundre Member) do not appear until section CL-1, about 35 km basinward from the extreme basinward limit of non-marine deposits (at section 5-41; see Fig. 6-1). These conglomerates are thickest at section CL-1, over the basinward margin of the thick shoreline-sand sheet of the Seebe; they are seen to drape this sand sheet as it pinches out further basinward. This basinward pinch-out is associated with the development of numerous, minor, mud-dominated cycles capped with thin conglomerates.

A similar basinward trend is present in the

Willmore-Wapiabi sedimentation episode; in this case, however, the transition is best revealed in correlation diagram D3 (Fig. 6-6), which also shows (at the basinward margin, section 5-45) a thick fining-upward cap over the toe of the shoreface and below the thickest transgressive conglomerate.

The significance of the highly bioturbated regression in the Sundre Member will be discussed in chapter 7.

It is noteworthy that none of the three regressive episodes is everywhere perfectly consistent with the conceptual model developed herein. Although this is in part due to the low density of outcrop control, the primary cause of deviation from the predicted norm probably is lateral variability associated with three-dimensionality of the shoreline and the direction of shoreline progradation. This topic is explored further in chapter 7.

CHAPTER 7. PALEOGEOGRAPHIC RECONSTRUCTIONS AND PALEOFLOW PATTERNS: DEFINITION OF LARGE-SCALE SHELF CIRCULATION DURING CARDIUM DEPOSITION

INTRODUCTION

A major objective of field work for this thesis was to measure the orientations and directions of paleoflow indicators (including paleoshoreline indicators) preserved in Cardium sediments. The purpose of this activity was two-fold:

1) Facies distributions and paleoflow indicators from a large number of control points would be used to establish the orientation and direction of progradation (i.e., the paleogeography) of the various Cardium shorelines which prograded through the Foothills belt.
2) The angular relationship between shoreline indicators and offshore flow indicators would be used to infer the dominant pattern of shelf circulation during Cardium deposition. This pattern would form the basis for an interpretation of

large-scale depositional processes.

The thrust of point 2 above was to provide a critical test of alternative depositional processes suggested for the emplacement of hummocky cross-stratified sands in a proximal offshore setting during shoreline progradation. The major alternatives suggested by previous workers have been described and discussed by Walker (1984b), who summarized the evidence for each of them. The hypothesized processes are:

1) storm-generated turbidity currents, and
2) storm-driven, geostrophically balanced bottom flows.

In this chapter, I shall first discuss shelf circulation and the processes of emplacement of hummocky cross-stratified sandstones in the Cardium Formation. Paleoflow data strongly suggest that shelf flows were in geostrophic balance. This finding has implications of extreme importance, especially regarding the origin of Bouma sequences preserved in shelf deposits, and also regarding the interpretation of inferred turbidity-current deposits in general.

Cardium paleogeography in the Foothills belt will then be discussed. These results are much more equivocal, due to extreme local variability in Cardium shoreline

orientation and the wide spacing of control points in this study.

PATTERNS OF SHELF CIRCULATION DETERMINED FROM PALEOFLOW DATA: IMPLICATIONS FOR LARGE-SCALE DEPOSITIONAL PROCESSES

The paleoflow data discussed in this section were principally derived from the 28 exposures which I measured in the northern and central Foothills of Alberta and adjacent British Columbia; very few data could be obtained in the southern sections measured by my McMaster colleagues. Data were obtained from regressive deposits associated with shoreline progradation, and from transgressive deposits (principally, transgressive conglomerates and thinning- and fining-upward sequences of hummocky beds capping several cycles). These data are summarized in appendix 5 and on the vertical graphic logs of appendix 2. Most paleoflow data were obtained from regressive intervals; these can be grouped into six categories:

1) Lower coastal plain flow indicators. Primarily, these indicators consist of trough cross-bedding and other tractional structures from fluvial channels (facies 4SF).

2) Shoreline orientation indicators. Most Cardium foreshore deposits consist of planar parallel lamination. Some occurrences reveal low-angle planar cross-bedding; the dip direction indicates the local offshore direction, oriented roughly 90° to the local shoreline. The dip direction is assumed to be the local gradient of the sea floor. A more reliable gradient direction was obtained at one location from large, asymmetrical load structures; the axial plane of these features is assumed to dip upslope.

3) Wave crest orientation indicators. The crest orientation of straight-crested symmetrical ripples typically is parallel to local wave propagation direction; waves are assumed generally to propagate in an onshore direction, roughly normal to the local shoreline orientation. Thus, symmetrical ripple crests are assumed to be parallel to the local shoreline.

4) Nearshore flow indicators. Trough cross-bedding from swaley cross-stratification (facies 3SW) is interpreted as forming in the nearshore flow, probably in response to storm-generated bottom flows.

5) Proximal offshore flow indicators. Paleoflow indicators from facies 3HA and association 2 are assumed to represent bottom flow directions from proximal offshore settings. These indicators consist primarily of sole marks

from the bases of hummocky beds and amalgamation units.

6) Distal offshore flow indicators. Current ripples and sole markings from association 1 represent bottom flow directions from the distal offshore region.

As I shall discuss in detail below, the various Cardium shorelines display great local variability in orientation and direction of progradation. In an attempt to determine the generalized pattern of shelf circulation (if such a pattern existed), I have compared offshore flow orientations with inferred shoreline orientation in all cycles (Fig. 7-1). Figure 7-1 is one of the major contributions of this field study, and is explained in detail below.

Figure 7-1 summarizes a great number of paleoflow readings. To remove the local shoreline vaiability, I have equally rotated all data from each cycle so that symmetrical ripple crests are aligned east-west (across the page), with the basinward direction to the south (bottom of the page). The basinward direction was determined from regional correlations, including thinning direction in non-marine splits. For example, if symmetrical ripple crests from one cycle were rotated 30° clockwise, so also were flow readings from the proximal and distal offshore. Symmetrical ripple crests were chosen as the local shoreline indicator, simply because of their usually

Figure 7-1. Comparison of vector mean orientations of symmetrical ripple crests (S) with vector mean flow orientations in the proximal offshore region (P) and the distal offshore region (D). See text for explanation.

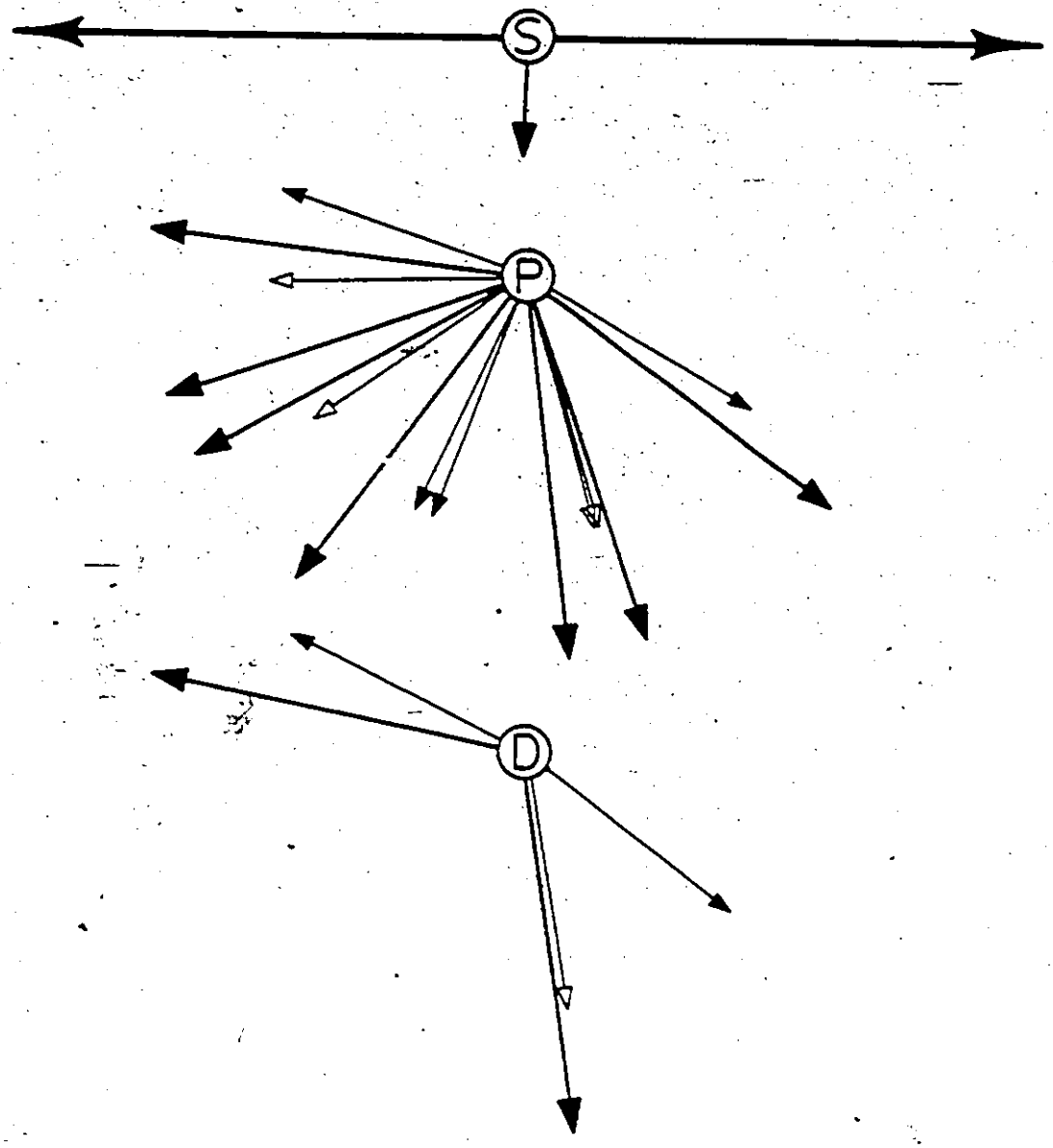
S
P
D

abundant occurrence in cycles.

The heaviest, longest arrows represent the vecter mean flow direction of a large number of readings; vector means were obtained using a computer program written by I. P. Martini (available at McMaster University). In cases represented by heavy arrows, both the vector mean orientation of symmetrical ripple crests and the vector mean orientation of the flow indicators in question were significant at greater than 75%. [In fact, both variables were significant at greater than 90% in all but one case; many were significant at greater than 95% or 99%.] The light arrows with filled heads represent cases where one vector mean was significant at greater than 75%; the other vector mean was obtained from one or a very few data, and significance was not calculated. The light arrows with empty heads represent cases involving vector means of one or a very few data; significance was not calculated for either vector mean in these cases.

Note that one heavy arrow extends from the symmetrical ripple axis in figure 7-1. This arrow indicates the downslope direction obtained from large asymmetrical load structures at section SC-1. This direction is nearly at right angles to the symmetrical ripple crests associated with this occurrence. This was the only opportunity presented to independently test the assumption that symmetrical ripples are oriented roughly at

right angles to sea-floor gradient and inferred shoreline trend; the 88° angular relationship supports this assumption.

Interpretation of Paleoflow Relationships

Maintaining the assumptions that symmetrical ripple crests show a statistically preferred shore-parallel orientation and that this orientation is normal to the slope of the sea-floor, the paleoflow relationships summarized in figure 7-1 do not support emplacement of hummocky cross-stratified sands in the proximal offshore region by sediment-laden turbidity currents. Such currents are driven by gravity operating upon the excess density due to sediment in the moving fluid; their motion is directed downslope. Paleoflow measurements from proximal offshore deposits in the Cardium generally do reveal an offshore component of flow, but they are widely dispersed. Measured paleoflow indicators from inferred turbidite-emplaced hummocky sandstones in the Jurassic Fernie-Kootenay transition (Hamblin & Walker, 1979) were much more coherent.

The widely scattered paleoflow data from hummocky sandstones in the Cardium Formation are much more consistent with an interpretation of sand emplacement by some sort of storm-forced bottom currents. I suggest it is

probable that these currents were commonly in geostrophic balance, as is suggested by the generalized direction of flow (obliquely offshore, to the right facing seaward). In the northern hemisphere, this flow orientation is consistent with an alongshore component of wind-sheared surface-water flow, also directed to the right (Fig. 7-2). Right-lateral wind shear (coupled with current-enforcing onshore wind and wave surge) is consistent with the generally accepted origin of hummocky cross-stratification; namely, origin due to major cyclonic storms. In the Cardium Formation in particular, situated in the northern hemisphere on the western margin of the Western Interior Seaway (Fig. 2-1), counterclockwise circulation in major cyclonic storms over the Seaway to the east would have produced these effects. Elsewhere, I have suggested that these cyclonic storms probably were hurricanes (Duke, 1985c).

At any one location on modern storm-dominated shelves, storm-forced currents generally display a wide variation in flow velocities and directions (see summary by Walker, 1984b). The wide variation in flow directions from hummocky sandstones in the Cardium may reflect this natural temporal variability; it may also indicate spatial variations imparted by irregularities (such as spits or embayments) developed along the ancient shorelines (see discussion below).

Data from distal offshore deposits (containing thin siltstones and sandstones which display Bouma sequences) are less abundant (Fig. 7-1), but also do not convincingly suggest a downslope direction of flow. In a review of storm-dominated shelves and shallow-marine deposits, Walker (1984b, p. 153) has asked the question, "is the geological evidence for turbidity currents [on the shelf] so strong that we must hypothesize a generating mechanism, or must we re-evaluate the geological evidence because studies of modern storm-dominated shorelines rule out the possibility of turbidity current generation?" Considering, specifically, Bouma sequences preserved in shallow-marine sequences, perhaps the answer to this question should be, "if ancient Bouma sequences apparently were formed by shelf flows which were not driven by gravity, a total re-evaluation of criteria for the recognition of turbidity-current deposits definitely is in order." This answer certainly is applicable to questionable shelf deposits; perhaps it should be extended to include all occurrences for which there does not exist independent evidence for deposition in deep water.

PALEOGEOGRAPHIC RECONSTRUCTIONS

As stated previously, the wide spacing of control

Figure 7-2. Development of a geostrophically balanced bottom flow along an east-facing shoreline in the northern hemisphere. From Walker (1984b, Fig. 2).

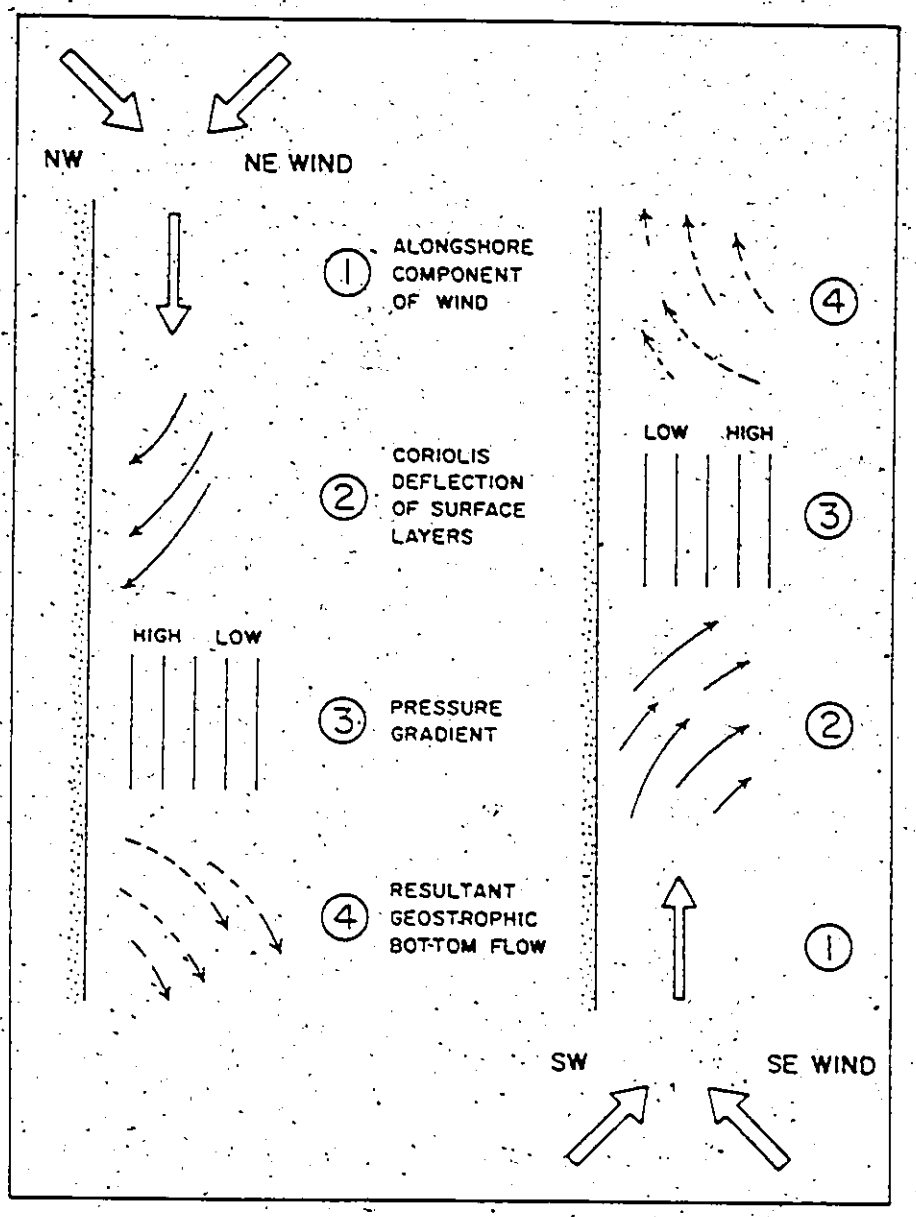
NW
NE WIND
1 ALONGSHORE COMPONENT OF WIND
2 CORIOLIS DEFLECTION OF SURFACE LAYERS
HIGH LOW
3 PRESSURE GRADIENT
4 RESULTANT GEOSTROPHIC BOTTOM FLOW
LOW HIGH
SW
SE WIND

points in this study does not permit a confident reconstruction of the apparently complex Cardium shorelines. Nevertheless, certain preliminary paleogeographic reconstructions are presented in this section. It should be noted by the reader that these represent a possible set of reconstructions based upon the data at hand; other reconstructions also are possible, but are considered less likely to the author. In August of 1985, I intend to return to the central Foothills to measure additional exposures in this area, in the hope that an increase in outcrop control in this critical region will permit a more rigorous definition of paleogeography for some intervals at least.

For the purposes of this thesis, I have chosen only to represent the paleogeography of the first two regressive episodes of sedimentation (i.e., the Seebe-Cutpick regression and the Sundre-Cutpick regression), and the intervening transgression (i.e., the Sundre transgression). These intervals were chosen for two reasons:

1) They illustrate the major process-oriented implications of the paleogeographic reconstructions in general, and
2) the data base for these reconstructions is relatively good.

These tentative reconstructions are presented as a series

of maps. These maps are based upon the pseudo-palinspastic reconstruction of the Cardium in the Foothills (discussed in chapter 6; see Fig. 6-1). The base map is reproduced at the same scale as the paleogeographic reconstructions in figure 7-3.

Note on each of the following paleogeographic reconstructions that the circles indicate those sections which serve as control points for the particular stratigraphic interval represented. The data represented on these maps are derived from the correlation diagrams of chapter 6. Additionally, some data from the subsurface Kakwa field are also presented on these maps. These data were kindly provided by Guy Plint at McMaster University (pers. comm., 1984 & 1985). The Kakwa field is indicated by the letter "K" on the following maps.

Seebe-Cutpick Regression and Sundre Transgression

The tentatively inferred maximum extent of the Cardium shoreline during Seebe time is presented as figure 7-4B. Note that this maximal regression represents the greatest basinward extent of any of the multiple shoreline oscillations associated with this regressive episode. The highly schematic shoreline orientations are based upon paleoflow data and inferred directions of shoreline progradation during Seebe time (Fig. 7-4A). The maximum

Figure 7-3. Location map and pseudo-palinspastic base map for tentative paleogeographic reconstructions. See text for discussion.

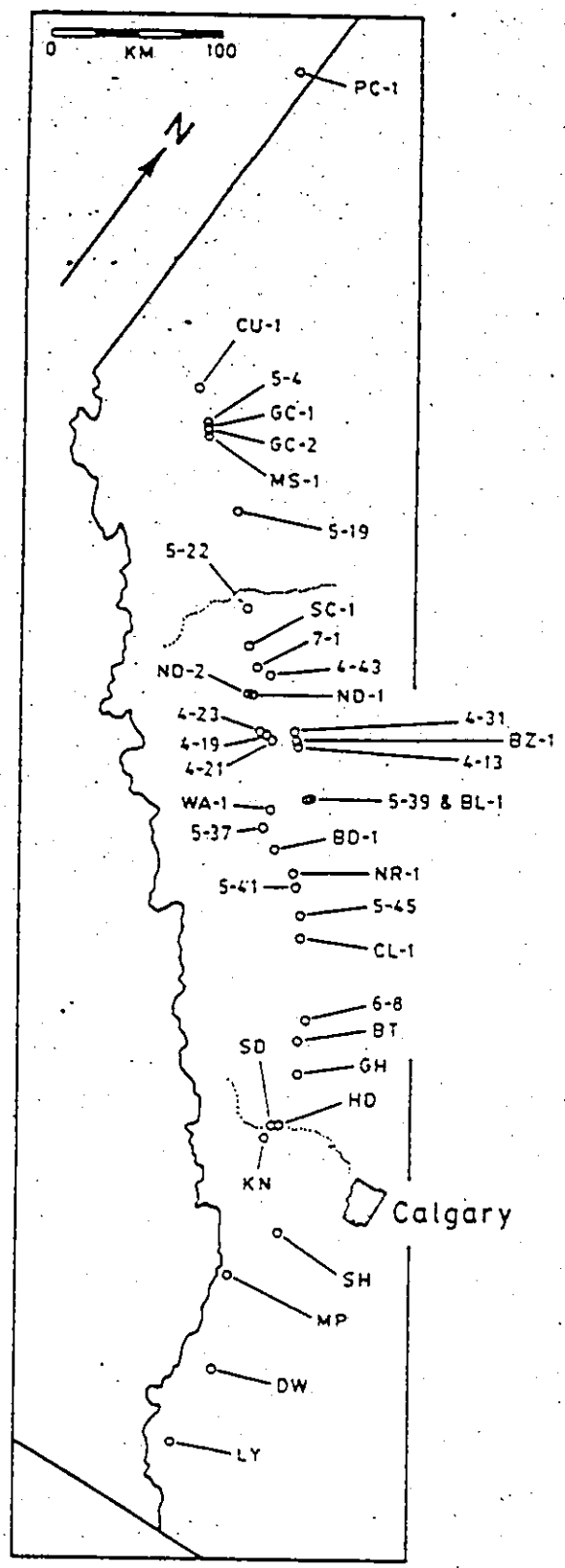
0 KM 100
N
PC-1
CU-1
5-4
GC-1
GC-2
MS-1
5-19
5-22
SC-1
7-1
4-43
ND-2
ND-1
4-23
4-19
4-21
4-31
BZ-1
4-13
WA-1
5-39 & BL-1
5-37
BD-1
5-41
NR-1
5-45
CL-1
6-8
BT
SD
GH
HD
KN
Calgary
SH
MP
DW
LY

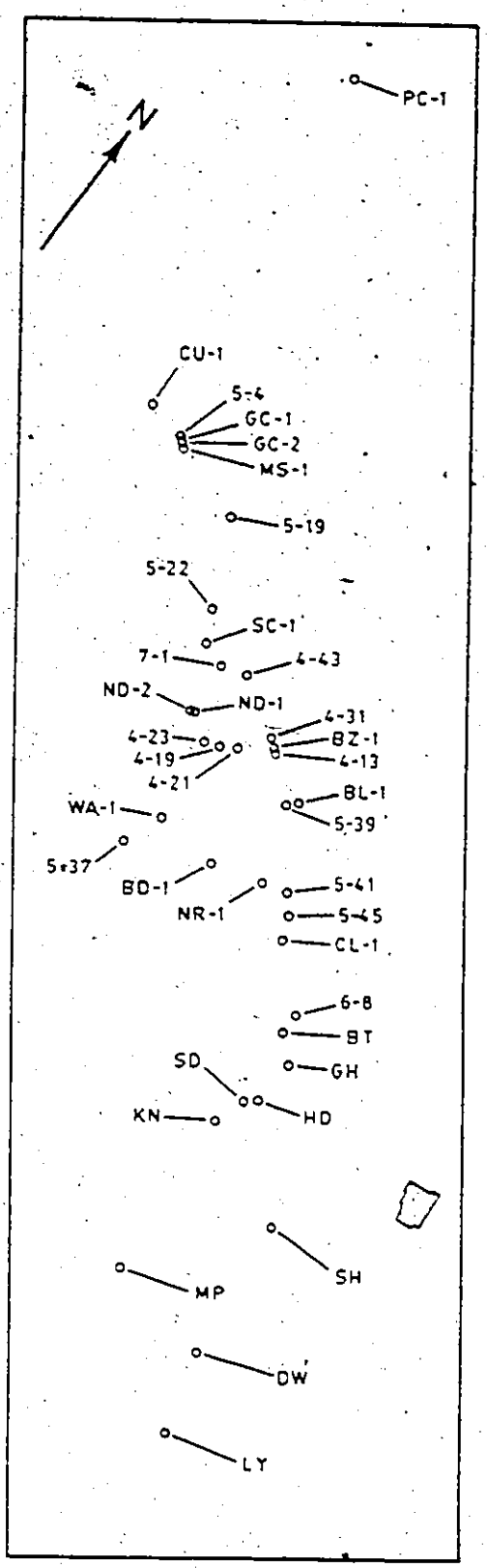
N
PC-1
CU-1
5-4
GC-1
GC-2
MS-1
5-19
5-22
SC-1
7-1
4-43
ND-2
ND-1
4-31
4-23
BZ-1
4-19
4-13
4-21
BL-1
WA-1
5-39
5-37
BD-1
NR-1
5-41
5-45
CL-1
6-8
BT
SD
GH
KN
HD
SH
MP
DW
LY

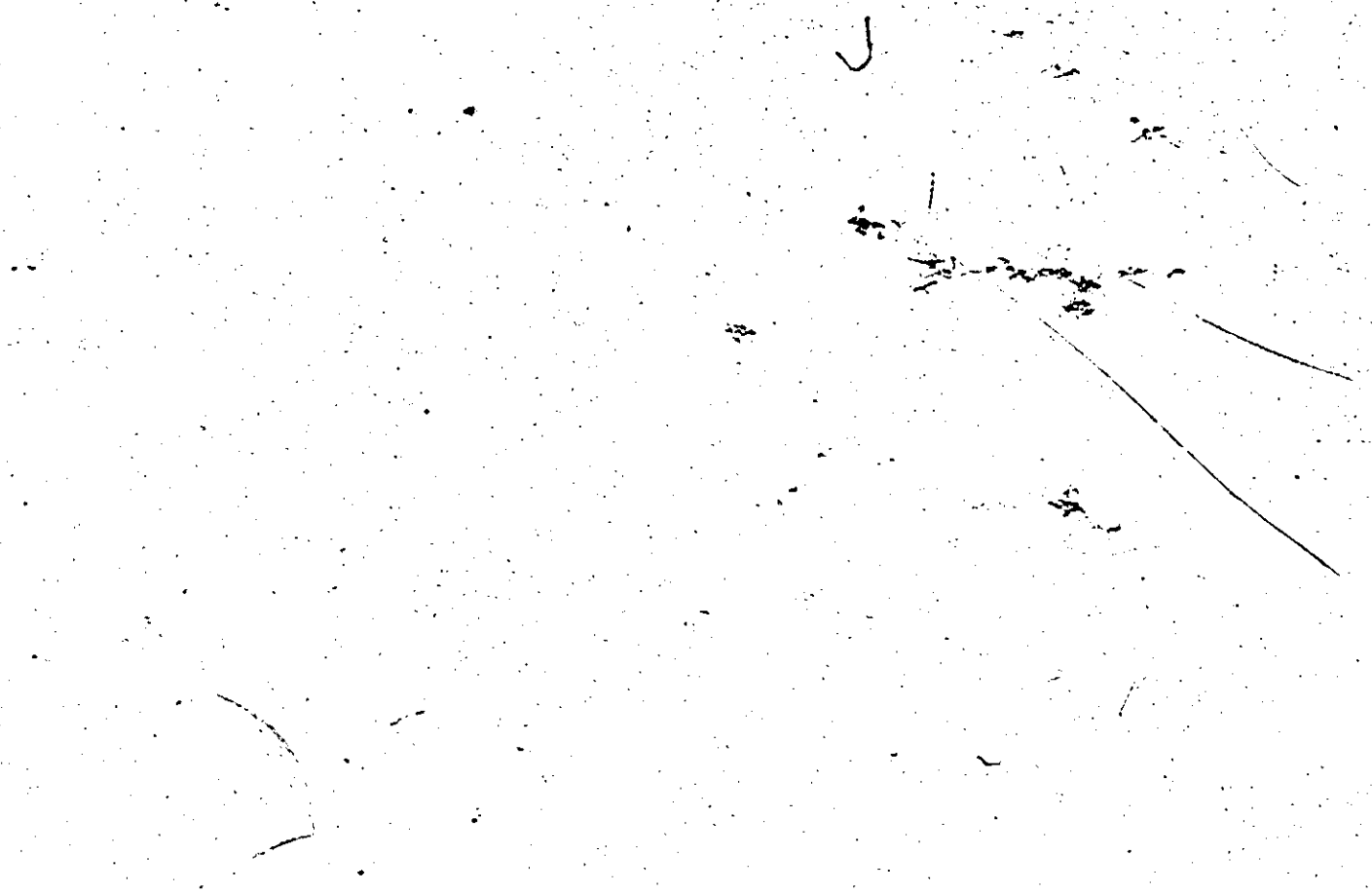

Figure 7-4. Data base (A) and paleogeographic reconstruction (B) of the Seebe-Cutpick regression. See text for discussion.

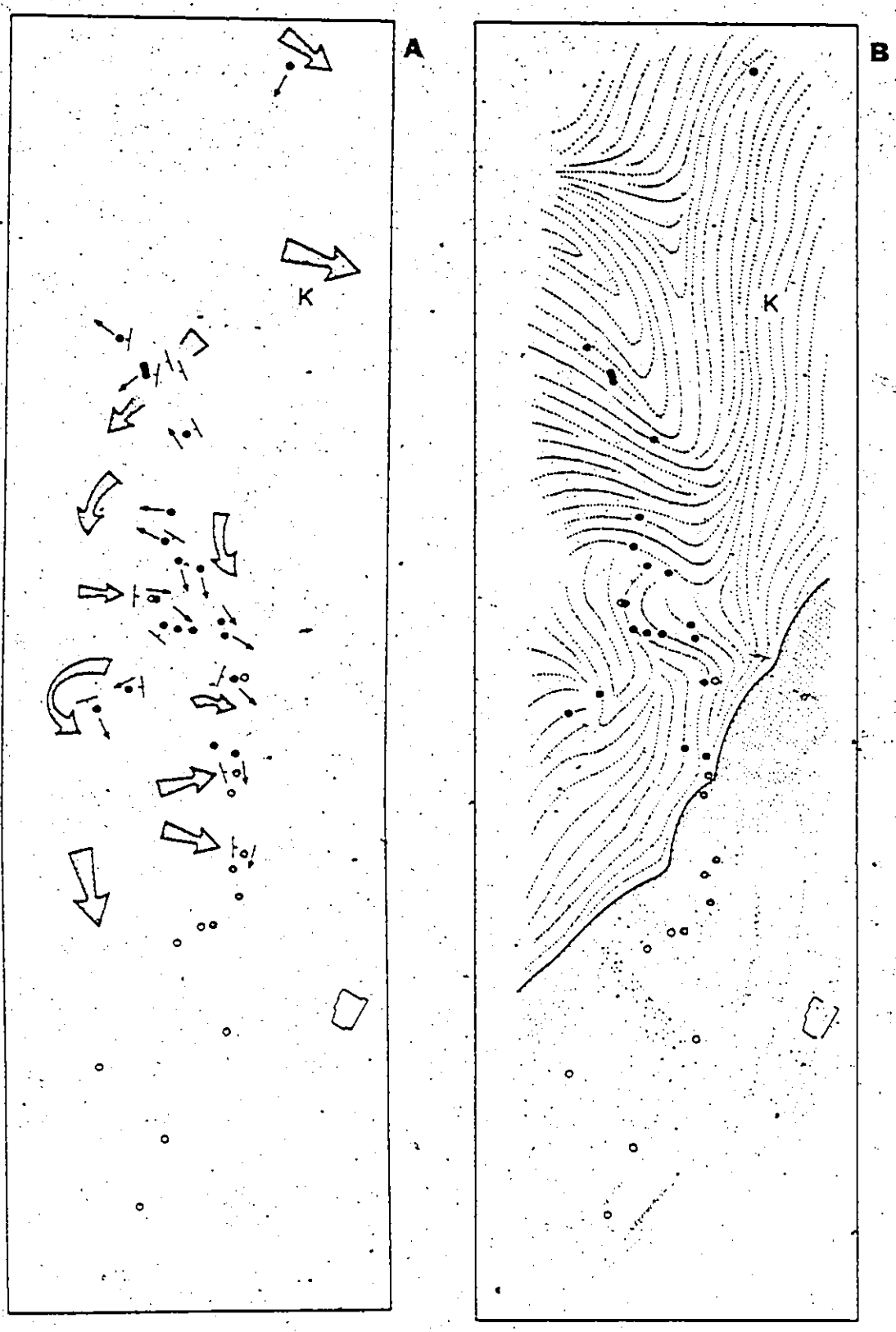
A
K
B
K

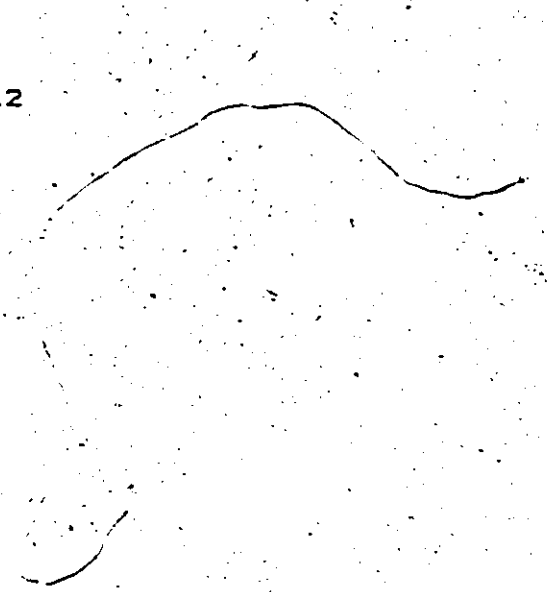

Figure 7-5. Paleogeographic reconstruction of the Sundre transgression. See text for discussion.

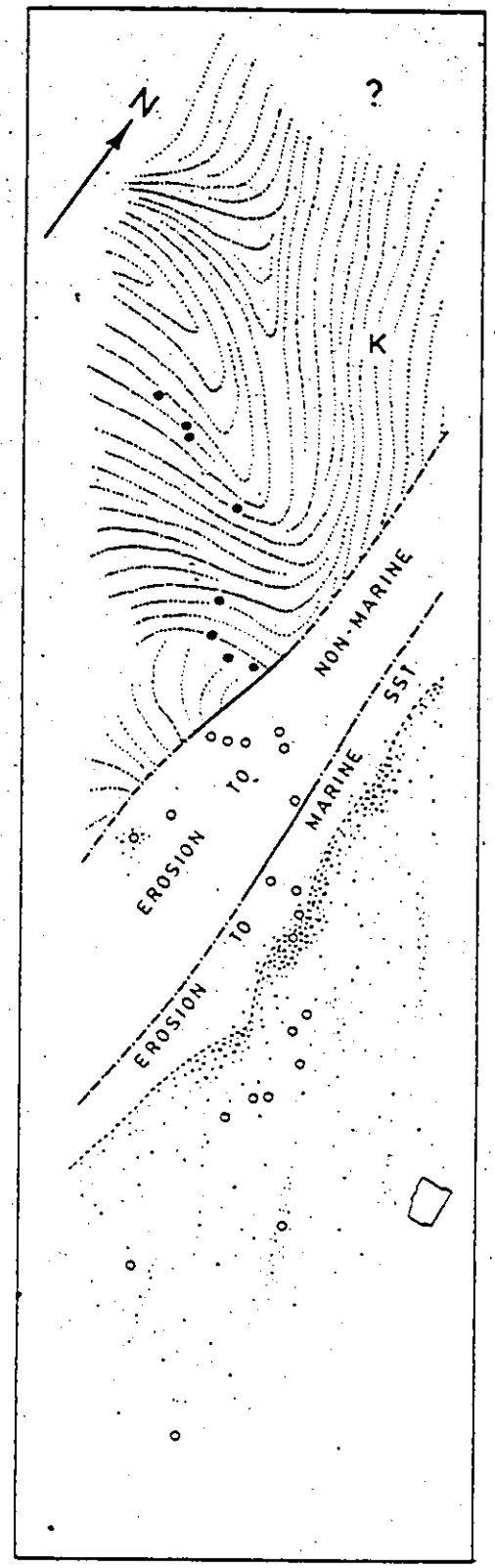
N
?
K
NON-MARINE
SSI.
MARINE
TO
EROSION
TO
EROSION

extent of the subsequent Sundre transgression is represented in figure 7-5.

Figure 7-4A shows summaries of inferred mean flow directions in the proximal offshore region of the prograding Seebe shoreline (small arrows). These arrows are summarized from the paleoflow data in appendix 2. The small dip and strike symbols indicate the inferred offshore direction and shoreline orientation, respectively. The large stippled arrows indicate a generalized local direction of progradation synthesized from several adjacent exposures. Within the circles representing control points for this interval, colors indicate the maximum proximality of preserved deposits: Black circles represent fully regressive cycles displaying non-marine deposits of association 4; yellow circles represent cycles capped with thick marine sandstones (association 3, not including facies 3PL); grey circles represent cycles terminating in association 1 or 2 (offshore muds and sands). Unfilled (white) circles indicate outcrops in which the uppermost part of the Seebe was not exposed.

The data summaries of figure 7-4A (plus additional data from fluvial channel deposits, not represented in this figure) were employed in constructing the cartoon diagram (Fig. 7-4B) illustrating successive positions of the Seebe shoreline. Note the inferrence of a highly irregular coast, which possibly displayed large cuspate structures

and/or spits. Note also that the final position of the shoreline has been extended a minimum of 10 km beyond the preserved limit of non-marine deposits, consistent with the conceptual model (chapter 6) involving complete transgressive erosion of underlying non-marine deposits over some large distance during retreat of the shoreface. This distance probably was as great as 30 to 40 km (see Fig. 7-5, discussed below).

In figure 7-4B, I have also indicated linear shelf ridges seaward of the final shoreline position, in the subsurface area around Calgary and in the southernmost Foothills outcrop belt. Such ridges probably formed during later stages of regression or early transgression, possibly during the multiple shoreline oscillations recorded in central Foothills exposures. Such ridges possibly constitute the subsurface Crossfield, Caroline, and Garrington sand bodies (Fig. 2-1).

Figure 7-5 shows the maximum extent of the transgression at the base of the Sundre. The maximum extent of the underlying Seebe shoreline is represented by the dashed line. As the shoreface transgressed over the Seebe-Cutpick deposits, erosion was sufficiently extensive to remove a thin interval of non-marine deposits inferred to have been deposited in a band roughly 30 km in width; these deposits were totally removed at section 5-45, and may possibly have been removed at the rooted tops of

sections 5-41 and NR-1, where the thin recessive interval in question is covered. Minor amounts of non-marine deposits were preserved northeast of these sections; they are recognized as the Lower Tongue of the Cutpick Member.

The inferred transgressive erosion of non-marine deposits from the top of the Cardium in locations adjacent to section 5-45 (and possibly further basinward) permits an explanation of the great lateral extent of shoreface sandstones, present as far south as sections CL-1, 6-8, and the northernmost southern Foothills exposures (Fig. 7-4B). This erosion also accommodates the appearance of a significant transgressive resedimented-lag conglomerate over the drowned shoreface, indicated by the control points colored red in figure 7-5. This conglomerate is present throughout the southern Foothills, and is especially thick at section CL-1. [The reader is referred to chapter 6 for an extended discussion of the processes involved in the development of this conglomeratic deposit.] The unfilled (white) circles in figure 7-5 indicate the absence of transgressive conglomerate over most of the transgressively eroded shelf terrace.

Sundre-Cutpick Regression

The symbols used in figure 7-6 are the same as and have the same significance as those in figure 7-4 discussed

above, with one addition. The control points colored blue (with a squiggle through their centers) indicate thick coarsening-upward intervals which are extensively bioturbated throughout their entire thickness (type 6 cycles; see chapter 5). Type 6 cycles in the central and northernmost southern Foothills are exclusively associated with the Sundre regression.

The areal distribution of type 6 cycles is compared with paleoflow data and the occurrence of major fluvial channels in the central Cutpick Member in figure 7-6. This distribution suggests that these cycles were formed to the east of the major sources of sediment to the Sundre shelf. Thus, these cycles were formed upstream of these fluvial sources (indicated by paleoflow data); they were not in the region of sediment deposition from the dominant geostrophically balanced shelf circulation (directed obliquely offshore with a strong right-lateral component of alongshore motion).

These observations offer an interpretive framework for the extensively bioturbated type 6 Cardium cycles; namely, these cycles represent deposition up-shelf (i.e., up the gradient of geostrophically balanced shelf circulation) from major sediment sources to the shelf. The associated reduction in sedimentation rate permitted the pervasive bioturbation which defines type 6 cycles.

Figure 7-6. Data base (A) and paleogeographic reconstruction (B) of the Sundre-Cutpick regression. See text for discussion.

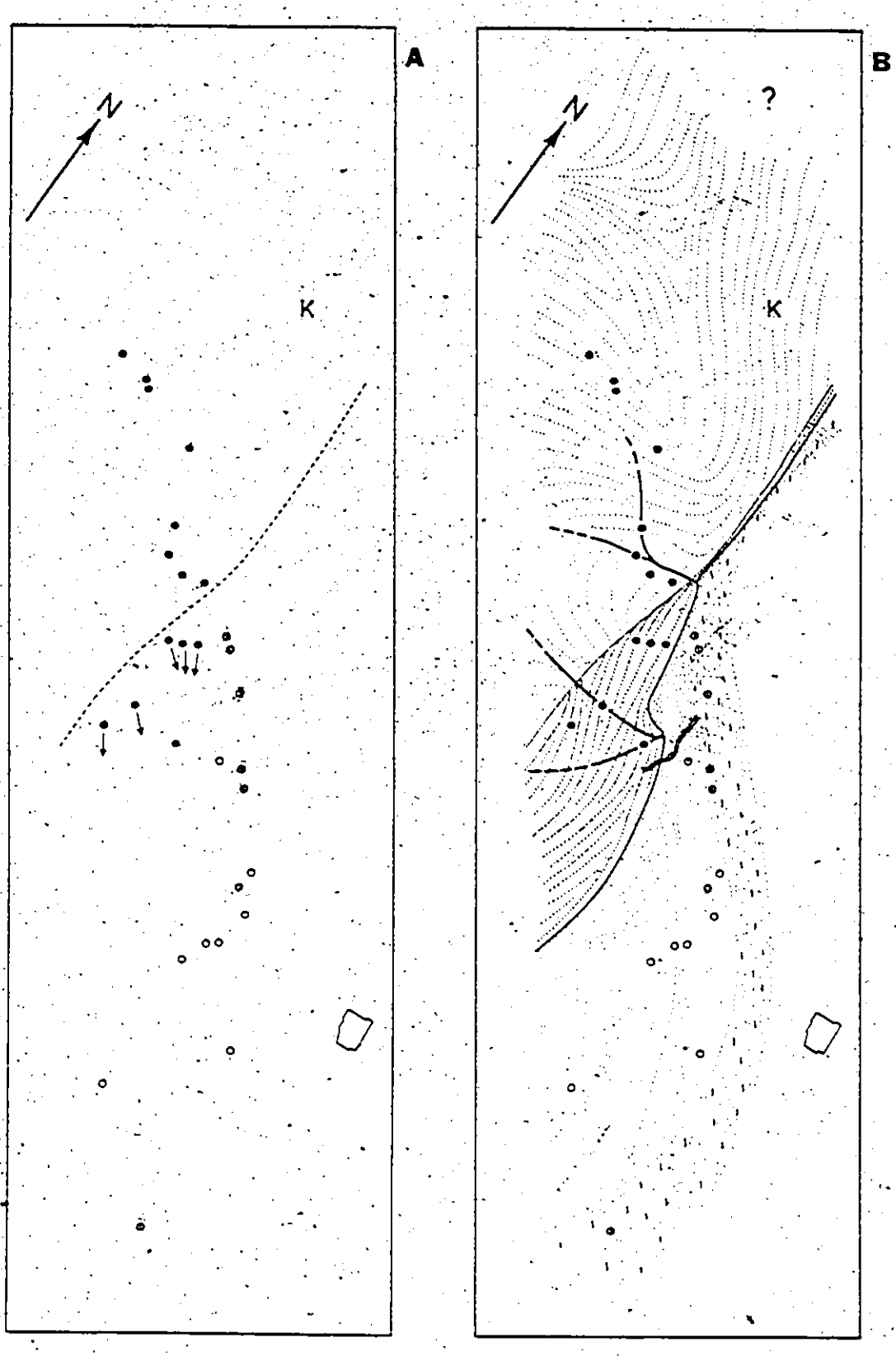
A
N
K
B
N
?
K

A TENTATIVE EXTENSION OF THE FINDINGS OF THIS THESIS TO SUBSURFACE CARDIUM FIELDS

The basic pattern of Cardium sedimentation advanced in this thesis involves formation of a regressive, coarsening-upward cycle by shoreline progradation, followed by the transgressive erosion of cycle-capping non-marine deposits and the deposition during transgression of resedimented-lag conglomerates over the drowned shoreface. This basic pattern of sedimentation can be tentatively extended to subsurface fields, offering a testable hypothesis for their formation.

A vertical sequence through the subsurface Pembina field consists of a thickening- and coarsening-upward sequence of shallow-marine sandstones and mudstones, erosionally overlain by a thick marine conglomerate; the conglomerate is capped with mudstones of the Wapiabi Formation (Krause & Nelson, 1984). In figure 7-7, I offer an interpretation of this basic field geometry. This figure shows an interpretive vertical cross-section through the center of the Pembina field. The occurrence of hydrocarbons in this field is indicated in black. The up-dip limit of the field is controlled by sandstone pinch-out; the down-dip hydrocarbon limit is effected by compaction and solution diagenesis of the carrier beds, which continue at depth (Nielsen & Porter, 1984). As

indicated in figure 7-7, I suggest that this geometry possibly results from transgressive erosion of non-marine deposits from the top of the Pembina regressive interval throughout the width of the field; the conglomerates are a resedimented-lag deposited over this transgression surface. As a test of this hypothesis, I indicate in figure 7-7 that non-marine deposits should be encountered <u>below</u> the transgression surface and <u>above</u> the sandstones in laterally contiguous deposits down-dip from the field of production.

This interpretation is consistent with the areal distribution of sediments in subsurface fields (Fig. 7-8). In this diagram, the lineations in the Pembina, Willesden Green, and Ferrier fields were observed by Nielsen & Porter (1984), Keith (1985), and Griffith (1981), respectively. I suggest that these lineations represent offlapping cyclicity associated with minor oscillations of a prograding shoreline. In my estimation, the elongate development at the eastern tip of Pembina probably represents the erosionally truncated vestige of a spit-bar system, as do the entire Ferrier and Willesden Green fields. The conglomerates capping these fields were deposited during the transgressive decapitation of these shoreline deposits; complete removal of inferred non-marine deposits in these fields accompanied this truncation. The shape and orientation of the inferred spit-bar developments is consistent with shelf and nearshore flows directed

Figure 7-7. Interpretive diagram of the Pembina field in vertical cross-section. See text for discussion. After Nielsen & Porter (1984, Fig. 13).

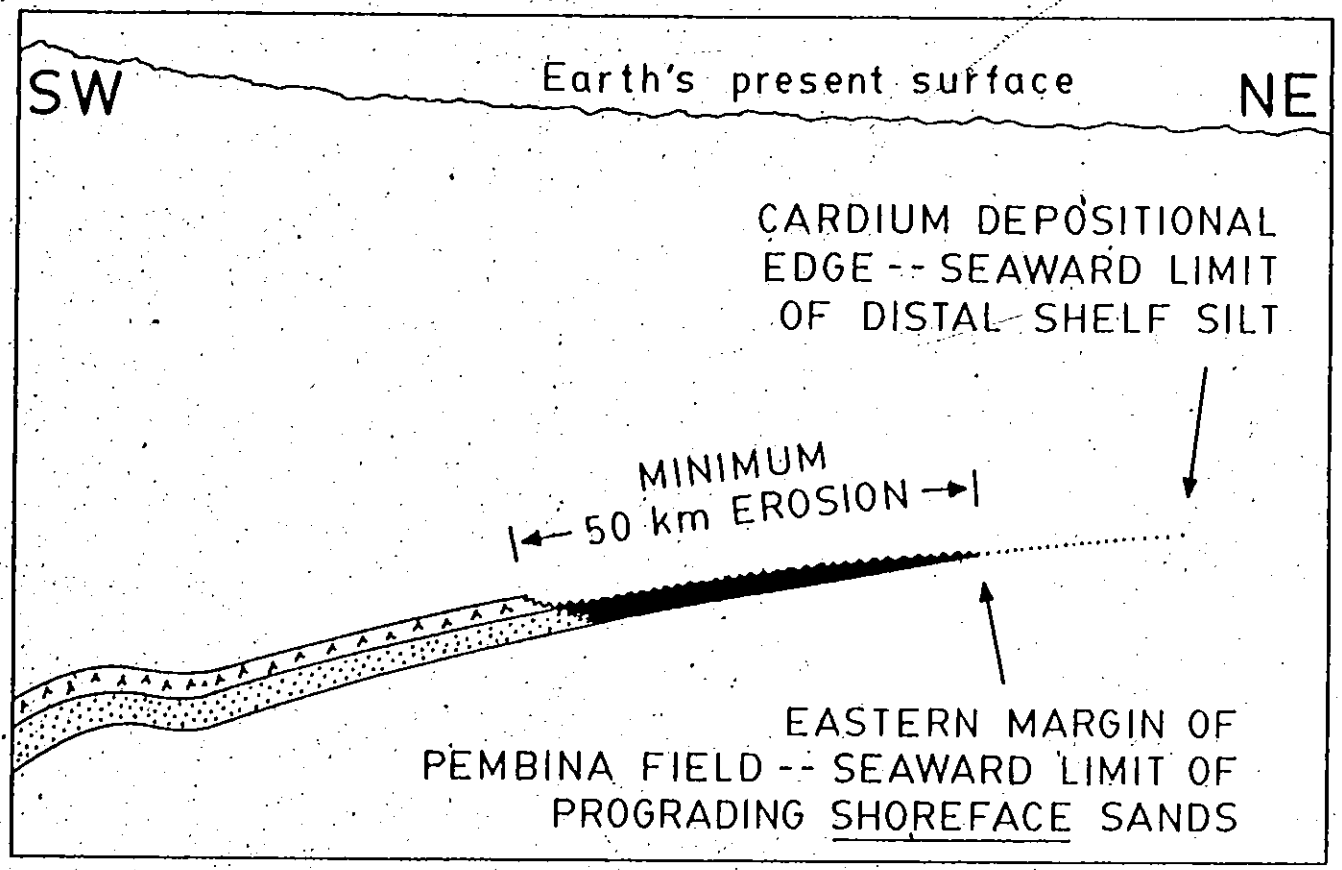
SW
Earth's present surface
NE
CARDIUM DEPOSITIONAL
EDGE -- SEAWARD LIMIT
OF DISTAL SHELF SILT
MINIMUM
50 km EROSION
EASTERN MARGIN OF
PEMBINA FIELD -- SEAWARD LIMIT OF
PROGRADING SHOREFACE SANDS

Figure 7-8. Interpretive diagram of subsurface Cardium paleogeography. See text for discussion.

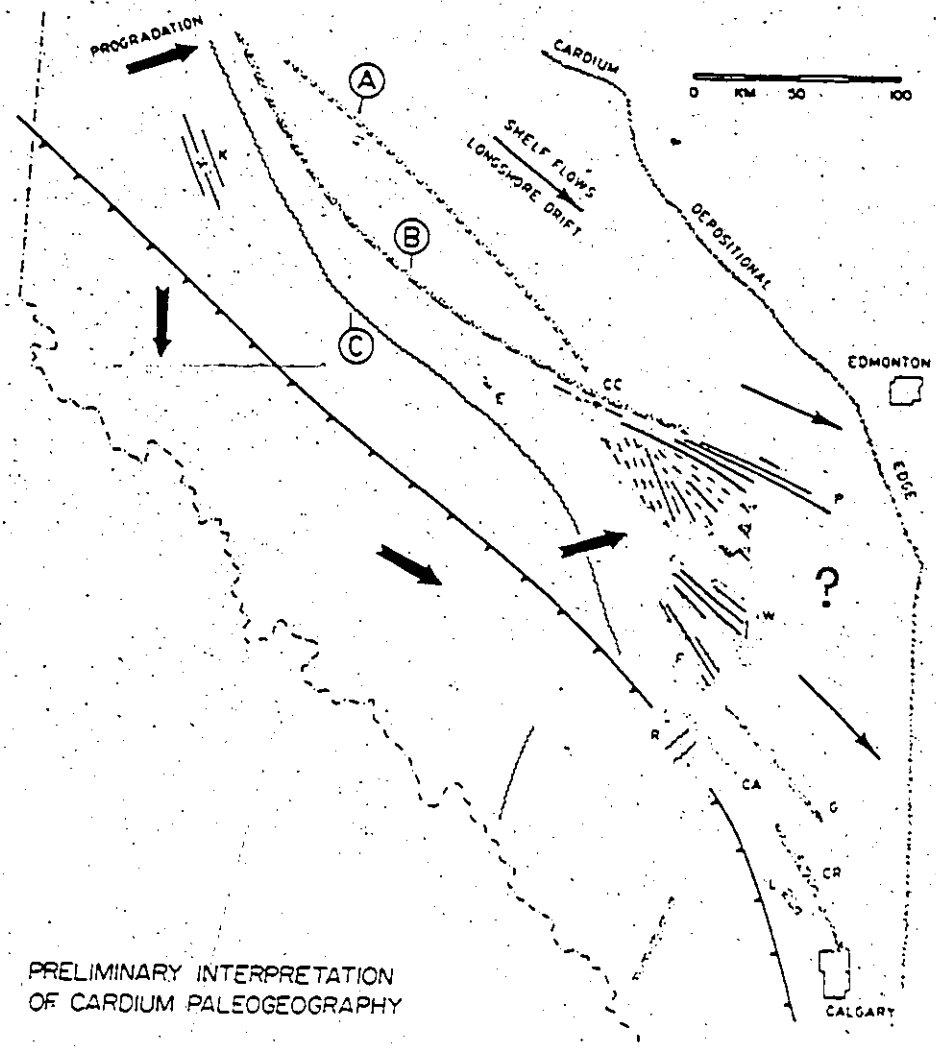

PRELIMINARY INTERPRETATION
OF CARDIUM PALEOGEOGRAPHY

alongshore to the southeast. The largest spit-bar system (at Pembina) is comparable in size to modern Cape Cod, Massachusetts.

In figure 7-8, the maximum shoreline extent probably lay somewhere between lines A and B; the shoreline probably curved to a north-south orientation in the region south of Pembina. The serrated line (C) provides a qualitative indication of the extent of transgressive removal of non-marine deposits.

In this hypothesis, the sand-filled channel at Ricinus (Walker, 1983b) probably was cut into the shoreface, or at least headed on the shoreface. The elongate bar-like fields (Crossfield, Garrington, Caroline) probably represent shelf sand ridges formed in response to geostrophically balanced shelf circulation.

CHAPTER 8. EXTENDED DISCUSSION OF WAVE-FORMED STRUCTURES AND SEQUENCES IN THE CARDIUM FORMATION

CHAPTER OUTLINE AND INTRODUCTION

The purpose of this chapter is to present a quantitative paleohydraulic analysis of various wave-formed primary physical structures in the Cardium Formation, with the intention of defining their environmental significance and the conditions of their origin as accurately as may be possible. In this context, the sequences of sedimentary structures defined in chapter 5 will also be re-evaluated quantitatively. This chapter is divided into four parts:

Part 1. The first section of the chapter (p. 531) presents a critical review of suggested generative processes for hummocky cross-stratification.

Part 2. In the second part (p. 592), the threshold-motion method for the paleohydraulic analysis of coarse-grained vortex ripples is discussed; this method is then tested against recent examples formed under known hydrodynamic conditions.

Part 3. In part 3 (p. 663), this method is applied to ancient orbital vortex ripples from the Cardium and two other Cretaceous units in Alberta. The results of this application are employed in an approximate determination of the conditions of formation of hummocky cross-stratification associated with these orbital ripples.

Part 4. The final section of the chapter (p. 689) places the above analysis into a broader stratigraphic context, in an attempt to determine quantitatively certain important parameters in Cardium shoreline sequences and in the Cardium basin as a whole.

NOTATION USED IN THIS CHAPTER

Ac dimensionless acceleration number

d_o bottom orbital diameter

d_o^T value of d_o at which the transition from orbital to anorbital ripples occurs for any given grain size

D sediment grain size

f_w wave friction factor

Fr Froude number

Fr' "densiometric" Froude number

g acceleration due to gravity

g' "densiometric" gravity term

h water depth

H wave height

L wave length

L_{deep} deep-water wave length

Re_d "orbital" Reynolds number

Re_b boundary Reynolds number

t thickness of a stratified underflow

T wave period

T^* value of T associated with incipient motion of sediment

U mean flow speed (unidirectional flow)

U_m maximum orbital speed at the bottom

U_m^* value of U_m associated with incipient motion of sediment

λ_H form-wavelength of hummocky cross-stratification (distance from hummock to hummock or swale to swale)

λ_m ripple or antidune spacing

λ_{max} maximum ripple spacing for any given grain size

ρ fluid density

ρ_s sediment density

$\Delta\rho$ excess fluid density due to suspended sediment

τ shear stress

τ_m maximum shear stress under an oscillatory flow

ν kinematic viscosity of fluid

PART 1

SUGGESTED PROCESSES FOR THE ORIGIN OF HUMMOCKY CROSS-STRATIFICATION: A CRITICAL REVIEW

INTRODUCTION

The inferred processes governing the origin of hummocky cross-stratification have recently received much attention in the geological literature (see appendix 9). Most previous workers have suggested formation by wave-generated bottom flows which are oscillatory or multidirectional, or by a combination of oscillatory/multidirectional and unidirectional bottom flow components.

A wide variety of generative agents has been invoked to account for the morphology, environmental distribution, and stratigraphic context of hummocky cross-stratification, as well as the suite of sedimentary structures with which it is commonly associated. Most previous workers have suggested an origin due to progressive surface gravity waves; however, several other types of wave phenomena have been suggested, as well as agents other than waves.

Herein I will critically review the various processes that have been suggested for the origin of

hummocky cross-stratification, and I will summarize and evaluate certain observational constraints that restrict the range of possible generative processes. The major emphasis of this review is placed upon small-scale features observable in individual exposures.

HUMMOCKY CROSS-STRATIFICATION: DESCRIPTION

General Description

Hummocky cross-stratification has never been observed during the process of formation in natural environments; in fact, it has never been recognized unequivocally from any recent sediments. The structure has never been formed experimentally, although similar smaller structures (probably genetically related) have been formed under purely oscillatory flows in laboratory apparata (see further discussion below). In the absence of appropriate field and laboratory studies, especially those involving stratification developed under aggradational conditions, all that is known of the characteristics of this structure (and virtually all that is known of its origin) has been inferred from studies of ancient sedimentary units.

There are now some 100 ancient stratigraphic units known to contain hummocky cross-stratification (Duke,

1985c). Most examples occur in coarse siltstone to very fine sandstone; examples formed in fine sandstone are also common (especially lower fine sandstone). The structure is very rarely observed in medium or coarse sandstone (Duke, 1985c), and pebbles or cobbles are occasionally observed within sandy laminae (Bourgeois, 1980; Duke, 1982b, Fig. 5a; Walker et al., 1983, Fig. 4; this thesis, Fig. 4-20C, 4-21A, & 4-21B).

Hummocky cross-stratified sandstones are characterized by gently curved, low-angle cross-stratification (Fig. 4-8). Within individual beds, curvature of laminae typically is both convex-upward (a "hummock") and concave-upward (a "swale"). Commonly, an individual lamina or lamina set may be traced over both a hummock and an adjacent swale (Fig. 4-12B & 4-20D). Cross-strata dip at maximum angles less than about 15°; higher angles of dip are extremely rare.

In plan view, hummocks and swales generally are three-dimensional and radially symmetrical (Fig. 4-19B). There typically is no preferred direction of cross-strata dip, nor does the angle of dip vary systematically with direction; consequently, vertical sections through hummocky beds appear very similar regardless of orientation.

Hierarchical Order of Discordant Surfaces in Hummocky Beds: Description and Preliminary Interpretation

Dott & Bourgeois (1982, p. 666 & Fig. 3, reproduced herein as Fig. 8-1) established a hierarchical order for discordant surfaces (boundaries between beds, lamina sets, and individual laminae) within hummocky cross-stratified beds, patterned after the terminology of Campbell (1966). With slight modification (Fig. 8-2), their system serves as a very useful observational guide for the examination of internal structures within hummocky beds. Dott & Bourgeois suggested the following three orders of surfaces:

1) First-order boundary. The sharp basal contacts of hummocky beds typically lie upon mudstone or bioturbated sandstone, and generally are erosional. Dott & Bourgeois (1982) suggested the term "first-order boundary" for such surfaces; these surfaces define hummocky beds, and as such may also be termed "bedding surfaces". I shall refer to these surfaces by the former term (first-order boundary).

It should be noted that the interpretational distinctions between first- and second-order boundaries can be very difficult under certain circumstances, especially cases involving boundaries between amalgamated sandstone beds (see "Major Facies Associations" below for a description of bedding relationships involving hummocky sandstones).

2) Second-order boundary. The term "second-order truncation" was used by Dott & Bourgeois (1982) for any internal discontinuity between hummocky sandstone laminae. These second-order boundaries define hummocky lamina sets, within which individual laminae lie upon one another without intersection.

Dott & Bourgeois (1982) clearly imply by their use of this term that all second-order lamina intersections within hummocky beds are erosional (i.e., truncating). This implication is made explicit in their description of the structure, and is reflected by the scour-and-drape genesis which they infer. As I shall demonstrate below, not all discordances between hummocky laminae are erosional. I therefore suggest that the name for internal discontinuities should be modified to "second-order boundary" or "lamina-set surfaces"; the term "truncation" can only be applied to certain of these boundaries (see below).

3) Third-order boundary. The boundaries between individual non-intersecting ("parallel") laminae within any lamina set were termed "third-order laminar surfaces" by Dott & Bourgeois (1982).

Figure 8-1. Hierarchical order of discordant surfaces in hummocky cross-stratified beds established by Dott & Bourgeois, 1982). See text for discussion. From Dott & Bourgeois (1982, Fig. 3).

IDEALIZED HUMMOCKY SEQUENCE

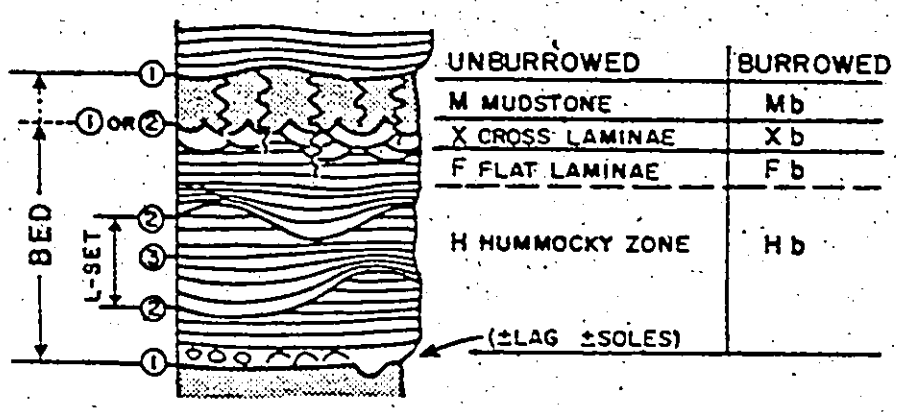

UNBURROWED	BURROWED
M MUDSTONE	Mb
X CROSS LAMINAE	Xb
F FLAT LAMINAE	Fb
H HUMMOCKY ZONE	Hb

Figure 8-2. Truncating, terminating, and truncating/terminating second-order boundaries within hummocky cross-stratification. In panel diagram, note laterally impersistent terminating boundary (dashed line). See text for discussion.

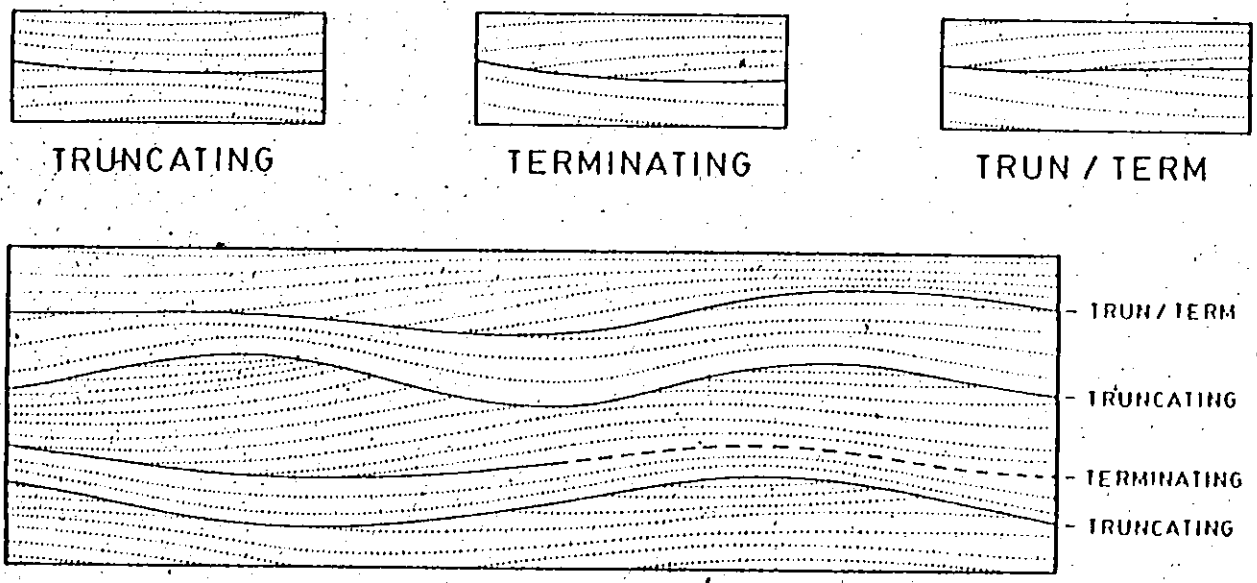
TRUNCATING
TERMINATING
TRUN / TERM
TRUN / TERM
TRUNCATING
TERMINATING
TRUNCATING

Classification of Second-Order Boundaries: Depositional Significance of Lamina Intersections Within Hummocky Beds

The system outlined above provides a basic framework for the interpretation of intersections between laminae, but does not provide for non-erosional second-order boundaries. Below I suggest a revision of the hierarchy in which four basic types of second-order boundaries (lamina-set surfaces, or lamina intersections) are recognized. The revised system is illustrated graphically in figure 8-2. Recognition of the different types of lamina intersections is crucial to the hydrodynamic interpretation and inferred genesis of hummocky cross-stratification. In particular, this recognition is important in the discussion of hummock growth, and the distinction between separate depositional events not marked by lithological changes or bioturbation.

Intersections between sandstone laminae within hummocky beds (definitionally, second-order boundaries) are varied, being of four major types described below. Note that all four types of intersections may be either angular or tangential.

1) Truncating intersections are those in which underlying laminae are erosionally truncated by overlying laminae that are parallel to the truncation surface, or

very nearly so (Fig. 8-2, 4-9A, & 4-13B). Even though truncating intersections separate sandstone from sandstone, they may represent the base of a separate depositional event (i.e., a temporally distinct episode of sand emplacement, rather than the shifting of hummocks and swales during a single depositional event -- see discussion below). In cases of extensive lateral exposure (a few tens of meters or more) revealing a continuously traceable truncating intersection, that intersection is probably best interpreted as the base of a separate event.

2) Terminating intersections are those in which overlying laminae non-erosionally terminate against underlying laminae that are parallel to the termination surface (Fig. 8-2 & 4-13C). In general, terminating intersections are not very extensive laterally. Typically, the surface of intersection is concave-upward, whereas the overlying sandstone laminae generally are convex-upward. Intersections of this type probably do not represent a separate depositional event. They are best interpreted as minor adjustments of bed topography (probably the lateral migration of a hummock into an adjacent swale) during a single episode of sand movement (i.e., during a single period of storm activity).

3) Truncating/terminating intersections are those in which overlying laminae both terminate against and

erosionally truncate underlying laminae (Fig. 8-2 & 4-20A). Neither set of laminae is parallel to the intersection surface. Whether a truncating/terminating intersection represents a separate depositional event probably depends upon the lateral extent of truncation. In extensive exposures, most intersections which locally appear to be of this type are seen to be laterally variable (see below).

4) Laterally variable intersections are those observed to alternate from one of the above types to another when traced over a short distance laterally (generally at least a few meters). With excellent lateral exposure on the order of several tens of meters, the tracing of intersections generally reveals that many are laterally variable and/or are not continuous across the entire outcrop. Laterally variable intersections (especially those which are not fully continuous) probably do not generally represent separate depositional events; however, examples which are both laterally continuous and predominantly truncating (i.e., laterally varying between the truncating and the truncating/terminating types, for the most part) do probably represent separate events.

The above descriptions suggest that each of the four types of intersections may be further classified as either continuous or discontinuous. This further categorization is of course subjective, in that it is

likely to be strongly influenced by the lateral extent of exposure. It should be emphasized that this classification scheme is entirely descriptive, not interpretational.

As stated by Dott & Bourgeois (1982, p. 666), "[in amalgamated sandstones] the distinction of a first-order from a second-order truncation surface may be difficult." Again, I advise use of the term "boundary" rather than "truncation surface". By their statement, they refer to the interpretational distinction between a separate depositional event and an erosional "pulse" within a single event, respectively. Herein, I prefer to restrict the hierarchical scheme to purely descriptive criteria; thus, in amalgamated sandstones, all discordant boundaries are of the second order, except those for which there is clear evidence of a major depositional discordance (e.g., surfaces which lie upon mudstone lenses or extensively bioturbated intervals -- see extensive discussion in the description of facies 3HA in chapter 4). Criteria for distinguishing between the four basic types of second-order lamina intersections (outlined above) may be used to evaluate the likelihood of separate depositional events in otherwise ambiguous cases.

In second-order boundaries involving intersections of one or a few thin laminae at very low angles (in many cases, approximately 1°), it often is difficult to distinguish between erosional and non-erosional contacts

(i.e., truncating and terminating intersections, respectively). This is especially true of tangential intersections. The distinction between locally truncating and locally terminating intersections is essential to the discussion of growth of hummocks as bedforms (see discussion below).

In vertical sections, hummocky laminae most commonly are fan-like within individual sets, with dip systematically decreasing both upward and toward the center of swales (Fig. 4-9A, 4-12E, & 4-13A). Exceptions to this generality are known (Hunter & Clifton, 1982, Fig. 6b; Walker et al., 1983, Fig. 2 & 6; this thesis, Fig. 4-13B). The possibility that hummocks grow vertically, with the dip on the sides of the hummock increasing vertically as individual laminae thicken toward the hummock crest, has been discussed by Hunter & Clifton (1982), Dott & Bourgeois (1982, 1983), and Walker et al. (1983). All agree that hummock growth (if it occurs) probably indicates that hummocks represent bedforms rather than artifacts of simple scour and drape. Both Hunter & Clifton (1982) and Walker et al. (1983) have illustrated and discussed examples of growing hummocks, but Dott & Bourgeois (1982, 1983) and Bourgeois (pers. comm., 1984) maintain that these examples generally include subtle truncation surfaces on the flanks of the hummock adjacent to the crest, and do not represent growing bedforms. My own examination both of hummocks in

the field, and published photographs of examples alleged to represent growing hummocks, suggests that the very subtle "truncations" recognized by Bourgeois are in most cases probably minor terminating intersections, not truncating intersections. The existence of terminating intersections (Fig. 4-13B & 4-13C) is consistent with, and probably supportive of, growth of hummocks as bedforms. Terminating intersections may also be reconciled with the inferred scour-and-drape genesis supported by Bourgeois, but only with difficulty (i.e., special pleading for anomalous deposition on the tops of hummocks only -- see further discussion below).

In some instances, the subtle intersections recognized by Bourgeois are in fact truncating, but these are extremely minor, probably do not represent any significant erosional period, and are also conceptually consistent with the growth of bedforms, especially those forming under natural polychromatic waves.

Major Facies Associations Involving Hummocky Cross-Stratification

Studies involving some 100 ancient examples of hummocky cross-stratification (summarized by Duke, 1985c) suggest that there are three major associations involving the structure. This tripartite classification is also

supported by the present study of Cardium Formation sandstones; the three categories are discussed below.

1) Interbedded lithologies. In this association (association 2 of chapter 4), hummocky cross-stratified sandstones are interbedded with either terrigenous or carbonate shales or mudstones. Sandstones are sharp-based, typically displaying directional sole marks. Sole marks generally are systematically aligned in most sequences (e.g., Fernie-Kootenay transition, Hamblin & Walker, 1979; Moosebar-Gates transition, Leckie & Walker, 1982), but occasionally are randomly oriented, or very poorly aligned (Hughley Shales, Gray & Benton, 1982; Medina Formation, Duke, 1982b and unpub. data).

Hummocky sandstones of association 1 generally range in thickness from about 10 cm to 250 cm. They typically are tabular or pinch and swell in thickness laterally; locally, they are lens-shaped. The fine-grained interbedded material commonly is extensively bioturbated, and typically contains very thin sandstone interbeds.

Dott and Bourgeois (1982) formulated an idealized divisional sequence for these sandstone/mudstone couplets (Fig. 8-1). Walker et al. (1983) suggested a modification of this sequence (Fig. 4-8) which, in descending order, consists of:

M - Shale/mudstone, commonly bioturbated.

X - Ripple cross-lamination. Ripples are usually symmetrical.

F - "Flat" lamination, often gently undulatory.

H - Hummocky cross-stratification.

P - Planar parallel lamination.

B - Basal division, consisting of one or more of the following: sharp base; directional sole marks; basal lag of pebbles, shells, and/or rip-up clasts of mudstone; a graded or apparently structureless basal zone. Rarely, large symmetrical ripples (λ_m approximately 1 m) are formed within basal conglomerates (see further discussion below).

Hummocky sandstone/mudstone couplets are associated with pot- and gutter-casts in numerous occurrences (e.g., Aigner, 1982; Duke, 1982b; chapters 4 & 5 of this thesis); these are usually no more than several tens of centimeters wide and several centimeters deep (Fig. 4-20D), but may be much larger (Fig. 5-39). Internally, pot- and gutter-casts typically contain hummocky cross-stratified sandstone.

High-angle cross-bedding, indicating reworking by tractional bottom flows due either to episodic storm processes or continuously-operating shallow-marine processes (fairweather waves, tidal currents, etc.)

generally is absent from this association. [Note, however, that this reflects a grain-size control in most instances -- see further discussion below.] Small-scale high-angle trough cross-lamination formed by current ripples is also generally very rare or absent from association 1. Thick intervals of planar parallel lamination generally also are absent; thin intervals occur at the bases of beds locally (division P above).

Occurrences of this association generally have been interpreted as representing an alternation between rapidly emplaced, storm-deposited sandstones and slowly deposited hemipelagic muds, suggesting sedimentation in water depths below fairweather wave base but above storm wave base (e.g., Hamblin & Walker, 1979; Dott & Bourgeois, 1982; Walker et al., 1983).

2) Amalgamated sandstones. This association consists of numerous sharp-based hummocky sandstones as above. Each sandstone bed is in erosional contact with the underlying sandstone bed (Fig. 4-17). Erosional surfaces can be traced many meters laterally, often across the entire width of outcrop. Erosion locally eliminates the upper parts of the previously emplaced sandstone/mudstone couplet; consequently, mudstone either is absent or is only locally present, typically forming isolated lenses within an amalgamated, hummocky cross-stratified sand body several

meters or tens or meters in thickness. Mudstone lenses often display abundant bioturbation, indicating a long period of quiescence prior to emplacement of the overlying sand bed. In many occurrences, abundant mudstone (rarely, sandstone) rip-up clasts and/or exotic pebbles are locally concentrated along certain sandstone laminae, usually above major second-order boundaries (i.e., above truncating intersections -- Fig. 8-2 & 4-20).

Occurrences of this facies generally have been interpreted as representing an environment similar to that of association 1, but with more energetic and/or frequent storm events, possibly indicating shallower water depth and/or closer proximity to source (e.g., Hamblin & Walker, 1979; Dott & Bourgeois, 1982; Walker et al., 1983). Deposition was probably still below fairweather wave base and above storm wave base.

3) Swaley cross-stratification. This term was introduced informally by Duke (1980) to distinguish a variant of hummocky cross-stratification in which swales are preferentially preserved, and hummocks are rare or absent (Fig. 4-22). Thick lenses of planar parallel lamination are common within this association.

Generally, swaley sandstones do not show evidence of amalgamation. Mudstone lenses are absent or extremely rare, as are mudstone rip-up clasts and bioturbation.

Erosional contacts cannot be traced more than a few meters laterally. Lenses of trough cross-bedding are present locally. Sand deposition apparently was largely continuous, not episodic as in associations 1 and 2.

The origin and environmental significance of swaley cross-stratification are unclear. All known occurrences of the structure are closely associated with more "traditional" varieties of hummocky cross-stratification (associations 1 and 2), suggesting a related genetic process probably involving storm waves. In the prograding shoreline sequences in which it occurs, swaley cross-stratification (where present) always overlies hummocky cross-stratification, and typically lies immediately below beach deposits. This typical pattern of facies sequences led Leckie & Walker (1982) to suggest an origin due to storm waves in water shallower than that for hummocky cross-stratification, and probably shallower than fairweather wave base.

INFERRED ORIGIN DUE TO PROGRESSIVE SURFACE GRAVITY WAVES: HISTORICAL PERSPECTIVE

As indicated above, the majority of previous workers have suggested an origin for hummocky cross-stratification due to progressive surface gravity

waves. Most have specifically inferred formation by exceptionally large storm-generated waves. The history of this interpretation dates from the nineteenth century, when it was originally advanced in a largely neglected paper by Grove Karl Gilbert.

Gilbert (1899) was the first to recognize, describe, illustrate, and interpret hummocky cross-stratification, from various stratigraphic levels within the Silurian Medina Formation in New York. He referred to the structure as a form of "giant ripple" and emphasized the large scale of examples, reporting forms with crest-to-crest wavelengths of 3 to 9 m, and trough-to-crest heights of 15 to 90 cm (Gilbert, 1899, p. 136). These measurements indicate low-angle cross-stratification of about 11° or less; Gilbert noted that some cross-strata are "so gently inclined that they might easily be confused with true bedding" (Gilbert, 1899, p. 139). He also described the complexity of intersections between laminae and the three-dimensional form of hummocks and swales (Gilbert, 1899, p. 135), and he reported the presence of convex-upward lamination over hummocks, forming smoothly sinusoidal cross-sectional profiles in some examples (Gilbert, 1899, p. 137 and Fig. 2c). His description of the structure is essentially identical to descriptions from twentieth-century studies. This pioneering recognition of hummocky cross-stratification has

been confirmed by recent work (Duke, 1982b).

Gilbert (1899, p. 139) interpreted the structure as the product of unusually large wave ripples generated beneath exceptionally large storm waves, and further suggested that the presence of the structure demonstrated an association with a large ocean. This conclusion is essentially identical to those advanced by most twentieth-century workers (see below).

Campbell (1966) was the first modern worker to re-discover the structure, which he termed "large-scale truncated wave-ripple laminae". Campbell referred to Gilbert's prior recognition of the structure, and agreed with the suggested wave origin.

Several other workers apparently recognized the structure independently during the 1960's and 70's. These include Michaelis & Dixon (1969), Goldring (1971), Howard (1972), and Broekman (1973). These authors suggested a variety of possible generative processes, including origin due to storms and/or waves.

The preferred term, hummocky cross-stratification, was introduced by Harms et al. (1975, p. 87), who inferred a probable origin beneath large storm waves. Subsequent workers have generally agreed with this interpretation, first advanced by Gilbert almost 100 years ago. In the past few years, however, a wide variety of "refinements" of the storm-wave origin have been advanced; many of these

conflict with one another to a varying degree. Below I critically evaluate some of these suggested processes.

INFERRED ORIGIN DUE TO PROGRESSIVE SURFACE GRAVITY WAVES: SOME RECENT SUGGESTIONS

The description of hummocky cross-stratification summarized in a preceding section supplies the basic observational constraints which must be fulfilled by any hypothetical generative process. These constraints have suggested a wave origin for hummocky cross-stratification to the majority of contemporary workers, including Harms et al. (1975), Hamblin & Walker (1979), Walker (1979), Bourgeois (1980), Kreisa (1981), Wright & Walker (1981), Aigner (1982), Aigner & Reineck (1982), Dott & Bourgeois (1982), Harms et al. (1982), Hunter & Clifton (1982), Leckie & Walker (1982), Mount (1982), Swift et al. (1983), Walker et al. (1983), Duke & Leckie (1984), Leckie & Duke (1984), Southard (1984), and Duke (1985a, 1985b, 1985c).

In this section, I discuss various processes suggested by modern workers for the origin of hummocky cross-stratification due to bottom shear stress generated by surface gravity waves. Alternative processes not involving wave-generated flows are considered in a later section.

Bottom flows generated by surface gravity waves include unidirectional, oscillatory (bidirectional), and multidirectional flows, and various combinations of these end-member flow classes. Additionally, oscillatory flow may be either monochromatic or polychromatic, reflecting the distribution of wave energy as a function of period. Various combinations and effects of these different flow components are involved in the following suggested processes. Seven wave-related processes, several of which are currently popular in the literature, will be discussed in this section. These involve generation of hummocky cross-stratification by:

1) Multidirectional- or oscillatory-flow flat-bed mantle over a pre-existing erosional topography;
2) Oscillatory- or multidirectional-flow flat bed with superimposed velocity fluctuations due to wave-wave interactions under a polychromatic wave spectrum;
3) Three-dimensional oscillatory-flow vortex ripples formed under a monochromatic wave spectrum;
4) Three-dimensional oscillatory-flow vortex ripples formed under a polychromatic wave spectrum;
5) Oscillatory-flow flat bed with superimposition of previously unrecognized low-amplitude, three-dimensional orbital ripples;
6) Combined-flow ("hummocky") megaripples;

7) Unidirectional-flow upper flat bed with superimposed wave-induced velocity fluctuations.

Some of the processes listed above are based upon qualitative concepts, rather than a rigorous quantitative analysis. At the time of this writing (Winter, 1984 - Spring, 1985), all of these suggestions are in a rather formative stage. There currently is a heated debate surrounding the origin of this structure, as is perhaps indicated by the large number of hypothetical modes of formation which have been suggested. The analysis offered herein is intended to stimulate a further critical evaluation of the numerous suggested processes.

Process 1: Generation by Multidirectional- or Oscillatory-Flow Flat-Bed Mantle Over Pre-Existing Erosional Topography

Harms et al. (1975, p. 88) were the first workers to explicitly suggest formation of hummocky cross-stratification by erratic, multidirectional flows generated beneath storm seas. Basically, this suggestion was inspired by the three-dimensional form of hummocks and swales, which they considered to be a variety of wave-formed (multidirectional-flow) flat bed in which the undulatory laminae represent deposition over a pre-existing erosional topography (Harms et al., 1975, p. 87-88).

In recent years, aspects of this theory for the origin of hummocky cross-stratification have been developed in greater detail by Dott & Bourgeois (1982, 1983), Bourgeois & Smith (1984), and Smith & Bourgeois (1984). These authors (most noteably Bourgeois) have maintained that the structure is purely a scour-and-drape phenomenon (see description summary above for further discussion), and that laminae merely drape a pre-existing erosional topography. Smith & Bourgeois (1984) specifically suggested that only breaking waves develop sufficient near-bed turbulence to account for both the scour typical of hummocky cross-stratification and the suspension required to form a centimeter-scale sand drape.

As discussed in the descriptive summary above, there is reasonable evidence to suggest that hummocky cross-stratification is <u>not</u> purely a scour-and-drape phenomenon, but rather that hummocks do grow as bedforms. If this indeed is the case, flow separation in the lee of hummocks may be responsible for some of the near-bed turbulence required for both scour and suspension of sand, as is clearly the case with simple vortex ripples. This hypothesis is strongly supported by experimental work reported by Southard (1984), in which very large vortex ripples were formed in very fine to fine sands (see further discussion in a later section). The assertion that only breaking waves are capable of significant scour and

suspension is contra-indicated by: 1) field studies in modern shallow-marine environments (see review by Clarke et al., 1982) showing significant sand suspension as high as 1 m above the bed by combined flows due to stable waves, and 2) studies of ancient hummocky sequences, indicating a proximal-shelf position for many examples (several tens to a few hundred kilometers from shore), far from the influence of breaking waves.

A further argument can be made against the general applicability of the scour-and-drape hypothesis. This argument is based upon the simple observation of lateral migration of hummocks as positive-relief features on the substrate, as is clearly indicated by preserved stratification overlying terminating intersections within many hummocky beds in ancient sequences. Figure 4-13C is an example in which a hummock has apparently migrated over an adjacent swale without any appreciable diminishment in the curvature of its convex-upward laminae. Thus, flow in the boundary layer was acting to preserve the form of these features as they migrated laterally. If individual laminae were deposited under relatively calm conditions (i.e., below the threshold for development of ripples), then they should appear as an upward-flattening drape over any convexity. On the other hand, if flow conditions were sufficiently energetic to produce flat-bed sand transport, and if there was no tendency in the flow to maintain or

amplify a positive feature on the bed, then the effect of an energetic wave-induced flow would be only to erosionally truncate any positive bed features, not to cause them to translate laterally while maintaining their topographic identity. Therefore, the process suggested by Bourgeois and co-workers probably cannot be accepted as generally applicable to all examples of hummocky cross-stratification.

Process 2: Generation Within the Oscillatory- or Multidirectional-Flow Flat-Bed Field by Superimposed Velocity Fluctuations Due to Wave-Wave Interactions

Under naturally occurring polychromatic wave spectra, both oscillatory- and multidirectional-dominant bottom flows are not strictly repetitive through time. Rather, wave-wave interactions in naturally occurring wave trains create spatially and temporally localized bottom-flow velocity fluctuations, involving irregularities in both speed and direction of the instantaneous bottom flow. Speed fluctuations may be either instantaneously unusually high, or they may be unusually low over extended lengths of time (on the order of a few nominal wave periods). This variation is in part a simple beating effect due to superimposition; another important factor is the rare positive re-enforcement of several wave forms,

possibly resulting in wave instability and local breaking (Smith & Bourgeois, 1984).

Under depositional conditions which would result in the formation of true flat bed under purely oscillatory or simply repetitive multidirectional flow, it is intuitively and conceptually reasonable to suppose that instantaneous velocity fluctuations of the sort described above may well be responsible for: 1) lateral thickening and thinning of laminae, 2) spatially localized shallow erosion, and 3) spatially localized flat-bed deposition. Such activity might well be responsible for formation of numerous examples of hummocky cross-stratification.

The differences between this suggested process and process 1 above may appear somewhat subtle, and are worth an elaboration. In process 1, hummocky cross-strata are envisioned to form as a simple drape over an irregular erosional surface (produced prior to sand deposition by any of a number of means). A polychromatic or multidirectional wave spectrum is not necessary for formation of the drape, although it may be considered necessary for production of the pre-existing topography at the base of the bed. In process 2, however, superimposed velocity fluctuations due to polychromatic and/or multidirectional waves are required to form the subtle undulations and truncations within laminae; pre-existing erosional topographic relief is not a necessary part of the formative process.

Clearly, these two processes are not mutually exclusive; both may be operating to form some examples of hummocky cross-stratification. What is not clear to me is the relative importance assigned to the two separate processes by their proponents (noteably, Bourgeois).

Process 3: Generation Under Monochromatic Oscillatory Flow by Three-Dimensional Vortex Ripples

Southard (1984) has reported laboratory formation under purely oscillatory flows of three-dimensional vortex ripples, with maximum ripple spacing of at least 1 m, in very fine to fine sands. These ripples appear to be scaled by bottom orbital diameter (d_o), thus making them <u>orbital</u> vortex ripples. This observation strongly suggests that hummocky cross-stratification is likely to be formed by oscillatory-flow vortex ripples in natural environments, as suggested by Southard (1984). The complex internal stratification within hummocky beds is in this model due to the temporal development and lateral migration of vortex ripples, and to their modification as wave conditions vary through time. Velocity fluctuations due to polychromatic wave spectra in natural environments would presumably also account for some of the complex internal stratification within hummocky beds (see below).

Process 4: Generation Under Polychromatic Oscillatory Flow by Three-Dimensional Vortex Ripples

The preliminary results of Southard's laboratory experiments (discussed above) strongly suggest that large three-dimensional vortex ripples formed under monochromatic oscillatory flow may be responsible for the formation of some examples of hummocky cross-stratification. Pending a complete report, however, it is not possible to determine the upper limit of vortex-ripple spacing in appropriate grain sizes under this type of flow. Southard (1984) reported ripples with maximum spacings in excess of 1 m; form-spacings within hummocky beds commonly attain a maximum of several meters.

I know of no laboratory study of substrate response to polychromatic oscillatory flow. We have virtually no data on the variation in ripple geometry (particularly, ripple spacing) under this important class of flow. Limited field observations by Miller & Komar (1980b) indicate a dramatic increase in ripple spacing under oscillatory flows which are even slightly polychromatic and/or multidirectional. Since most natural wave fields are both polychromatic and multidirectional, this observation of increased ripple spacing suggests yet another possibility for the origin of the meter-scale undulations which characterize hummocky

cross-stratification.

Process 5: Generation Within the Oscillatory-Flow Flat-Bed Field by Previously Unrecognized Low-Amplitude, Three-dimensional Orbital Ripples

Elsewhere, I have presented two independent paleohydraulic analyses of hummocky cross-stratification, from Pleistocene Lake Bonneville deposits (Duke, 1984) and Cretaceous marine deposits of Alberta (Duke & Leckie, 1984). Both analyses suggest the possible existence of low-amplitude, long-wavelength, three-dimensional orbital ripples within the wave-formed flat-bed field, and the formation of hummocky cross-stratification in these examples by these ripples. Presumably, such ripples (if they exist) have not been recognized previously because of the difficulty of detection in natural environments and the lack of experimental apparata large enough to permit their formation in the laboratory. The evidence for their existence is different in both cases, and will not be summarized here (but see part 2 of this chapter for a full development and critical discussion of the Alberta analysis).

Process 6: Generation by Combined-Flow Megaripples

Swift et al. (1983) have suggested a generalized

model for the formation of hummocky cross-stratification (or "hummocky megaripples", which they consider to be the generative bedform). Briefly summarized, the suggested process involves a unidirectional geostrophic flow with a roughly equal superimposed multidirectional component due to erratic, three-dimensional storm waves. The authors infer that such flows generate three-dimensional megaripples with greatly reduced angles of dip on the foresets (due to rotary "scrubbing" by the wave-induced flow component), and that hummocky cross-stratification is produced by the lateral migration and vertical growth of these hummocky megaripples. This hypothesis has recently been defended by Allen (1985). Allen's analysis is discussed separately below.

To clarify the terminology used in this document, note that megaripples and dunes are considered to be equivalent bedforms -- the term "megaripple" is reserved for examples generated by complex marine flows; "dune" refers to examples generated by purely unidirectional flows, such as flows in rivers or laboratory flumes. Together, the megaripple/dune bed phase and the sandwave bed phase constitute the two basic varieties of large ripples formed under unidirectional-dominant flows.

Combined-flow megaripples may be responsible for formation of some few examples of hummocky cross-stratification; however, they cannot be suggested as

a general generative agent for several reasons discussed below.

Mutually exclusive grain-size ranges of hummocky cross-stratification and megaripples. The single most compelling argument against the formation of hummocky cross-stratification by combined-flow megaripples involves their respective grain-size ranges. Most examples of hummocky cross-stratification are formed in coarse siltstone to very fine sandstone. Examples formed in fine sandstone (especially lower fine sandstone) are also common; those formed in medium to coarse sandstone are extremely rare (see above, also Duke, 1985c).

Large ripples do not form in sediments finer than about Ø.1 mm (i.e., finer than upper very fine sand -- Harms et al., 1984, p. 2-18). To a large degree, therefore, the grain-size ranges of large ripples and hummocky cross-stratification do not overlap. This difference is even more pronounced if we consider megaripples only. Rapid temporal velocity fluctuations characteristic of natural shallow-marine flows tend to inhibit development of megaripples on the low end of the grain-size range, where the stability field is restricted to a very narrow range of velocity. Megaripples are generally restricted to grain sizes greater than about Ø.2 mm (i.e., uppermost fine sand and coarser sizes --

Harms et al., 1982, Table 2-1). Thus, the grain-size ranges of megaripples and hummocky cross-stratification are almost completely mutually exclusive. This dissimilarity in grain sizes indicates that generation of hummocky cross-stratification by "hummocky megaripples" is inapplicable to almost all known examples of the structure, and suggests mutually exclusive generative processes for megaripples and hummocky cross-stratification. This discrepancy in grain-size ranges has previously been noted by Southard (1984).

Absence of a continuous spectrum between hummocky cross-stratification and trough cross-bedding in ancient sequences. In the shelf flows described by Swift et al. (1983), the wave-orbital (multidirectional) component decreases steadily with depth relative to the geostrophic (unidirectional) component. Likewise, depending upon local temporal and spatial variations in naturally variable shallow-marine flows, different storms would produce different combinations of unidirectional and multidirectional components of flow in the same depths of water. Thus, the model of Swift et al. (1983) predicts the presence of a continuum of structures intermediate between hummocky cross-stratification and trough cross-bedding in ancient shallow-marine sequences. No such spectrum of structures has been reported. The absence of such a

spectrum is consistent with the grain-size differences discussed above.

Mutually exclusive occurrence of hummocky cross-stratification and trough cross-bedding in ancient sequences. Due to natural variability in the relative strength of unidirectional and multidirectional components in shallow-marine flows such as those described by Swift et al. (1983), the process they propose would predict a close lateral and vertical association in ancient sequences between hummocky cross-stratification and trough cross-bedding (and possibly planar-tabular cross-bedding). However, high-angle trough cross-bedding produced by megaripples is conspicuously absent from most ancient occurrences of hummocky cross-stratification (as is high-angle planar-tabular cross-bedding produced by sandwaves -- but see further discussion under "process 6" below).

The mutually exclusive, non-gradational relationship between hummocky cross-stratification and trough cross-bedding in ancient sequences is fully consistent with the differences in grain-size ranges discussed above.

Inconsistency of observed and predicted vertical sequences involving hummocky cross-stratification. Swift et al. (1983, p. 1311) indicate that "hummocky megaripples"

on the Atlantic shelf occur laterally adjacent to normal megaripples formed by geostrophically balanced flows in slightly greater water depths (30 m or more), below the influence of surface storm waves. The same relationship should presumably exist in shelf sequences (both prograding and transgressive) preserved in the stratigraphic record. There have been over 100 studies of ancient prograding and transgressive sequences involving hummocky cross-stratification (many of which are summarized by Duke, 1985c); none reports trough cross-bedding formed in inferred deeper-water sediments adjacent to hummocky cross-stratification. The majority either do not report trough cross-bedding, or place it in shallow-water nearshore sands slightly coarser than the hummocky sands (Duke, 1985a, 1985b, 1985c -- but see reservation below).

Formation of high-angle cross-bedding by combined-flow megaripples. Swift et al. (1983, p. 1310) remark that very little information is available for combined-flow bedforms. However, the limited available studies indicate that megaripples formed by combined flows with significant unidirectional components exhibit fairly steep foresets (roughly 20°) and equally high-angle internal cross-bedding, not hummocky cross-stratification (see summaries by Clifton, 1976, and Harms et al:, 1982, chapter 2). There is at present no evidence for the rotary

"scrubbing" process suggested by Swift et al. (1983).

Absence of evidence for hummocky cross-stratification from locations studied. Evidence presented by Swift et al. (1983) for formation of hummocky cross-stratification by "hummocky megaripples" consists of three side-scan sonar records and the tracings of laminae from two box cores taken from the U.S. Atlantic shelf, where storm-induced combined flows composed of unidirectional and multidirectional components are well documented. Actual dip of cross-strata in the cores was not reported. The authors suggest that these cores and sonar records reveal hummocky cross-stratification and hummocky megaripples, respectively.

Elsewhere I have argued that these box cores probably have not penetrated hummocky cross-stratification, inasmuch as the internal cross-strata display apparent dips (i.e., minimal dips) as high as 31° (Duke, 1985c, Fig. 7). In light of the high-angle cross-strata displayed in the cores, the topography on the sonar records is best interpreted as slightly rounded and wave-reworked megaripples (Duke, 1985c). Alternatively, this topography may represent washed-out dunes formed under purely unidirectional flows near the transition to upper flat bed. High-angle cross-strata (in part) would be expected in either case.

The suggestion that these box cores have penetrated trough cross-bedding rather than hummocky cross-stratification is fully consistent with the reported grain size of the sediment (uppermost fine sand). Megaripples and trough cross-bedding are commonly observed in this size sediment, but hummocky cross-stratification is very rare.

Preservation potential of combined-flow megaripples formed by geostrophically balanced flows. The combined-flow megaripples described by Swift et al. (1983) generally occur superimposed upon the stoss sides of much larger sandwaves with spacings of about 100 to 200 m and heights of about 1 m. Stoss sides of sandwaves are composed of fine sand; troughs are composed of medium sand. Lee sides of Atlantic-Shelf sandwaves apparently are moderately steep, locally attaining the angle of repose (Swift et al., 1977, 1978).

Swift et al. (1983, p. 1312) state that these sandwaves would be "almost undetectable in outcrop". This contention remains to be demonstrated, especially in the progradational settings from which hummocky cross-stratification is most commonly reported. It seems probable that the troughs and inclined lee faces of the sandwaves are more likely to be preserved than are the megarippled stoss sides, as is generally the case with large sandwaves in ancient sequences. This is especially

likely in progradational settings, due to vertical aggradation of sediment and preferential preservation of the lower parts of the sandwaves. In such a situation, the resultant planar-tabular or compound cross-bedding would be detectable in outcrop, and would not resemble hummocky cross-stratification. Note, however, that stoss sides may well be generally preserved as relict features during periods of rapid deepening, when sandwaves are passively draped by distal shelf muds.

Sandwaves typically are the major bedform present on modern shelves dominated by geostrophically balanced flows, and "hummocky megaripples" apparently are closely associated with these larger bedforms in all or most occurrences (Swift et al., 1983, and references contained therein). A complete knowledge of the stratification produced by these bedforms (in combination) in a prograding shelf sequence, and the range of grain sizes in which they each are formed, is essential before we can properly evaluate the possibility of forming thick hummocky cross-stratified sequences on shelves dominated by tractional bedforms generated under geostrophically balanced flows.

Combined-flow megaripple model: Summary and discussion. Swift et al. (1983) have proposed a general model for formation of hummocky cross-stratification by

combined-flow megaripples. Their model cannot account for most ancient examples of this structure for the following major reasons:

1) Hummocky cross-stratification is generally formed in grain sizes much smaller than about Ø.1 - Ø.2 mm. Megaripples do not form in sediment of this size.

2) In the proposed model, natural variability of shallow marine flows and variation in the relative strength of flow components with depth would suggest the existence of a continuous spectrum within sands of a given grain size of structures intermediate between hummocky cross-stratification (formed by "hummocky megaripples") and trough cross-bedding (formed by normal megaripples). There is no evidence in ancient sequences for such a spectrum.

3) In the proposed model, natural variability of shallow marine flows would suggest common interbedding within sands of a given grain size of hummocky cross-stratification and trough cross-bedding; however, trough cross-bedding is conspicuously absent from hummocky associations in most occurrences.

4) Preserved structural sequences involving hummocky cross-stratification do not resemble those predicted by the model. In particular, the model predicts trough and/or planar-tabular cross-bedding in sediments deposited in deeper water adjacent to hummocky

cross-stratified deposits. This relationship is not generally reported from ancient sequences.

5) Swift et al. (1983) fail to present convincing evidence for the presence of hummocky cross-stratification within the recent examples of "hummocky megaripples" they describe. Their own evidence reveals the formation of high-angle trough cross-bedding instead.

6) The preservation potential of "hummocky megaripples" formed by combined unidirectional and oscillatory flows is probably very low, because they generally will occur superimposed upon the stoss sides of much larger sandwaves. The stoss sides of these larger bedforms probably are not generally preserved in prograding sequences. They may be preserved as relict features blanketed by mud in transgressive sequences.

Additionally, note that: 1) combined-flow megaripples are known to contain fairly high angles of cross-stratification much steeper than hummocky cross-strata (see summaries by Clifton, 1976, and Harms et al., 1982), and 2) there is at present no evidence for the total inhibition of slip-face development by the "rotary scrubbing mechanism" suggested by Swift et al. (1983).

In conclusion, a comparison of hummocky cross-stratification from ancient sequences and combined-flow megaripples from modern environments

eliminates the possibility of a common genesis. Therefore, the geological "double standard" of Swift et al. (1983) is a reasonable distinction to maintain.

Discussion of Allen's support of the combined-flow hypothesis. Allen (1985) has recently attempted to bring a quantitative analysis to the largely speculative debate over the origin of hummocky cross-stratification. He purports to demonstrate that an origin under purely oscillatory flow is impossible, thus indicating the necessity of a combined-flow involving oscillatory and unidirectional components. Unfortunately, Allen's conclusions overstep their analytical basis, which itself is not well-founded. His analysis proceeds from the false assumption that all proponents of oscillatory flow suggest formation at the transition from post-vortex ripples to wave-formed flat bed, as was tentatively suggested by Dott and Bourgeois (1982); however, this does not constitute the only possible oscillatory-flow origin. For example, Southard (1984) envisions an origin due to migration of vortex ripples on an aggrading bed, and I have suggested formation within the wave-formed flat-bed field (Duke, 1984; Duke & Leckie, 1984). How can we reconcile these suggestions (discussed in detail above) with Allen's analysis?

Let us start with Southard's idea. Allen's

refutation hangs on his assertion that the ratio of bottom orbital diameter (d_o) to the spacing of ripples (λ_m) is well-known over the appropriate range of grain size and near-bed flow parameters. Assuming a reasonable range of these parameters, calculated values of λ_m are far smaller than spacings observed in hummocky cross-stratification; thus, hummocky cross-stratification cannot be formed by purely oscillatory flow. However, Allen's empirical relationships are based upon a very limited set of data, collected mainly from small oscillating-bed devices (such as employed by Manohar, 1955); while this type of device may be useful for studies of incipient motion, the unrealistic geometry makes it unsuitable for studies of general motion and ripple growth at high Reynolds-numbers, for reasons involving unnatural accelerative forces, limitation of boundary-layer development, and the structure of generated turbulence (see further discussion in part 2 of this chapter). Additionally, the size of apparata employed in past experiments (including fixed-bed experiments) greatly restricts the maximum size that bedforms may attain.

Southard's experiments (see additional discussion above) in a large, fixed-bed, oscillating-flow water tunnel produced three-dimensional vortex ripples in very fine to fine sand with spacings of about 1 m. These spacings are much greater than those in the data set employed by Allen.

Southard's results demonstrate that an acceptable data base does not exist for the calculations Allen wishes to make.

My own suggestion for the origin of hummocky cross-stratification is based upon two unrelated paleohydraulic analyses of ancient sediments (Duke, 1984; Duke & Leckie, 1984). Both studies indicated formation of hummocky cross-stratification well within the wave-formed flat-bed field; they further indicate a near equality between the form-spacing of hummocky cross-stratification (λ_H) and the calculated value of d_o. This equivalence suggests that "flat bed" may not really be flat at all, but rather contains subtle undulations scaled by d_o which develop into hummocky cross-stratification as the bed aggrades. The near equality of d_o and λ_H are consistent with high Reynolds numbers and reduced inertial-lag effects. In evaluating these results, note that Clifton reported low-angle undulations within wave-worked sands described as flat in his older studies off the Oregon coast (Hunter & Clifton, 1982, p. 140).

I agree we must consider the fullest range of possibilities, including non-oscillatory flows. Allen implies that the only alternative to a strongly oscillatory-dominant flow is a combination of oscillatory and unidirectional flow. This ignores at least two other possibilities; namely, multidirectional flow and polychromatic oscillatory flow (see further discussion

elsewhere in this chapter). Neither of these flow classes necessarily involves a significant unidirectional component of flow. Thus, any future refutation of an origin under monochromatic oscillatory flow will not of necessity lead to the combined-flow hypothesis advocated by Allen.

Process 7: Generation Within the Unidirectional-Flow Upper Flat-Bed Field by Superimposed Wave-Induced Velocity Fluctuations

This process closely resembles that suggested by Swift et al. (1983), differing only in the replacement of megaripples with upper flat bed. This replacement is justified by and eliminates most of the difficulties described above. In this scenario, wave-induced second-order velocity fluctuations (either bidirectional or multidirectional) are responsible for the generation of irregularly-spaced mounds and scours within what would otherwise be planar parallel lamination deposited under unidirectional-flow upper flat-bed conditions.

Formation of hummocky cross-stratification by this process is supported by observed bedding sequences from the Late Proterozoic Johnnie Formation in S. E. California. My preliminary field work indicates that part of this formation is locally composed of a thick sequence of siltstones and very fine to coarse (pebbly) sandstones

interbedded with mudstone. Siltstone/sandstone beds are a few tens of centimeters thick; they possess sharp bases which generally display oriented directional sole marks, and tops which locally (rarely) display either symmetrical or asymmetrical ripples. In this interval, siltstones and very fine to fine sandstones generally are planar parallel laminated and/or hummocky cross-stratified (see Duke, 1985c, Fig. 1c & 1d), whereas medium and coarse sandstones display medium-scale trough cross-bedding and/or planar parallel lamination. Thus, hummocky cross-strata and trough cross-bedding are mutually exclusive on a bed-by-bed basis in this formation, and appear to be consistently segregated by grain size. This is the only example with which I am familiar (either from first-hand experience or from the literature) in which hummocky sandstones are intimately interbedded with trough cross-bedded sandstones; the rarity of such sequences probably reflects a generally higher level of sorting by grain size in shallow-marine environments than was present in the Johnnie basin.

It is reasonable to infer that the beds in this sequence were deposited by roughly the same class of flow (in this case, the inferred flows were unidirectional-dominant with minor oscillatory or multidirectional components). Unidirectional flows would have formed upper flat-bed parallel lamination in sediment finer than Ø.1 mm; but the superimposed wave-induced velocity fluctuations

modified the parallel lamination during deposition to form hummocky cross-stratification instead. Hydrodynamically similar flows formed planar parallel lamination or trough cross-bedding (depending upon flow strength and grain size) in the coarser sediments. The relatively weak wave-induced velocity fluctuations were not adequate to greatly modify parallel lamination in these grain sizes (formed by the strongest unidirectional flows in the basin), nor were they adequate to inhibit formation of steeply dipping foresets when megaripples were developed by slightly weaker unidirectional flows.

It is noteworthy that prominant convex-upward hummocks appear to be very rare or absent in the Johnnie; instead, hummocky beds are dominated by a multiplicity of very low-angle intersections of slightly curved laminae (Duke, 1985c, Fig. 1c & 1d). This morphological distinction is tentatively attributed to the dominance of a unidirectional component of flow in this unit, as compared to units like the Cardium, where a probable dominance by oscillatory flows is indicated by abundant symmetrical ripples (including conglomeratic symmetrical ripples), and hummocks are very well developed. This variation in the processes inferred to form hummocky cross-stratification may well prove to be the control over variation in the morphology of the structure in other stratigraphic units.

SUGGESTED GENERATIVE AGENTS OTHER THAN BOTTOM FLOWS RESULTING FROM PROGRESSIVE SURFACE GRAVITY WAVES

A wide variety of processes other than those involving progressive surface gravity waves have been suggested as possible generative agents for at least some examples of hummocky cross-stratification. The smoothly sinusoidal cross-sectional morphology of the structure, and the common association with small-scale symmetrical ripples have led most workers to suggest an origin involving some sort of naturally occurring wave phenomenon.

"Internal" Waves

Marsaglia & Klein (1983, p. 125) suggested the possibility that some examples of hummocky cross-stratification might be formed by "[breaking] internal waves separating stratified masses of opposite-flowing water". Breaking internal waves of this sort range greatly in scale, depth at which breaking occurs, speed of induced bottom flow, and nature of generation. They may be formed by shallow coastal jets, as for example, river-mouth surface jets of low-density fluid (due to reduced salinity), or storm-enhanced bottom rip currents of high-density fluid (due to increased suspended sediment). Wright & Coleman (1974) described their effects at the Mississippi River mouth.

On the deeper shelf (as far down as the shelf break, about 200 m) breaking internal waves may result from shoaling of meteorologically-induced interstratal waves propagating along surfaces of marked density stratification. The effects of these deeper breaking internal waves have not been extensively investigated. Southard & Stanley (1976) suggest that these waves may be capable of significant sediment transport, and formation of ripples or even sand waves, upslope of breaking.

I agree with the suggestion of Marsaglia & Klein (1983) that the possible significance of these waves in the formation of hummocky cross-stratification requires further study.

Helmholtz Waves

Marsaglia & Klein (1983) suggested the possibility that some sort of Helmholtz waves acting on the surface of a newly-deposited quick bed may be responsible for formation of some examples of hummocky cross-stratification. Experiments by Middleton (1967, p. 495) indicate that Helmholtz waves churn and shear underlying quick sediments, destroying existing stratification and producing a structureless and tabular bed instead. Conclusive evidence against formation by Helmholtz waves can be derived from the rock record. These ephemeral interstratal

waves must be formed during deposition from turbidity currents, and yet hummocky cross-stratification is conspicuously absent from deep-water sandy turbidites. In fact, the structure is only known from shallow-water environments. The logical conclusion is that hummocky cross-stratification is formed by surface gravity waves, and is not formed by Helmholtz waves.

Tsunamis

Dott & Bourgeois (1982) have suggested that tsunamis may be responsible for formation of some examples of hummocky cross-stratification. Previously, Goldring & Bridges (1973) had suggested tsunamis as a possible generative agent for "sublittoral sheet sandstones", most (possibly all) of which display hummocky cross-stratification (Duke, 1985c). Elsewhere I have argued (Duke, 1985c) that the paleogeographic and paleolatitudinal distributions of the structure strongly contra-indicate a principal origin due to tsunamis; these distributions support the preferred storm-origin hypothesis. It should be noted, however, that these distributions cannot eliminate the possibility of origin due to tsunamis for a relatively small percentage of known examples of the structure.

Wind

Marsaglia & Klein (1983) suggested that certain examples of hummocky and/or swaley cross-stratification could have been formed within eolian dunes, as the direct result of wind action. This interpretation is impossible, even if we disregard paleontological evidence (present in most examples) indicating subaqueous (generally submarine) origin. Firstly, the stratigraphic setting of hummocky and swaley cross-stratification (constrained between muddy offshore deposits and beach/nearshore deposits) generally eliminates eolian deposition (e.g., Harms et al., 1975; Hamblin & Walker, 1979; Dott & Bourgeois, 1982). Secondly, hummocky and swaley cross-stratification are distinctly dissimilar to structures found in eolian dunes. Even the dome dunes specifically suggested by Marsaglia & Klein (1983) contain an overwhelmingly predominant volume of high-angle cross-bedding (McKee, 1979). Hummocky and swaley cross-stratification are <u>never</u> characterized by predominant high-angle cross-bedding. Further, high-angle sets within dome dunes commonly exceed 1 to 3 m in thickness (McKee, 1979). In hummocky and swaley cross-stratification, the thickness of the <u>rare</u> high-angle sets is usually on the order of 1 to 10 cm; these thin sets were formed by wave ripples, small-scale current ripples, or (rarely) small submarine megaripples.

The characteristic hummock/swale morphology of hummocky cross-stratification, and the intersecting-swale morphology of swaley cross-stratification, are distinctive geometries not mimicked within any form of eolian dune.

Antidunes

The subject of a possible origin for hummocky cross-stratification due to three-dimensional antidunes has not been raised in the literature, despite the overall similarities between hummocky cross-strata and cross-strata known to be formed by antidunes in laboratory apparata and natural settings. This is presumably because the shallow-marine shelf-to-shoreface depositional setting of the structure intuitively precludes the possibility of forming antidunes with the appropriate characteristics. The possibility of such an origin is explored quantitatively below.

The equations relating antidune characteristics to generative flow parameters are well known, mainly from theoretical and experimental work of Kennedy (e.g., Kennedy, 1963). There are two general cases for which numerical solutions are easily obtained; these are examined below.

"Free-surface" antidunes. The first case involves antidunes forming below a free surface, as in open-channel flow. The spacing (λ_m) of free-surface antidunes is

directly related to the mean flow velocity (U) by the equation

$$U^2 = g \lambda_R / 2\pi \qquad (8\text{-}1)$$

where g is the acceleration due to gravity (980 cm/sec^2). A characteristic wavelength for the undulatory lamination in hummocky cross-stratified sandstones is approximately 250 cm. Substitution of this value for λ_R in expression 8-1 yields a free-surface mean flow velocity of 200 cm/sec.

Antidunes form only at Froude numbers (Fr) between 0.8 and 1.2, where Fr is given by

$$Fr^2 = U^2 / gh \qquad (8\text{-}2)$$

In expression 8-2, h is the depth of free-surface flow. Combining expressions 8-1 and 8-2, and solving for h yields

$$h = \lambda_R / 2\pi Fr^2 \qquad (8\text{-}3)$$

Note that the gravity terms cancel. Substituting in expression 8-3 the specified value for λ_R (250 cm) and the extreme values of Fr (0.8 and 1.2) yields a depth range of 28 to 62 cm. Less common (but by no means rare) wavelengths of 100 and 400 cm expand the depth range somewhat (11 to 99 cm).

This analysis suggests that hummocky cross-stratification, if formed by three-dimensional

free-surface antidunes, can only be formed in water depths less than about 100 cm by very high-speed flows on the order of 200 cm/sec. Such shallow depths and high mean flow speeds are completely inconsistent with the well established shelf-to-shoreface depositional environment inferred for the structure in numerous studies (summarized above). An origin due to free-surface antidunes can therefore be eliminated.

"Stratified-underflow" antidunes. The second case for which we can easily obtain numerical solutions involves antidunes formed under a two-layer stratified underflow, as, for example, a turbidity current. Antidunes of this sort are occasionally observed in deep-water turbidites (e.g., Blatt et al., 1980, Fig. 5-13); they bear a strong resemblance to hummocky cross-stratification.

In the case of an underflow, expressions 8-1 and 8-3 above are modified by the addition of a densiometric gravity term which can be written as

$$g' = \left[\Delta\rho / (\rho + \Delta\rho) \right] g \qquad (8\text{-}4)$$

where ρ is the density of the overlying fluid (for water, 1.0 g/cm^3) and $\Delta\rho$ is the excess density in the sediment-laden underflow. In natural subaqueous turbidity currents, typical values of $\Delta\rho$ rarely exceed 0.1 g/cm^3 (Blatt et al., 1980, p. 177-182). Substitution of the

values of ρ and $\Delta\rho$ specified above yields a g' value of 89 cm/sec^2.

The modified versions of relationships 8-1, 8-2, and 8-3 are

$$U^2 = g' \lambda_R / 2\pi \qquad (8\text{-}5)$$

$$(Fr')^2 = U^2 / g' t \qquad (8\text{-}6)$$

and

$$t = \lambda_R / 2\pi (Fr')^2 \qquad (8\text{-}7)$$

respectively. Again, the gravity terms cancel in 8-7. In the modified expressions, t is the thickness of the underflow. Solving expressions 8-5 and 8-7 for the assumed value of g', λ_R equal to 250 cm, and the extreme values of the densiometric Froude number (0.8 and 1.2) yields an underflow velocity U of 60 cm/sec, and a range of underflow thickness t of 28 to 62 cm. Under approximately these conditions, the antidune bed configuration would typically be superimposed upon upper flat bed or small ripples in the fine to very fine sand sizes (Harms et al., 1982, Fig. 2-4a).

Such modest underflow thicknesses and velocity are reasonably consistent with the concept of storm-generated shallow-shelf turbidity currents (or other types of underflow on the shelf). Note that these values explain

the rarity of antidunes within deep-water turbidites, which presumably are in general much thicker and/or faster flowing. What are some of the implications of this hypothetical process of formation?

There are several observations from hummocky beds supporting such an origin. In particular, purely unidirectional flows are consistent with the common observation of aligned sole marks at the bases of beds. Also, the high values of Froude number required for antidune formation imply extensive mixing between the two layers. The resulting entrainment of clear overlying fluid would cause the following two effects:

1) Entrainment would cause a slow decrease in flow velocity once the underflow had either passed by or been "turned off" by the generating agent (no matter how rapidly the underflow was turned off). Slowly waning clear-fluid flows passing over the newly-formed antidunes could commonly generate a suite of tractional bed configurations, thus modifying the antidunes and capping them (in very fine sands) with flat bed and/or small asymmetrical ripples. The "flat" lamination of division F might be formed in this way, as well as uncommon asymmetrical ripples in the overlying division X. The much more common symmetrical ripples of this division could simply represent syn- or post-depositional wave-reworking of the uppermost laminae

in the bed.

2) Alternatively, clear-fluid flow could re-suspend newly-deposited sand, resulting in erosional planing of the top of the bed. Hummocky sandstones commonly display sharp planar (or locally scoured) contacts with overlying mudstones, truncating underlying sandstone laminae.

There are several difficulties with this hypothetical origin of the structure. Firstly, variation in underflow speed and thickness from one depositional event to another would predict common interbedding of hummocky sandstones with beds of roughly equal thickness that do not display the structure, but rather display only parallel lamination and/or asymmetrical ripples, or two-dimensional antidunes. Such sequences have not been reported from the geologic record. Secondly, mixing at the interstratal contact would rapidly decrease overall mean flow speed and thicken the underflow, thus inhibiting the formation of antidunes; again, both lateral and vertical variation in structures would be the expected consequence. Thus, the general homogeniety and widespread lateral extent of reported occurrences of hummocky cross-stratification argues against a general origin due to three-dimensional antidunes formed by a stratified underflow.

In summary, the formation of hummocky cross-stratification by three-dimensional antidunes under a

high-Froude-number stratified underflow is hydrodynamically possible on the shoreface and proximal shelf, but is contra-indicated by the lack of association vertically and laterally with tractional structures formed by unidirectional flow. Further research into this possible mode of origin is strongly indicated.

SUMMARY AND DISCUSSION

In the preceding discussion, I have attempted to summarize and evaluate several of the many processes that have been suggested for the generation of hummocky cross-stratification, and to identify the most likely generative processes. In my opinion, evidence from ancient sequences strongly supports generative processes that involve formation within the wave-generated flat-bed and/or vortex-ripple field, and/or formation due to wave modification of unidirectional-flow upper flat bed. The most likely generative processes for at least some examples of hummocky cross-stratification include:

1) Generation within the oscillatory-flow vortex-ripple field by three-dimensional orbital vortex ripples formed under either a monochromatic wave spectrum (Southard, 1984) or a polychromatic wave spectrum (this paper).

2) Generation under oscillatory- or multidirectional-dominant flows within the wave-formed flat-bed field by flat-bed mantling of a pre-existing, storm-generated, hummocky erosional topography (Harms et al., 1975; Dott & Bourgeois, 1982).

3) Generation under oscillatory- or multidirectional-dominant flows within the wave-formed flat-bed field by superimposed velocity fluctuations due to wave-wave interactions under a natural polychromatic wave spectrum (Bourgeois & Smith, 1984; this paper).

4) Generation under oscillatory-dominant flows within the wave-formed flat-bed field by previously unrecognized, low-amplitude, three-dimensional orbital ripples (Duke, 1984; Duke & Leckie, 1984).

5) Generation within the unidirectional-flow upper flat-bed field by superimposed wave-induced velocity fluctuations (this paper).

Evidence supporting each of these processes is summarized and discussed above. Note that these processes are not necessarily mutually independent. For example, the vortex ripples of processes 3 and 4 might be significantly modified by very large velocity excursions (as were invoked in process 2) generated beneath a natural polychromatic and/or mutidirectional wave spectrum. Such excursions could result in rapid, localized transitions between the

vortex-ripple field and the flat-bed field, forming a complex stratification geometry. For another example, the "flat-bed" orbital ripples of process 5 might be genetically related to and intergradational with the vortex ripples of processes 3 and 4. The wide spectrum of stratification styles currently lumped together under the name "hummocky cross-stratification" (see examples figured by Dott & Bourgeois, 1982, and Walker et al., 1983) strongly suggests such a polygenetic and/or intergradational origin.

PART 2

PALEOHYDRAULIC ANALYSIS OF CONGLOMERATIC SYMMETRICAL RIPPLES

INTRODUCTION: SYMMETRICAL RIPPLES AS PALEOHYDRAULIC INDICATORS

For over a century, geologists have recognized that progressive surface gravity waves are capable of forming symmetrical ripples in sediment. Over the years, numerous laboratory and field studies have related ripple parameters to generative wave parameters. These studies have been summarized and expanded by Clifton (1976), J. R. L. Allen (1979), Dingler (1979), Miller and Komar (1980a, 1980b), P. A. Allen (1981, 1984), Southard (in Harms et al., 1982), and Clifton & Dingler (1984). Despite this interest, the usefulness of ancient symmetrical ripples in the determination of generative fluid-motion characteristics and paleobathymetry has remained extremely limited. At present, it is impossible to uniquely determine the conditions under which any ancient symmetrical ripples were formed, unless: 1) there exists independent evidence for water depth and wave parameters (see, for example, Clifton, 1976, p. 133-134, or Komar, 1974, p. 175-176), or 2) it is assumed that the

ripples in question were formed at or near the threshold of sediment motion. Below I discuss the threshold-motion method for the determination of generative fluid-motion characteristics for a certain broad class of symmetrical ripples.

PLEASE NOTE: The analysis presented herein is not original with this author. I have merely brought a slightly different approach to similar analyses presented by previous workers (see references above).

SYMMETRICAL RIPPLE MORPHOLOGY

Southard (in Harms et al., 1982, chapter 2) has reviewed the types of ripples generated in quartz-density sands by oscillatory flow, and the range of conditions under which each forms. These bedforms may be grouped into five categories: rolling-grain, vortex, post-vortex, reversing-crest, and transitory asymmetrical ripples. Typical flow-parallel profiles of these ripples are illustrated in figure 8-3. Vortex ripples are stable over a much wider range of flow conditions and sediment sizes than are the other varieties. In ancient sediments, vortex ripples are easily distinguished from the other ripple types by their high height-to-spacing ratio.

Vortex ripples can be either straight-crested and two-dimensionally symmetrical or equant, three-dimensional,

and radially symmetrical. Two-dimensional vortex ripples (Fig. 4-7C to 4-7F) are familiar to all sedimentologists; crests are aligned normal to the direction of wave propagation, and spacings generally are very uniform and easily measured in the field. In contrast, small three-dimensional vortex ripples are not commonly encountered in either modern or ancient deposits. Figure 4-7G shows ancient three-dimensional vortex ripples formed in fine sand; previously, these ripples have only been reported from laboratory experiments (Carstens et al., 1969; Lofquist, 1978; Southard, 1984). Their spacing is not readily characterized in the field without extensive plan-view exposure.

Straight-crested vortex ripples possess either smoothly rounded profiles (sinusoidal ripples) or relatively narrow, pointed crests and smooth, broad troughs (trochoidal ripples). Grain size ranges over a continuous spectrum from at least very fine sand to small pebble sizes. Likewise, spacing is continuously variable from a few centimeters to well over a meter; in the absence of a natural break in spacing or grain size, all symmetrical bedforms are herein referred to as "ripples" regardless of size.

In the remainder of this paper, only two-dimensional vortex ripples will be considered.

Figure 8-3. Typical flow-parallel profiles of ripples generated under oscillatory flow. From Harms et al. (1982, Fig. 2-9).

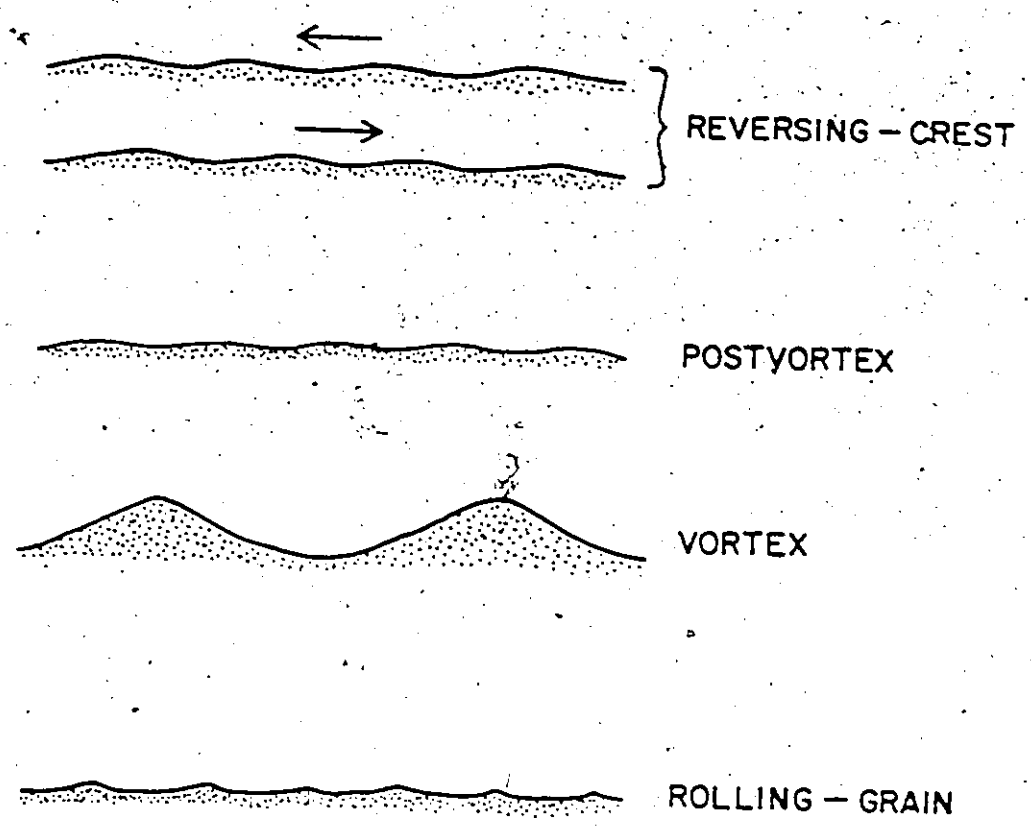
REVERSING – CREST
POSTVORTEX
VORTEX
ROLLING – GRAIN

CALCULATION OF BOTTOM ORBITAL DIAMETER FROM RIPPLE PARAMETERS

Figure 8-4 shows diagrammatically the relationship between the fluid-motion characteristics d_o, U_m, and T. For deep-water waves, these are related exactly by

$$d_o = U_m T / \pi \qquad (8\text{-}8)$$

This relationship is a very close approximation for intermediate- and shallow-water waves, in which water-particle orbitals are <u>not</u> closed loops. Through Airy (linear) wave theory, d_o is further related to generative wave parameters by

$$d_o = H / \sinh (2\pi h / L) \qquad (8\text{-}9)$$

The wave length L can be closely approximated by

$$L = L_{DEEP} \left[\tanh (2\pi h / L_{DEEP}) \right]^{1/2} \qquad (8\text{-}10)$$

from EcKart (1952), where

$$L_{DEEP} = g T^2 / 2\pi \qquad (8\text{-}11)$$

Straight-crested symmetrical vortex ripples fall into two categories with respect to d_o:

1) orbital ripples, for which $\lambda_m \propto d_o$;

2) anorbital ripples, for which $\lambda_m \propto D$.

Note, however, that a dispute exists in the literature regarding this two-fold classification. The disparate views have been summarized most recently by Clifton & Dingler (1984), who prefer the three-fold classification of Clifton (1976). This scheme involves the following third category of vortex ripples, additional to orbital and anorbital ripples:

3) suborbital ripples, for which ripple spacing depends upon both bottom orbital diameter and sediment grain size in some undetermined relationship.

Specifically, Clifton & Dingler (1984) contend that vortex ripple spacing increases in proportion to d_o (as orbital ripples) until a maximum spacing is achieved. Then, as d_o increases, spacing first decreases (suborbital ripples) and then stabilizes (anorbital ripples) at a value controlled by D. A further increase in d_o will not alter this final value of spacing.

Utilizing all available field and suitable experimental data, Clifton & Dingler (1984) presented a plot (their Fig. 5a, reproduced herein as Fig. 8-3.5) of two dimensionless groupings of variables (λ_r/D vs. d_o/D). This plot ostensibly supports their position by revealing a

Figure 8-3.5. Plot of dimensionless ripple spacing vs. bottom orbital diameter, from Clifton & Dingler (1984, Fig. 5a). Field observations are indicated by crosses; circles represent data from experimental apparata (wave channels and water tunnels only).

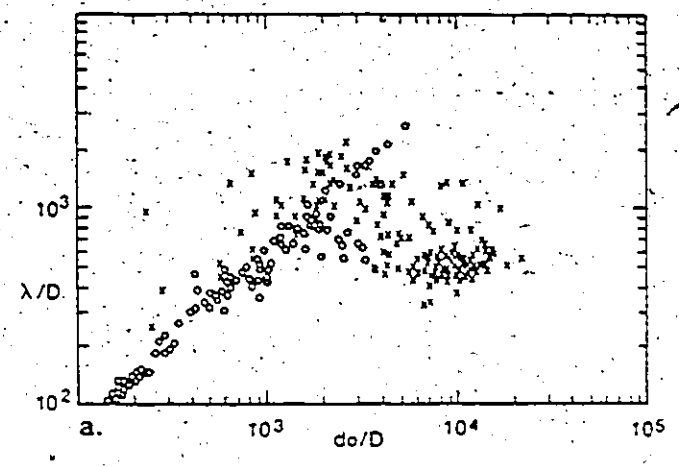
10^3
λ/D
10^2
a.
10^3
d_o/D
10^4
10^5

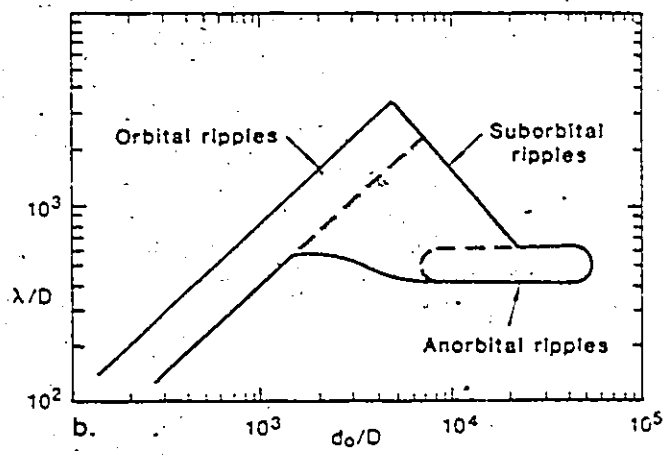
Orbital ripples
Suborbital ripples
10^3
λ/D
Anorbital ripples
10^2
b.
10^3
d_o/D
10^4
10^5

bell-shaped distribution of points. However, there are two problems with this plot: Firstly, the data are widely scattered, and the bell-shape is equivocal. Secondly, by choosing dimensionless variables, the pattern of variation for any given grain size cannot be resolved. It is quite possible that certain grain sizes do display a spacing decrease as d_o increases beyond the value associated with the maximum spacing, whereas other grain sizes do not display such a decrease. There is no *a priori* reason to suppose that the terminal ripple spacing is either less than or equal to the maximum ripple spacing in all grain sizes.

Given the disparity of opinion among the various workers in this field, and the lack (in my opinion) of substantive evidence one way or another, no attempt shall be made herein to evaluate the relative validity of the alternative views. At any rate, this distinction is not relevant to the analysis presented below, because those particular ripples discussed below are best interpreted as orbital ripples in either of the two systems of genetic classification. In the remainder of this chapter, I shall distinguish between only orbital and anorbital ripples. The reader should nonetheless bear in mind the uncertainties discussed in the paragraphs above.

Following an extensive review of field and laboratory data, Miller and Komar (1980) developed empirical relationships relating d_o to ripple properties. For two-dimensional (straight-crested) orbital ripples,

$$\lambda_R \simeq 0.65\, d_o \qquad (8\text{-}12)$$

Orbital ripples form at relatively low values of d_o; as d_o increases, λ_R increases to a maximum value determined by D. This maximum spacing is tentatively given by

$$\lambda_{MAX} \simeq 0.0028\,(10{,}000\,D)^{1.68} \qquad (8\text{-}13)$$

where both λ_{MAX} and D are in centimeters. Thus, ripples which possess a spacing less than λ_{MAX} are orbital ripples; those which possess a spacing equal to λ_{MAX} are anorbital ripples. Combining expressions 8-12 and 8-13 permits calculation of the critical value of d_o^T at which the transition from orbital to anorbital ripples occurs:

$$d_o^T = 0.0043\,(10{,}000\,D)^{1.68} \qquad (8\text{-}14)$$

Again, both d_o^T and D are given in centimeters. At values of d_o^T in excess of d_o, λ_R either remains constant or may actually decrease slightly. Again, this relationship is for two-dimensional, straight-crested ripples; it does not necessarily apply to three-dimensional ripples. In fact, recent experimental work reported by Southard (1984) indicates that the maximum spacing of three-dimensional

Figure 8-4. Diagrammatic relationship between fluid-motion characteristics under progressive surface gravity waves.

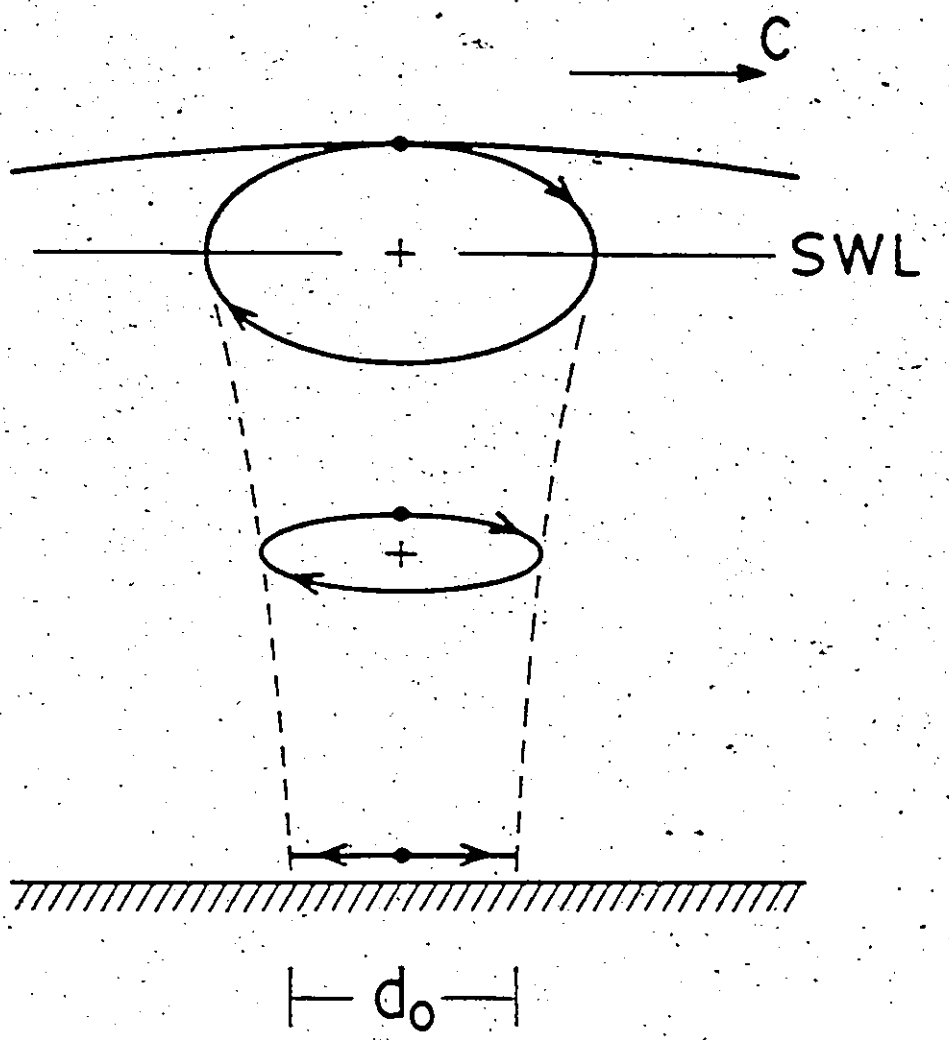

$$d_o = U_m T / \pi$$

vortex ripples may be much greater than that for two-dimensional ripples in some grain sizes.

The empirical relationships of expressions 8-12 through 8-14 were derived by Miller and Komar (1980) from experiments involving quartz-density particles no larger than coarse sand. Extrapolation of these results into gravel size ranges involves inherent uncertainties; however, in the absence of additional laboratory data, such extrapolation is required for the analysis of coarser deposits. Note, however, that these relationships can be tested for ripples formed in coarse sediment utilizing data from field studies of recent conglomeratic symmetrical ripples (see below).

Figure 8-5 shows the variation in d_o^T with grain size for quartz-density particles, as determined by expression 8-14. Note that d_o^T increases rapidly with grain size. Assuming that geologically significant oscillatory flows generated by stable (non-breaking) waves have maximum values of T and U_m equal to 20 s and 5 m/s, respectively, expression 8-8 can be used to calculate the maximum value of d_o^T for geologically significant flows. This figure is approximately 32 m; it probably represents a gross over-estimation. In expression 8-13, a d_o^T value of 32 m corresponds to a grain size of 0.31 cm, suggesting that for grain sizes greater than about 0.31 cm, all two-dimensional symmetrical ripples are orbital ripples.

For grain sizes less than 0.31 cm, the distinction between orbital and anorbital ripples can be determined from expression 8-13. In all cases involving orbital ripples, d_o can be determined from expression 8-12. These determinations require knowledge of D and λ_w only; these parameters are easily measured in ancient occurrences.

Note that the uncertainty in the determination of d_o from D and λ_w is sufficiently great (due to data scatter) that use of the more accurate Stokes theory in expressions 8-8 through 8-14 is not warranted.

Test of Method for Determining Bottom Orbital Diameter from Two-Dimensional Ripples Formed in Coarse Sediment

As stated above, the extrapolation of expressions 8-12 through 8-14 (developed largely from experimental studies) in application to naturally-occurring two-dimensional ripples formed in coarse sediment involves inherent uncertainties. It is therefore prudent to test these relationships against data from field studies of recent coarse-grained ripples.

To my knowledge, there is only one field study of actively forming conglomeratic symmetrical ripples involving simultaneous measurement of depth, sediment and ripple characteristics, and parameters of generative waves. This study was conducted by Gillie (1979) off the coast of

Figure 8-5. Variation in d_o^T with grain size for quartz-density particles. Heavy solid line indicates region in which this relationship is established from field and laboratory data; light lines are extrapolated values. Dashed line indicates theoretical values of d_o^T which probably are never achieved in natural flows. The d_o^T line separates the orbital and anorbital ripple fields.

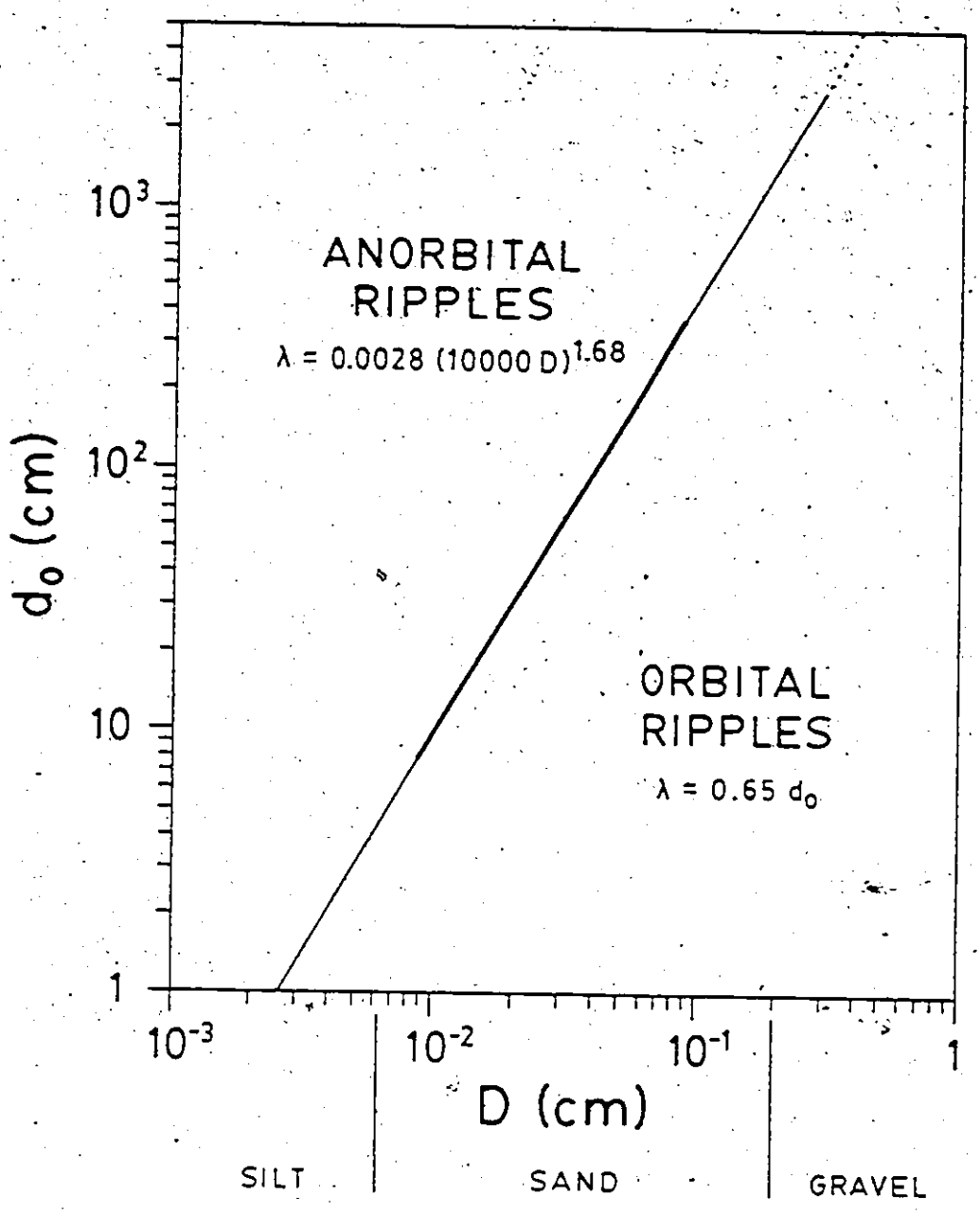
ANORBITAL
RIPPLES
λ = 0.0028 (10000 D)^1.68
ORBITAL
RIPPLES
λ = 0.65 d_o
d_o (cm)
10^3
10^2
10
1
10^-3
10^-2
10^-1
1
D (cm)
SILT
SAND
GRAVEL

New Zealand. Sinusoidal to trochoidal symmetrical ripples were observed during the process of formation in 18.3 m water depth; height and period of generative waves were also measured. These ripples were formed in quartz-density coarse to very coarse pebbly sand (mean grain size 0.09 cm, with abundant pebbles to 3.2 cm and larger).

Tables 8-1 and 8-2 summarize data from this study. In these tables, "calculated" values of d_o were derived by this author from depth and wave parameters using Airy wave theory; "predicted" values were obtained from grain size and ripple spacing using the relationships of expressions 8-12 to 8-14, as illustrated graphically in figure 8-6.

A graph of measured vs. predicted values of d_o is presented as figure 8-7. Note the very close agreement between the two sets of values. The relative error of any measurement is defined as

$$\text{relative error} = \frac{|\ \text{actual value} - \text{measured value}\ |}{\text{actual value}} \qquad (8\text{-}15)$$

Relative errors for individual measurements from these ripples are summarized in table 8-3. The mean relative error between predicted and measured values of d_o is 12.0%; the range of relative error is 5.3% to 19.6%. This close agreement suggests that the relationships of expressions 8-12 to 8-14 are applicable to straight-crested conglomeratic symmetrical ripples.

DETERMINATION OF FLOW CONDITIONS IN THE BOUNDARY LAYER

Unidirectional flow over flat beds of sediment can be either laminar or turbulent. Turbulent flows can be characterized as hydraulically smooth, transitional, or fully rough, depending upon the value of the boundary Reynolds number

$$Re_D = (\tau/\rho)^{1/2} D/\nu \qquad (8\text{-}16)$$

Specifically,

$Re_D < 5$ laminar or smooth turbulent flow

$5 < Re_D < 70$ transitional turbulent flow (8-17)

$Re_D > 70$ fully rough turbulent flow.

For oscillatory flow, the maximum shear stress is given by

$$\tau_m = (f_w/2)\,\rho\, U_m^2 \qquad (8\text{-}18)$$

and the maximum boundary Reynolds number becomes

$$Re_D = (f_w/2)^{1/2}\, U_m D/\nu \qquad (8\text{-}19)$$

Jonsson (1967) gives a graphical solution for the wave friction factor f_w, analogous to the Moody diagram used to determine the Darcy-Weisbach friction factor for steady, uniform unidirectional flow. The value of f_w is a function of Re_D and the inverse relative roughness d_o/D. This diagram is referred to herein as the Jonsson diagram,

Table 8-1. "Measured" values of generative wave parameters for recent ripples formed in a water depth of 18.3 m. Raw data (summarized as "observed" values) are from Gillie (1979, table 8.3). Assumed value of fluid property ρ is 1.025 g/cm^3 (seawater, 15°C). All ripple trains formed in quartz-density coarse to very coarse pebbly sand (mean grain size 0.09 cm, with abundant pebbles to 3.2 cm and larger). Numbers in parentheses are the average of a range of values.

"observed"

#	λ_m, cm	H, cm	T, s
1	90	100-150	12
2	85	100-150	12
3	85	100-150	12
4	130	150-200	11
5	70	100-150	8-10
6	70	100-150	8-10
7	85	125-175	11
8	105	100-150	10-12

"calculated"

#	d_o, cm	d_o/D	U_m, cm/s
1	123-184 (153)	1360-2040 (1700)	32.1-48.1 (40.1)
2	123-184 (153)	1360-2040 (1700)	32.1-48.1 (40.1)
3	123-184 (153)	1360-2040 (1700)	32.1-48.1 (40.1)
4	163-217 (190)	1810-2410 (2110)	46.4-61.9 (54.2)
5	61-140 (100)	680-1560 (1120)	19.1-55.0 (37.1)
6	61-140 (100)	680-1560 (1120)	19.1-55.0 (37.1)
7	135-190 (163)	1500-2110 (1810)	38.7-54.2 (46.4)
8	93-184 (139)	1040-2040 (1540)	24.5-57.7 (41.1)

Table 8-2. "Predicted" values of generative wave parameters and depth for recent ripples (from data of Gillie, 1979). "Depth" calculated in final column is based solely upon fluid-motion characteristics (d_o, U_m, and T) assuming the full range of stable wave height. See text for explanation and discussion.

"predicted" values

#	d_o, cm	T, s	U_M, cm/s	h, m
1	138	10.4	41.9	<96
2	131	9.9	41.4	<86
3	131	9.9	41.4	<86
4	200	13.9	45.1	<181
5	108	8.5	39.9	<61
6	108	8.5	39.9	<61
7	131	9.9	41.4	<86
8	162	11.7	43.2	<124

Figure 8-6. Mean spacing of two-dimensional symmetrical ripples (λ_m) vs. mean grain size (D) for recent ripples studied by Gillie (1979) and Yorath et al. (1979). On this diagram, the field of spacings which do not occur naturally is ruled; the line of separation represents λ_{max}, as determined by expression 8-13. Ripples from the Gillie study definitely are orbital ripples; those from the study of Yorath and co-workers approach the maximum value of spacing in their grain size, and may represent anorbital ripples. See text for further discussion.

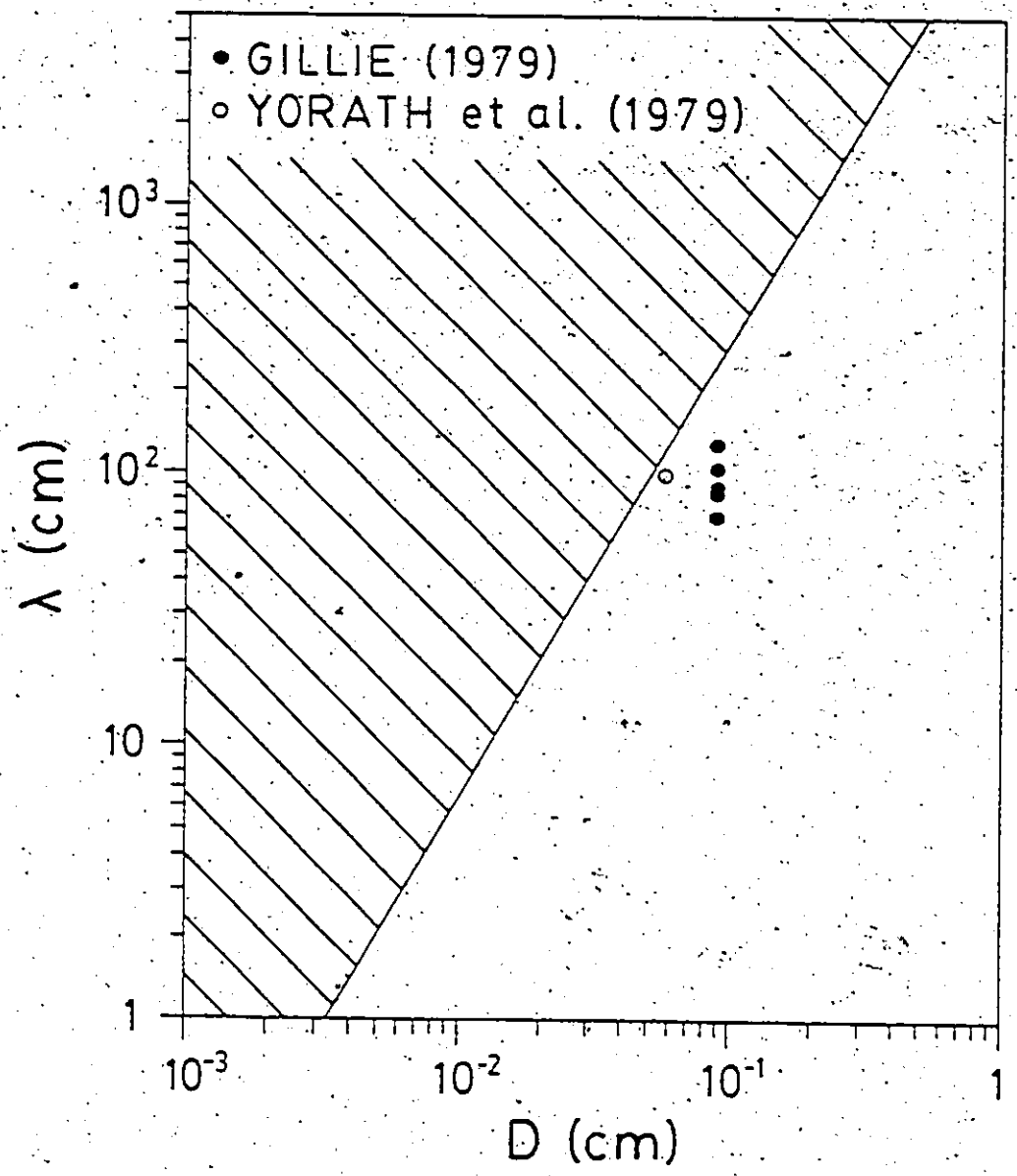
• GILLIE (1979)
○ YORATH et al. (1979)
λ (cm)
10³
10²
10
1
10⁻³
10⁻²
10⁻¹
1
D (cm)

Figure 8-7. Plot of "measured" vs. "predicted" values of d_o for recent ripples studied by Gillie (1979).

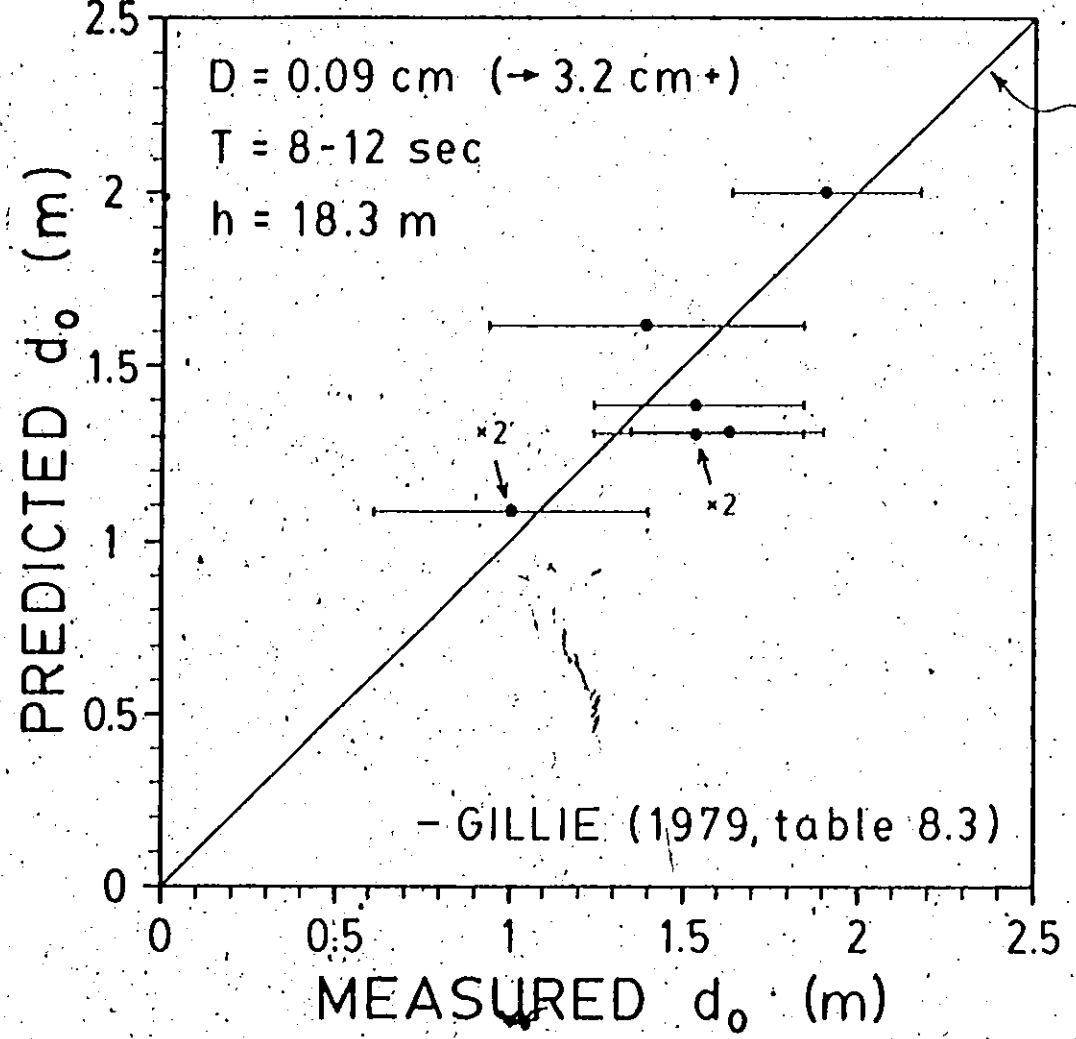

d_o (pred) = d_o (meas)

$\lambda = 0.65\ d_o$

MEAN RELATIVE ERROR = 12.0 %

614

Table 8-3. Relative error between measured and predicted values of generative fluid-motion characteristics, for recent ripples studied by Gillie (1979) and Yorath et al. (1979). See text for discussion.

n.a. = not applicable

	#	d_o	T	U_M
Gillie (1979)	1	9.8%	13.3%	4.5%
	2	14.4	17.5	3.2
	3	14.4	17.5	3.2
	4	5.3	26.4	16.8
	5	8.0	5.6	7.5
	6	8.0	5.6	7.5
	7	19.6	10.0	10.8
	8	16.5	6.4	5.1
	mean	12.0%	12.8%	7.3%
Yorath et al. (1979)		n.a.	9.2%	n.a.
mean of all data		12.0%	12.4%	7.3%

and is reproduced in slightly modified form as figure 8-8. [Note that the modifications to this figure involve simplification in the presentation of data, and the translation of variables to correspond to those used in this report.]

Use of the Jonsson diagram enables determination of flow conditions in the boundary layer from the measureable sediment parameter D, the assumed fluid parameter ρ_s, the calculable fluid-motion characteristic d_o, and the unknown fluid-motion characteristic U_m. A means for determination of U_m is outlined below. This technique assumes that flow conditions in the boundary layer are fully rough to transitional; this assumption can then be checked using the calculated value of U_m and the Jonsson diagram.

DATA SOURCES

There have been four detailed laboratory studies of the threshold of sediment motion under oscillatory flow in which grain sizes larger than medium sands were examined. These were conducted by Bagnold (1946), Manohar (1955), Rance & Warren (1968), and Dingler (1974, 1979). Of these studies, raw data are available for all except that of Rance & Warren (1968), who presented their data in dimensionless form. [Note: the experiments of Rance &

Warren (1968) were conducted at the Wallingford (England) Hydraulics Research Station; neither the personal files of the authors nor the station files preserve the original raw data (pers. comm., R. M. Shuttler, 1984).] The raw data from Manohar's study have been tabulated in appendix 9. Additionally, Manohar's data for quartz-density sediments has been converted to the units used in this report.

The initial-motion experiments of Bagnold (1946) and Dingler (1974, 1979) which utilized quartz-density sediments involve smooth and transitional flows only. This was determined in the Bagnold study by visualization of flow in the boundary layer, which was never observed to be turbulent. Dingler did not visually examine flow conditions in the boundary layer; conditions were calculated in his study by means of the Jonsson diagram. Additionally, Dingler did not explicitly state his definition of incipient motion (although he apparently used few-particle displacement as his criterion, as indicated by the close agreement with the Bagnold study). Bagnold explicitly stated use of this criterion; like Dingler, he did not investigate the onset of general sediment motion. For these reasons, their data are not examined in this report.

In contrast, the quartz-density data of Manohar (1955) did involve (in part) transitional and rough-turbulent flow conditions, which were visually

Figure 8-8. The Jonsson diagram for determination of f_w and flow conditions in an oscillatory boundary layer. After Jonsson (1967, Fig. 6).

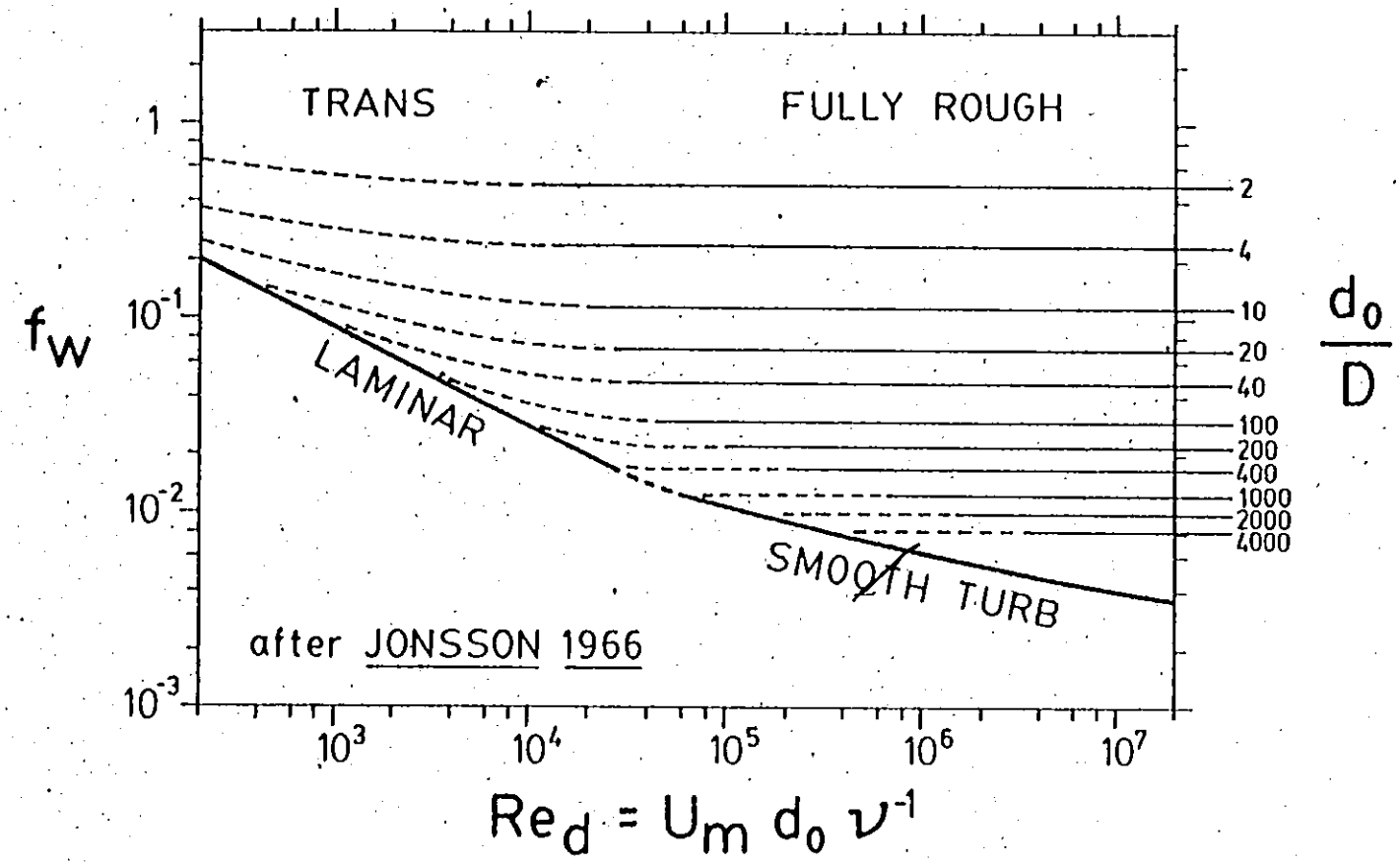
TRANS
FULLY ROUGH
LAMINAR
SMOOTH TURB
after JONSSON 1966
f_w
$\frac{d_0}{D}$
1
10^{-1}
10^{-2}
10^{-3}
2
4
10
20
40
100
200
400
1000
2000
4000
10^3
10^4
10^5
10^6
10^7
$Re_d = U_m\, d_0\, \nu^{-1}$

628

confirmed. Equally important, Manohar distinguished between few-particle displacement and many-particle displacement (general motion), and he presented data for both definitions of the threshold. The findings of Rance & Warren (1968) must also have been for fully-rough flow, given their use of granule- to pebble-size sediment; their results serve as a valuable confirmation of the results of Manohar (1955), which they closely approximate. This is of major importance in that the Manohar data were collected using an oscillating-bed device, whereas the Rance & Warren data were collected using the more reliable water-tunnel device (for discussions of experimental techniques, see Miller & Komar, 1980, and Harms et al., 1982, chapter 2). The unfortunate presentation (in dimensionless form only) of data from the Rance & Warren study, however, renders it impossible to further utilize their experimental results.

In the remainder of this analysis, I shall utilize only the data of Manohar (1955) to develop certain relationships pertaining to the onset of sediment motion under fully-rough turbulent oscillatory flow. These relationships shall be immediately applicable to the paleohydraulic analysis of conglomeratic symmetrical ripples. A discussion of possible problems arising from the use of data collected with an oscillating-bed device will be included at the end of this part of chapter 8.

THE DEFINITION OF INCIPIENT MOTION

When considering the geological significance of experimental studies of the threshold of sediment motion, it is important to understand the manner in which incipient motion was defined by the experimentalists. Both Manohar (1955) and Rance & Warren (1968) recognized that with fixed T and slowly increasing U_M, the following series of sediment-motion categories develops. First, at very low U_M values, no motion is observed. With increasing U_M, a broad band of conditions exists in which particles rock to and fro without actually moving position. At still higher U_M values, only a very small percentage of the particles are displaced downstream. Under these conditions, the few particles which move are those which project above the general level of a smooth, horizontal bed of sediment; the bulk of the sediment is never displaced downstream, and vortex ripples are not formed. Finally, with a small increase in U_M, many particles move during the course of one-half of the oscillation cycle. This latter category of sediment movement corresponds to the onset of general motion within the upper layer of grains in a horizontal, flat bed of sediment.

Thus, with fixed T and slowly increasing U_M, the sequence of sediment-motion categories may be designated as follows:

1) no motion

2) rocking motion

3) few-particle displacement

4) many-particle displacement

("general motion")

Note that both Manohar (1955) and Rance & Warren (1968) defined incipient motion as the onset of few-particle displacement. Only Manohar measured the onset of general motion.

The onset of few-particle displacement is not a geologically significant definition of incipient motion, because bedforms are not generated unless a significant fraction of the grains in the upper layer of sediment are able to be displaced from their original position. The onset of many-particle displacement, or incipient general motion, represents geologically significant incipient motion; when these conditions are maintained over several oscillation cycles, bedforms are developed. In some grain sizes, the first bedforms to develop are rolling-grain ripples; however, these are metastable structures under natural oscillatory flows. Over time, rolling-grain ripples are rapidly replaced in the sand sizes by straight-crested vortex ripples which are stable under incipient-motion conditions (Harms et al., 1982, chapter 2). It follows that straight-crested vortex ripples are

the stable bedform associated with incipient general-motion conditions (at least in the sand sizes -- see further discussion below); it is for this reason that the paleohydraulic analysis technique introduced herein is applicable to straight-crested vortex ripples only. [Three-dimensional vortex ripples occur only at significantly higher flow speeds for a given period -- see Harms et al., 1982, chapter 2.]

Manohar's (1955) examination of the onset of general motion is discussed in detail below.

EMPIRICAL RELATIONSHIP GOVERNING ONSET OF GENERAL MOTION UNDER TURBULENT FLOW

The quartz-density data of Manohar (1955) for both few- and many-particle displacement have been re-examined and grouped by maximum boundary Reynolds number (utilizing the Jonsson diagram, Fig. 8-8) as: 1) laminar or smooth, 2) transitional, or 3) fully rough.

Few-Particle Displacement

Manohar's data for few-particle displacement of quartz-density sediment are presented graphically in figure 8-9; a symbol key is included in the figure caption. The

Figure 8-9. Data of Manohar (1955) for incipient few-particle displacement of quartz-density sediment. Filled symbols represent runs in which boundary-layer flow was visually identified by Manohar as "laminar". Open symbols represent runs identified as "turbulent". Circles, diamonds, and squares represent rough turbulent, transitional turbulent, and smooth turbulent or laminar flow conditions, respectively, as calculated by this author. See text for discussion.

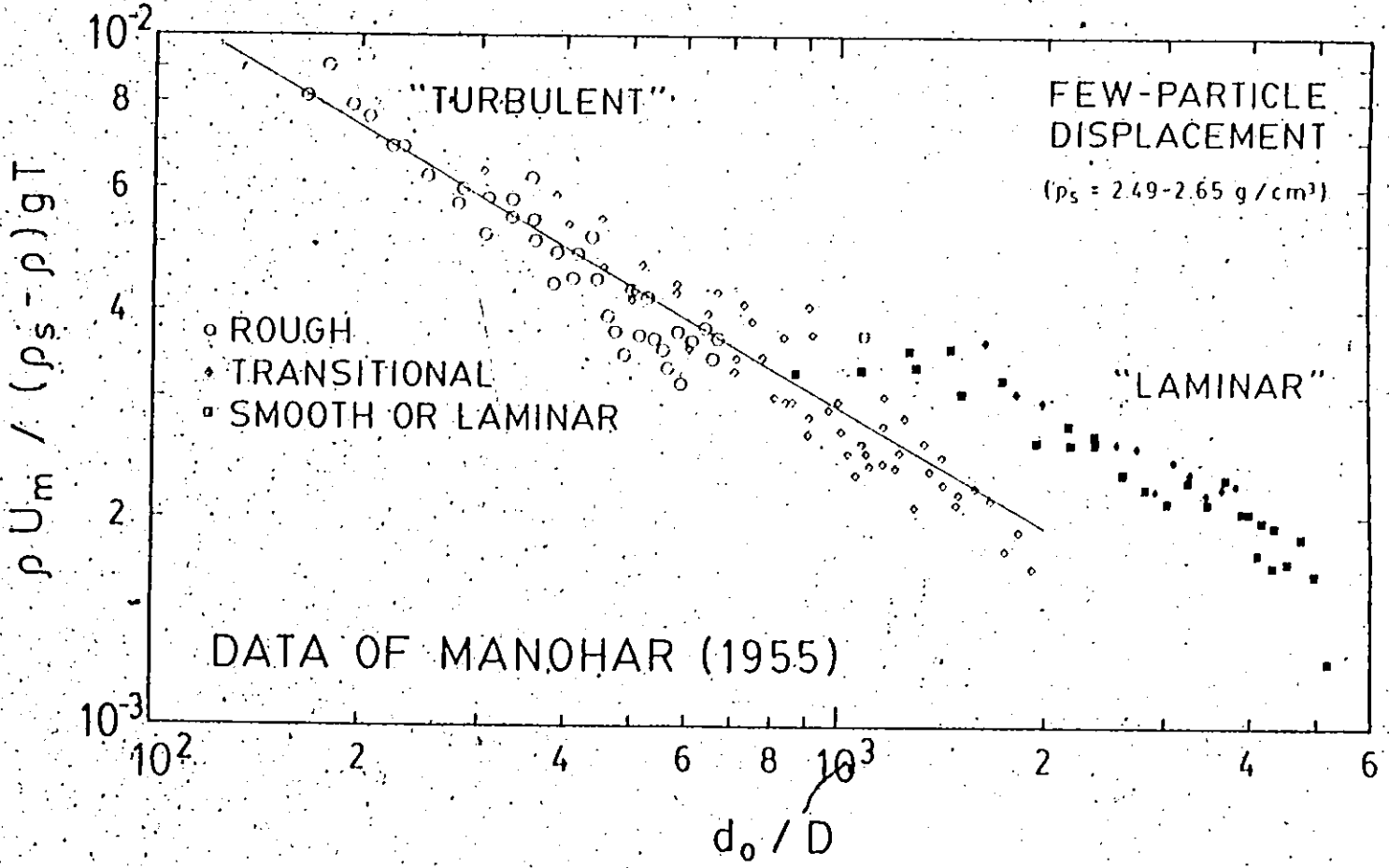
"TURBULENT"
FEW-PARTICLE DISPLACEMENT
(ρ_s = 2.49-2.65 g/cm³)
ROUGH
TRANSITIONAL
SMOOTH OR LAMINAR
"LAMINAR"
DATA OF MANOHAR (1955)
$\rho U_m / (\rho_s - \rho) g T$
d_o / D
10^{-2}
8
6
4
2
10^{-3}
10^2
2
4
6
8
10^3
2
4
6

626

grain-size range is 0.0235 to 0.1981 cm (upper fine to upper very coarse sand). In this figure, note that the calculated boundary-layer flow conditions are represented by the symbol shape, whereas the observed flow conditions (as determined visually by Manohar, using dye streaks) are indicated by symbol filling (filled symbols represent "laminar" flow, unfilled symbols represent "turbulent" flow, as classified by Manohar). Note the excellent agreement between calculated and observed flow conditions in over 130 data points -- with a single exception, all observed examples of turbulent flow correspond to calculated turbulent or transitional conditions, whereas all observed examples of laminar or smooth flow correspond to calculated laminar/smooth or transitional conditions.

The data of Manohar (1955) and Rance & Warren (1968) reveal good empirical trends for incipient few-particle displacement relating the dimensionless ratios

$$d_o/D \quad \text{and} \quad U_M/(\rho_s-\rho)gT^2.$$

The latter quantity represents the ratio of the acceleration forces to the effective gravity force acting on a grain under incipient motion conditions. To my knowledge, this particular dimensionless force ratio has not been assigned any name (as, for example, the Froude, Reynolds, or Prandtl numbers); for convenience, herein I shall refer to this ratio as the dimensionless acceleration

number, which I shall designate by the symbol Ac. Manohar's data (and the best-fit straight-line relationship) are illustrated in figure 8-9; figure 8-10 compares the relationships developed from the Manohar and the Rance & Warren data within the region of overlap between the two studies. Note that the best-fit straight line for the Rance & Warren study was determined using values obtained from a photographic enlargement of their dimensionless data presentation (Rance & Warren, 1968, Fig. 1). Figure 8-10 indicates the close agreement obtained from the two studies. Thus, the water-tunnel experiments of Rance & Warren (1968) serve to confirm the earlier results of oscillating-bed experiments by Manohar (1955) for the onset of few-particle displacement.

Many-Particle Displacement, or General Motion

Figure 8-11 presents a graph of d_o/D vs. Ac for the onset of general motion (many-particle displacement). Grain size in these experiments was 0.0147 to 0.1981 cm (lower fine to upper very coarse sand). Again, the data are those of Manohar (1955), and reveal a good correlation between d_o/D and Ac. Specifically, this graph displays only those data for which turbulent boundary-layer conditions were visually confirmed by Manohar. All of the points on the graph correspond to calculated rough or

Figure 8-10. Comparison of data trends for incipient few-particle displacement. Best-fit linear regression lines from data of Manohar (1955) and Rance & Warren (1968). See text for discussion.

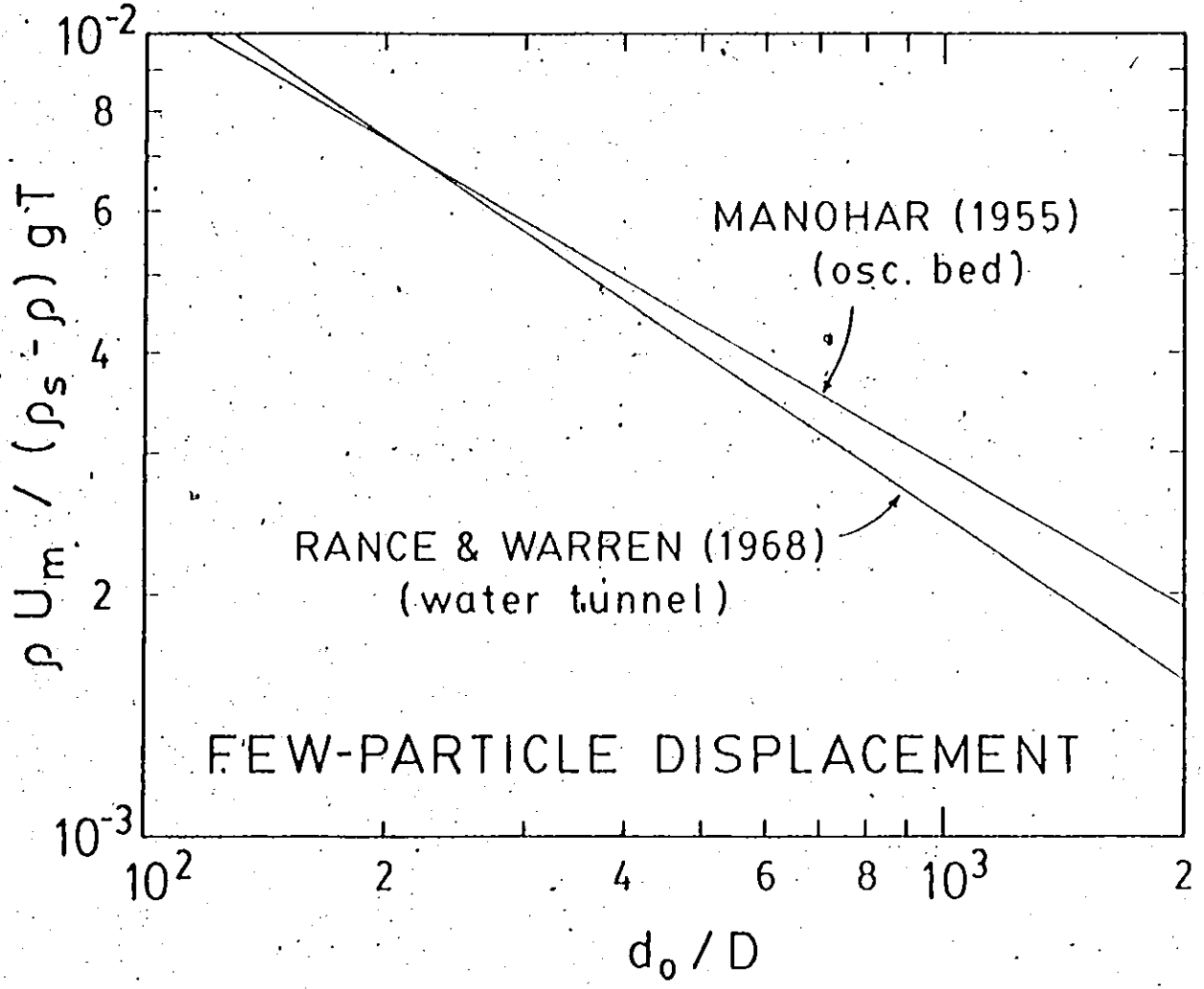
10^{-2}
8
6
4
2
10^{-3}
$\rho U_m / (\rho_s - \rho) g T$
MANOHAR (1955)
(osc. bed)
RANCE & WARREN (1968)
(water tunnel)
FEW-PARTICLE DISPLACEMENT
10^2
2
4
6
8
10^3
2
d_o / D

Figure 8-11. Data of Manohar (1955) for incipient many-particle displacement (i.e., onset of general motion) of quartz-density sediment. Symbols as in figure 8-9. See text for discussion.

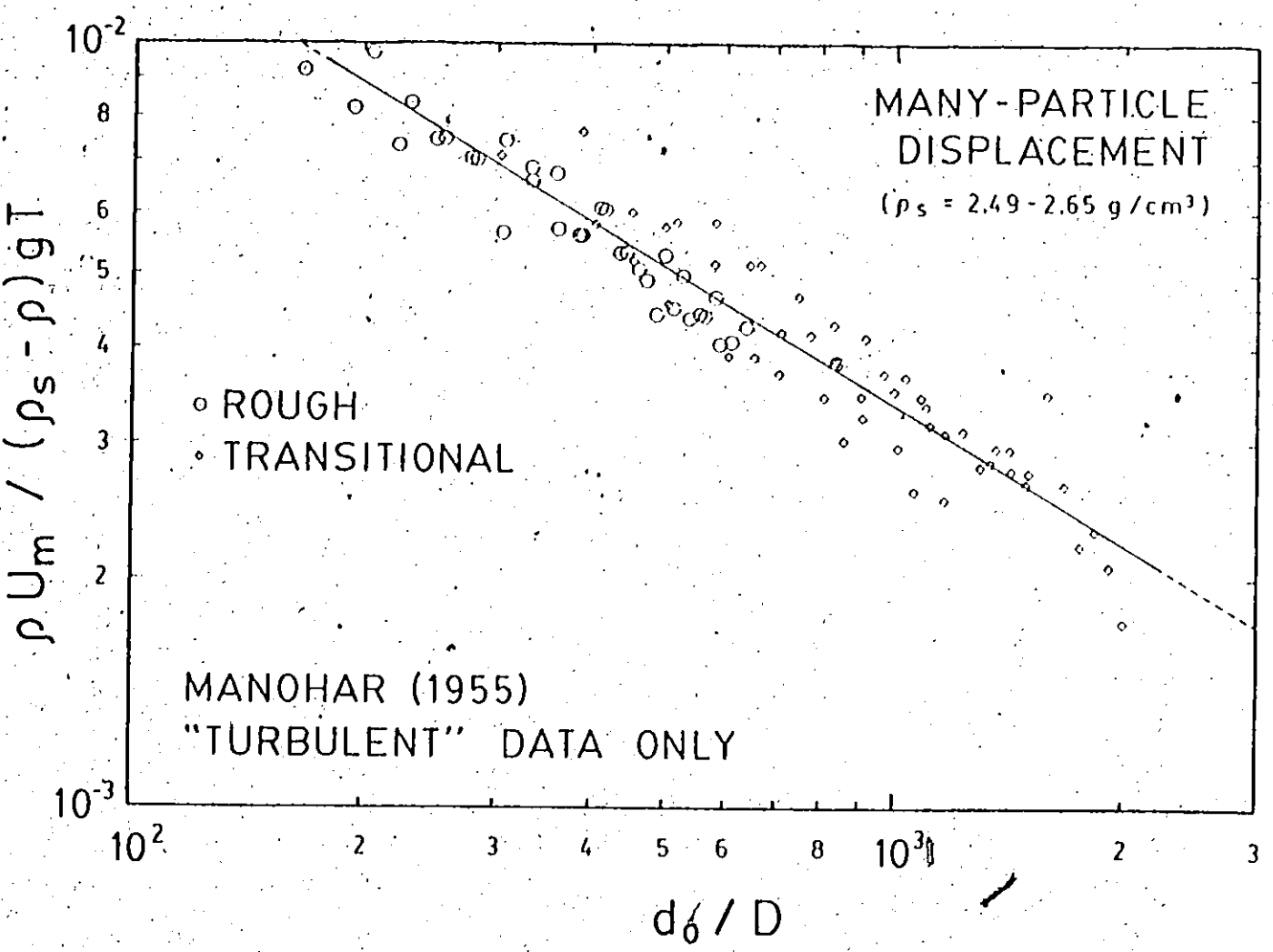
MANY-PARTICLE
DISPLACEMENT
(ρ_s = 2.49 - 2.65 g/cm³)
o ROUGH
• TRANSITIONAL
MANOHAR (1955)
"TURBULENT" DATA ONLY
$\rho U_m / (\rho_s - \rho) g T$
d_6 / D
10^{-2}
8
6
5
4
3
2
10^{-3}
10^2
2
3
4
5
6
8
10^3
2
3

transitional conditions, and all calculated rough-turbulent data points were visually identified as such by Manohar; thus, the correlation between observed and calculated conditions is perfect.

The best-fit (linear regression) straight-line relationship derived from these data for the onset of general sediment motion under fully-rough turbulent flows over a flat bed is

$$\log_{10}\left[\frac{\rho U_M^I}{(\rho_s-\rho) g T^I}\right] = -0.6669 - 0.6020 \log_{10}\left(\frac{d_o}{D}\right) \quad (8\text{-}20)$$

This expression can be re-arranged to yield

$$\frac{U_M^I}{T^I} = \frac{0.2153\ (\rho_s-\rho)\ g}{\rho\ (d_o/D)^{0.6020}} \quad (8\text{-}21)$$

As with the few-particle displacement data (Fig. 8-9), the general motion turbulent-flow data plot at d_o/D values less than about 2000. [Note: As was the case for few-particle motion, the laminar/smooth many-particle data would plot just to the upper right of the turbulent data, at d_o/D values greater than about 1000; these points have been omitted for clarity.] The positioning of the turbulent many-particle data suggests that the onset of general motion in fine to very coarse sands and coarser material takes place at values of d_o/D less than about 1000 to 2000. This relationship is valid for the range of periods investigated (about 2 to 15 s, depending on

mobility in the different grain sizes), which more-or-less covers the range of naturally occurring wave periods which initiate general motion in this size sediment.

CALCULATION OF U_m^2/T^2 FROM RIPPLE PARAMETERS

As stated previously, the maintenance of incipient general-motion conditions over a few oscillation periods is observed to lead to the development of stable, straight-crested vortex ripples in sand-sized material (Harms et al., 1982, chapter 2). Assuming this to be true in coarser grain sizes, we can utilize measureable sediment and ripple parameters to determine d_o/D, and expression 3-21 to determine U_m^2/T^2, which is the ratio of maximum bottom speed to wave period at incipient general-motion conditions, assuming only:

1) the fluid property ρ, and
2) rough-turbulent boundary-layer flow.

The latter assumption is verifiable by use of the Jonsson diagram, as shall be demonstrated in the following section, and is also verifiable for medium sands and coarser by simple inspection of the d_o/D value. This procedure is best illustrated and evaluated by means of an example, as seen at the end of the next section.

DETERMINATION OF U_M^* AND T^*

Figure 8-12 is a nomogram which can be used in conjunction with the previously mentioned relationships to uniquely determine U_M^* and T^* for ancient straight-crested orbital vortex ripples formed under fully rough oscillatory flow. This figure is a graph of U_M vs. T. Within the area of this graph, solid lines represent isograds (in meters) of d_o, as determined by expression 8-8. These lines have a negative slope. The dashed lines represent isograds (in m/s^2) of the ratio U_M/T; they have a positive slope. By locating the point of intersection of the appropriate isograds of d_o and U_M^*/T^* for a particular ripple train, it is a simple matter to read off the graph the values of U_M and T under which the ripples possibly formed [but see below the discussion of range of ambiguity]. Alternatively, these values of U_M and T may be calculated numerically by combining expressions 8-8 and 8-21 to obtain

$$U_M^I = \left[\frac{0.2153\ (\rho_s - \rho)\ g\ \pi\ d_o}{\rho\ (d_o/D)^{0.6020}} \right]^{1/2} \qquad (8\text{-}22)$$

and

$$T^I = \left[\frac{0.2153\ (\rho_s - \rho)\ g}{\rho\ d_o\ \pi\ (d_o/D)^{0.6020}} \right]^{-1/2} \qquad (8\text{-}23)$$

where d_o is measured in m, T in s, and U_M in m/s.

Note that these values are for incipient general motion conditions over an initially flat bed; as discussed above, maintenance of these conditions over several oscillation cycles would result in the formation of straight-crested vortex ripples having the observed spacing. Also note that a slightly decreased value of U_M, accompanied by a slight increase in T (as determined by the fixed value of d_o in expression 8-8), will not generate the ripples under consideration, because this combination of values results in a decrease in the ratio of acceleration forces to gravity force below the critical value for incipient motion. [Note that pre-existing ripples may remain active slightly below the threshold conditions, possibly at speeds reduced by as much as 20% (Bagnold, 1946, p. 10) -- but see further discussion below.] However, a slight increase in U_M and decrease in T with respect to the predicted values would also generate the observed ripples. A significant variation (constrained along the appropriate d_o isograd) toward high-U_M, low-T values will eventually enter the field of conditions in which three-dimensional orbital ripples or flat bed are stable (compare with Fig. 2-14 of Harms et al., 1982). In the absence of extensive field and/or laboratory data for coarse material, it is impossible to state the range of high-U_M, low-T conditions under which a given set of

Figure 2. Nomogram for determination of U_M^* and T^* for straight-crested orbital vortex ripples formed under rough-turbulent oscillatory flow. Isograds of d_o have a negative slope (solid-line diagonals). Isograds of U_M/T have a positive slope (dashed-line diagonals). Values of d_o, T, and U_M are in m, s, and m/s, respectively. See text for discussion.

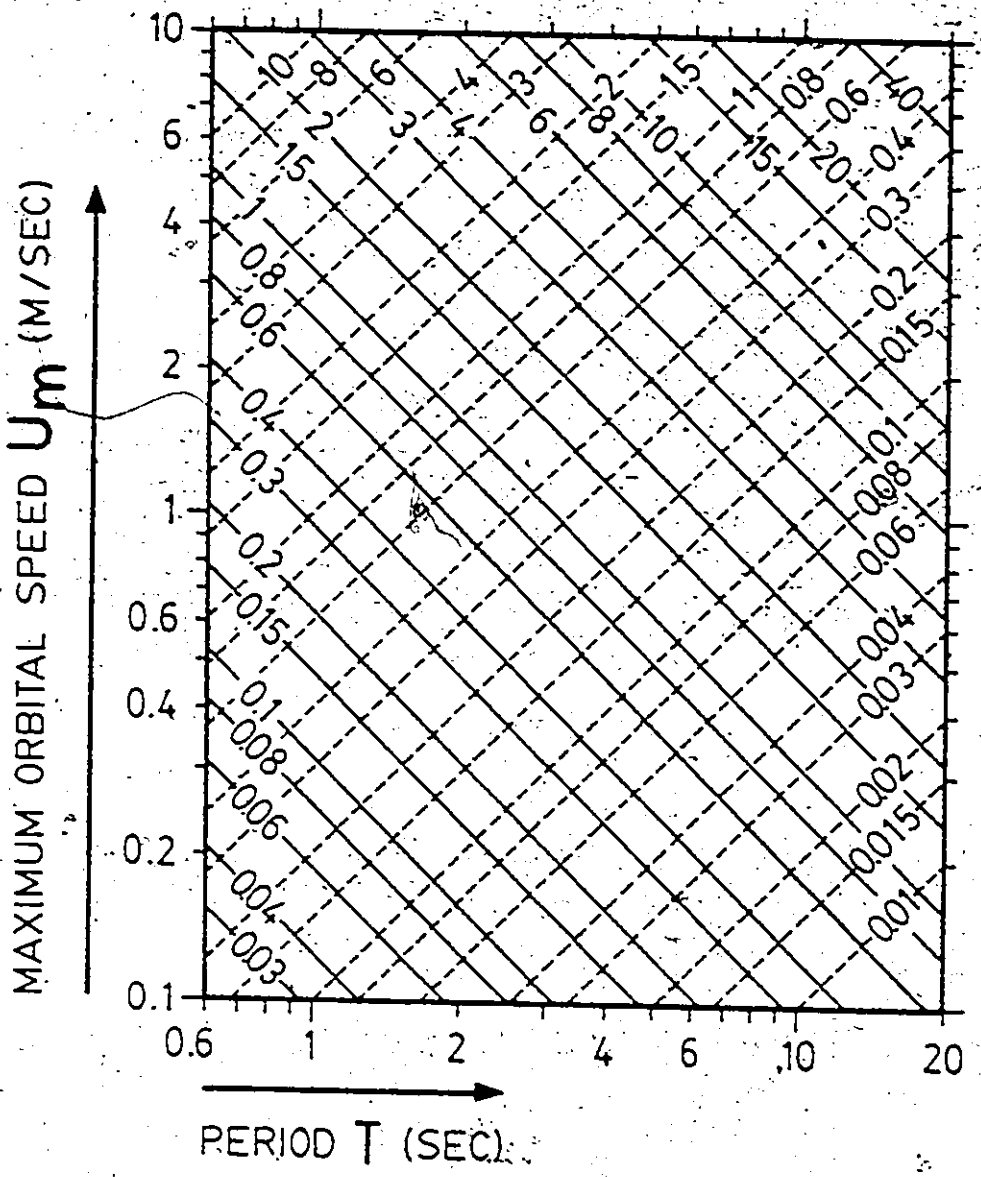
MAXIMUM ORBITAL SPEED U_m (M/SEC)
PERIOD T (SEC)
10
6
4
2
1
0.6
0.4
0.2
0.1
0.6
1
2
4
6
10
20
10
8
6
4
3
2
1.5
1
0.8
0.6
0.4
0.3
0.2
0.15
0.1
0.08
0.06
0.04
0.03
0.02
0.015
0.01

ripples would be formed; however, a test of the method against recent occurrences (see below) suggests that the range of ambiguity may be relatively small compared to measurement errors involved in field work in recent environments.

Despite the ambiguity described above, this method of paleohydraulic analysis represents a distinct improvement over similar existing techniques, as will be further discussed in a later section.

Example Illustrating Method for Determination of U_{wr} and T

To illustrate the method, let us take the example of the conglomeratic symmetrical ripples exposed in excellent plan view in the Cardium Formation outcrop at Seebe, Alberta. These ripples are formed in chert pebbles with a mean diameter (D) of 0.5 cm. Mean ripple spacing (λ_r) is 100 cm.

As discussed above, figure 8-5 indicates that ripples formed in sediment of this size are orbital ripples; expression 8-12 yields a d_o value of 154 cm. Thus, the ratio d_o/D is 300. Figure 8-11 and expression 8-20 indicate an Ac number of roughly 0.007 for this ratio of d_o/D, assuming viscosity of seawater and turbulent boundary-layer flow. [The low d_o/D ratio, much below 1000

to 2000, is consistent with fully rough turbulent flow in the experimental data set.] The assumption of turbulent flow can be tested once U_m^* is uniquely determined, using the Jonsson diagram (see below).

To uniquely determine both U_m^* and T^*, expressions 8-22 and 8-23 are employed. [Alternatively, figure 8-12 may be used, with a reduction in accuracy.] These expressions indicate a U_m^* value of 72 cm/s and a T^* value of 6.7 s. Insertion of this U_m^* value in the abscissa (Re_D) of the Jonsson diagram (Fig. 8-7) confirms turbulent flow in the boundary layer. As a further test, let us temporarily assume laminar or smooth boundary-layer flow. Note that laminar and smooth data plot <u>above</u> the equivalent turbulent data (for fixed d_o/D) on figure 8-11, corresponding to <u>higher</u> ratios of U_m^*/T^* (from Ac), and thus higher values of U_m^* from the intersecting isograds in figure 8-12. On the Jonsson diagram, however, higher U_m^* values must also indicate turbulent flow, which is inconsistent with the assumption of smooth flow. Thus, flow conditions for this example must have been turbulent.

TEST OF PALEOHYDRAULIC METHOD

The accuracy of this technique can be tested by applying it to recent examples of coarse-grained,

two-dimensional orbital vortex ripples for which both depth and generative wave parameters are well known, as well as sediment and ripple parameters. There are a few detailed studies of coarse-grained vortex ripples from natural environments; to date, there have been no laboratory studies utilizing fixed-bed devices of vortex ripples formed in coarse sediments. The stipulation of a fixed-bed device is required for the study of the ripple stability field; oscillating-bed devices are unsatisfactory for three reasons: 1) they produce unnatural acceleration forces on the bed at higher velocities and Reynolds numbers, 2) they generally prevent complete development of the boundary layer, and 3) the structure of turbulence in the boundary layer is unnatural due to the stillness of the overlying water. A more complete discussion is provided at the end of this part of chapter 8.

Recent Ripple Occurrences

Gillie (1979). As mentioned previously, Gillie (1979) simultaneously measured sediment, ripple, and generative wave parameters for active trochoidal to sinusoidal straight-crested conglomeratic symmetrical ripples forming at a depth of 18.3 m off the coast of New Zealand.

Table 8-1 summarizes the measured data of Gillie

(1979) for these ripples; "calculated" values of fluid-motion parameters (including U_m and T) were calculated by this author from depth and wave parameters, using Airy wave theory. Also presented (table 8-2) are predicted values of U_m and T, calculated using the method developed herein. I emphasize that with this method, the predicted values were calculated using only sediment and ripple parameters (as would be measureable in outcrop in an ancient occurrence). Note the very close agreement between predicted and measured values. The mean relative error (expression 8-15) between predicted and measured values of U_m and T is 9.9% and 12.8%, respectively. The relative error range is 2.2% to 17.7% (for U_m) and 5.6% to 26.4% (for T), as seen in table 8-3.

The differences between measured and predicted values of U_m and T for the data of Gillie and Yorath et al. (see below) are illustrated graphically in figures 8-13 and 8-14. Note that there is no systematic trend towards either higher or lower predicted values in these data sets.

Water depth can also be estimated from the predicted values of d_o, U_m, and T; to estimate depth, however, it is additionally necessary to assume a range of wave heights (H) for which waves are stable. This is a standard iterative precedure; I wrote a BASIC computer program to perform the iteration. This program and the results for examples discussed herein are available from

Figure 8-13. Plot of "measured" vs. "predicted" values of U_m for recent ripples studied by Gillie (1979) and Yorath et al. (1979).

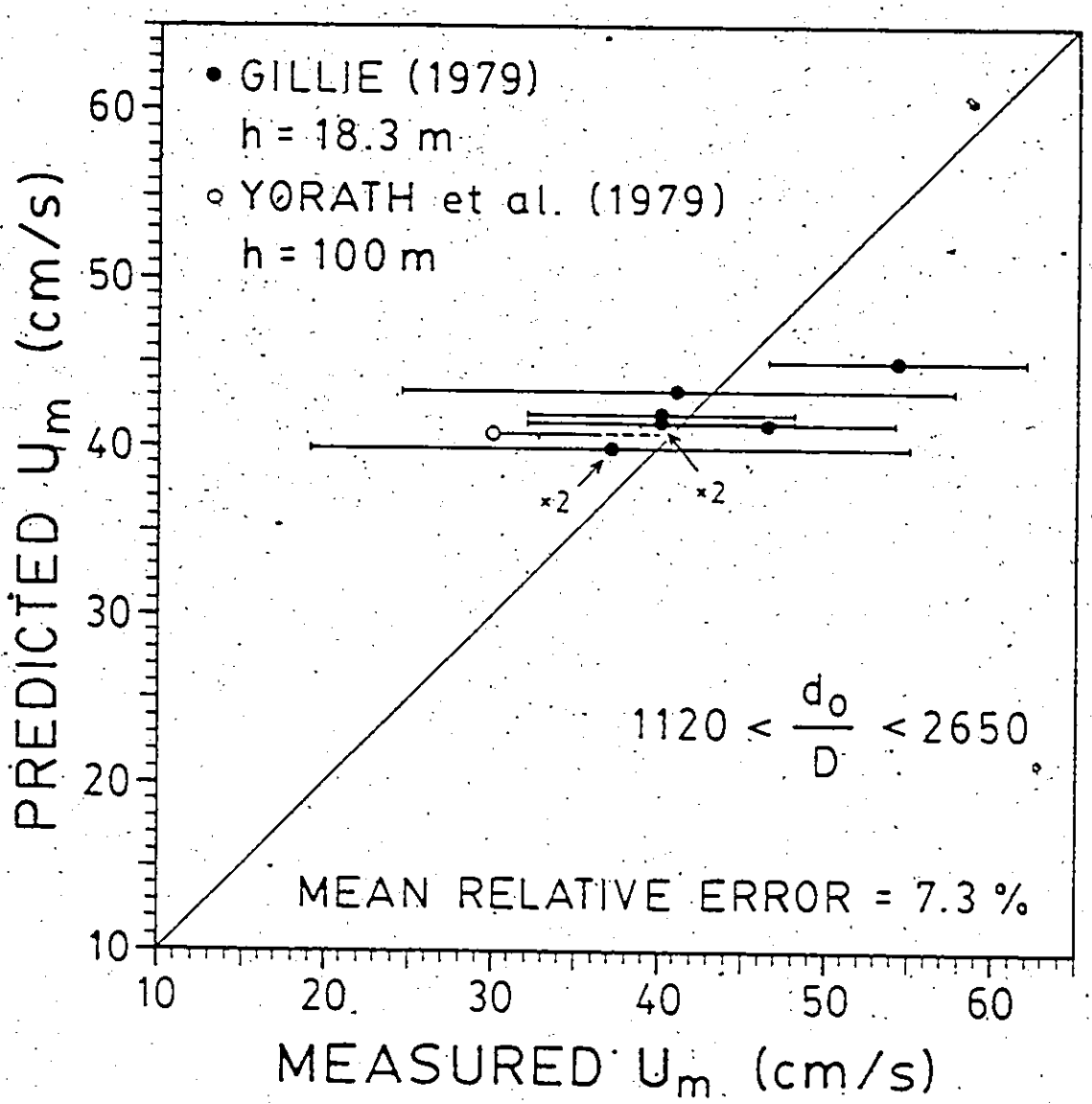
• GILLIE (1979)
h = 18.3 m
○ YORATH et al. (1979)
h = 100 m
×2
×2
1120 < d0/D < 2650
MEAN RELATIVE ERROR = 7.3 %
PREDICTED Um (cm/s)
MEASURED Um (cm/s)
10
20
30
40
50
60

Figure 8-14. Plot of "measured" vs. "predicted" values of T for recent ripples studied by Gillie (1979) and Yorath et al. (1979).

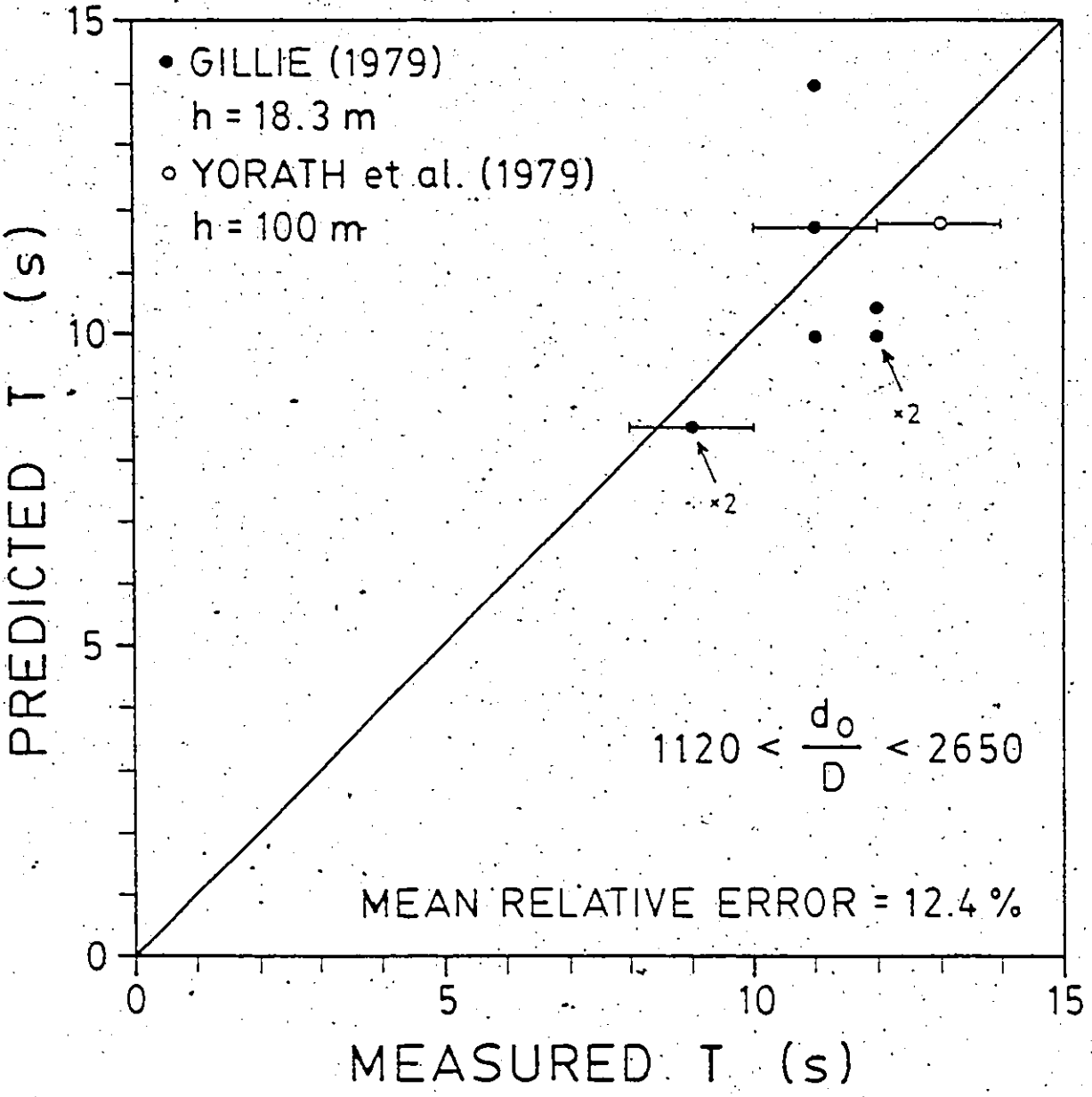
• GILLIE (1979)
h = 18.3 m
○ YORATH et al. (1979)
h = 100 m
×2
×2
1120 < d0/D < 2650
MEAN RELATIVE ERROR = 12.4 %
PREDICTED T (s)
MEASURED T (s)
0
5
10
15

the author. The predicted depth range (1 to 180 m) for the ripples from the Gillie study brackets the known depth (18.3 m), but has a huge relative error due to the assumption of the full range of stable wave heights. This depth range can be limited in some ancient occurrences by means of two methods:

1) If several different ripple trains occur within close stratigraphic proximity of one another, and if a disconformable relationship is not indicated, it can reasonably be assumed that all were formed in roughly the same water depth under waves possessing different characteristics. In such a situation, the minimum variation in extremes of paleodepth of any of the trains can be taken as applying to all of them. Thus, if the eight ripple trains observed in the Gillie study were ancient examples closely associated stratigraphically, their paleodepth range could be limited to 1 to 61 m (table 8-2).

2) If there is additional geological evidence which can be used to restrict the range of stable wave heights, the paleodepth range may be further restricted for even a single ripple train.

If it is not possible to make use of the two methods suggested above, the technique described herein can be used to establish only a fairly broad range of possible

paleodepths. As shall be seen in part 3 of this chapter, the possible depth range in some ancient occurrences is much less than that calculated from the Gillie data.

Yorath et al. (1979). Yorath et al. (1979) described large, trochoidal, straight-crested vortex ripples formed in coarse volcanic sand from the British Columbia shelf. Average ripple parameters and depth at this locality are:

$$\lambda_R = 100 \text{ cm}$$

$$D = 0.058 \text{cm}$$

$$\rho_s = 2.95 \text{ g/cm}^3$$

$$h = 100 \text{ m}$$

Yorath and co-workers calculated a range of d_o values associated with the observed variation in λ_R. Knowing the depth at which these ripples formed, and knowing that they formed under oceanic wave conditions, a U_M value in excess of approximately 30 cm/s was estimated by Yorath and co-workers. Over the range of wave periods between 5 and 20 s, U_M is relatively insensitive to T; thus, this lower-limit estimate of U_M is approximately valid for all oceanic wave conditions. The available wave record for the area was examined to define the co-variation in T and H for surface gravity waves over the site of deposition, and thus determine which waves were capable of generating the

appropriate d_o and U_M values in 100 m of water. Yorath and co-workers found that the vast majority of waves in the record capable of producing the appropriate values of d_o and U_M had periods of 12 to 14 s; they concluded that these ripples were probably formed under waves with periods of 12 to 14 s (average: 13 s).

Application of the technique introduced herein indicates the following values of generative fluid-motion characteristics for these ripples:

$$U_M = 40.8 \text{ cm/s}, \quad T = 11.8 \text{ s}.$$

The relative error (expression 8-15) for predicted and measured values of T is only 9.2%; relative error cannot be computed for U_M, because the authors did not calculate an upper limit for this parameter. The inability to estimate an upper limit reflects the absence of experimental data on wave-formed bed configurations in coarse material.

Test Results: Analysis and Implications

The test results summarized above indicate a close agreement (roughly 10% relative error) between measured values of fluid-motion characteristics, and values predicted by the paleohydraulic analysis technique discussed in this chapter. The technique has been tested over a wide range of wave periods (about 8 to 13 s), flow

speeds (about 35 to 55 cm/s) and water depths (18 to 100 m). Depending upon specific values of sediment size and ripple spacing, this technique can be tentatively employed for various sand and all gravel sizes.

It is possible that the close agreement between measured and predicted values in the tests performed above is strictly fortuitous; however, I think this to be an unlikely explanation of the test results. The need for further tests is most strongly indicated. In the event that further tests of the method suggest it to be generally applicable, the implications of the relatively high accuracy of the technique are three-fold:

1) In coarse sediments, two-dimensional symmetrical ripples are the stable bedform associated with the onset of general motion under oscillatory flow.

2) In coarse sediments, the bed-configuration field for two-dimensional symmetrical ripples is possibly restricted to a relatively narrow range of values of U_M and T; these values are within about 10% of the incipient general-motion values. Alternatively, it is possible that gradually waning storm conditions consistently rework rippled sediment such that the preserved ripples were in equilibrium with incipient general-motion conditions (approached during waning flow from higher values of U_M).

3) In coarse sediments, pre-existing

two-dimensional symmetrical ripples remain active and are not degraded by flows with bottom speeds slightly below the incipient general-motion threshold values; however, these ripples do not remain active at speeds roughly 10% below this threshold. Bagnold (1946) suggested continued ripple activity at a 20% reduction in speed; however, this estimate was based upon experimental study of the ripple stability field in an unreliable oscillating-bed device (see further discussion below).

Finally, it is noteworthy that the tested ripples were formed at d_o/D values between about 1000 and 4000. These values are within the transition region between rough-turbulent and laminar/smooth conditions (Fig. 8-11, and back-calculation using Fig. 8-8). However, values of d_o/D are calculated using mean grain size of sediment (D), whereas all of the recent ripples in question contained abundant coarser material, up to a few centimeters in diameter. I suggest that this coarse component is adequate to initiate turbulence within the boundary layer prior to the onset of general motion, a conclusion supported by the close agreement between measured and predicted values assuming rough-turbulent conditions. Thus, in naturally-occurring poorly-sorted coarse sediments, the relationships developed in this chapter are expected to obtain at higher d_o/D values than reflected by the

laboratory experiments utilizing well-sorted sediment; these relationships may obtain at d_o/D values as high as 4000 or greater.

SUMMARY AND DISCUSSION

Herein I have discussed a technique for the paleohydraulic analysis of coarse-grained, straight-crested, orbital symmetrical ripples. This technique is applicable to ripples formed under rough-turbulent boundary-layer flow; it permits accurate calculation of near-bed fluid-motion parameters based only upon sediment and ripple parameters measureable in outcrop. The method has been successfully tested utilizing data from recent studies. A broad range of possible paleodepths can also be calculated, assuming the full range of stable wave heights.

This method represents an improvement over other techniques which do not recognize the advantage of distinguishing between ripples formed under laminar or hydraulically smooth flows, and those formed under hydraulically rough turbulent flows.

Data from Oscillating-Bed Devices: A Cautionary Note

The relationships discussed in this chapter are developed primarily from experimental data collected by Manohar (1955) utilizing an oscillating-bed device. As noted previously, results obtained from devices of this sort can be held in question for the following reasons:

1) Acceleration forces. Unnatural acceleration forces operate on the bed, due to the oscillation of the bed itself within a body of still water. Other factors being equal, the magnitude of these acceleration forces increases with shorter periods of oscillation and/or higher values of maximum orbital speed. For a given period, ripples form at a higher speed than is required to initiate sediment motion; this is one reason why oscillating-bed devices are considered less reliable for the study of ripple parameters than for the study of incipient motion.

2) Incomplete boundary-layer development. Development of the entire oscillatory boundary layer (including both the growing and the collapsing stages) will be incomplete over the entire sediment tray if this tray is shorter than twice the bottom orbital diameter examined, as illustrated in figure 8-15. During the first half-stroke of oscillation (between time Ø and time T/2), the boundary layer first grows (time Ø to T/4) and then collapses (time

T/4 to T/2) as the tray moves right to left from one extreme position to the other (i.e., from the upper position to the middle position in Fig. 8-15). Complete development of both the growing and collapsing phase of the boundary layer occurs over the tray only to the right of the center-line (at lengths equal to or greater than d_o from the leading edge), as indicated by the hatchure below a conceptualized plot of maximum boundary-layer thickness (dotted line at middle position, Fig. 8-15). Left of the center-line, the growing phase of boundary-layer development is nowhere complete.

A mirror image of this situation exists for time T/2 to time T (middle position to lower position, Fig. 8-15). Thus, boundary-layer development over the full oscillation cycle is complete above the center-line of the tray only. This analysis indicates that the sediment tray must be over twice as long as the values of d_o examined in order to allow complete boundary-layer development over any part of the tray. Thus, a tray of length $3d_o$ will develop a complete boundary layer over a middle portion with length equal to d_o.

In the Manohar study in particular, the sediment tray was 198 cm long parallel to the direction of displacement. The maximum value of bottom orbital diameter studied was about 122 cm. Thus, complete development of the boundary layer did not occur at any point over the

Figure 8-15. Diagram illustrating boundary-layer development over an oscillating sediment tray of length $2d_o$. See text for discussion.

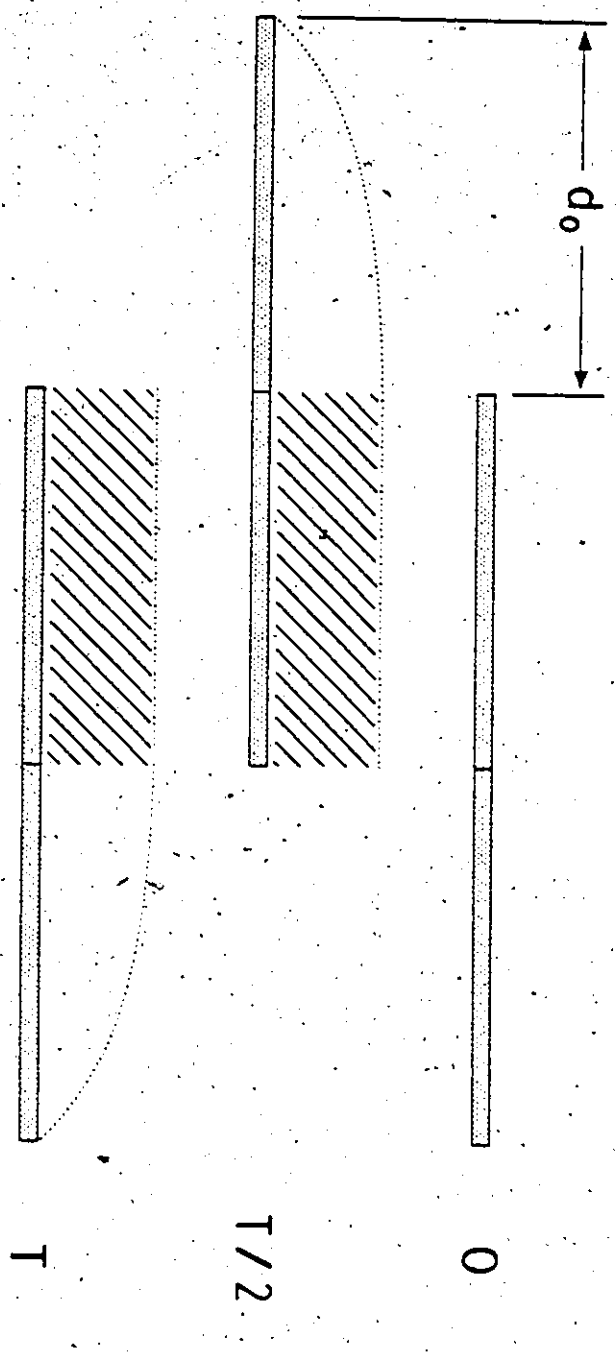
d_o
T
T/2
0

sediment tray in this run.

The possible complications arising from this incomplete boundary-layer development are not known; however, one may speculate as to the possible effects. In any grain size, the onset of sediment motion probably takes place under accelerating flow (i.e., during the growing phase of boundary-layer development) or at U_m (i.e., at the transition to the collapsing phase). Incomplete boundary-layer development due to the short sediment tray is most acute during the growing phase of the boundary layer: The leading edge of the tray enters still water with a non-zero forward velocity, resulting in an unnatural concentration of boundary shear stress directly at the bed. It is possible, however, that this undesired effect may not significantly alter data for incipient motion under turbulent flow; turbulence also results in a near-bed stress concentration. The possible influence of incomplete boundary-layer development on ripple initiation, morphology, and spacing cannot be estimated.

3) Lateral edge effects. In the Manohar study, the negative effective length of the sediment tray (relative to edge effects associated with incomplete boundary-layer development) bas been discussed under point 2 above. The flow-normal (lateral) width of the sediment tray was 29 cm. In such a narrow experimental set-up, lateral edge effects

certainly would be expected to affect the parameters of large ripples formed in the coarser grain sizes, especially in cases where the device was operated over several oscillation periods (thus permitting lateral propagation of edge effects). Extended periods of operation can be required to allow development of equilibrium ripple morphology (including spacing); this is especially true in the case of vortex ripples formed in coarse sediments. However, lateral edge effects probably would not influence the measured values for incipient motion; these effects cannot propagate beyond the zone of boundary-layer retardation unless sediment is in motion.

4) Turbulence structure. Even if complete boundary-layer development is attained, the structure of turbulence within the boundary layer over an oscillating bed probably is not the same as in natural oscillatory flows, for a variety of reasons. Firstly, turbulent eddies shed from the moving bed are not constrained to remain over the bed in oscillating-bed devices, due to the fact that the oscillating sediment tray must be contained within a much larger water tank. Thus, eddies may migrate into still water in a direction either parallel or perpedicular to the oscillating bed, and thereafter have little or no effect upon the flow over the bed. Secondly and more importantly, there is no shear within the still water

Figure 8-16. Schematic cartoon of vertical near-bed water motion and intergranular water motion resulting from natural wave-induced oscillatory flows.



overlying the developing boundary layer in oscillating-bed devices. In natural flows, however, the water above the boundary layer is continuously moving and shearing due to wave-induced orbital motion.

5) Other factors. The vertical component of near-bed water movement inherent to natural oscillatory flows can only be duplicated in the laboratory with a wave tank (Fig. 8-16). The same can be said for intergranular water flow within the bed induced by the varying hydrostatic pressure across the wave train (Fig. 8-16). Both of these secondary flow components can be expected to impart lift forces (both positive and negative) to the grains at the sediment-water interface; these forces are not duplicated in oscillating-bed devices.

In light of the numerous possible problems discussed above, (the consequences of which remain unknown), it is remarkable that the Manohar data are apparently in such good agreement with data collected from natural environments. This situation is even more remarkable when considered in light of recent experiments by Southard and students (mentioned above). These experiments in a fixed-bed laboratory apparatus indicate that very large symmetrical bedforms, both two- and three-dimensional, may develop in fine sand sizes under oscillatory flows (J. B. Southard, pers. comm., 1985). However, these structures

are only developed when the flow is allowed to continue over protracted periods of time. Such bedforms were not recognized in the Manohar study; similarly larger structures may be the stable bed configuration in coarser sediments, also. Possibly, the lengths of time required for their development were not achieved in the natural settings examined by Gillie (1979) and Yorath et al. (1979); this could explain the agreement with the Manohar data. The need for a new experimental data set, from large wave tanks and/or fixed bed laboratory apparata, is most strongly indicated.

PART 3

APPLICATION OF PALEOHYDRAULIC METHOD TO ANCIENT OCCURRENCES OF CONGLOMERATIC SYMMETRICAL RIPPLES, AND IMPLICATIONS FOR THE ORIGIN OF HUMMOCKY CROSS-STRATIFICATION

INTRODUCTION

Ancient examples of straight-crested symmetrical ripples formed within storm-emplaced conglomerates have been described from the Cardium Formation and other units of the western Canadian Cretaceous by Wright (1980), Wright & Walker (1982), Leckie (1983), Duke & Leckie (1984), and Leckie & Duke (1984). A preliminary discussion of the Cardium examples was presented in chapters 4 and 5 of this thesis. Photographs of several examples from the Cardium Formation are presented in figures 8-17 and 8-18.

In the above references, conglomeratic symmetrical ripples were interpreted as wave-formed orbital vortex ripples, and are associated with hummocky cross-stratified sandstones. In this part of chapter 9, I first demonstrate that an alternative interpretation (formation by antidunes) is hydrodynamically impossible. I then present a quantitative paleohydraulic analysis of these ripples.

Figure 8-17. Examples of conglomeratic symmetrical ripples from within a prograding shoreline sequence (cycle 2, section GC-2). All sections normal to bedding, roughly normal to ripple crests.

A) Crests of 13 individual ripples at four different stratigraphic horizons are numbered on this photo. Numbers appear below ripple crests. Good estimates of ripple-spacing can be determined for two trains (ripples 1 to 7 and 9 to 11). Parameters for these two trains are summarized in table 8-4 (trains 6 and 7, respectively). See details in photos B to E.

B) Note sinusoidal profile of ripples 3 to 7 in this photo. Field book (below ripple 4) for scale.

C) Close-up of ripples 3 and 4. Note sharp base of this conglomerate bed, which pinches down to 2 cm in the trough between these ripples.

D) An isolated symmetrical ripple (crest above number 8) and three laterally adjacent ripples (crests below numbers 9 to 11). The ripples in the train are formed in a layer of conglomerate above hummocky sandstone; this conglomerate dies out to the right, where it is replaced by additional hummocky sandstone.

E) Note sharp basal contact and structureless basal division of this conglomerate bed, and internal cross-strata within ripple 8 at top of bed.

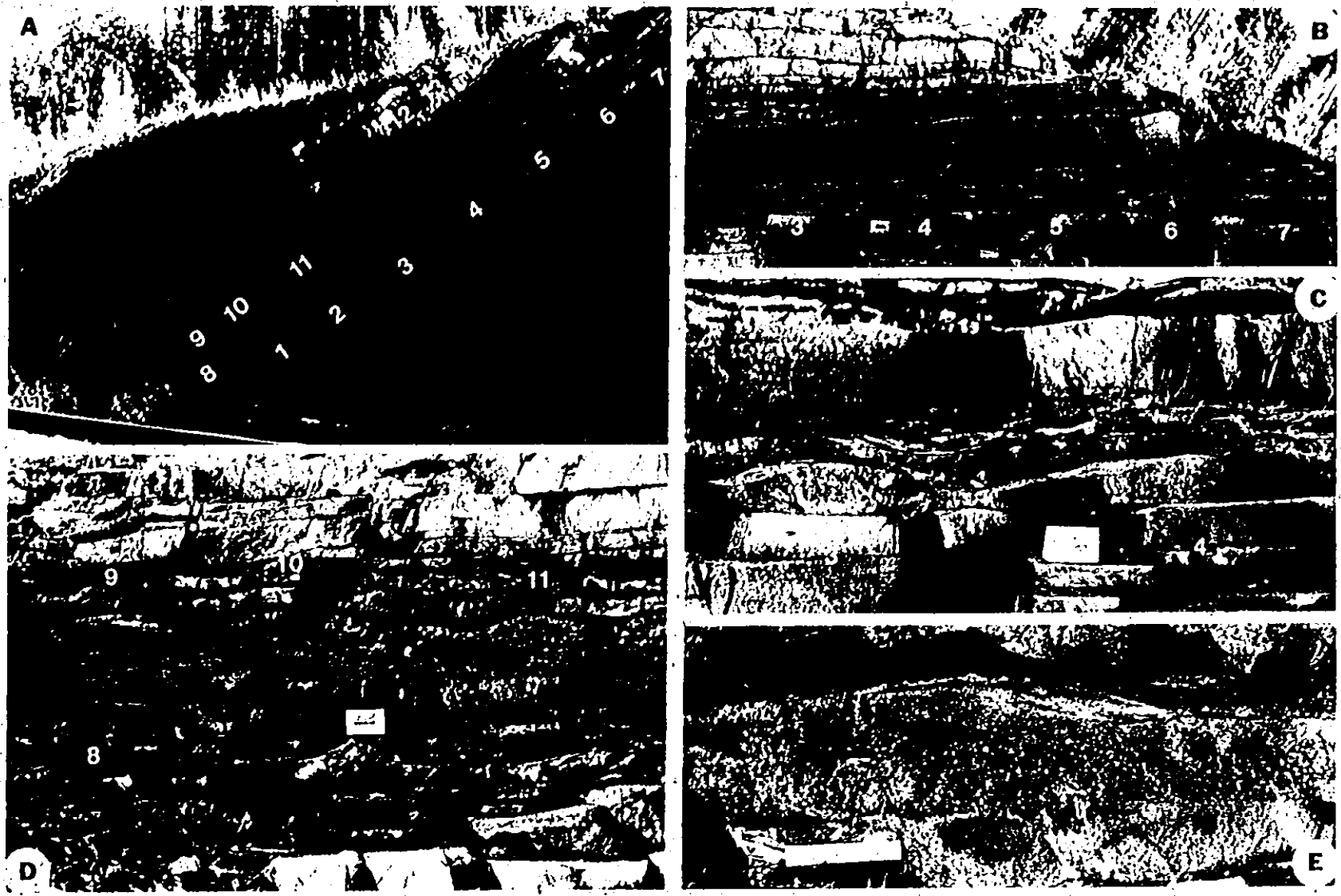
A
1
2
3
4
5
6
7
8
9
10
11
B
3
4
5
6
7
C
4
D
8
9
10
11
E

utilizing the method developed in part 2 of this chapter. Finally, I use the results of this analysis to estimate the conditions of formation of associated hummocky cross-stratified sandstones.

HUMMOCKY CROSS-STRATIFICATION AND CONGLOMERATIC SYMMETRICAL RIPPLES

As discussed in chapter 4 and part 1 of this chapter, most examples of hummocky cross-stratification are formed in coarse siltstone to fine sandstone. Hummocky sandstones are commonly mantled with small symmetrical ripples. A few studies have noted an association between hummocky sandstones and large, straight-crested symmetrical ripples formed in very coarse sandstone to sandy conglomerate (see references above).

I have examined conglomeratic symmetrical ripples and associated hummocky sandstones in two Upper Cretaceous units from southern Alberta, the Cardium Formation and the Chungo Sandstone Member of the overlying Wapiabi Formation. Additionally, D. A. Leckie has made available to me his observations of similar ripples and sandstones from the Chungo and the Lower Cretaceous Moosebar-Gates interval. Our collaboration shall soon be presented in a paper by Duke and Leckie.

Figure 8-18. Examples of conglomeratic symmetrical ripples capping a prograding shoreline sequence (cycle 7, section 4-19).

A) Section normal to bedding and roughly normal to ripple crests showing five ripples (indicated by numbers above crests) capping a prominent conglomerate bed (resistant bed at center right). Up is to the right. For scale, the cycle-capping conglomerate is 2.2 m in thickness, and the average ripple spacing is 1.7 m. See details in photos B to D.

B) Two of the ripples in photo A. Note sinusoidal profile. Slight asymmetry of ripple 2 is due to erosion and minor offset along minor fault (crack at left of photo). Tape is extended 30 cm.

C) Oblique plan view of ripples 1 to 3.

D) Close-up plan view of ripple 2. Crest is at center of photo, running from 2 o'clock to 8 o'clock. Note that coarsest clasts are concentrated in ripple trough (upper part of photo); some coarse clasts are also present on ripple crest.

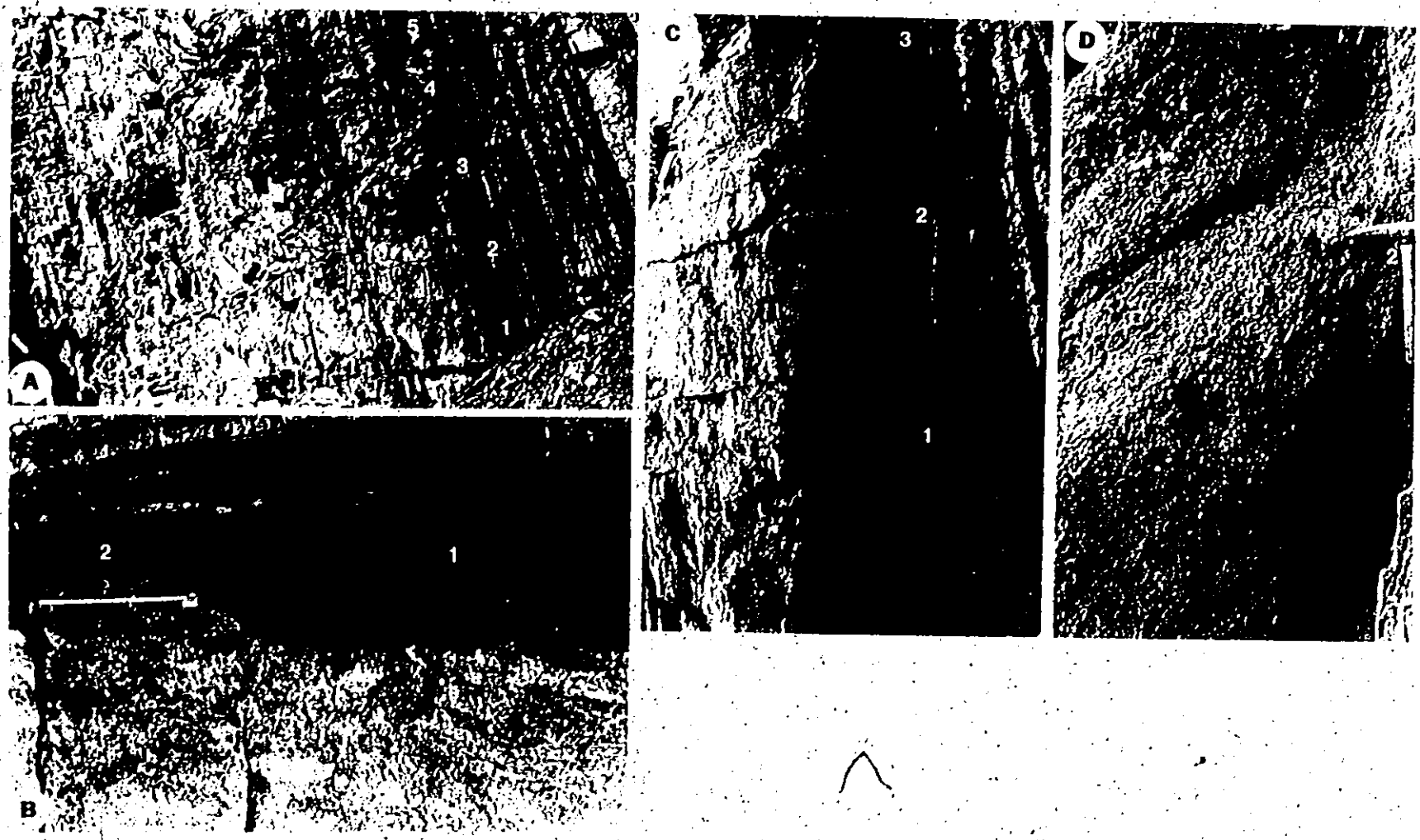
A
5
4
3
2
1
B
2
1
C
3
2
1
D
2

The following description of the conglomeratic symmetrical ripples examined for this joint study is summarized from the paper by Duke and Leckie currently in preparation. Sediment and ripple parameters are summarized in table 8-4.

The conglomeratic symmetrical ripples studied occur in sharp-based beds (Fig. 8-17C & 8-17E) which generally are structureless, graded, or imbricated in their lower portions (Fig. 8-17E); locally, bases display oriented directional sole marks (large flute casts). Average spacings and heights of the ripples are approximately 1 m and 15 cm, respectively (Table 8-4). They are sinusoidal or trochoidal in cross-section; all the Cardium examples are essentially sinusoidal (e.g., Fig. 8-17B & 8-17C). In plan view, conglomeratic symmetrical ripples are two-dimensional; crests are straight to sinuous, with tuning-fork bifurcations present locally. Wright & Walker (1981, Fig. 8) illustrated an excellent plan-view exposure of the two-dimensional ripples in the Cardium at the Seebe section.

Internal stratification of conglomeratic symmetrical ripples typically is absent or crudely developed; in most examples, internal laminae indicate vertical aggradation with little or no lateral migration of the bedform. Some examples show a strong component of lateral migration (Fig. 8-17E).

Table 8-4. Characteristic parameters of conglomeratic symmetrical ripples. Reference numbers (#) are the same as in table 8-5; "ht" indicates ripple height, measured from trough to crest. All ripples are formed in quartz-density material, and all values listed represent the mean of several measurements from a single ripple train.

Divisional sequences (modified from Walker et al., 1983):

M = mudstone, generally bioturbated

X = small-scale symmetrical ripples

F = "flat" lamination

H = hummocky cross-stratification

R = sandy conglomerate exhibiting large symmetrical ripples

B = sandy conglomerate (no ripples present)

Divisions are listed in ascending vertical sequence. Periods indicate sharp bases of depositional events; each sequence listed is erosionally truncated by a subsequent event. Divisions listed within parentheses are complexly interfingering or juxtaposed laterally, and are listed in their most common vertical sequence.

Rock unit, age, location	#	D, cm	λ_m, cm	ht, cm	Divisional Sequences
Chungo Member,	1	0.3	113	-	.BRM
Wapiabi Formation,	2	0.3	-	9	.BRH
U. Cret., S. Alta.	3	0.3	-	6	.B(RH)M
Cardium Formation,	4	0.5	100	7	.BRM
U. Cret., S. Alta.	5	1.8	169	30	.BRM
	6	1.0	120	12	.R(HFX)M
	7	1	101	10	.B(BH)(RH)(XM)
	8	1	-	-	.B(RH)(HF)XM
Moosebar and Gates	9	0.8	95	14	.BRM
Formations,	10	0.3	150	23	.BRM
L. Cret., Alta.	11	0.2	70	-	.BRM
and B. C.	12	0.3	75	12	.BRM
	13	0.5	120	18	.BRM
	14	0.5	116	13	.BRM
	15	0.6	115	12	.BRM
	16	0.8	69	5	.BRM
	17	0.2	97	9	.BRM

In the units studied, conglomeratic symmetrical ripples occur within prograding shoreline sequences, where they are closely associated both laterally and vertically with hummocky cross-stratification. The ripples typically occur within lower shoreface deposits, but also are present within upper shoreface and proximal shelf deposits. The overall stratigraphic position of conglomeratic symmetrical ripples is discussed in detail in part 4 of this chapter.

ORIGIN OF CONGLOMERATIC SYMMETRICAL RIPPLES

Recent ripples identical to the ancient ones described above have been reported from numerous modern shelves, in depths ranging from 5 to 100 m (Leckie & Duke, 1984; part 2 of this chapter). Gillie (1979) observed formation of conglomeratic symmetrical ripples under wave-generated oscillatory flows off the coast of New Zealand. Ancient examples also are best interpreted as wave ripples forming under purely oscillatory or strongly oscillatory-dominant flows.

Note that conglomeratic symmetrical ripples superficially resemble antidunes; however, formation by either free-surface or stratified-underflow antidunes is hydrodynamically impossible, as seen in the following quantitative analysis.

Quantitative Analysis Indicating Impossibility of an Origin for Conglomeratic Symmetrical Ripples by Antidunes

An alternative interpretation of conglomeratic symmetrical ripples involves formation by antidunes. The hydrodynamic conditions under which antidunes form were discussed in part 1 of this chapter; specific generative conditions can be inferred for ancient examples from bedform and sediment characteristics measureable in outcrop. There are two cases for which conditions are easily calculated: antidunes forming under free-surface flow, and antidunes forming under a stratified underflow (two-layer case).

Free-surface antidunes. The first case involves antidunes forming below a unidirectional free-surface flow, such as flow in an open channel. Expressions 8-1 to 8-3 (part 1 of this chapter) relate characteristics of this type of antidune to generating flow conditions.

Conglomeratic symmetrical ripples typically have spacings of about 100 cm. Insertion of a value of λ_m equal to 100 cm in expressions 8-1 to 8-3 yields

$$U = 125 \text{ cm/sec and } h = 11\text{-}25 \text{ cm.}$$

Such a shallow flow depth is completely inconsistent with the inferred proximal shelf to shoreface depositional setting of conglomeratic symmetrical ripples in these

units.

Stratified-underflow antidunes. The second case for which we can easily obtain numerical solutions involves antidunes formed under a stratified underflow (two-layer case), as, for example, a turbidity current. Expressions 8-4 to 8-7 relate the characteristics of this type of antidune to the generating flow conditions. In these expressions, t is the thickness of the underflow. Solving for λ_m equal to 100 cm, an assumed value of g' equal to 89 cm/s^2 (see part 1 of this chapter), and the extreme values of the densiometric Froude number (0.8 to 1.2), yields

$$U = 38 \text{ cm/sec and } t = 11\text{-}25 \text{ cm.}$$

Thus, antidunes of a specified spacing form at lower mean flow velocities under a stratified underflow than under free-surface flow, due to the greater ease with which vertical perturbations may develop along the density discontinuity. However, the mean grain size of quartz-density material typical of conglomeratic symmetrical ripples (roughly 1 cm) is far too large to be moved by such weak flows. Thus, stratified-underflow antidunes also cannot be responsible for the formation of these ripples.

Quantitative Paleohydraulic Analysis of Conglomeratic Symmetrical Ripples

By eliminating the possibility of an antidune origin for conglomeratic symmetrical ripples in the units studied (see above), the preferred wave-formed vortex-ripple interpretation remains as the only reasonable alternative. The method developed in part 2 of this chapter can now be applied in a paleohydraulic analysis of these bedforms.

Insertion of the measured values of sediment and ripple parameters (Table 8-4) into expressions 8-12 through 8-14 demonstrates that all of these bedforms are orbital (not suborbital or anorbital) ripples, as is illustrated graphically in figure 8-19.

Again, table 8-4 summarizes the measured sediment and ripple parameters in these occurrences. The inferred value of the fluid property ρ is 1.025 g/cm^3 (seawater, 15°C). Application of the technique discussed above predicts a range of U_M and T values which are summarized in table 8-5. Data from the Cardium examples show a good grouping between U_M values of 72 cm/s to 117 cm/s (average: 92 cm/s), and T values of 5.5 s to 7.0 s (average: 6.4 s).

Assuming a range of stable wave heights associated with these wave conditions, it is possible to calculate the total possible range of depth in which the ripples probably

Figure 8-19. Graph of λ_m vs. D for ancient conglomeratic symmetrical ripples. Hatchured area represents non-occurrence of ripple spacings. This plot indicates that these are orbital ripples; they plot well away from the line of maximum ripple spacing. See part 2 of this chapter for a complete discussion.

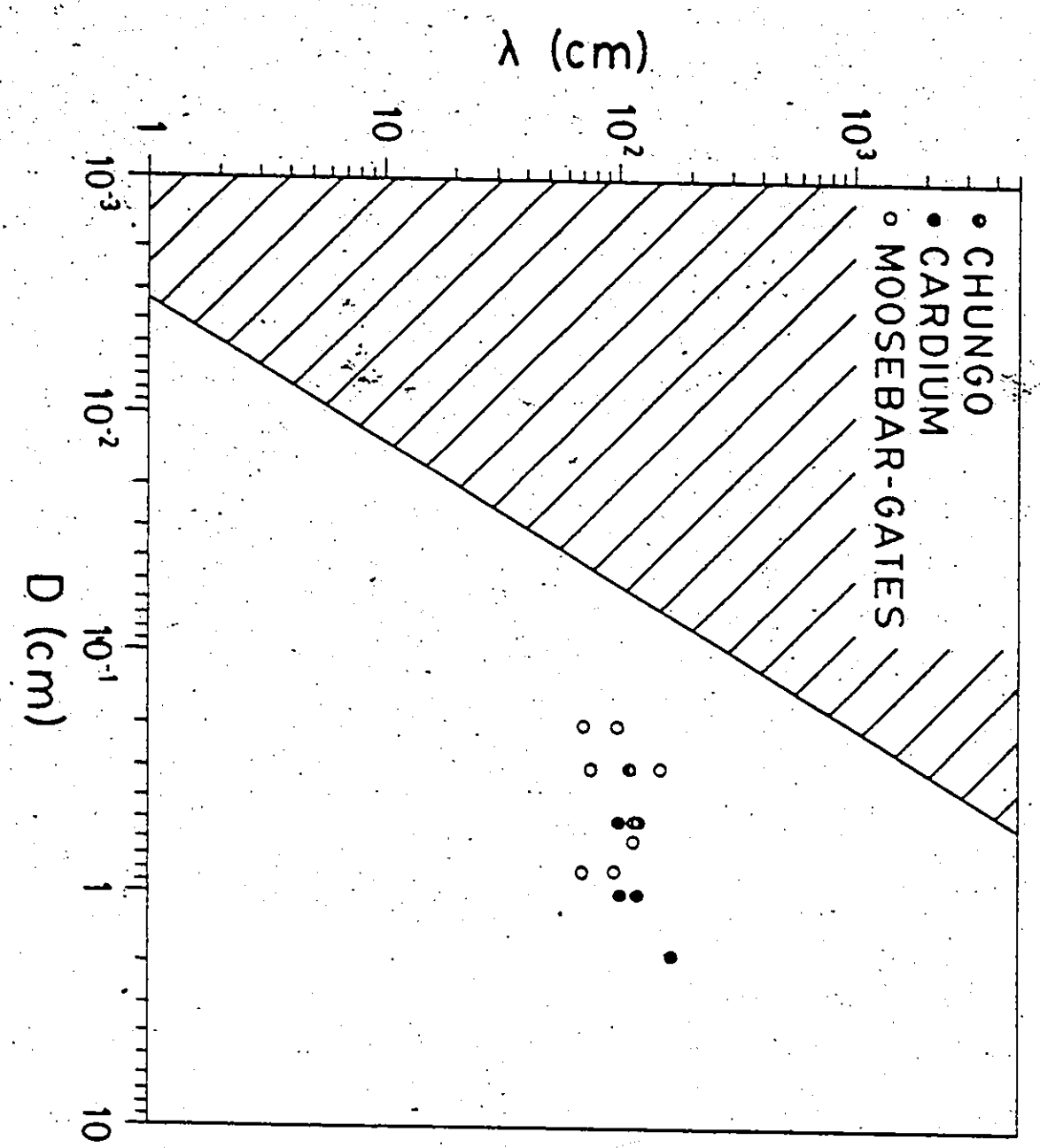
λ (cm)
1
10
10²
10³
D (cm)
10⁻³
10⁻²
10⁻¹
1
10
• CHUNGO
• CARDIUM
○ MOOSEBAR-GATES

Table 8-5. Calculated fluid-motion characteristics of conglomeratic symmetrical ripples. Values of U_M, T, and H have been calculated using the paleohydraulic analysis technique developed herein, utilizing measured parameters summarized in table 8-4. Assumed value of ρ is 1.025 g/cm³ (seawater, 15°C).

Rock unit, age, location	#	d_o, cm	d_o/D	U_M, cm/s	T, s	h, m
Chungo Member,	1	174	580	63	8.7	<56
Wapiabi Formation,	2	-	-	-	-	
U. Cret., S. Alta.	3	-	-	-	-	
Cardium Formation,	4	154	308	72	6.7	<29
U. Cret., S. Alta.	5	260	144	117	7.0	<26
	6	185	183	92	6.3	<22
	7	155	155	88	5.5	<16
	8	-	-	-	-	
Moosebar and Gates	9	146	195	80	5.7	<16
Formations,	10	231	924	63	11.5	<107
L. Cret., Alta.	11	108	470	53	6.4	<29
and B. C.	12	115	383	58	6.2	<26
	13	185	370	74	7.8	<41
	14	178	356	74	7.6	<38
	15	177	322	76	7.3	<34
	16	106	133	77	4.3	<10
	17	150	750	54	8.7	<10

formed (Table 8-5). The iterative procedure for calculation of H and h is available from the author on request. The calculated value of maximum depth of formation for these ripples ranges from 10 to 107 m; the Cardium values in particular range from 16 to 29 m (Table 8-5).

The maximum depth of formation of the Cardium ripple trains numbered 6 to 8 can be further restricted, due to their close stratigraphic grouping (see Fig. 5-38 and further discussion in part 4 of this chapter). Calculated wave parameters are available for ripple trains 6 and 7 only. These two ripple trains indicate maximum depths of 21 m and 15 m (Table 8-5). Because of their close stratigraphic positioning, they probably were formed in very similar water depths. Thus, the overlap between the two depth distributions probably encompasses the depth of formation; therefore, these ripples were probably formed in depths shallower than 15 m.

Similar values were calculated for the Chungo and Moosebar-Gates occurrences (Table 8-5).

STRUCTURAL SEQUENCES INVOLVING CONGLOMERATIC SYMMETRICAL RIPPLES AND HUMMOCKY CROSS-STRATIFICATION: SUMMARY

Beds exhibiting conglomeratic symmetrical ripples are closely associated both vertically and laterally with

complete and incomplete BPHFXM sequences (Dott and Bourgeois, 1982; Walker et al., 1983). Table 8-4 summarizes the sequence of structures observed in beds containing conglomeratic symmetrical ripples; these ripples are indicated as division R, and are distinguished from structureless, graded, or imbricated conglomerates (division B). Conglomeratic symmetrical ripples are commonly overlain by hummocky cross-stratified sandstone (division H). In turn, the hummocky interval in these beds is overlain by "flat" lamination (division F), centimeter-scale symmetrical ripples (division X), and/or bioturbated mudstone (division M), or is erosionally terminated by a subsequent depositional event. Conglomeratic symmetrical ripples (where present) always cap the basal conglomerate, yielding sequences which typically begin with a sharp base (.) overlain by division B overlain by division R. Note that planar parallel lamination (division P) was never observed in beds displaying these ripples.

I interpret the divisional sequences of table 8-4 as incomplete variations of the standard BPHFXM sequence. For occurrences displaying conglomeratic symmetrical ripples, I tentatively suggest the "idealized" conceptual sequence BRHFXM. This rare variant sequence is <u>not</u> intended to modify or replace the standard sequence. Further detailed study of divisional sequences in many more

examples is required to verify the general applicability of the BRHFXM variant proposed herein.

STRUCTURAL SEQUENCES INVOLVING CONGLOMERATIC SYMMETRICAL RIPPLES AND HUMMOCKY CROSS-STRATIFICATION: QUALITATIVE INTERPRETATION

The standard BPHFXM sequence is compared with the BRHFXM variant in figure 8-20. Walker et al. (1983) inferred that the BPHFXM sequence records a temporal transition from unidirectional- to oscillatory-dominant flow (Fig. 8-20A), but could not determine the relative importance of these two components in the formation of the hummocky division. Beds displaying oriented sole marks, graded bedding, imbrication, and conglomeratic symmetrical ripples within the basal conglomerate (Fig. 8-20B) probably also reflect initial deposition under waning unidirectional flow; in contrast to the standard BPHFXM sequence, the conglomeratic symmetrical ripples unquestionably indicate that transition to strongly oscillatory-dominant flow took place <u>prior</u> to formation of hummocky cross-stratification. The mantle of small symmetrical ripples (division X) overlying the hummocky division similarly indicates oscillatory flow <u>following</u> formation of hummocky cross-stratification. Flows that formed the small ripples

of division X were much less powerful than those required to form the large conglomeratic ripples of division R. Common gradational contacts between divisions and the preferred vertical sequence of divisions within beds suggest deposition as a single waning-flow event; therefore, in beds displaying conglomeratic symmetrical ripples within basal conglomerates, hummocky cross-stratification is best interpreted as resulting from waning, purely oscillatory or strongly oscillatory-dominant flow. This interpretation is strongly supported by the lateral juxtaposition of conglomeratic symmetrical ripples and hummocky sandstone in a few occurrences (Table 8-4).

Although some examples of hummocky cross-stratification are best interpreted as being formed by oscillatory flow, the structure may well be polygenetic in origin (see part 1 of this chapter). Extensive experimental and field research is required to determine the possible significance of other flow classes in the formation of hummocky cross-stratification. However, those examples which lie upon conglomeratic symmetrical ripples (and are therefore best interpreted as forming under oscillatory flow) may be subjected to quantitative paleohydraulic analysis (see below).

Figure 8-20. Comparison of standard BPHFXM sequence (A) with rare variant sequence (B). "U" and "O" refer to unidirectional and oscillatory fluid-motion components, respectively. See text for discussion.

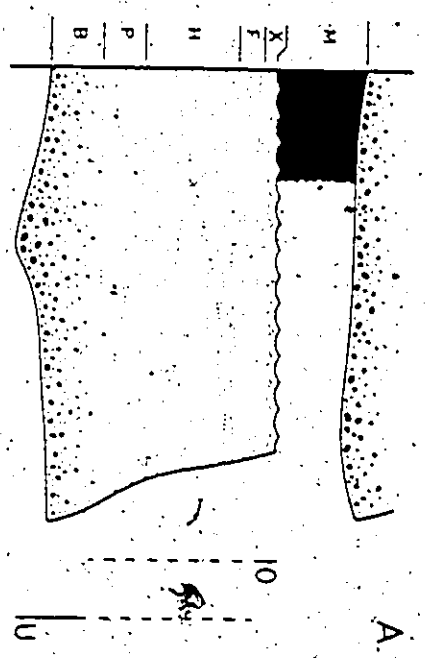
B
P
H
K
M
0
U
A

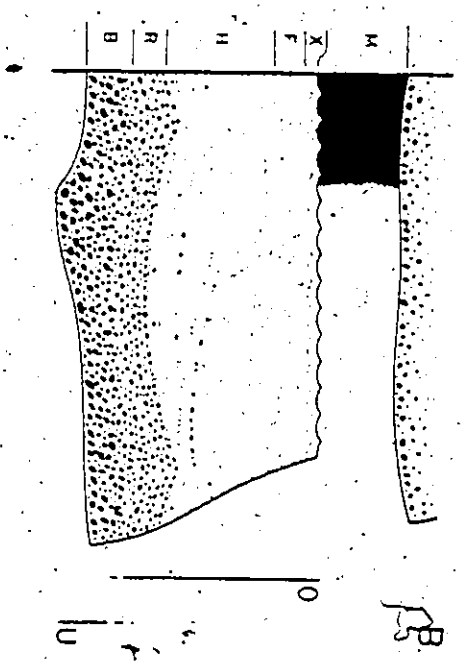
B
R
H
K
M
0
U
B

STRUCTURAL SEQUENCES INVOLVING CONGLOMERATIC SYMMETRICAL RIPPLES AND HUMMOCKY CROSS-STRATIFICATION: QUANTITATIVE INTERPRETATION

The quantitative paleohydraulic analysis of conglomeratic symmetrical ripples presented above permits approximate determination of the flow conditions that formed associated examples of hummocky cross-stratification. From the divisional sequences summarized in table 8-4, it is seen that the ripple occurrences numbered 2, 3, 6, 7, and 8 are immediately overlain by hummocky cross-stratified sandstone. Of this group, generative flow conditions may be calculated for ripple trains 6 and 7 only; both of these are from the Cardium Formation. The calculated flow conditions under which these ripple trains probably were formed are summarized in table 8-5. These conditions are illustrated on a graph of U_m vs. T in figure 8-21. This graph also illustrates conditions for other Cardium and Chungo examples; the Moosebar-Gates examples are plotted in figure 8-22. Note the diagonal arrows in these figures: These indicate the possible direction of displacement of these data points if the ancient ripples were formed under more energetic conditions than those which accompany the onset of general motion and ripple formation (for which conditions these calculations were made). As explained in part 2 of this chapter, each

of these points is constrained to the d_0 diagonal on which it is plotted; displacement along this diagonal opposite in sense to the arrows probably is impossible, due to reduction in the dimensionless acceleration number below the value required for general motion.

Also shown on these figures are the approximate bed-configuration boundaries for fine sand (after Harms et al., 1982, Fig. 2-10A). Inspection of figure 8-21 (specifically, the two points representing ripples which are immediately overlain by hummocky cross-stratified sandstone) reveals that these flow conditions correspond to the so-called "flat-bed" configuration field for oscillatory flows over fine sand. More energetic conditions (stronger than associated with the onset of general motion) would have placed these points deeper within the flat-bed field, as indicated by the arrows.

Assuming that the hummocky cross-stratification associated with ripple trains 6 and 7 was formed under roughly the same conditions as the underlying conglomeratic symmetrical ripples, these calculations suggest formation of these examples of hummocky cross-stratification within the wave-formed flat-bed field. These conclusions have been reported previously in abstract form by Duke & Leckie (1984), and are in agreement with the conclusions of another paleohydraulic analysis (performed by a different technique) from hummocky cross-stratified sands deposited

Figure 8-21. Calculated generative flow conditions (circles) for conglomeratic symmetrical ripples in the Cardium Formation and the Chungo Sandstone. Filled Cardium circles represent examples immediately overlain by hummocky cross-stratified sandstone. These points are superimposed upon the oscillatory-flow bed-configuration fields for fine sand (D = Ø.15-Ø.21 mm). See text for discussion.

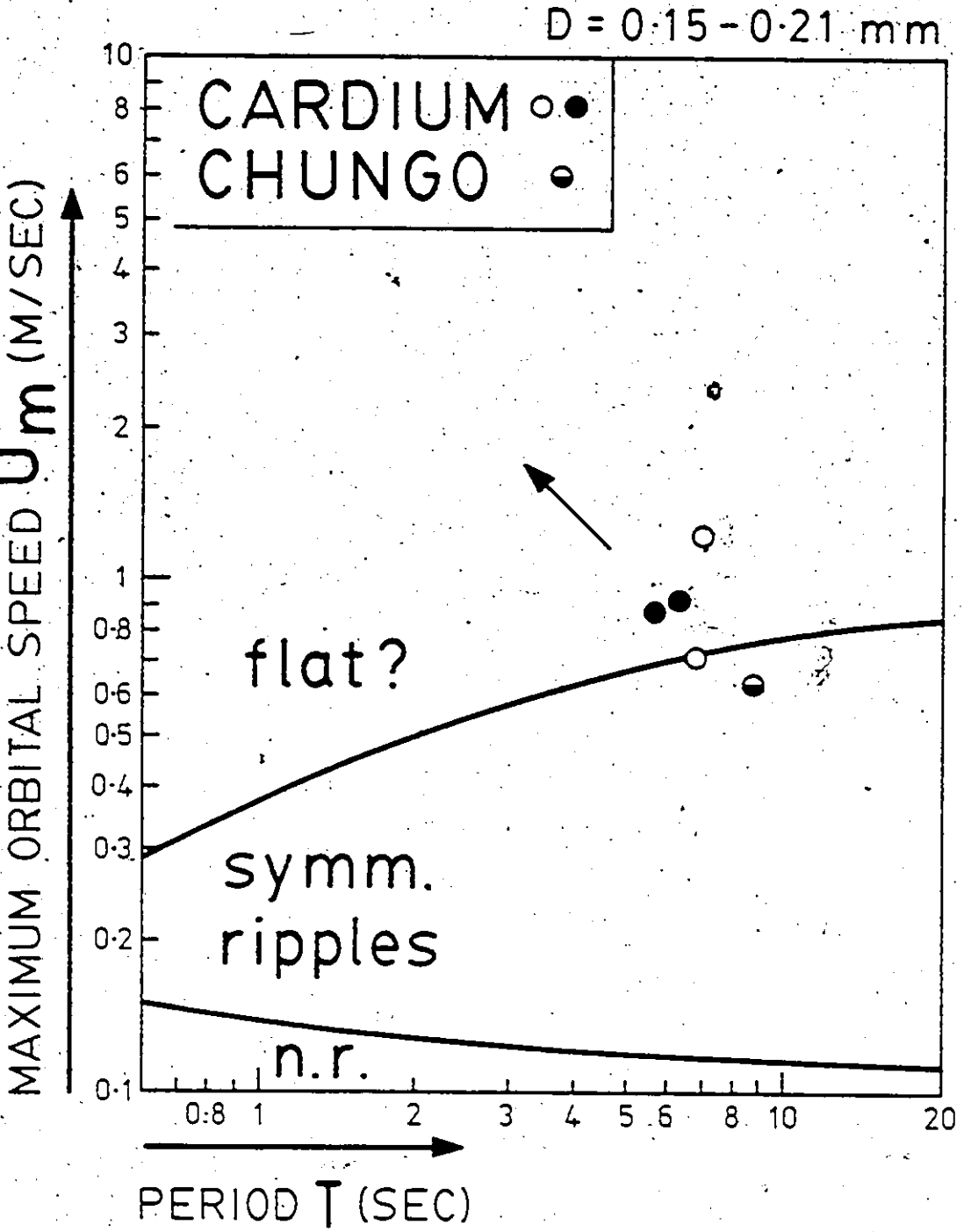
D = 0·15 - 0·21 mm
CARDIUM
CHUNGO
flat?
symm.
ripples
n.r.
MAXIMUM ORBITAL SPEED Um (M/SEC)
PERIOD T (SEC)
10
8
6
5
4
3
2
1
0·8
0·6
0·5
0·4
0·3
0·2
0·1
0·8
1
2
3
4
5
6
8
10
20

Figure 8-22. Calculated generative flow conditions (circles) for conglomeratic symmetrical ripples in the Moosebar-Gates transition. These points are superimposed upon the oscillatory-flow bed-configuration fields for fine sand (D = Ø.15-Ø.21 mm). See text for discussion.

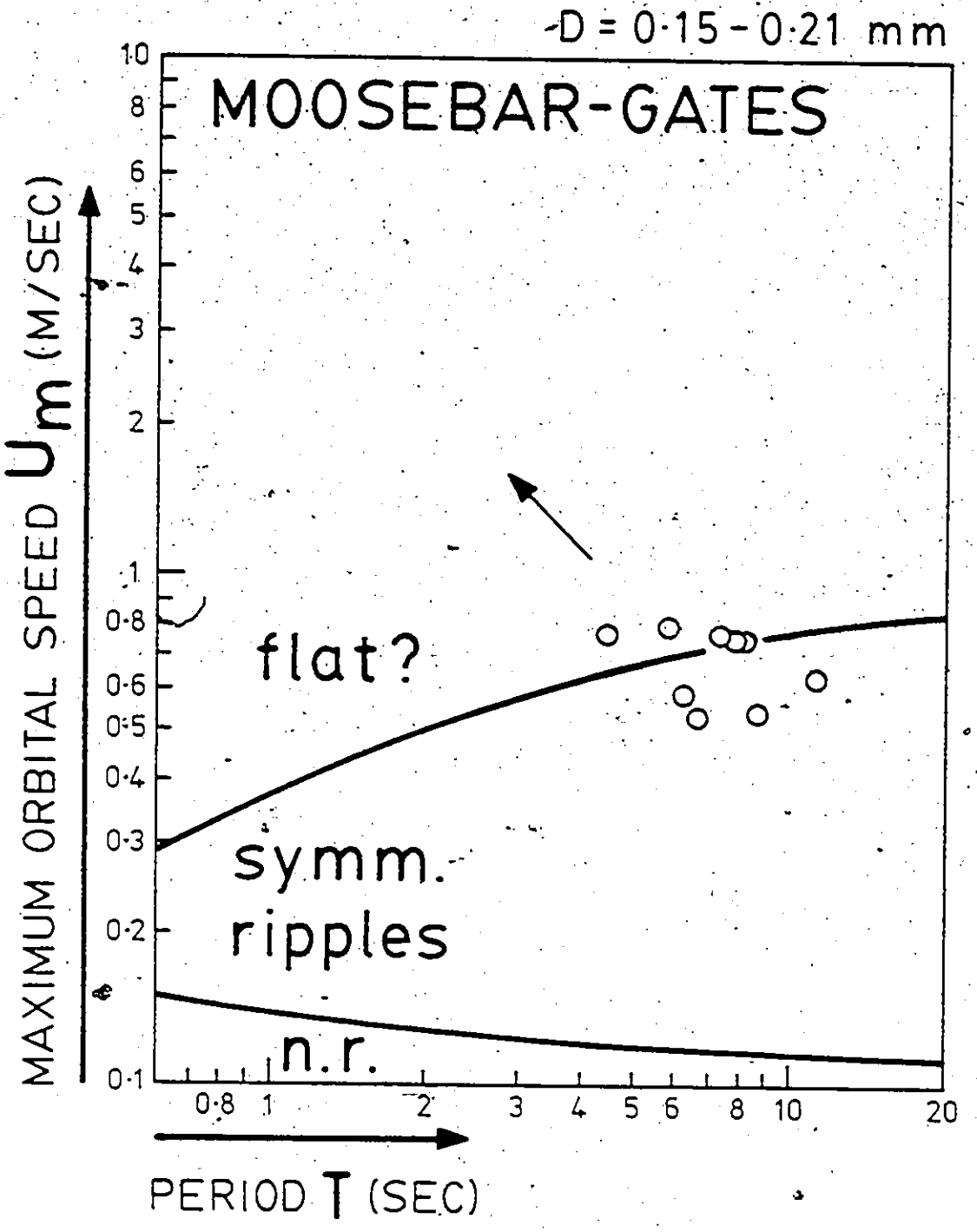
D = 0·15 - 0·21 mm
MOOSEBAR-GATES
MAXIMUM ORBITAL SPEED U_m (M/SEC)
10
8
6
5
4
3
2
1
0·8
0·6
0·5
0·4
0·3
0·2
0·1
flat?
symm.
ripples
n.r.
0·8
1
2
3
4
5
6
8
10
20
PERIOD T (SEC)

in Pleistocene Lake Bonneville (Duke, 1984).

This analysis suggests that hummocky cross-stratification may possibly be formed by low-amplitude, three-dimensional "undulations" developed within the so-called flat-bed field. Possible origins of these undulations include some sort of low-relief bedform (previously unrecognized) and/or a "beating" effect arising under natural polychromatic wave fields. The possible oscillatory-flow bedform associated with high values of the boundary Reynolds number (and, accordingly, low inertial-lag effects) would probably be an orbital ripple with a characteristic spacing approaching d_o. On the other hand, beating could result in rapidly varying, spatially localized, possibly non-periodic fluctuations in instantaneous bottom velocities. These velocity irregularities could result in both localized erosion and modification of the "flat-bed" bedform; however, pronounced beating effects probably would scale to some multiple of d_o.

Thus, the relationship between λ_H and d_o offers a test of the alternatives suggested above. The value of d_o can be obtained from conglomeratic symmetrical ripples, and thus can be compared to λ_H associated with these ripples. As was reported by Duke & Leckie (1984), this comparison indicates that λ_H values approximate the calculated values of d_o (plus or minus a maximum of 50%;

in several cases, 20%). In my opinion, these results favor the orbital ripple (bedform) origin, with the form-spacing of hummocky cross-stratification being scaled by bottom orbital diameter.

PART 4

ESTIMATED BATHYMETRY AND STORM-WAVE CLIMATE, AND THE HYDRAULIC SIGNIFICANCE OF VERTICAL STRUCTURAL SEQUENCES IN PROGRADING SHORELINE DEPOSITS IN THE CARDIUM FORMATION

INTRODUCTION

The preceding paleohydraulic analysis of conglomeratic symmetrical ripples in the Cardium Formation has major implications for the interpretation of Cardium shoreline sequences. In particular, this ahalysis provides: 1) a direct comparison of cycle thickness and calculated paleobathymetry within cycles, 2) a measure of the characteristic parameters of storm-generated waves incident at the Cardium shoreline, and 3) a framework for interpretation of the hydraulic significance of vertical structural sequences within Cardium cycles.

CYCLE THICKNESS AND PALEOBATHYMETRY

Returning to tables 8-4 and 8-5, note again that there are four different ripple trains from the Cardium Formation for which I was able to determine both: 1) the

generative fluid-motion characteristics U_M and T, and 2) maximum depth of formation. The first two Cardium examples (ripple trains 4 and 5) occur within thick transgressive resedimented-lag conglomerates capping Cardium cycles. [Train 4 occurs in the basal conglomerate of the Sundre Member, capping the second major sandstone in section 6-28 at the Seebe damsite; train 5 occurs in the Willmore Member, capping cycle 7 at section 4-19 on Thistle Creek.] The next two Cardium examples (ripple trains 6 and 7) both occur within a major regressive cycle. These trains both occur within cycle 2 in section GC-2, the Grande Cache railway roadcut (see Fig. 5-38 for a detailed vertical graphic log of this exposure). They occur in very close stratigraphic proximity (the 49 and 50 m levels, Fig. 5-38), roughly 6 and 7 m below the overlying contact between marine and non-marine deposits.

The maximum depths of formation calculated for the ripple trains in section GC-2 are 21 and 15 m; as discussed above in this chapter, their close stratigraphic proximity suggests that the shallower depth maximum probably is applicable to both trains. This depth limit is consistent with the depth estimate obtained by considering the total thickness of accumulated sediment between the ripples and the marine to non-marine transition. This interval is composed predominantly of well sorted sandstone; assuming no compaction and horizontal shoreline progradation, the

estimated depth of formation is 6 to 7 m.

Turning to the ripple trains occurring at transgressive cycle tops (examples 4 and 5), table 8-5 indicates somewhat greater maximum possible depths of formation (28 and 25 m, respectively). Again, these results are consistent with the inferred mode of formation: These ripple trains probably represent the final imprint of storm waves on these coarse deposits during transgressive inundation of the underlying cycles, prior to the deposition of muds over the transgressive shelf terrace upon which I infer they were formed. Thus, these ripples suggest an approximate maximum depth within Cardium cycles (i.e., at cycle boundaries) on the order of 25 to 30 m. This depth compares very favorably with the normative thickness of the marine portion of fully regressive (type 1) cycles in the Cardium (23.0 m). This normative thickness would be expected to fall somewhat short of the calculated maximum depth, due in part to compaction of the mud component of the cycle.

The preceding comparisons support one another, tentatively confirming the paleohydraulic analysis technique developed in this chapter, and suggesting that the maximum depth of deposition in most Cardium cycles was on the order of 25 to 30 m.

MAGNITUDE OF STORM WAVES INCIDENT AT CARDIUM SHORELINES

The calculations summarized in table 8-5 indicate that waves having periods on the order 5 to 7 s were responsible for formation of conglomeratic symmetrical ripples in shallow-marine deposits in the Cardium. Note that the values of period calculated for ripples formed in deeper water at cycle boundaries (6.7 to 7.0 s) are larger than those calculated for ripples formed in a more proximal, shallower setting (5.5 to 6.3 s). These values are fully consistent with the conceptual model for sedimentation developed in chapter 6. Specifically, the energy of larger, longer waves approaching a prograding Cardium shoreline would be drained over the shallow shelf terrace formed during the preceding transgression; the peak of the wave-energy spectrum would accordingly shift toward lower periods as waves approached the shoreline.

Conglomeratic symmetrical ripples are robust bedforms; they are the only wave-generated structures formed in coarse material which were recognized in this study. Accordingly, the wave periods associated with the formation of these ripples may represent the longest waves incident at the Cardium shoreline (or, possibly, the longest waves formed in the Cardium basin). It might be concluded, therefore, that no waves with periods longer than about 7 s were formed in the Alberta segment of the

Western Interior Seaway during Cardium deposition. These periods are greatly reduced relative to present-day oceanic waves, which have maximum periods on the order of 15 to 20 s. This may reflect reduced fetch and/or shallow water depths throughout the Seaway. Note, however, that the wave periods calculated from the ripples are not necessarily the maximum periods of high-energy waves associated with the deposition of the conglomerates in which the ripples were formed. Gillie (1979) observed that modern conglomeratic symmetrical ripples formed in storm-dominated shelf environments (at a depth of 18 m, comparable to the calculated depths of the Cardium examples) typically remain active during the waning stage of storm activity, and accordingly their characteristic parameters are imprinted by lower energy (and lower period) waves than those associated with the peak of storm activity.

TOWARD A HYDRODYNAMIC FRAMEWORK FOR THE INTERPRETATION OF VERTICAL SEQUENCES DEVELOPED IN PROGRADING SHORELINE DEPOSITS

The analysis presented in part 3 of this chapter indicated formation of hummocky cross-stratification within the oscillatory-flow "flat-bed" stability field by low-amplitude undulations (orbital ripples?) scaled by d_o.

Figure 8-23. A tentative framework for the interpretation of vertical structural sequences observed in prograding shoreline sequences in the Cardium Formation.

On the left is a diagram of stable bed configurations formed under oscillatory flows. NR = no ripple activity; RIP = symmetrical ripples; HCS = postulated field in which hummocky cross-stratification is formed (lower part of Southard's flat-bed field); FB = true flat bed (upper part of Southard's flat-bed field). The horizontal axis is wave period (in seconds); the vertical axis is maximum bottom orbital speed (in meters per second). Selected d_o diagonals are also drawn, as are representative points showing conditions under which examples of hummocky cross-stratification are thought to be formed (filled circles).

On the right is drawn a representation of a fully regressive Cardium cycle.

See text for explanation.

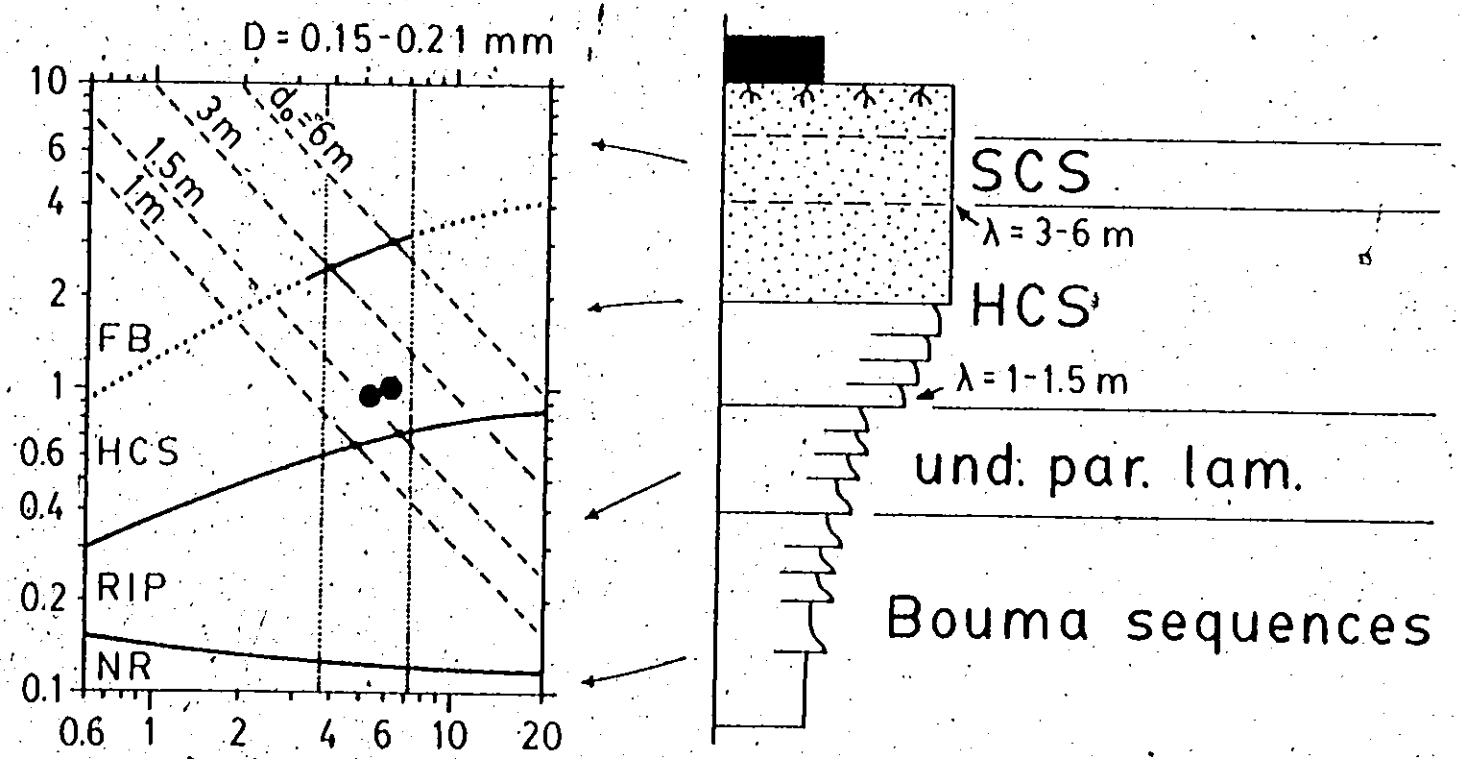
D = 0.15-0.21 mm
10
6
4
2
1
0.6
0.4
0.2
0.1
0.6
1
2
4
6
10
20
3m
1.5m
1m
d_0=6m
FB
HCS
RIP
NR
SCS
λ = 3-6 m
HCS
λ = 1-1.5 m
und. par. lam.
Bouma sequences

695

This tentative suggestion for the origin of the structure permits the development of a hydrodynamic interpretion of vertical structural sequences observed in Cardium cycles (Fig. 8-23).

On the left in figure 8-23, I have indicated a narrow band of wave periods on the oscillatory-flow bed configuration field for fine sand (modified from J. B. Southard's diagram in Harms et al., 1982, Fig. 2-10A). I have modified Southard's diagram to include my best estimate of the field for hummocky cross-stratification, as determined in this chapter; hummocky cross-stratification is drawn as occurring within the lower portion of Southard's flat-bed field. This band of wave periods (from about 4 to 7 s) is meant to represent the probable range of periods under which the Cardium Formation occurrences of hummocky cross-stratification were formed, based upon the calculated conditions of formation of conglomeratic symmetrical ripples (see part 3 of this chapter).

On the right in figure 8-23, I have drawn a representation of a fully regressive Cardium cycle. As was discussed in chapter 5, the scale of hummocky undulations generally increases upward through these cycles, with form-spacings increasing from about 1 to 1.5 m in the lowest hummocky bed, to about 3 to 6 m in the highest hummocky (or swaley) sandstone in a cycle. These dimensions correspond well with the values of d_o which

bound the hummocky bed-configuration field on the left.

Hummocky cross-stratification generally overlies undulatory parallel lamination (facies 1UP); the first hummocky bed represents an abrupt increase in the scale of wave-generated structures. I suggest that this abrupt break in scale, along with the gradual upward increase in form-spacing within hummocky beds, can best be explained by an upward increase in U_m accompanying the shoaling of waves of roughly constant period. The abrupt scale change from undulatory parallel lamination to hummocky cross-stratification represents the transition from deposition on an aggrading bed within the vortex-ripple field (undulatory parallel lamination) to deposition on an aggrading bed within the hummocky field (hummocky cross-stratification). The gradual upward increase in form-spacing within a sequence of hummocky sandstones represents variation within a single bed-configuration field (the hummocky field). This variation is controlled by the gradual increase in d_o which accompanies shoaling.

Likewise, the gradational upward transition common within swaley cross-stratified sandstones, from low-angle curved cross-strata to plane parallel lamination, probably reflects a gradational transition from the hummocky field to the true flat-bed field.

Additional field and laboratory investigations are required to test the hypothetical framework outlined above.

CHAPTER 9. SUMMARY OF THIS STUDY

This thesis presents the major conclusions of my study of the Turonian Cardium Formation. This investigation concentrated on primary physical and biogenic structures observed in 28 Cardium exposures in the Foothills belt of southern Alberta.

The major conclusions of this investigation can be grouped under four headings:

1) Internal stratigraphy of the Cardium Formation,
2) Large-scale sedimentology of the Cardium Formation,
3) Nature and origin of various wave-formed structures,
4) Improved technique for vertical facies analysis.

INTERNAL STRATIGRAPHY OF THE CARDIUM FORMATION

1) The cycle and member divisions established by Stott (1963, 1975) have been shown to be non-correlative and internally inconsistent; therefore, neither system is suitable as a basis of correlation.

2) A new member system has been erected for the Cardium Formation. The revised stratigraphy is based upon the

distinction between marine and non-marine deposits within lithostratigraphically correlative, thickening- and coarsening-upward cyclic sequences present in every exposure examined.

3) In the Foothills of southern Alberta, the revised member scheme consists of three marine members (Seebe, Sundre, and Willmore) and two non-marine members (Cutpick and Obstruction). The conglomeratic Baytree Member in the Peace River area and central British Columbia was not examined, and has not been modified in the revised stratigraphy.

LARGE-SCALE SEDIMENTOLOGY OF THE CARDIUM FORMATION

4) Vertically stacked thickening- and coarsening-upward cycles, several meters or tens of meters in thickness, constitute all or most of the thickness of each Cardium exposure examined.

5) Cardium cycles are composed primarily of mudstones, interbedded mudstones and very fine to fine decimeter-scale sandstones, thick very fine to fine sandstones several meters in thickness, and minor amounts of conglomerate.

6) All or most of the sediment in each Cardium cycle was deposited in shallow-marine environments, as evidenced by abundant shallow-marine trace and body fossils.

7) Hummocky cross-stratification is ubiquitous within marine sandstones of the Cardium Formation, suggesting a storm-dominated shallow-marine depositional environment.

8) The scale of hummocky cross-stratification and other inferred wave-generated structures generally increases upward through individual cycles.

9) Many Cardium cycles are capped with non-marine deposits, generally composed predominantly of rooted mudstones and thin coals.

10) The coarsening-upward tendency in Cardium cycles, the upward increase in scale of the dominant wave-formed structures in these cycles, and the transition to non-marine sedimentation in many cycles suggest that these developments were formed by prograding storm-dominated shorelines.

11) Paleoflow data indicate that the orientation of the Cardium shoreline varied greatly over short distances laterally, and that the dominant mode of transport of offshore sands was by storm-driven, geostrophically

balanced shelf circulation. Extensive sand/gravel transport by storm-generated turbidity currents on the shelf is not indicated.

12) A classification scheme for Cardium cycles, based upon improved Markov-chain analysis (see below), recognizes six basic cycle types.

13) The six cycle types consist of one fully regressive cycle type (i.e., cycles capped with non-marine deposits) and five related top-absent cycles (i.e., cycles truncated by transgression which do not display non-marine deposits).

14) Top-absent cycles display similar vertical facies sequences to those present in the lower parts of fully regressive cycles, suggesting that top-absent cycles represent prograding shoreline deposits truncated during transgression by a combination of transgressive erosion and/or non-deposition of the upper part of the shoreline sequence. Thus, most or all Cardium cycles can be interpreted as complete or superficially truncated prograding shoreline sequences.

15) Boundaries between vertically juxtaposed cycles represent transgression surfaces.

16) Transgression surfaces within the Cardium Formation typically are covered by marine conglomerates of variable thickness and lateral extent.

17) The areal distribution and internal structures of transgressive conglomerates suggest that they represent lag deposits which have been extensively remobilized and transported during transgression. Conglomerate commonly were transported by and deposited from a dispersion above the bed; I suggest the term resedimented-lag be applied to these deposits.

18) A conceptual model for Cardium sedimentation has been developed from the synthesis of a variety of observations. In this model, top-absent cycles originate as prograding shoreline deposits which are extensively eroded during a subsequent transgression. Non-marine deposits can be stripped from the top of a prograding sand sheet by the transgressing shoreface for several tens of kilometers landward of the final position of the shoreline. This process forms an extensive transgressive shelf terrace cut into the underlying regressive sand sheet.

19) The transgressive erosion mentioned above forms an extensive resedimented-lag conglomerate over the transgressively eroded shelf terrace. Transport of

this conglomerate during transgression by geostrophically balanced shelf circulation has an offshore component, resulting in the accumulation of a thick conglomerate body in a "hydrodynamic shadow" over the final profile of the drowned regressive shoreface.

20) The process described above results in formation of an extensive, asymmetrically tapered sand body capped with an offlapping, erosionally based conglomerate veneer.

21) Three major regressive episodes of sedimentation are recognized in Foothills exposures. Each of these is terminated by a regionally correlative transgression surface, locally accented by marine conglomerates. These three regressive-transgressive sedimentation episodes may possible correlate with similar developments in the subsurface.

NATURE AND ORIGIN OF VARIOUS WAVE-FORMED STRUCTURES

22) A detailed description of hummocky cross-stratification has identified a variety of near-bed flow conditions which may give rise to the structure.

23) A review of field and experimental data concerning the origin of symmetrical vortex ripples has permitted the

paleohydraulic analysis of vortex ripples formed under fully rough turbulent, oscillatory boundary-layer flow. This technique permits calculation of the generative flow parameters U_m (maximum orbital speed at the bottom) and T (period of oscillation). The technique relies solely upon measureable sediment and ripple characteristics and assumed fluid density; it is applicable to all ancient conglomeratic symmetrical ripples. The technique assumes formation at or near the threshold of motion; it has been successfully tested against modern conglomeratic symmetrical ripples formed under known hydraulic conditions.

24) A comparison of the calculated conditions of formation of conglomeratic symmetrical ripples closely associated stratigraphically with hummocky cross-stratification suggests that these examples of hummocky cross-stratification probably were formed within the oscillatory-flow "flat-bed" stability field, by previously unrecognized low-amplitude, three-dimensional orbital ripples with spacings approximating bottom orbital diameter.

IMPROVED TECHNIQUE FOR VERTICAL FACIES ANALYSIS

25) A "significance filter" has been developed to aid in the construction of normative vertical facies sequences based upon Markov-chain analysis of vertical facies successions. This statistical technique is applied following the selection (by means of standard techniques) of statistically acceptable transitions.

26) Analysis of vertical facies transitions within the Cardium Formation has demonstrated the validity of segregated Markov-chain analyses of non-ergodic data sets.

AFTERWORD

In August, 1985, following the oral defence of this thesis but prior to the final submission for binding, I spent two weeks in Alberta examining additional exposures of the Cardium Formation; and re-examining certain of the exposures described in this thesis. This additional work resulted in certain minor revisions to this study, which are summarized in a technical memorandum by the author available from either McMaster University (Geology Department Tech. Memo. 85-4) or the Pennsylvania State University (Geosciences Department, Geology Program Tech. Memo. 85-1). These essentially identical memoranda are listed in the references of this thesis.

During these two weeks of field work, it was my great pleasure to be accompanied by two other members of the McMaster Cardium Group: Guy Plint and Shelley Leggitt. Dr. Plint generously shared the expertise he has developed from his thorough studies of the Cardium in the subsurface; I deeply appreciate and acknowledge his important contributions to our understanding of this unit. Shelley provided spirited field assistance, as did Anne-Marie Plint.

REFERENCES CITED

Aigner, T., 1982, Calcareous tempestites: storm dominated stratification in Upper Muschelkalk limestones (middle Trias, S. W. Germany), in Einsele, G., and Seilacher, A., eds., Cyclic and Event Stratification: New York, Springer-Verlag, p.180-198.

Aigner, T., and Reineck, H. E., 1982, Proximality trends in modern storm sands from the Heligoland Bight (North Sea) and their implications for basin analysis: Senkenberg. Mar., v. 14, p. 183-215.

Allen, J. R. L., 1979, A model for the interpretation of wave ripple-marks using their wavelength, textural composition, and shape: Journal of the Geological Society of London, v. 136, p. 673-682.

Allen, P. A., 1981a, Wave-generated structures in the Devonian lacustrine sediments of south-east Shetland and ancient wave conditions: Sedimentology, v. 28, p. 369-379.

Allen, P. A., 1981b, Some guidelines in reconstructing ancient sea conditions from wave ripplemarks: Marine Geology, v. 43, p. M59-M67.

Allen, P. A., 1984, Reconstruction of ancient sea conditions with an example from the Swiss Molasse: Marine Geology, v. 60, p. 455-473.

Allen, P. A., 1985, Hummocky cross-stratification is not produced purely under progressive gravity waves: Nature, v. 313, p. 562-564.

Bagnold, R. A., 1946, Motion of waves in shallow water. Interaction between waves and sand bottoms: Proceedings of the Royal Society of London, Series A, v. 187, p. 1-15.

Beach, F. K., 1955, Cardium a turbidity current deposit: Journal of the Alberta Society of Petroleum Geologists, v. 3, p. 123-125.

Beach, F. K., 1956, Reply to DeWiel on turbidity current deposits: Journal of the Alberta Society of Petroleum Geologists, v. 4, p. 175-177.

Blatt, H., Middleton, G. V., and Murray, R., 1980, Origins of Sedimentary Rocks (2nd edition), New Jersey, Prentice-Hall, 782 p.

Bouma, A. H., 1962, Sedimentology of some flysch deposits: Amsterdam, Elsevier, 168 p.

Bourgeois, J., 1980, A transgressive shelf sequence exhibiting hummocky stratification: the Cape Sebastian Sandstone (Upper Cretaceous), southwestern Oregon: Journal of Sedimentary Petrology, v.50, p. 681-702.

Bourgeois, J., and Smith, J. D., 1984, Paleohydraulic significance of hummocky stratification (abs.): Canadian Society of Petroleum Geologists, Sedimentology of Shelf and Sandstones Symposium, Program and

Abstracts, p. 27.

Broekman, J. A., 1973, Sedimentary structures and paleoecology of the Pliocene Kritika Formation in a section near Kalithes (Rhodos, Greece): Nederlandse Akademie van Wetenschappen Proceedings, Series B (Physical Sciences), v. 76, p. 423-445.

Cairnes, D. D., 1907, Moose Mountain district of Southern Alberta: Geological Survey of Canada, Report No. 968.

Campbell, C. V., 1966, Truncated wave-ripple laminae: Journal of Sedimentary Petrology, v. 36, p. 820-828.

Campbell, C. V., 1971, Depositional Model -- Upper Cretaceous Gallop beach shoreline, Ship Rock Area, northwestern New Mexico: Journal of Sedimentary Petrology, v. 41, p. 395-409.

Carstens, M. R., Nielson, F. M., and Altinbileck, H. D., 1969, Bed forms generated in the laboratory under oscillatory flow: analytical and experimental study: U. S. Army Corps of Engineers, Coastal Engineering Resource Center, Technical Memorandum 28.

Clarke, T. L., Lesht, B., Swift, D. J. P., and Freeland, G. L., 1982, Sediment resuspension by surface wave action: an examination of possible mechanisms: Marine Geology, v. 49, p. 43-59.

Clifton, H. E., 1976, Wave-formed sedimentary structures - a conceptual model, in Davis, R. A., and Ethington, R. L., eds., Beach and Nearshore Sedimentation: Society

of Economic Paleontologists and Mineralogists, Special Publication No. 24, Tulsa, Oklahoma, p. 125-148.

Clifton, H. E., and Dingler, J. E., 1984, Wave-formed structures and paleoenvironmental reconstruction: Marine Geology, v. 60, p. 165-198.

Curray, J. R., 1964, Transgressions and regressions, in Miller, R. L., ed., Papers in Marine Geology -- Shepard Commemorative Volume: New York, Macmillan, p. 175-203.

Curray, J. R., and Moore, D. G. 1964, Holocene regressive littoral sand, Costa de Nayarit, Mexico, in van Straaten, L. M. J. U., ed., Deltaic and Shallow Marine Deposits: Amsterdam, Elsevier, p. 83-100

Curray, J. R., Emmel, F. J., and Crampton, P. J. S., 1969, Lagunas costeras, un simposio: Mem. Simp. Int. Lagunas Costeras, UNAM-UNESCO, Nov. 28-30, 1967, Mexico, D. F., p. 63-100

DeWeil, J. E. F., 1956, Viking and Cardium not turbidity current deposits: Journal of the Alberta Society of Petroleum Geologists, v. 4, p. 173-175.

Dingler, J. R., 1974, Wave-formed ripples in nearshore sands: Unpublished Ph.D. thesis, University of California, San Diego, California, 136 p.

Dingler, J. R., 1979, The threshold of grain motion under oscillatory flow in a laboratory wave channel: Journal of Sedimentary Petrology, v. 49, p. 287-294

Dott, R. H., Jr., and Bourgeois, J., 1982, Hummocky cross-

stratification -- importance of variable bedding sequences analogous to the Bouma sequence: Geological Society of America Bulletin, v. 94, p. 663-680.

Dott, R. H., Jr., and Bourgeois, J., 1983, Hummocky cross-stratification -- importance of variable bedding sequences analogous to the Bouma sequence: Reply: Geological Society of America Bulletin, v. 94, p. 1249-1251.

Duke, W. L., 1980, Upper Cretaceous (Turonian) Cardium Formation, southern Alberta: Department of Geology, McMaster University, Technical Memorandum 80-4, 59 p.

Duke, W. L., 1981, Internal stratigraphy and paleogeography of the Upper Cretaceous Cardium Formation in the Alberta Foothills (abs.): Abstracts of the Geological Association of Canada, v. 6, p. A-38.

Duke, W. L., 1982a, Hummocky cross-stratification, tropical hurricanes, and intense winter storms (abs.), Geological Society of America, Abstracts with Programs, v. 14, p. 478.

Duke, W. L., 1982b, The 'type locality' of hummocky cross-stratification: the storm-dominated Silurian Medina Formation in the Niagara Gorge, New York and Ontario: Proceedings of the Ontario Petroleum Institute, v. 21, p. 2.1-2.31.

Duke, W. L., 1984, Paleohydraulic analysis of hummocky cross-stratified sands indicates equivalence with

wave-formed flat bed: Pleistocene Lake Bonneville deposits, northern Utah (abs.): American Association of Petroleum Geologists Bulletin, v. 68, p. 472.

Duke, W. L., 1985a, Prograding shoreline sequence, Silurian Medina Formation, New York and Ontario: storm-dominated sedimentation in a very shallow epicontinental sea (abs.): Geological Society of America, Abstracts with Programs, v. 17, p. 16.

Duke, W. L., 1985b, The paleogeography of Paleozoic and Mesozoic storm depositional systems: a discussion: Journal of Geology, v. 93, p. 88-90.

Duke, W. L., 1985c, Hummocky cross-stratification, tropical hurricanes, and intense winter storms: Sedimentology, v. 32, p. 167-194.

Duke, W. L., 1985d, Cardium Formation in outcrop: summary of work conducted in August, 1985: Department of Geology, McMaster University, Technical Memorandum 85-4.

Duke, W. L., 1985e, Cardium Formation in outcrop: summary of work conducted in August, 1985: Department of Geosciences, The Pennsylvania State University, Geology Program Technical Memorandom 85-1.

Duke, W. L., Ainsworth, S. H., and Walker, R. G., 1980, Storm dominated coarsening-upward clastic sequences in the Cardium Formation, Upper Cretaceous, southern Alberta (abs.): Geological Society of America,

Abstracts with Programs, v. 12, p. 32.

Duke, W. L., and Leckie, D. A., 1984, Origin of Hummocky cross-stratification. Part 2. Paleohydraulic analysis indicates formation by orbital ripples within the wave-formed flat-bed field (abs.): Canadian Society of Petroleum Geologists, Shelf and Sands Symposium, Program and Abstracts, p. 32.

Eckart, C., 1952, The propogation of waves from deep to shallow water, in Gravity Waves: National Bureau of Standards, Circular No. 521, p. 165-173.

Frey, R. W., and Pemberton, S. G., Trace Fossil Facies Models, in Walker, R. G., ed., Facies Models (2nd edition), Geoscience Canada Reprint Series 1: Geological Association of Canada, p. 189-208.

Gilbert, G. K., 1899, Ripple-marks and cross-bedding: Geological Society of America Bulletin, v. 10, p. 135-140.

Gillie, 1979, Sand and gravel deposits of the coast and inner shelf, east coast, Northland Peninsula, New Zealand: Unpublished Ph.D. thesis, University of Canterbury, Christchurch, New Zealand.

Goldring, R., 1971, Shallow-water sedimentation as illustrated in the Upper Devonian Baggy Beds: Memoirs of the Geological Society of London, No. 5, 80 p.

Goldring, R., and Bridges, P., 1973, Sublittoral sheet sandstones: Journal of Sedimentary Petrology, v. 43,

p. 736-747.

Gray, D. I., and Benton, M. J., 1982, Multidirectional palaeocurrents as indicators of shelf storm beds, in Einsele, G., and Seilacher, A., eds., Cyclic and Event Stratification: New York, Springer-Verlag, p. 350-353.

Griffith, L. A., 1981, Depositional environment and conglomerate diagenesis of the Cardium Formation: Unpublished M.Sc. thesis, University of Calgary, Calgary, Alberta, 131 p.

Hamblin, A. P., 1978, Sedimentology of a prograding shallow marine slope and shelf sequence, Upper Jurassic Fernie-Kootenay transition, southern front ranges: Unpublished M.Sc. thesis, McMaster University, Hamilton, Ontario, Canada, 196 p.

Hamblin, A. P., Duke, W. L., and Walker, R. G., 1979, Hummocky cross-stratification -- indicator of storm-dominated shallow marine environments (abs.): American Association of Petroleum Geologists Bulletin, v. 63, p. 460-461.

Hamblin, A. P., and Walker, R. G., 1979, Storm-dominated shallow marine deposits: the Fernie-Kootenay (Jurassic) transition, southern Rocky Mountains: Canadian Journal of Earth Sciences, v. 16, p. 1673-1690.

Harms, J. C. Southard, J. B., Spearing, D. R., Walker, R. G., 1975, Depositional environments as interpreted from

primary sedimentary structures and stratification sequences: Society of Economic Paleontologists and Mineralogists, Short Course No. 2, 161 p.

Harms, J. C., Southard, J. B., and Walker, R. G., 1982, Structures and Sequences in Clastic Rocks: Society of Economic Paleontologists and Mineralogists, Short Course No. 9 (pages not consecutively numbered).

Harper, C. W., 1984, Improved methods of facies sequence analysis, in Walker, R. G., ed., Facies Models (2nd. edition), Geoscience Canada Reprint Series 1: Geological Association of Canada, p. 11-14.

Howard, J. D., 1972, Trace fossils as criteria for recognizing shorelines in the stratigraphic record, in Rigby, J. K., and Hamblin, W. K., eds., Recognition of Ancient Sedimentary Environments, Society of Economic Paleontologists and Mineralogists, Special Publication No. 16, p. 215-225.

Hunter, R. E., and Clifton, H. E., 1982, Cyclic deposits and hummocky cross-stratification of probable storm origin in Upper Cretaceous rocks of the Cape Sebastian area, southwestern Oregon: Journal of Sedimentary Petrology, v. 52, p. 127-143.

Jonsson, I. G., 1967, Wave boundary layers and friction factors: Proceedings of the 10th conference on Coastal Engineering, p. 127-148.

Keith, D. A. W., 1985, Sedimentology of the Cardium Forma-

tion, Willesden Green Field, Alberta: Unpublished M.Sc. thesis, McMaster University, Hamilton, Ontario, Canada, 233 p.

Kennedy, J. F., 1963, The mechanics of dunes and antidunes in erodible channels: Journal of Fluid Mechanics, v. 16, p. 521-544.

Komar, P. D., 1974, Oscillatory ripple marks and the evaluation of ancient wave conditions and environments: Journal of Sedimentary Petrology, v. 44, p. 169-180.

Komar, P. D., and Miller, M. C., 1973, The threshold of sediment movement under oscillatory water waves: Journal of Sedimentary Petrology, v. 43, p. 1101-1110.

Krauss, F. F., and Nelson, D. A., 1984, Storm event sedimentation: lithofacies association in the Cardium Formation, Pembina area, west-central Alberta, Canada, in Stott, D. F., and Glass D. J., eds., The Mesozoic of middle North America: Canadian Society of Petroleum Geologists, Memoir 9, p. 485-511.

Kreisa, R. D., 1981, Storm-dominated sedimentary structures in subtidal marine facies with examples from the Middle and Upper Ordivician of southwestern Virginia: Journal of Sedimentary Petrology, v. 51, p. 823-848.

Leckie, D. A., and Duke, W. L., 1984, Origin of hummocky cross-stratification. Part 1. Straight-crested symmetrical gravel dunes -- the coarse grained equivalent of hummocky cross-stratification (abs.):

Canadian Society of Petroleum Geologists, Shelf Sands and Sandstones Symposium, Program and Abstracts, p. 51.

Leckie, D. A., and Walker, R. G., 1982, Storm- and tide-dominated shorelines in Cretaceous Moosebar-lower Gates interval -- outcrop equivalents of Deep Basin gas trap in western Canada: American Association of Petroleum Geologists Bulletin, v. 66, p. 138-157.

Lofquist, K. E. B., 1978, Sand ripple growth in an oscillatory-flow water tunnel: U. S. Army Corps of Engineers, Coastal Engineering Resource Center, Technical Paper 78-5.

MacDonald, W. D., 1957, Cardium between Athabasca River and Peace River: Journal of the Alberta Society of Petroleum Geologists, v. 5, p. 82-88.

Malloch, C. S., 1911, Bighorn Coal Basin, Alberta: Geological Survey of Canada, Memoir 9E.

Manfrino, C., 1984, Stratigraphy and palynology of the Upper Lewis Shale, Pictured Cliffs Sandstone, and lower Fruitland Formation (Upper Cretaceous) near Durango, Colorado: The Mountain Geologist, v. 21, p. 115-132.

Manohar, M., 1955, Machanics of bottom sediment movement due to wave action, Beach Erosion Board Technical Memorandum No. 75, 105 p.

Marsaglia, K. M., and Klein, G. DeV., 1983, The paleogeography of Paleozoic and Mesozoic storm

depositional systems: Journal Geology, v. 91, p. 117-142.

McKee, E. D., 1979, Sedimentary structures in dunes, in McKee, E. D., ed., A study of global sand seas: U.S. Geological Survey Professional Paper 1052, p. 83-134.

Michaelis, E. R., 1957, Cardium sedimentation, Pembina River area: Journal of the Alberta Society of Petroleum Geologists, v. 5, p. 73-77.

Michaelis, E. R., and Dixon, G., 1969, Interpretation of depositional processes from sedimentary structures in the Cardium sand: Canadian Petroleum Geology Bulletin, v. 17, p. 410-443.

Middleton, G. V., 1967, Experiments on density and turbidity currents. III. Deposition of sediment: Canadian Journal of Earth Sciences, v. 4, p. 475-505.

Middleton, G. V., 1973, Johannes Walther's law of correlation of facies: Geological Society of America Bulletin, v. 84, p. 979-988.

Miller, M. C., and Komar, P. D., 1980a, Oscillation sand ripples generated by laboratory apparatus: Journal of Sedimentary Petrology, v. 50, p. 173-182.

Miller, M. C., and Komar, P. D., 1980b, A field investigation of the relationship between oscillation ripple spacing and the near-bottom water orbital motions: Journal of Sedimentary Petrology, v. 50, p. 183-191.

Mount, J. F., 1982, Storm-surge-ebb origin of hummocky

cross-stratified units of the Andrews Mountain Member, Campito Formation (Lower Cambrian), White-Inyo Mountains, eastern California: Journal of Sedimentary Petrology, v. 52, p. 941-958.

Nielson, A. R., 1957, Cardium stratigraphy, Pembina field: Journal of the Alberta Society of Petroleum Geologists, v. 5, p. 64-72.

Palmer, A. R., 1983, The decade of North American geology. 1983 geologic time scale: Geology, v. 11, p. 503-504.

Pemberton, S. G., and Frey, R. W., 1984, Ichnology of storm-influenced shallow-marine sequence: Cardium Formation (Upper Cretaceous) at Seebe, Alberta, in Stott, D. F., and Glass, D. J., eds., The Mesozoic in Middle North America: Canadian Society of Petroleum Geologists, Memoir 9, p. 281-304.

Pemberton, S. G., Frey, R. W., and Walker, R. G., 1984, Probable lobster burrows in the Cardium Formation (Upper Cretaceous) of southern Alberta, Canada, and comments on modern burrowing decapods: Journal of Paleontology, v. 58, p. 1422-1435.

Powers, D. W., and Easterling, R. G., 1982, Improved methodology for using embedded Markov chains to describe cyclical sediments: Journal of Sedimentary Petrology, v. 52, p. 913-924.

Rance, P. J., and Warren, N. F., 1968, The threshold of movement of coarse material in oscillatory flow:

Proceedings of the 11th Conference on Coastal Engineering, p. 487-491.

Rosenthal, L. R. P., 1983, Sedimentology of the Chungo Sandstone Member of the Upper Cretaceous Wapiabi Formation, Southern Alberta: Unpublished M.Sc. thesis, McMaster University, Hamilton, Ontario, Canada.

Rutherford, R. L., 1927, Geology along Bow River between Cochrane and Kananaskas, Alberta: Sci. Ind. Research Council, University of Alberta, Report 17.

Sinha, R. N., 1970, Cardium Formation, Edson area, Alberta: Geological Survey of Canada, Paper 68-30, 63 p.

Smith, J. D., and Bourgeois, J., 1984, A model for deposition seaward of the offshore bar due to storms of extreme intensity (abs.): Canadian Society of Petroleum Geologists, Sedimentology of Shelf Sands and Sandstones Symposium, Program and Abstracts, p. 64.

Southard, J. B., 1984, Laboratory studies of oscillatory-flow bed configurations and their bearing on stratification in shallow-marine sands (abs.): Canadian Society of Petroleum Geologists, Shelf Sands and Sandstones Symposium, Program and Abstracts, p. 65.

Southard, J. B., and Stanley, D. J., 1976, Shelf-break processes and sedimentation, in Stanley, D. J., and Swift, D. J. P., eds., Marine Sediment Transport and Environmental Management: New York, John Wiley and Sons, Inc., p. 351-378.

Stott, D. F., 1963, The Cretaceous Alberta Group and equivalent rocks, Rocky Mountain Foothills, Alberta: Geological Survey of Canada, Memoir 317, 306 p.

Stott, D. F., 1975, The Cretaceous System in northeastern British Columbia, in Caldwell, W. G. E., ed., The Cretaceous System in the Western Interior of North America, Geological Association of Canada, Special Paper No. 13, p. 441-468.

Swagor, N. S., Oliver, T. A., and Johnson, B. A., 1976, Carrot Creek Field, Central Alberta, in Leonard, ed., The Sedimentation of Selected Clastic Oil and Gas Resevoirs in Alberta, p. 78-95.

Swift, D. J. P., 1976, Coastal sedimentation, in Stanley, D. J., and Swift, J. P., eds., Marine Sediment Transport and Environmental Management: New York, John Wiley and Sons, p. 255-310.

Swift, D. J. P., Nelsen, T., McHone, J., Holliday, B., Palmer, H., and Shideler, G., 1977, Holocene evolution of the inner shelf of southern Virginia: Journal of Sedimentary Petrology, v. 47, p. 1454-1474.

Swift D. J. P., Parker, G., Lanfredi, N. W., Perillo, G., and Figge, K., 1978, Shoreface-connected sand ridges on American and European shelves: a comparison: Estuarine and Coastal Marine Science, v. 7, p. 257-273.

Swift, D. J. P., Figueiredo, A. G. Jr., Freeland, G. L., and Oertel, G. F., 1983, Hummocky cross-stratification

and megaripples: a geological double standard? Journal of Sedimentary Petrology, v. 53, p. 1295-1317.

Taylor, D. R., and Walker, R. G., 1984, Depositional environments and paleogeography in the Albian Moosebar Formation and adjacent fluvial Gladstone and Beaver Mines Formations, Alberta: Canadian Journal of Earth Sciences, v. 21, p. 698-714.

Walker, R. G., 1979a, Shallow marine sands, in Walker, R. G., ed., Facies Models, Geoscience Canada Reprint Series 1: Geological Association of Canada, p. 75-89.

Walker, R. G., 1983a, Cardium Formation 1. "Cardium, a turbidity current deposit" (Beach, 1955): a brief history of ideas: Canadian Petroleum Geology Bulletin, v. 31, p. 205-212.

Walker, R. G., 1983b, Cardium Formation 2. Sand-body geometry and stratigraphy in the Garrington-Caroline-Ricinus area, Alberta -- the "ragged blanket" model: Canadian Petroleum Geology Bulletin, v. 31, p. 14-26.

Walker, R. G., 1983c, Cardium Formation 3. Sedimentology and stratigraphy in the Garrington-Caroline area, Alberta: Canadian Petroleum Geology Bulletin, v. 31, p. 213-230.

Walker, R. G, 1984a, General Introduction: Facies, Facies Sequences and Facies Models, in Walker, R. G., ed., Facies Models (2nd edition), Geoscience Canada Reprint

Series 1: Geological Association of Canada, p. 1-10.

Walker, R. G., 1984b, Shelf and Shallow Marine Sands, in Walker, R. G., ed., Facies Models (2nd edition): Geological Association of Canada, Reprint Series 1, p. 141-170.

Walker, R. G., 1984c, Turbidites and Associated Coarse Clastic Deposits, in Walker, R. G., ed., Facies Models (2nd edition), Geoscience Canada Reprint Series 1: Geological Association of Canada, Reprint Series 1, p. 171-188.

Walker, R. G., 1985, Cardium Formation 5. Channel cut and filled by turbidity currents in the Cretaceous Western Interior Seaway, Ricinus Field, Alberta: American Association of Petroleum Geologists, (in press).

Walker, R. G., Duke, W. L., and Leckie, D. A., 1983, Hummocky stratification: significance of its variable bedding sequences: discussion: Geological Society of America Bulletin, v. 94, p. 1245-1249.

Whiteaves, J. F., 1895, Some of the Cretaceous fossils collected during Captain Palliser's explorations in British North America in 1857-60: Proceedings and Transactions of the Royal Society of Canada, 2nd series, v. 1, p. 110.

Wright, M. E., 1980, The Upper Cretaceous Cardium Formation at Seebe, Alberta: shallow marine storm deposits: Unpublished B.Sc. thesis, McMaster University,

Hamilton, Ontario, Canada, 117 p.

Wright, L. D., and Coleman, J. M., 1973, Variations in morphology of major river deltas as functions of ocean waves and river discharge regimes: American Association of Petroleum Geologists Bulletin, v. 57, p. 370-398.

Wright, M. E., and Walker, R. G., 1981, Cardium Formation (Upper Cretaceous) at Seebe, Alberta -- storm-transported sandstones and conglomerates in shallow marine depositional environments below fair-weather wave base: Canadian Journal of Earth Sciences, v. 18, p. 795-809.

Yorath, C. J., Bornhold, B. D., and Thomson, R. E., 1979, Oscillation ripples on the northeast Pacific continental shelf: Marine Geology, v. 31, p. 45-58.

Appendix 1 -- Field Guide to Exposures of the Cardium Formation Measured for this Thesis

This appendix provides precise directions to each section of the Cardium Formation which has been measured for this thesis. These sections were measured during four summer field seasons (1978-1981). Included herein are detailed location maps (Fig. A1-2 through A1-13, inclusive) for each of these 28 sections. The relative locations of these detailed maps are indicated on the small-scale general location map (Fig. A1-1). Additionally, a photograph of each measured section is included (Fig. A1-14 through A1-28, inclusive). This information should be adequate to locate all measured exposures in the field area, which occupies a belt through the foothills of Alberta and British Columbia some 560 km long and 50 km wide.

The individual directions to each exposure indicate the type of vehicle needed to reach each section at the time of completion of field work for this thesis. Road conditions may have changed since 1981. Note: A pair of hip-waders is recommended as an aid in examination of many of these sections.

Magnetic declinations indicated on the small-scale location maps were accurate in the early 1970's. At the time of completion of this thesis, declination had been reduced by approximately three-quarters of a degree throughout the field area.

This appendix is reproduced in exactly its present form as a McMaster University Departmental Technical Memorandum. Copies of this document are available from the Department of Geology at McMaster University. Interested readers should request a copy of:

Technical Memo 83-2:
Upper Cretaceous (Turonian) Cardium Formation, Southern Alberta: Field Guide to Exposures Measured by the Author (1978-1981), by W. L. Duke.

Note that this technical memo is not available through the McMaster University library system.

The following directions to the various measured sections are given in geographical order; sections are listed in sequence from northwest to southeast. Sections identified by number only (e.g. 5-45) were previously described by Stott (1963), and his scheme for the numbering of sections was used without modification.

With one exception, sections identified by letters and numbers (e.g. BD-1) have not previously been described. The exception to this system is section WA-1 on the south fork of Wapiabi Creek. Stott (1963) designated this as the type section of the Cardium Formation, but did not assign a number code for it.

Figure A1-1. General location map showing relative locations of the 28 Cardium exposures measured for this thesis. Measured sections are indicated by small filled circles. Boxes indicate locations of large-scale detailed location maps. The figure number for each of these maps is written beside the corresponding box. The inset shows the position of the general location map relative to northwestern states and provinces of the United States and Canada.

A1-5

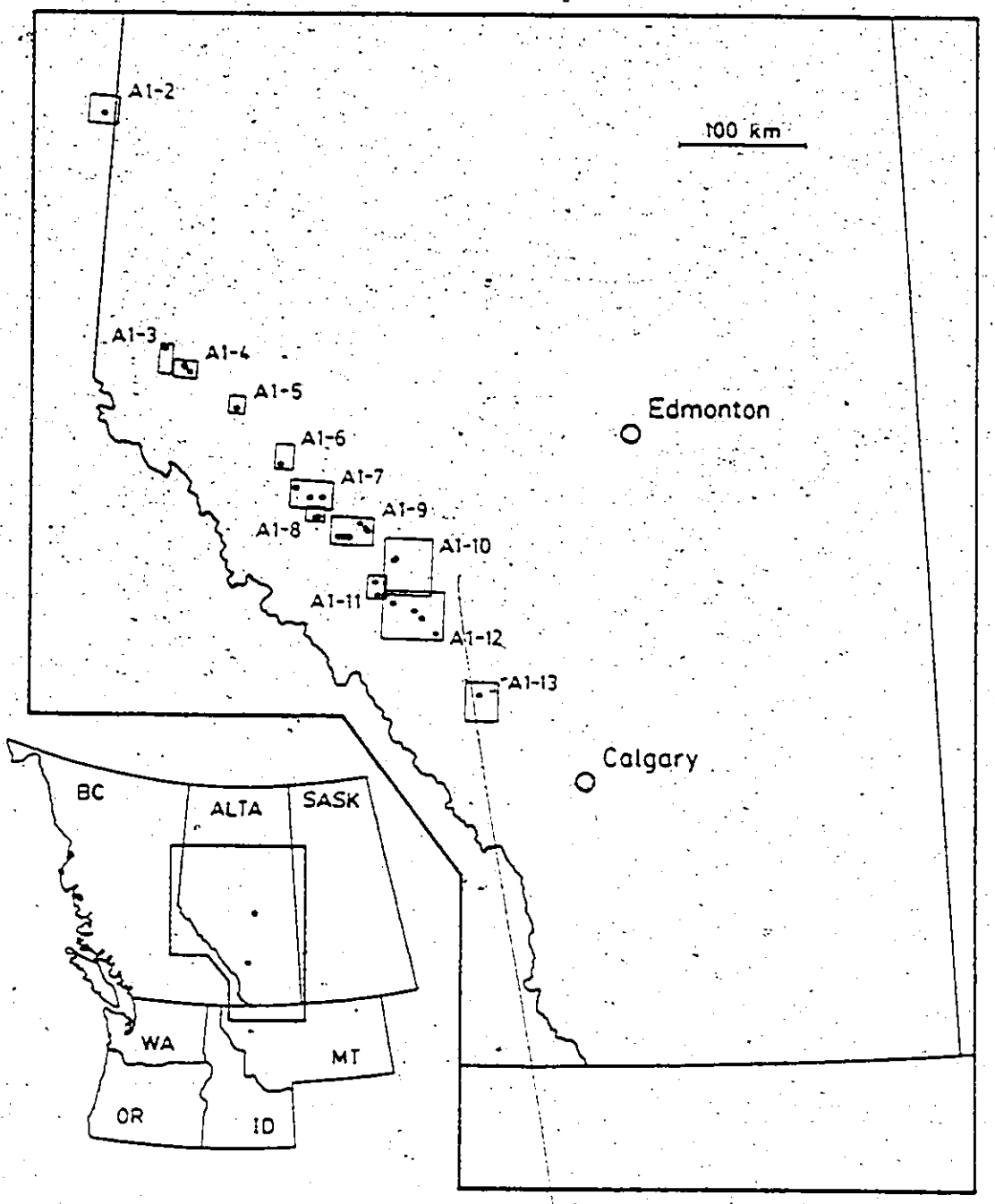
A1-2
100 km
A1-3
A1-4
A1-5
Edmonton
A1-6
A1-7
A1-9
A1-8
A1-10
A1-11
A1-12
A1-13
Calgary
BC
ALTA
SASK
WA
MT
OR
ID

Figure A1-2. Detailed map showing location of measured section PC-1.

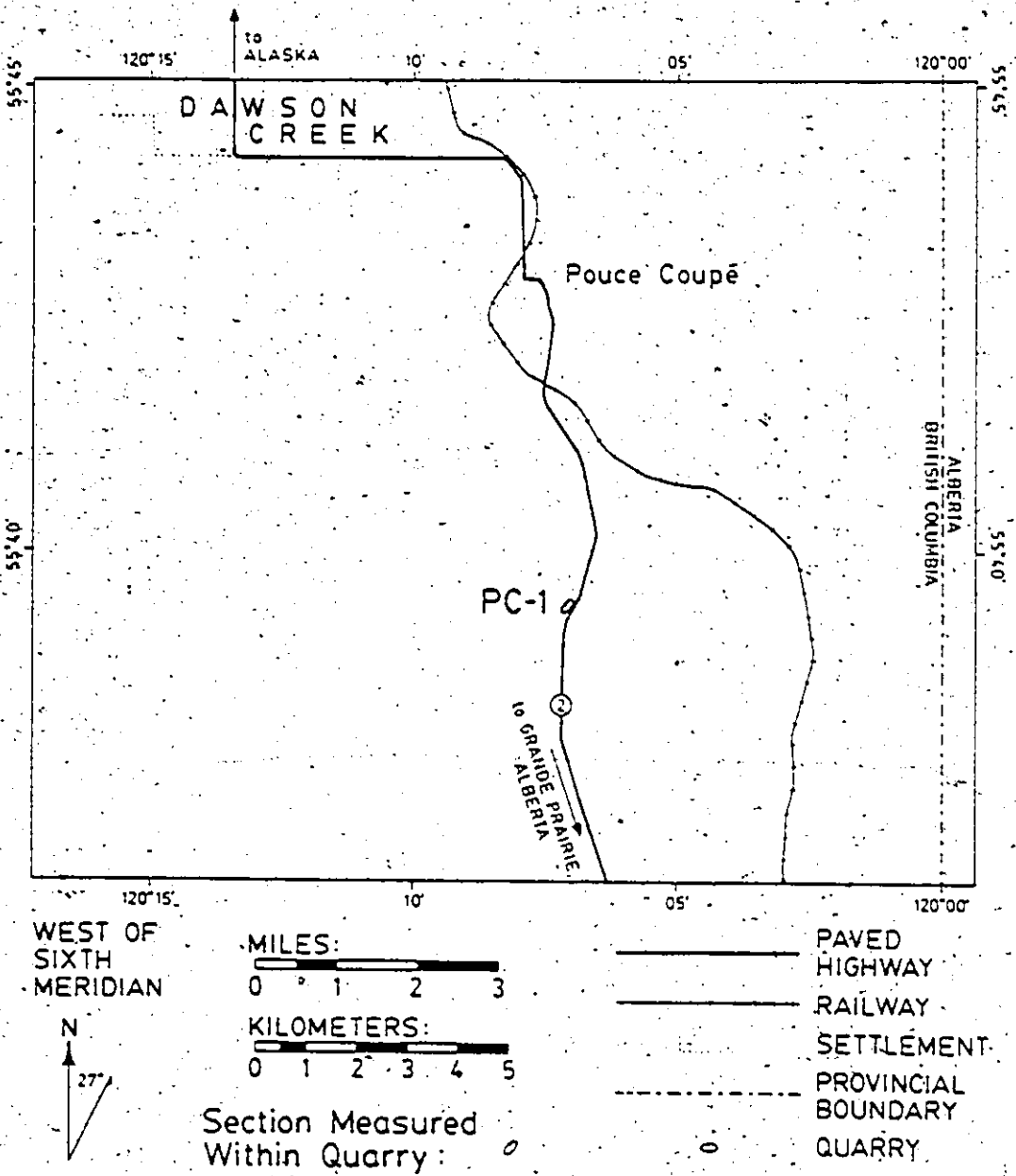
to ALASKA
120°15'
10'
05'
120°00'
55°45'
55°40'
DAWSON CREEK
Pouce Coupé
PC-1
to GRANDE PRAIRIE, ALBERTA
ALBERTA
BRITISH COLUMBIA
WEST OF SIXTH MERIDIAN
N
27°
MILES:
0 1 2 3
KILOMETERS:
0 1 2 3 4 5
Section Measured Within Quarry:
PAVED HIGHWAY
RAILWAY
SETTLEMENT
PROVINCIAL BOUNDARY
QUARRY
W L D 7/14/83

Figure A1-3. Detailed map showing location of measured section CU-1.

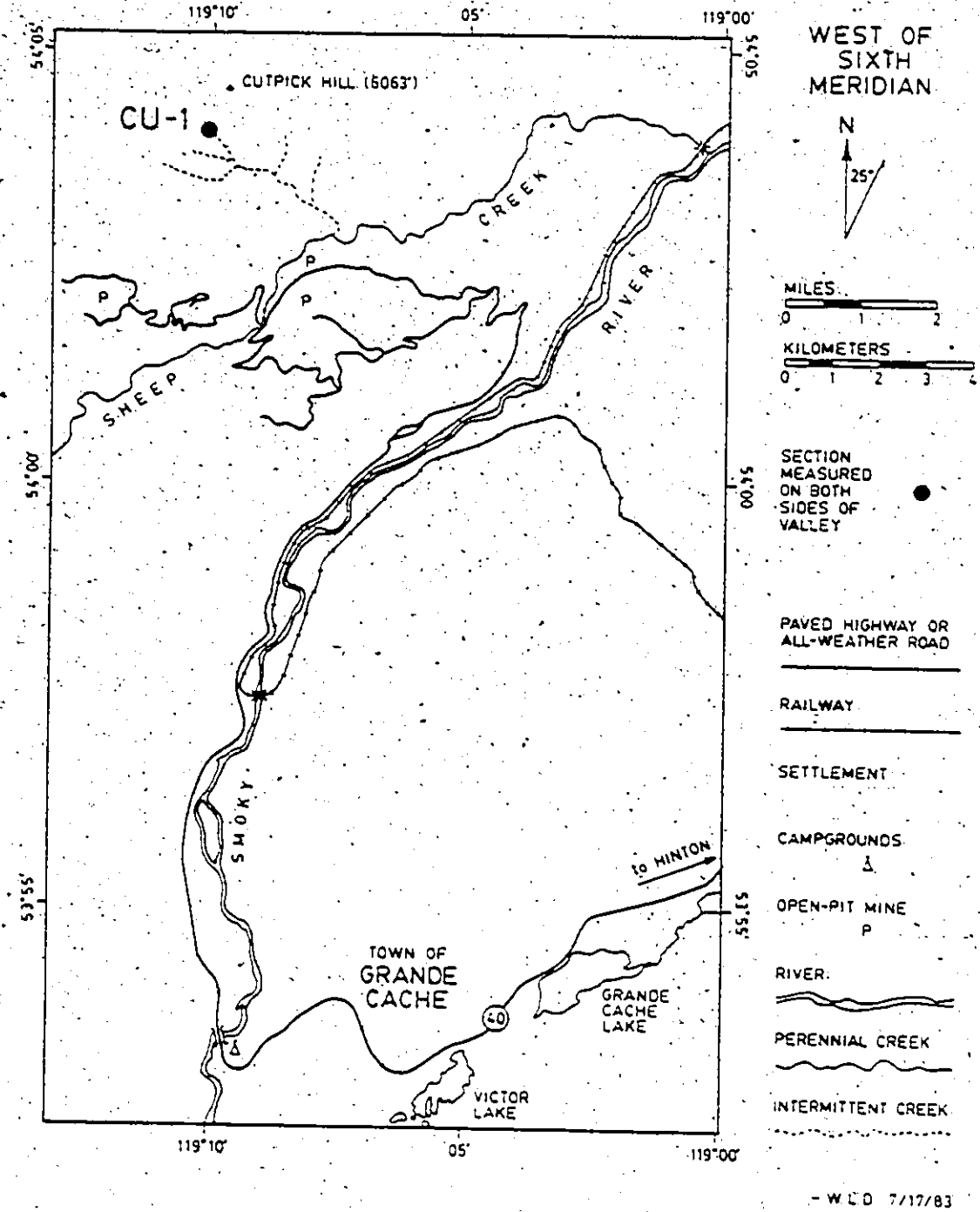
119°10'
05'
119°00'
54°05'
54°00'
53°55'
CUTPICK HILL (5063')
CU-1
SHEEP CREEK
SMOKY RIVER
P
TOWN OF GRANDE CACHE
TO HINTON
40
GRANDE CACHE LAKE
VICTOR LAKE
WEST OF SIXTH MERIDIAN
N
25°
MILES
0 1 2
KILOMETERS
0 1 2 3 4
SECTION MEASURED ON BOTH SIDES OF VALLEY
PAVED HIGHWAY OR ALL-WEATHER ROAD
RAILWAY
SETTLEMENT
CAMPGROUNDS
OPEN-PIT MINE
RIVER
PERENNIAL CREEK
INTERMITTENT CREEK
W.L.D. 7/17/83

Figure A1-4. Detailed map showing locations of measured sections 5-4, GC-1, GC-2, and MS-1.

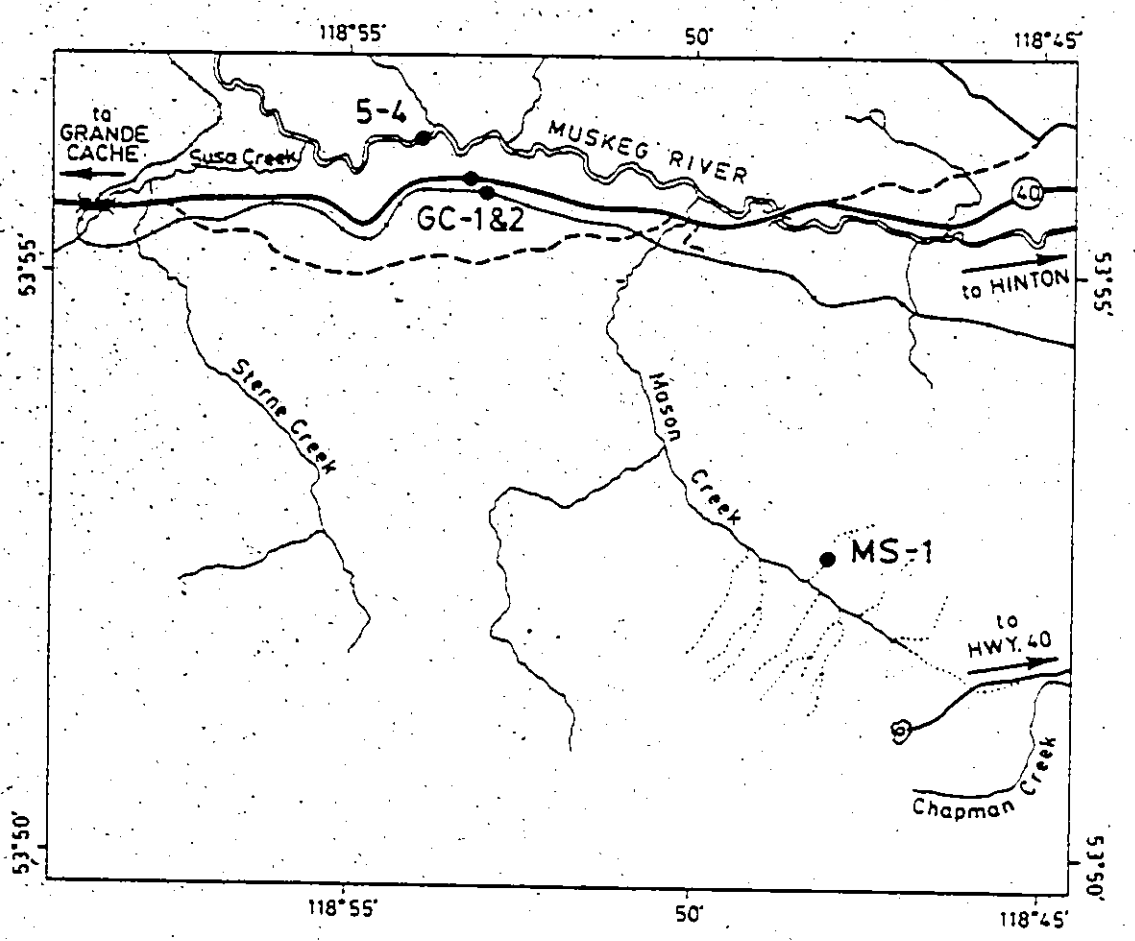

WEST OF SIXTH MERIDIAN

N

25°

MILES:
0 .1 2

KILOMETERS:
0 1 2 3

SECTION MEASURED:
● ON BOTH SIDES OF VALLEY

PAVED HIGHWAY
DRY-WEATHER ROAD
TRUCK TRAIL
RAILWAY
LOCALITY-little or no build-up
RIVER
PERENNIAL CREEK
INTERMITTENT CREEK
LAKE

- W.L.D. 6/29/83

Figure A1-5. Detailed map showing location of measured section 5-19.

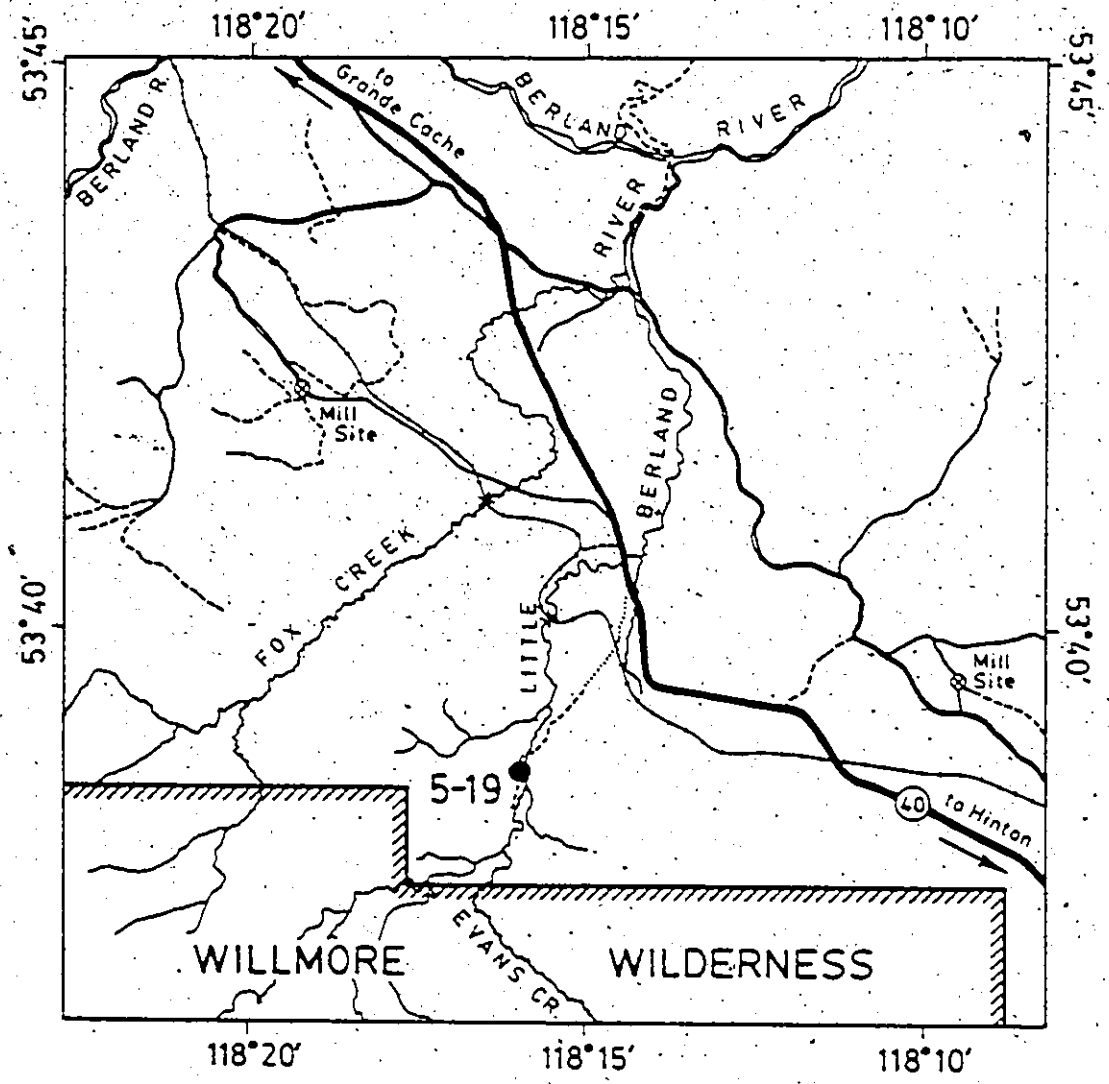
118°20'
118°15'
118°10'
53°45'
53°40'
BERLAND R.
to Grande Cache
BERLAND RIVER
RIVER
Mill Site
BERLAND
FOX CREEK
LITTLE
Mill Site
5-19
40
to Hinton
WILLMORE WILDERNESS
EVANS CR.
WEST OF SIXTH MERIDIAN
MILES:
0 1 2
KILOMETERS:
0 1 2 3 4
N
25°
SECTION MEASURED:
ON BOTH SIDES OF VALLEY
PAVED HIGHWAY
ALL-WEATHER ROAD
DRY-WEATHER ROAD
TRUCK TRAIL
RECLAIMED TRUCK TRAIL
RAILWAY
RIVER
MINOR RIVER, CREEK
W.L.D. 6/9/83

Figure A1-6. Detailed map showing location of measured section 5-22.

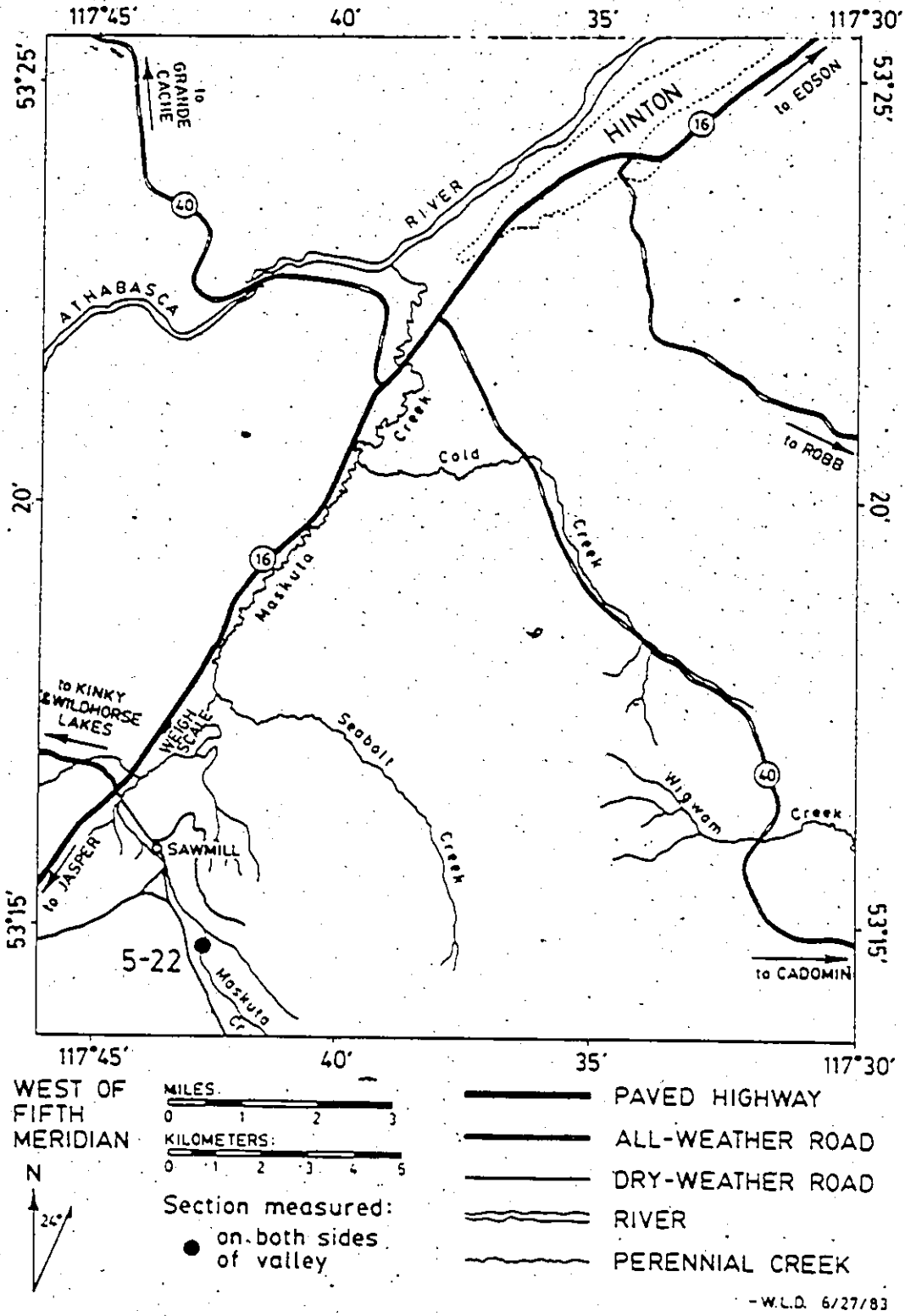
117°45'
40'
35'
117°30'
53°25'
20'
53°15'
to GRANDE CACHE
40
RIVER
ATHABASCA
HINTON
16
to EDSON
to ROBB
Cold
Creek
Creek
Muskuta
to KINKY & WILDHORSE LAKES
WEIGH SCALE
Seaboll
Creek
SAWMILL
to JASPER
5-22
Muskuta Cr.
Wigwam
Creek
to CADOMIN
WEST OF FIFTH MERIDIAN
MILES
0 1 2 3
KILOMETERS:
0 1 2 3 4 5
N
24°
Section measured:
on both sides of valley
PAVED HIGHWAY
ALL-WEATHER ROAD
DRY-WEATHER ROAD
RIVER
PERENNIAL CREEK
-W.L.D. 6/27/83

Figure A1-7. Detailed map showing locations of measured sections SC-1, 7-1, and 4-43.

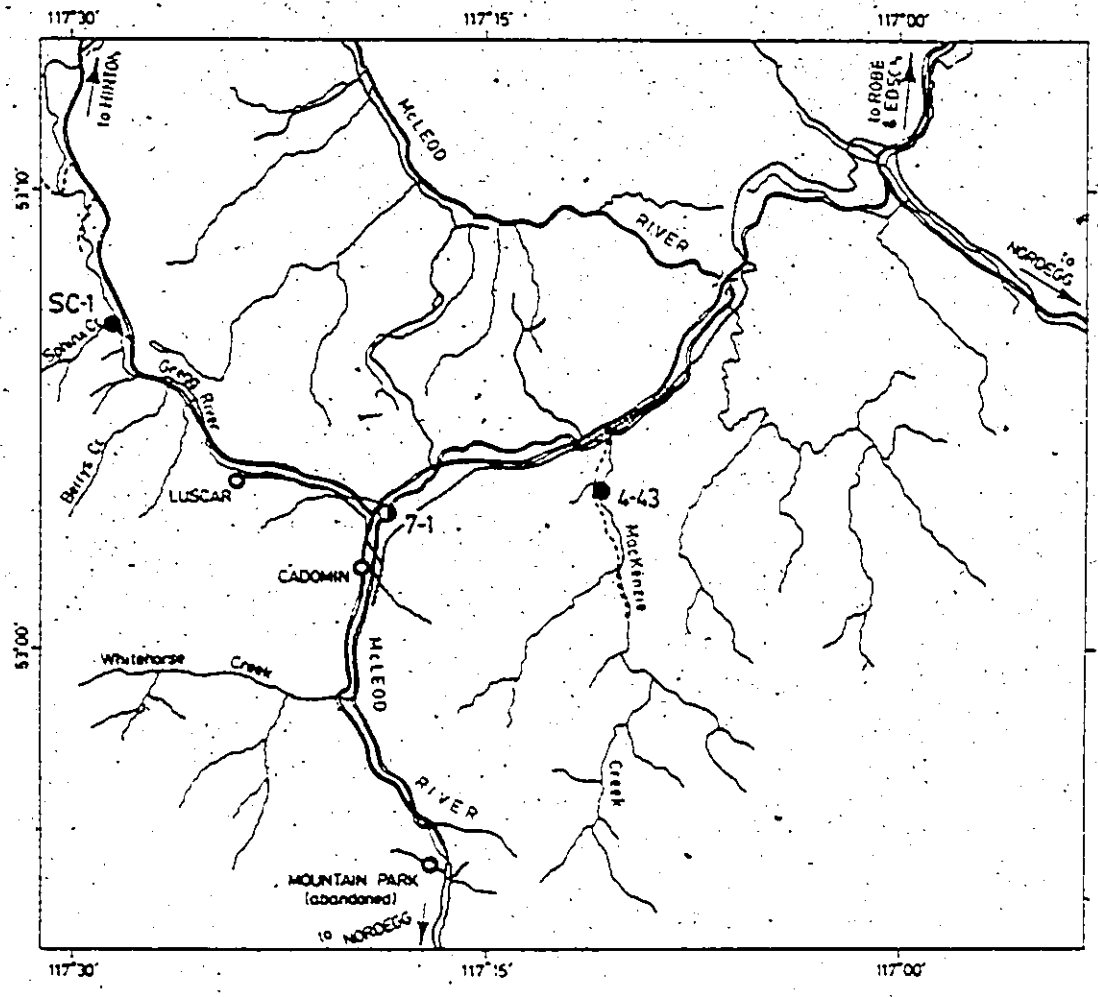

WEST OF FIFTH MERIDIAN

MILES 0 1 2 3 4 5

KILOMETERS 0 1 2 3 4 5 6 7 8

N

24°

SECTION MEASURED:

● on both sides of valley

◑ on east side of valley

All-Weather Road

Dry-Weather Road

Truck Trail

Railway

○ Settlement

River

Creek, Minor River

- W.L.D. 11/27/80

Figure A1-8. Detailed map showing locations of measured sections ND-2 and ND-1.

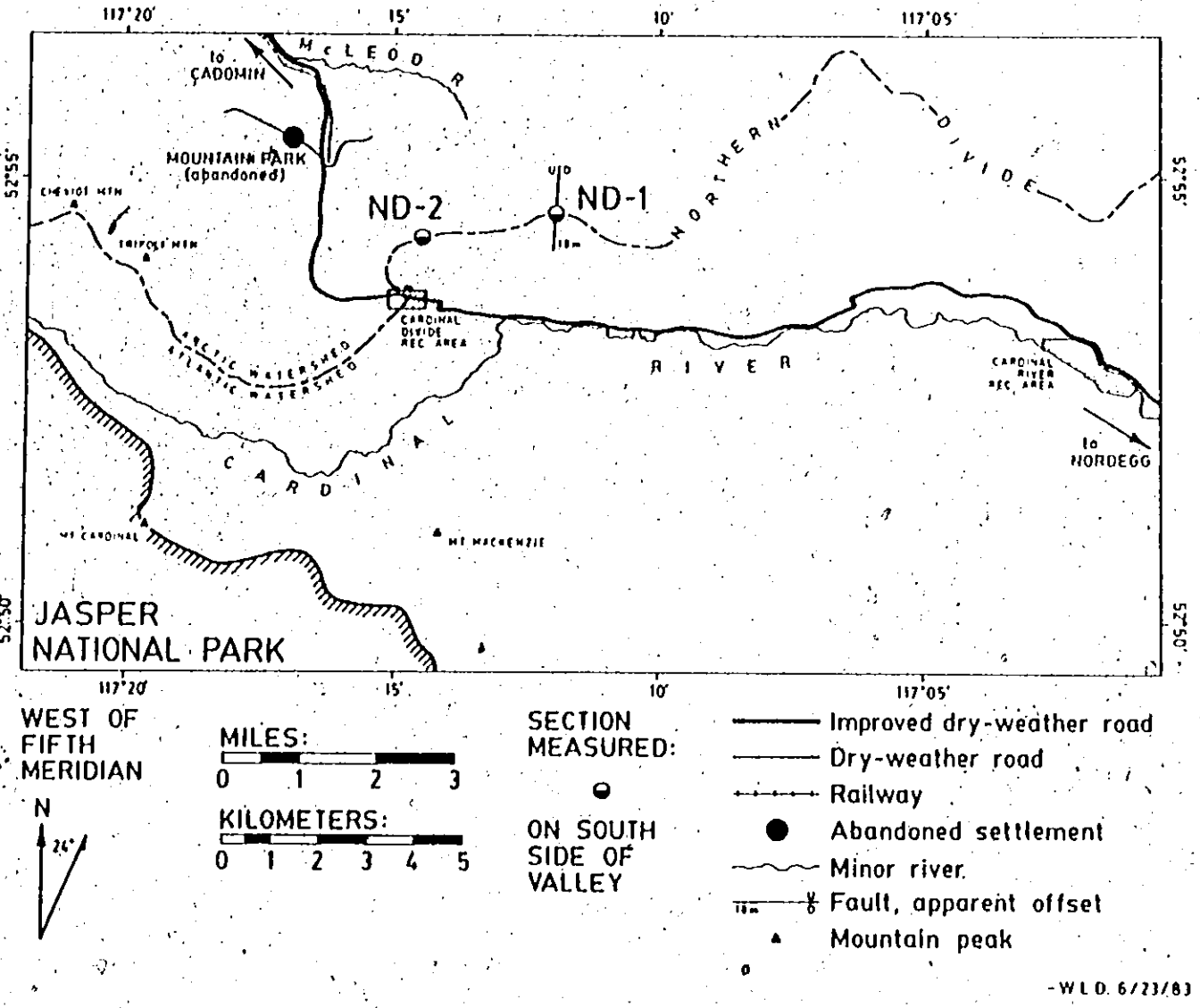
117°20'
15'
10'
117°05'
52°55'
52°50'
to CADOMIN
MCLEOD R
MOUNTAIN PARK (abandoned)
ND-2
ND-1
U/D
18m
NORTHERN DIVIDE
CHEVIOT MTN
TRIPOD MTN
ARCTIC WATERSHED
ATLANTIC WATERSHED
CARDINAL DIVIDE REC AREA
CARDINAL RIVER REC AREA
CARDINAL RIVER
to NORDEGG
MT CARDINAL
MT MACKENZIE
JASPER NATIONAL PARK
WEST OF FIFTH MERIDIAN
N
26°
MILES:
0 1 2 3
KILOMETERS:
0 1 2 3 4 5
SECTION MEASURED:
ON SOUTH SIDE OF VALLEY
Improved dry-weather road
Dry-weather road
Railway
Abandoned settlement
Minor river
Fault, apparent offset
Mountain peak
-W.L.D. 6/23/83

A1-19

Figure A1-9. Detailed map showing locations of measured sections 4-23, 4-19, 4-21, 4-31, BZ-1, and 4-13.

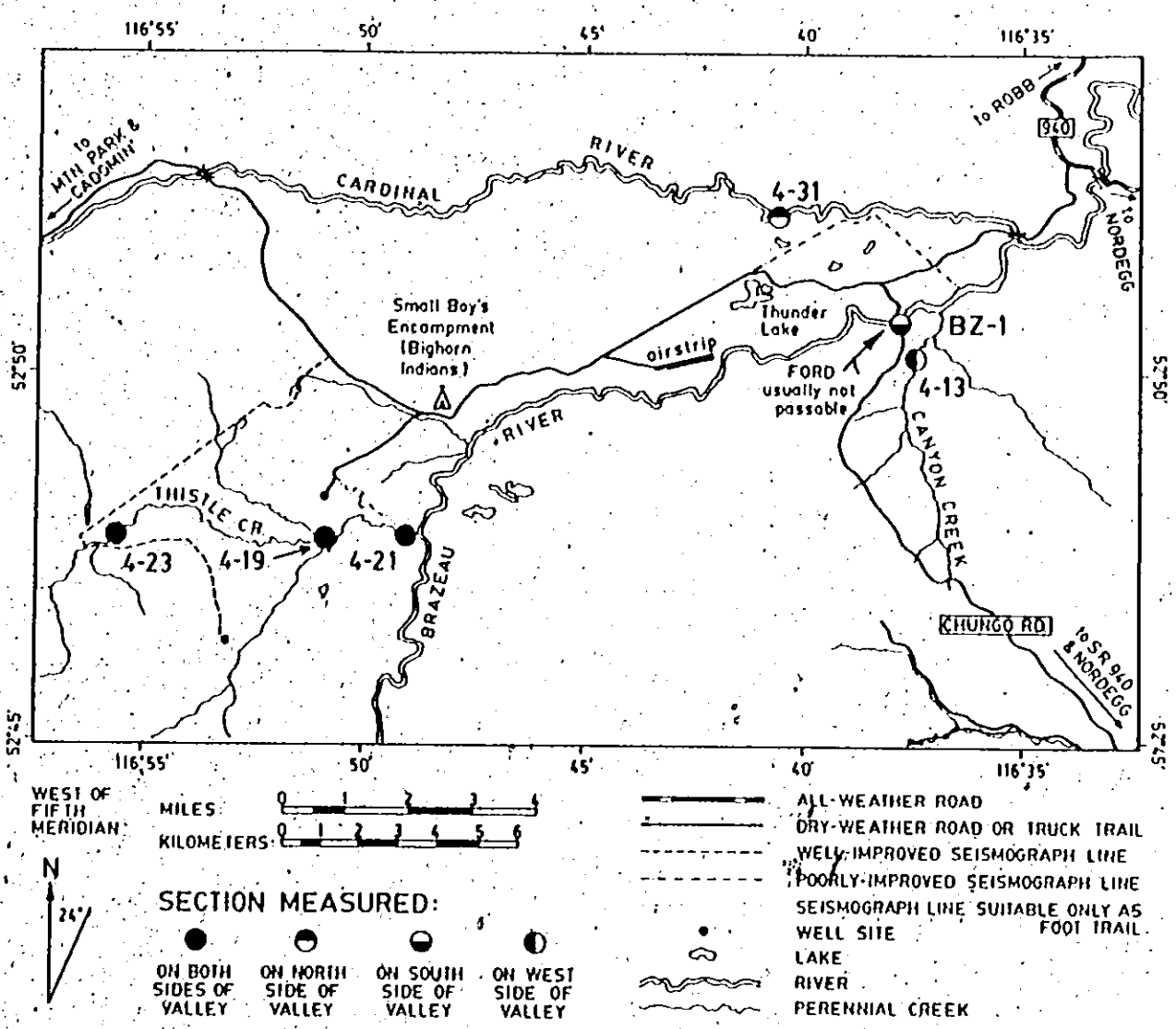
116°55'
50'
45'
40'
116°35'
52°50'
52°45'
to MTN PARK & CADOMIN
CARDINAL RIVER
4-31
to ROBB
960
to NORDEGG
Small Boy's Encampment (Bighorn Indians)
Thunder Lake
BZ-1
airstrip
FORD usually not passable
4-13
CANYON CREEK
RIVER
THISTLE CR.
4-23
4-19
4-21
BRAZEAU
CHUNGO RD.
to SR 940 & NORDEGG
WEST OF FIFTH MERIDIAN
MILES
KILOMETERS
N
24°
SECTION MEASURED:
ON BOTH SIDES OF VALLEY
ON NORTH SIDE OF VALLEY
ON SOUTH SIDE OF VALLEY
ON WEST SIDE OF VALLEY
ALL-WEATHER ROAD
DRY-WEATHER ROAD OR TRUCK TRAIL
WELL-IMPROVED SEISMOGRAPH LINE
POORLY-IMPROVED SEISMOGRAPH LINE
SEISMOGRAPH LINE SUITABLE ONLY AS FOOT TRAIL
WELL SITE
LAKE
RIVER
PERENNIAL CREEK
-W.E.D. 7/10/83

Figure A1-10. Detailed map showing locations of measured sections 5-39 and BL-1. These outcrops are so closely spaced that they have both been represented by the same filled circle.

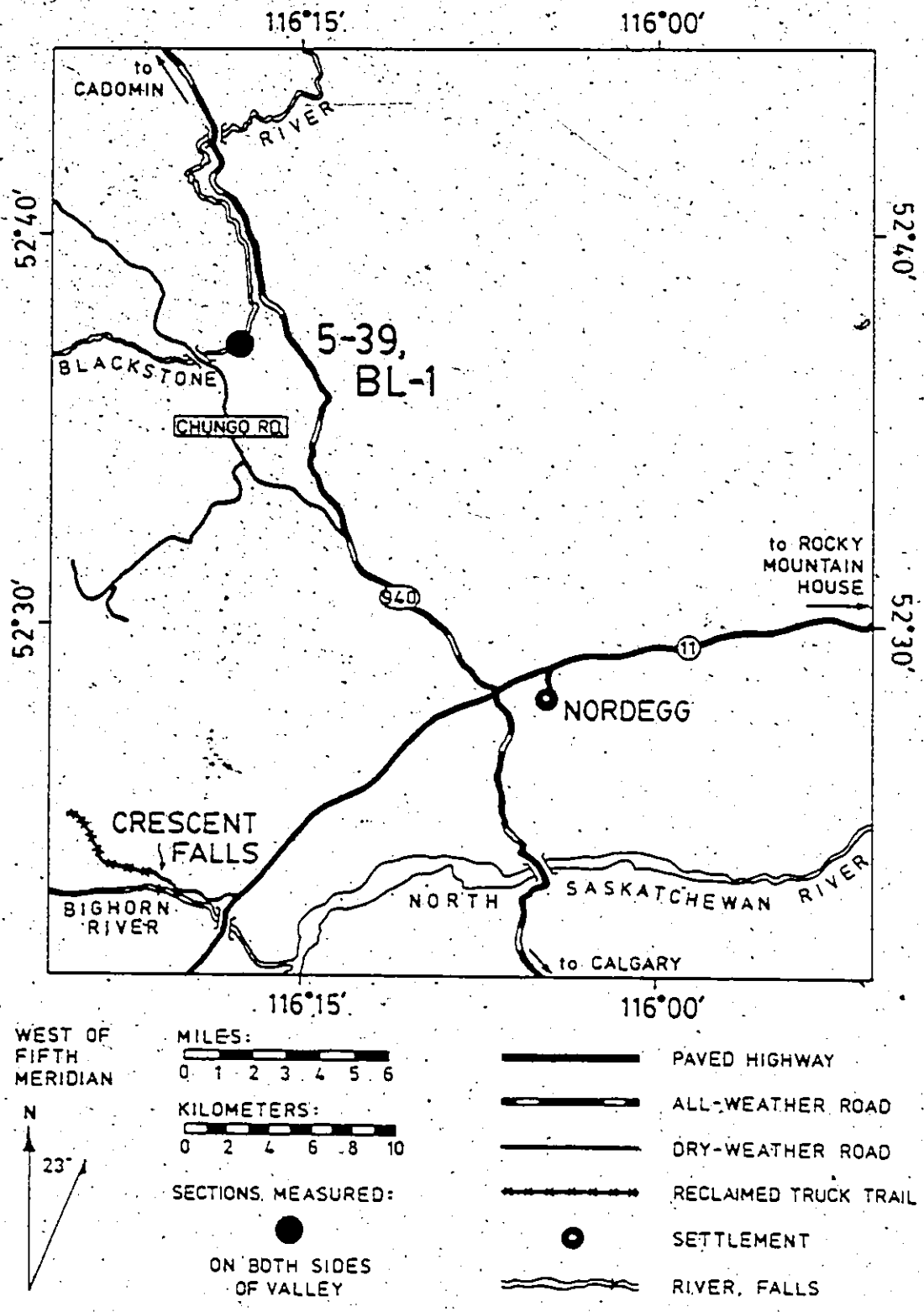
116°15'
116°00'
52°40'
52°30'
to CADOMIN
RIVER
5-39, BL-1
BLACKSTONE
CHUNGO RD.
940
to ROCKY MOUNTAIN HOUSE
11
NORDEGG
CRESCENT FALLS
BIGHORN RIVER
NORTH SASKATCHEWAN RIVER
to CALGARY
WEST OF FIFTH MERIDIAN
N
23°
MILES:
0 1 2 3 4 5 6
KILOMETERS:
0 2 4 6 8 10
SECTIONS MEASURED:
ON BOTH SIDES OF VALLEY
PAVED HIGHWAY
ALL-WEATHER ROAD
DRY-WEATHER ROAD
RECLAIMED TRUCK TRAIL
SETTLEMENT
RIVER, FALLS

– W.L.O. 6/25/83

Figure A1-11. Detailed map showing locations of measured sections WA-1 and 5-37. The route to Crescent Falls is shown in figures A1-10 and A1-12. It is proposed in this thesis that the type-section designation for WA-1 (Wapiabi Creek) be rescinded. Section 5-45 (Ram River) is herein designated the new type section, and section 5-37 (Littlehorn Creek) is the designated alternate.

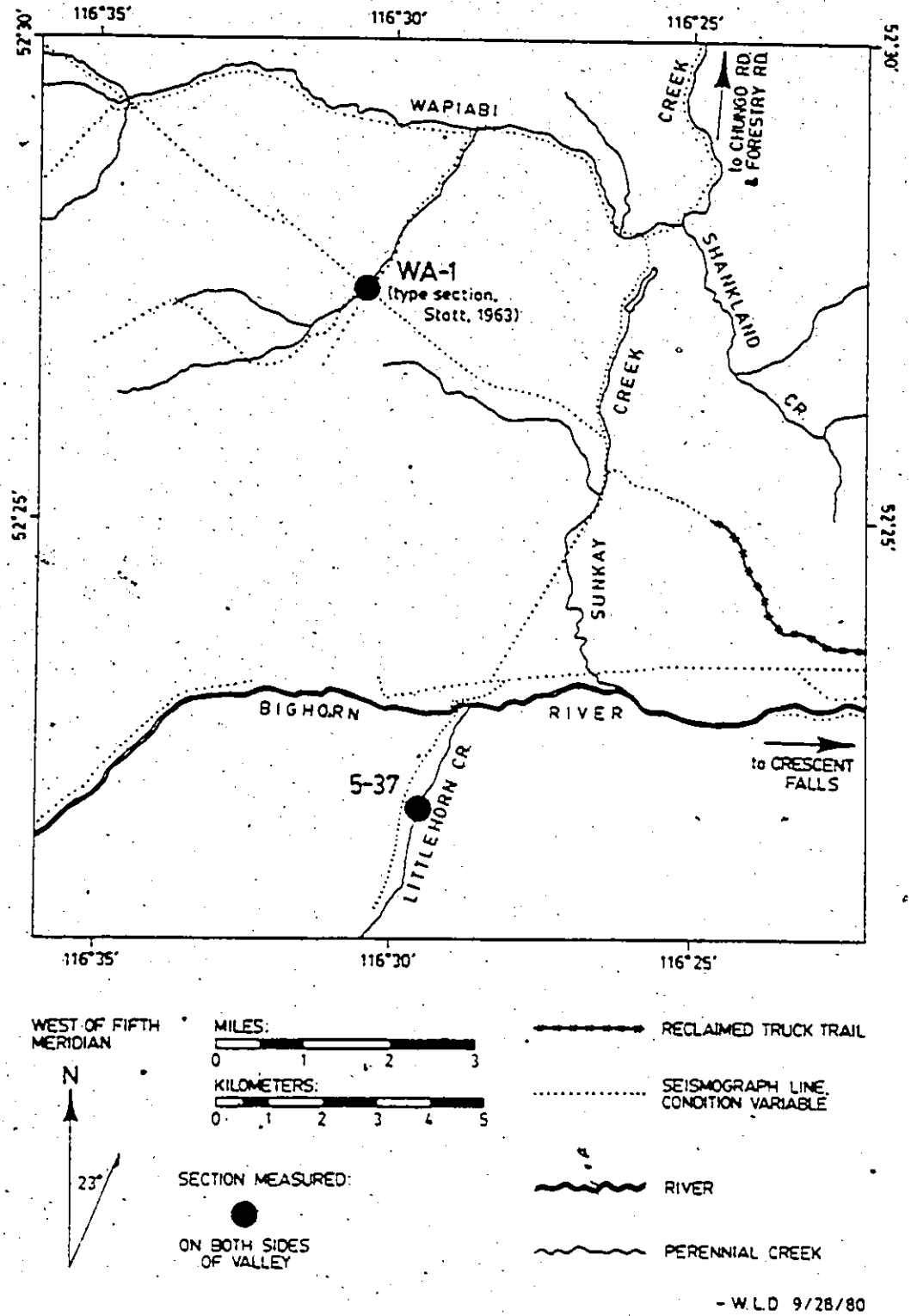
116°35'
116°30'
116°25'
52°30'
52°25'
WAPIABI
CREEK
to CHUNGO RD. & FORESTRY RD.
WA-1
(type section, Stott, 1963)
SHANKLAND CR.
CREEK
SUNKAY
BIGHORN
RIVER
to CRESCENT FALLS
5-37
LITTLEHORN CR.
WEST OF FIFTH MERIDIAN
N
23°
MILES:
0 1 2 3
KILOMETERS:
0 1 2 3 4 5
SECTION MEASURED:
ON BOTH SIDES OF VALLEY
RECLAIMED TRUCK TRAIL
SEISMOGRAPH LINE, CONDITION VARIABLE
RIVER
PERENNIAL CREEK
- W.L.D 9/26/80

Figure A1-12. Detailed map showing locations of measured sections BD-1, NR-1, 5-41 and 5-45. Section 5-45 is herein designated the new type section of the Cardium Formation.

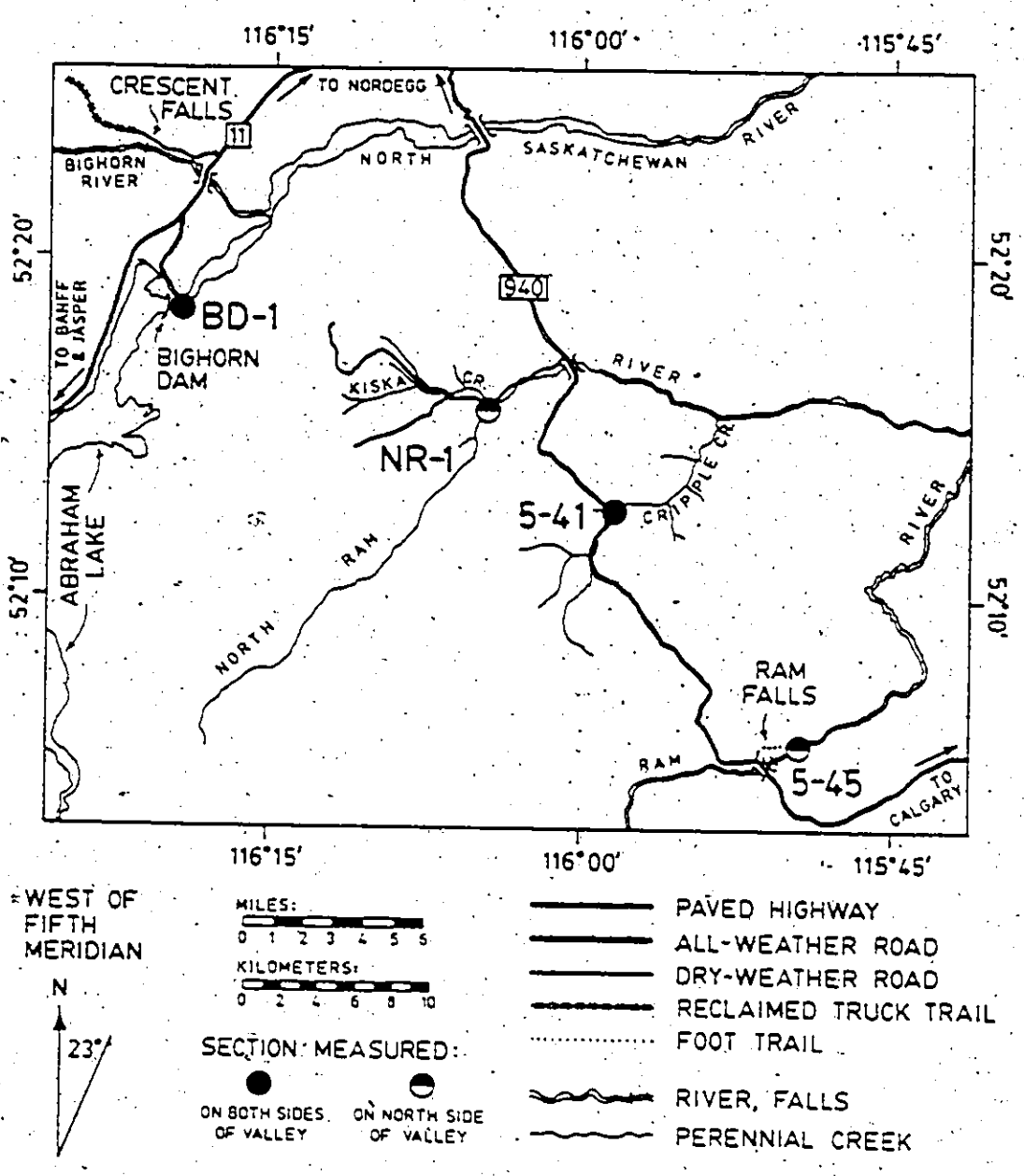
116°15'
116°00'
115°45'
52°20'
52°10'
CRESCENT FALLS
TO NORDEGG
11
BIGHORN RIVER
NORTH SASKATCHEWAN RIVER
940
TO BANFF & JASPER
BD-1
BIGHORN DAM
KISKA CR.
NR-1
5-41
CRIPPLE CR.
ABRAHAM LAKE
NORTH RAM RIVER
RAM FALLS
5-45
TO CALGARY
* WEST OF FIFTH MERIDIAN
N
23°
MILES: 0 1 2 3 4 5 6
KILOMETERS: 0 2 4 6 8 10
SECTION MEASURED:
ON BOTH SIDES OF VALLEY
ON NORTH SIDE OF VALLEY
PAVED HIGHWAY
ALL-WEATHER ROAD
DRY-WEATHER ROAD
RECLAIMED TRUCK TRAIL
FOOT TRAIL
RIVER, FALLS
PERENNIAL CREEK

- W. L.D. 6/7/83

Figure A1-13. Detailed map showing location of measured section 6-8.

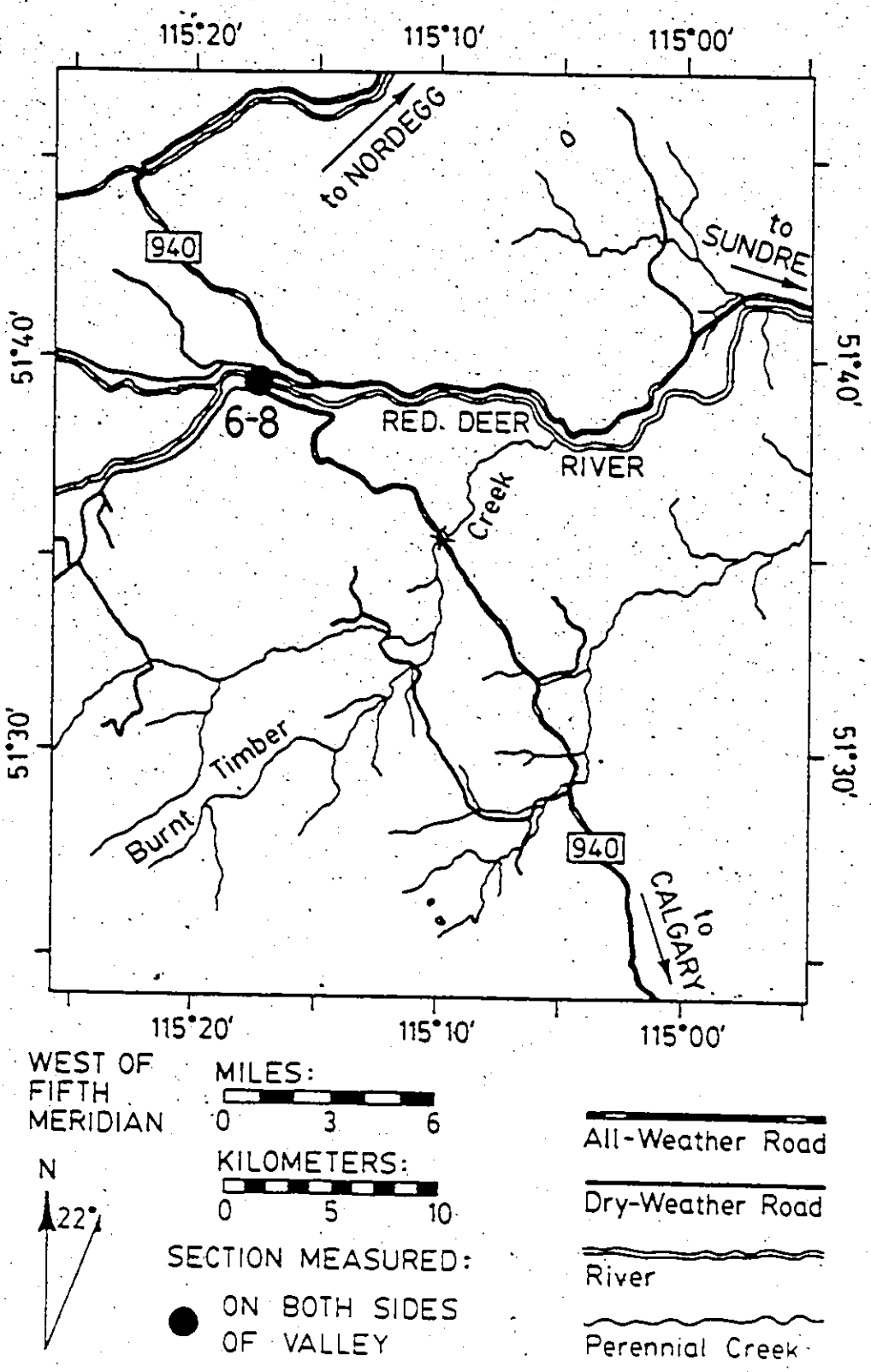
115°20'
115°10'
115°00'
51°40'
51°30'
to NORDEGG
940
to SUNDRE
6-8
RED. DEER
RIVER
Creek
Burnt Timber
940
to CALGARY
WEST OF FIFTH MERIDIAN
MILES:
0 3 6
KILOMETERS:
0 5 10
N
22°
SECTION MEASURED:
ON BOTH SIDES OF VALLEY
All-Weather Road
Dry-Weather Road
River
Perennial Creek

Section PC-1 (Pouce Coupé Quarry, Figure A1-2): Easily accessible by motorcar. This section was measured within a disused quarry located immediately west of Highway 2, approximately 7 km south of the village of Pouce Coupé, British Columbia. The quarry is visible from the road. This is the only section measured by the author located in the province of British Columbia, and it is the most northerly of all the sections measured for this study. A photograph of this exposure is presented as figure A1-14A.

Section CU-1 (Cutpick Hill, Figure A1-3): This section was visited by the author by means of a helicopter. It is not readily accessible by overland conveyance; however, it is accessible by motorcar and a difficult hike. From Grande Cache, drive north on the highway (route 40) to the open-pit coal mines (approximately 25 km). Stop at the first pit encountered (north of the road). Travel on foot due north, crossing Sheep Creek, and ascend in a northwesterly direction to the section on Cutpick Hill. The entire hike is approximately 4 km in length over open country; from Sheep Creek, the ascent to the section rises over 300 m. An excellent exposure of the Marshybank sandstone (Wapiabi Formation) is present above the Cardium interval. The upper beds

of the underlying Kaskapau Formation are also well exposed on the hill. An aerial photograph of this outcrop is presented as figure A1-14B.

Section 5-4 (Muskeg River, Figure A1-4): Easily accessible by motorcar and a short walk over steeply inclined terrain. Follow directions to section GC-1. Section 5-4 is located on the same thrust slice as GC-1, along strike to the northwest. From section GC-1, descend into the valley of the Muskeg by walking northwest (along strike) approximately 1 km. Section 5-4 is exposed in moderately dipping beds in both banks of the river. The lower half of the Cardium may be measured on either bank; the upper half is only exposed across the river in the northern bank. It is commonly very difficult to cross the Muskeg in the vicinity of the Cardium; a more favorable crossing is located a few hundred meters upstream (to the east). The upper beds of the underlying Kaskapau Formation and the lower beds of the overlying Wapiabi Formation are also exposed at section 5-4. Excellent exposures of the Marshybank and Chungo sandstones (Wapiabi Formation) are located immediately upstream (to the east). A photograph of this outcrop is presented as figure A1-14C.

Figure A1-14: Measured sections PC-1, CU-1, 5-4, and GC-1.

A) View of west wall of quarry in which section PC-1 was measured. Person (circled) for scale.

B) Aerial photograph of section CU-1 on Cutpick Hill.

C) View of section 5-4 on north side of Muskeg River.

D) View of section GC-1 on south side of Highway 40 roadcut.

A
B
C
D

Section GC-1 (Route 40 roadcut, Figure A1-4): Easily accessible by motorcar, this section is a roadcut of the Grande Cache-Hinton highway. Along route 40, drive 16.7 km east of the developed part of the town of Grande Cache (5.7 km east of the bridge over Susa Creek and the railroad tracks). The lower half of the Cardium Formation is exposed in moderately dipping beds on both sides of the road, although the exposure is best on the south side. A photograph of this exposure is presented as figure A1-14D.

Section GC-2 (Grande Cache-Hinton railway roadcut, Figure A1-4): Easily accessible by motorcar. Follow directions to section GC-1. Section GC-2 is located on the same thrust slice as GC-1, along strike to the southeast. From section GC-1, walk 100 m to the southeast. Section GC-2 is a roadcut of the Grande Cache-Hinton railway. The lower half of the Cardium Formation is exposed in moderately dipping beds on both sides of the railroad, although the exposure is best on the south side. A photograph of this exposure is presented as figure A1-15A.

Section MS-1 (Mason Creek, Figure A1-4): Section MS-1 was visited by helicopter; no attempt was made by the author to reach this section by automotive conveyance.

However, recent maps of this area indicate that a dry-weather road extends from the abandoned locality of Muskeg River (approximately 30 km east of Grande Cache on route 40) to another abandoned locality (unnamed) roughly 3 km SSE of the outcrop. From this locality it is possible to reach section MS-1 by following the creek bed. The upper beds of the underlying Kaskapau Formation are well exposed at this section. Approximately 70 m below the Cardium, a thick sandstone is present. This sandstone is apparently a fault-repeat of the major Cardium sandstone. An aerial photograph of this outcrop is presented as figure A1-15B.

Section 5-19 (Little Berland River, Figure A1-5): Accessible with difficulty by foot or off-road motorbike, this section is located near the forestry trunk road between Hinton and Grande Cache. From Hinton, drive north on route 40 approximately 40 km. A reclaimed truck trail diverges from the highway 5 km north of the railroad crossing in this vicinity (approximately 0.5 km south of the bridge over the Little Berland). Travel this road approximately 4 km to the south west (6 km on the odometer) to reach the section. This road was reclaimed in 1981, making it impassable to all vehicles other than off-road motorbikes; passage is difficult even by this means.

Figure A1-15: Measured sections GC-2, MS-1, 5-19, and 5-22.

A) View of section GC-2 on south side of Grande Cache-Hinton railway roadcut.

B) Aerial photograph of section MS-1 on the headwaters of Mason Creek.

C) Aerial photograph of section 5-19 on northwest side of Little Berland River.

D) View of section 5-22 on northeast side of Maskuta Creek.

A
B
C
D

The Cardium outcrop is most prominent in the north bank of the river approximately 0.5 km south of the ford of the truck trail through the Little Berland. [Note: Because this route was favored by local outdoorsmen as an access to the Willmore Wilderness, it is likely that it will soon be returned to its former state of repair.] Excellent exposures of the overlying Marshybank and Chungo Members of the Wapiabi Formation are present on the Little Berland north of the Cardium outcrop. An aerial photograph of this section is presented as figure A1-15C.

Section 5-22 (Maskuta Creek, Figure A1-6): Easily accessible by motorcar and a short walk. Drive southwest from Hinton along route 16 approximately 15 km. Immediately opposite the turn-off to Kinky and Wildhorse Lakes, turn left (southeast) onto the private road leading to Terris' Sawmill and Planer. Proceed along this road 2 km, passing by the mill and over a small bridge. Immediately after this bridge, take the first left turn and proceed another 2 km. Stop. Walk about 500 m to the east and descend into the valley of Maskuta Creek. The Cardium beds are very steeply dipping to overturned in this exposure. Note: After heavy rains, the road south of the sawmill may be

impassable to 2-wheel-drive vehicles. A photograph of this outcrop is presented as figure A1-15D.

Section SC-1 (Sphinx Creek, Figure A1-7): Easily accessible by motorcar and a short walk. From the Hinton area, drive south along route 40 (forestry trunk road) approximately 33 km from the junction with route 16. Section SC-1 is located a few hundred meters west of the highway, approximately 1.5 km north of one of the bridges over the Gregg River. From Luscar, the section is approximately 10 km northwest along route 40. The nearly vertical, overturned beds of the Cardium form a narrow prominence which is only momentarily visible from a car travelling along the highway. A photograph of this outcrop is presented as figure A1-16A.

Section 7-1 (McLeod River, Figure A1-7): Easily accessible by motorcar, this section is exposed in steeply dipping beds on the east side of the river approximately 300 m downstream from the junction of the Luscar and Cadomin Roads, only 3 km north of Cadomin. The river can usually be crossed easily on foot at this location. A photograph of this outcrop is presented as figure A1-16B.

Figure A1-16: Measured sections SC-1, 7-1, and 4-43.

A) View of section SC-1 on south side of Sphinx Creek. Person (circled) for scale.

B) Part of section 7-1 on east side of McLeod River. Person (circled) for scale.

C) Upper part of section 4-43 on west side of Mackenzie Creek. Scale bar is 1 m.

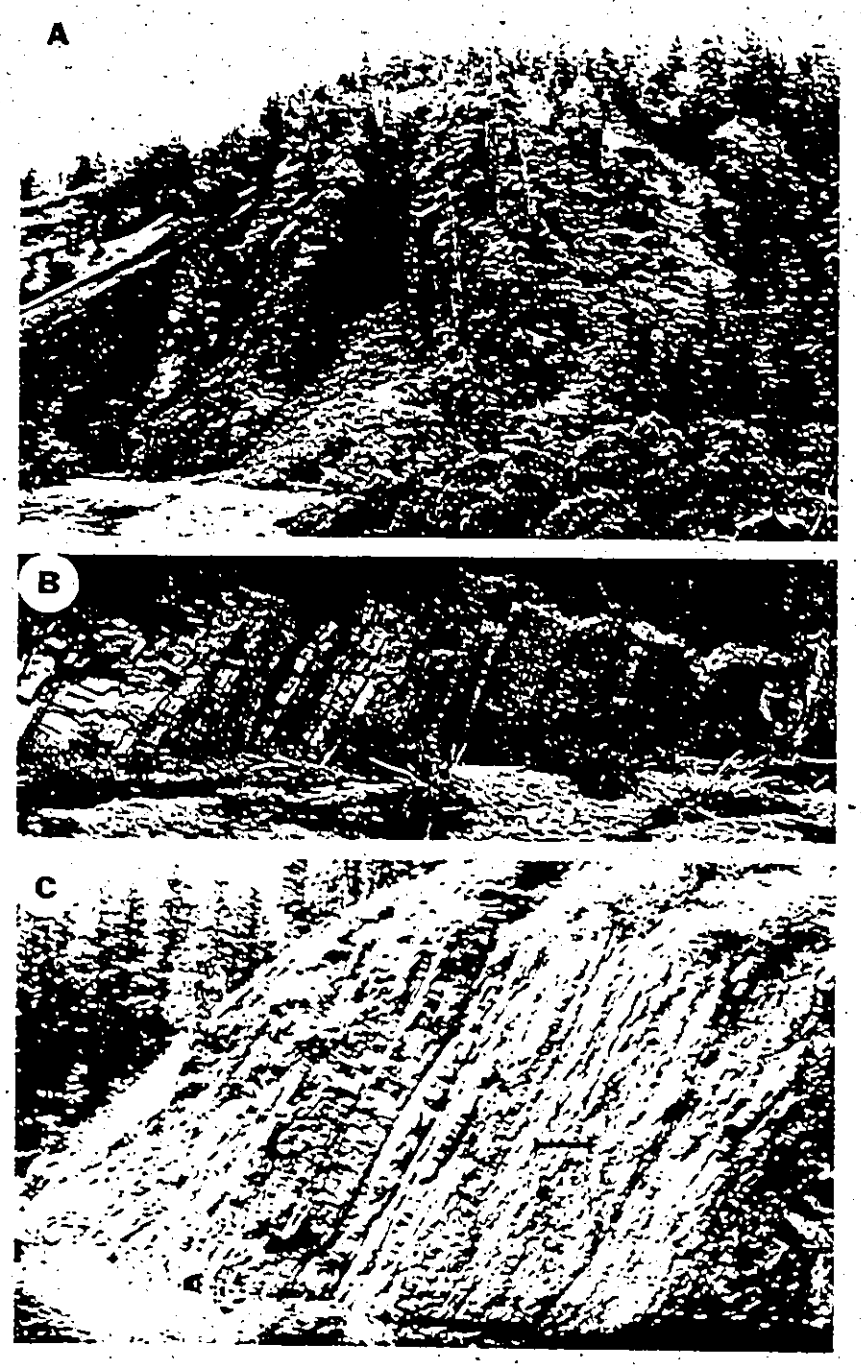
A
B
C

Section 4-43 (MacKenzie Creek, Figure A1-7): Accessible by motorcar and a long hike (about 4 km) or by 4-wheel-drive vehicle and a short walk. From Cadomin, drive approximately 11.5 km east toward Robb and turn off the road on a truck trail to the south. Drive 2 km (crossing railroad tracks and McLeod River) and walk east to the creek. Section 4-43 is well exposed in steeply dipping beds just south of the largest tributary of MacKenzie Creek in the vicinity. Excellent bedding-plane exposures of the highest conglomerate in the section may be viewed here; the creek is usually easily crossed on foot. A photograph of this outcrop is presented as figure A1-16C. This photograph shows the upper sandstone of the Cardium Formation on the west side of the creek. The excellent bedding-plane exposures of the overlying conglomerate occur on the east side of the creek.

Sections ND-1 and ND-2 (Northern Divide, Figure A1-8): Easily accessible by 4-wheel-drive vehicle. These sections are located on the steep face of a prominent cuesta formed by the sandstones of the Cardium Formation, which dip gently southward at this locality. The ridge of this cuesta locally forms the divide

between Arctic and Atlantic Ocean watersheds. To reach these sections, drive approximately 5 km south of the abandoned townsite of Mountain Park, south of Cadomin. At the height of land, a sign marks the position of the northern continental divide. This sign is near the center of the Cardinal Divide Recreation Area, where camping facilities may be found. From this area, follow the tire tracks up the sparsely vegetated dip slope to the north to the crest of the cuesta. Section ND-2 is near the terminus of this route; section ND-1 may be reached by driving approximately 3 km further east along the ridge. This latter section was measured across a north-south trending vertical fault having an apparent relative offset of approximately 18 m (west side upthrown). By correlating across this fault it is possible to construct a measured section at this location which is thicker than can be measured at any other point along the ridge. Figure A1-17A is an aerial photograph of this ridge. Figure A1-17B is a photograph of section ND-2 taken from ND-1. Figure A1-17C is a photograph of section ND-1 taken from section ND-2. Figure A1-17D shows the surface expression of the fault at ND-1.

Figure A1-17. Measured sections ND-1 and ND-2.

A) Aerial photograph of the cuesta formed by the Cardium Formation which locally constitutes the Northern Continental Divide between Arctic and Atlantic watersheds. View is toward the west; sections ND-1 and ND-2 were measured on the steep northern face.

B) Section ND-2 viewed from section ND-1. View is toward the west. Section ND-2 was measured on the extreme right (west) of the outcrop visible in this photograph (arrowed).

C) Section ND-1 viewed from section ND-2. View is toward the east. Arrow indicates position of fault across which beds were correlated, thus permitting measurement of a section which is thicker than the height of the exposure.

D) View of area of faulting on ridge of cuesta at section ND-1. View is toward the southwest. Person (circled) for scale.

A
B
C
D

Section 4-23 (Thistle Creek, Figure A1-9): Easily accessible by motorcar and a short walk. Follow same route as for section 4-21, but turn off the road to Cadomin 3 km further to the west (about 23 km from the forestry road). This turn is to the southwest on a well-improved seismic cut-line leading to an abandoned well site. This cut-line is passable by most larger motorcars. Travel this line about 8 km to the first difficult stream crossing. This is Thistle Creek, and the section is about 1 km downstream. The higher beds of the Blackstone and the lower beds of the Wapiabi are also exposed. The stream is easily crossed on foot to view exposures on both sides of the valley. A photograph of this outcrop is presented as figure A1-18A.

Section 4-19 (Thistle Creek, Figure A1-9): Accessible by 4-wheel-drive vehicle and a short hike or by motorcar and a longer hike. Follow directions to section 4-23, ford Thistle Creek, and continue approximately 3 km along this well-improved cut-line. Upon reaching the bend in the roadway (to the south), leave the road and descend to the creek in a northerly direction. Walk downstream along the creek bed (to the east). Section 4-19 is the first exposure of major sand bodies

encountered along this route. The overlying beds of the Wapiabi Formation are well-exposed east of this section, a photograph of which is presented as Figure A1-18B.

Section 4-21 (Thistle Creek, Figure A1-9): Accessible with some difficulty by 4-wheel-drive vehicle and a short hike. It is necessary to drive some distance down poorly-improved seismic cut-lines. From Nordegg, drive north 60 km on the forestry trunk road to the first left turn immediately north of the crossing of the Brazeau River. This turn (to the south) is marked by a sign which reads "Cardinal River 1". Drive approximately 20 km west to a southwest turn-off immediately west of the Indian settlement. This road runs to an abandoned well site 3 km to the southwest. A system of poorly-improved seismic cut-lines leads almost to the junction of Thistle Creek and the Brazeau River (about 2 km from the well site). Section 4-21 is located several hundred meters from the junction of the two waterways. It is highly recommended that a copy of Forest Cover Series Sheet No. 83C15 be procured before attempting to locate this section. Most cut-lines appear on this map. Copies are available at the Nordegg Forest Station. A photograph of this outcrop is presented as Figure A1-18C.

Figure A1-18. Measured sections 4-23, 4-19, 4-21, and 4-31.

A) View of section 4-23 on north side of Thistle Creek. Notebook (circled) in foreground for scale.

B) Upper half of section 4-19 on north side of Thistle Creek. Person (circled) in foreground for scale.

C) Lower portion of section 4-21 (at right) on south side of Thistle Creek. Note valley of Brazeau River in background on extreme left (east) side of photograph. The junction between Thistle Creek and the Brazeau is just a few hundred meters further east of the area shown in this photograph.

D) Aerial photograph of section 4-31 on north side of Cardinal River. The gravel bar from which this section was measured usually is exposed, except during times of unusually high water.

A
B
C
D

Section 4-31 (Cardinal River, Figure A1-9): Easily accessible by 4-wheel-drive vehicle and a short walk, or by motorcar and a slightly longer walk. From Nordegg, drive north 60 km on the forestry trunk road to the first left turn immediately north of the crossing of the Brazeau River. This turn (to the south) is marked by a sign which reads "Cardinal River 1". Drive approximately 10 km west to the Thunder Lake area and double-back to the northeast along a poorly-improved seismograph line. Travel this line approximately 1.5 km. Stop. Walk approximately 1 km to the northwest. The Cardium outcrop is best exposed across the river in the north bank; it may be necessary to walk some distance along the south bank in order to find a suitable place to descent into the valley of the Cardinal. A photograph of this outcrop is presented as Figure A1-18D. [Note: another excellent Cardium section outcrops at the end of the cut-line extending northeast from Thunder Lake. This section is easily accessible by 4-wheel-drive vehicle, because the cut-line descends almost to the river's edge at this location.]

Sections 4-13 (Canyon Creek) and BZ-1 (Brazeau River) (Figure A-19): Easily accessible by 4-wheel-drive vehicle and short walks. During dry periods, or when Chungo Road has recently been re-surfaced by a grader, these sections can be reached by motorcar. Detailed information on road conditions is available at the Nordegg Forestry Station. These sections must be approached from the south on Chungo Road; they cannot be approached from the north because the Chungo Road ford of the Brazeau River is invariably impassable. Follow directions to sections 5-39 and BZ-1; continue north on the Chungo Road. Section BZ-1 (highest beds of last cycle in Cardium, and lower Wapiabi beds) is best exposed in the south bank of the valley of the Brazeau, only a few hundred meters east of the Chungo Road "ford". Section 4-13 is visible in the steep west bank of Canyon Creek, approximately 1.5 km south of the junction of that creek and Brazeau River. It is most easily reached by walking down to the creek along the NE-SW running cut-line which joins the Chungo Road approximately 2.3 km south of the ford. Section 4-13 is exposed in a folded thrust-faulted sheet containing the upper beds of the Blackstone, the entire Cardium, and the lower beds of the Wapiabi, exposed in steeply dipping to overturned beds. To avoid confusion in the field, the reader should note that two additional

Figure A1-19. Measured sections 4-13, BZ-1, 5-39, and BL-1.

A) View of section 4-13 on thewest side of Canyon Creek. Beds are slightly overturned; up is to the right.

B) View of section BZ-1 on the south side of Brazeau River.

C) View of highest cycle of Cardium Formation within section 5-39, on south side of Blackstone River. Person (circled) for scale.

D) View of section BL-1 on north side of Blackstone River. Person (circled) for scale.

A
B
C
D

partial Cardium sections (highly sheared; not suitable for this study) are exposed immediately upstream of section 4-13. Photographs of sections 4-13 and BZ-1 are presented as figures A1-19A and A1-19B, respectively.

Sections 5-39 and BL-1 (Blackstone River, Figure A1-10: Easily accessible by 4-wheel-drive vehicle and a short walk; during dry periods, or when Chungo Road has recently been re-surfaced by a grader, these sections can be reached by motorcar. Contact the helpful people at the Nordegg Forestry Station for detailed information on road conditions. To reach these sections, travel 10 km north from Nordegg on the forestry road to the junction with Chungo Road (indicated by sign). Continue north 12 km on Chungo Road to the Blackstone River (first steel bridge). Park in the camping area on the south side of the river and the east side of the road. Walk about 2 km downstream on the south side of the river to reach section 5-39, which is excellently exposed in steeply dipping beds in the river valley. (Note: Do not be confused by the sandstones visible in the north bank between the parking area and the Cardium sections. These are not Cardium sands). Cycle #2 of section 5-39 is best observed on the north bank; the river is usually easy to walk across at this locality.

While on the north side one can observe section BL-1 (a fault repeat of cycle #1), which is only a few hundred meters further downstream from section 5-39. The higher beds of the Blackstone can be seen in both sections, and the lower beds of the Wapiabi can be observed at section 5-39. Photographs of sections 5-39 and BL-1 are presented as figures A1-19C and A1-19D, respectively.

Section WA-1 (Wapiabi Creek headwaters, south fork, Figure A1-11): This section was designated the type section of the Cardium Formation by Stott (1963). Unfortunately, it is not readily accessible by overland conveyance. Further, exposure is limited, numerous covered intervals are present, and cyclic development and facies sequences are fairly atypical of the Cardium in general. For these reasons, I suggest that the type-section designation be rescinded. Section 5-45 on Ram River is herein designated the new type section due to its excellent exposure and convenient location. Section 5-37 on Littlehorn Creek would be preferable were it not for the difficulty of access to this locality; section 5-37 is designated an alternate type section.

No attempt was made by the author to reach section WA-1 by overland conveyance; the section was visited by helicopter. Two alternative overland routes are suggested below; before attempting to reach this

section, contact the helpful people at the Nordegg Forestry Station.

The most promising route involves driving along several km of seismograph cut-lines of variable condition, parallel to and criss-crossing Wapiabi Creek. The route originates at the Chungo Road. Alternatively, follow the directions to Crescent Falls given under section 5-37 below; however, instead of turning off to the southwest (at the second sign) for the descent into the valley of the Bighorn River, continue northwest over the reclaimed truck trail (either on foot or by motorbike) and follow the cut-lines northwest to the section. A photograph of this outcrop is presented as figure A1-20A.

Section 5-37 (Littlehorn Creek, Figure A1-11): Located on Littlehorn Creek 2 km upstream (south) of the junction with Bighorn River, this section is not readily accessible by overland travel. The relative inaccessibility of this section is unfortunate because exposure of the Cardium is superlative. Also, section 5-37 is located only 2 km (approximately) below the McConnell thrust, making this section the most proximal to the Rocky Mountains of all the sections measured in this study.

The best overland route to section 5-37 is as follows: From the junction with the forestry road (S.R. 940) near Nordegg, travel southwest along the David Thompson Highway (route 11) some 16 km. Exit northwest to Crescent Falls (indicated by sign). This exit is approximately 2 km northeast of the bridge on route 11 over the Bighorn River. Travel along this road approximately 5 km to the turnoff to the southwest to Crescent Falls (again, indicated by a sign). Travel approximately 1.5 km further to Crescent Falls. It is possible to drive this far by conventional motorcar; further vehicular travel requires a 4-wheel-drive vehicle or an off-road motorbike and may be accomplished only during low stages of the Bighorn River. From Crescent Falls, section 5-37 is 10 km to the west. At least two different poorly-improved seismograph cut-lines extend west from Crescent Falls; these may be travelled by 4-wheel-drive vehicle no more than about 5 km during normal weather conditions. Both of these routes originate on the north side of Bighorn River and parallel the valley of the river toward the west. From Crescent Falls, drive west on the north side of the Bighorn approximately 1 km. Cross the river, continue west another 1 or 2 km before reaching a fork in the road. At this point, it is possible either to continue in a westerly direction on the south side of the Bighorn

or to re-cross the river to another route on the north side. It is not known which route is preferrable; in 1981, the more northerly route appeared to be more promising. Consult the helpful people at the Nordegg Forestry Station before attempting to drive to section 5-37. [Note: The preceding directions for overland travel to this section are tentative because the author reached this locality by helicopter only.]

Because of the great thickness of this section and its excellent exposure, section 5-37 is herein designated an alternate type section of the Cardium Formation. The type-section designation is reserved to the Ram River outcrop (section 5-45) due only to the greater ease of access to the latter. An aerial photograph of section 5-37 is presented as figure A1-20B.

Section BD-1 (Bighorn Damsite, North Saskatchewan River, Figure A1-12): Easily accessible by motorcar, this section forms the base upon which the Bighorn Dam was built. Drive 25 km west from Nordegg on the David Thompson Highway (Highway 11) and exit to the south at the Bighorn Damsite turnoff (indicated by sign). Park beside the visitor information building below the dam. The upper beds of the Cardium and the lower beds of the

Wapiabi may be observed at this section. A photograph of the outcrop is presented as figure A1-20C.

Section NR-1 (North Ram River, Figure A1-12): Easily accessible by motorcar, this section is located south of Nordegg near the forestry trunk road. From Nordegg, drive south approximately 25 km. Immediately north of the bridge over the North Ram River, turn west on a dry-weather road which runs parallel to the river. Drive 6 km west along this road, crossing five wooden bridges. Turn right (north) on a truck trail to a camping area. The outcrop is located to the north across the river, which is usually easily crossed on foot at this location. The Cardium forms a high ridge, with the best exposure along the river's edge. The outcrop is located just east of the junction with the Kiska Overlook Road, near the junction of Kiska Creek and the North Ram River. A photograph of this section is presented as figure A1-20D.

Section 5-41 (Cripple Creek, Figure A1-12): Easily accessible by motorcar, this section is located a few hundred meters east of the forestry trunk road approximately 35 km south of Nordegg. The low sandstone ridges of this section are visible from the forestry

Figure A1-20. Measured sections WA-1, 5-37, BD-1, and NR-1.

A) View of section WA-1 on the north side of the headwaters of Wapiabi Creek (south fork). Person (circled) for scale.

B) Aerial view of section 5-37 on Littlehorn Creek.

C) Photograph of section BD-1, taken from the top of the Bighorn Dam.

D) View of the limited exposure of section NR-1 on the north side of North Ram River. Notebook (circled) for scale.

A
B
C
D

Figure A1-21. Measured sections 5-41, 5-45, and 6-8.

A) View of lower sandstone within section 5-41 on north side of Cripple Creek. Person on sandstone for scale.

B) View of section 5-45 on south side of Ram River. Minor fault is indicated by dashed line.

C) View from bluff north of Red Deer River. Note outcrop of section 6-8 in the bluff. Also note that the bridge over the Red Deer River (circled) is built upon Cardium sandstones, which outcrop along the river's edge.

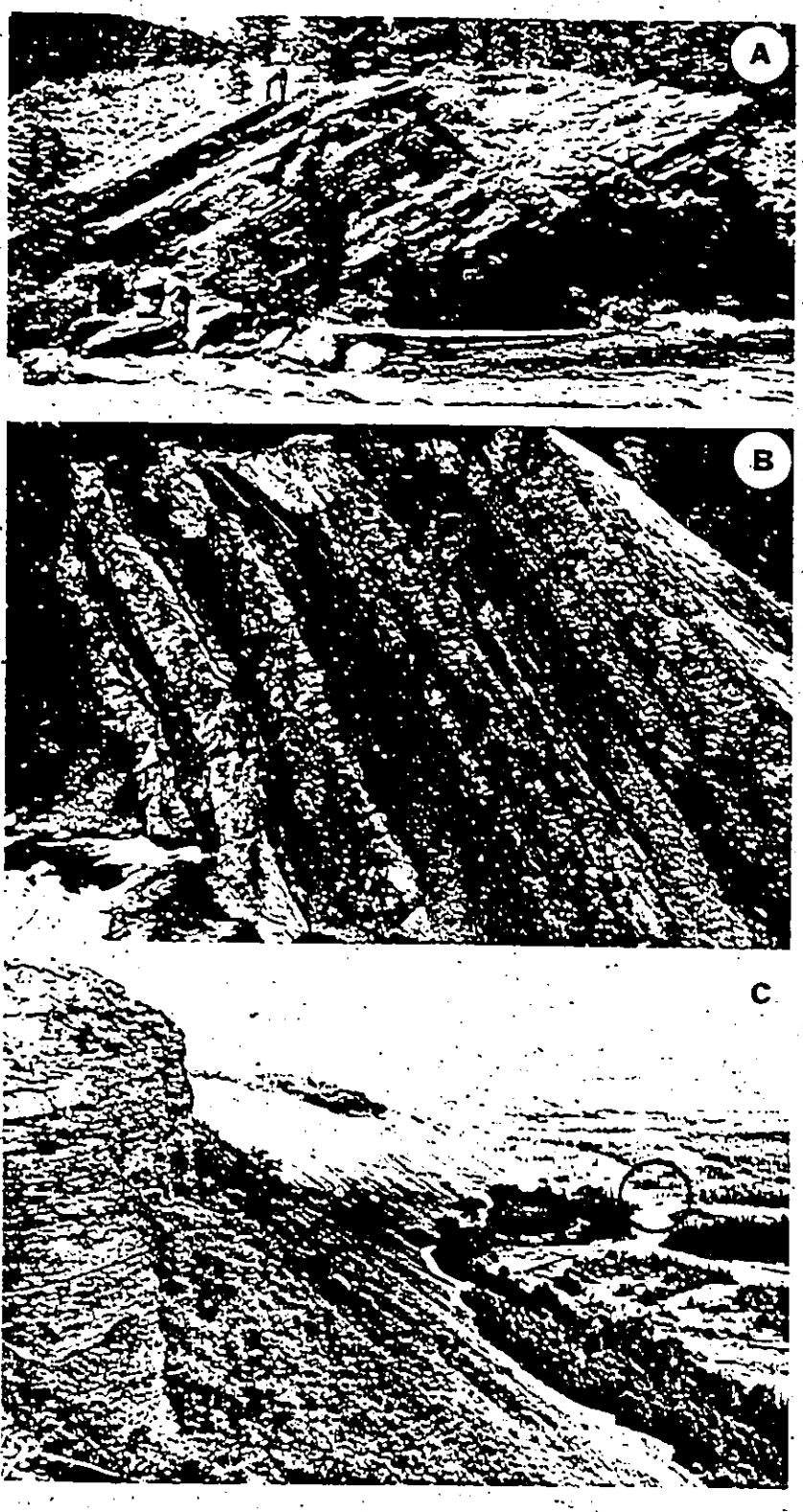
A
B
C

road near the Cripple Creek crossing. A photograph of this section is presented as figure A1-21A.

Section 5-45 (Ram River, Figure A1-12): Easily accessible by motorcar and a very short walk. Drive 50 km south along the forestry trunk road from Nordegg to the Ram Falls recreation area. The falls are formed in the highest thick sandstone body within the Cardium, and are located just east of the trunk road. The rocks of the falls section are somewhat tectonized, poorly accessible, and are not suitable as a measured section; however, approximately 1 km downstream of the falls, the Cardium is superbly exposed in steeply dipping beds. The higher part of the underlying shales of the Blackstone Formation and the overlying dark marine shales of the Wapiabi Formation are also exposed. Section 5-45 is herein designated the type section of the Cardium Formation. The outcrop is most accessible on the north side of the river valley. On this side, a minor fault forming a low angle with bedding traverses cycle #5; it can be seen on the opposite side of the valley, where it traverses cycle #4. A photograph of this outcrop is presented as figure A1-21B.

Section 6-8 (Red Deer River, Figure A1-13): Easily accessible by motorcar. Travel north along route 940 (forestry trunk road) approximately 80 km from the junction with route 1A (approximately 10 km west of Cochrane, or 30 km west of Calgary). The bridge at the Red Deer River crossing (beside the Mountain Air Lodge) is built upon Cardium outcrop, which is also exposed in the bluff immediately north of the river. A photograph of this outcrop is presented as figure A1-21C.

APPENDIX 2. MEASURED SECTIONS OF THE CARDIUM FORMATION

The following figures represent the sequence of facies observed in each of the Cardium exposures measured by the author. These figures also present and compare the stratigraphic divisions of Stott (1963) and this thesis. Paleoflow data obtained at these exposures is indicated to the right of the stratigraphic levels at which they were measured. These data are presented in map view, with north at the top of the page.

A key to these measured sections is presented as the first figure in this appendix (p. A2-4). This symbol key presents all facies symbols as they appear in this appendix and were presented in chapter 4, with a single exception: facies 4IF. The symbol key for facies 4IF is presented under the description of this facies in chapter 4 (p. 195).

Sections are presented in alphanumeric order (numerals listed first). Note that no measured section is presented for exposure ND-2; this section is a less completely exposed duplicate of section ND-1, with which it is in structural continuity (see appendix 1). No paleoflow data were obtained at section ND-2.

The stratigraphic terminology of Stott (1963) is abbreviated as follows:

WAP = Wapiabi Formation

STK = Sturrock Member of the Cardium Formation

LEY = Leyland Member of the Cardium Formation

CDL = Cardinal Member of the Cardium Formation

KIS = Kiska Member of the Cardium Formation

MSH = Moosehound Member of the Cardium Formation

RAM = Ram Member of the Cardium Formation

BLK = Blackstone Formation

KAS = Kaskapau Formation

The revised stratigraphic terminology of this thesis is abbreviated as follows:

WAR = Wapiabi Formation

OBS = Obstruction Member of the Cardium Formation

WIL = Willmore Member of the Cardium Formation

SUN = Sundre Member of the Cardium Formation

CUT = Cutpick Member of the Cardium Formation

SEE = Seebe Member of the Cardium Formation

BLK = Blackstone Formation

KAS = Kaskapau Formation

N.B.: In the revised stratigraphy, the letters "MB", "UT", and "LT" following a member name indicate the Main Body, Upper Tongue, and Lower Tongue of that member.

respectively. "TI" indicates the Transition Interval of the Seebe. "CCS" indicates the Canyon Creek Split (at section 4-13) or the Cripple Creek Split (at section 5-41) of the Cutpick. "GCS" indicates the Grande Cache Split of the Cutpick. "HS" indicates the Headwaters Split of the Cutpick. "LBS" indicates the Little Berland Split of the Cutpick.

Type of paleoflow measurement is indicated as follows:

a.r. = asymmetrical ripple

c.t. = s.t. = s.c. = small-scale channelling or terracing

e.r. = elongate erosional ridges

f.b. = fluted burrows

f.c. = flute cast

f.s. = fluted surface (bedding plane) with positive-relief longitudinal ridges resembling inverted flute casts

l.a. = lateral accretion surface, dip direction

l.p. = dip direction on low-angle inlined planar lamination (facies 3PL)

o.s. = oriented shells

o.f. = oriented plant fragments

p.l. = parting lineation

p.m. = prod mark

s.m. = oriented (non-directional) sole mark

t.b. = trough cross-bedding

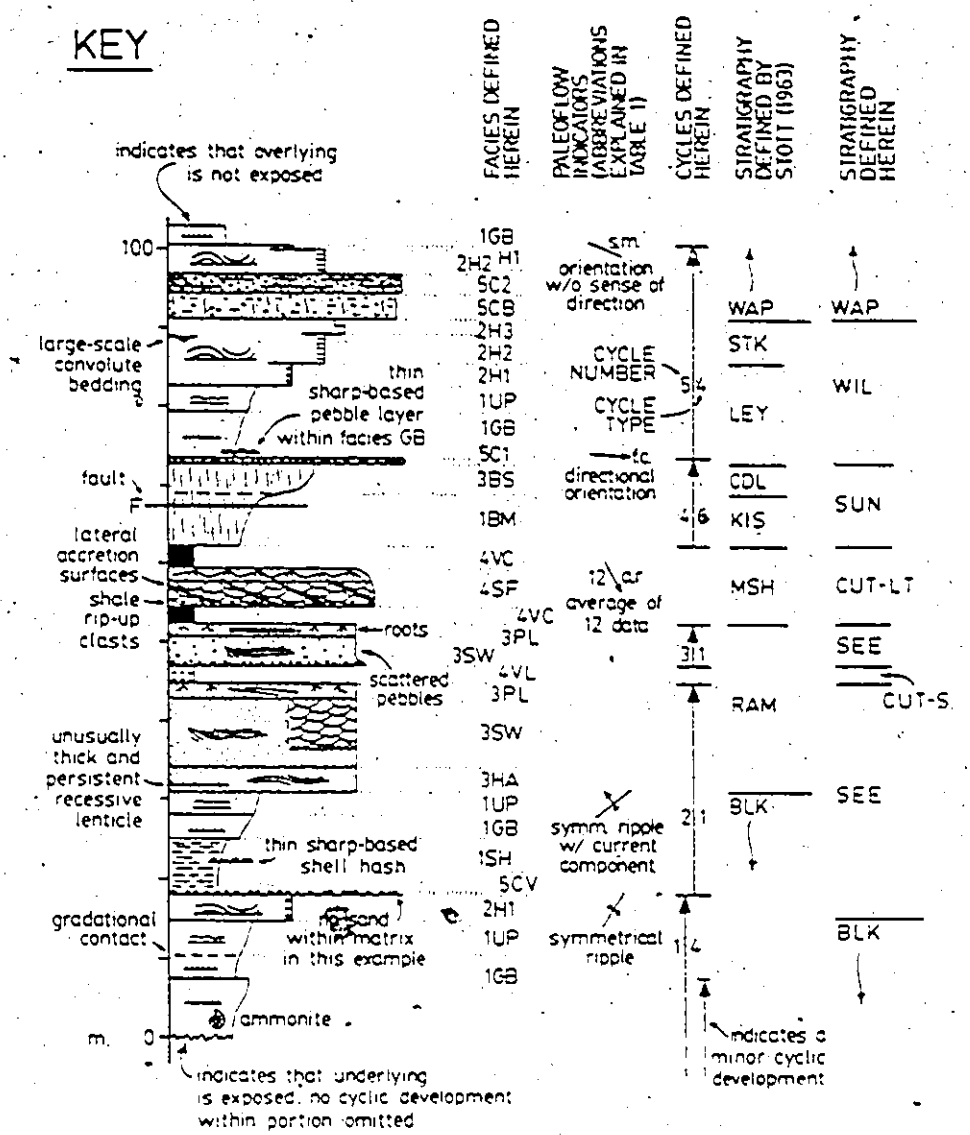
KEY
indicates that overlying is not exposed
100
large-scale convolute bedding
thin sharp-based pebble layer within facies GB
fault
F
lateral accretion surfaces
shale rip-up clasts
roots
scattered pebbles
unusually thick and persistent recessive lenticle
thin sharp-based shell hash
gradational contact
sand within matrix in this example
ammonite
m. 0
indicates that underlying is exposed, no cyclic development within portion omitted
FACIES DEFINED HEREIN
1GB
2H2 H1
5C2
5C8
2H3
2H2
2H1
1UP
1GB
5C1
3BS
1BM
4VC
4SF
4VC
3PL
3SW
4VL
3PL
3SW
3HA
1UP
1GB
1SH
5CV
2H1
1UP
1GB
PALEOFLOW INDICATIONS (ABBREVIATIONS EXPLAINED IN TABLE 1)
sm
orientation w/o sense of direction
CYCLE NUMBER
CYCLE TYPE
fc
directional orientation
12
cr
average of 12 data
symm. ripple w/ current component
symmetrical ripple
CYCLES DEFINED HEREIN
5
4
6
3
1
2
1
1
4
indicates a minor cyclic development
STRATIGRAPHY DEFINED BY STOTT (1963)
WAP
STK
LEY
CDL
KIS
MSH
RAM
BLK
STRATIGRAPHY DEFINED HEREIN
WAP
WIL
SUN
CUT-LT
SEE
CUT-S
SEE
BLK

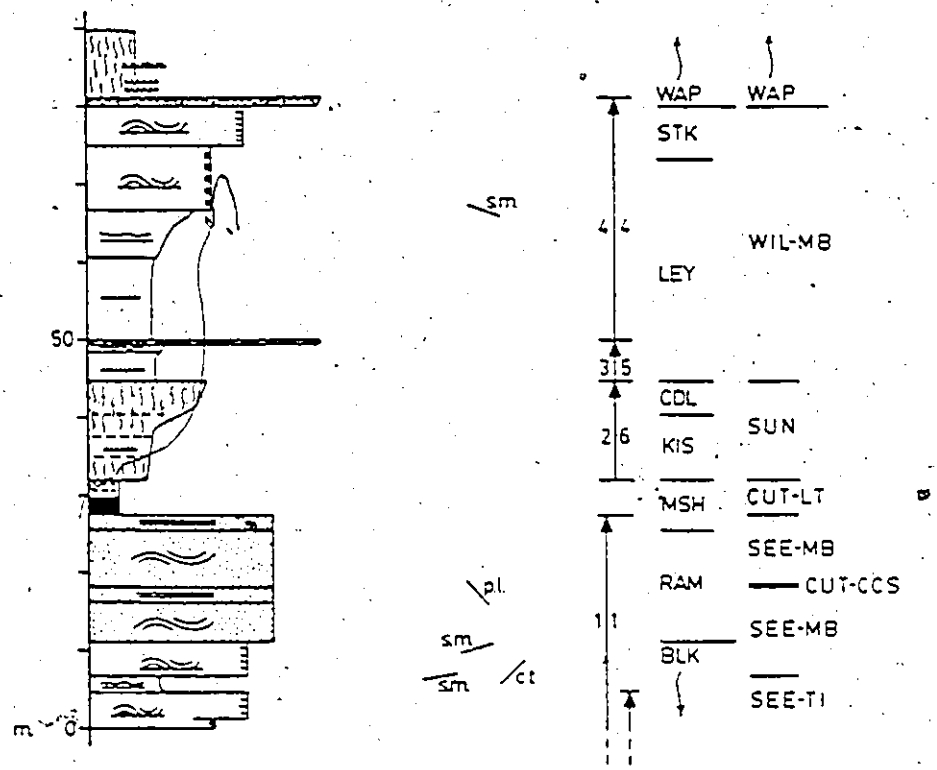

SECTION 4-13, CANYON CREEK

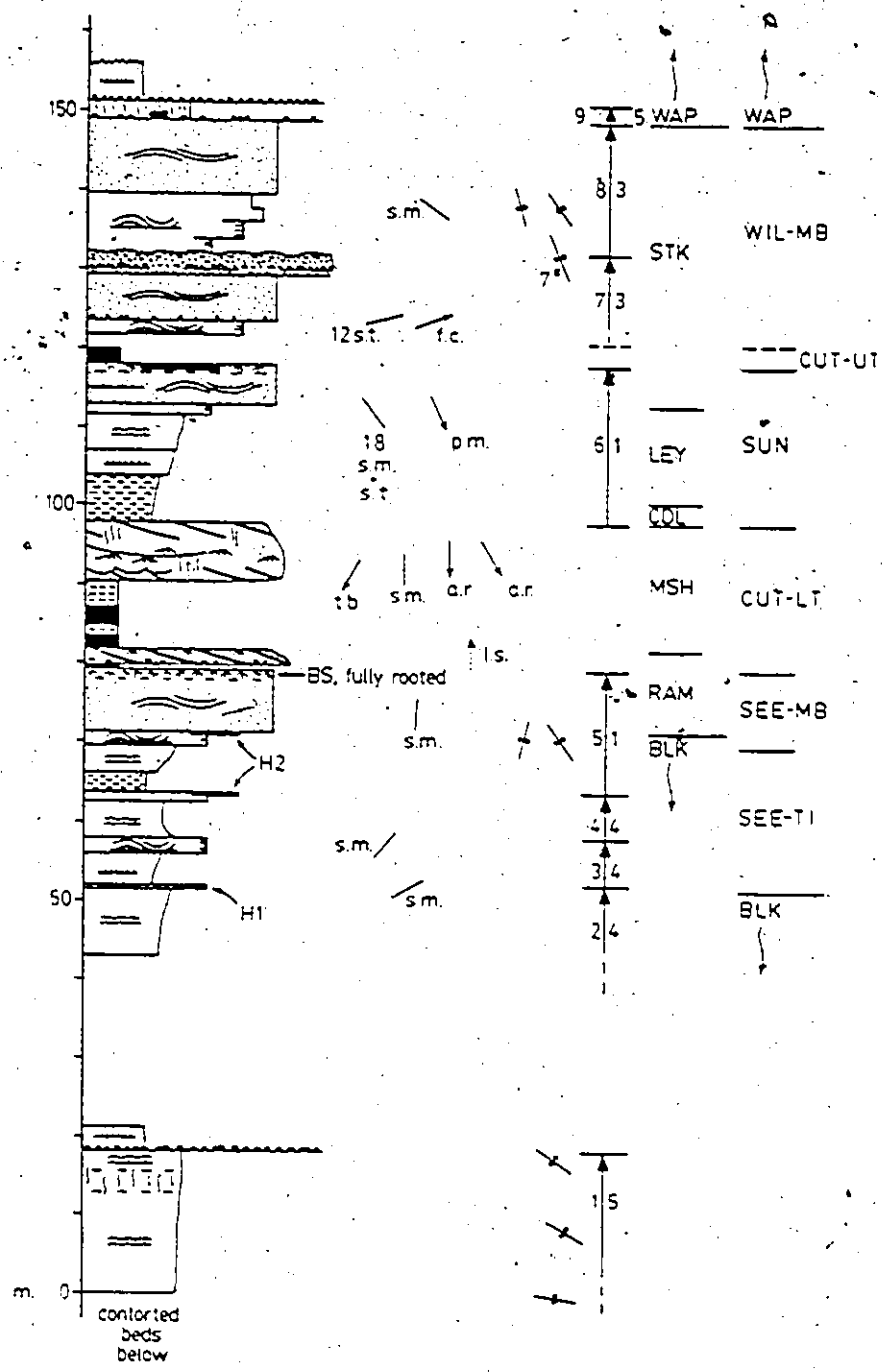

SECTION 4-19, THISTLE CREEK

*symmetrical wave ripples formed in conglomerate ($\lambda > 1$ m.)

N.B.: the interval between 110 m. and 132 m. is fault-repeated.

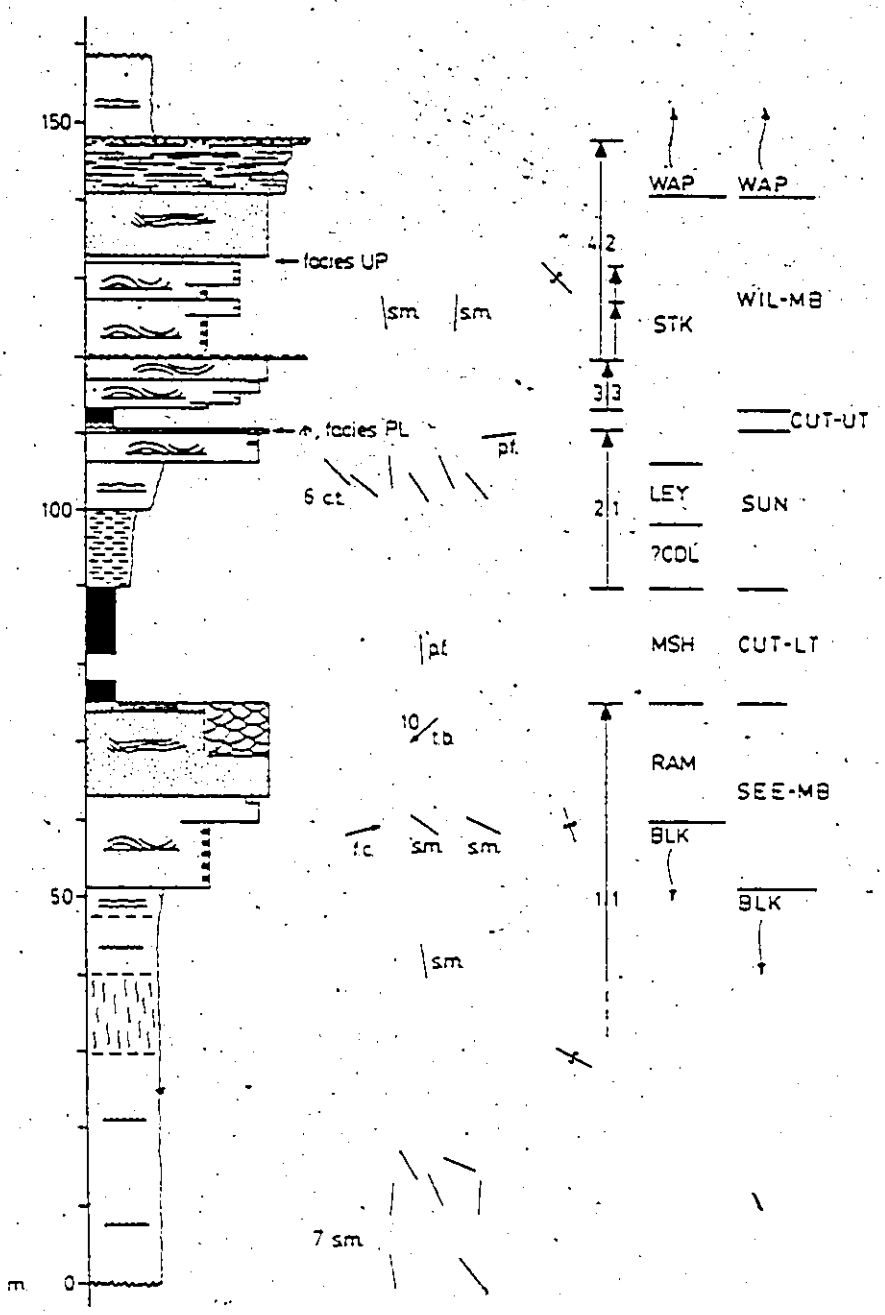

SECTION 4-21, THISTLE CREEK

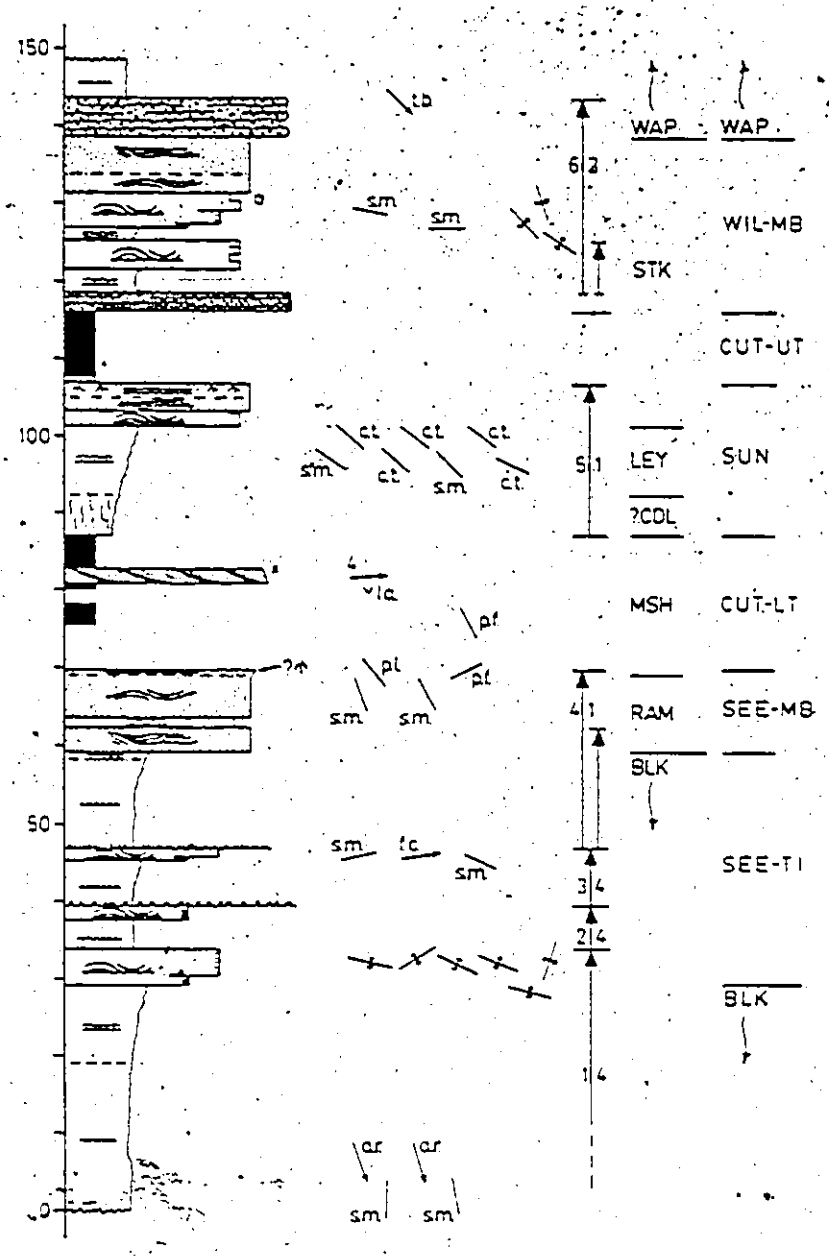

SECTION 4-23, THISTLE CREEK

* trough cross-bedding poorly developed; sandstones largely massive

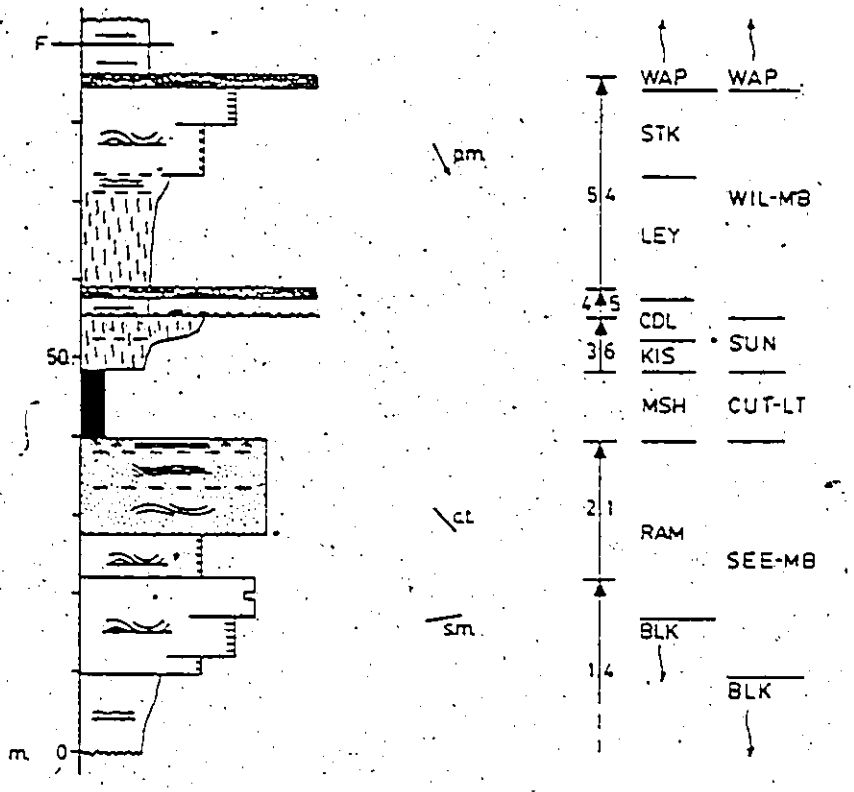

SECTION 4-31, CARDINAL RIVER

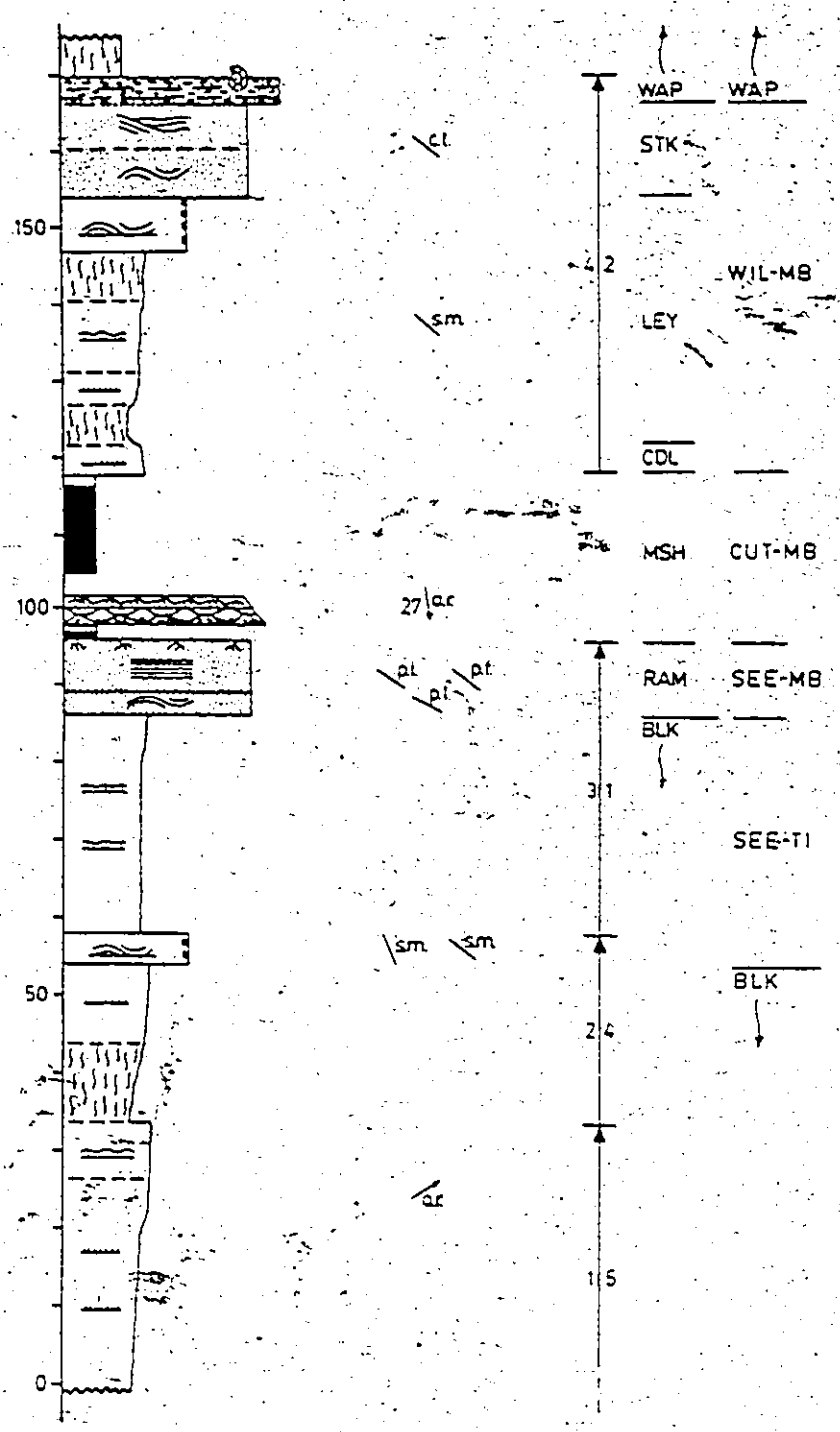

SECTION 4-43, MACKENZIE CREEK

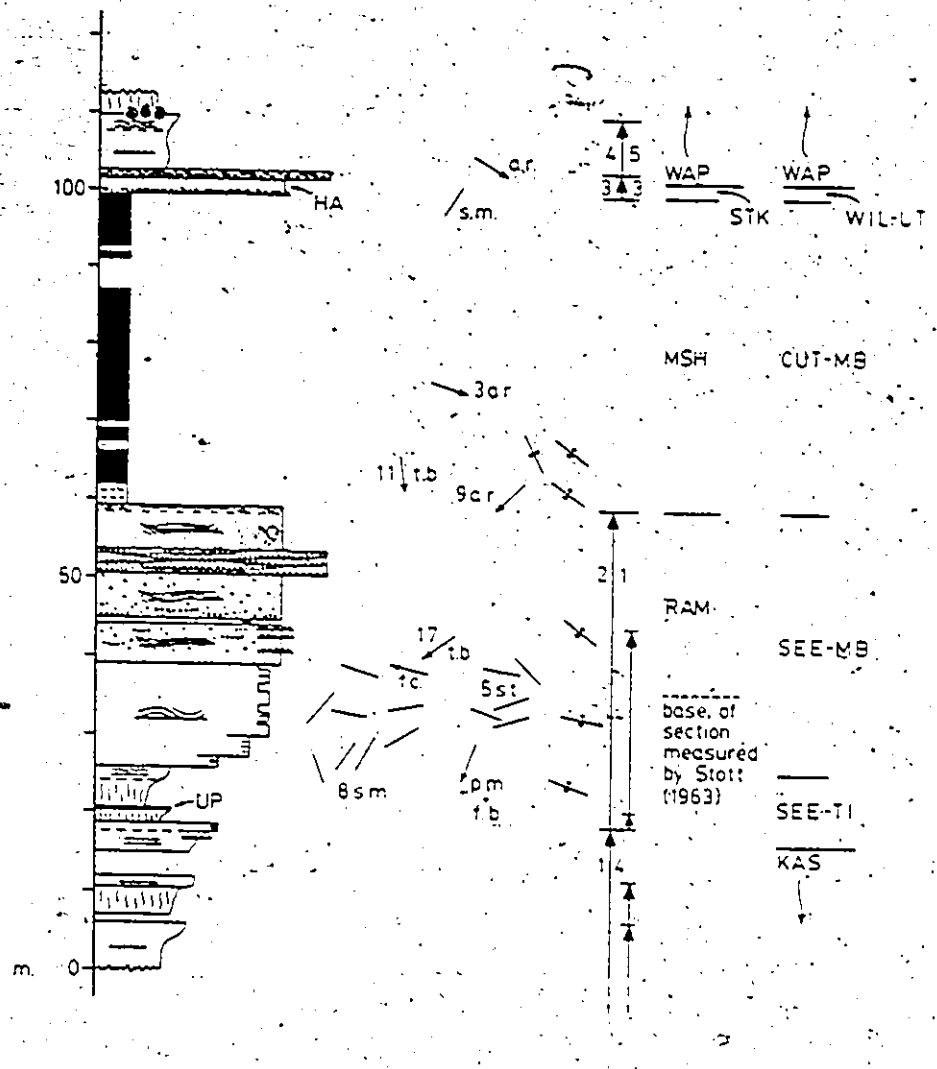

SECTION 5-4, MUSKEG RIVER

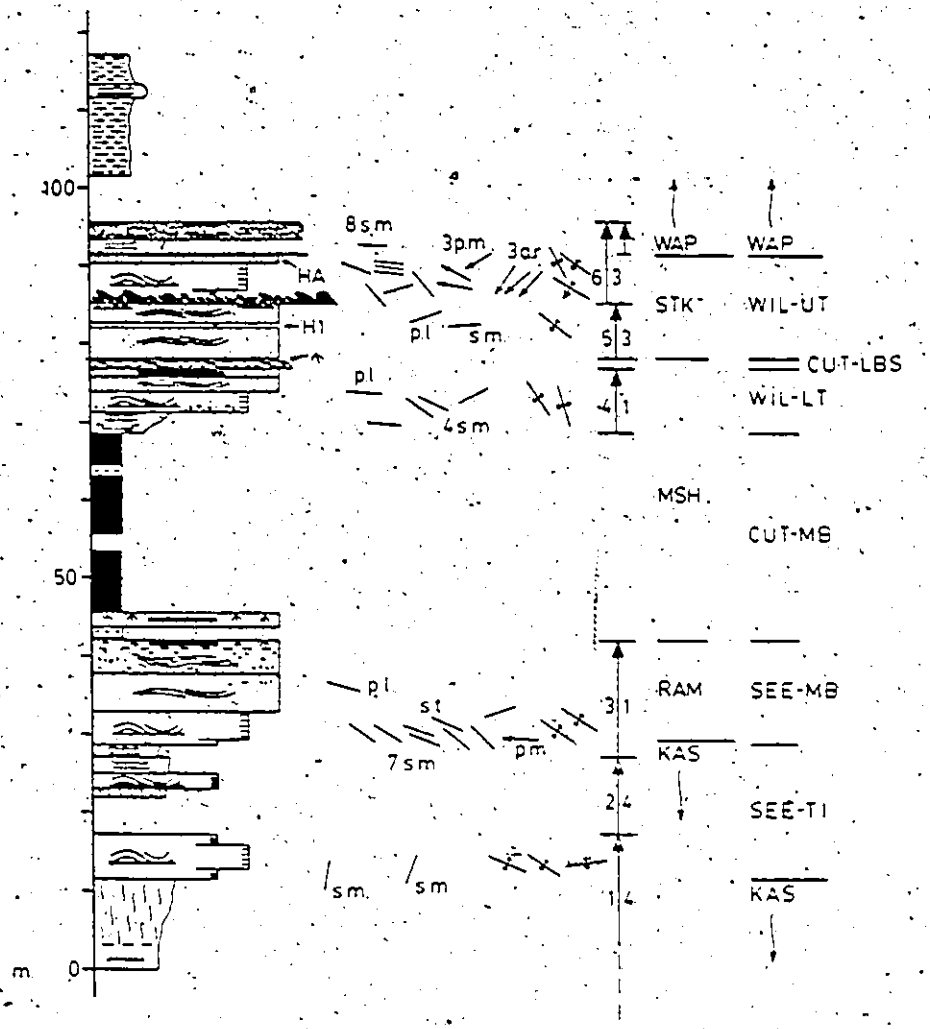

SECTION 5-19, LITTLE BERLAND RIVER

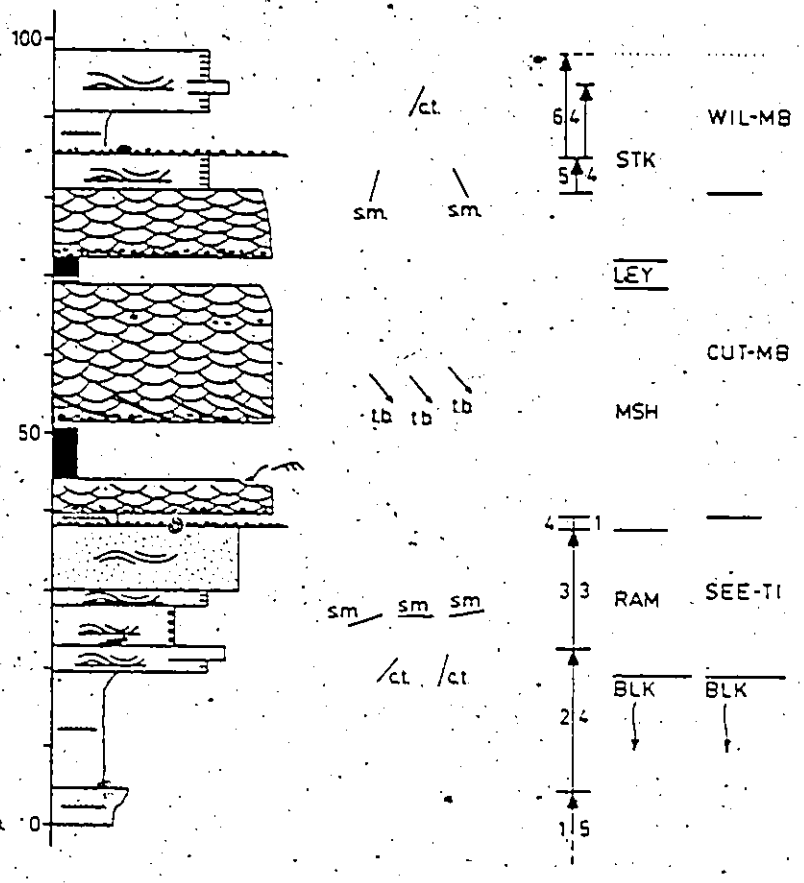

SECTION 5-22, MASKUTA CREEK

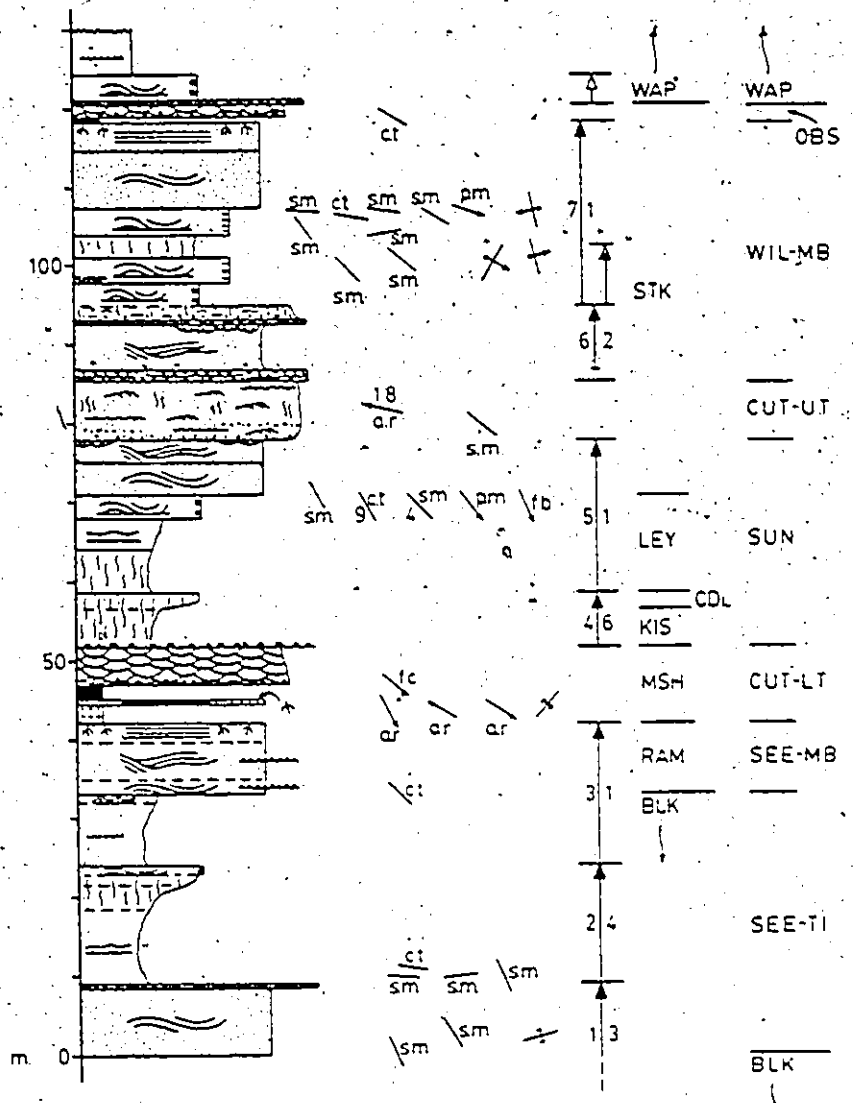

SECTION 5-37, LITTLEHORN CREEK

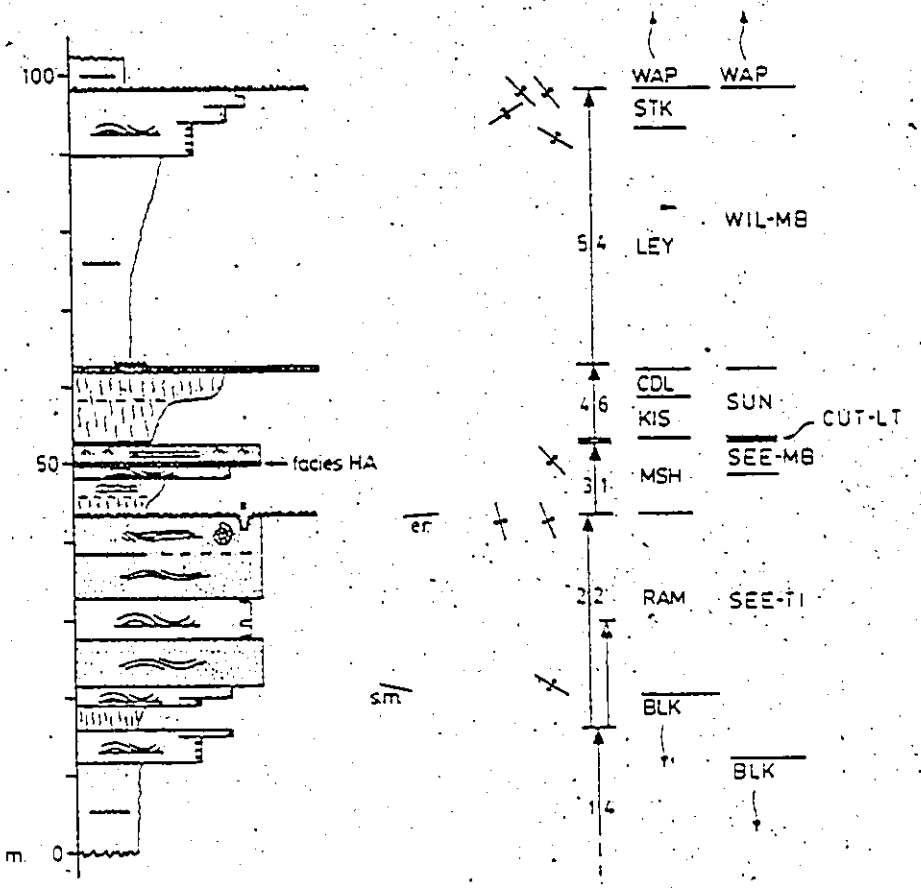

SECTION 5-39, BLACKSTONE RIVER

*pebble-lined burrow

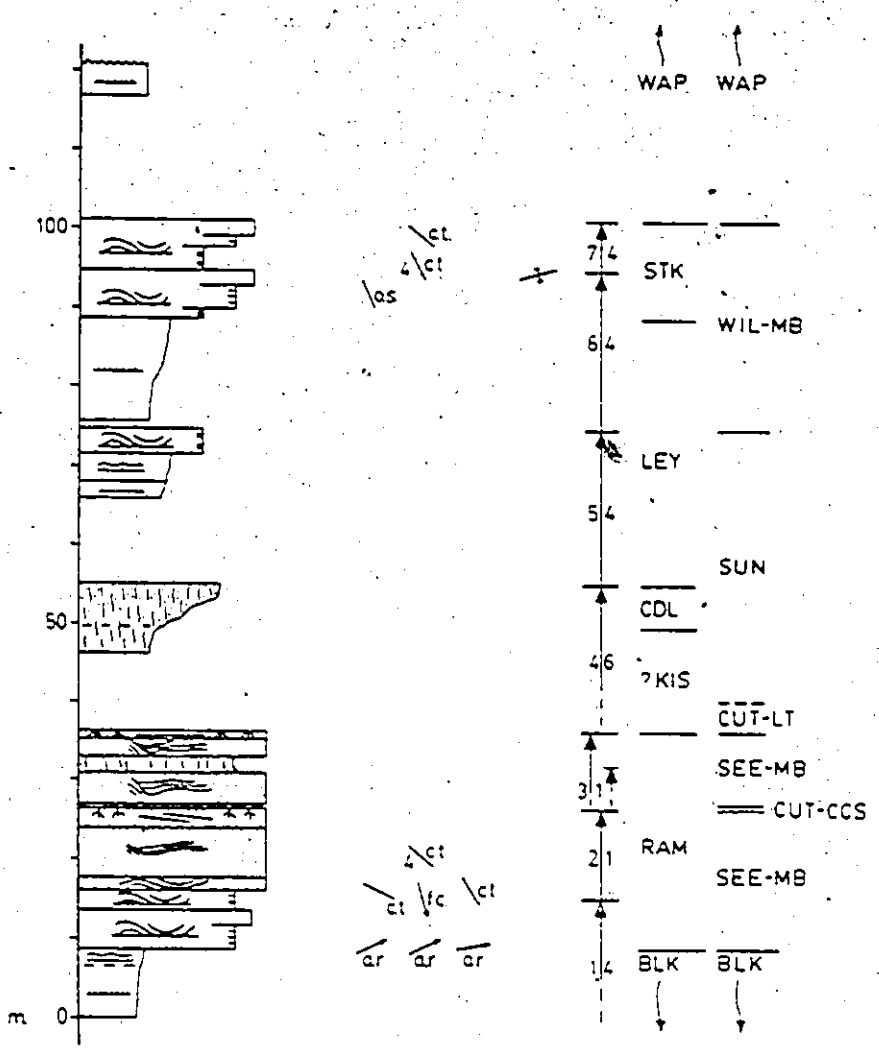

SECTION 5-41, CRIPPLE CREEK

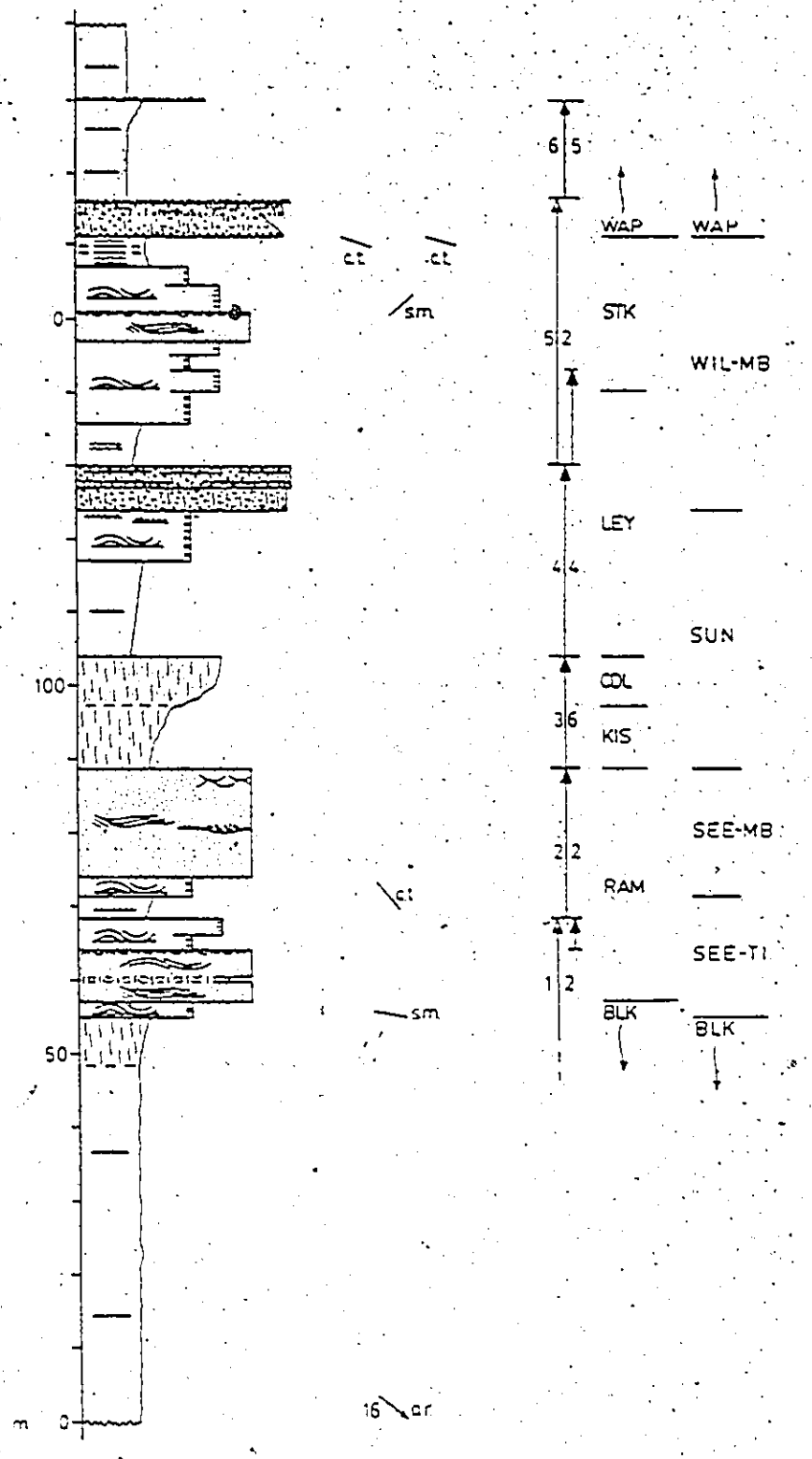

SECTION S-45, RAM RIVER FALLS

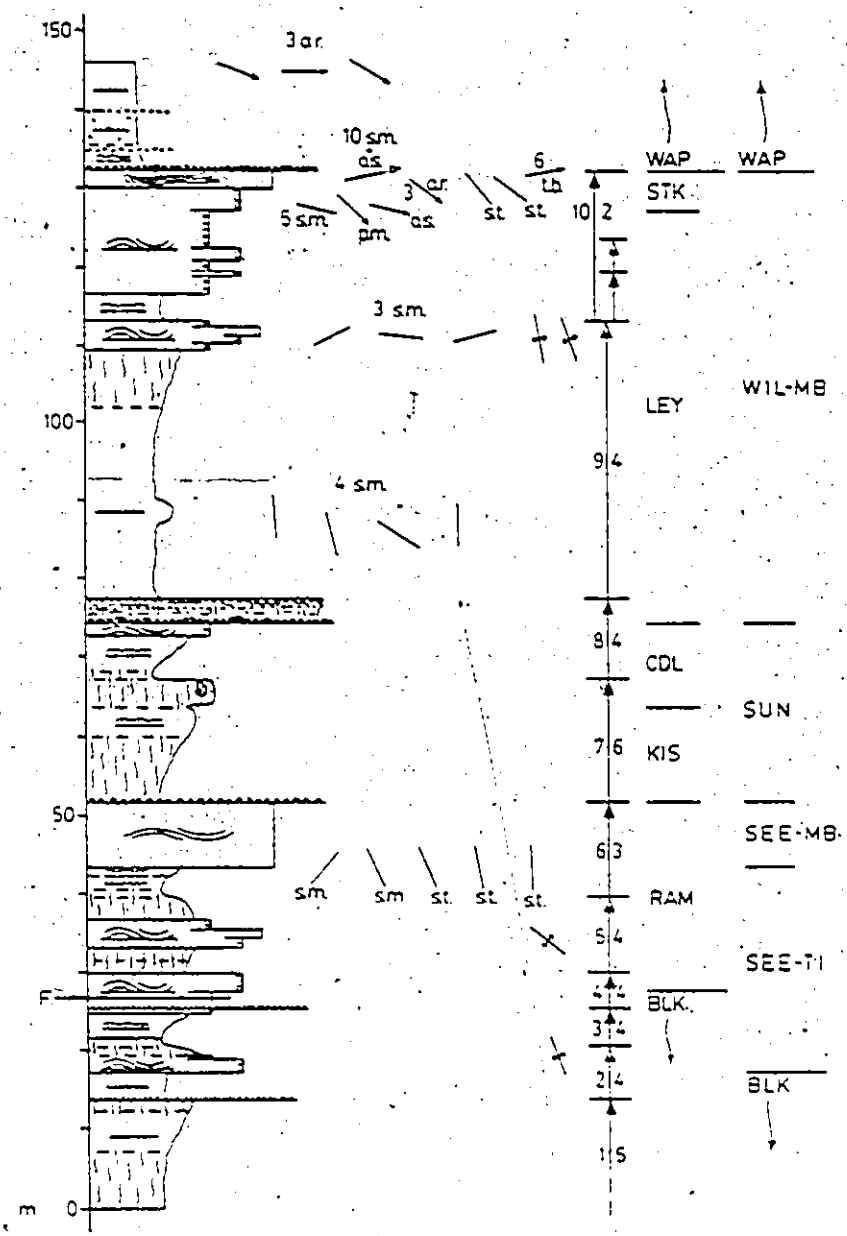

SECTION 6-8, RED DEER RIVER

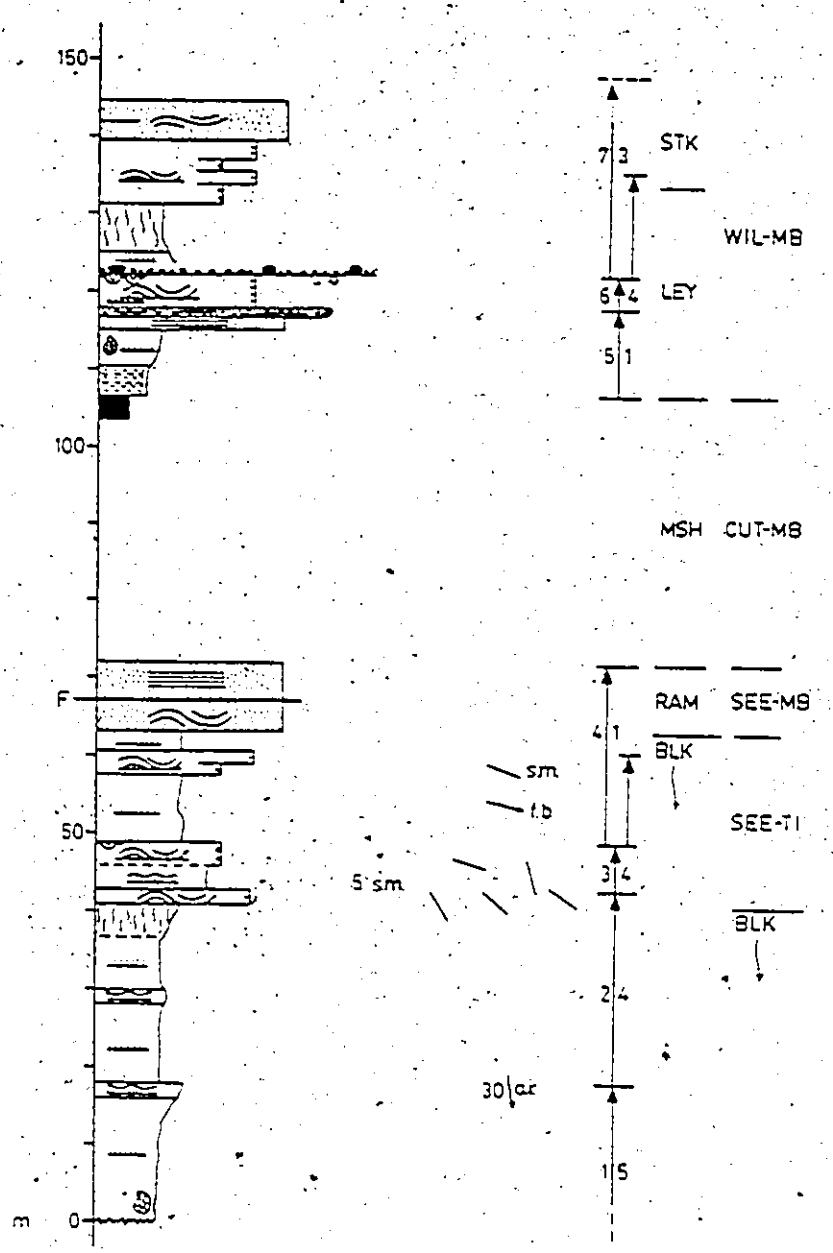

SECTION 7-1, MCLEOD RIVER

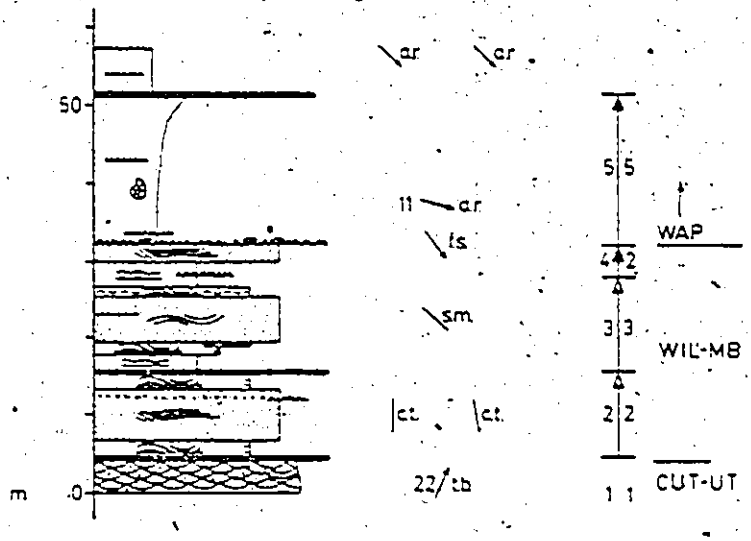

SECTION BD-1, BIGHORN DAMSITE, N. SASKATCHEWAN RIVER

* = reworked Ophiomorpha

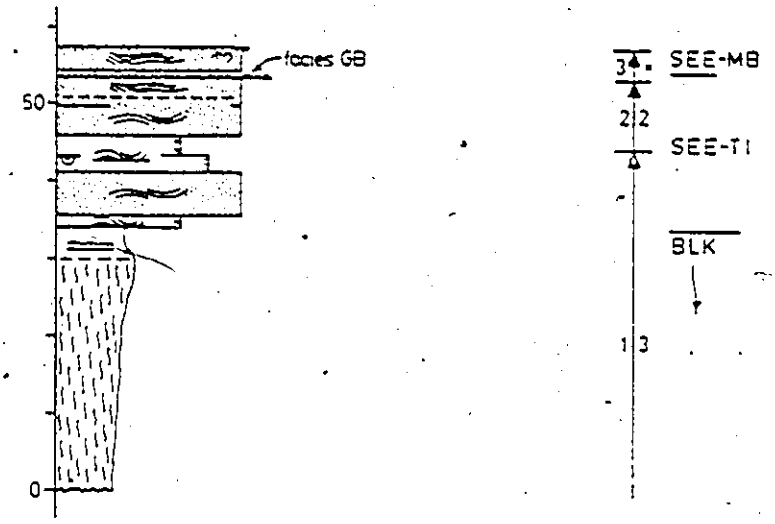

SECTION BL-1, BLACKSTONE RIVER

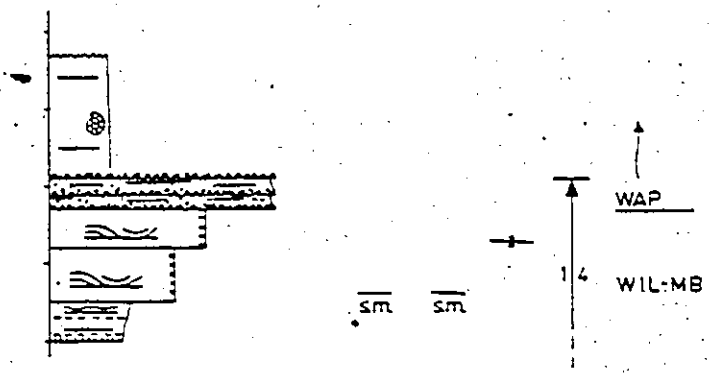

SECTION BZ-1, BRAZEAU RIVER

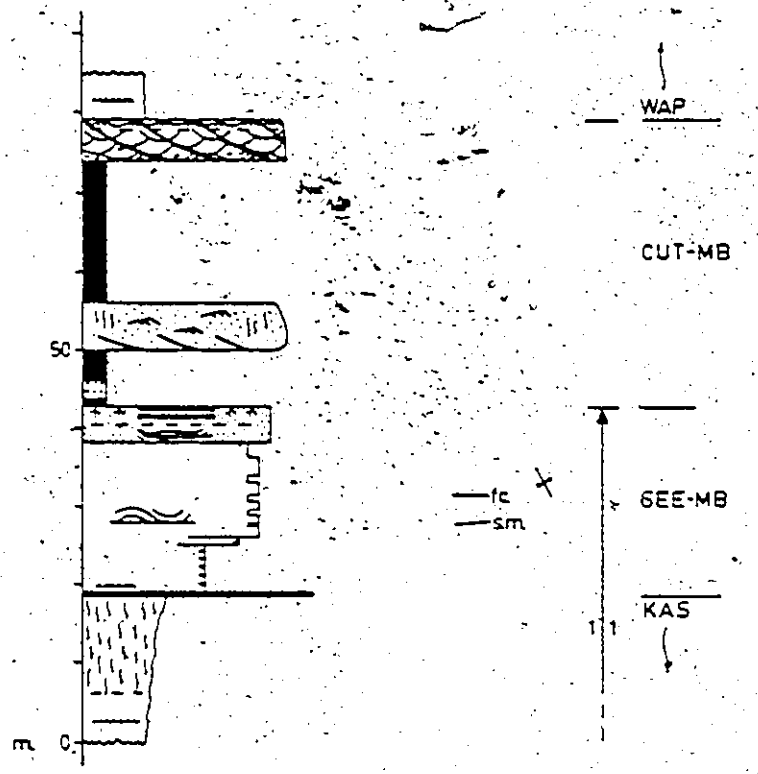

SECTION CU-1, CUTPICK HILL

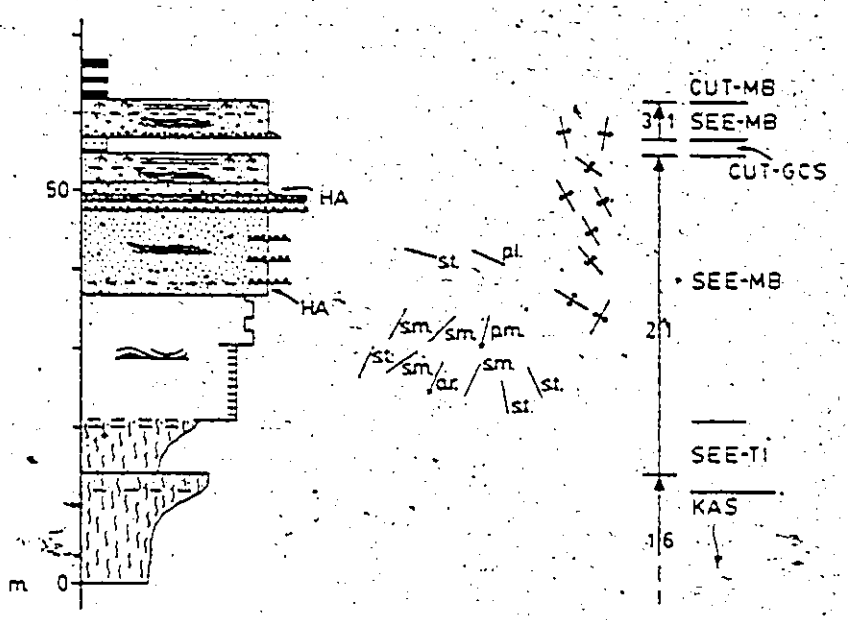

SECTION GC-1, GRANDE CACHE HIGHWAY ROADCUT

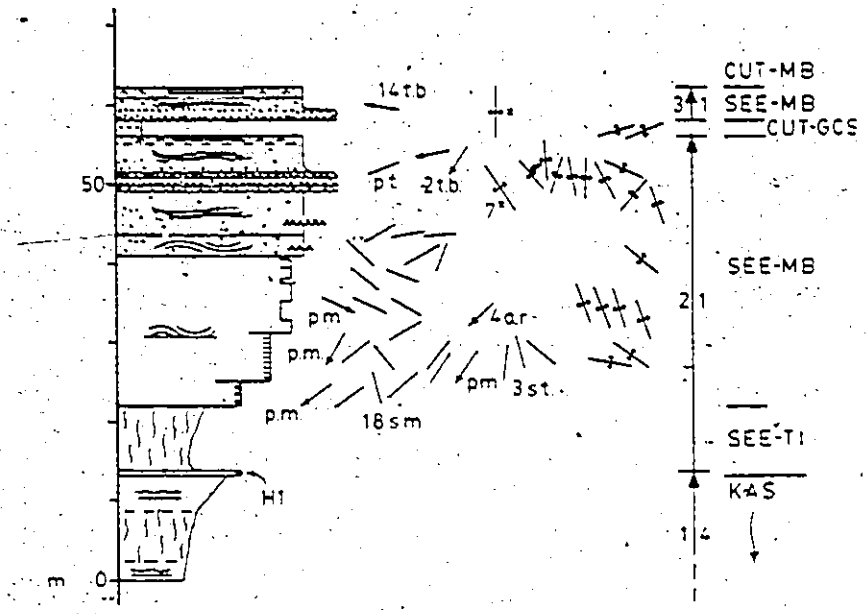

SECTION GC-7, GRANDE CACHE RAILWAY ROADCUT

*Symmetrical wave ripples formed in conglomerate ($\lambda > 1$ m)

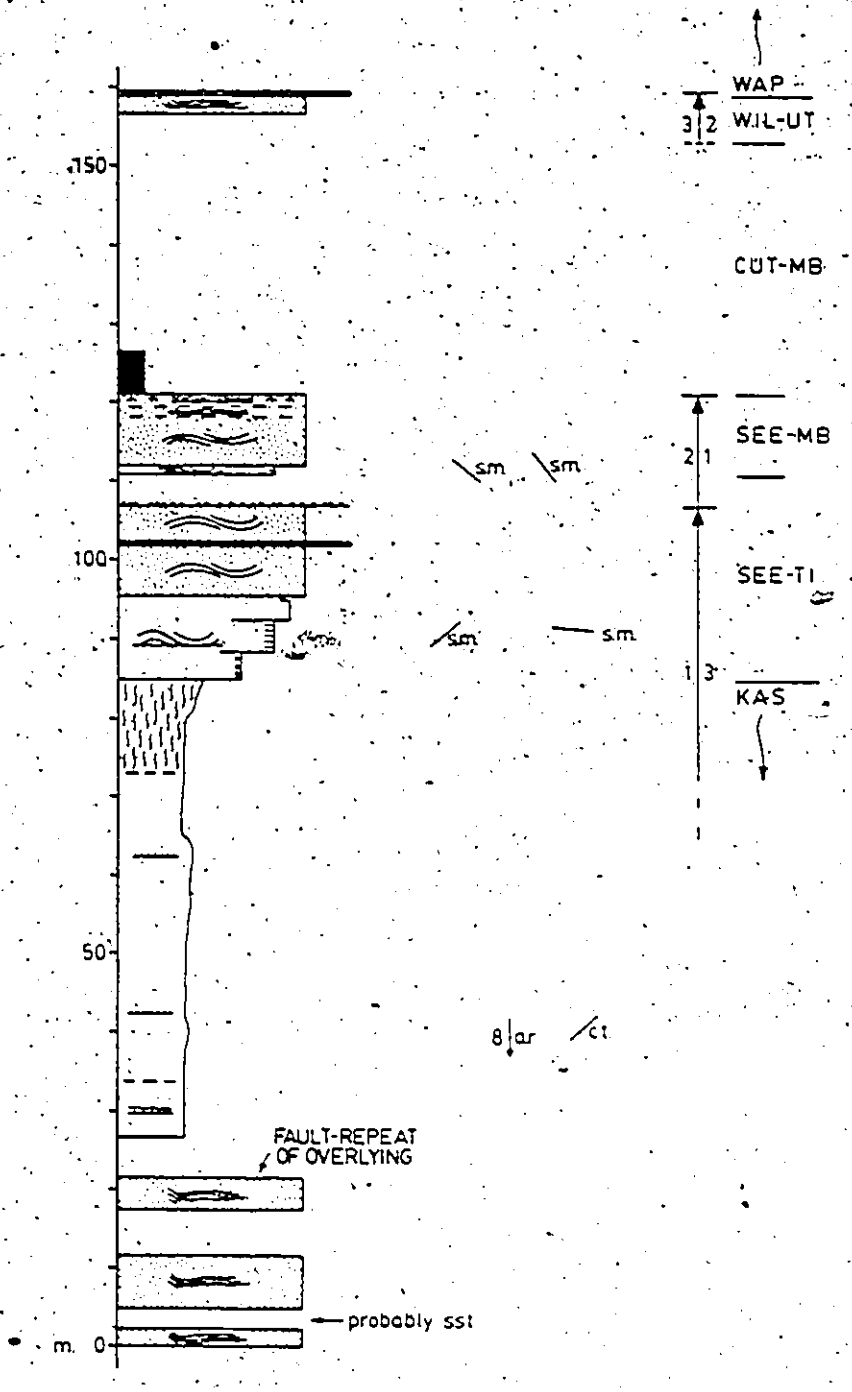

SECTION MS-1, MASON CREEK

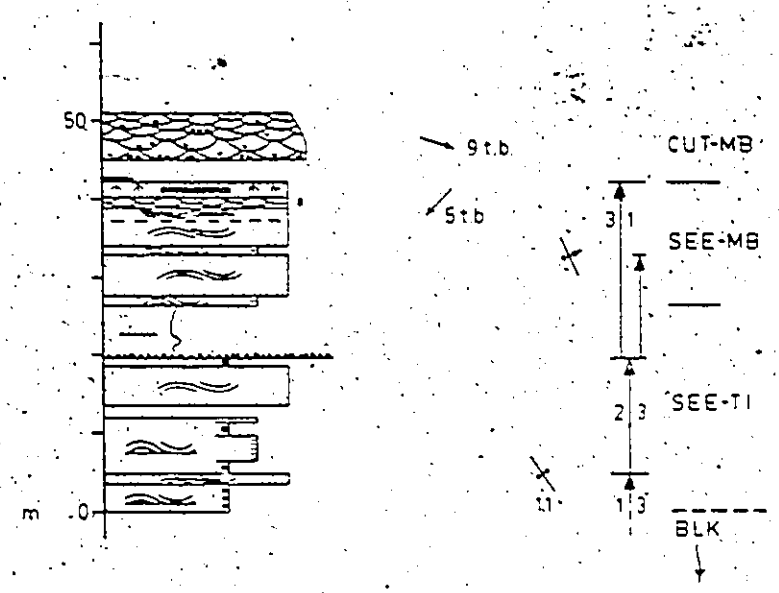

SECTION ND-1, NORTHERN DIVIDE

*largely continuous trough cross-bedded interval within swaley cross-stratified sandstone

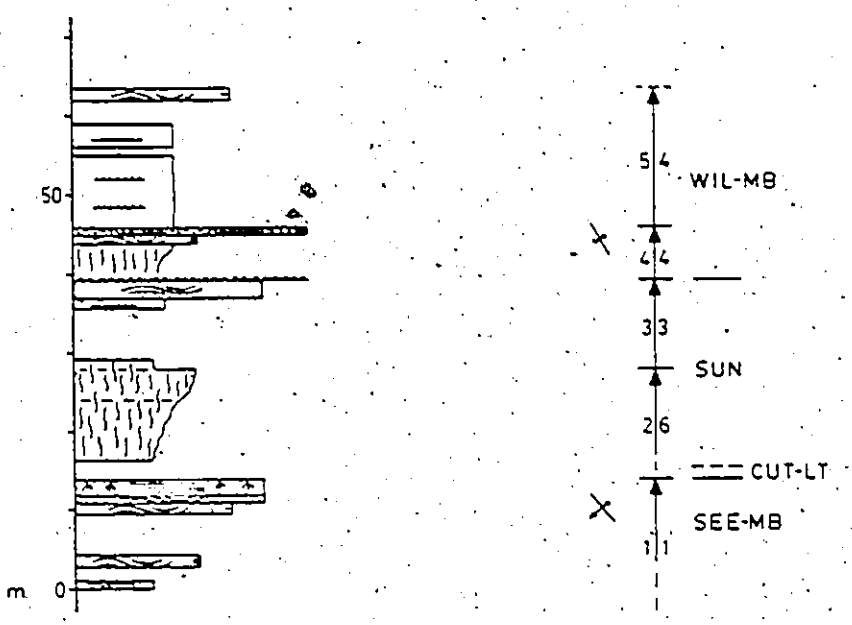

SECTION NR-1, N. RAM RIVER

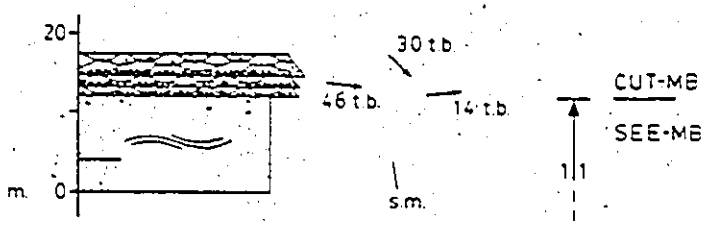

SECTION PC-1, POUCE COUPE QUARRY

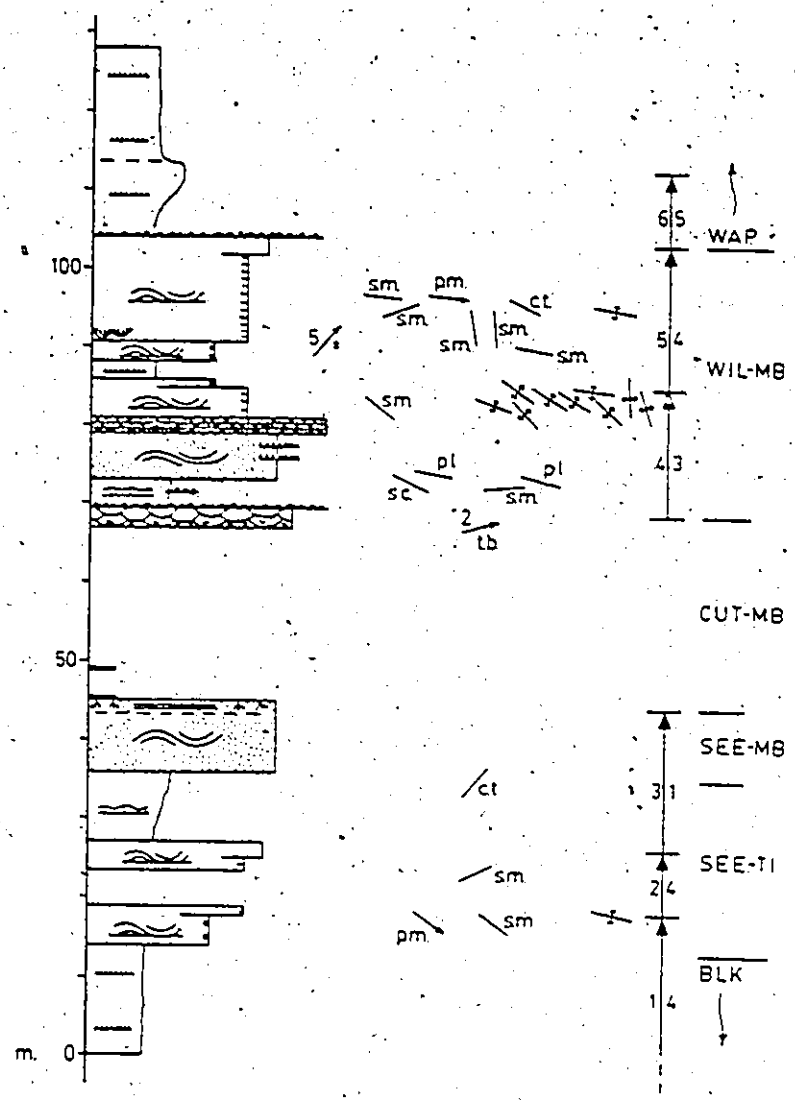

SECTION SC-1, SPHINX CREEK

*downslope direction from large asymmetrical load structures

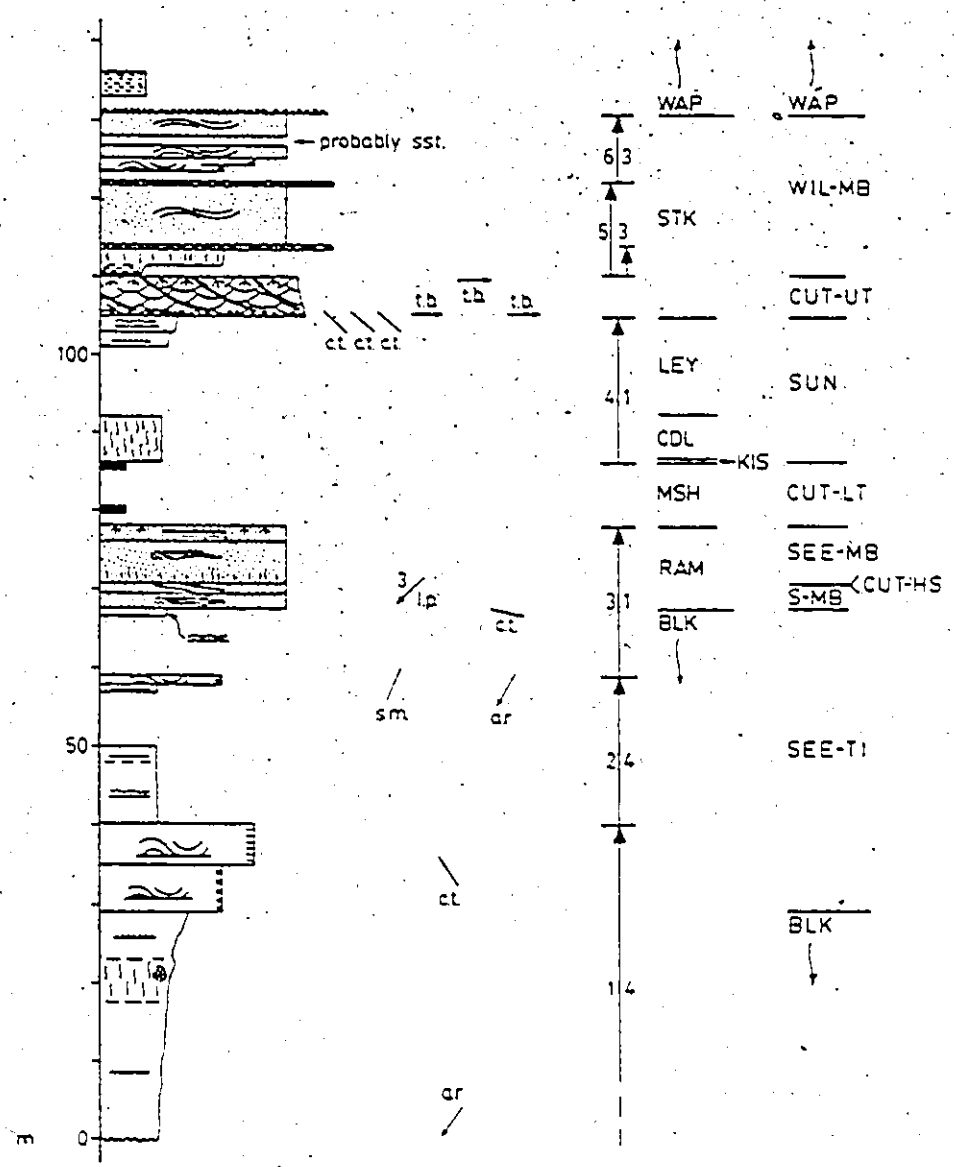

SECTION WA-1, S. FORK WAPIABI CREEK
TYPE SECTION, STOTT (1963)

APPENDIX 3. FACIES-TRANSITION DATA

The following tables summarize the facies-transition data used in chapter 5 to develop normative sequences for:

1) the Cardium Formation as a whole,
2) fully regressive cycles only (i.e., type 1 cycles only),
3) top-absent cycles only,
4) type 2 cycles only,
5) type 3 cycles only,
6) type 4 cycles only,
7) type 5 cycles only, and
8) type 6 cycles only.

The data tabulated herein and utilized in chapter 5 are summarized from the 28 Cardium exposures measured by this author. Facies sequences observed by other McMaster workers in southern Foothills exposures were not included in this summary.

In this appendix, the tables labelled "Cardium Formation" summarize all transitions observed. The tables labelled "Fully Regressive Cycles Only" include data from all cycles which display deposits from association 4 or facies 3PL. These data tables were used in constructing

the type 1 normative sequence (chapter 5). The tables labelled "Top-Absent Cycles Only" include data from all cycles which do not contain deposits from association 4 or facies 3PL.

The technique (developed in chapter 5) referred to as "artificial vertical juxtaposing of cycles" was utilized in the development of normative sequences for cycle types 2 through 6; these data are tabulated herein. This technique is explained in chapter 5.

All statistical techniques are explained in chapter 5. All calculations were conducted using a BASIC computer program (program "Markov") written by this author. The program was tested with data sets for which solutions were previously known.

There are 80 individual tables in this appendix; these are divided into eight groups of ten. Each group corresponds to one of the eight categories listed in the first paragraph of this appendix. Each group consists of the following ten types of tables, listed by their respective headings:

Facies Data. These tables list the number of occurrences of each facies in the data set examined. The mean thickness and range of thickness for each facies also are given, as is the total number of facies occurrences.

Thickness-of-Underlying Matrix. Each of these tables is a 19x19 matrix. These matrices give the mean thickness of any one facies (row) underlying any other facies (column). Thus, the element in row 1GB and column 1BM is the mean thickness (in meters) of all occurrences of facies 1GB which were observed to be immediately overlain by facies 1BM.

Thickness-of-Overlying Matrix. These 19x19 matrices give the mean thickness of any one facies (column) overlying any other facies (row). Thus, the element in row 1GB and column 1BM is the mean thickness (in meters) of all occurrences of facies 1BM which were observed to immediately overlie facies 1GB.

Observed Transitions. These tables give (at the top) the total number of facies transitions observed in the data set. The rest of the table is a 19x19 talley matrix listing the number of transitions from any one facies (row) to any other facies (column).

Observed Transition Probability. These matrices give the observed transition probability from any one facies (row) to any other facies (column). Possible values range from Ø to 1.

Expected (Random) Transitions. These matrices list the predicted number of transitions from any one facies

(row) to any other facies (column), assuming that all transitions occur randomly. Any non-negative value is possible.

Expected (Random) Transition Probability. These matrices list the predicted probability of any one facies (row) being overlain by any other facies (column), again assuming that all transitions occur randomly. Possible values range from Ø to 1.

Observed Minus Random Probability. These matrices list the difference between the values of observed and predicted (i.e., random) transition probability. Possible values range from -1 to 1.

Significance Test Values. These matrices list the statistical significance of the values in the difference matrices (i.e, the observed minus random probability matrices), utilizing the binomial probability method advocated by Harper (1984). Possible values range from Ø to 1. These values, when subtracted from unity and expressed as a percentage, represent the confidence values reported in chapter 5. Thus, an element with a listed value of, say, Ø.Ø3 represents a transition which is confident at 97%.

Values of Parameter r. These matrices list the values of the parameter r for the transition from any one

facies (row) to any other facies (column). In chapter 5, this parameter is referred to as the significance parameter; it was developed by the author for this thesis. Possible values range between -1 and 1.

PLEASE NOTE THE FOLLOWING:

1) The 19x19 matrices are divided into two parts for ease of reproduction.

2) In the last two matrices of each group (i.e., those listing confidence and significance values), the numbers 8 or 88 appear repeatedly as matrix elements. These numbers appear as place-savers only; they indicate that the respective calculation was not performed for that transition element, due to the prior determination of a negative residual (i.e., observed minus random) probability.

RUN DESIGNATION: CARDIUM FORMATION

FACIES DATA

FACIES	# OCCUR	MEAN THICKNESS (RANGE) IN METERS
1SH	8	5 (0.8 to 10)
1BM	52	5.2 (1 to 12.2)
1GB	75	7.1 (0.9 to 39.1)
1UP	63	4.1 (0.4 to 29.2)
2M1	64	2.5 (0.5 to 5.5)
2M2	75	2.5 (0.4 to 11.1)
2M3	24	3.6 (1 to 12.1)
3BS	19	2.7 (0.7 to 6.6)
3HA	54	4.5 (0.6 to 12.2)
3SW	40	4.5 (1.3 to 14.6)
3PL	32	1.9 (0.6 to 5.6)
4VL	16	1.5 (0.4 to 3.1)
4VC	48	3.4 (0.2 to 17.9)
4IF	3	7.2 (6.3 to 7.7)
4SF	14	4.9 (0.8 to 17.4)
5CV	30	0 (0 to 0)
5CB	4	2.6 (1.9 to 3)
5C1	13	0.4 (0.1 to 0.6)
5C2	20	2.5 (0.9 to 7.2)

TOTAL NUMBER OF FACIES OCCURRENCES: 674

RUN DESIGNATION: CARDIUM FORMATION

THICKNESS-OF-UNDERLYING MATRIX --

	1SH	1BM	1GB	1UP	2H1	2H2	2H3	3BS	3HA	3SW
1SH	0	0	4.8	7.5	0	0	0	0.8	0	0
1BM	0	0	5.2	4.5	6.4	4.1	0	5.4	0	0
1GB	0	11	0	5.1	6.6	5.2	0	0	1.9	0.9
1UP	1.8	6.3	4.1	0	4	2.1	6	3.7	7.3	3.5
2H1	0	0.9	1.8	2.2	0	2.6	6.5	0.9	3.2	2.4
2H2	0.4	1.7	2.4	3.9	2.4	0	3.2	3.2	4.9	1.8
2H3	0	0	0	2.9	2.1	1.7	0	0	4.5	6.4
3BS	0	2.6	5.5	0	1.4	1.8	0	0	0.7	2
3HA	0	0	0	0	3.5	5.6	6	6.5	0	3.9
3SW	0	14.6	0	3.2	0	5.3	0	3.3	9.3	0
3PL	0	0	0	0	0	0	0	0	1.9	1.2
4VL	0	2.3	1.2	0	0	0	0	0	0	1.7
4VC	4	3.6	4.3	0	2.1	0	0	0	3.5	0
4IF	7.5	0	0	0	0	0	0	0	0	0
4SF	0	0	5.2	0	0	8.6	0	0	0	0
5CV	0	0	0	0	0	0	0	0	0	0
5CB	0	0	0	0	1.9	0	0	0	0	0
5C1	0	0	0.5	0.3	0.2	0.3	0	0	0.3	0.7
5C2	0	2.1	2	4.2	2	2	0	0	0	2.4

	3PL	4VL	4VC	4IF	4SF	5CV	5CB	5C1	5C2
1SH	0	0	0	0	0	0	0	0	0
1BM	0	0	0	0	0	1.8	0	12.2	0
1GB	4.6	0	0	0	1.6	13.4	0	16.3	2.3
1UP	0	0	0	0	2	2.4	1.3	0.9	2
2H1	0	0	0	0	0	1.9	7	0	1.1
2H2	0	0	0	0	0	2.7	0	2	4.9
2H3	3.8	0	0	0	0	2.2	0	0	0
3BS	0	1.2	0	0	0	3	0	2	3.6
3HA	4.3	0	0	0	12.3	4.6	0	7.5	4.5
3SW	3.7	0	0	2.8	0	3	0	4.9	5.9
3PL	0	1.2	0	0	0	0	0	0	1.6
4VL	1.8	0	0	0	0	0	0	0	0
4VC	0	1.8	0	0	0.5	0	0	0	0
4IF	0	0	0	0	0	0	0	0	0
4SF	0	0	0	0	0	0	0	1.6	0
5CV	0	0	0	0	0	0	0	0	0
5CB	0	0	0	0	0	0	0	0	0
5C1	0	0	0	0	0	0	0	0	0
5C2	0	0	0	0	0	0	0	0	0

RUN DESIGNATION: -CARDIUM FORMATION

THICKNESS-OF-OVERLYING MATRIX

	1SH	1EM	1GB	1UP	2H1	2H2	2H3	3ES	3HA	3SW
1SH	0	0	3.9	3.6	0	0	0	2	0	0
1EM	0	0	4.5	3.5	2.6	2	0	3.2	0	0
1GB	0	6.8	0	3.3	2.9	1.7	0	0	3.1	2.1
1UP	4	5.3	11.7	0	2.6	2.9	3.1	3.5	5.3	2.9
2H1	0	4.6	5.8	6.3	0	2.6	3.3	2	4.1	5.6
2H2	2.7	2.4	3.1	2.4	2.1	0	3.6	2.9	4.8	4.6
2H3	0	0	0	5.2	3.1	3.2	0	0	4.1	5
3ES	0	2.7	8.3	0	0.6	4.7	0	0	3.6	2.4
3HA	0	0	0	0	1.4	1.6	5.1	1.2	0	4.3
3SW	0	8.6	0	1.3	0	2.1	0	1.4	3.6	0
3PL	0	0	0	0	0	0	0	0	7.3	5.4
4VL	0	3	3.9	0	0	0	0	0	0	0
4VC	4.8	5	8	0	0.6	0	0	0	2.9	0
4IF	5.9	0	0	0	0	0	0	0	0	0
4SF	0	0	0	0	0	4.8	0	0	0	0
5CV	0	4.5	7.6	1.8	2.6	0	0	0	0	0
5CB	0	0	0	0	2.9	0	0	0	0	0
5C1	0	0	17.5	5.6	4.8	2	0	0	4.5	7.5
5C2	0	12	11.6	4.4	3.1	3.8	0	0	0	4.6

	3PL	4VL	4VC	4IF	4SF	5CV	5CB	5C1	5C2
1SH	0	0	0	0	0	0	0	0	0
1EM	0	0	0	0	0	0	0	0.2	0
1GB	4.6	0	0	0	4.4	0	0	0.8	1.4
1UP	0	0	0	0	4.9	0	3	0.4	1.2
2H1	0	0	0	0	0	0	3	0	1
2H2	0	0	0	0	0	0	0	0.3	1.2
2H3	0.6	0	0	0	0	0	0	0	0
3ES	0	0	0.6	0	0	0	0	0.7	0.9
3HA	2.3	0	0	0	6.5	0	0	0.3	0
3SW	4.6	0	0	7.7	0	0	0	0.2	1.3
3PL	0	1.9	0	0	0.8	0	0	0	0
4VL	1.2	0	0	1.6	0	0	0	0	0
4VC	0	1.4	0	0	0.9	0	0	0	0.8
4IF	0	0	0	0	0	0	0	0	0
4SF	0	0	0	0	0	0	0	0	0
5CV	0	0	0	0	0	0	0	0	0
5CB	0	0	0	0	0	0	0	0	0
5C1	0	0	0	0	0	0	0	0	0
5C2	0	0	0	0	0	0	0	0	0



RUN DESIGNATION: CARDIUM FORMATION

TOTAL NUMBER OF FACIES TRANSITIONS OBSERVED: 596

OBSERVED TRANSITIONS --

	1SH	1BM	1GB	1UP	2H1	2H2	2H3	3BS	3HA	3SW
1SH	0	0	2	3	0	0	0	1	0	0
1BM	0	0	9	12	11	1	0	14	0	0
1GB	0	12	0	19	13	4	0	0	2	1
1UP	1	7	5	0	24	4	3	1	6	4
2H1	0	2	5	5	0	45	1	2	19	2
2H2	1	2	3	5	11	0	19	1	18	4
2H3	0	0	0	2	5	2	0	0	7	4
3BS	0	0	2	0	1	3	0	0	1	1
3HA	0	0	0	0	4	3	1	1	0	14
3SW	0	1	0	1	0	3	0	2	1	0
3PL	0	0	0	0	0	0	0	0	1	1
4VL	0	1	1	0	0	0	0	0	0	2
4VC	3	4	1	0	1	0	0	0	2	0
4IF	1	0	0	0	0	0	0	0	0	0
4SF	0	0	1	0	0	1	0	0	0	0
5CV	0	3	17	2	3	0	0	0	0	0
5CB	0	0	0	0	1	0	0	0	0	0
5C1	0	0	3	2	2	1	0	0	1	1
5C2	0	3	6	3	2	1	0	0	0	3

	3PL	4VL	4VC	4IF	4SF	5CV	5CB	5C1	5C2
1SH	0	0	0	0	0	0	0	0	0
1BM	0	0	0	0	0	2	0	1	0
1GB	1	0	0	0	1	1	0	1	1
1UP	0	0	0	0	1	1	1	1	1
2H1	0	0	0	0	0	5	1	0	1
2H2	0	0	0	0	0	2	0	1	3
2H3	1	0	0	0	0	2	0	0	0
3BS	0	0	1	0	0	1	0	1	1
3HA	10	0	0	0	1	9	0	2	3
3SW	17	0	0	1	0	4	0	4	5
3PL	0	4	17	0	1	0	0	0	1
4VL	2	0	9	1	0	0	0	0	0
4VC	0	12	0	1	7	0	0	0	1
4IF	0	0	1	0	0	0	0	0	1
4SF	0	0	0	0	0	2	0	1	0
5CV	0	0	0	0	0	0	1	0	0
5CB	0	0	0	0	0	0	0	1	2
5C1	0	0	0	0	0	0	1	0	0
5C2	0	0	0	0	0	1	0	0	0

RUN DESIGNATION: CARDIUM FORMATION

OBSERVED TRANSITION PROBABILITY --

	1SH	1BM	1GB	1UP	2H1	2H2	2H3	3BS	3HA	3SW
1SH	0	0	0.33	0.5	0	0	0	0.17	0	0
1BM	0	0	0.19	0.26	0.23	0.02	0	0.23	0	0
1GB	0	0.21	0	0.34	0.23	0.07	0	0	0.04	0.02
1UP	0.02	0.12	0.08	0	0.4	0.07	0.05	0.02	0.1	0.07
2H1	0	0.03	0.06	0.06	0	0.57	0.01	0.03	0.13	0.03
2H2	0.01	0.03	0.04	0.07	0.16	0	0.27	0.01	0.26	0.06
2H3	0	0	0	0.09	0.22	0.09	0	0	0.3	0.17
3BS	0	0.33	0.11	0	0.06	0.17	0	0	0.06	0.06
3HA	0	0	0	0	0.08	0.06	0.02	0.02	0	0.29
3SW	0	0.03	0	0.03	0	0.08	0	0.05	0.03	0
3PL	0	0	0	0	0	0	0	0	0.04	0.04
4VL	0	0.06	0.06	0	0	0	0	0	0	0.13
4VC	0.09	0.13	0.03	0	0.03	0	0	0	0.06	0
4IF	0.33	0	0	0	0	0	0	0	0	0
4SF	0	0	0.09	0	0	0.09	0	0	0	0
5CV	0	0.18	0.61	0.07	0.11	0	0	0	0	0
5CB	0	0	0	0	0.25	0	0	0	0	0
5C1	0	0	0.27	0.18	0.18	0.09	0	0	0.09	0.09
5C2	0	0.16	0.32	0.16	0.11	0.05	0	0	0	0.16

	3PL	4VL	4VC	4IF	4SF	5CV	5CB	5C1	5C2
1SH	0	0	0	0	0	0	0	0	0
1BM	0	0	0	0	0	0.04	0	0.02	0
1GB	0.02	0	0	0	0.02	0.02	0	0.02	0.02
1UP	0	0	0	0	0.02	0.02	0.02	0.02	0.02
2H1	0	0	0	0	0	0.06	0.01	0	0.01
2H2	0	0	0	0	0	0.03	0	0.01	0.04
2H3	0.04	0	0	0	0	0.09	0	0	0
3BS	0	0	0.06	0	0	0.06	0	0.06	0.06
3HA	0.21	0	0	0	0.02	0.19	0	0.04	0.06
3SW	0.44	0	0	0.03	0	0.1	0	0.1	0.13
3PL	0	0.16	0.68	0	0.04	0	0	0	0.04
4VL	0.13	0	0.56	0.06	0	0	0	0	0
4VC	0	0.38	0	0.03	0.22	0	0	0	0.03
4IF	0	0	0.33	0	0	0	0	0	0.33
4SF	0	0	0.55	0	0	0.18	0	0.09	0
5CV	0	0	0	0	0	0	0.04	0	0
5CB	0	0	0	0	0	0	0	0.25	0.5
5C1	0	0	0	0	0	0	0.09	0	0
5C2	0	0	0	0	0	0.05	0	0	0

RUN DESIGNATION: CARDIUM FORMATION

EXPECTED (RANDOM) TRANSITIONS --

	1SH	1BM	1GB	1UP	2H1	2H2	2H3	3BS	3HA	3SW
1SH	0	0.436	0.569	0.563	0.85	0.725	0.233	0.183	0.499	0.37
1BM	0.474	0	4.76	4.7	7.11	6.06	1.95	1.53	4.17	3.09
1GB	0.578	4.45	0	5.74	8.68	7.4	2.38	1.87	5.09	3.77
1UP	0.619	4.77	6.21	0	9.29	7.92	2.55	2	5.45	4.04
2H1	0.86	6.62	8.63	8.54	0	11	3.54	2.78	7.57	5.61
2H2	0.744	5.73	7.47	7.39	11.2	0	3.06	2.4	6.55	4.86
2H3	0.224	1.72	2.25	2.22	3.36	2.86	0	0.723	1.97	1.46
3BS	0.174	1.34	1.74	1.72	2.61	2.22	0.714	0	1.53	1.13
3HA	0.489	3.77	4.91	4.86	7.34	6.26	2.01	1.58	0	3.19
3SW	0.389	2.99	3.9	3.86	5.83	4.97	1.6	1.25	3.42	0
3PL	0.246	1.9	2.47	2.44	3.69	3.15	1.01	0.795	2.17	1.61
4VL	0.154	1.18	1.54	1.52	2.3	1.97	0.632	0.496	1.35	1
4VC	0.317	2.44	3.18	3.13	4.76	4.06	1.3	1.02	2.79	2.07
4IF	0.028	0.217	0.283	0.28	0.423	0.361	0.116	0.091	0.243	0.184
4SF	0.105	0.806	1.05	1.04	1.57	1.34	0.431	0.338	0.921	0.683
5CV	0.275	2.12	2.76	2.73	4.13	3.52	1.13	0.889	2.42	1.8
5CB	0.038	0.29	0.378	0.374	0.565	0.482	0.155	0.122	0.331	0.246
5C1	0.105	0.809	1.05	1.04	1.58	1.34	0.432	0.339	0.924	0.686
5C2	0.184	1.41	1.84	1.82	2.76	2.35	0.755	0.593	1.62	1.2

	3PL	4VL	4VC	4IF	4SF	5CV	5CB	5C1	5C2
1SH	0.382	0.154	0.336	0.028	0.105	0.294	0.038	0.124	0.193
1BM	2.53	1.29	2.81	0.256	0.876	2.46	0.315	1.03	1.61
1GB	3.08	1.37	3.42	0.288	1.07	3	0.384	1.26	1.97
1UP	3.3	1.68	3.66	0.308	1.14	3.21	0.411	1.35	2.11
2H1	4.59	2.33	5.09	0.428	1.59	4.46	0.571	1.88	2.93
2H2	3.97	2.02	4.41	0.37	1.37	3.86	0.494	1.62	2.53
2H3	1.19	0.606	1.33	0.111	0.414	1.16	0.149	0.489	0.762
3BS	0.926	0.471	1.03	0.086	0.321	0.901	0.115	0.379	0.591
3HA	2.61	1.33	2.9	0.243	0.904	2.54	0.325	1.07	1.67
3SW	2.07	1.05	2.3	0.193	0.718	2.02	0.258	0.849	1.32
3PL	0	0.667	1.46	0.122	0.455	1.28	0.164	0.538	0.838
4VL	0.819	0	0.91	0.076	0.284	0.797	0.102	0.335	0.523
4VC	1.69	0.859	0	0.138	0.586	1.64	0.211	0.692	1.08
4IF	0.15	0.076	0.167	0	0.052	0.146	0.019	0.062	0.096
4SF	0.559	0.284	0.62	0.052	0	0.543	0.07	0.229	0.357
5CV	1.47	0.746	1.63	0.127	0.509	0	0.183	0.601	0.937
5CB	0.201	0.102	0.223	0.019	0.07	0.195	0	0.082	0.128
5C1	0.56	0.285	0.622	0.052	0.194	0.545	0.07	0	0.358
5C2	0.979	0.498	1.09	0.091	0.339	0.953	0.122	0.401	0

RUN DESIGNATION: CARDIUM FORMATION

EXPECTED (RANDOM) TRANSITION PROBABILITY --

	1SH	1BM	1GB	1UP	2M1	2M2	2M3	3BS	3MA	3SW
1SH	0	0.07	0.09	0.09	0.14	0.12	0.04	0.03	0.08	0.06
1BM	0.01	0	0.1	0.1	0.15	0.13	0.04	0.03	0.09	0.07
1GB	0.01	0.08	0	0.1	0.16	0.13	0.04	0.03	0.09	0.07
1UP	0.01	0.08	0.1	0	0.15	0.13	0.04	0.03	0.09	0.07
2M1	0.01	0.08	0.11	0.11	0	0.14	0.04	0.04	0.1	0.07
2M2	0.01	0.08	0.11	0.11	0.16	0	0.04	0.03	0.09	0.07
2M3	0.01	0.07	0.1	0.1	0.15	0.12	0	0.03	0.09	0.06
3BS	0.01	0.07	0.1	0.1	0.15	0.12	0.04	0	0.09	0.06
3MA	0.01	0.08	0.1	0.1	0.15	0.13	0.04	0.03	0	0.07
3SW	0.01	0.08	0.1	0.1	0.15	0.13	0.04	0.03	0.09	0
3PL	0.01	0.08	0.1	0.1	0.15	0.13	0.04	0.03	0.09	0.06
4VL	0.01	0.07	0.1	0.1	0.14	0.12	0.04	0.03	0.08	0.06
4VC	0.01	0.08	0.1	0.1	0.15	0.13	0.04	0.03	0.09	0.06
4IF	0.01	0.07	0.09	0.09	0.14	0.12	0.04	0.03	0.08	0.06
4SF	0.01	0.07	0.1	0.09	0.14	0.12	0.04	0.03	0.08	0.06
5CV	0.01	0.08	0.1	0.1	0.15	0.13	0.04	0.03	0.09	0.06
5CB	0.01	0.07	0.09	0.09	0.14	0.12	0.04	0.03	0.08	0.06
5C1	0.01	0.07	0.1	0.09	0.14	0.12	0.04	0.03	0.08	0.06
5C2	0.01	0.07	0.1	0.1	0.15	0.12	0.04	0.03	0.09	0.06

	3PL	4VL	4VC	4IF	4SF	5CV	5CB	5C1	5C2
1SH	0.03	0.03	0.06	0	0.02	0.03	0.01	0.02	0.03
1BM	0.03	0.03	0.06	0.01	0.02	0.03	0.01	0.02	0.03
1GB	0.06	0.03	0.06	0.01	0.02	0.03	0.01	0.02	0.04
1UP	0.03	0.03	0.06	0.01	0.02	0.03	0.01	0.02	0.04
2M1	0.06	0.03	0.06	0.01	0.02	0.06	0.01	0.02	0.04
2M2	0.06	0.03	0.06	0.01	0.02	0.06	0.01	0.02	0.04
2M3	0.03	0.03	0.06	0	0.02	0.03	0.01	0.02	0.03
3BS	0.03	0.03	0.06	0	0.02	0.03	0.01	0.02	0.03
3MA	0.03	0.03	0.06	0.01	0.02	0.03	0.01	0.02	0.03
3SW	0.03	0.03	0.06	0	0.02	0.03	0.01	0.02	0.03
3PL	0	0.03	0.06	0	0.02	0.03	0.01	0.02	0.03
4VL	0.03	0	0.06	0	0.02	0.03	0.01	0.02	0.03
4VC	0.03	0.03	0	0	0.02	0.03	0.01	0.02	0.03
4IF	0.03	0.03	0.06	0	0.02	0.03	0.01	0.02	0.03
4SF	0.03	0.03	0.06	0	0	0.03	0.01	0.02	0.03
5CV	0.03	0.03	0.06	0	0.02	0	0.01	0.02	0.03
5CB	0.03	0.03	0.06	0	0.02	0.03	0	0.02	0.03
5C1	0.03	0.03	0.06	0	0.02	0.03	0.01	0	0.03
5C2	0.03	0.03	0.06	0	0.02	0.03	0.01	0.02	0

RUN DESIGNATION: CARDIUM FORMATION

OBSERVED MINUS RANDOM PROBABILITY --

	1SH	1BM	1GB	1UP	2H1	2H2	2H3	3BS	3HA	3SW
1SH	0	-0.07	0.24	0.41	-0.14	-0.12	-0.04	0.14	-0.08	-0.06
1BM	-0.01	0	0.09	0.16	0.08	-0.11	-0.04	0.2	-0.09	-0.07
1GB	-0.01	0.13	0	0.24	0.07	-0.06	-0.04	-0.03	-0.05	-0.05
1UP	0.01	0.04	-0.02	0	0.25	-0.06	0.01	-0.01	0.01	0
2H1	-0.01	-0.05	-0.05	-0.05	0	0.43	-0.03	-0.01	0.03	-0.04
2H2	0	-0.05	-0.07	-0.04	0	0	0.23	-0.02	0.17	-0.01
2H3	-0.01	-0.07	-0.1	-0.01	0.07	-0.03	0	-0.03	0.21	0.11
3BS	-0.01	0.26	0.01	-0.1	-0.09	0.05	-0.04	0	-0.03	0
3HA	-0.01	-0.08	-0.1	-0.1	-0.07	-0.07	-0.02	-0.01	0	0.22
3SW	-0.01	-0.05	-0.1	-0.07	-0.15	-0.05	-0.04	0.02	-0.06	0
3PL	-0.01	-0.08	-0.1	-0.1	-0.15	-0.13	-0.04	-0.03	-0.05	-0.02
4VL	-0.01	-0.01	-0.04	-0.1	-0.14	-0.12	-0.04	-0.03	-0.08	0.07
4VC	0.08	0.05	-0.07	-0.1	-0.12	-0.13	-0.04	-0.03	-0.03	-0.06
4IF	0.32	-0.07	-0.09	-0.09	-0.14	-0.12	-0.04	-0.03	-0.08	-0.06
4SF	-0.01	-0.07	-0.01	-0.09	-0.14	-0.03	-0.04	-0.03	-0.08	-0.06
5CV	-0.01	0.1	0.01	-0.03	-0.04	-0.13	-0.04	-0.03	-0.09	-0.06
5CB	-0.01	-0.07	-0.09	-0.09	0.11	-0.12	-0.04	-0.03	-0.08	-0.06
5C1	-0.01	-0.07	0.17	0.09	0.04	-0.03	-0.04	-0.03	0.01	0.03
5C2	-0.01	0.09	0.22	0.06	-0.04	-0.07	-0.04	-0.03	-0.09	0.1

	3PL	4VL	4VC	4IF	4SF	5CV	5CB	5C1	5C2
1SH	-0.05	-0.03	-0.06	0	-0.02	-0.05	-0.01	-0.02	-0.03
1BM	-0.05	-0.03	-0.06	-0.01	-0.02	-0.01	-0.01	0	-0.03
1GB	-0.04	-0.03	-0.06	-0.01	0	-0.03	-0.01	0	-0.02
1UP	-0.05	-0.03	-0.06	-0.01	0	-0.03	0.01	0	-0.02
2H1	-0.06	-0.03	-0.06	-0.01	-0.02	0	0	-0.02	-0.03
2H2	-0.06	-0.03	-0.06	-0.01	-0.02	-0.03	-0.01	-0.01	0
2H3	-0.01	-0.03	-0.06	0	-0.02	0.04	-0.01	-0.02	-0.03
3BS	-0.05	-0.03	0	0	-0.02	0.01	-0.01	0.04	0.03
3HA	0.16	-0.03	-0.06	-0.01	0	0.14	-0.01	0.02	0.03
3SW	0.39	-0.03	-0.06	0.03	-0.02	0.05	-0.01	0.06	0.1
3PL	0	0.13	0.62	0	0.02	-0.05	-0.01	-0.02	0.01
4VL	0.08	0	0.5	0.06	-0.02	-0.05	-0.01	-0.02	-0.03
4VC	-0.05	0.35	0	0.03	0.2	-0.05	-0.01	-0.02	0
4IF	-0.05	-0.03	0.27	0	-0.02	-0.05	-0.01	-0.02	0.3
4SF	-0.05	-0.03	0.49	0	0	0.13	-0.01	0.07	-0.03
5CV	-0.05	-0.03	-0.06	0	-0.02	0	0.03	-0.02	-0.03
5CB	-0.05	-0.03	-0.06	0	-0.02	-0.05	0	0.23	0.47
5C1	-0.05	-0.03	-0.06	0	-0.02	-0.05	0.08	0	-0.03
5C2	-0.05	-0.03	-0.06	0	-0.02	0	-0.01	-0.02	0

RUN DESIGNATION: CARDIUM FORMATION

SIGNIFICANCE TEST VALUES --

	1SH	1BM	1GB	1UP	2H1	2H2	2H3	3BS	3HA	3SW
1SH	0	0	0.1	0.01	0	0	0	0.17	0	0
1BM	0	0	0.04	0	0.09	0	0	0	0	0
1GB	0	0	0	0	0.1	0	0	0	0	0
1UP	0.45	0.2	0	0	0	0	0.43	0	0.46	0
2H1	0	0	0	0	0	0	0	0	0.26	0
2H2	0	0	0	0	0	0	0	0	0	0
2H3	0	0	0	0	0.26	0	0	0	0	0.05
3BS	0	0	0.33	0	0	0.37	0	0	0	0
3HA	0	0	0	0	0	0	0	0	0	0
3SW	0	0	0	0	0	0	0	0.33	0	0
3PL	0	0	0	0	0	0	0	0	0	0
4VL	0	0	0	0	0	0	0	0	0	0.25
4VC	0	0.25	0	0	0	0	0	0	0	0
4IF	0.05	0	0	0	0	0	0	0	0	0
4SF	0	0	0	0	0	0	0	0	0	0
5CV	0	0.07	0	0	0	0	0	0	0	0
5CB	0	0	0	0	0.45	0	0	0	0	0
5C1	0	0	0.09	0.26	0.47	0	0	0	0.6	0.49
5C2	0	0.14	0.01	0.3	0	0	0	0	0	0.1

	3PL	4VL	4VC	4IF	4SF	5CV	5CB	5C1	5C2
1SH	0	0	0	0	0	0	0	0	0
1BM	0	0	0	0	0	0	0	0	0
1GB	0	0	0	0	0	0	0	0	0
1UP	0	0	0	0	0	0	0.45	0	0
2H1	0	0	0	0	0	0	0	0	0
2H2	0	0	0	0	0	0	0	0	0
2H3	0	0	0	0	0	0.32	0	0	0
3BS	0	0	0	0	0	0.6	0	0.31	0.42
3HA	0	0	0	0	0	0	0	0.25	0.17
3SW	0	0	0	0	0	0.13	0	0.01	0.01
3PL	0	0.01	0	0	0.4	0	0	0	0.33
4VL	0.19	0	0	0	0	0	0	0	0
4VC	0	0	0	0	0	0	0	0	0
4IF	0	0	0.17	0	0	0	0	0	0.09
4SF	0	0	0	0	0	0.1	0	0.2	0
5CV	0	0	0	0	0	0	0.25	0	0
5CB	0	0	0	0	0	0	0	0.08	0.01
5C1	0	0	0	0	0	0	0.11	0	0
5C2	0	0	0	0	0	0	0	0	0

RUN DESIGNATION: CARDIUM FORMATION

TOTAL NUMBER OF FACIES TRANSITIONS OBSERVED: 595

VALUES OF PARAMETER P --

	1SH	1BM	1OB	1UP	2H1	2H2	2H3	3BS	3HA	3SW
1SH	88	88	0	0	38	88	88	-0.01	88	88
1BM	83	33	0.01	0.01	0.01	-0.01	83	0.01	88	88
1OB	88	0.01	88	0.03	0.01	0	88	88	0	-0.01
1UP	-0.01	0	0	88	0.03	0	0	-0.01	0	0
2H1	88	0	0	0	83	0.07	-0.01	0	0.01	0
2H2	-0.01	0	0	0	0.01	88	0.03	-0.01	0.02	0
2H3	88	88	88	0	0	0	88	38	0	0
3BS	83	0	0	88	-0.01	0	83	88	-0.01	-0.01
3HA	88	38	88	88	0	0	-0.01	-0.01	88	0.02
3SW	38	-0.01	88	-0.01	38	0	88	0	-0.01	88
3PL	83	88	88	88	88	88	88	38	-0.01	-0.01
4VL	38	-0.01	-0.01	38	38	38	83	83	88	0
4VC	0	0	-0.01	88	-0.01	83	33	88	0	88
4IF	-0.01	88	88	88	28	88	88	33	88	88
4SF	38	88	-0.01	88	88	-0.01	83	88	38	83
5CV	83	0	0.02	0	0	88	83	83	88	88
5C3	88	88	88	88	-0.01	88	88	88	88	88
5C1	88	83	0	0	0	-0.01	38	88	-0.01	-0.01
5C2	88	0	0	0	0	-0.01	88	88	88	0

	3PL	4VL	4VC	4IF	4SF	5CV	5C3	5C1	5C2
1SH	88	38	88	88	88	83	88	88	88
1BM	83	83	38	88	88	0	88	-0.01	88
1OB	-0.01	83	83	88	-0.01	-0.01	83	-0.01	-0.01
1UP	38	88	88	88	-0.01	-0.01	-0.01	-0.01	-0.01
2H1	83	83	83	33	83	0	-0.01	88	-0.01
2H2	38	83	98	88	98	0	88	-0.01	0
2H3	-0.01	88	98	38	98	0	38	88	88
3BS	83	38	-0.01	88	83	-0.01	88	-0.01	-0.01
3HA	0.01	88	88	88	-0.01	0.01	88	0	0
3SW	0.02	38	38	-0.01	38	0	83	0	0
3PL	88	0	0.02	28	-0.01	98	88	88	-0.01
4VL	0	83	0.01	-0.01	38	93	32	83	83
4VC	88	0.01	93	-0.01	0	33	88	88	-0.01
4IF	88	38	-0.01	38	33	38	33	88	-0.01
4SF	33	33	0	33	33	0	88	-0.01	83
5CV	38	88	83	38	38	33	-0.01	28	32
5C3	88	38	88	33	38	88	88	-0.01	0
5C1	93	83	38	83	88	38	-0.01	83	86
5C2	88	88	38	38	98	-0.01	88	88	88

RUN DESIGNATION: FULLY REGRESSIVE CYCLES ONLY

FACIES DATA --

FACIES	# OCCUR	MEAN THICKNESS (RANGE) IN METERS
1SH	4	5.5 (2.4 to 10)
1SM	10	6.1 (1.5 to 12.2)
1SS	15	5.2 (1 to 11.4)
1UP	25	4.4 (0.4 to 29.2)
2M1	13	3.1 (0.7 to 3.5)
2M2	19	2.7 (0.4 to 9.6)
2MC	7	6.5 (1.9 to 12.1)
2SS	4	1.8 (1 to 2.7)
3HA	24	4.4 (0.5 to 12.2)
3SW	24	4.1 (1.2 to 10.3)
3PL	22	1.9 (0.6 to 6.3)
4VL	16	1.5 (0.4 to 3.1)
4VC	48	3.4 (0.2 to 17.9)
4IF	3	7.2 (6.2 to 7.7)
4SF	14	4.9 (0.3 to 17.4)
5CV	2	0 (0 to 0)
5CD	3	0 (0 to 0)
5C1	2	0.2 (0.1 to 0.3)
5CC	7	2.2 (1.2 to 3.2)

TOTAL NUMBER OF FACIES OCCURRENCES: 231

RUN DESIGNATION: FULLY REGRESSIVE CYCLES ONLY

THICKNESS-OF-UNDERLYING MATRIX --

	1SM	1PM	1SS	1UP	2M1	2M2	2MC	3SS	3MA	3SW
1SM	0	0	4.3	6.2	0	0	0	0	0	0
1PM	0	0	12.4	3.6	8.1	0	0	6	0	0
1SS	0	0	0	5.6	0.5	6.7	0	0	2.5	0
1UP	0	0.4	0	0	3.5	2	7.6	0	9.8	1
2M1	0	0	3.6	0	0	2.4	8.5	0	3.2	0
2M2	0	0	1.6	0	0	0	4.8	3.2	2.1	0.6
2MC	0	0	0	0	0	0	0	0	0	6.4
3SS	0	0	0	0	0	2	0	0	0	2
3MA	0	0	0	0	0	3.5	0	6.5	0	3.6
3SW	0	0	0	3.2	0	3.1	0	1.9	9.5	0
3PL	0	0	0	0	0	0	0	0	1.9	1.2
4VL	0	0	0	0	0	0	0	0	0	1.7
4VC	5.9	2.7	4.3	0	0	0	0	0	0	0
4IF	7.8	0	0	0	0	0	0	0	0	0
4SF	0	0	3.2	0	0	0	0	0	0	0
5CV	0	0	0	0	0	0	0	0	0	0
5C3	0	0	0	0	0	0	0	0	0	0
5C1	0	0	0	0	0.2	0	0	0	0	0
5C2	0	0	0	0	0	0	0	0	0	2.9

	3PL	4VL	4VC	4IF	4SF	5CV	5C3	5C1	5C2
1SM	0	0	0	0	0	0	0	0	0
1PM	0	0	0	0	0	0	0	12.2	0
1SS	4.6	0	0	0	1.6	0	0	0	0
1UP	0	0	0	0	2	0	0	0	0
2M1	0	0	0	0	0	0	0	0	0
2M2	0	0	0	0	0	0	0	0	0
2MC	3.8	0	0	0	0	0	0	0	0
3SS	0	0	1.2	0	0	0	0	0	0
3MA	4.3	0	0	0	12.2	0	0	0	0
3SW	3.7	0	0	2.8	0	0	0	0	5.4
3PL	0	1.2	2.1	0	0	0	0	0	1.8
4VL	1.3	0	1.1	1.1	0	0	0	0	0
4VC	0	2.3	0	1.7	2.5	0	0	2	6.4
4IF	0	0	6.7	2	0	0	0	0	2.7
4SF	0	0	1.2	0	0	0	0	1.5	0
5CV	0	0	0	0	0	0	0	0	0
5C3	0	0	0	0	0	0	0	0	0
5C1	0	0	0	0	0	0	0	0	0
5C2	0	0	0	0	0	0	0	0	0

RUN DESIGNATION: FULLY REGRESSIVE CYCLES ONLY

THICKNESS-OF-OVERLYING MATRIX --

	1SH	1SM	1SS	1UP	2M1	2M2	2M3	3SS	3MA	3SW
1SH	0	0	7.9	4.9	0	0	0	0	0	0
1SM	0	0	7.4	[illegible]	[illegible]	0	0	[illegible]	0	0
1SS	0	[illegible]	0	[illegible]	[illegible]	1.3	0	0	0	0
1UP	0	[illegible]	0	0	[illegible]	2.9	[illegible]	0	[illegible]	2.6
2M1	0	0	0	0	[illegible]	2.6	[illegible]	0	[illegible]	0
2M2	0	0	[illegible]	0	0	0	[illegible]	[illegible]	[illegible]	[illegible]
2M3	0	0	0	0	0	0	0	0	[illegible]	0
3SS	0	0	0	0	0	[illegible]	0	0	0	[illegible]
3MA	0	0	0	0	0	[illegible]	0	[illegible]	0	[illegible]
3SW	0	0	0	[illegible]	0	[illegible]	0	2	[illegible]	0
3PL	0	0	0	0	0	0	0	0	[illegible]	[illegible]
4VL	0	0	0	0	0	0	0	0	0	0
4VC	6.8	[illegible]	[illegible]	0	0	0	0	0	0	0
4IF	[illegible]	0	0	0	0	0	0	0	0	0
4SF	0	0	0	0	0	0	0	0	0	0
5CV	0	0	0	0	0	0	0	0	0	0
5C3	0	0	0	0	0	0	0	0	0	0
5C1	0	0	0	0	4.3	0	0	0	0	0
5C2	0	0	0	0	0	0	0	0	0	4.1

	3PL	4VL	4VC	4IF	4SF	5CV	5C3	5C1	5C2
1SH	0	0	0	0	0	0	0	0	0
1SM	0	0	0	0	0	0	0	[illegible]	0
1SS	[illegible]	0	0	0	[illegible]	0	0	0	0
1UP	0	0	[illegible]	0	[illegible]	0	0	0	0
2M1	0	0	0	0	0	0	0	0	0
2M2	0	0	0	0	0	0	0	0	0
2M3	[illegible]	0	0	0	0	0	0	0	0
3SS	0	0	[illegible]	0	0	0	0	0	0
3MA	[illegible]	0	[illegible]	0	[illegible]	0	0	0	0
3SW	[illegible]	0	[illegible]	0	[illegible]	0	0	0	[illegible]
3PL	0	[illegible]	[illegible]	0	[illegible]	0	0	0	[illegible]
4VL	[illegible]	[illegible]	[illegible]	0	[illegible]	0	0	0	[illegible]
4VC	0	[illegible]	0	[illegible]	[illegible]	0	0	0	[illegible]
4IF	0	0	[illegible]	[illegible]	0	0	0	0	[illegible]
4SF	0	0	[illegible]	[illegible]	[illegible]	0	0	[illegible]	0
5CV	0	[illegible]	0	0	0	[illegible]	0	0	0
5C3	0	0	0	0	0	0	[illegible]	0	0
5C1	0	0	0	0	0	0	0	[illegible]	0
5C2	0	0	0	0	0	0	0	0	[illegible]

RUN DESIGNATION: FULLY REGRESSIVE CYCLES ONLY

TOTAL NUMBER OF FACIES TRANSITIONS OBSERVED: 215

OBSERVED TRANSITIONS --

	1SH	1BM	1GB	1UP	2M1	2M2	2MC	3BS	3MA	3SW
1SH	0	0	2	2	0	0	0	0	0	0
1BM	0	0	1	5	1	0	0	1	0	0
1GB	0	2	0	6	1	1	0	0	1	0
1UP	0	1	0	0	6	3	2	0	4	2
2M1	0	0	1	0	0	7	1	0	3	0
2M2	0	0	1	0	0	0	4	1	11	1
2MC	0	0	0	0	0	0	0	0	2	4
3BS	0	0	0	0	0	2	0	0	0	1
3MA	0	0	0	0	0	1	0	1	0	10
3SW	0	0	0	1	0	1	0	1	1	0
3PL	0	0	0	0	0	0	0	0	1	1
4VL	0	0	0	0	0	0	0	0	0	2
4VC	2	2	1	0	0	0	0	0	0	0
4IF	1	0	0	0	0	0	0	0	0	0
4SF	0	0	1	0	0	0	0	0	0	0
5CV	0	0	0	0	0	0	0	0	0	0
5CB	0	0	0	0	0	0	0	0	0	0
5C1	0	0	0	0	2	0	0	0	0	0
5C2	0	0	0	0	0	0	0	0	0	2

	3PL	4VL	4VC	4IF	4SF	5CV	5CB	5C1	5C2
1SH	0	0	0	0	0	0	0	0	0
1BM	0	0	0	0	0	0	0	1	0
1GB	1	0	0	0	1	0	0	0	0
1UP	0	0	0	0	1	0	0	0	0
2M1	0	0	0	0	0	0	0	0	0
2M2	0	0	0	0	0	0	0	0	0
2MC	1	0	0	0	0	0	0	0	0
3BS	0	0	1	0	0	0	0	0	0
3MA	10	0	0	0	1	0	0	0	0
3SW	17	0	0	1	0	0	0	0	2
3PL	0	4	17	0	1	0	0	0	1
4VL	2	0	0	1	0	0	0	0	0
4VC	0	12	0	1	1	0	0	0	1
4IF	0	0	1	0	0	0	0	1	0
4SF	0	0	0	0	0	2	0	1	0
5CV	0	0	0	0	0	0	0	0	0
5CB	0	0	0	0	0	0	0	0	0
5C1	0	0	0	0	0	0	0	0	0
5C2	0	0	0	0	0	0	0	0	0

RUN DESIGNATION: FULLY REGRESSIVE CYCLES ONLY

OBSERVED TRANSITION PROBABILITY --

	1SH	1BM	1GB	1UP	2H1	2H2	2H3	3BS	3HA	3SW
1SH	0	0	0.5	0.5	0	0	0	0	0	0
1BM	0	0	0.11	0.54	0.11	0	0	0.11	0	0
1GB	0	0.15	0	0.46	0.08	0.08	0	0	0.08	0
1UP	0	0.05	0	0	0.32	0.16	0.11	0	0.21	0.11
2H1	0	0	0.08	0	0	0.58	0.08	0	0.25	0
2H2	0	0	0.06	0	0	0	0.22	0.06	0.61	0.06
2H3	0	0	0	0	0	0	0	0	0.29	0.57
3BS	0	0	0	0	0	0.5	0	0	0	0.25
3HA	0	0	0	0	0	0.04	0	0.04	0	0.43
3SW	0	0	0	0.04	0	0.04	0	0.04	0.04	0
3PL	0	0	0	0	0	0	0	0	0.04	0.04
4VL	0	0	0	0	0	0	0	0	0	0.14
4VC	0.08	0.08	0.04	0	0	0	0	0	0	0
4IF	0.33	0	0	0	0	0	0	0	0	0
4SF	0	0	0.1	0	0	0	0	0	0	0
5CV	0	0	0	0	0	0	0	0	0	0
5C3	0	0	0	0	0	0	0	0	0	0
5C1	0	0	0	0	1	0	0	0	0	0
5C2	0	0	0	0	0	0	0	0	0	1

	3PL	4VL	4VC	4IF	4SF	5CV	5C3	5C1	5C2
1SH	0	0	0	0	0	0	0	0	0
1BM	0	0	0	0	0	0	0	0.11	0
1GB	0.08	0	0	0	0.08	0	0	0	0
1UP	0	0	0	0	0.05	0	0	0	0
2H1	0	0	0	0	0	0	0	0	0
2H2	0	0	0	0	0	0	0	0	0
2H3	0.14	0	0	0	0	0	0	0	0
3BS	0	0	0.25	0	0	0	0	0	0
3HA	0.43	0	0	0	0.04	0	0	0	0
3SW	0.71	0	0	0.04	0	0	0	0	0.08
3PL	0	0.16	0.68	0	0.04	0	0	0	0.04
4VL	0.14	0	0.64	0.07	0	0	0	0	0
4VC	0	0.46	0	0.04	0.27	0	0	0	0.04
4IF	0	0	0.33	0	0	0	0	0	0.33
4SF	0	0	0.6	0	0	0.2	0	0.1	0
5CV	0	0	0	0	0	0	0	0	0
5C3	0	0	0	0	0	0	0	0	0
5C1	0	0	0	0	0	0	0	0	0
5C2	0	0	0	0	0	0	0	0	0

RUN DESIGNATION: FULLY REGRESSIVE CYCLES ONLY.

EXPECTED (RANDOM) TRANSITIONS --

	1SH	1BM	1GB	1UP	2H1	2H2	2H3	3BS	3HA	3SW
1SH	0	0.039	0.127	0.263	0.181	0.28	0.124	0.07	0.443	0.445
1BM	0.119	0	0.289	0.597	0.411	0.636	0.281	0.159	1.01	1.01
1GB	0.173	0.256	0	0.87	0.6	0.928	0.41	0.231	1.47	1.48
1UP	0.253	0.447	0.638	0	0.903	1.41	0.621	0.35	2.22	2.23
2H1	0.162	0.277	0.395	0.814	0	0.869	0.384	0.216	1.37	1.38
2H2	0.25	0.426	0.607	1.25	0.864	0	0.591	0.333	2.11	2.13
2H3	0.093	0.159	0.227	0.468	0.323	0.499	0	0.124	0.789	0.794
3BS	0.053	0.09	0.128	0.264	0.182	0.281	0.124	0	0.445	0.447
3HA	0.034	0.569	0.811	1.67	1.15	1.79	0.789	0.445	0	2.84
3SW	0.348	0.594	0.847	1.75	1.21	1.86	0.824	0.465	2.95	0
3PL	0.38	0.648	0.924	1.91	1.31	2.03	0.899	0.507	3.21	3.23
4VL	0.195	0.332	0.474	0.979	0.675	1.04	0.461	0.26	1.65	1.66
4VC	0.403	0.686	0.979	2.02	1.39	2.16	0.953	0.537	3.41	3.43
4IF	0.039	0.067	0.095	0.197	0.136	0.21	0.093	0.052	0.332	0.334
4SF	0.136	0.232	0.33	0.682	0.47	0.727	0.321	0.181	1.15	1.16
5CV	0	0	0	0	0	0	0	0	0	0
5CB	0	0	0	0	0	0	0	0	0	0
5C1	0.026	0.044	0.063	0.131	0.09	0.139	0.062	0.035	0.22	0.222
5C2	0.026	0.045	0.064	0.133	0.091	0.141	0.062	0.035	0.223	0.225

	3PL	4VL	4VC	4IF	4SF	5CV	5CB	5C1	5C2
1SH	0.607	0.293	0.672	0.052	0.197	0.034	0	0.035	0.087
1BM	1.39	0.666	1.53	0.118	0.448	0.078	0	0.079	0.196
1GB	2.01	0.971	2.23	0.173	0.654	0.114	0	0.115	0.287
1UP	3.05	1.47	3.37	0.261	0.99	0.172	0	0.173	0.434
2H1	1.65	0.909	2.08	0.162	0.612	0.106	0	0.107	0.268
2H2	2.9	1.4	3.21	0.249	0.942	0.164	0	0.165	0.413
2H3	1.08	0.522	1.2	0.093	0.352	0.061	0	0.062	0.154
3BS	0.61	0.294	0.675	0.052	0.198	0.034	0	0.035	0.087
3HA	3.87	1.87	4.28	0.332	1.26	0.219	0	0.22	0.551
3SW	4.04	1.95	4.47	0.347	1.31	0.228	0	0.23	0.576
3PL	0	2.13	4.88	0.378	1.43	0.249	0	0.251	0.628
4VL	2.26	0	2.5	0.194	0.735	0.128	0	0.129	0.322
4VC	4.67	2.25	0	0.401	1.52	0.264	0	0.266	0.665
4IF	0.455	0.22	0.504	0	0.148	0.026	0	0.026	0.065
4SF	1.58	0.761	1.74	0.135	0	0.089	0	0.09	0.224
5CV	0	0	0	0	0	0	0	0	0
5CB	0	0	0	0	0	0	0	0	0
5C1	0.302	0.146	0.334	0.026	0.098	0.017	0	0	0.043
5C2	0.306	0.148	0.339	0.026	0.1	0.017	0	0.017	0

RUN DESIGNATION: FULLY REGRESSIVE CYCLES ONLY

EXPECTED (RANDOM) TRANSITION PROBABILITY --

	1SH	1BM	1GB	1UP	2M1	2M2	2M3	3BS	3HA	3SW
1SH	0	0.02	0.03	0.07	0.05	0.07	0.03	0.02	0.11	0.11
1BM	0.01	0	0.03	0.07	0.05	0.07	0.03	0.02	0.11	0.11
1GB	0.01	0.02	0	0.07	0.05	0.07	0.03	0.02	0.11	0.11
1UP	0.01	0.02	0.03	0	0.05	0.07	0.03	0.02	0.12	0.12
2M1	0.01	0.02	0.03	0.07	0	0.07	0.03	0.02	0.11	0.12
2M2	0.01	0.02	0.03	0.07	0.05	0	0.03	0.02	0.12	0.12
2M3	0.01	0.02	0.03	0.07	0.05	0.07	0	0.02	0.11	0.11
3BS	0.01	0.02	0.03	0.07	0.05	0.07	0.03	0	0.11	0.11
3HA	0.01	0.02	0.04	0.07	0.05	0.08	0.03	0.02	0	0.12
3SW	0.01	0.02	0.04	0.07	0.05	0.08	0.03	0.02	0.12	0
3PL	0.02	0.03	0.04	0.08	0.05	0.08	0.04	0.02	0.13	0.13
4VL	0.01	0.02	0.03	0.07	0.05	0.07	0.03	0.02	0.12	0.12
4VC	0.02	0.03	0.04	0.08	0.05	0.08	0.04	0.02	0.13	0.13
4IF	0.01	0.02	0.03	0.07	0.05	0.07	0.03	0.02	0.11	0.11
4SF	0.01	0.02	0.03	0.07	0.05	0.07	0.03	0.02	0.11	0.12
5CV	0	0	0	0	0	0	0	0	0	0
5CB	0	0	0	0	0	0	0	0	0	0
5C1	0.01	0.02	0.03	0.07	0.05	0.07	0.03	0.02	0.11	0.11
5C2	0.01	0.02	0.03	0.07	0.05	0.07	0.03	0.02	0.11	0.11

	3PL	4VL	4VC	4IF	4SF	5CV	5CB	5C1	5C2
1SH	0.15	0.07	0.17	0.01	0.05	0.01	0	0.01	0.02
1BM	0.15	0.07	0.17	0.01	0.05	0.01	0	0.01	0.02
1GB	0.15	0.07	0.17	0.01	0.05	0.01	0	0.01	0.02
1UP	0.16	0.08	0.18	0.01	0.05	0.01	0	0.01	0.02
2M1	0.16	0.08	0.17	0.01	0.05	0.01	0	0.01	0.02
2M2	0.16	0.08	0.18	0.01	0.05	0.01	0	0.01	0.02
2M3	0.15	0.07	0.17	0.01	0.05	0.01	0	0.01	0.02
3BS	0.15	0.07	0.17	0.01	0.05	0.01	0	0.01	0.02
3HA	0.17	0.08	0.19	0.01	0.05	0.01	0	0.01	0.02
3SW	0.17	0.08	0.19	0.01	0.05	0.01	0	0.01	0.02
3PL	0	0.09	0.2	0.02	0.06	0.01	0	0.01	0.03
4VL	0.16	0	0.18	0.01	0.05	0.01	0	0.01	0.02
4VC	0.18	0.09	0	0.02	0.06	0.01	0	0.01	0.03
4IF	0.15	0.07	0.17	0	0.05	0.01	0	0.01	0.02
4SF	0.16	0.08	0.17	0.01	0	0.01	0	0.01	0.02
5CV	0	0	0	0	0	0	0	0	0
5CB	0	0	0	0	0	0	0	0	0
5C1	0.15	0.07	0.17	0.01	0.05	0.01	0	0	0.02
5C2	0.15	0.07	0.17	0.01	0.05	0.01	0	0.01	0

RUN DESIGNATION: FULLY REGRESSIVE CYCLES ONLY

OBSERVED MINUS RANDOM PROBABILITY --

	1SH	1BM	1GB	1UP	2H1	2H2	2H3	3BS	3HA	3SW
1SH	0	-0.02	0.47	0.43	-0.05	-0.07	-0.03	-0.02	-0.11	-0.11
1BM	-0.01	0	0.08	0.49	0.06	-0.07	-0.03	0.89	-0.11	-0.11
1GB	-0.01	0.13	0	0.39	0.03	0.01	-0.03	-0.02	-0.03	-0.11
1UP	-0.01	0.03	-0.03	0	0.27	0.09	0.08	-0.02	0.09	-0.01
2H1	-0.01	-0.02	0.05	-0.07	0	0.31	0.05	-0.02	0.14	-0.12
2H2	-0.01	-0.02	0.03	-0.07	-0.05	0	0.19	0.04	0.49	-0.06
2H3	-0.01	-0.02	-0.03	-0.07	-0.05	-0.07	0	-0.02	0.18	0.46
3BS	-0.01	-0.02	-0.03	-0.07	-0.05	0.43	-0.03	0	-0.11	0.14
3HA	-0.01	-0.02	-0.04	-0.07	-0.05	-0.04	-0.03	0.02	0	0.31
3SW	-0.01	-0.02	-0.04	-0.03	-0.05	-0.04	-0.03	0.02	-0.08	0
3PL	-0.02	-0.03	-0.04	-0.06	-0.05	-0.06	-0.04	-0.02	-0.09	-0.09
4VL	-0.01	-0.02	-0.03	-0.07	-0.05	-0.07	-0.03	-0.02	-0.12	0.02
4VC	0.06	0.05	0	-0.08	-0.05	-0.08	-0.04	-0.02	-0.13	-0.13
4IF	0.32	-0.02	-0.03	-0.07	-0.05	-0.07	-0.03	-0.02	-0.11	-0.11
4SF	-0.01	-0.02	0.07	-0.07	-0.05	-0.07	-0.03	-0.02	-0.11	-0.12
5CV	0	0	0	0	0	0	0	0	0	0
5CB	0	0	0	0	0	0	0	0	0	0
5C1	-0.01	-0.02	-0.03	-0.07	0.93	-0.07	-0.03	-0.02	-0.11	-0.11
5C2	-0.01	-0.02	-0.03	-0.07	-0.05	-0.07	-0.03	-0.02	-0.11	0.89

	3PL	4VL	4VC	4IF	4SF	5CV	5CB	5C1	5C2
1SH	-0.15	-0.07	-0.17	-0.01	-0.05	-0.01	0	-0.01	-0.02
1BM	-0.15	-0.07	-0.17	-0.01	-0.05	-0.01	0	0.1	-0.02
1GB	-0.07	-0.07	-0.17	-0.01	0.03	-0.01	0	-0.01	-0.02
1UP	-0.16	-0.08	-0.18	-0.01	0	-0.01	0	-0.01	-0.02
2H1	-0.16	-0.08	-0.17	-0.01	-0.05	-0.01	0	-0.01	-0.02
2H2	-0.16	-0.08	-0.18	-0.01	-0.05	-0.01	0	-0.01	-0.02
2H3	-0.01	-0.07	-0.17	-0.01	-0.05	-0.01	0	-0.01	-0.02
3BS	-0.15	-0.07	0.09	-0.01	-0.05	-0.01	0	-0.01	-0.02
3HA	0.26	-0.08	-0.19	-0.01	-0.01	-0.01	0	-0.01	-0.02
3SW	0.54	-0.08	-0.19	0.03	-0.05	-0.01	0	-0.01	0.06
3PL	0	0.07	0.48	-0.02	-0.02	-0.01	0	-0.01	0.01
4VL	-0.02	0	0.46	0.06	-0.05	-0.01	0	-0.01	-0.02
4VC	-0.18	0.37	0	0.02	0.21	-0.01	0	-0.01	0.01
4IF	-0.15	-0.07	0.16	0	-0.05	-0.01	0	-0.01	0.21
4SF	-0.16	-0.08	0.43	-0.01	0	0.19	0	0.09	-0.02
5CV	0	0	0	0	0	0	0	0	0
5CB	0	0	0	0	0	0	0	0	0
5C1	-0.15	-0.07	-0.17	-0.01	-0.05	-0.01	0	0	-0.02
5C2	-0.15	-0.07	-0.17	-0.01	-0.05	-0.01	0	-0.01	0

RUN DESIGNATION: FULLY REGRESSIVE CYCLES ONLY

SIGNIFICANCE TEST VALUES --

	1SH	1BM	1GB	1UP	2H1	2H2	2H3	3BS	3HA	3SW
1SH	88	88	0.01	0.03	88	88	88	88	88	88
1BM	88	83	0.24	0	0.37	88	88	0.17	88	88
1GB	88	0.03	88	0	0.49	0.61	88	88	88	88
1UP	88	0.32	88	88	0	0.14	0.11	88	0.19	88
2H1	88	88	0.31	88	88	0	0.31	88	0.14	88
2H2	88	88	0.42	88	88	88	0	0.3	0	88
2H3	88	88	88	88	88	38	88	88	0.18	0
3BS	88	88	88	88	88	0.03	88	88	88	0.37
3HA	88	88	88	88	88	88	88	0.37	88	0
3SW	88	83	38	83	88	88	88	0.38	88	88
3PL	88	88	88	88	88	88	88	88	88	88
4VL	83	83	88	88	88	88	88	88	88	0.31
4VC	0.09	0.18	88	88	88	88	88	88	88	88
4IF	0.03	38	88	88	38	88	88	88	88	88
4SF	88	88	0.26	88	88	88	88	88	88	88
5CV	88	88	38	88	88	88	88	88	88	88
5CB	88	88	88	88	88	88	88	88	88	88
5C1	88	88	38	88	0	88	88	88	88	88
5C2	88	88	88	88	88	38	88	88	88	0.01

	3PL	4VL	4VC	4IF	4SF	5CV	5CB	5C1	5C2
1SH	88	88	88	88	88	88	88	88	88
1BM	88	88	88	88	88	88	88	0.09	88
1GB	88	88	88	88	0.49	88	88	88	88
1UP	88	88	88	88	88	88	88	88	88
2H1	88	88	88	88	88	88	88	88	88
2H2	88	88	88	88	88	88	88	88	88
2H3	88	88	88	88	88	83	88	88	88
3BS	88	88	0.53	88	88	88	88	88	88
3HA	0	88	88	88	88	88	88	88	88
3SW	0	83	88	0.21	88	88	88	83	0.08
3PL	88	0.18	0	88	88	88	88	88	0.53
4VL	88	88	0	0.13	88	88	88	88	38
4VC	88	0	88	0.41	0	38	88	88	0.55
4IF	88	88	0.43	88	88	88	88	88	0.06
4SF	88	88	0	38	88	0	88	0.1	88
5CV	88	88	38	83	88	88	83	83	88
5CB	88	88	88	88	83	88	88	38	83
5C1	83	38	88	88	38	88	83	38	88
5C2	88	88	88	38	88	88	38	83	88

RUN DESIGNATION: FULLY REGRESSIVE CYCLES ONLY

TOTAL NUMBER OF FACIES TRANSITIONS OBSERVED: 215.

VALUES OF PARAMETER P --

	1SH	1SM	1GB	1UP	2H1	2H2	2H3	3BS	3HA	3SW
1SH	88	88	0	0	88	38	88	88	36	88
1SM	88	88	-0.01	0.01	-0.01	83	88	-0.01	88	88
1GB	88	0	88	0.01	-0.01	-0.01	88	88	-0.01	88
1UP	88	-0.01	38	88	0.01	0	0	88	0.01	0
2H1	88	88	-0.01	88	88	0.02	-0.01	88	0	83
2H2	83	88	-0.01	83	88	88	0.01	-0.01	0.04	-0.01
2H3	88	88	88	88	88	88	36	88	0	0.01
3BS	88	33	83	33	38	0	83	33	88	-0.01
3HA	88	88	88	88	88	-0.01	88	-0.01	88	0.03
3SW	38	38	88	-0.01	33	-0.01	33	-0.01	-0.01	88
3PL	36	88	88	38	38	88	38	82	-0.01	-0.01
4VL	82	33	38	88	38	33	88	88	88	0
4VC	0	0	-0.01	88	83	88	88	88	88	38
4IF	-0.01	83	33	88	38	83	33	88	38	83
4SF	83	38	-0.01	38	88	88	88	38	88	88
5CV	88	88	83	83	88	33	33	88	88	88
5C3	33	88	88	88	38	38	88	38	83	38
5C1	38	88	38	33	0	88	83	38	88	88
5C2	88	88	88	83	88	88	38	88	88	0

	3PL	4VL	4VC	4IF	4SF	5CV	5C3	5C1	5C2
1SH	88	28	33	38	88	86	88	83	88
1SM	88	88	38	88	38	33	88	-0.01	88
1GB	-0.01	88	88	33	-0.01	83	38	88	38
1UP	38	33	83	83	-0.01	88	33	83	88
2H1	82	38	88	88	68	80	88	38	88
2H2	33	88	83	88	38	88	38	33	88
2H3	-0.01	88	88	88	83	89	38	38	83
3BS	83	33	-0.01	38	38	33	83	88	68
3HA	0.03	88	88	38	-0.01	38	33	88	88
3SW	0.07	83	38	-0.01	38	38	38	88	0
3PL	38	0.01	0.07	38	-0.01	33	82	88	-0.01
4VL	0	33	0.03	-0.01	83	83	33	38	82
4VC	38	0.04	33	-0.01	0.02	33	38	33	-0.01
4IF	82	88	-0.01	33	88	38	33	38	-0.01
4SF	38	28	0.01	38	38	0	88	-0.01	33
5CV	33	83	88	33	33	32	28	33	33
5C3	36	33	38	33	38	88	33	33	31
5C1	38	33	33	35	73	38	33	38	38
5C2	33	88	82	33	32	81	36	88	88

RUN DESIGNATION: TOP-ASCENT CYCLES ONLY

FACIES DATA --

FACIES	# OCCUR	MEAN THICKNESS (RANGE) IN METERS
1SH	3	4.2 (0.3 to 10)
1SM	43	4.9 (1 to 12)
1SS	62	7.5 (0.5 to 39.1)
1VF	43	4 (0.9 to 15)
2H1	71	2.4 (0.5 to 8.2)
2H2	57	2.8 (0.4 to 11.1)
2HC	17	2.5 (1 to 5.1)
2SS	19	3 (0.7 to 6.6)
2HA	30	4.6 (1 to 9.3)
2SW	16	3.1 (0.1 to 14.6)
3PL	3	0 (0 to 0)
4VL	3	0 (0 to 0)
4VC	0	0 (0 to 0)
4SF	3	0 (0 to 0)
4SF	0	0 (0 to 0)
5CV	29	0 (0 to 0)
5C3	4	2.6 (1.9 to 3)
5C1	11	0.4 (0.2 to 0.8)
5C2	15	2.6 (0.9 to 7.2)

TOTAL NUMBER OF FACIES OCCURRENCES: 517

RUN DESIGNATION: TOP-ASCENT CYCLES ONLY

THICKNESS-OF-UNDERLYING MATRIX --

	1SM	1SM	1SS	1UT	2M1	2M2	2M3	3S3	3M4	3S4
1SM	0	0	3.6	10	0	0	0	0.3	0	0
1SM	0	0	4.6	5.2	6.5	4.1	0	3.3	0	0
1SS	0	11	0	4.7	8.8	4.6	0	0	1.3	0.9
1UT	1.9	7.5	4.1	0	4.2	2.1	0	5.7	2.4	1.1
2M1	0	1.1	0.3	1.8	0	1.7	0	0.3	0.2	1.4
2M2	0.4	1.7	2.8	2.2	2.4	0	2.3	0	1.6	2.2
2M3	0	0	0	0.7	1.6	1.6	0	0	0.1	0
3S3	0	2.9	1.5	0	1.4	1.6	0	0	0.7	0
3M4	0	0	0	0	0.5	0.3	0	0	0	0.3
3S4	0	14.6	0	0	0	5.4	0	2.6	0	0
3PL	0	0	0	0	0	0	0	0	0	0
4VL	0	0	0	0	0	0	0	0	0	0
4VC	0	0	0	0	0	0	0	0	0	0
4IF	0	0	0	0	0	0	0	0	0	0
4SF	0	0	0	0	0	0	0	0	0	0
5SV	0	0	0	0	0	0	0	0	0	0
5C3	0	0	0	0	0	0	0	0	0	0
5C1	0	0	0.3	0.3	0	0.3	0	0	0.3	0.7
5C2	0	2.1	2	3.1	2.3	1	0	0	0	0

	3PL	4VL	4VC	4IF	4SF	5SV	5C3	5C1	5C2
1SM	0	0	0	0	0	0	0	0	0
1SM	0	0	0	0	0	1.3	0	0	0
1SS	0	0	0	0	0	13.4	0	16.3	2.3
1UT	0	0	0	0	0	2.4	1.3	0.9	2
2M1	0	0	0	0	0	1.9	7	0	1.1
2M2	0	0	0	0	0	2.7	0	2	4.9
2M3	0	0	0	0	0	2.3	0	0	0
3S3	0	0	0	0	0	0	0	2	0.6
3M4	0	0	0	0	0	4.6	0	7.3	4.4
3S4	0	0	0	0	0	0	0	4.9	6.2
3PL	0	0	0	0	0	0	0	0	0
4VL	0	0	0	0	0	0	0	0	0
4VC	0	0	0	0	0	0	0	0	0
4IF	0	0	0	0	0	0	0	0	0
4SF	0	0	0	0	0	0	0	0	0
5SV	0	0	0	0	0	0	0	0	0
5C3	0	0	0	0	0	0	0	1.6	0
5C1	0	0	0	0	0	0.4	0	0	0
5C2	0	0	0	0	0	4	0	0	0

RUN DESIGNATION: TOP-ABSENT CYCLES ONLY

THICKNESS-OF-OVERLYING MATRIX --

	1SH	1BM	1GB	1UP	2H1	2H2	2H3	3BS	3HA	3SW
1SH	0	0	4.6	1.8	0	0	0	2	0	0
1BM	0	0	4.2	3.5	2.5	2	0	3.4	0	0
1GB	0	5.9	0	3.3	3	1.9	0	0	2.3	3.1
1UP	4	5.7	11.7	0	2.6	3	3.7	3.5	7.1	5.2
2H1	0	1.5	3.1	3.3	0	2.6	0	2	3.9	3.6
2H2	2.4	2.4	3.4	3.7	2.1	0	2.2	0	4.8	4.3
2H3	0	0	0	1.6	2.5	3.3	0	0	5.3	0
3BS	0	1.1	3.3	0	0.3	1.2	0	0	3.6	0
3HA	0	0	0	0	1.4	1.8	5.1	0	0	4.5
3SW	0	3.6	0	0	0	2.2	0	0.7	0	0
3PL	0	0	0	0	0	0	0	0	0	0
4VL	0	0	0	0	0	0	0	0	0	0
4VC	0	0	0	0	0	0	0	0	0	0
4IF	0	0	0	0	0	0	0	0	0	0
4SF	0	0	0	0	0	0	0	0	0	0
5CV	0	5.1	3	2	2.3	0	0	0	0	0
5CB	0	0	0	0	0	0	0	0	0	0
5C1	0	0	17.5	5.3	0	2	0	0	4.5	7.5
5C2	0	12	11.6	5.8	1.3	3.8	0	0	0	0

	3PL	4VL	4VC	4IF	4SF	5CV	5CB	5C1	5C2
1SH	0	0	0	0	0	0	0	0	0
1BM	0	0	0	0	0	0	0	0	0
1GB	0	0	0	0	0	0	0	0.3	1.4
1UP	0	0	0	0	0	0	0	0.4	2.2
2H1	0	0	0	0	0	0	0	0	1
2H2	0	0	0	0	0	0	0	0.3	2.2
2H3	0	0	0	0	0	0	0	0	0
3BS	0	0	0	0	0	0	0	0.7	0.9
3HA	0	0	0	0	0	0	0	0.3	2
3SW	0	0	0	0	0	0	0	0.4	5.3
3PL	0	0	0	0	0	0	0	0	0
4VL	0	0	0	0	0	0	0	0	0
4VC	0	0	0	0	0	0	0	0	0
4IF	0	0	0	0	0	0	0	0	0
4SF	0	0	0	0	0	0	0	0	0
5CV	0	0	0	0	0	0	2.4	0	0
5CB	0	0	0	0	0	0	0	0.8	2.3
5C1	0	0	0	0	0	0	1.9	0	0
5C2	0	0	0	0	0	0	0	0	0

RUN DESIGNATION: TOP-ABSENT CYCLES ONLY

TOTAL NUMBER OF FACIES TRANSITIONS OBSERVED: 352

OBSERVED TRANSITIONS --

	1SH	1BM	1GB	1UP	2H1	2H2	2H3	3BS	3HA	3SW
1SH	0	0	1	1	0	0	0	1	0	0
1BM	0	0	8	7	10	1	0	10	0	0
1GB	0	10	0	13	12	3	0	0	1	1
1UP	1	6	5	0	18	1	1	1	2	2
2H1	0	1	2	4	0	38	0	2	7	2
2H2	1	2	2	4	11	0	15	0	7	3
2H3	0	0	0	1	4	1	0	0	5	0
3BS	0	4	2	0	1	1	0	0	1	0
3HA	0	0	0	0	4	2	1	0	0	4
3SW	0	1	0	0	0	2	0	1	0	0
3PL	0	0	0	0	0	0	0	0	0	0
4VL	0	0	0	0	0	0	0	0	0	0
4VC	0	0	0	0	0	0	0	0	0	0
4IF	0	0	0	0	0	0	0	0	0	0
4SF	0	0	0	0	0	0	0	0	0	0
5CV	0	3	14	1	3	0	0	0	0	0
5CB	0	0	0	0	0	0	0	0	0	0
5C1	0	0	3	2	0	1	0	0	1	1
5C2	0	3	6	2	1	1	[redacted]	0	0	0

	3PL	4VL	4VC	4IF	4SF	5CV	5CB	5C1	5C2
1SH	0	0	0	0	0	0	0	0	0
1BM	0	0	0	0	0	2	0	0	0
1GB	0	0	0	0	0	1	0	1	1
1UP	0	0	0	0	0	1	1	1	1
2H1	0	0	0	0	0	5	1	0	1
2H2	0	0	0	0	0	2	0	1	3
2H3	0	0	0	0	0	2	0	0	0
3BS	0	0	0	0	0	1	0	1	1
3HA	0	0	0	0	0	4	0	2	3
3SW	0	0	0	0	0	4	0	4	3
3PL	0	0	0	0	0	0	0	0	0
4VL	0	0	0	0	0	0	0	0	0
4VC	0	0	0	0	0	0	0	0	0
4IF	0	0	0	0	0	0	0	0	0
4SF	0	0	0	0	0	0	0	0	0
5CV	0	0	0	0	0	0	1	0	0
5CB	0	0	0	0	0	0	0	1	0
5C1	0	0	0	0	0	0	1	0	0
5C2	0	0	0	0	0	1	0	0	0

RUN DESIGNATION: TOP-ABSENT CYCLES ONLY

OBSERVED TRANSITION PROBABILITY --

	1SH	1BM	1GB	1UP	2H1	2H2	2H3	3BS	3HA	3SW
1SH	0	0	0.33	0.33	0	0	0	0.33	0	0
1BM	0	0	0.21	0.13	0.26	0.03	0	0.26	0	0
1GB	0	0.23	0	0.3	0.28	0.07	0	0	0.02	0.02
1UP	0.02	0.15	0.12	0	0.44	0.02	0.02	0.02	0.05	0.05
2H1	0	0.02	0.03	0.06	0	0.6	0	0.03	0.11	0.03
2H2	0.02	0.04	0.04	0.08	0.22	0	0.29	0	0.14	0.06
2H3	0	0	0	0.08	0.31	0.08	0	0	0.38	0
3BS	0	0.33	0.17	0	0.08	0.08	0	0	0.08	0
3HA	0	0	0	0	0.16	0.08	0.04	0	0	0.16
3SW	0	0.07	0	0	0	0.13	0	0.07	0	0
3PL	0	0	0	0	0	0	0	0	0	0
4VL	0	0	0	0	0	0	0	0	0	0
4VC	0	0	0	0	0	0	0	0	0	0
4IF	0	0	0	0	0	0	0	0	0	0
4SF	0	0	0	0	0	0	0	0	0	0
5CV	0	0.14	0.64	0.05	0.14	0	0	0	0	0
5CB	0	0	0	0	0	0	0	0	0	0
5C1	0	0	0.33	0.22	0	0.11	0	0	0.11	0.11
5C2	0	0.21	0.43	0.14	0.07	0.07	0	0	0	0

	3PL	4VL	4VC	4IF	4SF	5CV	5CB	5C1	5C2
1SH	0	0	0	0	0	0	0	0	0
1BM	0	0	0	0	0	0.05	0	0	0
1GB	0	0	0	0	0	0.02	0	0.02	0.02
1UP	0	0	0	0	0	0.02	0.02	0.02	0.02
2H1	0	0	0	0	0	0.08	0.02	0	0.02
2H2	0	0	0	0	0	0.04	0	0.02	0.06
2H3	0	0	0	0	0	0.15	0	0	0
3BS	0	0	0	0	0	0.08	0	0.08	0.08
3HA	0	0	0	0	0	0.36	0	0.08	0.12
3SW	0	0	0	0	0	0.27	0	0.27	0.2
3PL	0	0	0	0	0	0	0	0	0
4VL	0	0	0	0	0	0	0	0	0
4VC	0	0	0	0	0	0	0	0	0
4IF	0	0	0	0	0	0	0	0	0
4SF	0	0	0	0	0	0	0	0	0
5CV	0	0	0	0	0	0	0.05	0	0
5CB	0	0	0	0	0	0	0	0.33	0.67
5C1	0	0	0	0	0	0	0.11	0	0
5C2	0	0	0	0	0	0.07	0	0	0

RUN DESIGNATION: TOP-ABSENT CYCLES ONLY

EXPECTED (RANDOM) TRANSITIONS --

	1SH	1BM	1GB	1UP	2H1	2H2	2H3	3BS	3HA	3SW
1SH	0	0.254	0.373	0.3	0.686	0.456	0.134	0.118	0.195	0.103
1BM	0.211	0	3.13	4.13	3.35	6.28	1.84	1.62	2.69	1.41
1GB	0.249	4.14	0	4.89	9.87	7.43	2.18	1.91	3.18	1.67
1UP	0.231	3.84	5.63	0	9.16	6.89	2.02	1.78	2.95	1.55
2H1	0.4	6.65	9.74	7.85	0	11.7	3.5	3.08	5.11	2.69
2H2	0.385	5.87	7.43	5.98	12.1	0	2.66	2.34	3.89	2.05
2H3	0.069	1.15	1.68	1.35	2.74	2.06	0	0.531	0.882	0.464
3BS	0.063	1.05	1.54	1.24	2.51	1.89	0.354	0	0.809	0.425
3HA	0.136	2.26	3.3	2.66	5.38	4.05	1.19	1.04	0	0.911
3SW	0.079	1.31	1.92	1.55	3.12	2.35	0.688	0.606	1.01	0
3PL	0	0	0	0	0	0	0	0	0	0
4VL	0	0	0	0	0	0	0	0	0	0
4VC	0	0	0	0	0	0	0	0	0	0
4IF	0	0	0	0	0	0	0	0	0	0
4SF	0	0	0	0	0	0	0	0	0	0
5CV	0.121	2.01	2.94	2.37	4.78	3.6	1.05	0.928	1.54	0.81
5CB	0.015	0.256	0.374	0.302	0.61	0.459	0.134	0.118	0.196	0.103
5C1	0.047	0.782	1.14	0.922	1.36	1.4	0.411	0.361	0.6	0.316
5C2	0.074	1.23	1.8	1.45	2.93	2.21	0.646	0.568	0.944	0.497

	3PL	4VL	4VC	4IF	4SF	5CV	5CB	5C1	5C2
1SH	0	0	0	0	0	0.226	0.031	0.086	0.118
1BM	0	0	0	0	0	3.11	0.421	1.18	1.63
1GB	0	0	0	0	0	3.68	0.498	1.39	1.92
1UP	0	0	0	0	0	3.42	0.462	1.29	1.79
2H1	0	0	0	0	0	5.91	0.8	2.24	3.09
2H2	0	0	0	0	0	4.51	0.61	1.7	2.36
2H3	0	0	0	0	0	1.02	0.138	0.386	0.533
3BS	0	0	0	0	0	0.937	0.127	0.354	0.49
3HA	0	0	0	0	0	2.01	0.271	0.756	1.05
3SW	0	0	0	0	0	1.16	0.158	0.44	0.609
3PL	0	0	0	0	0	0	0	0	0
4VL	0	0	0	0	0	0	0	0	0
4VC	0	0	0	0	0	0	0	0	0
4IF	0	0	0	0	0	0	0	0	0
4SF	0	0	0	0	0	0	0	0	0
5CV	0	0	0	0	0	0	0.241	0.675	0.933
5CB	0	0	0	0	0	0.227	0	0.086	0.119
5C1	0	0	0	0	0	0.693	0.094	0	0.363
5C2	0	0	0	0	0	1.09	0.148	0.413	0

RUN DESIGNATION: TOP-ABSENT CYCLES ONLY

EXPECTED (RANDOM) TRANSITION PROBABILITY --

	1SH	1BM	1GB	1UP	2H1	2H2	2H3	3BS	3HA	3SW
1SH	0	0.08	0.12	0.1	0.2	0.15	0.04	0.04	0.07	0.02
1BM	0.01	0	0.13	0.11	0.22	0.17	0.05	0.04	0.07	0.04
1GB	0.01	0.1	0	0.11	0.23	0.17	0.05	0.04	0.07	0.04
1UP	0.01	0.09	0.14	0	0.22	0.17	0.05	0.04	0.07	0.04
2H1	0.01	0.11	0.15	0.12	0	0.19	0.06	0.05	0.08	0.04
2H2	0.01	0.1	0.15	0.12	0.24	0	0.05	0.05	0.08	0.04
2H3	0.01	0.09	0.13	0.1	0.21	0.16	0	0.04	0.07	0.04
3BS	0.01	0.09	0.13	0.1	0.21	0.16	0.05	0	0.07	0.04
3HA	0.01	0.09	0.13	0.11	0.22	0.16	0.05	0.04	0	0.04
3SW	0.01	0.09	0.13	0.1	0.21	0.16	0.05	0.04	0.07	0
3PL	0	0	0	0	0	0	0	0	0	0
4VL	0	0	0	0	0	0	0	0	0	0
4VC	0	0	0	0	0	0	0	0	0	0
4IF	0	0	0	0	0	0	0	0	0	0
4SF	0	0	0	0	0	0	0	0	0	0
5CV	0.01	0.09	0.13	0.11	0.22	0.16	0.05	0.04	0.07	0.04
5CB	0.01	0.09	0.12	0.1	0.2	0.15	0.04	0.04	0.07	0.02
5C1	0.01	0.09	0.13	0.1	0.21	0.16	0.05	0.04	0.07	0.04
5C2	0.01	0.09	0.13	0.1	0.21	0.16	0.05	0.04	0.07	0.04

	3PL	4VL	4VC	4IF	4SF	5CV	5CB	5C1	5C2
1SH	0	0	0	0	0	0.03	0.01	0.03	0.04
1BM	0	0	0	0	0	0.08	0.01	0.03	0.04
1GB	0	0	0	0	0	0.09	0.01	0.03	0.04
1UP	0	0	0	0	0	0.08	0.01	0.03	0.04
2H1	0	0	0	0	0	0.09	0.01	0.04	0.05
2H2	0	0	0	0	0	0.09	0.01	0.03	0.05
2H3	0	0	0	0	0	0.08	0.01	0.03	0.04
3BS	0	0	0	0	0	0.08	0.01	0.03	0.04
3HA	0	0	0	0	0	0.08	0.01	0.03	0.04
3SW	0	0	0	0	0	0.08	0.01	0.03	0.04
3PL	0	0	0	0	0	0	0	0	0
4VL	0	0	0	0	0	0	0	0	0
4VC	0	0	0	0	0	0	0	0	0
4IF	0	0	0	0	0	0	0	0	0
4SF	0	0	0	0	0	0	0	0	0
5CV	0	0	0	0	0	0	0.01	0.03	0.04
5CB	00	0	0	0	0	0.08	0	0.03	0.04
5C1	0	0	0	0	0	0.03	0.01	0	0.04
5C2	0	0	0	0	0	0.08	0.01	0.03	0

RUN DESIGNATION: TOP-ABSENT CYCLES ONLY

OBSERVED MINUS RANDOM PROBABILITY --

	1SH	1BM	1GB	1UP	2M1	2M2	2M3	3BS	3MA	3SW
1SH	0	-0.08	0.21	0.23	-0.2	-0.15	-0.04	0.29	-0.07	-0.03
1BM	-0.01	0	0.08	0.07	0.04	-0.14	-0.05	0.22	-0.07	-0.04
1GB	-0.01	0.13	0	0.19	0.05	-0.1	-0.05	-0.04	-0.05	-0.02
1UP	0.01	0.06	-0.02	0	0.22	-0.15	-0.03	-0.02	-0.02	0.01
2M1	-0.01	-0.09	-0.12	-0.06	0	0.41	-0.06	-0.02	0.03	-0.01
2M2	0.01	-0.06	-0.11	-0.04	-0.02	0	0.24	-0.05	0.06	0.02
2M3	-0.01	-0.09	-0.13	-0.02	0.1	-0.08	0	-0.04	0.31	-0.04
3BS	-0.01	0.24	0.04	-0.1	-0.13	-0.08	-0.05	0	0.01	-0.04
3MA	-0.01	-0.09	-0.13	-0.11	-0.06	-0.08	-0.01	-0.04	0	0.12
3SW	-0.01	-0.02	-0.13	-0.1	-0.21	-0.03	-0.05	0.03	-0.07	0
3PL	0	0	0	0	0	0	0	0	0	0
4VL	0	0	0	0	0	0	0	0	0	0
4VC	0	0	0	0	0	0	0	0	0	0
4IF	0	0	0	0	0	0	0	0	0	0
4SF	0	0	0	0	0	0	0	0	0	0
5CV	-0.01	0.05	0.31	-0.06	-0.08	-0.16	-0.05	-0.04	-0.07	-0.04
5CB	-0.01	-0.09	-0.12	-0.1	-0.2	-0.15	-0.04	-0.04	-0.07	-0.03
5C1	-0.01	-0.09	0.2	0.12	-0.21	-0.05	-0.05	-0.04	0.04	-0.07
5C2	-0.01	0.12	0.3	0.04	-0.14	-0.09	-0.05	-0.04	-0.07	-0.04

	3PL	4VL	4VC	4IF	4SF	5CV	5CB	5C1	5C2
1SH	0	0	0	0	0	-0.03	-0.01	-0.03	-0.04
1BM	0	0	0	0	0	-0.03	-0.01	-0.03	-0.04
1GB	0	0	0	0	0	-0.07	-0.01	-0.01	-0.02
1UP	0	0	0	0	0	-0.06	0.01	-0.01	-0.02
2M1	0	0	0	0	0	-0.01	0.01	-0.04	-0.03
2M2	0	0	0	0	0	-0.05	-0.01	0.01	0.01
2M3	0	0	0	0	0	0.07	-0.01	-0.03	-0.04
3BS	0	0	0	0	0	0	-0.01	0.05	0.04
3MA	0	0	0	0	0	0.28	-0.01	0.05	0.08
3SW	0	0	0	0	0	0.19	-0.01	0.24	0.16
3PL	0	0	0	0	0	0	0	0	0
4VL	0	0	0	0	0	0	0	0	0
4VC	0	0	0	0	0	0	0	0	0
4IF	0	0	0	0	0	0	0	0	0
4SF	0	0	0	0	0	0	0	0	0
5CV	0	0	0	0	0	0	0.04	-0.03	-0.04
5CB	0	0	0	0	0	-0.08	0	0.3	0.62
5C1	0	0	0	0	0	-0.03	0.1	0	-0.04
5C2	0	0	0	0	0	-0.01	-0.01	-0.02	0

RUN DESIGNATION: TOP-ABSENT CYCLES ONLY

SIGNIFICANCE TEST VALUES --

	1SH	1BM	1GB	1UP	2M1	2M2	2M3	3BS	3HA	3SW
1SH	88	88	0.32	0.27	88	88	88	0.12	88	88
1BM	88	88	0.11	0.12	0.32	83	88	0	88	88
1GB	88	0.01	88	0	0.27	83	88	88	88	88
1UP	0.34	0.16	88	88	0	88	88	88	88	0.49
2M1	83	88	88	88	88	0	88	38	0.24	88
2M2	0.4	88	88	88	88	88	0	88	0.11	0.33
2M3	88	88	88	88	0.28	88	88	88	0	88
3BS	88	0.02	0.47	88	88	88	88	88	0.38	88
3HA	88	88	88	88	88	88	88	88	88	0.82
3SW	88	88	88	88	88	88	88	0.46	88	88
3PL	88	88	88	88	38	88	88	88	88	88
4VL	88	83	88	83	88	88	88	88	88	88
4VC	88	88	88	88	88	83	88	38	88	88
4IF	88	83	88	83	88	88	88	88	88	88
4SF	88	88	88	88	88	88	88	88	88	88
5CV	83	0.32	0	83	38	88	88	88	88	88
5CB	88	88	88	88	88	83	88	88	88	88
5C1	88	88	0.1	0.23	88	88	83	88	0.48	0.31
5C2	88	0.13	0.01	0.42	88	88	88	88	88	88

	3PL	4VL	4VC	4IF	4SF	5CV	5CB	5C1	5C2
1SH	88	88	88	88	83	88	88	88	88
1BM	88	88	88	88	38	88	88	88	88
1GB	88	88	88	88	38	88	88	88	88
1UP	88	88	88	88	38	88	0.34	88	88
2M1	88	88	88	88	88	88	0.47	88	88
2M2	88	88	38	88	38	88	88	88	0.47
2M3	88	88	83	88	88	0.28	88	88	88
3BS	83	83	88	83	88	88	88	0.31	0.39
3HA	88	83	88	88	88	0	88	0.17	0.08
3SW	88	88	88	88	88	0.03	88	0	0.02
3PL	88	38	88	83	88	88	88	88	88
4VL	88	38	88	88	88	83	88	88	88
4VC	88	38	88	88	38	88	88	88	88
4IF	83	88	88	88	83	88	88	88	88
4SF	88	88	83	88	88	83	88	88	88
5CV	88	33	38	88	88	38	0.2	88	88
5CB	88	88	88	33	38	88	88	0.09	0
5C1	88	88	88	88	38	88	0.39	88	88
5C2	88	88	38	88	88	88	88	83	83

RUN DESIGNATION: TOP-ABSENT CYCLES ONLY

TOTAL NUMBER OF FACIES TRANSITIONS OBSERVED: 352

VALUES OF PARAMETER r --

	1SH	1BM	1GB	1UP	2H1	2H2	2H3	3BS	3HA	3SW
1SH	88	88	-0.01	-0.01	38	38	88	-0.01	88	88
1BM	88	83	0.01	0.01	0.02	-0.01	83	0.02	88	88
1GB	88	0.02	88	0.03	0.02	0	88	88	-0.01	-0.01
1UP	-0.01	0.01	0	38	0.04	-0.01	-0.01	-0.01	0	0
2H1	88	-0.01	0	0	88	0.1	83	0	0.01	0
2H2	-0.01	0	0	0	0.02	88	0.03	88	0.01	0
2H3	88	88	88	-0.01	0	-0.01	88	88	0	88
3BS	83	0	0	88	-0.01	-0.01	88	88	-0.01	88
3HA	88	88	88	83	0	0	-0.01	88	83	0
3SW	88	-0.01	88	88	88	0	88	-0.01	83	88
3PL	88	88	88	88	38	38	88	88	88	88
4VL	88	88	88	38	38	33	88	88	88	88
4VC	38	38	88	88	88	33	88	38	38	88
4IF	88	38	83	83	88	88	83	88	88	88
4SF	38	38	38	33	38	88	88	88	88	88
5CV	88	0	0.03	-0.01	0	38	38	38	83	88
5CB	88	38	38	88	38	88	88	38	88	88
5C1	88	88	0	0	33	-0.01	88	88	-0.01	-0.01
5C2	88	0	0.01	0	-0.01	-0.01	38	88	88	38

	3PL	4VL	4VC	4IF	4SF	5CV	5CB	5C1	5C2
1SH	88	88	88	88	83	88	88	88	83
1BM	83	83	38	88	38	0	88	38	38
1GB	88	88	88	83	88	-0.01	88	-0.01	-0.01
1UP	88	88	88	88	88	-0.01	-0.01	-0.01	-0.01
2H1	38	88	88	88	88	0	-0.01	88	-0.01
2H2	88	88	88	88	88	0	83	-0.01	0
2H3	38	88	88	88	88	0	88	88	88
3BS	38	38	88	88	88	-0.01	88	-0.01	-0.01
3HA	38	88	88	83	88	0.02	88	0	0
3SW	38	38	88	88	88	0	88	0	0
3PL	88	88	88	88	88	88	88	88	88
4VL	88	88	88	88	88	88	88	88	88
4VC	88	88	88	88	88	88	88	88	88
4IF	88	88	88	88	88	88	88	88	88
4SF	88	88	88	88	88	88	88	88	88
5CV	88	88	88	88	88	88	-0.01	88	88
5CB	88	88	88	88	88	88	88	-0.01	0
5C1	88	88	88	88	88	88	-0.01	88	88
5C2	88	88	88	88	88	-0.01	88	88	88

RUN DESIGNATION: TYPE 2 CYCLES ONLY, ARTIFICIALLY JUXTAPOSED

FACIES DATA --

FACIES	# OCCUR	MEAN THICKNESS (RANGE) IN METERS
1SH	0	0 (0 to 0)
1SM	4	5.4 (3.2 to 6.5)
1GB	6	2.6 (0.9 to 4.2)
1UP	8	3.4 (0.9 to 9.4)
2M1	15	2.8 (0.5 to 7.1)
2M2	13	2.1 (0.7 to 3.6)
2M3	3	3.7 (2.4 to 5.1)
3BS	1	0.7 (0.7 to 0.7)
3MA	6	4.8 (2.5 to 6.3)
3SW	15	4.9 (2.1 to 14.6)
3PL	0	0 (0 to 0)
4VL	0	0 (0 to 0)
4VC	0	0 (0 to 0)
4IF	0	0 (0 to 0)
4SF	0	0 (0 to 0)
5CV	4	0 (0 to 0)
5C3	2	2.5 (1.9 to 3)
5C1	4	0.3 (0.3 to 0.4)
5C2	4	4.6 (2.6 to 7.2)

TOTAL NUMBER OF FACIES OCCURRENCES: 85

RUN DESIGNATION: TYPE 2 CYCLES ONLY, ARTIFICIALLY JUXTAPOSED

THICKNESS-OF-UNDERLYING MATRIX --

	1SH	1BM	1GB	1UP	2H1	2H2	2H3	3BS	3HA	3SW
1SH	0	0	0	0	0	0	0	0	0	0
1BM	0	0	5.3	0	5.4	0	0	0	0	0
1GB	0	3.9	0	2.6	3	0	0	0	0	0.9
1UP	0	9.4	1.8	0	3.7	0	3	0	0	2.1
2H1	0	0	0	2.5	0	2.6	0	0	4.8	2.4
2H2	0	0	2.1	2.7	2.2	0	1.7	0	1.5	2.2
2H3	0	0	0	3.7	0	0	0	0	3.8	0
3BS	0	0	0	0	0	0	0	0	0.7	0
3HA	0	0	0	0	3.6	0	6	0	0	4.9
3SW	0	14.6	0	0	0	5.4	0	2.6	0	0
3PL	0	0	0	0	0	0	0	0	0	0
4VL	0	0	0	0	0	0	0	0	0	0
4VC	0	0	0	0	0	0	0	0	0	0
4IF	0	0	0	0	0	0	0	0	0	0
4SF	0	0	0	0	0	0	0	0	0	0
5CV	0	0	0	0	0	0	0	0	0	0
5CB	0	0	0	1.9	0	0	0	0	0	0
5C1	0	0	0	0.3	0.3	0.3	0	0	0	0
5C2	0	0	0	7.2	3.7	0	0	0	0	0

	3PL	4VL	4VC	4IF	4SF	5CV	5CB	5C1	5C2
1SH	0	0	0	0	0	0	0	0	0
1BM	0	0	0	0	0	0	0	0	0
1GB	0	0	0	0	0	0	0	0	0
1UP	0	0	0	0	0	0	1.3	0	0
2H1	0	0	0	0	0	0	0	0	0
2H2	0	0	0	0	0	0	0	2	0
2H3	0	0	0	0	0	0	0	0	0
3BS	0	0	0	0	0	0	0	0	0
3HA	0	0	0	0	0	0	0	0	0
3SW	0	0	0	0	0	3	0	4	6.2
3PL	0	0	0	0	0	0	0	0	0
4VL	0	0	0	0	0	0	0	0	0
4VC	0	0	0	0	0	0	0	0	0
4IF	0	0	0	0	0	0	0	0	0
4SF	0	0	0	0	0	0	0	0	0
5CV	0	0	0	0	0	0	0	0	0
5CB	0	0	0	0	0	0	0	0	3
5C1	0	0	0	0	0	0	0.4	0	0
5C2	0	0	0	0	0	0	0	0	0

RUN DESIGNATION: TYPE 2 CYCLES ONLY, ARTIFICIALLY JUXTAPOSED

THICKNESS-OF-OVERLYING MATRIX --

	1SH	1BM	1GB	1UP	2H1	2H2	2H3	3BS	3HA	3SW
1SH	0	0	0	0	0	0	0	0	0	0
1BM	0	0	4.2	0	3.4	0	0	0	0	0
1GB	0	5.9	0	5.4	2.6	0	0	0	0	3.1
1UP	0	6.4	0.9	0	2.4	0	3.7	0	0	5.2
2H1	0	0	0	1.8	0	2	0	0	5.6	8.6
2H2	0	0	3	0.9	2.3	0	2.4	0	6	4.3
2H3	0	0	0	1.6	0	0	0	0	4.1	0
3BS	0	0	0	0	0	0	0	0	3.6	0
3HA	0	0	0	0	2.1	0	5.1	0	0	4.3
3SW	0	3.2	0	0	0	2.9	0	0.7	0	0
3PL	0	0	0	0	0	0	0	0	0	0
4VL	0	0	0	0	0	0	0	0	0	0
4VC	0	0	0	0	0	0	0	0	0	0
4IF	0	0	0	0	0	0	0	0	0	0
4SF	0	0	0	0	0	0	0	0	0	0
5CV	0	0	2.4	0	0	0	0	0	0	3.7
5CB	0	0	0	5.8	0	0	0	0	0	0
5C1	0	0	0	3.2	2.3	2	0	0	0	0
5C2	0	0	0	3	3.4	0	0	0	0	0

	3PL	4VL	4VC	4IF	4SF	5CV	5CB	5C1	5C2
1SH	0	0	0	0	0	0	0	0	0
1BM	0	0	0	0	0	0	0	0	0
1GB	0	0	0	0	0	0	0	0	0
1UP	0	0	0	0	0	0	3	0	0
2H1	0	0	0	0	0	0	0	0	0
2H2	0	0	0	0	0	0	0	0.3	0
2H3	0	0	0	0	0	0	0	0	0
3BS	0	0	0	0	0	0	0	0	0
3HA	0	0	0	0	0	0	0	0	0
3SW	0	0	0	0	0	0	0	0.3	3.3
3PL	0	0	0	0	0	0	0	0	0
4VL	0	0	0	0	0	0	0	0	0
4VC	0	0	0	0	0	0	0	0	0
4IF	0	0	0	0	0	0	0	0	0
4SF	0	0	0	0	0	0	0	0	0
5CV	0	0	0	0	0	0	0	0	0
5CB	0	0	0	0	0	0	0	0	2.6
5C1	0	0	0	0	0	0	1.9	0	0
5C2	0	0	0	0	0	0	0	0	0

RUN DESIGNATION: TYPE 2 CYCLES ONLY, ARTIFICIALLY JUXTAPOSED

TOTAL NUMBER OF FACIES TRANSITIONS OBSERVED: 81

OBSERVED TRANSITIONS --

	1SH	1BM	1GB	1UP	2H1	2H2	2H3	3BS	3HA	3SW
1SH	0	0	0	0	0	0	0	0	0	0
1BM	0	0	1	0	3	0	0	0	0	0
1GB	0	2	0	2	1	0	0	0	0	1
1UP	0	1	1	0	2	0	1	0	0	2
2H1	0	0	0	1	0	10	0	0	2	2
2H2	0	0	1	1	5	0	1	0	1	3
2H3	0	0	0	1	0	0	0	0	2	0
3BS	0	0	0	0	0	0	0	0	1	0
3HA	0	0	0	0	1	0	1	0	0	4
3SW	0	1	0	0	0	2	0	1	0	0
3PL	0	0	0	0	0	0	0	0	0	0
4VL	0	0	0	0	0	0	0	0	0	0
4VC	0	0	0	0	0	0	0	0	0	0
4IF	0	0	0	0	0	0	0	0	0	0
4SF	0	0	0	0	0	0	0	0	0	0
5CV	0	0	2	0	0	0	0	0	0	1
5CB	0	0	0	1	0	0	0	0	0	0
5C1	0	0	0	1	1	1	0	0	0	0
5C2	0	0	0	1	1	0	0	0	0	0

	3PL	4VL	4VC	4IF	4SF	5CV	5CB	5C1	5C2
1SH	0	0	0	0	0	0	0	0	0
1BM	0	0	0	0	0	0	0	0	0
1GB	0	0	0	0	0	0	0	0	0
1UP	0	0	0	0	0	0	1	0	0
2H1	0	0	0	0	0	0	0	0	0
2H2	0	0	0	0	0	0	0	1	0
2H3	0	0	0	0	0	0	0	0	0
3BS	0	0	0	0	0	0	0	0	0
3HA	0	0	0	0	0	0	0	0	0
3SW	0	0	0	0	0	4	0	3	3
3PL	0	0	0	0	0	0	0	0	0
4VL	0	0	0	0	0	0	0	0	0
4VC	0	0	0	0	0	0	0	0	0
4IF	0	0	0	0	0	0	0	0	0
4SF	0	0	0	0	0	0	0	0	0
5CV	0	0	0	0	0	0	0	0	0
5CB	0	0	0	0	0	0	0	0	1
5C1	0	0	0	0	0	0	1	0	0
5C2	0	0	0	0	0	0	0	0	0

RUN DESIGNATION: TYPE 2 CYCLES ONLY, ARTIFICIALLY JUXTAPOSED

OBSERVED TRANSITION PROBABILITY --

	1SH	1BM	1OB	1UP	2H1	2H2	2H3	3BS	3HA	3SW
1SH	0	0	0	0	0	0	0	0	0	0
1BM	0	0	0.25	0	0.75	0	0	0	0	0
1OB	0	0.33	0	0.33	0.17	0	0	0	0	0.17
1UP	0	0.13	0.13	0	0.25	0	0.13	0	0	0.25
2H1	0	0	0	0.07	0	0.67	0	0	0.13	0.13
2H2	0	0	0.08	0.08	0.33	0	0.08	0	0.08	0.25
2H3	0	0	0	0.33	0	0	0	0	0.67	0
3BS	0	0	0	0	0	0	0	0	1	0
3HA	0	0	0	0	0.17	0	0.17	0	0	0.67
3SW	0	0.07	0	0	0	0.14	0	0.07	0	0
3PL	0	0	0	0	0	0	0	0	0	0
4VL	0	0	0	0	0	0	0	0	0	0
4VC	0	0	0	0	0	0	0	0	0	0
4IF	0	0	0	0	0	0	0	0	0	0
4SF	0	0	0	0	0	0	0	0	0	0
5CV	0	0	0.67	0	0	0	0	0	0	0.33
5CB	0	0	0	0.5	0	0	0	0	0	0
5C1	0	0	0	0.25	0.25	0.25	0	0	0	0
5C2	0	0	0	0.5	0.5	0	0	0	0	0

	3PL	4VL	4VC	4IF	4SF	5CV	5CB	5C1	5C2
1SH	0	0	0	0	0	0	0	0	0
1BM	0	0	0	0	0	0	0	0	0
1OB	0	0	0	0	0	0	0	0	0
1UP	0	0	0	0	0	0	0.13	0	0
2H1	0	0	0	0	0	0	0	0	0
2H2	0	0	0	0	0	0	0	0.08	0
2H3	0	0	0	0	0	0	0	0	0
3BS	0	0	0	0	0	0	0	0	0
3HA	0	0	0	0	0	0	0	0	0
3SW	0	0	0	0	0	0.29	0	0.21	0.21
3PL	0	0	0	0	0	0	0	0	0
4VL	0	0	0	0	0	0	0	0	0
4VC	0	0	0	0	0	0	0	0	0
4IF	0	0	0	0	0	0	0	0	0
4SF	0	0	0	0	0	0	0	0	0
5CV	0	0	0	0	0	0	0	0	0
5CB	0	0	0	0	0	0	0	0	0.5
5C1	0	0	0	0	0	0	0.25	0	0
5C2	0	0	0	0	0	0	0	0	0

RUN DESIGNATION: TYPE 2 CYCLES ONLY, ARTIFICIALLY JUXTAPOSED

EXPECTED (RANDOM) TRANSITIONS --

	1SM	1BM	1GB	1UP	2H1	2H2	2H3	3BS	3HA	3SW
1SM	0	0	0	0	0	0	0	0	0	0
1BM	0	0	0.243	0.401	0.793	0.709	0.141	0.046	0.292	0.721
1GB	0	0.289	0	0.689	1.21	1.08	0.214	0.07	0.444	1.1
1UP	0	0.401	0.514	0	1.67	1.5	0.297	0.097	0.617	1.52
2H1	0	0.828	1.07	1.77	0	3.13	0.621	0.202	1.29	3.18
2H2	0	0.709	0.908	1.5	2.96	0	0.525	0.171	1.09	2.69
2H3	0	0.141	0.18	0.297	0.587	0.525	0	0.034	0.216	0.534
3BS	0	0.046	0.059	0.097	0.191	0.171	0.034	0	0.071	0.174
3HA	0	0.292	0.374	0.617	1.22	1.09	0.216	0.071	0	1.11
3SW	0	0.766	0.982	1.62	3.2	2.86	0.567	0.185	1.18	0
3PL	0	0	0	0	0	0	0	0	0	0
4VL	0	0	0	0	0	0	0	0	0	0
4VC	0	0	0	0	0	0	0	0	0	0
4IF	0	0	0	0	0	0	0	0	0	0
4SF	0	0	0	0	0	0	0	0	0	0
5CV	0	0.142	0.182	0.3	0.594	0.531	0.105	0.034	0.219	0.54
5CB	0	0.093	0.119	0.196	0.387	0.346	0.069	0.022	0.143	0.352
5C1	0	0.19	0.243	0.401	0.793	0.709	0.141	0.046	0.292	0.721
5C2	0	0.095	0.121	0.2	0.396	0.354	0.07	0.023	0.146	0.36

	3PL	4VL	4VC	4IF	4SF	5CV	5CB	5C1	5C2
1SM	0	0	0	0	0	0	0	0	0
1BM	0	0	0	0	0	0.138	0.093	0.19	0.185
1GB	0	0	0	0	0	0.285	0.141	0.289	0.282
1UP	0	0	0	0	0	0.396	0.196	0.401	0.391
2H1	0	0	0	0	0	0.828	0.409	0.838	0.819
2H2	0	0	0	0	0	0.7	0.346	0.709	0.692
2H3	0	0	0	0	0	0.139	0.069	0.141	0.137
3BS	0	0	0	0	0	0.045	0.022	0.046	0.045
3HA	0	0	0	0	0	0.289	0.143	0.292	0.285
3SW	0	0	0	0	0	0.737	0.374	0.766	0.748
3PL	0	0	0	0	0	0	0	0	0
4VL	0	0	0	0	0	0	0	0	0
4VC	0	0	0	0	0	0	0	0	0
4IF	0	0	0	0	0	0	0	0	0
4SF	0	0	0	0	0	0	0	0	0
5CV	0	0	0	0	0	0	0.069	0.142	0.139
5CB	0	0	0	0	0	0.092	0	0.093	0.09
5C1	0	0	0	0	0	0.188	0.093	0	0.185
5C2	0	0	0	0	0	0.094	0.046	0.095	0

RUN DESIGNATION: TYPE 2 CYCLES ONLY, ARTIFICIALLY JUXTAPOSED

EXPECTED (RANDOM) TRANSITION PROBABILITY --

	1SH	1BM	1GB	1UP	2H1	2H2	2H3	3BS	3HA	3SW
1SH	0	0	0	0	0	0	0	0	0	0
1BM	0	0	0.06	0.1	0.2	0.18	0.04	0.01	0.07	0.18
1GB	0	0.05	0	0.1	0.2	0.18	0.04	0.01	0.07	0.18
1UP	0	0.05	0.06	0	0.21	0.19	0.04	0.01	0.08	0.19
2H1	0	0.06	0.07	0.12	0	0.21	0.04	0.01	0.09	0.21
2H2	0	0.05	0.07	0.12	0.23	0	0.04	0.01	0.08	0.21
2H3	0	0.05	0.06	0.1	0.2	0.18	0	0.01	0.07	0.18
3BS	0	0.05	0.06	0.1	0.19	0.17	0.03	0	0.07	0.17
3HA	0	0.05	0.06	0.1	0.2	0.18	0.04	0.01	0	0.19
3SW	0	0.05	0.07	0.12	0.23	0.2	0.04	0.01	0.08	0
3PL	0	0	0	0	0	0	0	0	0	0
4VL	0	0	0	0	0	0	0	0	0	0
4VC	0	0	0	0	0	0	0	0	0	0
4IF	0	0	0	0	0	0	0	0	0	0
4SF	0	0	0	0	0	0	0	0	0	0
5CV	0	0.05	0.06	0.1	0.2	0.18	0.04	0.01	0.07	0.18
5CB	0	0.05	0.06	0.1	0.19	0.17	0.03	0.01	0.07	0.18
5C1	0	0.05	0.06	0.1	0.2	0.18	0.04	0.01	0.07	0.18
5C2	0	0.05	0.06	0.1	0.2	0.18	0.04	0.01	0.07	0.18

	3PL	4VL	4VC	4IF	4SF	5CV	5CB	5C1	5C2
1SH	0	0	0	0	0	0	0	0	0
1BM	0	0	0	0	0	0.05	0.02	0.05	0.05
1GB	0	0	0	0	0	0.05	0.02	0.05	0.05
1UP	0	0	0	0	0	0.05	0.02	0.05	0.05
2H1	0	0	0	0	0	0.06	0.03	0.06	0.05
2H2	0	0	0	0	0	0.05	0.03	0.05	0.05
2H3	0	0	0	0	0	0.05	0.02	0.05	0.05
3BS	0	0	0	0	0	0.04	0.02	0.05	0.04
3HA	0	0	0	0	0	0.05	0.02	0.05	0.05
3SW	0	0	0	0	0	0.05	0.03	0.05	0.05
3PL	0	0	0	0	0	0	0	0	0
4VL	0	0	0	0	0	0	0	0	0
4VC	0	0	0	0	0	0	0	0	0
4IF	0	0	0	0	0	0	0	0	0
4SF	0	0	0	0	0	0	0	0	0
5CV	0	0	0	0	0	0	0.02	0.05	0.05
5CB	0	0	0	0	0	0.05	0	0.05	0.04
5C1	0	0	0	0	0	0.05	0.02	0	0.05
5C2	0	0	0	0	0	0.05	0.02	0.05	0

RUN DESIGNATION: TYPE 2 CYCLES ONLY, ARTIFICIALLY JUXTAPOSED

OBSERVED MINUS RANDOM PROBABILITY --

	1SH	1BM	1GB	1UP	2H1	2H2	2H3	3BS	3HA	3SW
1SH	0	0	0	0	0	0	0	0	0	0
1BM	0	0	0.19	-0.1	0.55	-0.18	-0.04	-0.01	-0.07	-0.18
1GB	0	0.28	0	0.23	-0.03	-0.18	-0.04	-0.01	-0.07	-0.01
1UP	0	0.08	0.07	0	0.04	-0.19	0.09	-0.01	-0.08	0.06
2H1	0	-0.06	-0.07	-0.03	0	0.46	-0.04	-0.01	0.04	-0.08
2H2	0	-0.05	0.01	-0.04	0.15	0	0.04	-0.01	0	0.02
2H3	0	-0.05	-0.06	0.23	-0.2	-0.18	0	-0.01	0.6	-0.18
3BS	0	-0.05	-0.06	-0.1	-0.19	-0.17	-0.03	0	0.93	-0.17
3HA	0	-0.05	-0.06	-0.1	-0.03	-0.18	0.13	-0.01	0	0.48
3SW	0	0.02	-0.07	-0.12	-0.23	-0.06	-0.04	0.06	-0.08	0
3PL	0	0	0	0	0	0	0	0	0	0
4VL	0	0	0	0	0	0	0	0	0	0
4VC	0	0	0	0	0	0	0	0	0	0
4IF	0	0	0	0	0	0	0	0	0	0
4SF	0	0	0	0	0	0	0	0	0	0
5CV	0	-0.05	0.61	-0.1	-0.2	-0.18	-0.04	-0.01	-0.07	0.15
5CB	0	-0.05	-0.06	0.4	-0.19	-0.17	-0.03	-0.01	-0.07	-0.18
5C1	0	-0.05	-0.06	0.15	0.05	0.07	-0.04	-0.01	-0.07	-0.18
5C2	0	-0.05	-0.06	0.4	0.3	-0.18	-0.04	-0.01	-0.07	-0.18

	3PL	4VL	4VC	4IF	4SF	5CV	5CB	5C1	5C2
1SH	0	0	0	0	0	0	0	0	0
1BM	0	0	0	0	0	-0.05	-0.02	-0.05	-0.05
1GB	0	0	0	0	0	-0.05	-0.02	-0.05	-0.05
1UP	0	0	0	0	0	-0.05	0.11	-0.05	-0.05
2H1	0	0	0	0	0	-0.06	-0.03	-0.06	-0.05
2H2	0	0	0	0	0	-0.05	-0.03	0.03	-0.05
2H3	0	0	0	0	0	-0.05	-0.02	-0.05	-0.05
3BS	0	0	0	0	0	-0.04	-0.02	-0.05	-0.04
3HA	0	0	0	0	0	-0.05	-0.02	-0.05	-0.05
3SW	0	0	0	0	0	0.24	-0.03	0.16	0.16
3PL	0	0	0	0	0	0	0	0	0
4VL	0	0	0	0	0	0	0	0	0
4VC	0	0	0	0	0	0	0	0	0
4IF	0	0	0	0	0	0	0	0	0
4SF	0	0	0	0	0	0	0	0	0
5CV	0	0	0	0	0	0	-0.02	-0.05	-0.05
5CB	0	0	0	0	0	-0.05	0	-0.05	0.46
5C1	0	0	0	0	0	-0.05	0.23	0	-0.05
5C2	0	0	0	0	0	-0.05	-0.02	-0.05	0

RUN DESIGNATION: TYPE 2 CYCLES ONLY, ARTIFICIALLY JUXTAPOSED

SIGNIFICANCE TEST VALUES --

	1SH	1BM	1GB	1UP	2H1	2H2	2HC	3BS	3HA	3SW
1SH	33	38	89	33	38	38	88	33	93	39
1BM	38	38	0.22	98	0.03	38	33	88	88	38
1GB	33	0.03	33	0.11	39	33	38	38	33	38
1UP	33	0.34	0.09	33	0.33	38	0.29	88	38	0.47
2H1	38	88	89	88	33	0	88	98	0.4	38
2H2	33	88	0.01	83	0.15	98	0.41	38	88	0.33
2HC	98	38	98	0.27	88	38	98	88	0.31	83
3BS	38	33	38	98	38	98	33	38	0.07	39
3HA	38	88	88	88	88	38	0.22	38	38	0.31
3SW	88	0.31	88	83	98	88	88	0.13	38	93
3PL	38	38	83o	93	38	83	93	98	33	33
4VL	33	33	38	38	38	33	33	39	38	83
4VC	38	33	93	39	33	33	39	98	39	23
4IF	38	38	38	33	28	33	33	33	23	33
4SF	38	38	38	39	38	33	33	38	98	38
5CV	98	83	0.01	38	33	88	33	38	88	0.45
5C3	38	98	39	0.19	98	88	38	98	39	39
5C1	33	33	38	0.04	0.39	0.39	39	33	88	83
5C2	38	38	93	0.19	0.36	38	88	38	98	38

	3PL	4VL	4VC	4IF	4SF	5CV	5C3	5C1	5C2
1SH	38	38	88	88	98	98	38	83	38
1BM	88	83	33	88	98	38	83	88	38
1GB	39	33	38	38	38	88	38	89	38
1UP	38	33	38	93	28	38	0.13	38	38
2H1	38	38	88	88	88	38	38	38	88
2H2	38	33	83	38	83	88	38	0.46	38
2HC	38	88	88	88	33	33	38	39	33
3BS	38	38	83	88	38	38	88	88	88
3HA	88	88	88	89	88	88	88	88	88
3SW	38	38	88	88	38	0	88	0.03	0.03
3PL	98	88	88	98	83	88	88	38	88
4VL	38	33	38	88	38	38	33	33	93
4VC	38	38	88	38	38	38	33	38	93
4IF	38	38	33	38	38	98	38	33	33
4SF	38	39	83	39	33	98	38	39	33
5CV	83	88	33	33	38	38	38	33	83
5C3	38	83	88	38	38	93	33	38	0.33
5C1	33	38	38	88	93	38	0.08	88	39
5C2	98	98	98	83	33	38	93	33	33

RUN DESIGNATION: TYPE 2 CYCLES ONLY, ARTIFICIALLY JUXTAPOSED

TOTAL NUMBER OF FACIES TRANSITIONS OBSERVED: 81

VALUES OF PARAMETER = --

	1SH	1SM	1GS	1UP	2M1	2M2	2M3	3BS	3HA	3SW
1SH	38	33	33	33	33	33	33	33	33	33
1SM	33	33	-0.01	33	0.01	33	33	33	33	33
1GS	33	0	33	0	-0.01	33	33	33	33	-0.01
1UP	33	-0.01	-0.01	33	0	33	-0.01	33	33	0
2M1	33	33	33	-0.01	33	0.1	33	33	0	0
2M2	33	33	-0.01	-0.01	0.04	33	-0.01	33	-0.01	0.01
2M3	33	33	33	-0.01	33	33	33	33	0	33
3BS	33	33	33	33	33	33	33	33	-0.01	33
3HA	33	33	33	33	-0.01	33	-0.01	33	33	0.03
3SW	33	-0.01	33	33	33	0	33	-0.01	33	33
3PL	33	33	33	33	33	33	33	33	33	33
4VL	33	33	33	33	33	33	33	33	33	33
4VC	33	33	33	33	33	33	33	33	33	33
4IF	33	33	33	33	33	33	33	33	33	33
4SF	33	33	33	33	33	33	33	33	33	33
5CV	33	33	0	33	33	33	33	33	33	-0.01
5CB	33	33	33	-0.01	33	33	33	33	33	33
5C1	33	33	33	-0.01	-0.01	-0.01	33	33	33	33
5C2	33	33	33	-0.01	-0.01	33	33	33	33	33

	3PL	4VL	4VC	4IF	4SF	5CV	5CB	5C1	5C2
1SH	33	33	33	33	33	33	33	33	33
1SM	33	33	33	33	33	33	33	33	33
1GS	33	33	33	33	33	33	33	33	33
1UP	33	33	33	33	33	33	-0.01	33	33
2M1	33	33	33	33	33	33	33	33	33
2M2	33	33	33	33	33	33	-0.01	33	33
2M3	33	33	33	33	33	33	33	33	33
3BS	33	33	33	33	33	33	33	33	33
3HA	33	33	33	33	33	33	33	33	33
3SW	33	33	33	33	33	0.03	33	0.01	0.01
3PL	33	33	33	33	33	33	33	33	33
4VL	33	33	33	33	33	33	33	33	33
4VC	33	33	33	33	33	33	33	33	33
4IF	33	33	33	33	33	33	33	33	33
4SF	33	33	33	33	33	33	33	33	33
5CV	33	33	33	33	33	33	33	33	33
5CB	33	33	33	33	33	33	33	33	-0.01
5C1	33	33	33	33	33	33	-0.01	33	33
5C2	33	33	33	33	33	33	33	33	33

RUN DESIGNATION: TYPE 3 CYCLES ONLY, ARTIFICIALLY JUXTAPOSED

FACIES DATA --

FACIES	# OCCUR	MEAN THICKNESS (RANGE) IN METERS
1SH	1	0.8 (0.8 to 0.8)
1SM	5	5.1 (1.1 to 11.8)
1GB	5	9.4 (1.3 to 39.1)
1UP	5	3.8 (1.1 to 6.9)
2H1	18	2.1 (0.6 to 5.1)
2H2	16	2.1 (0.5 to 4.1)
2H3	3	2.7 (1.7 to 3.5)
3BS	1	2 (2 to 2)
3HA	25	4.7 (1 to 9.3)
3SW	0	0 (0 to 0)
3PL	0	0 (0 to 0)
4VL	0	0 (0 to 0)
4VC	0	0 (0 to 0)
4IF	0	0 (0 to 0)
4SF	0	0 (0 to 0)
5CV	10	0 (0 to 0)
5CB	0	0 (0 to 0)
5C1	4	0.5 (0.2 to 0.7)
5C2	3	2 (1.2 to 2.8)

TOTAL NUMBER OF FACIES OCCURRENCES: 96

RUN DESIGNATION: TYPE 3 CYCLES ONLY, ARTIFICIALLY JUXTAPOSED

THICKNESS-OF-UNDERLYING MATRIX --

	1SH	1BM	1OB	1UP	2H1	2H2	2H3	3BS	3HA	3SW
1SH	0	0	0	0	0	0	0	8.8	0	0
1BM	0	0	1.1	0	0	0	0	0	0	0
1OB	0	21	0	1.7	0	0	0	0	1.3	0
1UP	0	0	6.9	0	4	0	0	0	2.4	0
2H1	0	2.5	1.1	0	0	2	0	0	2.6	0
2H2	0	0	0	1.3	2.7	0	2.6	0	1.6	0
2H3	0	0	0	0	0	0	0	0	2.7	0
3BS	0	0	0	0	0	0	0	0	0	0
3HA	0	0	0	0	3.4	3.8	0	0	0	0
3SW	0	0	0	0	0	0	0	0	0	0
3PL	0	0	0	0	0	0	0	0	0	0
4VL	0	0	0	0	0	0	0	0	0	0
4VC	0	0	0	0	0	0	0	0	0	0
4IF	0	0	0	0	0	0	0	0	0	0
4SF	0	0	0	0	0	0	0	0	0	0
5CV	0	0	0	0	0	0	0	0	0	0
5CB	0	0	0	0	0	0	0	0	0	0
5C1	0	0	0	0	0	0	0	0	0.5	0
5C2	0	0	0	0	2.8	2	0	0	0	0

	3PL	4VL	4VC	4IF	4SF	5CV	5CB	5C1	5C2
1SH	0	0	0	0	0	0	0	0	0
1BM	0	0	0	0	0	0	0	0	0
1OB	0	0	0	0	0	0	0	0	0
1UP	0	0	0	0	0	0	0	0	0
2H1	0	0	0	0	0	1.1	0	0	0
2H2	0	0	0	0	0	0	0	0	0
2H3	0	0	0	0	0	0	0	0	0
3BS	0	0	0	0	0	0	0	2	0
3HA	0	0	0	0	0	4.6	0	7.3	4.3
3SW	0	0	0	0	0	0	0	0	0
3PL	0	0	0	0	0	0	0	0	0
4VL	0	0	0	0	0	0	0	0	0
4VC	0	0	0	0	0	0	0	0	0
4IF	0	0	0	0	0	0	0	0	0
4SF	0	0	0	0	0	0	0	0	0
5CV	0	0	0	0	0	0	0	0	0
5CB	0	0	0	0	0	0	0	0	0
5C1	0	0	0	0	0	0	0	0	0
5C2	0	0	0	0	0	0	0	0	0

RUN DESIGNATION: TYPE 3 CYCLES ONLY, ARTIFICIALLY JUXTAPOSED

THICKNESS-OF-OVERLYING MATRIX --

	1SH	1BM	1GB	1UP	2H1	2H2	2H3	3BS	3HA	3SW
1SH	0	0	0	0	0	0	0	2	0	0
1BM	0	0	1.7	4	3	0	0	0	0	0
1GB	0	0	0	1.1	0	0	0	0	2.3	0
1UP	0	0	39.1	0	1.5	0	0	0	7.1	0
2H1	0	1.1	2.3	0	0	2	0	0	3.2	0
2H2	0	0	0	3.2	2.3	0	2.7	0	4.6	0
2H3	0	0	0	0	0	0	0	0	6.1	0
3BS	0	0	0	0	0	0	0	0	0	0
3HA	0	0	0	0	1.1	1.8	0	0	0	0
3SW	0	0	0	0	0	0	0	0	0	0
3FL	0	0	0	0	0	0	0	0	0	0
4VL	0	0	0	0	0	0	0	0	0	0
4VC	0	0	0	0	0	0	0	0	0	0
4IF	0	0	0	0	0	0	0	0	0	0
4SF	0	0	0	0	0	0	0	0	0	0
5CV	8.8	0	2.8	5.3	2.1	0	0	0	0	0
5CB	0	0	0	0	0	0	0	0	0	0
5C1	0	0	0	0	0	0	0	0	0	0
5C2	0	0	0	0	1.8	3.8	0	0	0	0

	3FL	4VL	4VC	4IF	4SF	5CV	5CB	5C1	5C2
1SH	0	0	0	0	0	0	0	0	0
1BM	0	0	0	0	0	0	0	0	0
1GB	0	0	0	0	0	0	0	0	0
1UP	0	0	0	0	0	0	0	0	0
2H1	0	0	0	0	0	0	0	0	0
2H2	0	0	0	0	0	0	0	0	0
2H3	0	0	0	0	0	0	0	0	0
3BS	0	0	0	0	0	0	0	0.7	0
3HA	0	0	0	0	0	0	0	0.4	2
3SW	0	0	0	0	0	0	0	0	0
3FL	0	0	0	0	0	0	0	0	0
4VL	0	0	0	0	0	0	0	0	0
4VC	0	0	0	0	0	0	0	0	0
4IF	0	0	0	0	0	0	0	0	0
4SF	0	0	0	0	0	0	0	0	0
5CV	0	0	0	0	0	0	0	0	0
5CB	0	0	0	0	0	0	0	0	0
5C1	0	0	0	0	0	0	0	0	0
5C2	0	0	0	0	0	0	0	0	0

RUN DESIGNATION: TYPE 3 CYCLES ONLY, ARTIFICIALLY JUXTAPOSED

TOTAL NUMBER OF FACIES TRANSITIONS OBSERVED: 81

OBSERVED TRANSITIONS --

	1SH	1BM	1GB	1UP	2M1	2M2	2M3	3BS	3MA	3SW
1SH	0	0	0	0	0	0	0	1	0	0
1BM	0	0	1	1	2	0	0	0	0	0
1GB	0	2	0	1	0	0	0	0	1	0
1UP	0	0	1	0	1	0	0	0	2	0
2M1	0	1	1	0	0	10	0	0	3	0
2M2	0	0	0	1	4	0	3	0	6	0
2M3	0	0	0	0	0	0	0	0	3	0
3BS	0	0	0	0	0	0	0	0	0	0
3MA	0	0	0	0	3	2	0	0	0	0
3SW	0	0	0	0	0	0	0	0	0	0
3PL	0	0	0	0	0	0	0	0	0	0
4VL	0	0	0	0	0	0	0	0	0	0
4VC	0	0	0	0	0	0	0	0	0	0
4IF	0	0	0	0	0	0	0	0	0	0
4SF	0	0	0	0	0	0	0	0	0	0
5CV	1	0	1	2	4	0	0	0	0	0
5CB	0	0	0	0	0	0	0	0	0	0
5C1	0	0	0	0	0	0	0	0	2	0
5C2	0	0	0	0	1	1	0	0	0	0

	3PL	4VL	4VC	4IF	4SF	5CV	5CB	5C1	5C2
1SH	0	0	0	0	0	0	0	0	0
1BM	0	0	0	0	0	0	0	0	0
1GB	0	0	0	0	0	0	0	0	0
1UP	0	0	0	0	0	0	0	0	0
2M1	0	0	0	0	0	1	0	0	0
2M2	0	0	0	0	0	0	0	0	0
2M3	0	0	0	0	0	0	0	0	0
3BS	0	0	0	0	0	0	0	1	0
3MA	0	0	0	0	0	0	0	3	3
3SW	0	0	0	0	0	0	0	0	0
3PL	0	0	0	0	0	0	0	0	0
4VL	0	0	0	0	0	0	0	0	0
4VC	0	0	0	0	0	0	0	0	0
4IF	0	0	0	0	0	0	0	0	0
4SF	0	0	0	0	0	0	0	0	0
5CV	0	0	0	0	0	0	0	0	0
5CB	0	0	0	0	0	0	0	0	0
5C1	0	0	0	0	0	0	0	0	0
5C2	0	0	0	0	0	0	0	0	0

RUN DESIGNATION: TYPE 3 CYCLES ONLY, ARTIFICIALLY JUXTAPOSED

OBSERVED TRANSITION PROBABILITY --

	1SH	1BM	1GB	1UP	2H1	2H2	2H3	3BS	3HA	3SW
1SH	0	0	0	0	0	0	0	1	0	0
1BM	0	0	0.25	0.25	0.5	0	0	0	0	0
1GB	0	0.5	0	0.25	0	0	0	0	0.25	0
1UP	0	0	0.25	0	0.25	0	0	0	0.5	0
2H1	0	0.06	0.06	0	0	0.56	0	0	0.28	0
2H2	0	0	0	0.07	0.29	0	0.21	0	0.43	0
2H3	0	0	0	0	0	0	0	0	1	0
3BS	0	0	0	0	0	0	0	0	0	0
3HA	0	0	0	0	0.15	0.1	0	0	0	0
3SW	0	0	0	0	0	0	0	0	0	0
3PL	0	0	0	0	0	0	0	0	0	0
4VL	0	0	0	0	0	0	0	0	0	0
4VC	0	0	0	0	0	0	0	0	0	0
4IF	0	0	0	0	0	0	0	0	0	0
4SF	0	0	0	0	0	0	0	0	0	0
5CV	0.13	0	0.13	0.25	0.5	0	0	0	0	0
5C3	0	0	0	0	0	0	0	0	0	0
5C1	0	0	0	0	0	0	0	0	1	0
5C2	0	0	0	0	0.5	0.5	0	0	0	0

	3PL	4VL	4VC	4IF	4SF	5CV	5C3	5C1	5C2
1SH	0	0	0	0	0	0	0	0	0
1BM	0	0	0	0	0	0	0	0	0
1GB	0	0	0	0	0	0	0	0	0
1UP	0	0	0	0	0	0	0	0	0
2H1	0	0	0	0	0	0.06	0	0	0
2H2	0	0	0	0	0	0	0	0	0
2H3	0	0	0	0	0	0	0	0	0
3BS	0	0	0	0	0	0	0	1	0
3HA	0	0	0	0	0	0.45	0	0.15	0.15
3SW	0	0	0	0	0	0	0	0	0
3PL	0	0	0	0	0	0	0	0	0
4VL	0	0	0	0	0	0	0	0	0
4VC	0	0	0	0	0	0	0	0	0
4IF	0	0	0	0	0	0	0	0	0
4SF	0	0	0	0	0	0	0	0	0
5CV	0	0	0	0	0	0	0	0	0
5C3	0	0	0	0	0	0	0	0	0
5C1	0	0	0	0	0	0	0	0	0
5C2	0	0	0	0	0	0	0	0	0

RUN DESIGNATION: TYPE 3 CYCLES ONLY, ARTIFICIALLY JUXTAPOSED

EXPECTED (RANDOM) TRANSITIONS --

	1SH	1BM	1GB	1UP	2H1	2H2	2H3	3BS	3HA	3SW
1SH	0	0.032	0.043	0.054	0.282	0.163	0.032	0.81	0.274	0
1BM	0.043	0	0.177	0.222	0.827	0.665	0.131	0.043	1.12	0
1GB	0.043	0.134	0	0.224	0.837	0.673	0.133	0.043	1.13	0
1UP	0.044	0.136	0.181	0	0.846	0.68	0.134	0.044	1.15	0
2H1	0.253	0.724	0.965	1.21	0	3.62	0.716	0.253	6.11	0
2H2	0.173	0.537	0.716	0.895	3.34	0	0.531	0.173	4.53	0
2H3	0.032	0.1	0.133	0.166	0.62	0.499	0	0.032	0.841	0
3BS	0.81	0.032	0.043	0.054	0.282	0.163	0.032	0	0.274	0
3HA	0.284	0.881	1.18	1.47	5.49	4.41	0.872	0.284	0	0
3SW	0	0	0	0	0	0	0	0	0	0
3PL	0	0	0	0	0	0	0	0	0	0
4VL	0	0	0	0	0	0	0	0	0	0
4VC	0	0	0	0	0	0	0	0	0	0
4IF	0	0	0	0	0	0	0	0	0	0
4SF	0	0	0	0	0	0	0	0	0	0
3CV	0.094	0.29	0.387	0.484	1.81	1.45	0.287	0.094	2.45	0
3CB	0	0	0	0	0	0	0	0	0	0
3C1	0.022	0.067	0.09	0.112	0.418	0.336	0.066	0.022	0.566	0
3C2	0.021	0.066	0.089	0.111	0.413	0.332	0.066	0.021	0.56	0

	3PL	4VL	4VC	4IF	4SF	3CV	3CB	3C1	3C2
1SH	0	0	0	0	0	0.114	0	0.042	0.032
1BM	0	0	0	0	0	0.467	0	0.173	0.13
1GB	0	0	0	0	0	0.473	0	0.175	0.131
1UP	0	0	0	0	0	0.478	0	0.177	0.133
2H1	0	0	0	0	0	2.55	0	0.944	0.708
2H2	0	0	0	0	0	1.89	0	0.7	0.525
2H3	0	0	0	0	0	0.35	0	0.13	0.097
3BS	0	0	0	0	0	0.114	0	0.042	0.032
3HA	0	0	0	0	0	3.1	0	1.15	0.862
3SW	0	0	0	0	0	0	0	0	0
3PL	0	0	0	0	0	0	0	0	0
4VL	0	0	0	0	0	0	0	0	0
4VC	0	0	0	0	0	0	0	0	0
4IF	0	0	0	0	0	0	0	0	0
4SF	0	0	0	0	0	0	0	0	0
3CV	0	0	0	0	0	0	0	0.378	0.284
3CB	0	0	0	0	0	0	0	0	0
3C1	0	0	0	0	0	0.236	0	0	0.066
3C2	0	0	0	0	0	0.234	0	0.087	0

RUN DESIGNATION: TYPE I CYCLES ONLY, ARTIFICIALLY JUXTAPOSED

EXPECTED (RANDOM) TRANSITION PROBABILITY --

	1SH	1BM	1GB	1UP	2H1	2H2	2H3	3BS	3HA	3SW
1SH	0	0.03	0.04	0.03	0.2	0.16	0.03	0.01	0.27	0
1BM	0.01	0	0.04	0.06	0.24	0.17	0.03	0.01	0.28	0
1GB	0.01	0.03	0	0.06	0.21	0.17	0.03	0.01	0.28	0
1UP	0.01	0.03	0.03	0	0.21	0.17	0.03	0.01	0.29	0
2H1	0.01	0.04	0.03	0.07	0	0.12	0.04	0.01	0.34	0
2H2	0.01	0.04	0.03	0.06	0.24	0	0.04	0.01	0.32	0
2H3	0.01	0.03	0.04	0.06	0.21	0.17	0	0.01	0.28	0
3BS	0.01	0.03	0.04	0.03	0.2	0.16	0.03	0	0.27	0
3HA	0.01	0.04	0.06	0.07	0.27	0.22	0.04	0.01	0	0
3SW	0	0	0	0	0	0	0	0	0	0
3PL	0	0	0	0	0	0	0	0	0	0
4VL	0	0	0	0	0	0	0	0	0	0
4VC	0	0	0	0	0	0	0	0	0	0
4IF	0	0	0	0	0	0	0	0	0	0
4SF	0	0	0	0	0	0	0	0	0	0
5CV	0.01	0.04	0.03	0.06	0.23	0.18	0.04	0.01	0.31	0
5CB	0	0	0	0	0	0	0	0	0	0
5C1	0.01	0.03	0.04	0.06	0.21	0.17	0.03	0.01	0.28	0
5C2	0.01	0.03	0.04	0.06	0.21	0.17	0.03	0.01	0.28	0

	3PL	4VL	4VC	4IF	4SF	5CV	5CB	5C1	5C2
1SH	0	0	0	0	0	0.11	0	0.04	0.03
1BM	0	0	0	0	0	0.12	0	0.04	0.03
1GB	0	0	0	0	0	0.12	0	0.04	0.03
1UP	0	0	0	0	0	0.12	0	0.04	0.03
2H1	0	0	0	0	0	0.14	0	0.03	0.04
2H2	0	0	0	0	0	0.13	0	0.03	0.04
2H3	0	0	0	0	0	0.12	0	0.04	0.03
3BS	0	0	0	0	0	0.11	0	0.04	0.03
3HA	0	0	0	0	0	0.16	0	0.06	0.04
3SW	0	0	0	0	0	0	0	0	0
3PL	0	0	0	0	0	0	0	0	0
4VL	0	0	0	0	0	0	0	0	0
4VC	0	0	0	0	0	0	0	0	0
4IF	0	0	0	0	0	0	0	0	0
4SF	0	0	0	0	0	0	0	0	0
5CV	0	0	0	0	0	0	0	0.05	0.04
5CB	0	0	0	0	0	0	0	0	0
5C1	0	0	0	0	0	0.12	0	0	0.03
5C2	0	0	0	0	0	0.12	0	0.04	0

RUN DESIGNATION: TYPE I CYCLES ONLY, ARTIFICIALLY JUXTAPOSED

OBSERVED MINUS RANDOM PROBABILITY --

	1SH	1BM	1OB	1UP	2H1	2H2	2H3	3BS	3HA	3SW
1SH	0	-0.03	-0.04	-0.05	-0.2	-0.16	-0.03	0.99	-0.27	0
1BM	-0.01	0	0.21	0.19	0.29	-0.17	-0.03	-0.01	-0.28	0
1OB	-0.01	0.47	0	0.19	-0.21	-0.17	-0.03	-0.01	-0.03	0
1UP	-0.01	-0.03	0.2	0	0.34	-0.17	-0.03	-0.01	0.21	0
2H1	-0.01	0.02	0.01	-0.07	0	0.36	-0.04	-0.01	-0.06	0
2H2	-0.01	-0.04	-0.05	0.01	0.05	0	0.17	-0.01	0.11	0
2H3	-0.01	-0.03	-0.04	-0.06	-0.21	-0.17	0	-0.01	0.72	0
3BS	-0.01	-0.03	-0.04	-0.05	-0.2	-0.16	-0.03	0	-0.27	0
3HA	-0.01	-0.04	-0.06	-0.07	-0.12	-0.12	-0.04	-0.01	0	0
3SW	0	0	0	0	0	0	0	0	0	0
3PL	0	0	0	0	0	0	0	0	0	0
4VL	0	0	0	0	0	0	0	0	0	0
4VC	0	0	0	0	0	0	0	0	0	0
4IF	0	0	0	0	0	0	0	0	0	0
4SF	0	0	0	0	0	0	0	0	0	0
5CV	0.12	-0.04	0.08	0.19	0.27	-0.18	-0.04	-0.01	-0.31	0
5CB	0	0	0	0	0	0	0	0	0	0
5C1	-0.01	-0.03	-0.04	-0.06	-0.21	-0.17	-0.03	-0.01	0.72	0
5C2	-0.01	-0.03	-0.04	-0.06	0.29	0.33	-0.03	-0.01	-0.28	0

	3PL	4VL	4VC	4IF	4SF	5CV	5CB	5C1	5C2
1SH	0	0	0	0	0	-0.11	0	-0.04	-0.03
1BM	0	0	0	0	0	-0.12	0	-0.04	-0.03
1OB	0	0	0	0	0	-0.12	0	-0.04	-0.03
1UP	0	0	0	0	0	-0.12	0	-0.04	-0.03
2H1	0	0	0	0	0	-0.08	0	-0.05	-0.04
2H2	0	0	0	0	0	-0.13	0	-0.05	-0.04
2H3	0	0	0	0	0	-0.12	0	-0.04	-0.03
3BS	0	0	0	0	0	-0.11	0	0.96	-0.03
3HA	0	0	0	0	0	0.29	0	0.09	0.11
3SW	0	0	0	0	0	0	0	0	0
3PL	0	0	0	0	0	0	0	0	0
4VL	0	0	0	0	0	0	0	0	0
4VC	0	0	0	0	0	0	0	0	0
4IF	0	0	0	0	0	0	0	0	0
4SF	0	0	0	0	0	0	0	0	0
5CV	0	0	0	0	0	0	0	-0.03	-0.04
5CB	0	0	0	0	0	0	0	0	0
5C1	0	0	0	0	0	-0.12	0	0	-0.03
5C2	0	0	0	0	0	-0.12	0	-0.04	0

RUN DESIGNATION: TYPE 3 CYCLES ONLY, ARTIFICIALLY JUXTAPOSED

SIGNIFICANCE TEST VALUES --

	1SH	1BM	1OB	1UP	2H1	2H2	2H3	3BS	3HA	3SW
1SH	83	33	33	38	88	33	38	0.01	38	33
1BM	38	33	0.15	0.22	0.2	33	33	38	33	88
1OB	88	0.31	33	0.22	38	33	83	38	38	38
1UP	83	38	0.19	83	0.31	33	83	33	0.33	33
2H1	38	0.52	0.5	38	38	0	33	38	88	38
2H2	33	83	33	0.38	0.44	38	0.32	33	0.23	38
2H3	38	38	38	38	38	38	88	88	0.02	33
3BS	33	38	88	33	88	33	33	38	38	38
3HA	88	88	88	88	88	38	88	38	88	38
3SW	33	33	88	33	33	83	38	38	88	88
3PL	38	88	38	38	38	38	88	38	38	33
4VL	33	38	38	83	38	38	88	38	38	38
4VC	38	88	38	88	88	38	38	38	38	88
4IF	83	33	83	88	33	38	38	38	38	38
4SF	88	88	38	38	88	33	38	88	88	38
5CV	0.03	33	0.04	0.03	0.09	38	33	98	88	98
5CB	38	38	38	88	88	33	83	88	88	33
5C1	83	33	38	38	38	88	38	88	0.08	33
5C2	88	38	38	38	0.38	0.31	38	88	38	38

	3PL	4VL	4VC	4IF	4SF4	5CV	5CB	5C1	5C2
1SH	88	80	83	88	88	38	88	38	38
1BM	38	83	88	33	38	38	33	88	38
1OB	38	88	88	88	38	88	38	83	38
1UP	38	38	88	38	38	98	38	33	88
2H1	33	83	88	38	38	33	33	38	33
2H2	83	33	38	88	38	83	88	38	38
2H3	88	38	28	88	38	38	38	38	33
3BS	88	83	38	88	83	88	88	0.04	88
3HA	38	38	33	88	38	0	88	0.11	0.04
3SW	38	33	38	98	38	38	83	38	88
3PL	38	38	88	88	38	88	38	33	33
4VL	38	38	38	38	38	38	38	38	38
4VC	88	38	28	88	38	38	38	38	38
4IF	33	38	38	33	33	38	38	38	33
4SF	88	38	33	38	88	38	88	88	38
5CV	83	88	38	88	33	88	88	83	88
5CB	38	38	38	38	38	38	33	38	38
5C1	83	38	88	88	83	38	38	38	38
5C2	88	88	88	38	38	38	38	33	33

RUN DESIGNATION: TYPE 3 CYCLES ONLY, ARTIFICIALLY JUXTAPOSED

TOTAL NUMBER OF FACIES TRANSITIONS OBSERVED: 41

VALUES OF PARAMETER F --

	1SH	1SM	1GS	1UP	2M1	2M2	2MC	2BS	2HA	2SW
1SH	38	38	38	38	30	83	86	-0.02	38	38
1SM	38	33	-0.02	-0.02	-0.01	33	83	88	88	88
1GS	83	-0.01	33	-0.02	32	83	88	38	-0.02	86
1UP	33	33	-0.02	33	-0.02	38	83	38	-0.01	33
2M1	38	-0.02	-0.02	38	38	0.09	86	88	0.03	38
2M2	33	32	38	-0.02	0.02	38	0.01	88	0.04	85
2MC	38	38	88	38	38	36	33	33	0.01	38
2BS	33	38	38	83	88	38	83	33	88	88
2HA	38	88	86	38	0.01	-0.01	88	83	83	38
2SW	83	38	83	38	33	88	33	38	83	33
3PL	38	32	33	38	86	33	88	38	33	38
4VL	38	33	33	33	38	83	33	33	38	83
4VC	38	88	33	88	38	38	38	38	38	38
4IF	83	88	83	33	38	33	33	33	88	38
4SF	38	88	38	83	88	33	38	86	33	38
5CV	-0.02	86	-0.02	-0.01	0.02	88	88	88	38	88
5C3	33	88	38	88	86	38	38	88	88	33
5C1	38	88	88	86	83	28	36	38	-0.01	33
5C2	38	38	83	38	-0.02	-0.02	38	33	33	38

	3PL	4VL	4VC	4IF	4SF	5CV	5C3	5C1	5C2
1SH	88	83	83	83	38	33	36	38	38
1SM	38	86	83	88	33	88	38	38	38
1GS	38	85	88	33	28	86	38	38	38
1UP	38	33	33	88	38	33	38	38	38
2M1	38	38	38	38	38	-0.02	88	38	38
2M2	33	38	38	38	38	33	88	38	38
2MC	88	83	38	88	33	88	38	38	83
2BS	38	38	88	33	33	38	38	-0.02	38
2HA	38	38	88	38	38	0.08	38	0.01	0.01
2SW	38	38	38	38	38	38	38	38	38
3PL	38	88	38	38	38	88	38	38	38
4VL	38	38	38	38	38	38	38	38	38
4VC	38	88	38	88	88	38	38	38	38
4IF	38	88	88	88	38	38	38	88	38
4SF	38	88	88	88	38	38	38	88	38
5CV	38	88	38	38	38	38	88	88	38
5C3	88	38	38	38	38	88	88	38	38
5C1	38	38	38	88	38	88	38	38	38
5C2	38	38	38	38	38	38	38	38	38

RUN DESIGNATION: TYPE 4 CYCLES ONLY, ARTIFICIALLY JUXTAPOSED

FACIES DATA --

FACIES	# OCCUR	MEAN THICKNESS (RANGE) IN METERS
1SH	0	0 (0 to 0)
1BM	17	4.5 (1 to 12)
1GS	38	7.6 (1 to 27.1)
1UP	28	4.5 (1.8 to 10)
2M1	39	2.4 (0.5 to 8.2)
2M2	28	2.9 (0.4 to 11.1)
2M3	11	2 (1 to 3)
3BS	4	1.8 (1.1 to 2.9)
3HA	0	0 (0 to 0)
3SW	0	0 (0 to 0)
3PL	0	0 (0 to 0)
4VL	0	0 (0 to 0)
4VC	0	0 (0 to 0)
4IF	0	0 (0 to 0)
4SF	0	0 (0 to 0)
5CV	0	0 (0 to 0)
5CS	2	2.7 (2.4 to 3)
5C1	1	0.8 (0.8 to 0.8)
5C2	5	2.1 (1 to 4)

TOTAL NUMBER OF FACIES OCCURRENCES: 164

RUN DESIGNATION: TYPE 4 CYCLES ONLY, ARTIFICIALLY JUXTAPOSED

THICKNESS-OF-UNDERLYING MATRIX --

	1SM	1BM	1GB	1UP	2M1	2M2	2M3	3BS	3MA	3SW
1SM	0	0	0	0	0	0	0	0	0	0
1BM	0	0	5	5.1	5.4	4.1	0	2.4	0	0
1GB	0	11.4	0	6.2	9.1	7.4	0	0	0	0
1UP	0	5.2	4.8	0	4.4	2.1	0	0	0	0
2M1	0	0	1.7	1.6	0	3	0	0.9	0	0
2M2	0	2	2	3.6	2.4	0	3	0	0	0
2M3	0	3	1.9	0	1.3	1.7	0	0	0	0
3BS	0	2	0	0	1.4	1.6	0	0	0	0
3MA	0	0	0	0	0	0	0	0	0	0
3SW	0	0	0	0	0	0	0	0	0	0
3PL	0	0	0	0	0	0	0	0	0	0
4VL	0	0	0	0	0	0	0	0	0	0
4VC	0	0	0	0	0	0	0	0	0	0
4IF	0	0	0	0	0	0	0	0	0	0
4SF	0	0	0	0	0	0	0	0	0	0
5CV	0	0	0	0	0	0	0	0	0	0
5CB	0	0	0	0	0	0	0	0	0	0
5C1	0	0	0.8	0	0	0	0	0	0	0
5C2	0	1.6	1.1	3	0	0	0	0	0	0

	3PL	4VL	4VC	4IF	4SF	5CV	5CB	5C1	5C2
1SM	0	0	0	0	0	0	0	0	0
1BM	0	0	0	0	0	0	0	0	0
1GB	0	0	0	0	0	0	0	0	0
1UP	0	0	0	0	0	0	0	0	0
2M1	0	0	0	0	0	2.1	7	0	1.1
2M2	0	0	0	0	0	2.7	0	0	4.9
2M3	0	0	0	0	0	2.2	0	0	0
3BS	0	0	0	0	0	0	0	0	0
3MA	0	0	0	0	0	0	0	0	0
3SW	0	0	0	0	0	0	0	0	0
3PL	0	0	0	0	0	0	0	0	0
4VL	0	0	0	0	0	0	0	0	0
4VC	0	0	0	0	0	0	0	0	0
4IF	0	0	0	0	0	0	0	0	0
4SF	0	0	0	0	0	0	0	0	0
5CV	0	0	0	0	0	0	0	0	0
5CB	0	0	0	0	0	0	0	2.4	3
5C1	0	0	0	0	0	0	0	0	0
5C2	0	0	0	0	0	0	0	0	0

RUN DESIGNATION: TYPE 4 CYCLES ONLY, ARTIFICIALLY JUXTAPOSED

THICKNESS-OF-OVERLYING MATRIX --

	1SH	1BM	1CB	1UP	2HI	2HZ	2HS	3BS	3HA	3SW
1SH	0	0	0	0	0	0	0	0	0	0
1BM	0	0	4.9	3.6	1.8	2	0	1.5	0	0
1CB	0	6.3	0	4.2	3.1	1.9	0	0	0	0
1UP	0	3.4	4.4	0	2.7	3	0	0	0	0
2HI	0	0	9.4	3.8	0	3.3	0	2	0	0
2HZ	0	5.9	11.1	5.4	5.9	0	2	0	0	0
2HS	0	12	2.2	0	1.6	4.1	0	0	0	0
3BS	0	1.1	0	0	0.8	1.2	0	0	0	0
3HA	0	0	0	0	0	0	0	0	0	0
3SW	0	0	0	0	0	0	0	0	0	0
3PL	0	0	0	0	0	0	0	0	0	0
4VL	0	0	0	0	0	0	0	0	0	0
4VC	0	0	0	0	0	0	0	0	0	0
4IF	0	0	0	0	0	0	0	0	0	0
4SF	0	0	0	0	0	0	0	0	0	0
5CV	0	0	4	2.5	2.9	0	0	0	0	0
5CB	0	0	0	0	0	0	0	0	0	0
5C1	0	0	24.4	0	0	0	0	0	0	0
5C2	0	4.7	7.8	9.5	0	0	0	0	0	0

	3PL	4VL	4VC	4IF	4SF	5CV	5CB	5C1	5C2
1SH	0	0	0	0	0	0	0	0	0
1BM	0	0	0	0	0	0	0	0	0
1CB	0	0	0	0	0	0	0	0	0
1UP	0	0	0	0	0	0	0	0	0
2HI	0	0	0	0	0	0	3	0	1
2HZ	0	0	0	0	0	0	0	0	2.2
2HS	0	0	0	0	0	0	0	0	0
3BS	0	0	0	0	0	0	0	0	0
3HA	0	0	0	0	0	0	0	0	0
3SW	0	0	0	0	0	0	0	0	0
3PL	0	0	0	0	0	0	0	0	0
4VL	0	0	0	0	0	0	0	0	0
4VC	0	0	0	0	0	0	0	0	0
4IF	0	0	0	0	0	0	0	0	0
4SF	0	0	0	0	0	0	0	0	0
5CV	0	0	0	0	0	0	2.4	0	0
5CB	0	0	0	0	0	0	0	0.8	3
5C1	0	0	0	0	0	0	0	0	0
5C2	0	0	0	0	0	0	0	0	0

RUN DESIGNATION: TYPE 4 CYCLES ONLY, ARTIFICIALLY JUXTAPOSED

TOTAL NUMBER OF FACIES TRANSITIONS OBSERVED: 158

OBSERVED TRANSITIONS --

	1SH	1BM	1GB	1UP	2H1	2H2	2H3	3BS	3HA	3SW
1SH	0	0	0	0	0	0	0	0	0	0
1BM	0	0	4	4	5	1	0	2	0	0
1GB	0	4	0	6	11	3	0	0	0	0
1UP	0	3	2	0	14	1	0	0	0	0
2H1	0	0	3	3	0	18	0	2	0	0
2H2	0	2	4	2	2	0	11	0	0	0
2H3	0	1	2	0	3	2	0	0	0	0
3BS	0	2	0	0	1	1	0	0	0	0
3HA	0	0	0	0	0	0	0	0	0	0
3SW	0	0	0	0	0	0	0	0	0	0
3PL	0	0	0	0	0	0	0	0	0	0
4VL	0	0	0	0	0	0	0	0	0	0
4VC	0	0	0	0	0	0	0	0	0	0
4IF	0	0	0	0	0	0	0	0	0	0
4SF	0	0	0	0	0	0	0	0	0	0
5CV	0	0	4	1	2	0	0	0	0	0
5CB	0	0	0	0	0	0	0	0	0	0
5C1	0	0	1	0	0	0	0	0	0	0
5C2	0	1	2	1	0	0	0	0	0	0

	3PL	4VL	4VC	4IF	4SF	5CV	5CB	5C1	5C2
1SH	0	0	0	0	0	0	0	0	0
1BM	0	0	0	0	0	0	0	0	0
1GB	0	0	0	0	0	0	0	0	0
1UP	0	0	0	0	0	0	0	0	0
2H1	0	0	0	0	0	4	1	0	1
2H2	0	0	0	0	0	2	0	0	3
2H3	0	0	0	0	0	2	0	0	0
3BS	0	0	0	0	0	0	0	0	0
3HA	0	0	0	0	0	0	0	0	0
3SW	0	0	0	0	0	0	0	0	0
3PL	0	0	0	0	0	0	0	0	0
4VL	0	0	0	0	0	0	0	0	0
4VC	0	0	0	0	0	0	0	0	0
4IF	0	0	0	0	0	0	0	0	0
4SF	0	0	0	0	0	0	0	0	0
5CV	0	0	0	0	0	0	1	0	0
5CB	0	0	0	0	0	0	0	1	1
5C1	0	0	0	0	0	0	0	0	0
5C2	0	0	0	0	0	1	0	0	0

RUN DESIGNATION: TYPE 4 CYCLES ONLY, ARTIFICIALLY JUXTAPOSED

OBSERVED TRANSITION PROBABILITY --

	1SH	1BM	1GB	1UP	2M1	2M2	2M3	3BS	3HA	3SW
1SH	0	0	0	0	0	0	0	0	0	0
1BM	0	0	0.25	0.25	0.31	0.06	0	0.13	0	0
1GB	0	0.17	0	0.25	0.46	0.13	0	0	0	0
1UP	0	0.15	0.1	0	0.7	0.05	0	0	0	0
2M1	0	0	0.15	0.09	0	0.33	0	0.06	0	0
2M2	0	0.08	0.15	0.08	0.08	0	0.42	0	0	0
2M3	0	0.1	0.2	0	0.3	0.2	0	0	0	0
3BS	0	0.5	0	0	0.25	0.25	0	0	0	0
3HA	0	0	0	0	0	0	0	0	0	0
3SW	0	0	0	0	0	0	0	0	0	0
3PL	0	0	0	0	0	0	0	0	0	0
4VL	0	0	0	0	0	0	0	0	0	0
4VC	0	0	0	0	0	0	0	0	0	0
4IF	0	0	0	0	0	0	0	0	0	0
4SF	0	0	0	0	0	0	0	0	0	0
5CV	0	0	0.5	0.13	0.25	0	0	0	0	0
5C3	0	0	0	0	0	0	0	0	0	0
5C1	0	0	1	0	0	0	0	0	0	0
5C2	0	0.2	0.4	0.2	0	0	0	0	0	0

	3PL	4VL	4VC	4IF	4SF	5CV	5C3	5C1	5C2
1SH	0	0	0	0	0	0	0	0	0
1BM	0	0	0	0	0	0	0	0	0
1GB	0	0	0	0	0	0	0	0	0
1UP	0	0	0	0	0	0	0	0	0
2M1	0	0	0	0	0	0.12	0.03	0	0.03
2M2	0	0	0	0	0	0.08	0	0	0.12
2M3	0	0	0	0	0	0.2	0	0	0
3BS	0	0	0	0	0	0	0	0	0
3HA	0	0	0	0	0	0	0	0	0
3SW	0	0	0	0	0	0	0	0	0
3PL	0	0	0	0	0	0	0	0	0
4VL	0	0	0	0	0	0	0	0	0
4VC	0	0	0	0	0	0	0	0	0
4IF	0	0	0	0	0	0	0	0	0
4SF	0	0	0	0	0	0	0	0	0
5CV	0	0	0	0	0	0	0.13	0	0
5C3	0	0	0	0	0	0	0	0.5	0.5
5C1	0	0	0	0	0	0	0	0	0
5C2	0	0	0	0	0	0.2	0	0	0

RUN DESIGNATION: TYPE 4 CYCLES ONLY, ARTIFICIALLY JUXTAPOSED

EXPECTED (RANDOM) TRANSITIONS --

	1SH	1BM	1GB	1UP	2H1	2H2	2H3	3BS	3HA	3SW
1SH	0	0	0	0	0	0	0	0	0	0
1BM	0	0	2.77	1.89	5.03	3.86	1.14	0.397	0	0
1GB	0	2.29	0	3.1	8.26	5.03	1.86	0.652	0	0
1UP	0	1.8	3.57	0	6.49	3.95	1.46	0.512	0	0
2H1	0	3.84	7.62	5.19	0	8.42	3.12	1.09	0	0
2H2	0	2.54	5.03	3.42	9.13	0	2.06	0.721	0	0
2H3	0	0.86	1.7	1.16	3.1	1.88	0	0.244	0	0
3BS	0	0.329	0.652	0.444	1.18	0.721	0.267	0	0	0
3HA	0	0	0	0	0	0	0	0	0	0
3SW	0	0	0	0	0	0	0	0	0	0
3PL	0	0	0	0	0	0	0	0	0	0
4VL	0	0	0	0	0	0	0	0	0	0
4VC	0	0	0	0	0	0	0	0	0	0
4IF	0	0	0	0	0	0	0	0	0	0
4SF	0	0	0	0	0	0	0	0	0	0
5CV	0	0.679	1.35	0.916	2.44	1.49	0.551	0.193	0	0
5CB	0	0.163	0.322	0.219	0.585	0.356	0.132	0.046	0	0
5C1	0	0.681	0.16	0.109	0.291	0.177	0.066	0.023	0	0
5C2	0	0.414	0.82	0.558	1.49	0.987	0.336	0.118	0	0

	3PL	4VL	4VC	4IF	4SF	5CV	5CB	5C1	5C2
1SH	0	0	0	0	0	0	0	0	0
1BM	0	0	0	0	0	0.917	0.196	0.098	0.5
1GB	0	0	0	0	0	1.5	0.322	0.16	0.82
1UP	0	0	0	0	0	1.18	0.253	0.126	0.644
2H1	0	0	0	0	0	2.52	0.54	0.268	1.37
2H2	0	0	0	0	0	1.66	0.356	0.177	0.907
2H3	0	0	0	0	0	0.564	0.121	0.06	0.307
3BS	0	0	0	0	0	0.216	0.046	0.023	0.118
3HA	0	0	0	0	0	0	0	0	0
3SW	0	0	0	0	0	0	0	0	0
3PL	0	0	0	0	0	0	0	0	0
4VL	0	0	0	0	0	0	0	0	0
4VC	0	0	0	0	0	0	0	0	0
4IF	0	0	0	0	0	0	0	0	0
4SF	0	0	0	0	0	0	0	0	0
5CV	0	0	0	0	0	0	0.095	0.047	0.243
5CB	0	0	0	0	0	0.187	0	0.011	0.058
5C1	0	0	0	0	0	0.053	0.011	0	0.029
5C2	0	0	0	0	0	0.271	0.058	0.029	0

RUN DESIGNATION: TYPE 4 CYCLES ONLY, ARTIFICIALLY JUXTAPOSED

EXPECTED (RANDOM) TRANSITION PROBABILITY --

	1SH	1BM	1GB	1UP	2H1	2H2	2H3	3BS	3HA	3SW
1SH	0	0	0	0	0	0	0	0	0	0
1BM	0	0	0.17	0.12	0.31	0.19	0.07	0.02	0	0
1GB	0	0.1	0	0.13	0.34	0.21	0.08	0.03	0	0
1UP	0	0.09	0.18	0	0.32	0.2	0.07	0.03	0	0
2H1	0	0.11	0.22	0.15	0	0.25	0.09	0.03	0	0
2H2	0	0.1	0.19	0.13	0.33	0	0.08	0.03	0	0
2H3	0	0.09	0.17	0.12	0.31	0.19	0	0.02	0	0
3BS	0	0.08	0.16	0.11	0.3	0.18	0.07	0	0	0
3HA	0	0	0	0	0	0	0	0	0	0
3SW	0	0	0	0	0	0	0	0	0	0
3PL	0	0	0	0	0	0	0	0	0	0
4VL	0	0	0	0	0	0	0	0	0	0
4VC	0	0	0	0	0	0	0	0	0	0
4IF	0	0	0	0	0	0	0	0	0	0
4SF	0	0	0	0	0	0	0	0	0	0
5CV	0	0.08	0.17	0.11	0.3	0.19	0.07	0.02	0	0
5CB	0	0.08	0.16	0.11	0.29	0.18	0.07	0.02	0	0
5C1	0	0.08	0.16	0.11	0.29	0.18	0.07	0.02	0	0
5C2	0	0.08	0.16	0.11	0.3	0.18	0.07	0.02	0	0

	3PL	4VL	4VC	4IF	4SF	5CV	5CB	5C1	5C2
1SH	0	0	0	0	0	0	0	0	0
1BM	0	0	0	0	0	0.06	0.01	0.01	0.03
1GB	0	0	0	0	0	0.06	0.01	0.01	0.03
1UP	0	0	0	0	0	0.06	0.01	0.01	0.03
2H1	0	0	0	0	0	0.07	0.02	0.01	0.04
2H2	0	0	0	0	0	0.06	0.01	0.01	0.03
2H3	0	0	0	0	0	0.06	0.01	0.01	0.03
3BS	0	0	0	0	0	0.05	0.01	0.01	0.03
3HA	0	0	0	0	0	0	0	0	0
3SW	0	0	0	0	0	0	0	0	0
3PL	0	0	0	0	0	0	0	0	0
4VL	0	0	0	0	0	0	0	0	0
4VC	0	0	0	0	0	0	0	0	0
4IF	0	0	0	0	0	0	0	0	0
4SF	0	0	0	0	0	0	0	0	0
5CV	0	0	0	0	0	0	0.01	0.01	0.03
5CB	0	0	0	0	0	0.05	0	0.01	0.03
5C1	0	0	0	0	0	0.05	0.01	0	0.03
5C2	0	0	0	0	0	0.05	0.01	0.01	0

RUN DESIGNATION: TYPE 4 CYCLES ONLY, ARTIFICIALLY JUXTAPOSED

OBSERVED MINUS RANDOM PROBABILITY --

	1SH	1BM	1GB	1UP	2M1	2M2	2M3	3BS	3HA	3SW
1SH	0	0	0	0	0	0	0	0	0	0
1BM	0	0	0.08	0.13	0	-0.13	-0.07	0.11	0	0
1GB	0	0.07	0	0.12	0.12	-0.08	-0.08	-0.03	0	0
1UP	0	0.06	-0.06	0	0.28	-0.15	-0.07	-0.03	0	0
2M1	0	-0.11	-0.07	-0.06	0	0.28	-0.09	0.03	0	0
2M2	0	-0.02	-0.04	-0.03	-0.27	0	0.24	-0.03	0	0
2M3	0	0.01	0.03	-0.12	-0.01	0.01	0	-0.02	0	0
3BS	0	0.42	-0.16	-0.11	-0.03	0.07	-0.07	0	0	0
3HA	0	0	0	0	0	0	0	0	0	0
3SW	0	0	0	0	0	0	0	0	0	0
3PL	0	0	0	0	0	0	0	0	0	0
4VL	0	0	0	0	0	0	0	0	0	0
4VC	0	0	0	0	0	0	0	0	0	0
4IF	0	0	0	0	0	0	0	0	0	0
4SF	0	0	0	0	0	0	0	0	0	0
5CV	0	-0.08	0.33	0.02	-0.03	-0.19	-0.07	-0.02	0	0
5CB	0	-0.08	-0.14	-0.11	-0.29	-0.18	-0.07	-0.02	0	0
5C1	0	-0.08	0.04	-0.11	-0.29	-0.18	-0.07	-0.02	0	0
5C2	0	0.12	0.24	0.09	-0.3	-0.18	-0.07	-0.02	0	0

	3PL	4VL	4VC	4IF	4SF	5CV	5CB	5C1	5C2
1SH	0	0	0	0	0	0	0	0	0
1BM	0	0	0	0	0	-0.06	-0.01	-0.01	-0.03
1GB	0	0	0	0	0	-0.06	-0.01	-0.01	-0.03
1UP	0	0	0	0	0	-0.06	-0.01	-0.01	-0.03
2M1	0	0	0	0	0	0.03	0.01	-0.01	-0.01
2M2	0	0	0	0	0	0.02	-0.01	-0.01	0.09
2M3	0	0	0	0	0	0.14	-0.01	-0.01	-0.03
3BS	0	0	0	0	0	-0.03	-0.01	-0.01	-0.03
3HA	0	0	0	0	0	0	0	0	0
3SW	0	0	0	0	0	0	0	0	0
3PL	0	0	0	0	0	0	0	0	0
4VL	0	0	0	0	0	0	0	0	0
4VC	0	0	0	0	0	0	0	0	0
4IF	0	0	0	0	0	0	0	0	0
4SF	0	0	0	0	0	0	0	0	0
5CV	0	0	0	0	0	0	0.12	-0.01	-0.03
5CB	0	0	0	0	0	-0.03	0	0.49	0.47
5C1	0	0	0	0	0	-0.03	-0.01	0	-0.03
5C2	0	0	0	0	0	0.15	-0.01	-0.01	0

RUN DESIGNATION: TYPE 4 CYCLES ONLY, ARTIFICIALLY JUXTAPOSED

SIGNIFICANCE TEST VALUES --

	1SH	1BM	1GB	1UP	2H1	2H2	2H3	3BS	3HA	3SW
1SH	88	38	38	88	88	38	33	88	33	33
1BM	38	88	0.23	0.12	83	88	88	0.34	38	33
1GB	38	0.21	38	0.08	0.16	88	38	38	38	33
1UP	33	0.27	38	38	0	33	33	88	38	88
2H1	88	38	88	88	38	0	33	0.27	88	33
2H2	38	88	88	83	38	88	0	33	38	88
2H3	88	0.61	0.33	38	38	0.5*	33	88	38	38
3BS	33	0.83	38	83	33	0.33	38	38	38	83
3HA	38	38	38	88	38	33	38	38	28	38
3SW	88	33	88	33	33	88	28	38	38	88
3PL	38	38	38	38	38	38	38	38	38	38
4VL	33	83	38	83	28	33	38	88	88	88
4VC	88	88	83	38	88	38	88	88	88	38
4IF	88	38	38	88	88	88	88	38	88	38
4SF	88	38	88	38	88	38	88	38	38	38
5CV	83	38	0.83	0.61	83	33	38	38	38	88
5CB	38	88	38	38	83	38	38	38	88	38
5C1	38	38	0.16	83	38	88	83	38	38	38
5C2	33	0.34	0.13	0.44	38	38	88	38	38	38

	3PL	4VL	4VC	4IF	4SF	5CV	5CB	5C1	5C2
1SH	83	33	88	88	88	38	38	33	38
1BM	88	88	88	88	38	88	88	88	88
1GB	38	38	88	38	88	88	88	88	38
1UP	38	38	38	38	38	38	83	38	38
2H1	88	88	88	88	38	0.21	0.3	88	38
2H2	38	38	38	88	88	0.47	88	38	0.04
2H3	88	88	88	83	83	0.12	83	88	38
3BS	88	38	88	38	38	88	38	38	88
3HA	88	88	88	38	38	38	88	38	38
3SW	38	33	38	83	38	38	38	33	38
3PL	88	88	38	38	38	83	38	38	38
4VL	33	38	38	38	38	38	33	33	38
4VC	38	38	83	38	33	33	38	33	38
4IF	38	33	33	33	38	38	88	38	88
4SF	38	88	88	38	38	88	88	88	88
5CV	88	33	38	38	88	88	0.08	83	38
5C3	33	38	88	38	33	38	38	0.02	0.06
5C1	38	38	38	88	38	38	88	38	38
5C2	38	83	88	38	38	0.23	38	38	38

RUN DESIGNATION: TYPE 4 CYCLES ONLY, ARTIFICIALLY JUXTAPOSED

TOTAL NUMBER OF FACIES TRANSITIONS OBSERVED: 150

VALUES OF PARAMETER P --

	ISH	IBM	IGB	IUP	ZH1	ZH2	ZHC	CBS	ZHA	ZSW
ISH	00	00	00	00	00	00	00	00	00	00
IBM	00	00	0	0	0.01	-0.02	00	-0.01	00	00
IGB	00	0	00	0.02	0.05	0	00	00	00	00
IUP	00	0	-0.01	00	0.07	-0.02	00	00	00	00
ZH1	00	00	0.01	0	00	0.1	00	-0.01	00	00
ZH2	00	-0.01	0	-0.01	-0.01	00	0.05	00	00	00
ZHC	00	-0.02	-0.01	00	0	-0.01	00	00	00	00
CBS	00	-0.01	00	00	-0.02	-0.02	00	00	00	00
ZHA	00	00	00	00	00	00	00	00	00	00
ZSW	00	00	00	00	00	00	00	00	00	00
ZPL	00	00	00	00	00	00	00	00	00	00
4VL	00	00	00	00	00	00	00	00	00	00
4VC	00	00	00	00	00	00	00	00	00	00
4IF	00	00	00	00	00	00	00	00	00	00
4SF	00	00	00	00	00	00	00	00	00	00
SCV	00	00	0	-0.02	-0.01	00	00	00	00	00
SC3	00	00	00	00	00	00	00	00	00	00
SC1	00	00	-0.02	00	00	00	00	00	00	00
SC2	00	-0.02	-0.01	-0.02	00	00	00	00	00	00

	ZPL	4VL	4VC	4IF	4SF	SCV	SC3	SC1	SC2
ISH	00	00	00	00	00	00	00	00	00
IBM	00	00	00	00	00	00	00	00	00
IGB	00	00	00	00	00	00	00	00	00
IUP	00	00	00	00	00	00	00	00	00
ZH1	00	00	00	00	00	0	-0.02	00	-0.02
ZH2	00	00	00	00	00	-0.01	00	00	0
ZHC	00	00	00	00	00	-0.01	00	00	00
CBS	00	00	00	00	00	00	00	00	00
ZHA	00	00	00	00	00	00	00	00	00
ZSW	00	00	00	00	00	00	00	00	00
ZPL	00	00	00	00	00	00	00	00	00
4VL	00	00	00	00	00	00	00	00	00
4VC	00	00	00	00	00	00	00	00	00
4IF	00	00	00	00	00	00	00	00	00
4SF	00	00	00	00	00	00	00	00	00
SCV	00	00	00	00	00	00	-0.02	00	00
SC3	00	00	00	00	00	00	00	-0.02	-0.02
SC1	00	00	00	00	00	00	00	00	00
SC2	00	00	00	00	00	-0.02	00	00	00

RUN DESIGNATION: TYPE 5 CYCLES ONLY, ARTIFICIALLY JUXTAPOSED

0

FACIES DATA --

FACIES	# OCCUR	MEAN THICKNESS (RANGE) IN METERS
1SH	0	0 (0 to 0)
1BM	4	3.7 (1.3 to 7)
1GB	10	10.2 (2.3 to 23.9)
1UP	7	4.3 (0.9 to 13)
2H1	0	0 (0 to 0)
2H2	0	0 (0 to 0)
2H3	0	0 (0 to 0)
3BS	0	0 (0 to 0)
3HA	0	0 (0 to 0)
3SW	0	0 (0 to 0)
3PL	0	0 (0 to 0)
4VL	0	0 (0 to 0)
4VC	0	0 (0 to 0)
4IF	0	0 (0 to 0)
4SF	0	0 (0 to 0)
5CV	3	0 (0 to 0)
5C3	0	0 (0 to 0)
5C1	2	0.4 (0.3 to 0.4)
5C2	2	1.8 (1.4 to 2.2)

TOTAL NUMBER OF FACIES OCCURRENCES: 28

RUN DESIGNATION: TYPE 3 CYCLES ONLY, ARTIFICIALLY JUXTAPOSED

THICKNESS-OF-UNDERLYING MATRIX --

	1SH	1BM	1GB	1UP	2H1	2H2	2H3	3BS	3HA	3SW
1SH	0	0	0	0	0	0	0	0	0	0
1BM	0	0	7	2.7	0	0	0	0	0	0
1GB	0	5.2	0	4.3	0	0	0	0	0	0
1UP	0	7.6	4.7	0	0	0	0	0	0	0
2H1	0	0	0	0	0	0	0	0	0	0
2H2	0	0	0	0	0	0	0	0	0	0
2H3	0	0	0	0	0	0	0	0	0	0
3BS	0	0	0	0	0	0	0	0	0	0
3HA	0	0	0	0	0	0	0	0	0	0
3SW	0	0	0	0	0	0	0	0	0	0
3PL	0	0	0	0	0	0	0	0	0	0
4VL	0	0	0	0	0	0	0	0	0	0
4VC	0	0	0	0	0	0	0	0	0	0
4IF	0	0	0	0	0	0	0	0	0	0
4SF	0	0	0	0	0	0	0	0	0	0
5CV	0	0	0	0	0	0	0	0	0	0
5CB	0	0	0	0	0	0	0	0	0	0
5C1	0	0	8.4	0	0	0	0	0	0	0
5C2	0	1.4	0	2.2	0	0	0	0	0	0

	3PL	4VL	4VC	4IF	4SF	5CV	5CB	5C1	5C2
1SH	0	0	0	0	0	0	0	0	0
1BM	0	0	0	0	0	1.3	0	0	0
1GB	0	0	0	0	0	13.4	0	18.3	2.3
1UP	0	0	0	0	0	2.4	0	8.9	2
2H1	0	0	0	0	0	0	0	0	0
2H2	0	0	0	0	0	0	0	0	0
2H3	0	0	0	0	0	0	0	0	0
3BS	0	0	0	0	0	0	0	0	0
3HA	0	0	0	0	0	0	0	0	0
3SW	0	0	0	0	0	0	0	0	0
3PL	0	0	0	0	0	0	0	0	0
4VL	0	0	0	0	0	0	0	0	0
4VC	0	0	0	0	0	0	0	0	0
4IF	0	0	0	0	0	0	0	0	0
4SF	0	0	0	0	0	0	0	0	0
5CV	0	0	0	0	0	0	0	0	0
5CB	0	0	0	0	0	0	0	0	0
5C1	0	0	0	0	0	0	0	0	0
5C2	0	0	0	0	0	0	0	0	0

RUN DESIGNATION: TYPE 5 CYCLES ONLY, ARTIFICIALLY JUXTAPOSED

THICKNESS-OF-OVERLYING MATRIX --

	1SM	1BM	1CB	1UP	2M1	2M2	2M3	3BS	3MA	3SW
1SM	0	0	0	0	0	0	0	0	0	0
1BM	0	0	5.2	2.4	0	0	0	0	0	0
1CB	0	1.3	0	3.1	0	0	0	0	0	0
1UP	0	2.7	3.6	0	0	0	0	0	0	0
2M1	0	0	0	0	0	0	0	0	0	0
2M2	0	0	0	0	0	0	0	0	0	0
2M3	0	0	0	0	0	0	0	0	0	0
3BS	0	0	0	0	0	0	0	0	0	0
3MA	0	0	0	0	0	0	0	0	0	0
3SW	0	0	0	0	0	0	0	0	0	0
3PL	0	0	0	0	0	0	0	0	0	0
4VL	0	0	0	0	0	0	0	0	0	0
4VC	0	0	0	0	0	0	0	0	0	0
4IF	0	0	0	0	0	0	0	0	0	0
4SF	0	0	0	0	0	0	0	0	0	0
5CV	0	0	15.3	0	0	0	0	0	0	0
5CB	0	0	0	0	0	0	0	0	0	0
5C1	0	0	13.4	0	0	0	0	0	0	0
5C2	0	7	0	13	0	0	0	0	0	0

	3PL	4VL	4VC	4IF	4SF	5CV	5CB	5C1	5C2
1SM	0	0	0	0	0	0	0	0	0
1BM	0	0	0	0	0	0	0	0	0
1CB	0	0	0	0	0	0	0	9.3	1.4
1UP	0	0	0	0	0	0	0	9.4	2.2
2M1	0	0	0	0	0	0	0	0	0
2M2	0	0	0	0	0	0	0	0	0
2M3	0	0	0	0	0	0	0	0	0
3BS	0	0	0	0	0	0	0	0	0
3MA	0	0	0	0	0	0	0	0	0
3SW	0	0	0	0	0	0	0	0	0
3PL	0	0	0	0	0	0	0	0	0
4VL	0	0	0	0	0	0	0	0	0
4VC	0	0	0	0	0	0	0	0	0
4IF	0	0	0	0	0	0	0	0	0
4SF	0	0	0	0	0	0	0	0	0
5CV	0	0	0	0	0	0	0	0	0
5CB	0	0	0	0	0	0	0	0	0
5C1	0	0	0	0	0	0	0	0	0
5C2	0	0	0	0	0	0	0	0	0

RUN DESIGNATION: TYPE 5 CYCLES ONLY, ARTIFICIALLY JUXTAPOSED

TOTAL NUMBER OF FACIES TRANSITIONS OBSERVED: 25

OBSERVED TRANSITIONS --

	1SH	1BM	1GB	1UP	2M1	2M2	2M3	3BS	3HA	3SW
1SH	0	0	0	0	0	0	0	0	0	0
1BM	0	0	1	1	0	0	0	0	0	0
1GB	0	1	0	4	0	0	0	0	0	0
1UP	0	2	2	0	0	0	0	0	0	0
2M1	0	0	0	0	0	0	0	0	0	0
2M2	0	0	0	0	0	0	0	0	0	0
2M3	0	0	0	0	0	0	0	0	0	0
3BS	0	0	0	0	0	0	0	0	0	0
3HA	0	0	0	0	0	0	0	0	0	0
3SW	0	0	0	0	0	0	0	0	0	0
3PL	0	0	0	0	0	0	0	0	0	0
4VL	0	0	0	0	0	0	0	0	0	0
4VC	0	0	0	0	0	0	0	0	0	0
4IF	0	0	0	0	0	0	0	0	0	0
4SF	0	0	0	0	0	0	0	0	0	0
5CV	0	0	3	0	0	0	0	0	0	0
5CB	0	0	0	0	0	0	0	0	0	0
5C1	0	0	2	0	0	0	0	0	0	0
5C2	0	1	0	1	0	0	0	0	0	0

	3PL	4VL	4VC	4IF	4SF	5CV	5CB	5C1	5C2
1SH	0	0	0	0	0	0	0	0	0
1BM	0	0	0	0	0	1	0	0	0
1GB	0	0	0	0	0	1	0	1	1
1UP	0	0	0	0	0	1	0	1	1
2M1	0	0	0	0	0	0	0	0	0
2M2	0	0	0	0	0	0	0	0	0
2M3	0	0	0	0	0	0	0	0	0
3BS	0	0	0	0	0	0	0	0	0
3HA	0	0	0	0	0	0	0	0	0
3SW	0	0	0	0	0	0	0	0	0
3PL	0	0	0	0	0	0	0	0	0
4VL	0	0	0	0	0	0	0	0	0
4VC	0	0	0	0	0	0	0	0	0
4IF	0	0	0	0	0	0	0	0	0
4SF	0	0	0	0	0	0	0	0	0
5CV	0	0	0	0	0	0	0	0	0
5CB	0	0	0	0	0	0	0	0	0
5C1	0	0	0	0	0	0	0	0	0
5C2	0	0	0	0	0	0	0	0	0

RUN DESIGNATION: TYPE 5 CYCLES ONLY, ARTIFICIALLY JUXTAPOSED

OBSERVED TRANSITION PROBABILITY --

	1SH	1BM	1GB	1UP	2H1	2H2	2H3	3BS	3HA	3SW
1SH	0	0	0	0	0	0	0	0	0	0
1BM	0	0	0.33	0.67	0	0	0	0	0	0
1GB	0	0.13	0	0.5	0	0	0	0	0	0
1UP	0	0.29	0.29	0	0	0	0	0	0	0
2H1	0	0	0	0	0	0	0	0	0	0
2H2	0	0	0	0	0	0	0	0	0	0
2H3	0	0	0	0	0	0	0	0	0	0
3BS	0	0	0	0	0	0	0	0	0	0
3HA	0	0	0	0	0	0	0	0	0	0
3SW	0	0	0	0	0	0	0	0	0	0
3PL	0	0	0	0	0	0	0	0	0	0
4VL	0	0	0	0	0	0	0	0	0	0
4VC	0	0	0	0	0	0	0	0	0	0
4IF	0	0	0	0	0	0	0	0	0	0
4SF	0	0	0	0	0	0	0	0	0	0
5CV	0	0	1	0	0	0	0	0	0	0
5CB	0	0	0	0	0	0	0	0	0	0
5C1	0	0	1	0	0	0	0	0	0	0
5C2	0	0.5	0	0.5	0	0	0	0	0	0

	3PL	4VL	4VC	4IF	4SF	5CV	5CB	5C1	5C2
1SH	0	0	0	0	0	0	0	0	0
1BM	0	0	0	0	0	0.33	0	0	0
1GB	0	0	0	0	0	0.13	0	0.13	0.13
1UP	0	0	0	0	0	0.14	0	0.14	0.14
2H1	0	0	0	0	0	0	0	0	0
2H2	0	0	0	0	0	0	0	0	0
2H3	0	0	0	0	0	0	0	0	0
3BS	0	0	0	0	0	0	0	0	0
3HA	0	0	0	0	0	0	0	0	0
3SW	0	0	0	0	0	0	0	0	0
3PL	0	0	0	0	0	0	0	0	0
4VL	0	0	0	0	0	0	0	0	0
4VC	0	0	0	0	0	0	0	0	0
4IF	0	0	0	0	0	0	0	0	0
4SF	0	0	0	0	0	0	0	0	0
5CV	0	0	0	0	0	0	0	0	0
5CB	0	0	0	0	0	0	0	0	0
5C1	0	0	0	0	0	0	0	0	0
5C2	0	0	0	0	0	0	0	0	0

RUN DESIGNATION: TYPE 5 CYCLES ONLY, ARTIFICIALLY JUXTAPOSED

EXPECTED (RANDOM) TRANSITIONS---

	1SH	1BM	1OB	1UP	2H1	2H2	2H3	3BS	3HA	3SW
1SH	0	0	0	0	0	0	0	0	0	0
1BM	0	0	1.36	0.858	0	0	0	0	0	0
1OB	0	1.75	0	3.26	0	0	0	0	0	0
1UP	0	1.24	3.66	0	0	0	0	0	0	0
2H1	0	0	0	0	0	0	0	0	0	0
2H2	0	0	0	0	0	0	0	0	0	0
2H3	0	0	0	0	0	0	0	0	0	0
3BS	0	0	0	0	0	0	0	0	0	0
3HA	0	0	0	0	0	0	0	0	0	0
3SW	0	0	0	0	0	0	0	0	0	0
3PL	0	0	0	0	0	0	0	0	0	0
4VL	0	0	0	0	0	0	0	0	0	0
4VC	0	0	0	0	0	0	0	0	0	0
4IF	0	0	0	0	0	0	0	0	0	0
4SF	0	0	0	0	0	0	0	0	0	0
5CV	0	0.443	1.31	0.826	0	0	0	0	0	0
5CB	0	0	0	0	0	0	0	0	0	0
5C1	0	0.284	0.839	0.53	0	0	0	0	0	0
5C2	0	0.284	0.839	0.53	0	0	0	0	0	0

	3PL	4VL	4VC	4IF	4SF	5CV	5CB	5C1	5C2
1SH	0	0	0	0	0	0	0	0	0
1BM	0	0	0	0	0	0.344	0	0.221	0.221
1OB	0	0	0	0	0	1.31	0	0.837	0.837
1UP	0	0	0	0	0	0.926	0	0.594	0.594
2H1	0	0	0	0	0	0	0	0	0
2H2	0	0	0	0	0	0	0	0	0
2H3	0	0	0	0	0	0	0	0	0
3BS	0	0	0	0	0	0	0	0	0
3HA	0	0	0	0	0	0	0	0	0
3SW	0	0	0	0	0	0	0	0	0
3PL	0	0	0	0	0	0	0	0	0
4VL	0	0	0	0	0	0	0	0	0
4VC	0	0	0	0	0	0	0	0	0
4IF	0	0	0	0	0	0	0	0	0
4SF	0	0	0	0	0	0	0	0	0
5CV	0	0	0	0	0	0	0	0.212	0.212
5CB	0	0	0	0	0	0	0	0	0
5C1	0	0	0	0	0	0.212	0	0	0.136
5C2	0	0	0	0	0	0.212	0	0.136	0

RUN DESIGNATION: TYPE 5 CYCLES ONLY, ARTIFICIALLY JUXTAPOSED

-- EXPECTED (RANDOM) TRANSITION PROBABILITY --

	1SH	1BM	1OB	1UP	2H1	2H2	2H3	3BS	3HA	3SW
1SH	0	0	0	0	0	0	0	0	0	0
1BM	0	0	0.45	0.29	0	0	0	0	0	0
1OB	0	0.22	0	0.41	0	0	0	0	0	0
1UP	0	0.18	0.52	0	0	0	0	0	0	0
2H1	0	0	0	0	0	0	0	0	0	0
2H2	0	0	0	0	0	0	0	0	0	0
2H3	0	0	0	0	0	0	0	0	0	0
3BS	0	0	0	0	0	0	0	0	0	0
3HA	0	0	0	0	0	0	0	0	0	0
3SW	0	0	0	0	0	0	0	0	0	0
3PL	0	0	0	0	0	0	0	0	0	0
4VL	0	0	0	0	0	0	0	0	0	0
4VC	0	0	0	0	0	0	0	0	0	0
4IF	0	0	0	0	0	0	0	0	0	0
4SF	0	0	0	0	0	0	0	0	0	0
5CV	0	0.15	0.44	0.28	0	0	0	0	0	0
5CB	0	0	0	0	0	0	0	0	0	0
5C1	0	0.14	0.42	0.26	0	0	0	0	0	0
5C2	0	0.14	0.42	0.26	0	0	0	0	0	0

	3PL	4VL	4VC	4IF	4SF	5CV	5CB	5C1	5C2
1SH	0	0	0	0	0	0	0	0	0
1BM	0	0	0	0	0	0.11	0	0.07	0.07
1OB	0	0	0	0	0	0.16	0	0.1	0.1
1UP	0	0	0	0	0	0.13	0	0.08	0.08
2H1	0	0	0	0	0	0	0	0	0
2H2	0	0	0	0	0	0	0	0	0
2H3	0	0	0	0	0	0	0	0	0
3BS	0	0	0	0	0	0	0	0	0
3HA	0	0	0	0	0	0	0	0	0
3SW	0	0	0	0	0	0	0	0	0
3PL	0	0	0	0	0	0	0	0	0
4VL	0	0	0	0	0	0	0	0	0
4VC	0	0	0	0	0	0	0	0	0
4IF	0	0	0	0	0	0	0	0	0
4SF	0	0	0	0	0	0	0	0	0
5CV	0	0	0	0	0	0	0	0.07	0.07
5CB	0	0	0	0	0	0	0	0	0
5C1	0	0	0	0	0	0.11	0	0	0.07
5C2	0	0	0	0	0	0.11	0	0.07	0

RUN DESIGNATION: TYPE 3 CYCLES ONLY, ARTIFICIALLY JUXTAPOSED

OBSERVED MINUS RANDOM PROBABILITY --

	1SH	1BM	1OB	1UP	2H1	2H2	2H3	3BS	3HA	3SW
1SH	0	0	0	0	0	0	0	0	0	0
1BM	0	0	-0.12	0.04	0	0	0	0	0	0
1OB	0	-0.09	0	0.09	0	0	0	0	0	0
1UP	0	0.11	-0.23	0	0	0	0	0	0	0
2H1	0	0	0	0	0	0	0	0	0	0
2H2	0	0	0	0	0	0	0	0	0	0
2H3	0	0	0	0	0	0	0	0	0	0
3BS	0	0	0	0	0	0	0	0	0	0
3HA	0	0	0	0	0	0	0	0	0	0
3SW	0	0	0	0	0	0	0	0	0	0
3PL	0	0	0	0	0	0	0	0	0	0
4VL	0	0	0	0	0	0	0	0	0	0
4VC	0	0	0	0	0	0	0	0	0	0
4IF	0	0	0	0	0	0	0	0	0	0
4SF	0	0	0	0	0	0	0	0	0	0
5CV	0	-0.15	0.56	-0.28	0	0	0	0	0	0
5CB	0	0	0	0	0	0	0	0	0	0
5C1	0	-0.14	0.58	-0.26	0	0	0	0	0	0
5C2	0	0.34	-0.42	0.24	0	0	0	0	0	0

	3PL	4VL	4VC	4IF	4SF	5CV	5CB	5C1	5C2
1SH	0	0	0	0	0	0	0	0	0
1BM	0	0	0	0	0	0.22	0	-0.07	-0.07
1OB	0	0	0	0	0	-0.03	0	0.03	0.03
1UP	0	0	0	0	0	0.01	0	0.06	0.06
2H1	0	0	0	0	0	0	0	0	0
2H2	0	0	0	0	0	0	0	0	0
2H3	0	0	0	0	0	0	0	0	0
3BS	0	0	0	0	0	0	0	0	0
3HA	0	0	0	0	0	0	0	0	0
3SW	0	0	0	0	0	0	0	0	0
3PL	0	0	0	0	0	0	0	0	0
4VL	0	0	0	0	0	0	0	0	0
4VC	0	0	0	0	0	0	0	0	0
4IF	0	0	0	0	0	0	0	0	0
4SF	0	0	0	0	0	0	0	0	0
5CV	0	0	0	0	0	0	0	-0.07	-0.07
5CB	0	0	0	0	0	0	0	0	0
5C1	0	0	0	0	0	-0.11	0	0	-0.07
5C2	0	0	0	0	0	-0.11	0	-0.07	0

RUN DESIGNATION: TYPE 5 CYCLES ONLY, ARTIFICIALLY JUXTAPOSED

SIGNIFICANCE TEST VALUES --

	1SM	1BM	1GB	1UP	2M1	2M2	2M3	3BS	3MA	3SW
1SM	33	38	38	38	33	33	86	33	33	88
1BM	38	83	38	0.34	33	88	88	36	36	83
1GB	38	38	38	0.43	38	38	38	88	38	33
1UP	33	0.37	38	33	33	38	33	88	38	88
2M1	33	38	88	88	38	38	38	88	38	88
2M2	33	33	36	83	58	38	53	38	38	88
2M3	38	38	88	88	38	33	38	38	88	38
3BS	88	33	88	88	83	83	33	38	38	38
3MA	38	38	53	88	38	38	83	38	88	38
3SW	33	33	38	88	38	88	38	38	38	88
3PL	38	38	38	36	88	38	83	38	38	38
4VL	83	33	38	58	38	38	33	38	38	38
4VC	58	88	58	38	58	38	83	88	38	38
4IF	38	88	83	38	38	38	38	38	38	33
4SF	38	38	33	88	88	38	33	88	38	38
5CV	33	38	0.39	85	38	38	33	38	38	38
5CB	38	38	38	38	38	33	83	88	88	38
5C1	38	38	0.13	38	38	88	38	38	38	38
5C2	38	0.26	38	0.45	88	38	88	36	38	38

	3PL	4VL	4VC	4IF	4SF	5CV	5CB	5C1	5C2
1SM	88	38	38	38	38	88	38	38	88
1BM	88	88	38	33	38	0.3	38	38	38
1GB	38	38	88	88	38	38	88	0.37	0.37
1UP	33	33	38	88	38	0.62	38	0.44	0.44
2M1	38	88	88	88	88	38	38	38	88
2M2	88	38	38	33	38	88	38	38	38
2M3	38	38	88	38	38	88	88	88	88
3BS	38	38	53	88	38	38	38	38	88
3MA	38	33	88	38	38	38	38	38	33
3SW	38	38	38	38	38	38	38	38	38
3PL	88	38	88	38	38	38	38	88	33
4VL	38	38	38	38	38	38	38	83	38
4VC	38	83	38	38	38	88	38	38	83
4IF	38	88	33	38	38	38	83	88	33
4SF	88	88	38	38	88	33	38	88	88
5CV	33	38	88	38	38	38	38	38	33
5CB	38	88	88	88	88	88	38	38	88
5C1	33	38	38	33	33	38	38	33	33
5C2	38	38	88	88	38	88	33	83	83

RUN DESIGNATION: TYPE 5 CYCLES ONLY, ARTIFICIALLY JUXTAPOSED

TOTAL NUMBER OF FACIES TRANSITIONS OBSERVED: 25

VALUES OF PARAMETER r --

	1SH	1BM	1GB	1UP	2M1	2M2	2M3	3BS	3MA	3SW
1SH	88	88	88	88	88	88	88	88	88	88
1BM	88	88	-0.02	-0.02	88	88	88	88	88	88
1GB	88	-0.02	88	0.1	88	88	88	88	88	88
1UP	88	0.02	0.02	88	88	88	88	88	88	88
2M1	88	88	88	88	88	88	88	88	88	88
2M2	88	88	88	88	88	88	88	88	88	88
2M3	88	88	88	88	88	88	88	88	88	88
3BS	88	88	88	88	88	88	88	88	88	88
3MA	88	88	88	88	88	88	88	88	88	88
3SW	88	88	88	88	88	88	88	88	88	88
3PL	88	88	88	88	88	88	88	88	88	88
4VL	88	88	88	88	88	88	88	88	88	88
4VC	88	88	88	88	88	88	88	88	88	88
4IF	88	88	88	88	88	88	88	88	88	88
4SF	88	88	88	88	88	88	88	88	88	88
5CV	88	88	0.06	88	88	88	88	88	88	88
5CB	88	88	88	88	88	88	88	88	88	88
5C1	88	88	0.02	88	88	88	88	88	88	88
5C2	88	-0.02	88	-0.02	88	88	88	88	88	88

	3PL	4VL	4VC	4IF	4SF	5CV	5CB	5C1	5C2
1SH	88	88	88	88	88	88	88	88	88
1BM	88	88	88	88	88	-0.02	88	88	88
1GB	88	88	88	88	88	-0.02	88	-0.02	-0.02
1UP	88	88	88	88	88	-0.02	88	-0.02	-0.02
2M1	88	88	88	88	88	88	88	88	88
2M2	88	88	88	88	88	88	88	88	88
2M3	88	88	88	88	88	88	88	88	88
3BS	88	88	88	88	88	88	88	88	88
3MA	88	88	88	88	88	88	88	88	88
3SW	88	88	88	88	88	88	88	88	88
3PL	88	88	88	88	88	88	88	88	88
4VL	88	88	88	88	88	88	88	88	88
4VC	88	88	88	88	88	88	88	88	88
4IF	88	88	88	88	88	88	88	88	88
4SF	88	88	88	88	88	88	88	88	88
5CV	88	88	88	88	88	88	88	88	88
5CB	88	88	88	88	88	88	88	88	88
5C1	88	88	88	88	88	88	88	88	88
5C2	88	88	88	88	88	88	88	88	88

RUN DESIGNATION: TYPE 6 CYCLES ONLY, ARTIFICIALLY JUXTAPOSED

FACIES DATA --

FACIES	# OCCUR	MEAN THICKNESS (RANGE) IN METERS
1SH	0	0 (0 to 0)
1SM	10	6 (2.9 to 12)
1GB	1	2.7 (2.7 to 2.7)
1UP	1	3.7 (3.7 to 3.7)
2M1	0	0 (0 to 0)
2M2	0	0 (0 to 0)
2M3	0	0 (0 to 0)
3BS	9	3.9 (2 to 6.6)
3HA	0	0 (0 to 0)
3SW	0	0 (0 to 0)
3PL	0	0 (0 to 0)
4VL	0	0 (0 to 0)
4VC	0	0 (0 to 0)
4IF	0	0 (0 to 0)
4SF	0	0 (0 to 0)
5CV	1	0 (0 to 0)
5C3	0	0 (0 to 0)
5C1	0	0 (0 to 0)
5C2	1	0.9 (0.9 to 0.9)

TOTAL NUMBER OF FACIES OCCURRENCES: 23

RUN DESIGNATION: TYPE 6 CYCLES ONLY; ARTIFICIALLY JUXTAPOSED

THICKNESS-OF-UNDERLYING MATRIX --

	1SH	1BM	1GB	1UP	2M1	2M2	2M3	3BS	3HA	3SW
1SH	0	0	0	0	0	0	0	0	0	0
1BM	0	0	3	8.3	0	0	0	6.1	0	0
1GB	0	2.7	0	0	0	0	0	0	0	0
1UP	0	0	0	0	0	0	0	3.7	0	0
2M1	0	0	0	0	0	0	0	0	0	0
2M2	0	0	0	0	0	0	0	0	0	0
2M3	0	0	0	0	0	0	0	0	0	0
3BS	0	4	0	0	0	0	0	0	0	0
3HA	0	0	0	0	0	0	0	0	0	0
3SW	0	0	0	0	0	0	0	0	0	0
3PL	0	0	0	0	0	0	0	0	0	0
4VL	0	0	0	0	0	0	0	0	0	0
4VC	0	0	0	0	0	0	0	0	0	0
4IF	0	0	0	0	0	0	0	0	0	0
4SF	0	0	0	0	0	0	0	0	0	0
5CV	0	0	0	0	0	0	0	0	0	0
5CB	0	0	0	0	0	0	0	0	0	0
5C1	0	0	0	0	0	0	0	0	0	0
5C2	0	6.9	0	0	0	0	0	0	0	0

	3PL	4VL	4VC	4IF	4SF	5CV	5CB	5C1	5C2
1SH	0	0	0	0	0	0	0	0	0
1BM	0	0	0	0	0	0	0	0	0
1GB	0	0	0	0	0	0	0	0	0
1UP	0	0	0	0	0	0	0	0	0
2M1	0	0	0	0	0	0	0	0	0
2M2	0	0	0	0	0	0	0	0	0
2M3	0	0	0	0	0	0	0	0	0
3BS	0	0	0	0	0	3	0	0	3.6
3HA	0	0	0	0	0	0	0	0	0
3SW	0	0	0	0	0	0	0	0	0
3PL	0	0	0	0	0	0	0	0	0
4VL	0	0	0	0	0	0	0	0	0
4VC	0	0	0	0	0	0	0	0	0
4IF	0	0	0	0	0	0	0	0	0
4SF	0	0	0	0	0	0	0	0	0
5CV	0	0	0	0	0	0	0	0	0
5CB	0	0	0	0	0	0	0	0	0
5C1	0	0	0	0	0	0	0	0	0
5C2	0	0	0	0	0	0	0	0	0

RUN DESIGNATION: TYPE 6 CYCLES ONLY, ARTIFICIALLY JUXTAPOSED

THICKNESS-OF-OVERLYING MATRIX --

	1SH	1BM	1GB	1UP	2M1	2M2	2M3	3BS	3MA	3SW
1SH	0	0	0	0	0	0	0	0	0	0
1BM	0	0	2.7	3.7	0	0	0	3.9	0	0
1GB	0	2.9	0	0	0	0	0	0	0	0
1UP	0	0	0	0	0	0	0	3.5	0	0
2M1	0	0	0	0	0	0	0	0	0	0
2M2	0	0	0	0	0	0	0	0	0	0
2M3	0	0	0	0	0	0	0	0	0	0
3BS	0	3.5	0	0	0	0	0	0	0	0
3MA	0	0	0	0	0	0	0	0	0	0
3SW	0	0	0	0	0	0	0	0	0	0
3PL	0	0	0	0	0	0	0	0	0	0
4VL	0	0	0	0	0	0	0	0	0	0
4VC	0	0	0	0	0	0	0	0	0	0
4IF	0	0	0	0	0	0	0	0	0	0
4SF	0	0	0	0	0	0	0	0	0	0
5CV	0	3.4	0	0	0	0	0	0	0	0
5CB	0	0	0	0	0	0	0	0	0	0
5C1	0	0	0	0	0	0	0	0	0	0
5C2	0	0.4	0	0	0	0	0	0	0	0

	3PL	4VL	4VC	4IF	4SF	5CV	5CB	5C1	5C2
1SH	0	0	0	0	0	0	0	0	0
1BM	0	0	0	0	0	0	0	0	0
1GB	0	0	0	0	0	0	0	0	0
1UP	0	0	0	0	0	0	0	0	0
2M1	0	0	0	0	0	0	0	0	0
2M2	0	0	0	0	0	0	0	0	0
2M3	0	0	0	0	0	0	0	0	0
3BS	0	0	0	0	0	0	0	0	8.9
3MA	0	0	0	0	0	0	0	0	0
3SW	0	0	0	0	0	0	0	0	0
3PL	0	0	0	0	0	0	0	0	0
4VL	0	0	0	0	0	0	0	0	0
4VC	0	0	0	0	0	0	0	0	0
4IF	0	0	0	0	0	0	0	0	0
4SF	0	0	0	0	0	0	0	0	0
5CV	0	0	0	0	0	0	0	0	0
5CB	0	0	0	0	0	0	0	0	0
5C1	0	0	0	0	0	0	0	0	0
5C2	0	0	0	0	0	0	0	0	0

RUN DESIGNATION: TYPE 6 CYCLES ONLY, ARTIFICIALLY JUXTAPOSED

TOTAL NUMBER OF FACIES TRANSITIONS OBSERVED: 22

OBSERVED TRANSITIONS --

	1SH	1BM	1GB	1UP	2M1	2M2	2M3	3BS	3HA	3SW
1SH	0	0	0	0	0	0	0	0	0	0
1BM	0	0	1	1	0	0	0	0	0	0
1GB	0	1	0	0	0	0	0	0	0	0
1UP	0	0	0	0	0	0	0	0	0	0
2M1	0	0	0	0	0	0	0	1	0	0
2M2	0	0	0	0	0	0	0	0	0	0
2M3	0	0	0	0	0	0	0	0	0	0
3BS	0	0	0	0	0	0	0	0	0	0
3HA	0	0	0	0	0	0	0	0	0	0
3SW	0	0	0	0	0	0	0	0	0	0
3PL	0	0	0	0	0	0	0	0	0	0
4VL	0	0	0	0	0	0	0	0	0	0
4VC	0	0	0	0	0	0	0	0	0	0
4IF	0	0	0	0	0	0	0	0	0	0
4SF	0	0	0	0	0	0	0	0	0	0
5CV	0	1	0	0	0	0	0	0	0	0
5CB	0	0	0	0	0	0	0	0	0	0
5C1	0	0	0	0	0	0	0	0	0	0
5C2	0	1	0	0	0	0	0	0	0	0

	3PL	4VL	4VC	4IF	4SF	5CV	5CB	5C1	5C2
1SH	0	0	0	0	0	0	0	0	0
1BM	0	0	0	0	0	0	0	0	0
1GB	0	0	0	0	0	0	0	0	0
1UP	0	0	0	0	0	0	0	0	0
2M1	0	0	0	0	0	0	0	0	0
2M2	0	0	0	0	0	0	0	0	0
2M3	0	0	0	0	0	0	0	0	0
3BS	0	0	0	0	0	1	0	0	1
3HA	0	0	0	0	0	0	0	0	0
3SW	0	0	0	0	0	0	0	0	0
3PL	0	0	0	0	0	0	0	0	0
4VL	0	0	0	0	0	0	0	0	0
4VC	0	0	0	0	0	0	0	0	0
4IF	0	0	0	0	0	0	0	0	0
4SF	0	0	0	0	0	0	0	0	0
5CV	0	0	0	0	0	0	0	0	0
5CB	0	0	0	0	0	0	0	0	0
5C1	0	0	0	0	0	0	0	0	0
5C2	0	0	0	0	0	0	0	0	0

RUN DESIGNATION: TYPE 6 CYCLES ONLY, ARTIFICIALLY JUXTAPOSED

OBSERVED TRANSITION PROBABILITY --

	1SH	1BM	1GB	1UP	2H1	2H2	2H3	3BS	3HA	3SW
1SH	0	0	0	0	0	0	0	0	0	0
1BM	0	0	0.1	0.1	0	0	0	0.8	0	0
1GB	0	1	0	0	0	0	0	0	0	0
1UP	0	0	0	0	0	0	0	1	0	0
2H1	0	0	0	0	0	0	0	0	0	0
2H2	0	0	0	0	0	0	0	0	0	0
2H3	0	0	0	0	0	0	0	0	0	0
3BS	0	0.75	0	0	0	0	0	0	0	0
3HA	0	0	0	0	0	0	0	0	0	0
3SW	0	0	0	0	0	0	0	0	0	0
3PL	0	0	0	0	0	0	0	0	0	0
4VL	0	0	0	0	0	0	0	0	0	0
4VC	0	0	0	0	0	0	0	0	0	0
4IF	0	0	0	0	0	0	0	0	0	0
4SF	0	0	0	0	0	0	0	0	0	0
5CV	0	1	0	0	0	0	0	0	0	0
5C3	0	0	0	0	0	0	0	0	0	0
5C1	0	0	0	0	0	0	0	0	0	0
5C2	0	1	0	0	0	0	0	0	0	0

	3PL	4VL	4VC	4IF	4SF	5CV	5C3	5C1	5C2
1SH	0	0	0	0	0	0	0	0	0
1BM	0	0	0	0	0	0	0	0	0
1GB	0	0	0	0	0	0	0	0	0
1UP	0	0	0	0	0	0	0	0	0
2H1	0	0	0	0	0	0	0	0	0
2H2	0	0	0	0	0	0	0	0	0
2H3	0	0	0	0	0	0	0	0	0
3BS	0	0	0	0	0	0.13	0	0	0.13
3HA	0	0	0	0	0	0	0	0	0
3SW	0	0	0	0	0	0	0	0	0
3PL	0	0	0	0	0	0	0	0	0
4VL	0	0	0	0	0	0	0	0	0
4VC	0	0	0	0	0	0	0	0	0
4IF	0	0	0	0	0	0	0	0	0
4SF	0	0	0	0	0	0	0	0	0
5CV	0	0	0	0	0	0	0	0	0
5C3	0	0	0	0	0	0	0	0	0
5C1	0	0	0	0	0	0	0	0	0
5C2	0	0	0	0	0	0	0	0	0

RUN DESIGNATION: TYPE 6 CYCLES ONLY, ARTIFICIALLY JUXTAPOSED

EXPECTED (RANDOM) TRANSITIONS --

	1SH	1BM	1GB	1UP	2H1	2H2	2H3	3BS	3HA	3SW
1SH	0	0	0	0	0	0	0	0	0	0
1BM	0	0	8.59	8.59	0	0	0	7.59	0	0
1GB	0	8.566	0	0.027	0	0	0	0.034	0	0
1UP	0	8.566	0.027	0	0	0	0	0.034	0	0
2H1	0	0	0	0	0	0	0	0	0	0
2H2	0	0	0	0	0	0	0	0	0	0
2H3	0	0	0	0	0	0	0	0	0	0
3BS	0	6.74	0.027	0.027	0	0	0	0	0	0
3HA	0	0	0	0	0	0	0	0	0	0
3SW	0	0	0	0	0	0	0	0	0	0
3PL	0	0	0	0	0	0	0	0	0	0
4VL	0	0	0	0	0	0	0	0	0	0
4VC	0	0	0	0	0	0	0	0	0	0
4IF	0	0	0	0	0	0	0	0	0	0
4SF	0	0	0	0	0	0	0	0	0	0
5CV	0	0.566	0.027	0.027	0	0	0	0.034	0	0
5CB	0	0	0	0	0	0	0	0	0	0
5C1	0	0	0	0	0	0	0	0	0	0
5C2	0	0.566	0.027	0.027	0	0	0	0.034	0	0

	3PL	4VL	4VC	4IF	4SF	5CV	5CB	5C1	5C2
1SH	0	0	0	0	0	0	0	0	0
1BM	0	0	0	0	0	0.59	0	0	0.59
1GB	0	0	0	0	0	0.027	0	0	0.027
1UP	0	0	0	0	0	0.027	0	0	0.027
2H1	0	0	0	0	0	0	0	0	0
2H2	0	0	0	0	0	0	0	0	0
2H3	0	0	0	0	0	0	0	0	0
3BS	0	0	0	0	0	0.327	0	0	0.327
3HA	0	0	0	0	0	0	0	0	0
3SW	0	0	0	0	0	0	0	0	0
3PL	0	0	0	0	0	0	0	0	0
4VL	0	0	0	0	0	0	0	0	0
4VC	0	0	0	0	0	0	0	0	0
4IF	0	0	0	0	0	0	0	0	0
4SF	0	0	0	0	0	0	0	0	0
5CV	0	0	0	0	0	0	0	0	0.027
5CB	0	0	0	0	0	0	0	0	0
5C1	0	0	0	0	0	0	0	0	0
5C2	0	0	0	0	0	0.027	0	0	0

RUN DESIGNATION: TYPE 6 CYCLES ONLY, ARTIFICIALLY JUXTAPOSED

EXPECTED (RANDOM) TRANSITION PROBABILITY --

	1SH	1BM	1GB	1UP	2H1	2H2	2H3	3BS	3HA	3SW
1SH	0	0	0	0	0	0	0	0	0	0
1BM	0	0	0.06	0.06	0	0	0	0.76	0	0
1GB	0	0.57	0	0.03	0	0	0	0.33	0	0
1UP	0	0.57	0.03	0	0	0	0	0.33	0	0
2H1	0	0	0	0	0	0	0	0	0	0
2H2	0	0	0	0	0	0	0	0	0	0
2H3	0	0	0	0	0	0	0	0	0	0
3BS	0	0.84	0.04	0.04	0	0	0	0	0	0
3HA	0	0	0	0	0	0	0	0	0	0
3SW	0	0	0	0	0	0	0	0	0	0
3PL	0	0	0	0	0	0	0	0	0	0
4VL	0	0	0	0	0	0	0	0	0	0
4VC	0	0	0	0	0	0	0	0	0	0
4IF	0	0	0	0	0	0	0	0	0	0
4SF	0	0	0	0	0	0	0	0	0	0
5CV	0	0.57	0.03	0.03	0	0	0	0.33	0	0
5CB	0	0	0	0	0	0	0	0	0	0
5C1	0	0	0	0	0	0	0	0	0	0
5C2	0	0.57	0.03	0.03	0	0	0	0.33	0	0

	3PL	4VL	4VC	4IF	4SF	5CV	5CB	5C1	5C2
1SH	0	0	0	0	0	0	0	0	0
1BM	0	0	0	0	0	0.06	0	0	0.06
1GB	0	0	0	0	0	0.03	0	0	0.03
1UP	0	0	0	0	0	0.03	0	0	0.03
2H1	0	0	0	0	0	0	0	0	0
2H2	0	0	0	0	0	0	0	0	0
2H3	0	0	0	0	0	0	0	0	0
3BS	0	0	0	0	0	0.04	0	0	0.04
3HA	0	0	0	0	0	0	0	0	0
3SW	0	0	0	0	0	0	0	0	0
3PL	0	0	0	0	0	0	0	0	0
4VL	0	0	0	0	0	0	0	0	0
4VC	0	0	0	0	0	0	0	0	0
4IF	0	0	0	0	0	0	0	0	0
4SF	0	0	0	0	0	0	0	0	0
5CV	0	0	0	0	0	0	0	0	0.03
5CB	0	0	0	0	0	0	0	0	0
5C1	0	0	0	0	0	0	0	0	0
5C2	0	0	0	0	0	0.03	0	0	0

RUN DESIGNATION: TYPE 6 CYCLES ONLY, ARTIFICIALLY JUXTAPOSED

OBSERVED MINUS RANDOM PROBABILITY --

	1SH	1BM	1GB	1UP	2H1	2H2	2H3	3BS	3HA	3SW
1SH	0	0	0	0	0	0	0	0	0	0
1BM	0	0	0.04	0.04	0	0	0	0.04	0	0
1GB	0	0.43	0	-0.03	0	0	0	-0.03	0	0
1UP	0	-0.57	-0.03	0	0	0	0	0.03	0	0
2H1	0	0	0	0	0	0	0	0	0	0
2H2	0	0	0	0	0	0	0	0	0	0
2H3	0	0	0	0	0	0	0	0	0	0
3BS	0	-0.09	-0.04	-0.04	0	0	0	0	0	0
3HA	0	0	0	0	0	0	0	0	0	0
3SW	0	0	0	0	0	0	0	0	0	0
3PL	0	0	0	0	0	0	0	0	0	0
4VL	0	0	0	0	0	0	0	0	0	0
4VC	0	0	0	0	0	0	0	0	0	0
4IF	0	0	0	0	0	0	0	0	0	0
4SF	0	0	0	0	0	0	0	0	0	0
5CV	0	0.43	-0.03	-0.03	0	0	0	-0.03	0	0
5CB	0	0	0	0	0	0	0	0	0	0
5C1	0	0	0	0	0	0	0	0	0	0
5C2	0	0.43	-0.03	-0.03	0	0	0	-0.03	0	0

	3PL	4VL	4VC	4IF	4SF	5CV	5CB	5C1	5C2
1SH	0	0	0	0	0	0	0	0	0
1BM	0	0	0	0	0	-0.06	0	0	-0.06
1GB	0	0	0	0	0	-0.03	0	0	-0.03
1UP	0	0	0	0	0	-0.03	0	0	-0.03
2H1	0	0	0	0	0	0	0	0	0
2H2	0	0	0	0	0	0	0	0	0
2H3	0	0	0	0	0	0	0	0	0
3BS	0	0	0	0	0	0.09	0	0	0.09
3HA	0	0	0	0	0	0	0	0	0
3SW	0	0	0	0	0	0	0	0	0
3PL	0	0	0	0	0	0	0	0	0
4VL	0	0	0	0	0	0	0	0	0
4VC	0	0	0	0	0	0	0	0	0
4IF	0	0	0	0	0	0	0	0	0
4SF	0	0	0	0	0	0	0	0	0
5CV	0	0	0	0	0	0	0	0	-0.03
5CB	0	0	0	0	0	0	0	0	0
5C1	0	0	0	0	0	0	0	0	0
5C2	0	0	0	0	0	-0.03	0	0	0

RUN DESIGNATION: TYPE 6 CYCLES ONLY, ARTIFICIALLY JUXTAPOSED

SIGNIFICANCE TEST VALUES --

	1SH	1BM	1OB	1UP	2H1	2H2	2H3	3BS	3HA	3SW
1SH	38	38	38	38	88	98	88	33	33	38
1BM	38	83	0.46	0.46	33	33	33	0.56	38	38
1OB	38	0.57	38	33	33	33	38	38	33	38
1UP	33	33	33	33	38	38	38	0.35	38	33
2H1	38	88	38	38	38	38	38	88	88	38
2H2	33	33	38	33	38	38	33	88	88	33
2H3	33	38	38	38	88	38	98	33	38	33
3BS	33	33	33	38	38	38	33	38	38	38
3HA	88	38	88	38	38	38	38	38	88	38
3SW	83	38	83	38	38	38	38	38	33	38
3PL	98	38	88	38	38	38	88	38	88	88
4VL	33	83	38	33	38	88	38	38	38	83
4VC	88	38	88	88	88	38	88	88	38	38
4IF	38	88	38	38	38	38	38	88	88	38
4SF	38	88	38	83	38	88	88	88	88	38
5CV	38	0.57	38	38	88	88	88	88	88	88
5CB	38	88	38	38	83	33	38	38	88	88
5C1	38	38	38	38	88	88	88	38	88	33
5C2	33	0.57	38	38	88	38	33	83	88	33

	3PL	4VL	4VC	4IF	4SF	5CV	5CB	5C1	5C2
1SH	38	88	88	88	88	83	38	83	88
1BM	88	98	88	88	98	98	93	88	88
1OB	38	38	83	88	33	88	38	98	88
1UP	88	33	83	33	38	88	38	38	88
2H1	88	83	88	88	38	93	88	88	88
2H2	83	38	38	88	33	88	38	38	88
2H3	38	38	88	88	38	83	38	38	38
3BS	83	33	38	38	38	0.23	38	38	0.23
3HA	38	83	88	38	83	38	38	38	38
3SW	88	88	38	88	38	83	88	88	38
3PL	38	38	38	88	38	38	38	88	38
4VL	38	38	38	33	38	33	38	38	33
4VC	38	33	88	88	83	83	38	38	38
4IF	38	38	38	83	88	38	38	88	83
4SF	38	38	88	38	38	83	38	38	38
5CV	38	83	38	88	38	38	88	38	38
5CB	88	38	88	38	38	38	38	38	38
5C1	38	88	38	83	38	38	38	38	38
5C2	38	38	38	38	38	38	88	38	38

RUN DESIGNATION: TYPE 6 CYCLES ONLY, ARTIFICIALLY JUXTAPOSED

TOTAL NUMBER OF FACIES TRANSITIONS OBSERVED: 22

VALUES OF PARAMETER F --

	1SH	1BM	1GB	1UP	2H1	2H2	2H3	3BS	3HA	3SW
1SH	33	38	38	38	33	83	88	33	88	38
1BM	88	83	-0.05	-0.05	83	38	88	0.26	88	88
1GB	38	-0.05	33	38	33	38	88	88	38	38
1UP	88	83	38	83	38	88	88	-0.05	38	38
2H1	88	38	38	38	38	38	88	88	83	38
2H2	38	83	83	33	38	38	33	38	38	88
2H3	38	38	38	38	33	38	38	38	33	38
3BS	33	0.17	38	33	38	33	33	33	38	38
3HA	38	38	38	38	88	38	38	83	38	38
3SW	83	88	38	33	38	38	38	33	88	38
3PL	38	88	38	88	38	38	33	38	38	33
4VL	38	88	88	88	83	38	83	88	88	88
4VC	38	38	33	38	33	38	38	88	38	38
4IF	88	83	38	88	88	88	88	83	88	88
4SF	38	38	83	88	88	38	83	38	83	38
5CV	83	-0.05	88	33	33	38	83	33	88	38
5C3	88	38	38	88	38	33	83	38	88	38
5C1	88	83	38	83	83	33	33	38	38	38
5C2	38	-0.05	38	38	38	38	88	88	38	38

	3PL	4VL	4VC	4IF	4SF	5CV	5C3	5C1	5C2
1SH	38	33	38	33	33	83	83	38	88
1BM	88	38	88	88	33	88	33	33	88
1GB	38	88	88	83	83	88	38	38	38
1UP	38	88	33	38	38	38	38	38	88
2H1	38	88	88	88	88	88	33	38	33
2H2	33	33	33	38	33	38	33	38	38
2H3	38	33	38	38	38	88	33	33	83
3BS	33	33	33	33	33	-0.05	38	83	-0.05
3HA	38	38	33	38	33	38	38	33	38
3SW	33	33	38	38	88	83	38	33	33
3PL	33	33	33	88	33	83	38	88	33
4VL	83	88	38	38	33	38	83	38	83
4VC	38	38	38	83	33	38	38	33	83
4IF	33	33	83	88	38	33	83	33	33
4SF	38	83	88	38	38	33	38	38	33
5CV	38	38	83	33	38	38	38	38	83
5C3	38	33	38	33	38	38	88	38	38
5C1	33	38	33	33	38	33	33	33	33
5C2	88	88	38	33	38	38	83	38	88

APPENDIX 4. FABRIC DATA FROM CONGLOMERATES IN THE CARDIUM FORMATION

The following conglomerate fabric data generally take the following form:

1.Ø / 255 N 14 +51

This indicates that the measured pebble has a long-axis length of 1.Ø cm. The strike and dip of the AB-plane of the pebble are 255 N 14. The long axis of the pebble rakes at 51° within the AB-plane, measured clockwise (+) from a position above the bed. Sense of rake is always taken from a position <u>above</u> the bed, even if the bed is overturned. [Counterclockwise rake measurements are indicated by a negative sign (-).]

TABLE

Section 4-23, Thistle Creek (40 m level)

Regional Bedding Orientation: 323 SW 17

348 E 85	318 S 16	275 N 51
347 E 65	347 W 42	31 E 80
355 W 22	218 W 16	293 W 55
288 E 44	262 N 64	82 N 10
354 E 54	142 SW 22	201 W 11
027 W 32	349 E 29	154 W 80
119 W 29	313 N 26	319 W 22
101 N 21	318 W 9	200 E 60
300 NE 5	175 W 25	100 S 50
118 E 29	265 S 15	342 W 50
176 E 26	320 S 30	230 N 20
155 E 85	315 S 15	340 W 43
153 E 75	290 N 36	342 W 23
108 S 31	162 E 22	356 W 27
001 W 40	305 VERT	230 E 22
313 W 34	300 N 24	026 W 34
222 W 56	290 SW 51	338 W 25
285 S 29	190 E 24	

TABLE

Section 4-19, Thistle Creek (131 m level)

Regional Bedding Orientation: 147 NE 79

6.5 / 293 N 65 +82	0.8 / 332 N 80 -58
7.0 / 233 S 17 ±90	1.0 / 133 N 81 -77
3.2 / 335 N 48 +38	1.2 / 252 S 46 -70
1.3 / 261 W 32 +18	1.1 / 120 S 83 ±90
2.7 / 165 W 85 -09	1.3 / 144 N 82 +58
1.6 / 158 N 78 -17	1.3 / 148 N 75 +42
1.4 / 148 N 79 +86	0.8 / 107 S 74 +77
1.2 / 172 W 65 +81	0.6 / 252 N 32 -51
1.2 / 153 N 82 ±90	1.0 / 147 S 87 ±90
1.0 / 252 N 56 -70	0.5 / 134 N 76 +66
0.8 / 132 S 85 +83	0.5 / 178 W 78 +14
3.0 / 308 N 63 -85	0.7 / 225 S 58 ±00
0.6 / 303 N 76 +04	0.7 / 313 N 66 +22
1.5 / 323 N 79 +24	1.2 / 174 W 79 +75
0.7 / 246 N 68 ±00	1.0 / 204 N 82 ±90
0.8 / 242 N 37 +01	1.0 / 256 S 42 ±90
0.8 / 247 S 44 -02	0.8 / 148 S 86 +14
0.5 / 228 N 85 ±00	1.2 / 285 N 60 -15
1.4 / 262 N 82 +80	1.9 / 305 N 53 -72
0.9 / 180 E 63 ±90	2.6 / 344 N 59 +68
1.0 / 175 E 69 +85	3.3 / 345 N 52 -15
3.0 / 306 N 88 -81	3.0 / 334 N 76 +82
0.8 / 150 S 74 -78	2.1 / 335 N 52 +86
0.8 / 253 N 80 -69	2.0 / 325 N 61 -22
1.5 / 308 N 82 +87	1.2 / 013 E 36 -65
3.5 / 184 E 78 ±90	1.3 / 007 E 75 +67
0.5 / 146 N 76 -78	1.2 / 345 S 65 -52
2.8 / 172 W 75 -84	1.2 / 151 N 80 -26

0.6 / 260 N 69 -81	1.6 / 172 E 78 -33
1.4 / 146 N 23 +28	1.8 / 312 N 68 -18
0.8 / 168 W 42 -55	1.6 / 310 N 74 -15
0.7 / 288 N 85 -79	1.5 / 353 E 64 -75
0.5 / 175 E 61 -85	1.2 / 332 N 74 -08
2.6 / 165 VERT -75	1.5 / 326 N 80 -27
2.1 / 176 W 55 -78	1.5 / 356 E 65 +14
1.2 / 307 N 66 -84	0.9 / 344 N 66 -13
1.2 / 253 N 44 -04	1.0 / 331 N 35 -44
1.0 / 180 E 81 +22	1.2 / 012 E 15 -62
2.3 / 168 W 84 -68	0.9 / 015 E 20 -65
1.8 / 319 N 46 -73	1.0 / 330 N 75 -75
1.4 / 312 N 58 -78	1.1 / 293 S 72 -49
1.0 / 158 S 68 -85	1.2 / 009 E 10 -74
1.3 / 329 N 82 +58	1.4 / 345 N 78 +75
1.0 / 246 N 66 -84	2.6 / 339 N 72 +87
2.5 / 323 N 38 +79	1.0 / 330 S 76 -02

Regional Bedding Orientation: 148 NE 72

1.7 / 317 N 57 -75	1.8 / 146 S 88 -72
1.0 / 359 E 42 -82	1.9 / 148 S 85 -79
0.8 / 014 S 45 ±90	0.6 / 129 S 57 -04
0.9 / 138 S 58 -72	0.6 / 092 S 55 -69
2.0 / 000 E 75 +09	0.5 / 078 S 68 -16
1.0 / 010 E 58 -38	0.9 / 105 N 74 -09
0.8 / 061 S 61 -12	1.1 / 139 N 69 -59
0.9 / 130 S 85 -76	0.8 / 126 S 83 -77
0.8 / 062 S 70 -80	0.6 / 350 E 63 -80
1.0 / 130 S 86 -81	1.8 / 095 S 46 -67
2.5 / 121 N 68 -62	1.1 / 048 S 65 +75
0.9 / 098 S 56 +13	0.7 / 016 N 05 -67
1.1 / 135 S 88 -36	0.8 / 060 S 49 -01

1.2 / 054 S 58 -90

1.6 / 112 N 61 -52

1.0 / 131 VERT -60

TABLE

Section 4-23, Thistle Creek (142 m level)

137 W 27	012 W 65	160 E 07
178 W 25	177 W 59	032 E 40
169 W 33	025 W 36	175 W 51
054 W 40	160 W 35	004 W 27
094 N 11	015 W 70	100 N 31
179 W 68	033 W 42	027 W 57
110 N 28	003 W 36	060 N 50
008 W 41	005 W 32	110 S 64
172 W 42	008 W 37	136 S 70
006 W 30	085 N 20	114 S 30
065 E 20	135 E 22	069 S 44
035 W 38	030 W 45	130 S 32
150 W 46	135 S 40	138 W 18
032 W 41	030 W 47	104 S 29
075 S 33	090 N 26	030 W 34
162 W 41	118 S 80	038 W 21
105 S 45	100 N 35	019 W 14
095 N 44	038 W 84	135 S 27
080 S 52	150 E 23	050 W 46
064 N 50	036 W 34	136 W 57

TABLE

Section 4-25, Thistle Creek (143 m level)

Regional Bedding Orientation:

001 E 20	069 S 23	126 S 13
250 E 26	107 S 25	320 S 14
107 S 27	194 E 70	266 S 30
296 S 36	120 S 21	239 N 60
290 S 30	115 S 15	299 S 25
009 E 09	194 W 05	156 W 15
294 S 35	073 S 30	348 S 76
253 S 65	006 E 15	305 S 65
345 W 12	342 W 09	322 SW 30
188 E 15	122 N 65	350 W 35
310 S 10	316 N 15	324 W 25
292 S 08	210 E 50	135 S 35
144 S 20	161 W 10	164 W 25
193 E 17	162 W 14	145 E 34
152 S 40	197 E 34	125 S 70
054 E 60	310 N 52	220 E 34
109 S 55	105 S 34	231 E 17
209 E 56	344 E 58	108 N 24
134 S 79	121 S 21	140 S 23
132 S 10	073 S 60	185 E 55
184 W 24	186 E 58	125 S 60
188 E 35	130 S 25	210 E 08
168 E 45	146 S 75	135 S 18
350 E 53	099 S 37	348 W 30
329 S 44	181 W 33	116 N 16
315 S 36	185 W 22	150 W 15
127 S 37	011 W 37	152 E 12
146 N 52	026 W 40	208 S 44
096 S 20	228 E 47	060 S 35

290 S 46
265 S 15
017 E 30

203 E 58
170 W 20

203 E 34
130 N 24

TABLE

Section 6-8, Red Deer River (75 m level)

Regional Bedding Orientation: 151 NE 50

1.4 / 348 E 16 -15	0.6 / 335 S 13 -22
0.6 / 341 S 30 -74	5.1 / 351 E 12 -36
0.3 / 018 S 31 -60	1.4 / 026 S 15 -29
1.0 / 353 E 43 -03	1.2 / 044 S 12 -68
0.7 / 007 E 50 -04	0.9 / 205 N 34 -06
1.5 / 345 S 51 -63	1.2 / 353 E 12 +58
2.2 / 008 E 49 +26	1.0 / 327 S 05 +65
1.7 / 336 N 15 -36	0.5 / 335 S 09 +34
2.0 / 316 N 10 00	0.6 / 005 E 50 -33
0.8 / 018 S 22 -71	3.2 / 003 E 37 +03
7.0 / 328 N 23 ±90	2.0 / 332 S 21 -06
2.4 / 325 N 65 -16	1.3 / 164 N 20 +19
1.6 / 358 N 55 -69	2.0 / 024 S 83 -84
1.2 / 026 S 67 +25	2.2 / 337 S 29 +26
0.8 / 344 N 28 +22	2.1 / 340 S 74 -09
1.6 / 324 N 74 ±90	0.6 / 307 N 61 -17
1.7 / 360 E 12 +01	1.1 / 297 N 27 +57
2.1 / 157 W 25 -06	1.3 / 012 E 41 ±90
0.5 / 013 E 09 -34	1.2 / 329 S 45 +73
0.7 / 225 N 53 -21	0.7 / 079 S 51 -53
1.3 / 349 W 73 -09	0.7 / 086 S 88 +37
1.0 / 332 N 34 -83	0.8 / 298 N 32 -50
0.7 / 350 E 26 -21	1.0 / 014 E 05 +79
0.7 / 337 N 46 -35	1.7 / 295 N 21 -19
0.9 / 004 E 44 -28	1.3 / 190 N 18 -06
1.4 / 096 S 32 +06	1.1 / 008 E 55 +21
1.4 / 313 N 50 -33	0.8 / 354 E 50 -19
1.3 / 305 N 70 ±90	0.6 / 338 N 55 -24
1.6 / 322 N 17 -29	0.9 / 053 S 35 ±90

1.0 / 025 S 34 +70
1.5 / 058 S 27 -84
0.6 / 307 N 31 -61
0.7 / 312 N 48 -30
1.5 / 280 N 67 -23
0.7 / 337 N 47 -67
1.2 / 321 N 61 -32
0.8 / 275 N 63 -38
1.0 / 328 N 35 -75
0.7 / 147 N 21 -18
1.2 / 302 N 29 +85
1.6 / 342 N 35 -48
1.1 / 314 N 38 -18
1.7 / 338 N 45 -14
2.0 / 335 N 32 -40
1.8 / 320 N 44 -36
3.2 / 009 E 12 +78
1.4 / 359 E 50 +05
1.3 / 308 N 65 -47
0.7 / 290 S 76 -65
1.5 / 343 E 72 +40
1.4 / 342 E 33 -76
1.6 / 339 E 31 -44
2.9 / 028 W 73 +24
2.2 / 348 E 50 -74
2.8 / 146 W 46 -13
2.0 / 058 S 24 -72
2.7 / 324 E 50 -78
2.4 / 358 E 66 +52
1.2 / 026 E 18 ±90
0.9 / 065 N 75 -54
2.6 / 305 N 42 -15
1.2 / 042 E 19 -12

2.0 / 280 N 21 - 8
0.7 / 272 N 20 +32
2.8 / 332 N 49 -09
1.6 / 014 E 75 +82
2.4 / 002 E 63 -57
1.0 / 317 N 29 +42
1.3 / 005 E 54 -79
1.3 / 317 E 63 -09
1.5 / 038 E 14 -06
1.6 / 328 E 78 -83
0.8 / 272 S 72 -56
1.4 / 324 E 64 -04
1.3 / 332 E 40 -34
0.9 / 042 E 76 -79
1.0 / 298 N 55 -52
1.3 / 323 E 21 ±00
2.0 / 083 S 13 +66
1.9 / 306 S 72 -01
2.5 / 300 N 55 -71
1.7 / 346 E 34 +60
3.8 / 325 E 85 +19
2.0 / 333 E 50 -07
2.3 / 328 E 54 -74
2.0 / 359 E 44 -82
1.1 / 036 E 22 -85
1.2 / 360 E 42 -51
2.3 / 328 N 32 -12
2.7 / 353 E 27 -36
1.7 / 022 E 58 +40
1.5 / 348 E 25 +42
2.2 / 308 N 46 -17
2.5 / 356 E 40 -27
1.7 / 352 E 51 -64

4.7 / 035 E 55 +42
1.6 / 258 N 54 -41
2.4 / 328 E 84 +09

1.2 / 031 E 21 -84
1.5 / 351 E 45 +44

TABLE

Section 6-8, Red Deer River (135 m level)

Regional Bedding Orientation: 153 NE 38

0.6 / 024 E 21 ±90	1.2 / 147 E 45 +06
0.8 / 342 E 32 +03	1.0 / 353 E 39 -37
1.2 / 085 N 55 +21	0.9 / 078 S 80 +12
1.0 / 078 S 31 -70	0.8 / 138 E 52 -12
3.5 / 105 N 70 +25	1.7 / 023 E 72 -80
1.0 / 348 E 50 +86	1.0 / 095 S 24 +44
1.7 / 124 S 12 -69	0.9 / 319 E 35 -09
1.3 / 022 E 56 -78	1.0 / 002 E 55 -30
1.3 / 012 E 22 -81	1.1 / 005 E 21 +07
1.1 / 075 N 48 +17	1.4 / 052 N 80 -13
1.0 / 107 N 50 -10	0.7 / 342 E 30 -25
1.5 / 098 S 64 -12	1.2 / 332 E 25 -66
1.4 / 040 W 67 -55	1.6 / 322 E 24 -54
1.2 / 135 S 30 +70	2.3 / 327 E 36 -44
1.2 / 172 E 78 -58	1.0 / 317 E 58 -46
1.1 / 205 W 50 +09	0.9 / 095 S 15 -78
0.6 / 333 E 30 +70	0.9 / 358 E 30 -82
1.3 / 087 S 14 -19	1.8 / 134 N 58 +66
1.2 / 325 E 12 +85	1.5 / 216 W 31 -10
1.0 / 276 N 15 -02	1.4 / 355 E 42 -54
1.2 / 094 N 78 -14	1.0 / 353 E 22 -78
0.6 / 324 E 16 -78	1.1 / 355 E 52 ±90
1.1 / 122 S 24 +41	0.8 / 201 W 50 -20
1.2 / 312 N 45 ±00	1.9 / 293 E 28 -06
0.9 / 329 E 32 -18	1.2 / 330 E 27 ±90
2.6 / 225 W 36 -21	0.8 / 078 S 60 +03
1.2 / 323 E 25 -42	1.0 / 324 E 24 -59
1.0 / 025 E 41 -58	1.1 / 325 E 26 -46

2.0 / 274 N 36 -12	1.2 / 148 E 65 +24
1.1 / 075 S 72 -78	0.5 / 072 W 76 -06
0.8 / 022 W 86 -26	1.4 / 004 E 56 -39
1.3 / 028 E 44 -21	0.7 / 023 E 45 +27
2.0 / 102 S 75 -61	1.7 / 130 N 75 -56
1.5 / 093 S 50 -70	1.4 / 168 E 64 -45
0.9 / 094 S 39 -48	0.8 / 100 E 30 -46
0.8 / 097 S 32 -62	0.8 / 122 N 82 +78
1.8 / 150 S 81 -47	0.9 / 092 S 48 -75
1.5 / 063 N 48 +27	1.0 / 138 E 65 -36
1.0 / 095 S 05 +71	0.8 / 358 E 45 -76
0.8 / 012 N 78 ±00	1.2 / 320 E 45 -29
1.3 / 074 S 78 ±90	2.5 / 332 E 42 -44
1.2 / 323 E 24 -58	1.0 / 009 E 79 +03
1.0 / 357 E 78 -63	1.2 / 112 N 44 -15
0.9 / 312 N 30 -25	1.5 / 318 E 44 -08
1.2 / 002 W 69 -49	1.0 / 358 E 65 -64
1.4 / 317 N 44 -24	1.1 / 008 E 76 -65
1.6 / 349 E 41 -52	1.4 / 348 E 35 +52
1.3 / 072 N 53 +51	1.6 / 315 N 44 -24
1.0 / 127 S 20 -01	1.4 / 327 E 32 -55
1.1 / 141 E 71 -06	1.8 / 184 W 64 -06
2.1 / 270 N 48 -60	1.4 / 338 E 36 -11

TABLE

Section GC-1, Grande Cache Highway Roadcut,
Route 40 (47.5 m level)

Regional Bedding Orientation: 135 NE 42.

1.0 / 268 N 44 +24	1.5 / 019 E 13 +41
2.5 / 089 N 41 +71	1.5 / 125 NE 42 +58
1.5 / 076 N 26 +14	2.5 / 112 N 13 -74
1.0 / 283 N 52 -84	1.0 / 065 SE 67 +39
1.0 / 091 S 31 -85	1.0 / 064 SE 60 +42
1.5 / 023 SE 21 -09	2.0 / 185 E 27 -74
1.5 / 006 W 31 -41	1.0 / 115 N 55 +56
1.5 / 132 NE 18 +53	2.0 / 065 NE 42 +17
1.0 / 154 NE 32 +54	1.0 / 141 NE 20 +69
1.0 / 259 N 25 -32	1.0 / 114 NE 31 +65
1.5 / 123 NE 44 +88	1.0 / 181 E 24 -32
1.0 / 162 NE 46 -59	1.0 / 110 N 55 +48
1.5 / 184 E 58 -47	1.0 / 076 N 45 +59
1.5 / 268 N 21 -67	1.0 / 060 NW 46 -11
1.5 / 154 NE 28 -46	1.0 / 292 N 55 -74
1.0 / 143 NE 51 -57	1.0 / 096 N 38 +45
1.5 / 146 NE 46 +58	1.0 / 070 NW 57 +40
1.0 / 166 NE 55 +04	2.0 / 143 NE 38 +12
1.0 / 272 N 25 +23	1.5 / 318 N 29 -11
1.5 / 130 NE 41 +63	1.5 / 127 NE 44 +14
1.0 / 116 NE 55 -12	1.0 / 136 NE 26 -36
1.5 / 122 NE 27 -64	1.0 / 103 N 38 +16
1.0 / 310 N 43 +58	1.0 / 286 N 60 +52
1.0 / 138 NE 57 -08	1.0 / 290 N 45 +90
1.5 / 014 E 48 +01	2.0 / 359 E 37 -24
1.5 / 145 NE 27 +36	1.0 / 068 SE 24 -24
1.0 / 294 N 44 +56	1.0 / 204 E 14 +31
1.5 / 100 N 64 +54	1.5 / 192 E 19 -49

1.0 / 164 SW 11 -31
1.0 / 120 N 40 +67
1.0 / 323 NE 38 -21
1.0 / 300 N 44 -31
1.0 / 134 SW 51 +01
1.0 / 195 E 25 +24
1.0 / 087 N 16 +42

1.0 / 154 SE 42 +24
1.0 / 122 N 27 -46
1.0 / 163 E 44 -08
1.5 / 290 N 19 +87
1.5 / 179 E 24 +76
1.0 / 185 E 24 -37
1.0 / 157 NE 22 -36

TABLE

Section GC-1, Grande Cache Highway Roadcut,
Route 40 (49 m level)

Regional Bedding Orientation: 135 NE 42

1.0 / 357 E 32 -14
2.0 / 193 E 24 -64
3.5 / 168 NE 29 -69
1.5 / 141 NE 35 -61
1.5 / 167 NE 39 -57
2.0 / 027 W 24 -16
2.0 / 161 NE 39 +34
2.0 / 134 NE 30
2.5 / 075 S 23 -42
3.0 / 170 E 43 +81
1.5 / 168 NE 27 +24
1.5 / 152 NE 35 -18
1.0 / 156 NE 29 -45
1.0 / 065 NW 30 +14
2.0 / 092 N 18 +25
2.0 / 250 N 42 -10
1.5 / 330 NE 31 -54
1.0 / 178 E 60 -29
1.5 / 152 NE 24 -09
1.0 / 134 NE 25 -57
1.5 / 322 NE 26 -27
1.5 / 140 NE 25 -43
2.5 / 123 NE 25 -45
3.5 / 189 E 26 -30
1.5 / 129 NE 55 +32
1.5 / 173 E 31 -54
2.5 / 305 N 27 -41
1.5 / 334 NE 24 +13
1.5 / 313 SW 31 -02
1.5 / 331 NE 20 +14
1.0 / 326 NE 39 -31
4.5 / 124 NE 27 -05
4.0 / 141 NE 44 -09
1.0 / 145 NE 42 -88
4.0 / 136 NE 42 -14
4.5 / 145 Ne 37 -05
2.0 / 266 N 37 +88
1.5 / 157 NE 71 +09
1.0 / 331 NE 68 -77
2.0 / 082 N 21 +87
2.0 / 218 SW 38 -42
1.5 / 143 NE 19 -06
1.5 / 154 NE 30 -26
2.0 / 320 NE 26 +14
1.0 / 300 N 33 -84
1.0 / 164 E 54 +34
1.5 / 033 NW 27 +27
1.5 / 138 NE 11 +13
1.0 / 316 NE 37 -69
1.5 / 094 N 37 +29
1.5 / 304 N 22 +71
1.5 / 108 N 30 -09
5.0 / 126 NE 41 -04
2.0 / 108 N 20 +28
1.5 / 332 NE 41 -02
1.5 / 092 N 46 +39

1.5 / 150 NE 49 -02
2.0 / 105 N 22 +50
1.5 / 041 NW 18 +50
2.0 / 125 NE 54 -12
1.5 / 156 NE 35 +54
1.5 / 023 SE 39 -26
1.5 / 152 NE 36 -54

1.0 / 357 E 52 -32
2.5 / 321 NE 37 -26
4.0 / 312 NE 39 -07
1.0 / 088 N 40 -35
4.5 / 277 N 43 +14
1.0 / 199 E 25 +51
2.5 / 136 NE 21 -08

TABLE

Section GC-1, Grande Cache Highway Roadcut,
Route 40 (49.5 m level)

Regional Bedding Orientation: 135 NE 42

3.0 / 185 W 21 +32	4.0 / 308 N 25 -49
1.5 / 156 NE 47 -46	1.0 / 301 N 17 -56
1.0 / 164 NE 51 -51	1.0 / 311 N 54 -56
1.5 / 346 NE 23 +49	1.5 / 330 NE 38 -36
1.5 / 326 NE 44 -24	1.0 / 327 NE 45 -41
1.5 / 161 E 89 +44	1.5 / 278 N 41 -64
1.5 / 178 S 33 -59	1.5 / 318 E 28 -30
1.5 / 131 NE 40 +56	1.5 / 149 NE 36 -60
1.0 / 143 NE 60 -72	1.5 / 133 NE 47 +19
1.5 / 195 W 32 +66	1.5 / 141 SW 34 +59
2.5 / 315 NE 31 -81	1.0 / 274 S 25 -46
1.5 / 128 NE 23 -37	5.0 / 332 NE 29 +11
1.5 / 342 NE 44 -01	5.0 / 350 E 14 ±90
1.0 / 002 W 19 +04	5.0 / 131 NE 24 +13
1.0 / 052 NW 64 +19	2.0 / 278 N 24 +04
1.5 / 131 NE 75 +19	1.5 / 226 NW 64 +46
1.0 / 116 NE 12 +62	1.5 / 322 NE 38 -31
3.5 / 192 E 17 -20	1.5 / 144 NE 49 -11
2.0 / 174 E 51 -11	1.5 / 154 NE 29 +10
3.0 / 123 NE 26 +70	1.5 / 097 N 31 +59
2.0 / 302 NE 31 -59	2.0 / 136 NE 35 -31
2.0 / 129 NE 31 -59	1.5 / 127 NE 32 +25
1.5 / 128 NE 35 -19	1.0 / 342 E 40 -29
1.5 / 105 N 66 +30	2.0 / 047 NW 55 +27
1.5 / 025 SE 30 -62	2.0 / 359 W 46 +55
2.0 / 305 NE 78 +25	1.0 / 139 VERT +69
1.0 / 116 NE 41 +77	2.0 / 222 NW 37 -74
1.0 / 128 NE 63 +29	2.0 / 282 N 57 +36

1.0 / 020 SE 45 +46
1.5 / 133 NE 45 +58
1.0 / 115 NE 44 +36
1.5 / 120 NE 49 -10
1.0 / 284 N 54 +54
1.0 / 129 NE 39 +51
2.0 / 142 NE 57 -19
1.0 / 145 NE 21 +13
2.5 / 155 NE 39 +06
1.0 / 300 N 60 -72
1.5 / 235 NW 57 +08
1.5 / 107 N 67 -03
1.0 / 148 NE 23 -29
1.5 / 113 NE 69 +81
1.5 / 137 SW 70 +35
1.5 / 119 NE 45 -29
1.5 / 101 N 62 + 28
1.0 / 110 E 56 -26
2.0 / 106 E 24 -16
1.5 / 353 E 16 +90
1.0 / 123 NE 61 +19
1.0 / 267 N 72 +65

1.0 / 073 NW 67 -24
1.0 / 146 NE 34 -70
1.0 / 119 NE 81 -51
1.0 / 138 W 43 +71
1.0 / 127 NE 76 -69
1.0 / 120 NE 39 -29
1.0 / 141 NE 26 +14
1.5 / 269 N 42 +35
1.5 / 134 SW 37 22
1.0 / 168 E 25 -18
1.0 / 198 E 26 -37
1.0 / 167 NE 58 -10
1.5 / 154 NE 31 - 1
1.0 / 169 E 45 -29
1.5 / 083 N 51 -08
1.0 / 176 E 39 -51
1.0 / 344 E 54 -32
1.0 / 150 NE 19 +59
1.0 / 353 E 43 -34
1.5 / 014 E 65 -29
1.5 / 142 NE 46 -31
1.0 / 149 NE 41 -32

TABLE

Section GC-1, Grande Cache Highway Roadcut,
Route 40 (57.5 m level)

Regional Bedding Orientation: 135 NE 39

1.0 / 145 NE 44 +31	1.0 / 139 NE 25 -71
2.0 / 323 NE 31 -26	1.5 / 144 NE 22 -71
1.0 / 081 N 34 +34	0.5 / 191 E 22 +51
0.5 / 181 E 43 +44	1.0 / 150 NE 39 -30
1.0 / 260 N 21 -78	1.5 / 255 N 14 -74
1.5 / 137 NE 29 -35	1.0 / 145 NE 24 +28
1.0 / 249 N 53 -21	2.5 / 123 N 47 ±90
0.5 / 272 N 50 -08	2.0 / 286 N 54 +59
1.0 / 115 N 44 +42	1.0 / 146 NE 68 +03
1.0 / 169 E 80 -36	2.0 / 137 NE 45 +82
0.5 / 350 E 25 -51	1.0 / 045 NW 16 +77
1.0 / 138 NE 40 -20	0.5 / 148 NE 54 -19
0.5 / 179 E 49 -26	1.5 / 122 NE 40 -32
0.5 / 006 E 38 +86	2.0 / 316 NE 35 +14
0.5 / 278 N 41 ±90	2.0 / 104 N 46 -24
2.0 / 077 N 36 +79	2.0 / 286 N 32 -49
1.5 / 138 NE 37 +21	2.5 / 091 N 15 +26
1.0 / 154 NE 55 -42	1.0 / 181 W 32 -33
1.0 / 354 E 18 +32	1.0 / 090 N 31 +43
1.0 / 212 NW 13 -43	1.5 / 169 N 36 -20
0.5 / 210 SE 24 -54	1.5 / 114 N 42 -72
1.0 / 060 NW 16 -76	2.0 / 132 NE 48 +66
1.5 / 150 E 58 +07	1.0 / 289 N 52 +34
2.0 / 141 NE 39 +88	1.0 / 350 E 54 -54
1.0 / 141 NE 61 +49	1.0 / 059 NW 58 +75
1.5 / 316 NE 44 +84	1.0 / 115 N 48 -20
2.0 / 126 NE 29 +31	2.5 / 002 N 51 +24
2.0 / 124 NE 31 -40	2.0 / 102 S 24 -16

1.5 / 022 NW 27 +86
1.0 / 139 NE 34 -26
1.5 / 068 NW 37 +64
1.0 / 311 NE 37 -49
1.5 / 115 N 31 +64
1.5 / 321 NE 32 +87
1.5 / 082 N 18 -64
1.0 / 132 NE 14 -60
1.0 / 152 NE 36 -67
1.0 / 039 NW 73 +45
1.0 / 283 N 42 -89
2.0 / 284 N 47 -32
1.5 / 314 NE 40 -05
1.5 / 119 N 26 +10
1.0 / 145 NE 21 +50
1.0 / 137 NE 26 -42
1.0 / 032 NW 43 +64
1.0 / 232 NW 40 -85
1.5 / 130 NE 29 +81
2.0 / 081 N 30 +61
1.0 / 118 N 56 +28
2.0 / 131 NE 41 -26
2.0 / 281 N 50 +21
1.5 / 117 N 32 -59
1.5 / 307 N 49 +89
2.0 / 124 NE 48 +54
0.5 / 039 SE 42 +34
1.5 / 133 NE 32 -50
1.0 / 060 NW 24 +65
1.0 / 263 N 65 -78
1.0 / 122 NE 25 -70
1.0 / 351 E 31 +35
1.0 / 346 E 26 +64
1.0 / 271 N 24 +46
1.5 / 141 NE 61 +75
1.5 / 161 E 34 -34
1.5 / 030 NW 31 +8
1.5 / 294 N 38 +71
1.0 / 340 E 48 +27
1.5 / 032 NW 16 +18
1.5 / 344 NE 40 +24
1.0 / 020 NW 44 +55
1.0 / 060 NW 62 +65
0.5 / 210 W 21 +30

TABLE

Section GC-2, Grande Cache Railway (49 m level)

Regional Bedding Orientation: 138 NE 32

1.1 / 340 E 64 ±90	1.1 / 290 N 37 +32
1.0 / 271 N 51 -87	0.9 / 287 N 40 +20
1.4 / 322 E 72 +40	0.8 / 282 N 20 +52
0.9 / 330 E 54 +66	1.0 / 306 N 54 +71
1.6 / 286 N 63 -34	0.8 / 294 N 31 -69
1.0 / 310 N 49 +88	0.7 / 283 N 45 -61
1.5 / 314 N 46 +06	0.6 / 261 N 15 -22
1.0 / 305 N 15 +73	0.7 / 278 N 34 +24
1.0 / 342 E 36 -58	1.2 / 327 E 60 +24
1.1 / 335 E 45 +18	0.9 / 278 N 58 -48
1.1 / 322 E 52 +61	1.0 / 312 N 45 -15
1.2 / 320 E 45 +10	0.9 / 309 N 38 +14
1.8 / 313 N 28 +19	1.2 / 314 N 41 -44
1.0 / 310 N 46 +09	1.0 / 310 N 40 +10
0.9 / 295 N 46 +19	1.0 / 302 N 40 +34
1.0 / 326 E 47 -52	0.8 / 311 N 45 -85
1.7 / 305 N 37 +49	1.0 / 290 N 38 +85
0.8 / 310 N 35 ±90	1.0 / 295 N 44 -82
0.9 / 303 N 56 -50	1.1 / 300 N 25 +38
1.2 / 308 N 34 +05	1.0 / 309 N 46 -55
1.0 / 309 N 46 +23	1.1 / 311 N 39 -05
1.0 / 288 N 35 -70	1.1 / 329 E 33 -81
1.1 / 283 N 44 +77	1.3 / 310 N 29 +42
0.7 / 323 E 65 -39	1.2 / 315 N 30 +43
1.1 / 096 S 48 +27	0.9 / 307 N 32 +86
1.0 / 285 N 42 -80	1.2 / 323 E 53 -07
0.7 / 284 N 42 -89	0.7 / 312 N 46 -14
1.0 / 311 N 56 -74	0.8 / 309 N 45 -09

0.6 / 312 N 46 +46	1.2 / 335 E 42 +85
1.1 / 269 N 44 +05	1.0 / 302 N 70 -12
0.9 / 290 N 39 +83	0.9 / 347 E 46 +90
0.9 / 283 N 35 +73	0.9 / 299 N 40 -81
1.0 / 327 E 20 -30	0.9 / 305 N 39 -72
0.6 / 294 N 14 -27	0.8 / 276 N 14 +67
0.6 / 325 E 30 -74	1.1 / 355 N 34 -85
1.1 / 306 N 38 -76	0.8 / 305 N 44 -45
1.1 / 288 N 44 -86	1.2 / 316 N 71 -02
1.1 / 321 N 13 +03	

TABLE

Section GC-2, Grande Cache Railway (58 m level)

Regional Bedding Orientation: 138 NE 32

1.0 / 305 N 24 -84	1.0 / 255 N 55 ±90
1.2 / 319 E 27 -71	1.5 / 246 N 34 -63
0.8 / 240 N 71 -80	0.9 / 264 N 20 -81
0.8 / 312 N 50 -48	2.0 / 219 W 84 -05
1.2 / 218 W 55 -53	1.0 / 285 N 82 -05
1.0 / 253 N 31 +39	0.9 / 304 N 24 -87
0.9 / 210 W 10 +85	1.1 / 286 N 81 -84
0.9 / 317 E 42 -76	1.0 / 026 E 04 +37
1.0 / 275 N 50 -78	1.0 / 271 N 41 -13
1.5 / 278 N 22 -15	1.4 / 282 N 20 +67
1.0 / 220 W 30 -24	0.8 / 261 N 23 -70
1.0 / 325 E 05 +78	0.7 / 320 E 31 -10
1.3 / 338 E 35 -34	0.8 / 335 E 35 -17
1.7 / 268 N 44 -02	1.0 / 183 W 85 +11
1.2 / 267 N 42 +22	1.5 / 192 W 88 +20
1.5 / 302 N 62 +04	0.8 / 281 N 88 -06
0.8 / 255 N 48 -72	1.5 / 166 W 45 -23
0.8 / 255 N 48 -86	0.8 / 333 E 25 -68
0.8 / 194 W 36 ±90	2.1 / 258 N 53 -36
1.0 / 294 N 44 +54	1.0 / 284 N 22 -01
0.9 / 349 E 66 +71	1.0 / 322 E 12 -20
0.9 / 128 S 22 -09	0.8 / 312 N 34 ±90
0.8 / 342 E 18 +55	2.4 / 274 N 21 -88
0.8 / 285 N 78 -28	0.6 / 344 E 76 +56
1.0 / 152 W 37 -30	0.8 / 317 W 64 -21
0.7 / 305 S 80 +80	1.0 / 235 N 45 -22
1.0 / 320 E 26 ±00	1.4 / 250 N 65 +72
1.4 / 344 E 55 -01	0.9 / 214 W 22 -49

1.4 / 006 E 10 +50
0.8 / 244 N 78 -07
1.1 / 312 N 26 +24
0.8 / 205 W 38 +02
2.0 / 350 E 24 -77
3.5 / 308 S 52 -03
1.3 / 172 W 35 -85
0.9 / 272 N 65 +02
0.6 / 160 W 15 -68
1.0 / 158 W 08 -30
1.5 / 245 S 16 +03
0.8 / 300 N 85 +76
1.0 / 292 N 55 +82
1.0 / 235 S 56 +02
0.9 / 235 N 58 -04
1.0 / 235 N 34 -67
1.2 / 205 E 61 -41
2.0 / 276 N 22 +75
1.0 / 265 S 60 ±00
0.7 / 220 E 85 +29
0.8 / 263 S 88 -64
1.0 / 247 S 64 +16
0.8 / 270 N 18 -71

0.8 / 273 N 35 -72
1.0 / 260 N 48 -35
1.0 / 328 E 20 -73
1.1 / 132 S 30 -16
0.8 / 305 N 48 +05
1.0 / 207 W 68 -46
1.0 / 278 N 38 +32
1.5 / 037 E 43 +45
2.3 / 257 N 28 +61
1.2 / 276 N 25 +76
0.7 / 280 N 80 +75
0.8 / 282 N 45 -44
1.5 / 278 N 24 +77
1.5 / 278 N 42 -46
1.4 / 295 S 70 +02
1.2 / 165 W 25 -65
1.0 / 207 W 25 +61
1.1 / 328 E 48 +67
1.9 / 065 S 10 ±00
0.7 / 320 E 38 +50
0.8 / 355 E 35 +23
0.9 / 120 S 20 ±90
0.8 / 338 E 38 +76

TABLE

Section GC-2, Grande Cache Railway (51 m level)

Regional Bedding Orientation: 138 NE 32

2.0 / 323 E 43 -68	1.9 / 355 E 35 +85
2.2 / 332 E 42 -05	1.0 / 353 E 30 -73
1.1 / 330 E 37 -15	1.4 / 263 N 15 +43
1.6 / 318 E 36 -23	1.5 / 331 E 36 -75
1.6 / 328 E 10 +15	1.0 / 284 N 30 -09
2.7 / 162 W 32 -21	0.6 / 303 N 43 -04
1.9 / 146 S 18 -63	1.0 / 328 E 45 +08
3.5 / 267 N 10 -05	1.1 / 257 N 76 +35
1.2 / 306 N 44 -06	1.2 / 300 N 30 -85
1.1 / 302 N 62 +16	1.5 / 001 E 49 +64
1.6 / 270 N 40 -46	0.9 / 252 N 40 ±90
1.3 / 245 N 35 +55	2.1 / 258 N 45 -82
0.9 / 317 N 42 +34	1.9 / 289 S 80 -78
2.2 / 258 N 60 ±90	1.0 / 225 W 14 -37
0.7 / 265 N 35 -76	1.4 / 231 N 42 -54
0.8 / 032 E 26 +56	0.9 / 290 S 48 +79
1.1 / 043 E 25 +58	0.8 / 212 N 78 +28
0.8 / 227 S 68 +84	0.9 / 307 N 26 -80
2.5 / 316 W 05 +30	2.2 / 313 N 25 +09
1.2 / 222 W 85 -75	1.2 / 328 E 34 -67
0.8 / 233 N 72 +07	1.1 / 245 S 74 +08
1.2 / 295 N 14 -81	1.0 / 231 N 75 -23
1.3 / 230 N 68 -15	1.2 / 158 W 25 -48
1.0 / 010 E 28 +73	1.0 / 265 N 13 -40
1.0 / 290 N 15 +11	1.0 / 007 E 39 +80
1.1 / 335 E 85 +70	1.0 / 269 S 59 +76
0.9 / 040 E 25 +60	0.8 / 209 W 85 +29
1.3 / 304 N 35 +85	1.0 / 317 E 56 +76

0.8 / 327 E 38 -80
1.0 / 305 N 48 -54
1.5 / 322 E 42 -60
0.8 / 268 N 28 -86
1.8 / 204 E 76 +78
0.8 / 256 N 46 +35
0.9 / 234 S 84 +36
1.5 / 255 N 69 -80
1.3 / 284 S 82 -72
1.4 / 272 N 84 -80
1.4 / 276 N 50 +61
1.8 / 292 N 44 +67
0.9 / 234 S 84 +36
1.5 / 255 N 69 -80
1.3 / 284 S 82 -72
1.4 / 272 N 84 -80
1.4 / 276 N 50 +61
1.8 / 292 N 44 +67
1.3 / 329 W 70 +09
0.9 / 322 W 67 -76
1.0 / 327 E 75 -67
1.0 / 281 S 56 +75
4.5 / 307 N 27 +14
1.8 / 249 N 23 -16
1.2 / 258 N 50 +44
0.7 / 254 N 68 +87
1.1 / 309 VERT -14
0.9 / 225 N 80 +15

1.0 / 159 W 50 +50
1.5 / 234 N 38 +36
6.8 / 315 N 44 +16
1.2 / 344 E 75 +34
0.9 / 318 E 51 -73
1.4 / 316 E 78 +15
1.0 / 336 E 74 -78
1.5 / 289 N 80 -86
1.0 / 310 N 56 ±90
1.0 / 263 N 48 -41
1.0 / 250 N 54 ±90
1.2 / 256 N 63 +36
1.0 / 336 E 74 -78
1.5 / 289 N 80 -86
1.0 / 310 N 56 ±90
1.0 / 263 N 48 -41
1.0 / 250 N 54 ±90
1.2 / 256 N 63 +36
2.0 / 284 N 30 -34
1.5 / 290 S 76 +08
1.5 / 278 N 14 -42
1.0 / 348 E 40 +24
1.9 / 212 E 45 +29
1.4 / 012 E 40 -54
2.2 / 342 E 36 +58
3.5 / 340 E 35 ±90
1.3 / 195 E 58 +72
1.0 / 234 E 71 +05

TABLE

Section SC-1, Sphinx Creek (80 m level)

Regional Bedding Orientation: 122 SW 79 OVERTURNED

1.5 / 133 SW 66 -49	1.5 / 116 N 78 +34
6.0 / 308 S 83 +42	2.5 / 104 S 86 +24
2.0 / 082 N 52 -36	3.5 / 304 S 86 -53
1.5 / 277 S 53 -76	2.5 / 306 N 84 +49
2.0 / 300 N 82 -31	5.0 / 304 N 88 -25
1.0 / 096 N 76 +34	1.0 / 093 N 80 -50
1.0 / 112 VERT +02	1.0 / 277 S 70 -57
1.0 / 304 N 71 -52	2.0 / 118 N 82 +18
1.5 / 132 NE 81 -50	2.0 / 302 N 89 +49
1.0 / 270 N 68 -51	2.0 / 292 S 77 -64
1.0 / 116 S 74 +37	1.0 / 094 N 70 +74
1.5 / 310 N 87 -48	1.0 / 307 N 66 +88
2.0 / 100 N 38 +13	1.5 / 109 S 73 -57
1.5 / 299 S 61 -06	1.0 / 096 S 69 +31
1.0 / 124 S 79 +69	1.0 / 077 S 71 -36
1.5 / 288 S 88 -54	1.5 / 109 S 51 -29
1.0 / 284 S 76 -34	3.5 / 325 NE 87 -44
1.5 / 300 S 81 -25	1.0 / 131 NE 55 +24
1.0 / 132 SE 70 +66	1.0 / 144 NE 26 +11
1.0 / 151 SE 83 -56	1.0 / 270 S 52 -52
1.0 / 094 N 78 -46	1.5 / 196 E 68 +84
1.0 / 115 N 57 -59	1.5 / 315 SW 57 -19
1.0 / 097 N 87 -51	2.0 / 102 N 71 -15
1.0 / 100 N 66 -23	1.5 / 120 S 75 -32
1.0 / 096 N 64 -27	1.0 / 326 NE 80 +71
1.0 / 123 NW 69 +48	1.5 / 172 E 71 +83
1.0 / 279 S 76 +30	1.0 / 270 N 67 -80
1.5 / 108 S 70 -35	1.0 / 284 S 71 -66

2.0 / 264 S 89 -89
2.5 / 315 NE 75 +78
2.0 / 020 W 41 +86
1.0 / 317 SW 68 +24
1.5 / 081 N 61 -34
2.0 / 310 SW 68 +76
1.0 / 087 N 78 +56
1.5 / 142 NE 69 -61
1.0 / 071 N 65 -69
1.5 / 117 SW 76 +01
2.0 / 290 S 72 -45
1.0 / 147 SW 67 +17
1.5 / 118 VERT -39
1.0 / 135 SW 60 -26
1.0 / 320 SW 80 +80
1.5 / 141 NE 84 +88
2.0 / 310 SW 80 -21
1.0 / 240 SE 47 +81
1.0 / 317 SW 79 +81
1.5 / 132 NE 84 -10
1.0 / 120 N 71 +09
1.5 / 071 SE 72 +24

1.5 / 104 S 69 +38
1.0 / 180 E 18 +65
1.0 / 289 S 66 +24
1.0 / 100 S 66 -16
1.0 / 140 NE 25 +09
1.5 / 135 NE 54 +19
0.5 / 270 N 68 -16
1.0 / 309 NE 45 +22
1.5 / 286 N 66 +90
1.0 / 260 N 56 +74
1.0 / 110 S 89 +14
2.0 / 098 S 57 +50
1.5 / 247 NW 42 +82
1.5 / 124 SW 61 +16
1.0 / 102 S 69 +39
1.5 / 110 S 76 +59
1.0 / 158 NE 65 -32
1.0 / 297 S 77 -59
1.0 / 132 SW 71 +19
2.0 / 100 N 70 +66
2.5 / 104 N 72 -14
1.0 / 125 S 73 -57

TABLE

Section NR-1, North Ram River (39 m level)

Regional Bedding Orientation: 140, SW 44

337 SW 20	330 S 40	146 W 40
156 SW 51	014 W 54	116 NE 36
146 SW 42	341 SW 56	140 SW 39
336 SW 53	010 W 19	176 E 06
145 SW 50	184 W 41	003 W 50
344 SW 46	164 W 54	323 SW 44
135 SW 55	133 SW 55	061 S 26
310 SW 41	324 SW 56	331 SW 51
324 SW 46	316 SW 46	338 SW 34
014 W 66	344 SW 45	324 SW 30
326 NE 56	165 W 39	085 S 69
344 SW 51	047 SE 40	049 NW 04
165 W 65	065 NW 57	021 S 44
255 E 30	247 E 58	128 S 41
321 SW 49	323 SW 49	151 SW 38
323 SW 56	324 SW 44	304 S 55
181 W 45	194 W 74	005 W 45
155 W 53		

APPENDIX 5. VECTOR MEANS OF PALEOFLOW DATA

Paleoflow data obtained for this thesis (other than conglomerate fabric data) have been presented graphically on the measured sections of appendix 2. In most cases (i.e., wherever adequate space was available on the figures of appendix 2), individual paleoflow data were each presented at the stratigraphic level at which they were obtained. In cases involving exceptionally abundant data, adequate space for the presentation of individual measurements was not available on certain of the measured sections of appendix 2, and vector means of groups of data were presented. In each case, the data represented by a vector mean orientation or direction were obtained from roughly the same stratigraphic level in a single section.

This appendix summarizes vector means and chi-squared significance values of selected paleoflow data obtained for this thesis. The data summaries presented herein include those data represented by vector means on the figures of appendix 2; additionally, vector means have been provided for sections with abundant data that nonetheless were presented individually in appendix 2. The data summarized in this appendix were employed in the construction of the figures in chapter 7.

Vector means and chi-squared significance values

reported herein were obtained using a modified version of a FORTRAN program written by I. P. Martini (program "VM"), available at the Department of Geology at McMaster University.

Vector means listed below are classified as "directions" or "orientations". Vector mean directions are determined from directional data (e.g., dip directions from foresets on asymmetrical current ripples). Vector mean orientations are determined from oriented, directionless data (e.g., crest orientations of symmetrical wave ripples). In a few instances, vector mean directions were obtained from data sets which actually include a small percentage of coherent orientational data points (e.g., 5 asymmetrical ripples plus 2 sole marks). In several instances, vector mean orientations were obtained from data sets which actually include a small percentage of coherent directional data points (e.g., 7 sole marks plus 1 flute cast).

SECTION 4-13

Seebe Member, orientation of flow indicators

Number of measurements: 4

Vector mean orientation: 89°-269°

Value of chi-squared significant at greater than 97.5%

SECTION 4-19

Seebe Member, orientation of symmetrical ripple crests

Number of measurements: 5

Vector mean orientation: 135°-315°

Value of chi squared significant at greater than 97.5%

Cutpick Member, Lower Tongue, facies 4IF flow directions

Number of measurements: 4

Vector mean direction: flow toward 180°

Value of chi squared significant at greater than 95.0%

Sundre Member, orientation of sole marks and gutter-casts

Number of measurements: 18

Vector mean orientation: 143°-323°

Value of chi-squared significant at greater than 99.5%

Willmore Member, orientation of gutter-casts

Number of measurements: 12

Vector mean orientation: 76°-256°

Value of chi squared significant at greater than 99.5%

SECTION 4-21

Upper Blackstone Frm., orientation of sole marks

Number of measurements: 7

Vector mean orientation: 166°-346°

Value of chi squared significant at greater than 99.5%

Sundre Member, gutter-cast orientation

Number of measurements: 6

Vector mean orientation: 152°-332°

Value of chi squared significant at greater than 99.5%

SECTION 4-23

Upper Blackstone Frm., direction from asymmetrical ripples and sole marks

Number of measurements: 4

Vector mean direction: flow toward 16°°

Value of chi squared significant at greater than 97.5%

Seebe Member, orientation of symmetrical ripple crests

Number of measurements: 6

Vector mean orientation: 87°-267°

Value of chi squared significant at greater than 97.5%

Seebe Member, orientation of various flow indicators

Number of measurements: 7

Vector mean orientation: 123°-303°

Value of chi squared significant at greater than 99.5%

SECTION 4-43

Seebe Member, orientation of various flow indicators

Number of measurements: 5

Vector mean orientation: 131°-311°

Value of chi squared significant at greater than 99.0%

Cutpick Member, direction from asymmetrical ripples in fluvial channel sandstone

Number of measurements: 27

Vector mean direction: flow toward 169°

Value of chi squared significant at greater than 99.5%

Willmore Member, orientation of symmetrical ripple crests

Number of measurements: 14

Vector mean orientation: 113°-293°

Value of chi squared significant at greater than 99.5%

SECTION 5-4

Seebe Member and lagoonal deposits in lower Cutpick Member, orientation of symmetrical ripple crests

Number of measurements: 6

Vector mean orientation: 124°-304°

Value of chi squared significant at greater than 99.5%

Seebe Member, direction from sole marks and other flow indicators (other than high-angle cross-bedding, see below)

Number of measurements: 15

Vector mean direction: flow toward 251°

Value of chi squared significant at greater than 99.5%

Seebe Member, direction of irregular, high-angle trough cross-bedding in swaley sandstone

Number of measurements: 17

Vector mean direction: flow toward 245°

Value of chi squared significant at greater than 99.5%

Cutpick Member, direction of lagoonal asymmetrical ripples

Number of measurements: 9

Vector mean direction: flow toward 226°

Value of chi squared significant at greater than 99.5%

Cutpick Member, direction of trough cross-bedding in fluvial channel sandstone

Number of measurements: 11

Vector mean direction: flow toward 172°

Value of chi squared significant at greater than 90.0%

SECTION 5-19

Seebe Member, orientation of symmetrical ripple crests

Number of measurements: 5

Vector mean orientation: 115°-295°

Value of chi squared significant at greater than 99.5%

Seebe Member, orientation of sole marks and other flow indicators

Number of measurements: 12

Vector mean orientation: 121°-301°

Value of chi squared significant at greater than 99.5%

Willmore Member, Lower Tongue, orientation of sole marks and parting lineation

Number of measurements: 5

Vector mean orientation: 98°-278°

Value of chi squared significant at greater than 97.5%

Willmore Member, Upper Tongue, direction from various flow indicators

Number of measurements: 16

Vector mean direction: flow toward 266°

Value of chi squared significant at greater than 99.5%

SECTION 5-22

Seebe Member, orientation of various flow indicators

Number of measurements: 5

Vector mean orientation: 60°-240°

Value of chi squared significant at greater than 95.0%

SECTION 5-41

Seebe Member, direction from various flow indicators

Number of measurements: 10

Vector mean direction: flow toward 122°

Value of chi squared significant at greater than 99.5%

Willmore Member, orientation of various flow indicators

Number of measurements: 6

Vector mean orientation: 149°-329°

Value of chi squared significant at greater than 99.5%

SECTION 5-45

Upper Blackstone Frm., asymmetrical ripples

Number of measurements: 16

Vector mean direction: flow toward 127°

Value of chi squared significant at greater than 99.5%

Seebe Member, orientation of symmetrical ripple crests

Number of measurements: 15

Vector mean orientation: 116°-296°

Value of chi squared significant at greater than 75.0%

Willmore Member, orientation of flow indicators

Number of measurements: 3

Vector mean orientation: 117°-297°

Value of chi squared significant at greater than 90.0%

SECTION 6-8

Seebe Member, orientation of sole marks and gutter-casts

Number of measurements: 5

Vector mean orientation: 162°-342°

Value of chi squared significant at greater than 95.0%

Willmore Member, direction from various flow indicators

Number of measurements: 35

Vector mean direction: flow toward 101°

Value of chi squared significant at greater than 99.5%

SECTION 7-1

Upper Blackstone Frm., direction from asymmetrical ripples

Number of measurements: 30

Vector mean direction: flow toward 172°

Value of chi squared significant at greater than 99.5%

Seebe Member, orientation of sole marks

Number of measurements: 7

Vector mean orientation: 127°-307°

Value of chi squared significant at greater than 99.5%

SECTION GC-1

Seebe Member below Grande Cache Split of Cutpick Member, orientation of symmetrical ripple crests

Number of measurements: 7

Vector mean orientation: 126°-306°

Value of chi squared significant at greater than 95.0%

Seebe Member, direction from sole marks and other flow indicators

Number of measurements: 11

Vector mean direction: flow toward 209°

Value of chi squared significant at greater than 99.0%

SECTION GC-2

Seebe Member and lagoonal deposits of Grande Cache Split of Cutpick Member, orientation of symmetrical ripple crests

Number of measurements: 20

Vector mean orientation: 152°-332°

Value of chi squared significant at greater than 99.5%

Seebe Member, direction of irregular, high-angle trough cross-bedding in highest swaley sandstone

Number of measurements: 14

Vector mean direction: flow toward 276°

Value of chi squared significant at greater than 99.5%

SECTION MS-1

Upper Blackstone Frm., direction from asymmetrical ripples plus 1 elongate scour

Number of measurements: 9

Vector mean direction: flow toward 134°

Value of chi squared significant at greater than 99.5%

SECTION ND-1

Lower Seebe Member, orientation of symmetrical ripple crests

Number of measurements: 11

Vector mean orientation: 145°-325°

Value of chi squared significant at greater than 99.5%

Seebe Member, direction of irregular, high-angle trough cross-bedding in swaley sandstone

Number of measurements: 5

Vector mean direction: flow toward 224°

Value of chi squared significant at greater than 97.5%

Cutpick Member, direction of trough cross-bedding in fluvial channel sandstone

Number of measurements: 9

Vector mean direction: flow toward 108°

Value of chi squared significant at greater than 99.5%

SECTION PC-1

Cutpick Member, lowest story of multi-story channel sandstone, direction from trough cross-bedding

Number of measurements: 14

Vector mean direction: flow toward 84°

Value of chi squared significant at greater than 95.0%

Cutpick Member, central story of multi-story channel sandstone, direction from trough cross-bedding

Number of measurements: 46

Vector mean direction: flow toward 96°

Value of chi squared significant at greater than 99.5%

Cutpick Member, highest story of multi-story channel sandstone, direction from trough cross-bedding

Number of measurements: 30

Vector mean direction: flow toward 133°

Value of chi squared significant at greater than 99.5%

GRAND VECTOR MEAN OF THESE DATA FROM SECTION PC-1: Flow direction toward 109°, with chi squared significant at greater than 99.5%

SECTION SC-1

Cutpick Member, direction from trough cross-bedding in fluvial channel sandstone

Number of measurements: 7

Vector mean direction: flow toward 92°

Value of chi squared significant at greater than 75.0%

Willmore Member, orientation of symmetrical ripple crests

Number of measurements: 10

Vector mean orientation: 129°-309°

Value of chi squared significant at greater than 99.5%

Willmore Member, orientation of various flow indicators (does not include asymmetric load structures)

Number of measurements: 12

Vector mean orientation: 111°-291°

Value of chi squared significant at greater than 99.5%

SECTION WA-1

Seebe Member, orientation of various flow indicators

Number of measurements: 4

Vector mean orientation: 28°-208°

Value of chi squared significant at less than 75.0%

EXPLANATORY NOTE: SIGNIFICANCE OF SYMBOLISM IN THE TENTATIVE PALEOGEOGRAPHIC RECONSTRUCTIONS PRESENTED IN CHAPTER 7

Tentative paleogeographic reconstructions for Cardium shorelines in the Foothills were presented as a series of cartoons in chapter 7 (i.e., Fig. 7-4, 7-5, & 7-6). The somewhat involved symbolism employed in these diagrams is clarified herein. The significance of the symbols themselves is explained in the text of chapter 7. The derivation of their orientation is discussed below. For the purposes of this discussion, I shall refer specifically to figure 7-4.

In part A of this figure, those symbols which resemble strike and dip symbols represent my best estimate of the local orientation of the Cardium shoreline and the inferred offshore direction. The estimation of shoreline orientation is largely based upon the vector mean orientation of wave-formed symmetrical ripple crests, assuming that these crestal orientations are roughly parallel to the local trend of the associated shoreline. This assumption is supported by the generally good coherence of symmetrical ripple crest orientations from any one regressive interval at any one exposure (see above data). This coherence is consistent with the inference of formation by shoaling waves with rays oriented roughly

perpendicular to the shoreline (by wave refraction). Coherence is not consistent with formation far from shore by storm waves; ripples formed by such waves would be expected to show a poor coherence resulting from variations in storm track orientation, etc.

In a few instances, inferred shoreline orientation and offshore direction are based solely or in part upon mean strike and dip direction of low-angle planar lamination interpreted as foreshore deposits. In one case, symmetrical ripple data were supplemented by oriented load structures, as discussed in chapter 7.

In cases where symmetrical ripple data alone were utilized to determine shoreline orientation, the offshore direction was inferred from the vector mean orientation of directional flow indicators from the bases of hummocky cross-stratified sandstones (or amalgamation couplets). This determination of the offshore direction was based upon the assumption that the storm-generated flows which deposited the hummocky beds possessed a component of flow generally directed offshore (not onshore). In cases where flow was essentially parallel to the shoreline, the context of shoreline orientations and offshore directions determined from surrounding exposures was used to resolve the ambiguity.

The small arrows on figure 7-4A represent vector mean orientations of proximal offshore flows, as discussed in

chapter 7.

The large stippled arrows of figure 7-4A represent crudely generalized directions of shoreline progradation determined by optically smoothing the data discussed above. The shoreline is assumed to have prograded generally in the offshore direction.

APPENDIX 6. SUMMARY OF THE EXISTING STRATIGRAPHIC SYSTEM FOR THE CARDIUM FORMATION IN FOOTHILLS EXPOSURES

Figure 3-1 illustrates the member scheme for the Cardium Formation as defined by Stott (1963, 1975). The definition of each of these units is summarized below; these definitions and descriptions are extracted from Stott (1963, 1975).

Ram Member. "The massive sandstone at the base of the Cardium Formation comprises the Ram member.... The basal contact with the Blackstone Formation is gradational but an arbitrary boundary is drawn at the base of the lower massive sandstone unit" (Stott, 1963, p. 63). Stott (1963, p. 63) observed that "fine uniform laminae are typical of the Ram sand"; thus, in the definition statement the word "massive" is taken to mean "thick", as opposed to "apparently structureless". It follows, therefore, that the base of the Cardium Formation and the Ram member is arbitrarily placed at the base of the lowest thick sandstone. The required thickness is not specified.

The upper contact of the Ram is defined (where overlain by the Moosehound member) by the sharp contrast

with the overlying carbonaceous sandstones and shales; where overlain by the marine shales of the Kiska member, the contact is similarly well defined.

Moosehound Member. "The Moosehound member comprises a sequence of non-marine shales, siltstone, sandstone, and some coal that lies between the overlying concretionary shales of the Kiska member and the underlying thickly bedded sandstones of the Ram member.... In areas where the Kiska member is replaced by non-marine beds, the Moosehound sediments are overlain by the Cardinal member. North of the McLeod River, the Cardinal is not recognized, and the Moosehound is overlain by marine shales of the Leyland member or by marine sandstones of the Sturrock member" (Stott, 1963, p. 68).

Note that the preceding defininition statement firmly indicates that Moosehound sediments are exclusively non-marine.

Kiska Member. "The marine shales lying on the Moosehound member in the type section but on the basal Ram member in some sections and lying below the siltstone and sandstone of the Cardinal member are included in the Kiska member" (Stott, 1963, p. 72).

Cardinal Member. "The Cardinal member comprises beds of massive, argillaceous siltstone and sandstone that

occur in the middle of the Cardium.... The upper boundary is well defined with an abrupt change...to the shales of the overlying Leyland member and in may places is marked by pebbles.... The lower boundary is drawn at the base of the massive siltstone" (Stott, 1963, p. 73).

Leyland Member. "A shale unit below the upper sandstone of the Cardium Formation is named the Leyland member.... The upper boundary is drawn at the base of the thickly bedded sandstones of the Sturrock member.... The lower boundary is placed at the base of the marine shale and may be marked by pebble beds." (Stott, 1963, p. 74-75).

Sturrock Member. "The uppermost fine-grained sandstone of the Cardium Formation is designated as the Sturrock member.... The lower boundary is drawn at the base of thickly bedded sandstone.... As defined, the Sturrock member consists of sandstone with minor quantities of shale and some carbonaceous sediments. The non-marine beds in the upper part of the formation west of the Bighorn and Nikanassin Ranges have been included in the member.... The top of the Sturrock member is usually concretionary and forms a resistant massive bed.... Pebbles may be embedded in the sand but more commonly lie above the fine-grained sandstone." (Stott, 1963, p. 77-81). From this description, it is apparent that the Sturrock member

consists of both marine and non-marine beds, and that the conglomerates which cap the Cardium Formation were included by Stott within the basal Wapiabi Formation.

Baytree Member. Stott (1975, p. 462, also Fig. 9) indicates that "coarse-grained, conglomeratic sandstone of the Baytree Member" overlies the Moosehound Member in N. E. British Columbia and N. W. Alberta. No depositional environment was inferred for these coarse deposits. Field work for this thesis did not include examination of the Baytree Member.

APPENDIX 7. SUMMARY OF THE REVISED STRATIGRAPHIC SYSTEM FOR THE CARDIUM FORMATION IN FOOTHILLS EXPOSURES

Figure 3-1 compares the existing member scheme for the Cardium Formation (defined by Stott, 1963, 1975) and the revised member scheme defined in this thesis. The definitions and descriptions of Stott's stratigraphic units are summarized in appendix 6. The definitions and descriptions of the revised units are summarized below; these decriptions emphasize criteria for their recognition and mapping in the field.

In the following discussion, no distinction is made between the Blackstone and Kaskapau Formations. References to the Blackstone Formation contained in this appendix apply equally to the Kaskapau Formation in the northern Foothills.

The type section for the Cardium Formation designated by Stott (1963) is not completely exposed; several critical transitions are covered (see vertical graphic log for section WA-1 in appendix 2). Also, vertical facies sequences at section WA-1 are not wholly typical of the formation in general. For these reasons, coupled with the extreme inaccessibility of this section, I

suggest abandonment of this exposure as the type section. In its place, I propose that section 5-45 on the Ram River be formally designated as the new type section of the Cardium Formation. This is an exceptionally thick section, completely and very well exposed. Vertical facies sequences are completely typical of the formation in general; a well developed thinning- and fining-upward cycle cap is also present, as are thick resedimented-lag transgressive conglomerates. Section 5-45 is easily accessible by the Forestry Trunk Road from either Edmonton or Calgary. Unfortunately, no non-marine deposits are present at section 5-45; for this reason, I have chosen to designate section 5-37 on Littlehorn Creek as the principal reference section of the Cardium Formation. This is the only exposure examined by the author in which all the members of the Cardium Formation are exposed (with the exception of the Baytree Member of British Columbia and north-central Alberta, which was not examined in this study). Section 5-37 also is exceptionally thick and completely and excellently exposed, and displays the Obstruction Member and both tongues of the Cutpick Member; the Upper Tongue of the Cutpick at this section displays an occurrence of the rare interbedded-fill channel deposits (facies 4IF). Unfortunately, access to section 5-37 is relatively difficult.

Directions to these and all other sections measured

for this study are presented in appendix 1.

REVISED MEMBER STRATIGRAPHY

Seebe Member. The Seebe Member is present in all outcrops examined in this study; it consists of the marine deposits above the Blackstone Formation and below the Cutpick or Sundre Members. Detailed discussion of the Blackstone-Seebe contact is presented under a separate heading below.

The Seebe-Cutpick contact (throughout the northern and central Foothills) is easily distinguished by the transition to non-marine deposits.

In the southern Foothills and the southern part of the central Foothills, where non-marine deposits are not present, the marine Sundre Member lies directly upon the marine Seebe Member. The Seebe-Sundre contact can be traced with absolute certainty only by comparison and correlation of the constituent cycles in these members (see correlation diagrams of chapter 6). In isolated exposures, however, this contact commonly can be recognized by the following three criteria:

1) The top of the major sandstone in the Cardium in the southern Foothills typically represents the

Seebe-Sundre boundary.

2) In this area, the Seebe-Sundre contact typically is overlain by the major conglomerate in the lower half of the formation.

3) The uppermost Seebe sandstone in this area typically is less extensively bioturbated than the coarse sediments contained in the overlying Sundre cycle(s).

As has been discussed in chapters 3 and 6 of this thesis, small splits of non-marine deposits locally extend into the underlying Seebe Member from the overlying Cutpick Member where the latter unit is present in the northern and central Foothills.

The Seebe Member derives its name from an occurrence which is well exposed and conveniently accessible from Calgary. This exposure is at the Seebe Damsite (section 6-28) on the Bow River, the boundary between the southern and central Foothills. This exposure has been described in detail by Wright & Walker (1981). Excellently exposed, thick occurrences of the Seebe Member are also present in the new type section (section 5-45) and the principal reference section (section 5-37). At sections 6-28 and 5-45, the Seebe is immediately overlain by the marine Sundre Member; section 5-37 displays an excellent transition from the marine Seebe Member to the

non-marine deposits of the Cutpick Member.

Cutpick Member. The Cutpick Member is the major non-marine (lagoonal and fluvial) development in Foothills exposures. This member is present throughout the northern Foothills and most of the central Foothills; where present, the Cutpick always lies directly upon the Seebe Member (but see discussion of tonguing relationships below). Most occurrences of the Cutpick are dominated by soft, coaly shales; these occurrences are less resistant than surrounding marine strata. Thus, exposures of the Cutpick generally are poor and patchy. Large fluvial channel sandstones in the Cutpick are exceptions to this generality (e.g., the well exposed non-marine interval at section 5-22 on Maskuta Creek is dominated by fluvial sandstones).

In the northern Foothills, the Cutpick Member is vertically continuous, and is in this area referred to informally as the Main Body of the Cutpick. In the central Foothills, the Cutpick is divided by the marine Sundre Member into two major tongues of non-marine sediments, informally designated the Upper and Lower Tongues of the Cutpick. The Cutpick Member is not present in the southern Foothills or the southernmost exposures in the central Foothills. The Lower Tongue of the Cutpick is everywhere overlain by the Sundre Member. The Upper Tongue and Main Body of the Cutpick are everywhere overlain by the Willmore

Member (except in the extreme northern Foothills, where the Cutpick is directly overlain by the Wapiabi Formation). These relationships (and those involving the minor splits of the Cutpick, discussed below) are best appreciated by inspecting the correlation diagrams of chapter 6.

Several minor splits of the Cutpick protrude into the underlying Seebe Member in the northern and central Foothills; these have been thoroughly discussed in various chapters of the thesis. In the southern part of the northern Foothills, where outcrop is particularly scarce, I have recognized a single non-marine split of the Cutpick which protrudes into the overlying Willmore Member (the Little Berland Split of the Cutpick Member). This split defines the Upper Tongue, Lower Tongue, and Main Body of the Willmore Member, as shall be discussed in detail below. Note that the minor splits of the Cutpick protruding into the Seebe Member have <u>not</u> been used to similarly sub-divide the Seebe Member; such an attempt at sub-division would be overly complicated and non-productive.

The Cutpick Member derives its name from the excellent exposure of the Main Body of the Cutpick on Cutpick Hill at section CU-1. This section is exposed in a small, steeply sloping ravine; hence, even the non-resistant mudstones of the Cutpick Member are well exposed at this locality. In fact, this occurrence is the thickest continuous exposure of the Cutpick Member observed

in the sections examined by this author, with the single exception of the occurrence on Maskuta Creek (section 5-22) where the Cutpick Member is anomalously coarse, being dominated by thick fluvial channel sandstones. Additionally, the Cutpick Hill section displays a rare occurrence of facies 4IF (interbedded channel-fill deposits).

The principal reference section of the Cardium Formation (section 5-37) presents an opportunity to examine the two major tongues of the Cutpick Member, and to examine their relationship with the intervening Sundre Member. The most convenient localities for the inspection of the Cutpick Member are the sections in the viscinity of Grande Cache, where a minor non-marine split protruding into the Seebe Member may also be examined.

Sundre Member. The marine Sundre Member is defined in the central Foothills (i.e., in the northernmost area of its extent), where it is completely enveloped by the non-marine Cutpick Member. Here, the Sundre is underlain and overlain by the Lower Tongue and Upper Tongue of the Cutpick, respectively; further to the northwest, the Sundre pinches out, being replaced by the Main Body of the Cutpick Member. By the comparison and correlation of cycles within laterally adjacent exposures, the Sundre Member can be traced with confidence to the southwest, beyond the maximum

extent of the non-marine deposits of the Cutpick Member. The Sundre is present throughout the southern Foothills, where it is underlain by the marine Seebe Member and overlain by the marine Willmore Member.

Within individual exposures in the southern Foothills, the marine Sundre Member typically can be distinguished from the vertically adjacent marine members by the following criteria:

1) The sediments of the Sundre Member commonly are more extensively bioturbated than the surrounding strata.
2) The Sundre Member commonly is bounded by the two major conglomerates present <u>within</u> the Cardium Formation. The lower of these conglomerates is included in the Sundre Member; the upper conglomerate is included in the overlying Willmore Member. Note that a third major conglomerate typically is present at the base of the Wapiabi Formation.
3) The Sundre Member consists of one or two marine cycles which occupy roughly the middle third of the thickness of the Cardium Formation.

The conglomerates (mentioned above) present locally at the contact between the Sundre Member and an underlying member are always included in the Sundre Member, for reasons that shall be discussed separately below.

Similarly, conglomerates present at the upper contact of the Sundre are always included in the overlying Willmore Member (see below).

The Sundre Member derives its name from a well exposed, easily accessible, relatively thick occurrence on the Red Deer River (section 6-8). The name "Red Deer" has been pre-empted by prior usage; the community of Sundre, Alberta, is the first settlement immediately downstream of this exposure on the Red Deer River.

Another excellent exposure of the Sundre Member is present in the new type section of the Cardium Formation (section 5-45). The principal reference section (section 5-37) illustrates the definition of the Sundre Member by means of the surrounding non-marine strata; this relationship is also clearly evident in the more easily accessible sections on Thistle Creek.

Willmore Member. The marine Willmore Member has been traced throughout the Alberta Foothills to where it pinches out in the extreme northern Foothills near the British Columbia border; in this northern area, the non-marine Cutpick Member is directly overlain by the Wapiabi Formation, and the Willmore is absent. Where present, the Willmore is the uppermost member of the Cardium Formation, except in the inner central Foothills west of the Bighorn and Nikanassin Ranges; in this area, a

transition to non-marine depositional environments is present at the top of the Cardium, and the Willmore Member is overlain by the non-marine Obstruction Member.

The Willmore Member overlies the non-marine Main Body and Upper Tongue of the Cutpick Member throughout most of the northern and central Foothills. Where the Cutpick pinches out in the southern central Foothills, the Willmore overlies the marine Sundre Member, from which it can be distinguished by the comparison and correlation of the constituent cycles. In the southern Foothills, a major conglomerate commonly is present at the Sundre-Willmore contact; further north, this conglomerate locally is also present at the Cutpick-Willmore contact. This conglomerate is included in the Willmore Member for reasons discussed in detail below. The basal conglomerate of the Willmore Member is the highest major conglomerate within the fully marine Cardium Formation in the southern Foothills. Another major conglomerate typically is present at the Willmore-Wapiabi contact throughout the Alberta Foothills; this conglomerate is included in the overlying Wapiabi Formation for reasons discussed in detail below.

In the southernmost northern Foothills, the non-marine Little Berland Split of the Cutpick Member protrudes into the overlying Willmore Member; due to the extreme scarcity of outcrop in this region, this split was only recognized at section 5-19 on the Little Berland

River. At this section, this split defines two separate tongues of the Willmore Member, referred to informally as the Upper and Lower Tongues. In exposures to the southeast of section 5-19, the Little Berland Split is not present; the two tongues of the Willmore are vertically juxtaposed, thus forming the Main Body of the Willmore Member. In exposures to the northwest of section 5-19, the Lower Tongue of the Willmore is not present (being replaced by non-marine deposits of the Cutpick Member); however, the Upper Tongue of the Willmore Member continues throughout most of the northern Foothills, where it directly overlies the Cutpick Member.

The Willmore Member derives its name from the exposure on the Little Berland River (section 5-19), at which section the Lower and Upper Tongues of the member have been defined. The name "Berland" has been pre-empted by prior usage; the name "Willmore" is derived from the Willmore Wilderness, the boundary of which is located only 2 km from section 5-19.

The Willmore Member is well developed and exposed at the type section of the Cardium Formation (section 5-45). A superb example of a thinning- and fining-upward cycle cap is developed in the Willmore at this locality, as are the major transgressive conglomerates found at the lower and upper contacts of the member. At the principal reference section (section 5-37), a transition to the

non-marine Obstruction Member can be observed.

Obstruction Member. The non-marine Obstruction Member is the thinnest and most areally restricted member of the Cardium Formation. Stott (1963) reports that non-marine beds are present at the top of the Cardium in exposures in the inner central Foothills west of the Bighorn and Nikanassin Ranges; I have examined only one complete Cardium section in this area, the principal reference section (section 5-37, Littlehorn Creek). In this exposure, the marine beds of the Willmore Member are overlain by the non-marine Obstruction Member, which in turn is overlain by a transgressive conglomerate included at the base of the Wapiabi Formation (see further discussion under a separate heading below).

The name "Littlehorn" has been pre-empted by prior usage. The exposure on Littlehorn Creek is directly below the McConnell thrust (locally, the structural boundary between the Foothills and the Front Ranges); the name "Obstruction" is derived from a peak in the Front Ranges near the Littlehorn Creek locality.

EXTENDED DISCUSSION OF FORMATIONAL BOUNDARIES AND OTHER PARTICULARS OF THE REVISED STRATIGRAPHIC SYSTEM

Blackstone-Seebe Contact

The contact between the Blackstone and Cardium Formations can conveniently be defined in either of two ways, as shall be discussed in detail below. I shall commense this discussion by first demonstrating that the "transition beds" of the lowermost Cardium cycle in any exposure (formerly included by Stott, 1963, in the underlying Blackstone Formation) are best included in the Seebe Member of the Cardium Formation.

Stott's definitional criterion for the base of the Cardium is discussed in appendix 6. Stott defines the base of the Cardium as the base of the first "massive" (i.e., thick) sandstone bed; thickness was not specified. Inspection of Stott's measured sections clearly indicates that his criterion is <u>not</u> meant to included decimeter-scale sandstones from the lowermost cycle in any exposure, but rather is meant to indicate beds with thicknesses typically greater than 1 m. These thicker sandstones generally are representative of association 3 (thick shoreface-attached sandstones).

The decimeter-scale sandstones of the transition interval are hummocky cross-stratified, and can be classed

in association 2. These deposits are not typical of any other beds in the mudstone-dominated Blackstone Formation; however, these beds are completely typical of the other sandstones in the Cardium Formation, and in fact are typical of other sandstones which generally are present higher in the Seebe Member. Thus, it is logical to assign these decimeter-scale sandstones to the Cardium Formation, rather than the Blackstone Formation. This re-assignment will be of value to exploration geologists; it will improve the significance of isopach maps and other geometrical constructs derived from data obtained strictly from the Cardium Formation.

Note that the thinner sandstones of association 1 (which typically occur below the transition beds) cannot be distinguished in the field from similar beds occurring at a variety of stratigraphic levels throughout the Blackstone Formation. Thus, it is reasonable to place these beds within the Blackstone Formation (but see additional remarks below).

In accordance with the above discussion, two new criteria for the distinction of the Blackstone and Cardium Formations can be suggested. These two criteria represent different approaches to the definition of stratigraphic units; they are summarized and compared below. The two different definitional criteria are as follows:

1) The basal Seebe Member of the Cardium Formation can be defined so as to consist of all (and only) those deposits from association 2 and higher-numbered associations below the Cutpick and/or Sundre Members. Alternatively,

2) The base of the Seebe Member can be drawn at the base of the lowest occurrence of deposits from association 2 or higher-numbered associations.

The distinction between these two criteria is best illustrated diagrammatically. Figure 6-8 (pg. 405) provides an illustration of this distinction from correlative cycles in the Grande Cache area of Alberta. In this figure, non-marine deposits of the Cutpick Member (including the Grande Cache Split) are represented by a dark stipple pattern. Below these non-marine deposits, the light stipple pattern represents marine sandstones of associations 2 and 3, and the white (non-stippled) areas represent mudstone-dominated deposits of association 1.

According to criterion 1 suggested above, the lightly stippled intervals of figure 6-8 represent the Seebe Member of the Cardium, and the white intervals represent the upper part of the Kaskapau (=Blackstone) Formation. This distinction between these two stratigraphic units results in lithostratigraphically correlative subdivisions of the rocks, with numerous

interdigitations between the Seebe and the Kaskapau in this area. Note that one of these interdigitations of the Kaskapau into the Seebe occurs at a relatively high position within the Seebe, above the minor transgression surface in section MS-1.

While this criterion for the distinction of the Seebe results in strictly correlative stratigraphic units, it also results in exceedingly complicated interdigitations of the two formations. Correlations of these interdigitations are highly tentative in all but the most closely spaced sections (such as those in the Grande Cache area). In the absence of adequate outcrop control, this criterion is of little use sedimentologically.

A more simple criterion for the boundary between the Seebe and the underlying formation follows the example of Stott (1963). The formational boundary is drawn at the base of the transition interval in each exposure (i.e., at the base of the first decimeter- or meter-scale hummocky or bioturbated sandstone encountered in a complete exposure). In figure 6-8, this definitional boundary is represented by the solid line near the base of the measured sections. This definitional boundary is a true lithostratigraphically correlative surface between sections S-4, GC-1, and GC-2; however, it crosses lithostratigraphically correlative beds between sections GC-2 and MS-1. Although imprecise, this definition of the formational boundary has the following

advantages: 1) it is a simple criterion easily mapped in the field, and 2) it permits a crude or approximate correlation of the formational boundary between widely spaced exposures. The use of the first criterion would not permit the correlation of this boundary between any but the most closely spaced exposures, such as those in figure 6-8.

The second, definitional boundary between the formations has been employed in the correlation diagrams of chapter 6, and has been located on the measured sections of appendix 2. The use of this definition of the formational boundary results in the recognition of two informal sub-divisions of the Seebe Member of the Cardium Formation. These are:

1) the "Transition Interval", and
2) the "Main Body" of the Seebe.

The Main Body of the Seebe consists of the uppermost sandstone-dominated interval of the member (i.e., that part of the Seebe which does not include mudstone-dominated interdigitations of the Blackstone Formation defined by criterion 2 discussed above). The underlying Transition Interval of the Seebe is that part of the member which <u>does</u> include such interdigitations; accordingly, the Transition Interval of the Seebe includes that part of the member in which true lithostratigraphic relationships (involving interdigitations and, possibly, isolated lenses) cannot

generally be confidently determined.

Cardium-Wapiabi Contact

Following Stott (1963), the Cardium-Wapiabi contact has been drawn at the base of the last major transgressive conglomerate (or the base of the Wapiabi shales and mudstones in sections where this conglomerate is not present). The last conglomerate has been included at the base of the Wapiabi Formation for two reasons. Firstly, this definition of the contact avoids the stratigraphic difficulties which would arise if these conglomerates were to be included in the underlying Cardium Formation. Specifically, if these conglomerates were to be included in the Willmore Member, this member would, as a result, completely surround the thin non-marine deposits of the Obstruction Member. This stratigraphic relationship would obscure the significance of the regionally extensive transgression which occurs at the base of the Wapiabi Formation as defined in this thesis. Secondly, the base of the last major transgressive conglomerate associated with Cardium sedimentation does indeed appear to represent a major lithostratigraphically correlative surface throughout the Foothills. These conglomerates appear to rest erosionally on a wide variety of facies, including both marine and non-marine deposits (see correlation diagrams of

chapter 6). Thus, this surface is eminently suitable as a formational boundary.

Major Trangressive Conglomerates

As with the basal conglomerates of the Wapiabi Formation, the other two major transgressive conglomerates associated with Cardium sedimentation (i.e., those at the base of the Sundre and Willmore Members) also overlie a variety of facies and appear to be regionally correlative. [Note, however, that they do not extend over as great an area as do the basal Wapiabi conglomerates.] Additionally, the basal Willmore conglomerates also overlie both marine deposits (Sundre Member) and non-marine deposits (Cutpick Member). Thus, these major transgressive conglomerates have been included as the basal beds of the members for the same stratigraphic and sedimentological reasons discussed with regard to the Cardium-Wapiabi contact above.

APPENDIX 8: AN ANNOTATED HISTORY AND BIBLIOGRAPHY OF HUMMOCKY CROSS-STRATIFICATION

The following list of references is by no means complete. I have included most of those papers which I believe to be very influential (for better or for worse), or which address important issues that all students of hummocky cross-stratification should consider. In addition to these papers, the book Cyclic and Event Stratification (1982, G. Einsele & A. Seilacher, ed., published by Springer-Verlag) is must reading.

A more encyclopedic list of references is presented by Duke (1985c).

Gilbert (1899) -- First recognition, description, illustration, and interpretation of hummocky cross-stratification. Has a surprisingly modern ring to it.

Campbell (1966) -- First modern re-discovery of the structure.

Goldring (1971) -- Best published description to date of any hummocky cross-stratified unit. Very lengthy.

Goldring & Bridges (1973) -- Still the best description of the tops of sharp-based hummocky cross-stratified beds, which were referred to as "sublittoral sheet sandstones".

Harms et al. (1975, p.87-91) -- Introduction of preferred term (hummocky cross-stratification). First description of bedding characteristics, vertical facies sequences.

de Raaf et al. (1977) -- A good description of a variety of ancient wave-formed structures, also wave-formed "offshore bar" geometry.

Hamblin & Walker (1979) -- First description of amalgamated hummocky cross-stratification. Presented convincing paleoflow data suggesting introduction of sands into the basin by storm-generated turbidity currents.

Bourgeois (1980) -- Numerical calculations of wave climate and paleobathymetry in an unusually thick transgressive sequence dominated by hummocky cross-stratification.

Kreisa (1981) -- First detailed description of hummocky cross-stratification from mixed siliciclastic-carbonate sediments. Includes a detailed discussion of vertical sequences within beds. First paper

to specify the inferred type of generating storm (tropical hurricanes).

Wright & Walker (1981) -- Suggestion of turbidity-current deposition of shallow-marine conglomerate beds associated with hummocky cross-stratified sandstones. This interpretation has been brought into question in this thesis.

Dott & Bourgeois (1982) -- Excellent detailed description and categorization of bedding sequences, from a variety of units. Introduced the hFXM sequence.

Harms et al. (1982) -- A recent summary of sequences and processes involving hummocky cross-stratification. Includes a state-of-the-art analysis of wave-formed structures and sequences (by J. B. Southard).

Hunter & Clifton (1982) -- Another excellent, detailed description of hummocky cross-stratification and structural sequences within hummocky sandstones. This paper was published before the Dott & Bourgeois (1982) paper, and recognized a similar structural sequence from the same unit. Strong on near-bed processes and comparison with recent sediments. Includes a comment by Clifton representing the first publication of a tentative recognition of recent hummocky cross-stratification.

Leckie & Walker (1982) -- First published description of swaley cross-stratification, suggesting formation by storms in depths above fairweather wave base.

Mount (1982) -- A good description of complex vertical structural sequences within hummocky cross-stratified sandstones.

Marsalia & Klein (1983) -- A limited data base produced this questionable analysis of the paleogeographic distribution of hummocky cross-stratification. Emphasized origin by winter storms. See discussion by Duke (1985a).

Swift et al. (1983) -- Suggested an origin for hummocky cross-stratification involving combined-flow "hummocky megaripples". Many problems with this hypothetical origin. See limited comments by Duke (1985c), and extensive discussion in chapter 8 of this thesis.

Walker et al. (1983) -- Discussion and modification of standard sequence of Dott & Bourgeois (1982), to suggest the BPHFXM sequence. See also the reply by Dott & Bourgeois (1983).

Taylor & Walker (1984) -- Good description and photographs of an excellent exposure of swaley cross-stratification.

Walker (1984, Facies Models, 2nd Edition, p.

141-170) -- A recent summary of sequences and processes involving hummocky cross-stratification. Includes an excellent, provocative discussion of storm-dominated shelves.

Allen (1985) -- Purports to demonstrate that hummocky cross-stratification cannot form under purely oscillatory flow. There are several difficulties with Allen's analysis (see criticisms in chapter 8 of this thesis).

Cotter (1985, Sedimentology, in press) -- Takes up where de Raaf et al. (1977) left off, interpreting their "offshore bars" as shelf sand ridges. Includes an excellent description of hummocky cross-stratified beds, employing a slightly different usage of the term "swaley cross-stratification" from that advocated in this thesis.

Duke (1985a) -- Discussion of paleogeographic analysis and various alternative processes for the origin of hummocky cross-stratification suggested by Marsaglia & Klein (1983).

Duke (1985b) -- Paleogeographic analysis of over 100 tabulated examples of hummocky cross-stratification indicates principal origin due to hurricanes, secondary origin due to winter storms. Includes a discussion of storm distribution during non-glacial episodes. First

worker to suggest an origin for swaley cross-stratification by wave processes which operate quasi-continuously.

APPENDIX 9. TABULATION OF THE DATA OF MANOHAR (1955) FOR THE ONSET OF INCIPIENT AND GENERAL MOTION OF SEDIMENT UNDER OSCILLATORY FLOW

The following tables present threshold-motion data obtained by Manohar (1955) using an oscillating-bed device. I have tabulated his data for sediments of quartz density and very similar densities only. These sediments consisted of quartz sands and glass beads.

The tables in this appendix fall into two groups. The first group reports data for the onset of few-particle displacement, or incipient motion. The second group reports data for the onset of many-particle displacement, or general sediment motion. All of Manohars's data have been translated into the variables and units employed in chapter 8 of this thesis.

Also listed are wave friction factors and boundary Reynolds numbers. These were calculated by the author using the Jonsson diagram (Fig. 8-8). See chapter 8, part 2 for further discussion.

FEW-PARTICLE DISPLACEMENT (incipient motion)

D = 0.0235 cm (upper fine sand)

ρ_s = 2.49 g/cm^3

ν = 0.9776 X 10^{-2} cm^2/s

μ = 0.9756 X 10^{-2} g/(cm·s)

ρ = 0.99797 g/cm^3

water temperature : 21.1°C

d_o (cm)	T (s)	U_m (cm/s)	d_o/D	$U_m d_o/\nu$	f_w	Re_D
121.9	14.511	26.39	5187	3.291 X 10^5	7.6 X 10^{-3}	4
106.7	11.508	29.13	4540	3.179 X 10^5	8.0 X 10^{-3}	4
81.3	9.106	28.05	3460	2.333 X 10^5	8.5 X 10^{-3}	4
61.0	7.653	25.04	2596	1.562 X 10^5	9.3 X 10^{-3}	4
25.4	4.072	19.60	1081	5.092 X 10^4	1.2 X 10^{-2}	4
20.4	3.666	17.48	868.1	3.648 X 10^4	1.4 X 10^{-2}	4
116.9	12.296	29.87	4974	3.572 X 10^5	7.9 X 10^{-3}	5
40.7	5.236	24.42	1732	1.017 X 10^5	1.1 X 10^{-2}	4
76.2	8.491	28.19	3243	2.197 X 10^5	8.9 X 10^{-3}	4
55.5	6.807	25.61	2362	1.454 X 10^5	9.7 X 10^{-3}	4
35.5	5.007	22.27	1511	8.087 X 10^4	1.1 X 10^{-2}	4
111.8	11.301	31.08	4757	3.554 X 10^5	8.0 X 10^{-3}	5
91.4	9.802	29.29	3889	2.738 X 10^5	8.5 X 10^{-3}	5
71.1	8.502	26.27	3026	1.911 X 10^5	9.0 X 10^{-3}	4
50.8	6.308	25.30	2162	1.314 X 10^5	9.2 X 10^{-3}	4
30.5	4.440	21.58	1298	6.733 X 10^4	1.2 X 10^{-2}	4
101.6	11.301	28.24	4323	2.935 X 10^5	8.0 X 10^{-3}	4
45.7	6.160	23.31	1945	1.090 X 10^5	1.0 X 10^{-2}	4
86.4	9.002	30.15	3677	2.665 X 10^5	8.8 X 10^{-3}	5
96.5	10.777	28.13	4106	2.777 X 10^5	8.0 X 10^{-3}	4
66.0	8.004	25.91	2809	1.749 X 10^5	9.1 X 10^{-3}	4

All "laminar" according to Manohar.

FEW-PARTICLE DISPLACEMENT (incipient motion)

D = 0.0280 cm (lower medium sand)

ρ_s = 2.65 g/cm^3

ν = 0.9285 X 10^{-2} cm^2/s

μ = 0.9261 X 10^{-2} g/(cm-sec)

ρ = 0.99746 g/cm^3

water temperature : 23.3°C

d_o (cm)	T (s)	U_m (cm/s)	d_o/D	$U_m d_o/\nu$	f_w	Re_D
121.9	11.004	34.80	4354	4.569 X 10^5	8.0 X 10^{-3}	7
106.7	9.593	34.94	3811	4.015 X 10^5	8.6 X 10^{-3}	7
81.3	8.457	30.20	2904	2.664 X 10^5	9.0 X 10^{-3}	6
61.0	6.785	28.24	2179	1.855 X 10^5	9.5 X 10^{-3}	6
25.4	*3.481	22.92	907.1	6.269 X 10^4	1.3 X 10^{-2}	6
20.4	*3.110	20.61	728.6	4.528 X 10^4	1.5 X 10^{-2}	5
16.9	10.686	34.37	4175	4.327 X 10^5	7.9 X 10^{-3}	7
40.7	4.724	27.07	1454	1.187 X 10^5	1.1 X 10^{-2}	6
76.2	7.616	31.43	2721	2.579 X 10^5	9.4 X 10^{-3}	6
55.5	6.030	28.92	1982	1.729 X 10^5	1.0 X 10^{-2}	6
35.5	4.425	25.20	1268	9.635 X 10^4	1.1 X 10^{-2}	6
111.8	10.300	34.10	3993	4.106 X 10^5	8.0 X 10^{-3}	7
91.4	8.715	32.95	3264	3.244 X 10^5	8.8 X 10^{-3}	7
71.1	7.306	30.57	2539	2.341 X 10^5	9.2 X 10^{-3}	6
50.8	5.686	28.07	1814	1.536 X 10^5	1.0 X 10^{-2}	6
30.5	*4.002	23.94	1089	7.864 X 10^4	1.2 X 10^{-2}	6
101.6	9.420	33.88	3629	3.707 X 10^5	8.7 X 10^{-3}	7
45.7	4.947	29.02	1632	1.428 X 10^5	1.1 X 10^{-2}	6
86.4	8.300	32.70	3086	3.043 X 10^5	9.0 X 10^{-3}	7
96.5	9.267	32.71	3446	3.400 X 10^5	8.5 X 10^{-3}	6
66.0	6.943	29.86	2357	2.123 X 10^5	9.4 X 10^{-3}	6

* "turbulent" according to Manohar

Flow conditions were "laminar" according to Manohar, except where period value is marked with an asterisk.

FEW-PARTICLE DISPLACEMENT (incipient motion)

D = 0.0610 cm (lower coarse sand)

ρ_s = 2.54 g/cm^3

ν = 0.9776 X 10^{-2} cm^2/s

μ = 0.9756 X 10^{-2} g/(cm·s)

ρ = 0.99797 g/cm^3

water temperature = 21.1°C

d_o (cm)	T (s)	U_m (cm/s)	d_o/D	$U_m d_o/\nu$	f_w	Re_p
121.9	13.036	29.38	1998	3.663 X 10^5	1.0 X 10^{-2}	13
106.7	11.101	30.20	1749	3.296 X 10^5	1.1 X 10^{-2}	14
91.4	9.350	30.71	1498	2.871 X 10^5	1.1 X 10^{-2}	14
76.2	7.507	31.89	1249	2.486 X 10^5	1.2 X 10^{-2}	15
61.0	6.545	29.28	1000	1.827 X 10^5	1.3 X 10^{-2}	15
45.7	4.955	28.97	749.2	1.354 X 10^5	1.4 X 10^{-2}	15
30.5	3.907	24.52	500.0	7.650 X 10^4	1.5 X 10^{-2}	13
116.9	11.968	30.69	1916	3.670 X 10^5	1.0 X 10^{-2}	14
96.5	9.506	31.89	1582	3.148 X 10^5	1.1 X 10^{-2}	15
71.1	7.005	31.89	1166	2.319 X 10^5	1.2 X 10^{-2}	15
50.8	5.357	29.79	832.8	1.548 X 10^5	1.4 X 10^{-2}	16
35.5	4.107	27.16	582.0	9.863 X 10^4	1.5 X 10^{-2}	15
111.8	11.004	31.92	1833	3.650 X 10^5	1.0 X 10^{-2}	14
86.4	8.537	31.79	1416	2.809 X 10^5	1.1 X 10^{-2}	15
66.0	7.298	28.41	1082	1.918 X 10^5	1.2 X 10^{-2}	14
40.7	4.456	28.69	667.2	1.194 X 10^5	1.5 X 10^{-2}	16
81.3	8.086	31.59	1333	2.627 X 10^5	1.2 X 10^{-2}	15
55.9	5.600	31.36	916.4	1.793 X 10^5	1.3 X 10^{-2}	16
101.6	9.958	32.05	1666	3.331 X 10^5	1.1 X 10^{-2}	15

All "turbulent" according to Manohar.

FEW-PARTICLE DISPLACEMENT (incipient motion)

D = 0.0786 cm (upper coarse sand)

ρ_s = 2.63 g/cm^3

ν = 0.9392 X 10^{-2} cm^2/s

μ = 0.9370 X 10^{-2} g/(cm·s)

ρ = 0.9976 g/cm^3

water temperature : 22.8°C

d_o (cm)	T (s)	U_m (cm/s)	d_o/D	$U_m d_o/\nu$	f_w	Re_D
121.9	-----	-----	1551	----------	----------	--
106.7	9.448	35.48	1358	4.03 X 10^5	1.2 X 10^{-2}	23
91.4	8.097	35.46	1163	3.45 X 10^5	1.2 X 10^{-2}	23
76.2	7.205	33.23	969.5	2.695 X 10^5	1.3 X 10^{-2}	22
61.0	5.900	32.48	776.1	2.109 X 10^5	1.4 X 10^{-2}	23
45.7	4.593	31.26	581.4	1.521 X 10^5	1.5 X 10^{-2}	23
30.5	3.189	30.05	388.0	9.758 X 10^4	1.7 X 10^{-2}	23
116.9	10.455	35.13	1487	4.372 X 10^5	1.1 X 10^{-2}	22
96.5	8.702	34.84	1228	3.579 X 10^5	1.2 X 10^{-2}	23
71.1	7.247	30.82	904.6	2.333 X 10^5	1.3 X 10^{-2}	21
50.8	5.007	31.87	646.3	1.724 X 10^5	1.4 X 10^{-2}	22
35.5	3.580	31.15	451.7	1.177 X 10^5	1.6 X 10^{-2}	23
111.8	9.879	35.55	1422	4.231 X 10^5	1.2 X 10^{-2}	23
86.4	8.246	32.92	1099	3.028 X 10^5	1.2 X 10^{-2}	21
66.0	6.614	31.35	839.7	2.203 X 10^5	1.4 X 10^{-2}	22
40.7	4.134	30.93	517.8	1.340 X 10^5	1.5 X 10^{-2}	22
81.3	8.004	31.91	1034	2.762 X 10^5	1.2 X 10^{-2}	21
55.9	5.661	31.02	711.2	1.846 X 10^5	1.4 X 10^{-2}	22
101.6	9.787	32.61	1293	3.527 X 10^5	1.2 X 10^{-2}	21

All "turbulent" according to Manohar.

FEW-PARTICLE DISPLACEMENT (incipient motion)

D = 0.1006 cm (lower very coarse sand)

ρ_s = 2.60 g/cm^3

ν = 0.9285 X 10^{-2} cm^2/s

μ = 0.9261 X 10^{-2} g/(cm·s)

ρ = 0.99746 g/cm^3

water temperature : 23.3°C

d_o (cm)	T (s)	U_m (cm/s)	d_o/D	$U_m d_o/\nu$	f_w	Re_D
121.9	10.134	37.79	1212	4.961 X 10^5	1.2 X 10^{-2}	32
106.7	9.593	34.94	1061	4.015 X 10^5	1.2 X 10^{-2}	29
91.4	8.055	35.65	908.5	3.509 X 10^5	1.3 X 10^{-2}	31
76.2	-----	-----	757.5	----------	----------	--
61.0	5.872	32.64	606.4	2.144 X 10^5	1.5 X 10^{-2}	31
45.7	4.440	32.34	454.3	1.592 X 10^5	1.6 X 10^{-2}	31
30.5	3.095	30.96	303.2	1.017 X 10^5	1.9 X 10^{-2}	33
116.9	10.200	36.01	1162	4.534 X 10^5	1.2 X 10^{-2}	30
96.5	-----	-----	959.2	----------	----------	--
71.1	6.586	33.92	706.8	2.597 X 10^5	1.4 X 10^{-2}	31
50.8	4.878	32.72	504.9	1.790 X 10^5	1.6 X 10^{-2}	32
35.5	------	-----	352.9	----------	----------	--
111.8	9.666	36.34	1111	4.376 X 10^5	1.2 X 10^{-2}	31
86.4	7.634	35.56	858.8	3.309 X 10^5	1.4 X 10^{-2}	32
66.0	6.209	33.39	656.1	2.373 X 10^5	1.5 X 10^{-2}	31
40.7	3.903	32.76	404.6	1.436 X 10^5	1.7 X 10^{-2}	33
81.3	7.349	34.75	808.2	3.043 X 10^5	1.3 X 10^{-2}	30
55.9	-----	-----	555.7	----------	----------	--
101.6	8.690	36.73	1010	4.019 X 10^5	1.2 X 10^{-2}	31

All "turbulent" according to Manohar.

FEW-PARTICLE DISPLACEMENT (incipient motion)

D = 0.1829 cm (upper very coarse sand)

ρ_s = 2.60 g/cm^3

ν = 0.9525 X 10^{-2} cm^2/s

μ = 0.9503 X 10^{-2} g/(cm-s)

ρ = 0.99772 g/cm^3

water temperature : 22.2°C

d_o (cm)	T (s)	U_m (cm/s)	d_o/D	$U_m d_o/\nu$	f_w	Re_D
121.9	8.160	46.93	666.5	6.006 X 10^5	1.5 X 10^{-2}	78
106.7	7.552	44.39	583.3	4.973 X 10^5	1.6 X 10^{-2}	76
91.4	6.525	44.01	499.7	4.223 X 10^5	1.6 X 10^{-2}	76
76.2	5.610	42.67	416.6	3.361 X 10^5	1.6 X 10^{-2}	73
61.0	4.586	41.79	333.5	2.676 X 10^5	1.9 X 10^{-2}	72
45.7	3.820	37.58	249.9	1.803 X 10^5	2.1 X 10^{-2}	74
30.5	2.732	35.07	166.8	1.123 X 10^5	2.5 X 10^{-2}	75
116.9	7.854	46.76	639.1	5.739 X 10^5	1.5 X 10^{-2}	78
96.5	6.785	44.68	527.6	4.527 X 10^5	1.6 X 10^{-2}	76
71.1	5.407	41.31	388.7	3.084 X 10^5	1.7 X 10^{-2}	73
50.8	4.217	37.85	277.7	2.019 X 10^5	2.0 X 10^{-2}	72
35.5	2.992	37.27	194.1	1.389 X 10^5	2.3 X 10^{-2}	76
111.8	7.844	44.78	611.3	5.256 X 10^5	1.5 X 10^{-2}	74
86.4	6.793	39.96	472.4	3.625 X 10^5	1.6 X 10^{-2}	69
66.0	5.108	40.59	360.9	2.813 X 10^5	1.8 X 10^{-2}	74
40.7	3.433	37.25	222.5	1.592 X 10^5	2.1 X 10^{-2}	74
81.3	6.042	42.27	444.5	3.608 X 10^5	1.6 X 10^{-2}	73
55.9	4.654	37.73	305.6	2.214 X 10^5	1.8 X 10^{-2}	69
101.6	7.588	42.06	555.5	4.486 X 10^5	1.6 X 10^{-2}	73

All "turbulent" according to Manohar.

FEW-PARTICLE DISPLACEMENT (incipient motion)

D = 0.1981 cm (upper very coarse sand)

ρ_s = 2.63 g/cm^3

ν = 0.9525 X 10^{-2} cm^2/s

μ = 0.9503 X 10^{-2}g/(cm·s)

ρ = 0.99772 g/cm^3

water temperature : 22.2°C

d_o (cm)	T (s)	U_m (cm/s)	d_o/D	$U_m d_o/\nu$	f_w	Re_D
121.9	-----	-----	615.3	----------	----------	--
106.7	7.570	44.28	538.6	4.960 X 10^5	1.6 X 10^{-2}	82
91.4	6.749	42.55	461.4	4.083 X 10^5	1.6 X 10^{-2}	79
76.2	5.845	40.96	384.7	3.277 X 10^5	1.8 X 10^{-2}	81
61.0	4.537	42.24	307.9	2.705 X 10^5	1.9 X 10^{-2}	86
45.7	3.607	39.80	230.7	1.910 X 10^5	2.0 X 10^{-2}	83
30.5	2.440	39.27	154.0	1.257 X 10^5	2.5 X 10^{-2}	91
116.9	8.537	43.02	590.1	5.280 X 10^5	1.5 X 10^{-2}	77
96.5	7.392	41.01	487.1	4.155 X 10^5	1.6 X 10^{-2}	76
71.1	5.075	44.01	358.9	3.285 X 10^5	1.8 X 10^{-2}	87
50.8	4.002	39.88	356.4	2.127 X 10^5	1.8 X 10^{-2}	79
35.5	2.774	40.20	179.2	1.498 X 10^5	2.4 X 10^{-2}	92
111.8	8.128	43.21	564.4	5.072 X 10^5	1.5 X 10^{-2}	78
86.4	5.754	47.17	436.1	4.279 X 10^5	1.6 X 10^{-2}	88
66.0	4.871	42.57	333.2	2.950 X 10^5	1.7 X 10^{-2}	82
40.7	3.235	39.52	205.5	1.689 X 10^5	2.1 X 10^{-2}	84
81.3	5.978	42.73	410.4	3.647 X 10^5	1.7 X 10^{-2}	82
55.9	4.274	41.09	282.2	2.411 X 10^5	1.9 X 10^{-2}	83
101.6	7.340	43.39	512.9	4.639 X 10^5	1.5 X 10^{-2}	78

All "turbulent" according to Minohar.

MANY-PARTICLE DISPLACEMENT (onset of general motion)

$D = 0.0147$ cm (lower fine sand)

$\rho_s = 2.65$ g/cm^3

$\nu = 0.9393 \times 10^{-2}$ cm^2/s

$\mu = 0.9370 \times 10^{-2}$ g/(cm·s)

$\rho = 0.9976$ g/cm^3

water temperature : 22.8°C

d_o (cm)	T (s)	U_m (cm/s)	d_o/D	$U_m d_o/\nu$	f_w	Re_D
121.9	15.104	25.35	8293	3.289×10^5	6.0×10^{-3}	2
106.7	11.424	29.34	7259	3.333×10^5	6.7×10^{-3}	3
81.3	10.134	25.20	5531	2.181×10^5	7.5×10^{-3}	2
61.0	7.616	25.16	4150	1.634×10^5	8.0×10^{-3}	2
25.4	4.304	18.54	1728	5.013×10^4	1.1×10^{-2}	2
20.4	4.015	15.96	1388	3.466×10^4	1.2×10^{-2}	2
116.9	12.928	28.41	7952	3.536×10^5	6.1×10^{-3}	3
40.7	5.512	23.20	2769	1.005×10^5	9.1×10^{-3}	2
76.2	8.812	27.17	5184	2.204×10^5	8.0×10^{-3}	3
55.9	6.785	25.88	3803	1.540×10^5	8.6×10^{-3}	3
35.5	4.995	22.33	2415	8.439×10^4	9.6×10^{-3}	2
112.3	10.965	32.18	7639	3.847×10^5	6.5×10^{-3}	3
91.4	9.308	30.85	6218	3.002×10^5	7.0×10^{-3}	3
71.1	8.887	25.13	4837	1.902×10^5	7.9×10^{-3}	2
50.8	6.997	22.81	3456	1.234×10^5	8.5×10^{-3}	2
30.5	4.999	19.17	2075	6.225×10^4	1.0×10^{-2}	2
101.6	10.686	29.87	6912	3.231×10^5	6.9×10^{-3}	3
45.7	6.491	22.12	3109	1.076×10^5	9.0×10^{-3}	2
86.4	9.910	27.39	5878	2.519×10^5	7.1×10^{-3}	3
96.5	10.118	29.96	6565	3.078×10^5	6.8×10^{-3}	3
66.0	8.004	25.91	4490	1.821×10^5	7.9×10^{-3}	3

All "laminar" according to Manohar.

MANY-PARTICLE DISPLACEMENT (onset of general motion)

D = 0.0235 cm (upper fine sand)

ρ_s = 2.49 g/cm^3

ν = 0.8812 X 10^{-2} cm^2/s

μ = 0.8785 X 10^{-2} g/(cm-s)

ρ = 0.99690 g/cm^3

water temperature : 25.6°C

d_o (cm)	T (s)	U_m (cm/s)	d_o/D	$U_m d_o/\nu$	f_w	Re_D
121.9	12.823	29.87	5187	4.132 X 10^5	7.9 X 10^{-3}	5
106.7	9.711	34.52	4540	4.180 X 10^5	7.9 X 10^{-3}	5
81.3	8.004	31.91	3460	2.944 X 10^5	8.6 X 10^{-3}	5
61.0	6.405	29.92	2596	2.071 X 10^5	9.1 X 10^{-3}	5
25.4	3.670	21.74	1081	6.266 X 10^4	1.2 X 10^{-2}	4
20.4	3.202	20.02	868.1	4.635 X 10^4	1.4 X 10^{-2}	5
116.9	10.005	36.71	4974	4.869 X 10^5	7.9 X 10^{-3}	6
40.7	4.672	27.37	1732	1.264 X 10^5	1.1 X 10^{-2}	5
76.2	7.700	31.09	3243	2.688 X 10^5	8.8 X 10^{-3}	5
55.9	6.209	28.28	2379	1.794 X 10^5	9.7 X 10^{-3}	6
35.5	4.504	24.76	1511	9.974 X 10^4	1.1 X 10^{-2}	4
112.3	10.403	33.91	4779	4.321 X 10^5	7.9 X 10^{-3}	5
91.4	8.311	34.55	3889	3.584 X 10^5	8.4 X 10^{-3}	5
71.1	6.897	32.39	3026	2.613 X 10^5	9.0 X 10^{-3}	5
50.8	5.507	28.98	2162	1.671 X 10^5	9.9 X 10^{-3}	5
30.5	4.107	23.33	1298	8.075 X 10^4	1.2 X 10^{-2}	4
101.6	~~10.517~~	30.94	4323	3.567 X 10^5	8.1 X 10^{-2}	5
45.7	5.507	26.07	1945	1.352 X 10^5	1.0 X 10^{-2}	4
86.4	7.709	35.21	3677	3.452 X 10^5	8.8 X 10^{-3}	6
96.5	9.802	30.93	4106	3.387 X 10^5	8.0 X 10^{-3}	5
66.0	7.005	29.60	2809	2.217 X 10^5	9.2 X 10^{-3}	5

All "laminar" according to Manohar.

MANY-PARTICLE DISPLACEMENT (onset of general motion)

D = 0.0280 cm (lower medium sand)

ρ_s = 2.65 g/cm^3

ν = 0.9285 cm^2/s

μ = 0.9261 g/(cm·s)

ρ = 0.99746 g/cm^3

water temperature : 23.3°C

d_o (cm)	T (s)	U_m (cm/s)	d_o/D	$U_m d_o/\nu$	f_w	Re_D
121.9	10.053	38.09	4354	5.000 X 10^5	8.0 X 10^{-3}	7
106.7	9.133	36.70	3811	4.217 X 10^5	8.7 X 10^{-3}	7
81.3	7.409	34.47	2904	3.018 X 10^5	9.1 X 10^{-3}	7
61.0	6.190	30.96	2179	2.034 X 10^5	9.5 X 10^{-3}	6
25.4	*3.214	24.83	907.1	6.792 X 10^4	1.3 X 10^{-2}	6
20.4	*2.869	22.34	728.6	4.908 X 10^4	1.5 X 10^{-2}	6
116.9	10.420	35.24	4175	4.437 X 10^5	8.0 X 10^{-3}	7
40.7	4.570	27.98	1454	1.226 X 10^5	1.1 X 10^{-2}	6
76.2	7.298	32.80	2721	2.692 X 10^5	9.2 X 10^{-3}	7
55.9	5.791	30.33	1996	1.826 X 10^5	1.0 X 10^{-2}	6
35.5	4.217	26.45	1268	1.011 X 10^5	1.2 X 10^{-2}	6
112.3	9.787	36.05	4011	4.360 X 10^5	8.0 X 10^{-3}	7
91.4	8.344	34.41	3264	3.387 X 10^5	9.0 X 10^{-3}	7
71.1	6.905	32.35	2539	2.477 X 10^5	9.0 X 10^{-3}	7
50.8	5.417	29.46	1814	1.612 X 10^5	1.0 X 10^{-2}	6
30.5	*3.831	25.01	1089	8.215 X 10^4	1.3 X 10^{-2}	6
101.6	8.976	35.56	3629	3.891 X 10^5	8.5 X 10^{-3}	7
45.7	4.778	30.05	1632	1.479 X 10^5	1.1 X 10^{-2}	7
86.4	7.588	35.77	3086	3.329 X 10^5	9.0 X 10^{-3}	7
96.5	9.002	33.68	3446	3.500 X 10^5	8.8 X 10^{-3}	7
66.0	6.379	32.50	2357	2.310 X 10^5	9.7 X 10^{-3}	7

* "turbulent" according to Manohar

Flow conditions were "laminar" according to Manohar, except where period value is marked with an asterisk.

MANY-PARTICLE DISPLACEMENT (onset of general motion)

D = 0.0610 cm (lower coarse sand)

ρ_s = 2.54 g/cm^3

ν = 0.9776 X 10^{-2} cm^2/s

μ = 0.9756 X 10^{-2} g/(cm·s)

ρ = 0.99797 g/cm^3

water temperature : 21.1°C

d_o (cm)	T (s)	U_m (cm/s)	d_o/D	$U_m d_o/\nu$	f_w	Re_D
121.9	11.991	31.94	1998	3.983 X 10^5	1.0 X 10^{-2}	14
106.7	10.005	33.60	1749	3.656 X 10^5	1.1 X 10^{-2}	16
91.4	8.300	34.60	1498	3.235 X 10^5	1.1 X 10^{-2}	16
76.2	-----	-----	1249	----------	----------	--
61.0	6.001	31.93	1000	1.992 X 10^5	1.2 X 10^{-2}	15
45.7	4.504	31.88	749.2	1.490 X 10^5	1.4 X 10^{-2}	17
30.5	3.316	28.90	500.0	9.016 X 10^4	1.6 X 10^{-2}	16
116.9	10.796	34.02	1916	4.068 X 10^5	1.0 X 10^{-2}	15
96.5	8.655	35.03	1582	3.458 X 10^5	1.1 X 10^{-2}	16
71.1	6.511	34.31	1166	2. 95 X 10^5	1.2 X 10^{-2}	17
50.8	4.955	32.21	832.8	1.673 X 10^5	1.4 X 10^{-2}	17
35.5	3.554	31.38	582.0	1.139 X 10^5	1.5 X 10^{-2}	17
111.8	10.005	35.11	1833	4.015 X 10^5	1.0 X 10^{-2}	16
86.4	7.796	34.82	1416	3.077 X 10^5	1.1 X 10^{-2}	16
66.0	6.302	32.90	1082	2.221 X 10^5	1.3 X 10^{-2}	17
40.7	4.054	31.54	667.2	1.313 X 10^5	1.5 X 10^{-2}	17
81.3	7.709	33.13	1333	2.755 X 10^5	1.2 X 10^{-2}	16
55.9	5.302	33.12	916.4	1.894 X 10^5	1.3 X 10^{-2}	17
101.6	8.912	35.82	1666	3.722 X 10^5	1.1 X 10^{-2}	17

All "turbulent" according to Manohar.

MANY-PARTICLE DISPLACEMENT (onset of general motion)

D = 0.0786 cm (upper coarse sand)

ρ_s = 2.63 g/cm^3

ν = 0.9393 X 10^{-2} cm^2/s

μ = 0.9370 X 10^{-2} g/(cm·s)

ρ = 0.9976 g/cm^3

water temperature : 22.8°C

d_o (cm)	T (s)	U_m (cm/s)	d_o/D	$U_m d_o/\nu$	f_w	Re_D
121.9	-----	-----	1551	----------	----------	--
106.7	8.400	39.91	1358	4.356 X 10^5	1.2 X 10^{-2}	26
91.4	7.607	37.75	1163	3.529 X 10^5	1.2 X 10^{-2}	25
76.2	6.353	37.68	969.5	2.937 X 10^5	1.3 X 10^{-2}	25
61.0	5.361	35.75	776.1	2.231 X 10^5	1.4 X 10^{-2}	25
45.7	4.167	34.45	581.4	1.610 X 10^5	1.5 X 10^{-2}	25
30.5	2.793	34.31	388.0	1.070 X 10^5	1.7 X 10^{-2}	27
116.9	9.267	39.63	1487	4.739 X 10^5	1.1 X 10^{-2}	25
96.5	7.786	38.94	1228	3.844 X 10^5	1.2 X 10^{-2}	25
71.1	6.347	35.19	904.6	2.559 X 10^5	1.3 X 10^{-2}	24
50.8	4.460	36.27	646.3	1.885 X 10^5	1.5 X 10^{-2}	26
35.5	3.400	32.80	451.7	1.191 X 10^5	1.6 X 10^{-2}	25
111.8	8.887	39.52	1422	4.520 X 10^5	1.2 X 10^{-2}	26
86.4	7.100	38.23	1099	3.379 X 10^5	1.2 X 10^{-2}	25
66.0	5.807	35.71	839.7	2.411 X 10^5	1.4 X 10^{-2}	25
40.7	3.696	34.59	517.8	1.440 X 10^5	1.6 X 10^{-2}	26
81.3	6.593	38.74	1034	3.222 X 10^5	1.2 X 10^{-2}	25
55.9	5.108	34.38	711.2	1.966 X 10^5	1.4 X 10^{-2}	24
101.6	8.423	37.89	1293	3.938 X 10^5	1.2 X 10^{-2}	25

All "turbulent" according to Manohar.

MANY-PARTICLE DISPLACEMENT (onset of general motion)

D = 0.1006 cm (lower very coarse sand)

ρ_s = 2.60 g/cm^3

ν = 0.9285 X 10^{-2} cm^2/s

μ = 0.9261 X 10^{-2} g/(cm·s)

ρ = 0.99746 g/cm^3

water temperature : 23.3°C

d_o (cm)	T (s)	U_m (cm/s)	d_o/D	$U_m d_o/\nu$	f_w	Re_D
121.9	-----	-----	1212	----------	----------	--
106.7	9.041	37.08	1061	4.261 X 10^5	1.2 X 10^{-2}	31
91.4	7.498	38.30	908.5	3.770 X 10^5	1.3 X 10^{-2}	33
76.2	-----	-----	757.5	----------	----------	—
61.0	5.585	34.31	606.4	2.254 X 10^5	1.5 X 10^{-2}	32
45.7	4.189	34,27	454.3	1.687 X 10^5	1.6 X 10^{-2}	33
30.5	2.922	32.79	303.2	1.077 X 10^5	1.9 X 10^{-2}	35
116.9	9.578	38.34	1162	4.827 X 10^5	1.2 X 10^{-2}	32
96.5	-----	-----	959.2	----------	----------	--
71.1	6.190	36.09	706.8	2.764 X 10^5	1.5 X 10^{-2}	34
50.8	4.710	33.88	504.9	1.854 X 10^5	1.6 X 10^{-2}	33
35.5	-----	-----	352.9	----------	----------	--
111.8	8.378	41.92	1111	5.048 X 10^5	1.2 X 10^{-2}	35
86.4	7.222	37.58	858.8	3.497 X 10^5	1.3 X 10^{-2}	33
66.0	5.818	35.64	656.1	2.533 X 10^5	1.5 X 10^{-2}	33
40.7	3.740	34.19	404.6	1.499 X 10^5	1.7 X 10^{-2}	34
81.3	6.852	37.28	808.2	3.264 X 10^5	1.4 X 10^{-2}	34
55.9	-----	-----	555.7	----------	----------	--
101.6	8.267	38.61	1010	4.225 X 10^5	1.2 X 10^{-2}	32

All "turbulent" according to Manohar.

MANY-PARTICLE DISPLACEMENT (onset of general motion)

$D = 0.1829$ cm (upper very coarse sand)

$\rho_s = 2.60$ g/cm^3

$\nu = 0.9525 \times 10^{-2}$ cm^2/s

$\mu = 0.9503 \times 10^{-2}$ g/(cm·s)

$\rho = 0.99772$ g/cm^3

water temperature : 22.2°C

d_o (cm)	T (s)	U_m (cm/s)	d_o/D	$U_m d_o/\nu$	f_w	Re_D
121.9	-----	-----	666.5	----------	----------	--
106.7	6.756	49.62	583.3	5.558×10^5	1.5×10^{-2}	83
91.4	5.872	48.90	499.7	4.692×10^5	1.6×10^{-2}	84
76.2	5.007	47.81	416.6	3.825×10^5	1.7×10^{-2}	85
61.0	4.274	44.84	333.5	2.872×10^5	1.9×10^{-2}	84
45.7	3.491	41.13	249.9	1.973×10^5	2.0×10^{-2}	79
30.5	2.596	36.91	166.8	1.182×10^5	2.5×10^{-2}	80
116.9	7.392	49.68	639.1	6.097×10^5	1.5×10^{-2}	83
96.5	6.221	48.73	527.6	4.937×10^5	1.6×10^{-2}	84
71.1	5.027	44.43	388.7	3.317×10^5	1.8×10^{-2}	80
50.8	3.785	42.16	277.7	2.249×10^5	2.0×10^{-2}	81
35.5	2.936	37.99	194.1	1.416×10^5	2.2×10^{-2}	77
111.8	7.392	47.51	611.3	5.562×10^5	1.5×10^{-2}	79
86.4	5.928	45.79	472.4	4.153×10^5	1.6×10^{-2}	79
66.0	4.796	43.23	360.9	2.995×10^5	1.8×10^{-2}	79
40.7	3.324	38.47	222.5	1.644×10^5	2.1×10^{-2}	76
81.3	5.512	46.34	444.5	3.955×10^5	1.6×10^{-2}	80
55.9	4.440	39.55	305.6	2.321×10^5	1.9×10^{-2}	74
101.6	6.756	47.24	555.5	5.039×10^5	1.6×10^{-2}	81

All "turbulent" according to Manohar.

MANY-PARTICLE DISPLACEMENT (onset of general motion)

D = 0.1981 cm (upper very coarse sand)

ρ_s = 2.63 g/cm^3

ν = 0.9525 X 10^{-2} cm^2/s

μ = 0.9503 X 10^{-2} g/(cm·s)

ρ = 0.99772 g/cm^3

water temperature : 22.2°C

d_o (cm)	T (s)	U_m (cm/s)	d_o/D	$U_m d_o/\nu$	f_w	Re_D
121.9	-----	-----	615.3	----------	----------	—
106.7	6.905	48.55	538.6	5.439 X 10^5	1.5 X 10^{-2}	87
91.4	5.939	48.35	461.4	4.640 X 10^5	1.6 X 10^{-2}	90
76.2	5.154	46.45	384.7	3.716 X 10^5	1.7 X 10^{-2}	89
61.0	4.002	47.89	307.9	3.067 X 10^5	1.8 X 10^{-2}	94
45.7	3.272	43.88	230.7	2.105 X 10^5	2.0 X 10^{-2}	91
30.5	2.130	44.99	154.0	1.441 X 10^5	2.5 X 10^{-2}	105
116.9	7.516	48.86	590.1	5.997 X 10^5	1.6 X 10^{-2}	91
96.5	6.531	46.42	487.1	4.703 X 10^5	1.6 X 10^{-2}	86
71.1	4.537	49.23	358.9	3.675 X 10^5	1.8 X 10^{-2}	97
50.8	3.642	43.82	256.4	2.337 X 10^5	2.0 X 10^{-2}	91
35.5	2.559	43.58	179.2	1.624 X 10^5	2.3 X 10^{-2}	97
111.8	7.044	49.86	564.4	5.852 X 10^5	1.5 X 10^{-2}	90
86.4	5.635	48.17	436.1	4.369 X 10^5	1.6 X 10^{-2}	90
66.6	4.333	47.85	333.2	3.316 X 10^5	1.8 X 10^{-2}	94
40.7	2.862	44.68	205.5	1.909 X 10^5	2.1 X 10^{-2}	95
81.3	5.108	50.00	410.4	4.268 X 10^5	1.6 X 10^{-2}	93
55.9	3.939	44.58	282.2	2.616 X 10^5	2.0 X 10^{-2}	93
101.6	6.635	48.11	512.9	5.132 X 10^5	1.5 X 10^{-2}	87

All "turbulent" according to Manohar.